NASA TECHNICAL MEMORANDUM

NASA TM X-3534

NASA TM X-3534

TRANSONIC WIND-TUNNEL INVESTIGATION OF THE MANEUVER POTENTIAL OF THE NASA SUPERCRITICAL WING CONCEPT

Phase I

James B. Hallissy and Theodore G. Ayers

Langley Research Center
Hampton, Va. 23665

NATIONAL AERONAUTICS AND SPACE ADMINISTRATION · WASHINGTON, D. C. · SEPTEMBER 1977

1. Report No.	2. Government Accession No.	3. Recipient's Catalog No.
NASA TM X-3534		

4. Title and Subtitle	5. Report Date
TRANSONIC WIND-TUNNEL INVESTIGATION OF THE MANEUVER POTENTIAL OF THE NASA SUPERCRITICAL WING CONCEPT - PHASE I	September 1977
	6. Performing Organization Code

7. Author(s)	8. Performing Organization Report No.
James B. Hallissy and Theodore G. Ayers	L-11064
	10. Work Unit No. 517-51-03-00

9. Performing Organization Name and Address	11. Contract or Grant No.
NASA Langley Research Center Hampton, VA 23665	
	13. Type of Report and Period Covered Technical Memorandum

12. Sponsoring Agency Name and Address	14. Sponsoring Agency Code
National Aeronautics and Space Administration Washington, DC 20546	

15. Supplementary Notes

16. Abstract

An investigation was conducted in the NASA Langley 8-foot transonic pressure tunnel at Mach numbers from 0.60 to 0.975 with a variable-wing-sweep airplane model in order to evaluate a series of wings designed to demonstrate the maneuver potential of the NASA supercritical airfoil concept. Both conventional and supercritical wing designs for several planform configurations were investigated with wing sweep angles from 16.0° to 72.5°, depending on Mach number and wing configuration. The supercritical wing configurations showed significant improvements over the conventional configurations in drag-divergence Mach number and in drag level at transonic maneuver conditions.

17. Key Words (Suggested by Author(s))	18. Distribution Statement
F-111 Supercritical airfoil Variable sweep Transonic maneuver	Unclassified - Unlimited Subject Category 02

19. Security Classif. (of this report)	20. Security Classif. (of this page)	21. No. of Pages	22. Price*
Unclassified	Unclassified	293	$9.25

* For sale by the National Technical Information Service, Springfield, Virginia 22161

TRANSONIC WIND-TUNNEL INVESTIGATION OF THE MANEUVER POTENTIAL OF THE NASA SUPERCRITICAL WING CONCEPT

PHASE I

James B. Hallissy and Theodore G. Ayers
Langley Research Center

SUMMARY

The first phase of a wind-tunnel investigation to evaluate a series of wings designed to demonstrate the maneuver potential of the NASA supercritical airfoil concept has been conducted at Mach numbers from 0.60 to 0.975 with an F-111 airplane model. Both conventional and supercritical wing designs for several planform configurations were investigated with wing sweep angles from 16.0° to 72.5°, depending on Mach number and wing configuration.

The test results indicated that the supercritical wing configurations exhibited substantially lower drag levels at transonic maneuvering conditions and significantly higher drag-divergence Mach numbers at cruise lift coefficients than did the conventional configurations of the same planforms. The supercritical wing configurations generally had more negative pitching-moment coefficients than did the conventional configurations of the same planform, but there was little difference in longitudinal stability for low wing sweep angles and Mach numbers below drag divergence. Aerodynamic range factor maximums for the supercritical wing configurations evaluated in this phase of the investigation were somewhat lower than for the conventional wing configurations of the same planform.

INTRODUCTION

The emphasis on fighter aircraft capable of achieving high maneuver load factors for air-to-air combat at high subsonic speeds has created a need for basic research in the areas of buffet and high-lift drag at transonic speeds. The stringent requirements placed on these aircraft are such that methods must be found to reduce the drag and buffeting associated with shock-induced boundary-layer separation of the wing flow at high maneuvering lift coefficients. Although twist, camber, and sweep have a favorable effect on the wing flow characteristics, as do maneuver strakes, the use of these design methods alone does not fully solve the basic supercritical-flow problem.

Two-dimensional wind-tunnel test results obtained for integral supercritical airfoils have indicated that substantial improvements in aircraft performance at high subsonic speeds might be achieved by special shaping of the airfoil to improve the supercritical flow above the upper surface. Significant increases in the drag-rise Mach number, the maximum lift coefficient for buffet

onset, and the Mach number for buffet onset at a given lift coefficient have been demonstrated for the supercritical airfoil, as compared with an NACA 6-series airfoil of comparable thickness. (See ref. 1.) Corroborative results from three-dimensional wind-tunnel and flight tests are presented in references 2 to 5.

Because these indicated extensions of the buffet boundaries could provide significant improvements in the maneuverability of a fighter airplane, the National Aeronautics and Space Administration (NASA) initiated an exploratory wind-tunnel investigation to define the aerodynamic improvements that could result from direct substitution of a supercritical airfoil on a variable-wing-sweep multimission airplane model. Results of this investigation are presented in reference 6.

Following the exploratory investigation of reference 6, NASA, in a cooperative effort with the General Dynamics Corporation, initiated a wind-tunnel program to demonstrate the aerodynamic advantages in aircraft maneuverability that could be realized through application of supercritical airfoil technology to the F-111 airplane. In anticipation of an eventual full-scale flight validation of the wind-tunnel results, program objectives and constraints were established for a practical design. The objectives of the program were as follows: (1) To maximize the transonic maneuver capability of the F-111 without degrading cruise performance, (2) to minimize penalties on the sea-level dash and supersonic performance, and (3) to maintain existing F-111 take-off and landing performance. The design constraints imposed on the configuration generally limited major airframe modifications to the outboard wing panels and the wing glove. The new wing design was to be a practical wet-wing configuration with a high-lift system capable of providing satisfactory landing and take-off characteristics. Modifications to the glove lines were permitted only as far forward as the crew escape module, which could not in any way be altered. The new wing was to be designed within the structural and physical limits of the existing wing pivot and carry-through structure. Extensions of the wing chord forward of those for the basic wing were limited by stability requirements, whereas rearward chord extensions and maximum wing sweep angles were restricted by the tailplane and fuselage structural geometry. The F-111 airplane was selected for this program because its outer wing panel was easily replaced and its variable-sweep wing provided capability for a wide flight envelope, including sea-level supersonic flight, transonic maneuvering, and flight speeds exceeding Mach 2. The variable sweep capability allowed the leading edge to be swept behind the Mach line, thereby minimizing possible drag penalties associated with the large leading-edge radius of the supercritical airfoil in supersonic flow.

The present report has been prepared to document the first phase of the wind-tunnel development program associated with the full-scale flight demonstration of the maneuver potential of supercritical wings.

SYMBOLS

The results presented herein are referred to the body-axis system, with the exception of the lift and drag coefficients which are referred to the stability-axis system. The moment center is located at fuselage station 56.688 ($0.45\bar{c}_{ref}$)

on the model reference line. Data coefficients for all configurations are based on the geometry of the model with wing planform B and with a leading-edge sweep angle of 16.0°.

b	wing span, cm
c	wing local chord, cm
c_r	wing root chord, at model center line, cm
c_t	wing tip chord, cm
$\bar{c}$	wing mean aerodynamic chord, cm
$\bar{c}_{ref}$	reference mean aerodynamic chord (planform B), 13.310 cm
C_D	drag coefficient, Drag/qS_{ref}
C_L	lift coefficient, Lift/qS_{ref}
C_m	pitching-moment coefficient about moment center, $\text{Pitching moment}/qS_{ref}\bar{c}_{ref}$
L/D	lift-drag ratio, C_L/C_D
M	free-stream Mach number
q	free-stream dynamic pressure, N/cm^2
S	wing area, including fuselage intercept, cm^2
S_{ref}	wing reference area, including fuselage intercept, 974.03 cm^2
t/c	ratio of wing thickness to wing chord
w/w_∞	average duct internal mass-flow ratio
x	distance aft of wing leading edge, measured in direction parallel to wing reference plane
y	distance outboard of model's vertical plane of symmetry
z	distance above wing reference plane, measured in direction perpendicular to wing reference plane
α	angle of attack, referred to wing reference plane (+1° with respect to model reference line), deg
δ_h	horizontal-tail deflection angle, referred to wing reference plane (positive when trailing edge is down), deg
Λ	wing leading-edge sweep angle, deg

Subscripts:

i	internal
l	lower surface
max	maximum value
min	minimum value
u	upper surface

Abbreviations:

B.L.	buttock line
F.S.	fuselage station

Model-component designations:

B_{80}	basic F-111 D fuselage with Triple Plow II inlet cowl; aft fuselage lines refaired to accommodate sting and annular engine nozzles
G_{17}	basic F-111 glove; leading-edge sweep of 70.0°
G_{43}	glove for wing W_{31}; double delta with leading-edge sweep of 70.0°/66.2°
G_{47}	glove for wing W_{32}; similar to glove G_{43} but refaired around wing root to match supercritical airfoil contours
G_{49}	glove for supercritical wings W_{34}, W_{35}, and W_{37}; leading-edge sweep of 70.0°
G_{50}	glove for conventional wings W_{36} and W_{38}; leading-edge sweep of 70.0°
H_{13}	F-111 horizontal stabilizer
I_{71}	double-cone translating inlet spike for proper mass flow at $M = 1.2$
N_{32}^{b}	modified F-111 nozzles with subsonic-transonic nozzle plug b; $w/w_{\infty} \approx 0.8$ at $M_{\infty} = 0.8$
N_{32}^{c}	modified F-111 nozzles with subsonic-transonic nozzle plug c; $w/w_{\infty} \approx 0.7$ at $M_{\infty} = 0.8$
N_{32}^{d}	modified F-111 nozzles with subsonic-transonic nozzle plug d; $w/w_{\infty} \approx 0.6$ at $M_{\infty} = 0.8$
V_{29}	basic F-111 twin ventral fins
V_{38}	basic F-111 vertical stabilizer

W_x outboard wing panel (see figs. 3 to 5 and tables 1 to 11)

X_{24} infrared detector mounted on top of vertical stabilizer

X_{25} dorsal antenna forward of vertical stabilizer

X_{168} fuselage-nacelle fairing to smooth model cross-sectional area distribution

MODEL DESCRIPTION

The general arrangement of the airplane model used for this investigation is shown in figure 1, and model photographs are presented as figure 2. The baseline configuration was a 1/24-scale model of the F-111 D airplane, with an inboard wing pivot located longitudinally at fuselage station 51.610 cm and laterally 7.440 cm outboard of the model plane of symmetry. Provisions were made for manually varying the leading-edge sweep angles of the outboard wing panels from 16.0° to 72.5°. The wing incidence angle could be varied at the pivot, from 1° to -3° with respect to the model reference plane, although for the present investigation the wing incidence angle was a constant 1°.

Eleven wing configurations were investigated in addition to the basic F-111 wing (W_{29}). Design variables for these wings included planform, tip shape, and airfoil section. Details of the alternate wing planforms - designated "A," "A-1," "B," and "C" - are shown in figures 3 and 4, and a summary of wing geometric characteristics is presented in table 1. Because of the emphasis on increased maneuverability, the planform area of these alternate wings was increased from that of the basic wing, and the span and aspect ratio were decreased accordingly so as to limit bending moments at the wing pivot to the allowable stress levels for the existing wing pivot and carry-through structure. Because the physical depth at the pivot station was held constant for all wings, the longer chords of the alternate planform wings, as compared with the basic wing, resulted in lower wing thickness ratios. These longer chords also restricted the maximum sweep angle because of physical interference with the tailplane and fuselage structure. (Refer to table 1.) Geometric details of planforms A and A-1 were the same except for their position relative to the pivot; planform A-1 was, for stability reasons, moved 0.30 m (full scale) aft relative to the pivot such that its leading edge coincided with the leading edge of the basic F-111 wing.

The tip planform shape for wing W_{32} was varied as shown in figure 5. The round tip shape of wing W_{32} was also incorporated into conventional wing W_{31}, whereas a square tip shape was used for all wings with planforms A-1, B, and C, except wing W_{32a} (planform A-1, round tip). Coordinates for these wing-tip planform shapes are given in table 2.

Supercritical airfoil configurations with planforms A, A-1, B, and C were investigated. In order to separate planform effects from airfoil effects, conventional airfoil configurations with planforms A, A-1, and B were investigated in addition to the basic F-111 wing configuration. The supercritical wing configurations utilized a twist distribution having more washout at the tip than

the conventional wings of the same planform. (See table 1.) It should be noted that local incidence angles for the supercritical wings are defined by a reference line which passes through the leading edge and bisects the airfoil at the 35-percent-chord station. All wing incidence angles shown in table 1 are specified relative to the wing reference plane ($+1^{\circ}$ for this investigation). Tabulated airfoil coordinates for all wings tested are presented in tables 3 to 11.

Following preliminary analyses of the data presented herein, wing W_{34} (planform B, supercritical airfoil) was selected for further development testing. A series of minor changes to the wing surface contours were made to reduce or eliminate local flow irregularities that were identified through pressure measurements and flow visualization using the techniques established in reference 7. The resulting configuration was designated "W_{34e}," and its airfoil geometry is tabulated in table 7.

The wide variation in wing geometry required the use of several different glove shapes. A double-delta glove configuration, shown in figure 3, was used with planform A wings to accommodate their forward leading-edge location. The break in the glove leading edge occurred just aft of the crew escape module. Glove contours near the wing-glove leading-edge intercept were slightly different for the supercritical wings than for the conventional wings because of the larger leading-edge radius of the supercritical airfoil. Except for these differences, the external lines of the various gloves were the same.

The model was equipped with flow-through ducts and interchangeable nozzle plugs to allow variation of the mass-flow ratio. A cross-sectional area distribution for the wind-tunnel model with 100-percent-capture-ratio area removed is shown in figure 6.

Early in the test program, a fuselage side fairing - designated X_{168} and shown in figure 7 - was added to smooth the cross-sectional area distribution and to reduce the pressure gradients near the wing cusp. This fairing remained on the model for the tests with wings W_{32}, W_{32a}, W_{32b}, and W_{32c}, and for some configurations with wing W_{31}. The reader is cautioned to note the presence or absence of this fairing, as indicated in the figure legend or key.

APPARATUS AND PROCEDURES

Facility

The investigation was conducted in the NASA Langley 8-foot transonic pressure tunnel, which is a single-return tunnel having a rectangular slotted test section to permit continuous operation through the transonic speed range. The stagnation temperature and dew point were maintained at values sufficient to avoid condensation effects throughout the test.

Boundary-Layer Transition

Transition was fixed on the model with 0.25-cm-wide bands of carborundum grit sized according to the procedures established in reference 8. Transition

strips were located on the fuselage 3.8 cm aft of the nose with No. 120 carborundum grit; transition strips were located on the ventral fins, the horizontal and vertical tails, and the exterior portions of the engine inlets 1 cm aft of their respective leading edges with No. 150 carborundum grit. Transition on the model wing was fixed with one of several grit patterns designated as types a, b, c, d, e, and f, which are shown in figure 8.

For most configurations the wing-upper-surface boundary-layer trip was located near the leading edge, as in type b transition. Flow-visualization studies conducted with various upper-surface trip locations indicated that attached laminar flow could generally be maintained on the wing upper surface ahead of an aft-located trip for conditions which produced supercritical flow. At these conditions, however, some laminar separation was observed ahead of the trip on the inboard portions of the wing. Based on these observations, the development work on the selected wing configuration was conducted with the wing-upper-surface transition locations shown as types c, d, e, and f in figure 8 for free-stream Mach numbers of 0.80 and above. For these transition types, trips on the inboard region of the wing were located about 5 percent chord at the wing-glove juncture and angled rearward to intersect the aft trip at a point 5.1, 7.6, and 10.2 cm outboard of the wing-glove juncture for wing sweeps of 16.0°, 26.0°, and 30.0°, respectively. For the 35.0° sweep configuration with the selected wing, flow-visualization results showed the wing shock to be swept forward of the aft-trip location near the wing tip at a Mach number of 0.90. In order to reduce the potential for shock-induced separation at these conditions, the trip was angled forward near the tip (type f transition), thus insuring a turbulent boundary layer at the shock location.

For the high-sweep configurations, the trips were placed near the wing leading edge on both upper and lower surfaces (type a transition) because attached laminar flow could not be maintained to a trip location determined by the method of reference 9.

For all rearward trip locations, the model surface was kept exceptionally smooth to maintain laminar flow ahead of the trip, as required by the method of reference 9.

Measurements

Six-component static aerodynamic force and moment measurements were obtained by means of an electrical strain-gage balance located within a fuselage cavity. Total and static pressures were measured at the exit of both ducts to determine internal duct drag and mass-flow ratio. Additional pressures were measured at the fuselage base and nozzle-exit plug bases. Data were obtained at Mach numbers from 0.60 to 0.975, at angles of attack up to about 20°, and for Reynolds number per meter from 13×10^6 to 18×10^6. The angle of sideslip was zero throughout the investigation.

Corrections

The drag coefficient C_D has been corrected for internal flow through the ducts. The internal drag correction applied to the data is presented with the corresponding mass-flow ratios in figure 9. The drag data have also been adjusted to the condition of free-stream static pressure acting over the fuselage cavity and nozzle-exit plug bases. The measured angles of attack have been corrected for tunnel-flow angularity and for model-support sting and balance deflections occurring upstream of the angle measurement device as a result of aerodynamic loads on the model.

Because of the high loads imposed on the model during this investigation and the need to obtain data at angles of attack where severe model buffeting occurred, a model-sting arrangement was chosen in which the sting diameter was increased by a tapered section immediately aft of the model base. The proximity of sting taper to the model base produced a positive pressure field which affected the axial and pitching-moment measurements at subsonic and transonic speeds. No attempt was made to correct the drag data or the pitching-moment data for this pressure gradient; therefore, these data are invalid insofar as absolute values are concerned. The buoyancy effects, however, would be the same for all configurations having the same wing sweep, and the incremental drag values are therefore judged to be accurate.

PRESENTATION OF RESULTS

The results of this investigation are presented in the following figures:

	Figure
Longitudinal aerodynamic characteristics of model:	
$\Lambda = 16.0^\circ$ for -	
Configuration with wing W_{31}	10
Configuration with wing W_{34e}	11
$\Lambda = 26.0^\circ$ for -	
Configuration with wing W_{31}	12
Configuration with wing W_{32}	13
Configuration with wing W_{32a}	14
Comparison of configurations with wings W_{29}, W_{36}, and W_{38}	15
Comparison of configurations with wings W_{29}, W_{34}, W_{35}, and W_{37}	16
Configuration with wing W_{34e}	17
$\Lambda = 30.0^\circ$ for -	
Comparison of configurations with wings W_{29}, W_{36}, and W_{38}	18
Comparison of configurations with wings W_{29}, W_{34}, W_{35}, and W_{37}	19
$\Lambda = 35.0^\circ$ for -	
Configuration with wing W_{36}	20
Comparison of configurations with wings W_{34}, W_{35}, and W_{37}	21
Configuration with wing W_{34e}	22
$\Lambda = 45.0^\circ$ for -	
Configuration with wing W_{32}	23
$\Lambda = \Lambda_{max}$ for -	
Configuration with wing W_{29}, $\Lambda = 72.5^\circ$	24
Configuration with wing W_{31}, $\Lambda = 63.7^\circ$	25

Figure

Configuration with wing W_{32}, $\Lambda = 63.7^\circ$ 26
Configuration with wing W_{36}, $\Lambda = 58.0^\circ$ 27
Comparison of configurations with wings W_{34}, $\Lambda = 58.0^\circ$ and wing W_{37}, $\Lambda = 54.8^\circ$ 28

Effect of fuselage side fairing X_{168} on the longitudinal aerodynamic characteristics of model with wing W_{31}:
$\Lambda = 26.0^\circ$ 29
$\Lambda = 63.7^\circ$ 30

Effect of wing-tip planform on longitudinal aerodynamic characteristics of model with wing W_{32}, $\Lambda = 26.0^\circ$ 31

Effect of horizontal-tail deflection on longitudinal aerodynamic characteristics of model with wing W_{32}, $\Lambda = 26.0^\circ$ 32

Effect of internal mass-flow ratio on longitudinal aerodynamic characteristics:
Configuration with wing W_{34}, $\Lambda = 26.0^\circ$ 33
Configuration with wing W_{36}, $\Lambda = 26.0^\circ$ 34

Summary of longitudinal aerodynamic characteristics:
Variation of C_m with M, $\Lambda = 26.0^\circ$, for -
$C_L = 0.465$ 35
$C_L = 0.670$ 36
Variation of C_D with M, $\Lambda = 26.0^\circ$, for -
$C_L = 0.465$ 37
$C_L = 0.670$ 38
Variation of $M(L/D)_{max}$ with M, $\Lambda = 26.0^\circ$ 39
Variation of $C_{D,min}$ with M, $\Lambda = \Lambda_{max}$ 40

DISCUSSION OF RESULTS

Aerodynamic design objectives of primary interest in the present investigation were to increase transonic maneuverability and to obtain cruise efficiency equal to or better than the basic configuration. The maneuver condition of interest was specified as a load factor of 5.5g, a Mach number of 0.90, and an altitude of 3048 m which corresponds to $C_L = 0.670$. The subsonic cruise condition was specified as $C_L = 0.465$ at an altitude of 10 668 m. Discussion of the test results has been centered about these two flight conditions.

The scope of this investigation was such that the acquisition of horizontal-tail-effectiveness data for all configurations throughout the test envelope was prohibitive, and only very limited data were obtained (fig. 32). Because the tail-deflection data are limited and because the effects of the pressure gradient resulting from the proximity of the sting taper are unknown, no attempt has been made to provide trimmed drag data for this report.

Early in the test program, flow-visualization studies using the fluorescent-oil film technique described in reference 7 revealed some minor boundary-layer separation in the wing lower-surface cusp region adjacent to the fuselage. A possible cause was the superposition of the adverse pressure gradient normally found in that region of the supercritical airfoil's lower surface on the pressure gradients associated with a local fuselage indentation. (Refer to figs. 1 and 7.) The flow field was further complicated by the presence of low energy air from the inlet boundary-layer plow. In an attempt to reduce the severity of this separation, a fuselage side fairing (X_{168}) was added to the model, as shown in figure 7. The fairing was relatively ineffective, however, and was later removed. Most of the data presented herein are for configurations without the fairing. In order to provide readers with incremental values, data are presented in figures 29 and 30 for the model with and without the fairing for wing sweep angles of 26.0° and 63.7°, respectively.

Pitching-Moment Characteristics

The measured pitching-moment coefficients for the various wings utilized in this investigation are summarized for a wing sweep angle of 26.0° in figures 35 and 36 for lift coefficients of 0.465 and 0.670, respectively. As would be expected, the aft-loading characteristics of the supercritical airfoils produced more negative pitching moments than did the conventional airfoils for wing configurations of the same planform. A comparison of the pitching-moment coefficient slopes $\left(C_{m_{C_L}}\right)$ from the basic data (figs. 12 to 17) indicates that, for Mach numbers below their respective drag divergence and for a wing sweep angle of 26.0°, the supercritical wing configurations exhibited stability comparable to or slightly less than for the corresponding conventional wing configuration. All of the wings tested exhibited pitching moments that were generally unstable or neutrally stable for the selected center-of-gravity location at cruise flight conditions and wing sweep angles of 16.0°, 26.0°, and 30.0°. Stability levels for the low-sweep configurations with wings W_{31} and W_{32} (planform A) were not acceptable for a flight vehicle; consequently, these wings were given no further consideration in the development program. This unacceptable stability level was overcome by positioning the wing panels farther aft on the airframe and by eliminating the additional glove area required by the planform A configuration. This new planform was designated planform A-1.

Cruise Drag Characteristics

The drag characteristics of the wings used in the present investigation are summarized in figure 37 for a wing sweep angle of 26.0° and a cruise lift coefficient of 0.465. The aerodynamic range factors $M(L/D)_{max}$ for the various wings are presented in figure 39. In all cases the alternate wing configurations exhibited higher cruise Mach numbers than the basic configuration (W_{29}). Drag-divergence Mach numbers ranged from about 0.76 for wing configuration W_{29} to 0.89 for wing configuration W_{32}. In every case where the comparison is available, the supercritical wing configurations W_{32}, W_{34}, and W_{37} showed a significantly higher drag-divergence Mach number than did the conventional wing configurations of the same planform (W_{31}, W_{36}, and W_{38}, respectively). The sub-

sonic drag levels of the supercritical wings, however, were higher than for the corresponding conventional configurations. This higher subsonic level, coupled with the drag creep associated with early supercritical airfoil designs, resulted in lower maximum values of aerodynamic range factor for these supercritical configurations than for the conventional configurations, even though the cruise Mach numbers were significantly higher. Analyses of data for the various tip shapes on the planform A supercritical wing (fig. 31) indicate higher maximum range factors for the round-tipped configuration (W_{32}). Practical considerations for a leading-edge high-lift system, however, favored development of a square-tip configuration. Through additional refinement and testing of the planform B supercritical wing (resulting in the designation W_{34e}), the maximum range factors were improved to a level nearly equal to that of the basic wing W_{29}. In addition, the Mach number at which the range factor reached its maximum was 0.10 higher for wing W_{34e} than for wing W_{29}.

It should be noted that the drag creep exhibited by these supercritical wings is typical of configurations based on early supercritical airfoil designs. More recently, two-dimensional tests of an improved supercritical airfoil have shown that the drag creep has been almost completely eliminated (ref. 10).

Maneuver Drag Characteristics

The drag characteristics at the maneuver lift coefficient of 0.670 are summarized in figure 38 for a sweep angle of 26.0°. The trends are similar to those for the cruise lift coefficient, that is, the supercritical wing configurations have significantly lower drag levels than the conventional configurations at the Mach numbers where extensive supercritical flow exists over the wings but have higher subsonic drag levels than the corresponding conventional configurations.

For the 0.90 Mach number maneuver condition, with 26.0° wing sweep, the alternate conventional wing configurations (W_{31}, W_{36}, and W_{38}) exhibited somewhat lower drag levels than did the basic configuration. Of these configurations, wing W_{31} showed the lowest drag level, a 25-percent reduction from the basic configuration, with wings W_{36} and W_{38} showing considerably smaller drag reductions (less than 7 percent). The supercritical wing configurations showed significantly greater drag reductions than any of the alternate conventional wings. The configuration with wing W_{32} showed a reduction in drag coefficient of 0.0520, or 43 percent, relative to the untrimmed drag level of the basic configuration. Supercritical wing W_{37} and the refined wing W_{34e} exhibited somewhat smaller drag reductions of 37 percent and 33 percent, respectively. It should be noted that for the specified maneuver criteria the conventional wing configurations are operating well above drag divergence, whereas the supercritical wings were designed to operate efficiently in this mixed flow environment. It is recognized that the trim penalties for these supercritical wing configurations will generally be somewhat greater than for the basic or the conventional wing configurations because of the more negative pitching moments. However, unpublished data on similar wind-tunnel model configurations indicate that the trim penalties will not be of sufficient magnitude to offset the significant drag reductions shown by the supercritical airfoils operating in their design environment.

High-Sweep Minimum Drag Characteristics

The minimum drag characteristics for the configurations with high wing sweep angles are summarized in figure 40. It can be noted that the drag levels for the supercritical wing configurations sometimes differed from those for the corresponding conventional configuration, but there was no significant difference in the rate of drag increase with Mach number over the range of this investigation.

CONCLUDING REMARKS

The first phase of a wind-tunnel investigation to evaluate a series of wings designed to demonstrate the maneuver potential of the NASA supercritical airfoil has been conducted at Mach numbers from 0.60 to 0.975 with an F-111 airplane model. Both conventional and supercritical wing designs for several planform configurations were investigated with wing sweep angles from 16.0° to 72.5°, depending on Mach number and wing configuration.

The following conclusions are indicated:

1. The supercritical wing configurations showed substantially lower drag levels at transonic maneuvering conditions than did the conventional wing configurations.

2. Drag-divergence Mach numbers for the supercritical wing configurations were significantly higher than the corresponding conventional wing configurations.

3. Aerodynamic range factor maximums for the supercritical wing configurations evaluated in this phase of the investigation were somewhat lower than for the conventional wing configurations of the same planform.

4. The supercritical airfoil configurations generally had more negative pitching moments than did the conventional airfoil configurations of the same planform.

5. For low wing sweep angles and Mach numbers below drag divergence, little difference was noted in longitudinal stability between the supercritical wing configuration and the conventional wing configuration.

Langley Research Center
National Aeronautics and Space Administration
Hampton, VA 23665
May 19, 1977

REFERENCES

1. Whitcomb, Richard T.: Review of NASA Supercritical Airfoils. ICAS Paper No. 74-10, Aug. 1974.

2. Ferris, James C.: Static Aerodynamic Characteristics of a Model With a 17-Percent-Thick Supercritical Wing. NASA TM X-2551, 1972.

3. Bartlett, Dennis W.; and Re, Richard J.: Wind Tunnel Investigation of Basic Aerodynamic Characteristics of a Supercritical-Wing Research Airplane Configuration. NASA TM X-2470, 1972.

4. Supercritical Wing Technology - A Progress Report on Flight Evaluations. NASA SP-301, 1972.

5. Palmer, W. E.; Elliott, D. W.; and White, J. E.: Flight and Wind Tunnel Evaluation of a 17-Percent-Thick Supercritical Airfoil on a T-2C Airplane. NR71H-150 (Contract N00019-70-C-0474), North American Rockwell Corp., July 31, 1971.
   Volume I - Basic Report. (Available from DDC as AD 517 436L.)
   Volume II - Flight Measured Wing Rake Profiles and Surface Pressures. (Available from DDC as AD 517 437L.)

6. Ayers, Theodore G.: A Wind Tunnel Investigation of the Application of the NASA Supercritical Airfoil to a Variable-Wing-Sweep Fighter Airplane. NASA TM X-2759, 1973.

7. Loving, Donald L.; and Katzoff, S.: The Fluorescent-Oil Film Method and Other Techniques for Boundary-Layer Flow Visualization. NASA MEMO 3-17-59L, 1959.

8. Braslow, Albert L.; and Knox, Eugene C.: Simplified Method for Determination of Critical Height of Distributed Roughness Particles for Boundary-Layer Transition at Mach Numbers From 0 to 5. NACA TN 4363, 1958.

9. Blackwell, James A., Jr.: Preliminary Study of Effects of Reynolds Number and Boundary-Layer Transition Location on Shock-Induced Separation. NASA TN D-5003, 1969.

10. Harris, Charles D.: Aerodynamic Characteristics of the 10-Percent-Thick NASA Supercritical Airfoil 33 Designed for a Normal-Force Coefficient of 0.7. NASA TM X-72711, 1975.

TABLE 1.- SUMMARY OF WING GEOMETRIC CHARACTERISTICS

Wing	Planform (a)	Tip shape	Airfoil	Root incidence, deg (b)	Twist, deg (c)	Sweep angle, deg								
						16.0	26.0	30.0	35.0	45.0	54.8	58.0	63.7	72.5
W_{29}	F-111		Conventional	0	-4.00		X	X						X[d]
W_{31}	A	Rounded	Conventional	-2.13	-2.37	X	X						X[d]	
W_{32}	A	Rounded	Supercritical	-4.50	-4.00		X			X			X[d]	
W_{32a}	A-1	Rounded	Supercritical	-4.50	-4.00		X							
W_{32b}	A	Intermediate	Supercritical	-4.50	-4.50		X							
W_{32c}	A	Square	Supercritical	-4.50	-4.50		X							
W_{34}	B	Square	Supercritical	-3.58	-5.32		X	X	X			X[d]		
W_{34e}	B	Square	Supercritical	-3.58	-5.32	X	X		X					
W_{35}	C	Square	Supercritical	-3.67	-6.33		X	X	X					
W_{36}	B	Square	Conventional	-2.13	-2.37		X	X	X			X[d]		
W_{37}	A-1	Square	Supercritical	-4.50	-4.00		X	X	X		X[d]			
W_{38}	A-1	Square	Conventional	-2.13	-2.37		X	X						

[a]Refer to figures 3 and 4.

[b]Root incidence was measured relative to wing reference plane at B.L. 7.440 cm for wing W_{29} and at B.L. 13.123 cm for all other wings.

[c]Wing W_{29} was twisted uniformly about 26.146-percent-chord line. All other wings were twisted about leading edge.

[d]Maximum attainable sweep angle.

TABLE 2.- WING-TIP PLANFORM GEOMETRY

[All linear dimensions in cm]

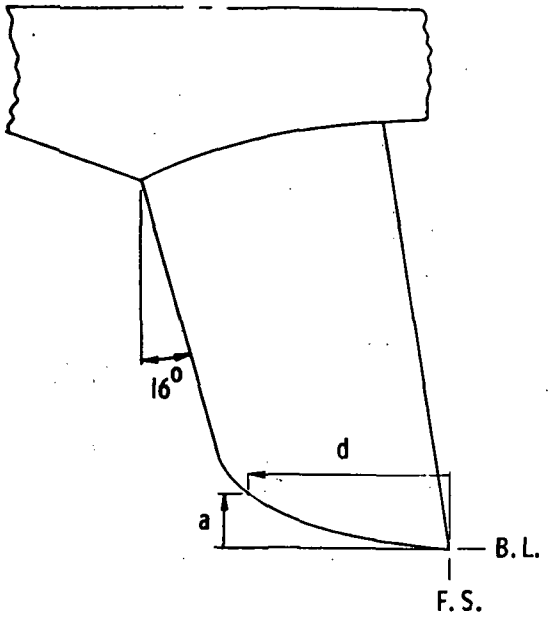

Trailing-edge tip coordinates

Wing	F.S.	B.L.
W_{29}	62.474	40.005
W_{31}	67.023	36.195
W_{32}	67.023	36.195
W_{32b}	67.023	36.195
W_{32c}	67.023	36.195
W_{34}	65.710	37.676
W_{35}	64.321	38.418
W_{36}	65.710	37.676
W_{37}, W_{38}	68.060	36.195

Wing W_{29}

a	d
0	0.531
0	2.077
.010	2.657
.056	3.223
.157	3.779
.323	4.409
.528	4.871
.836	5.278
1.270	5.542

Wing W_{31}

a	d
0	0
.107	1.158
.254	2.370
.424	3.602
.635	4.841
.927	6.098
1.334	7.412
1.992	8.809
2.858	10.206
3.897	11.486
4.646	12.227
6.823	13.165
7.727	14.069

Wing W_{32}, W_{32a}

a	d
0	0
.030	.930
.107	1.865
.213	3.135
.477	4.898
.741	6.064
1.270	7.638
1.801	8.913
2.329	9.724
3.388	11.090
4.445	12.116
5.504	12.909
6.563	13.503
7.620	13.981
8.679	14.344

TABLE 2.- Concluded

Wing W_{32b}

a	d
0	0
.043	1.196
.074	2.360
.127	3.546
.211	4.793
.348	6.002
.572	7.249
.856	8.509
1.323	9.926
1.989	11.196
2.570	11.981
3.038	12.405
4.318	13.094

Wing W_{32c}

a	d
0	0
0	9.484
.048	10.266
.127	10.721
.211	11.059
.351	11.399
.561	11.760
.782	11.981
1.059	12.149
1.308	12.230

Wing W_{34}

a	d
0	0
0	4.539
.025	5.451
.079	6.370
.185	7.292
.249	7.767
.371	8.265
.561	8.773
.747	9.050
1.270	9.444

Wing W_{35}

a	d
0	0
0	3.005
.025	3.747
.058	4.496
.117	5.233
.234	6.033
.444	6.830
.810	7.493
1.270	7.831

Wing W_{36}

a	d
0	0
0	4.542
.043	5.471
.102	6.383
.224	7.313
.307	7.795
.429	8.280
.620	8.778
.805	9.070
1.270	9.431

Wings W_{37}, W_{38}

a	d
0	0
0	7.107
.048	8.313
.107	9.515
.160	10.117
.254	10.742
.338	11.087
.460	11.400
.655	11.748
1.270	12.217

TABLE 3.- AIRFOIL COORDINATES FOR WING W_{29}

$(x/c)_u$ and l	y = 10.548 cm c = 13.127 cm	
	$(z/c)_u$	$(z/c)_l$
0.0000	0.0025	0.0025
.0075	.0128	-.0066
.0124	.0163	-.0093
.0250	.0230	-.0137
.0500	.0337	-.0205
.0700	.0406	-.0246
.1000	.0490	-.0298
.1500	.0586	-.0356
.1999	.0646	-.0385
.2999	.0693	-.0408
.4000	.0708	-.0399
.4998	.0689	-.0366
.5998	.0617	-.0296
.6999	.0509	-.0203
.7498	.0441	-.0157
.7997	.0368	-.0112
.8498	.0290	-.0070
.8997	.0211	-.0031
.9497	.0128	.0006
1.0000	.0046	.0039
L.E. radius: 0.0085c		

$(x/c)_u$ and l	y = 33.138 cm c = 5.519 cm	
	$(z/c)_u$	$(z/c)_l$
0.0000	0.0713	0.0713
.0051	.0815	.0621
.0101	.0861	.0594
.0304	.0985	.0548
.0502	.1072	.0534
.0704	.1141	.0534
.0999	.1224	.0534
.1500	.1339	.0548
.2002	.1431	.0566
.3000	.1569	.0603
.3999	.1661	.0663
.5002	.1698	.0759
.6001	.1694	.0888
.7000	.1652	.1031
.7501	.1624	.1100
.8003	.1588	.1169
.8500	.1546	.1233
.9001	.1505	.1293
.9498	.1459	.1353
1.0000	.1422	.1404
L.E. radius: 0.0115c		

TABLE 4.- AIRFOIL COORDINATES FOR WING W_{31}

$(x/c)_u$ and l	y = 7.440 cm c = 15.133 cm	
	$(z/c)_u$	$(z/c)_l$
0.0000	-0.0164	-0.0164
.0262	.0203	-.0203
.0525	.0378	-.0210
.0755	.0500	-.0210
.1004	.0594	-.0210
.1514	.0727	-.0210
.2011	.0769	-.0210
.3014	.0769	-.0210
.3097	.0769	-.0210
.4015	.0769	-.0210
.5022	.0769	-.0148
.6014	.0752	-.0059
.7007	.0700	.0055
.8021	.0601	.0175
.9008	.0468	.0269
.9597	.0354	.0344
1.0000	.0309	.0299
L.E. radius: 0.0060c		

$(x/c)_u$ and l	y = 9.314 cm c = 14.920 cm	
	$(z/c)_u$	$(z/c)_l$
0.0000	-0.0099	-0.0099
.0323	.0180	-.0203
.0511	.0329	-.0213
.0752	.0443	-.0213
.1003	.0546	-.0213
.1512	.0669	-.0213
.2007	.0734	-.0213
.3008	.0773	-.0213
.3994	.0798	-.0184
.5003	.0802	-.0092
.6008	.0780	0
.7016	.0717	.0111
.8015	.0613	.0209
.9009	.0490	.0284
1.0000	.0349	.0339
L.E. radius: 0.0061c		

$(x/c)_u$ and l	y = 11.219 cm c = 14.702 cm	
	$(z/c)_u$	$(z/c)_l$
0.0000	-0.0099	-0.0099
.0252	.0183	-.0183
.0504	.0332	-.0202
.0757	.0425	-.0206
.0987	.0498	-.0209
.1493	.0612	-.0190
.1980	.0695	-.0176
.3010	.0767	-.0152
.4000	.0810	-.0112
.4997	.0834	-.0032
.6011	.0802	.0060
.6997	.0741	.0162
.8004	.0638	.0252
.8998	.0515	.0316
1.0000	.0373	.0363
L.E. radius: 0.0054c		

TABLE 4.- Continued

$(x/c)_u$ and l	y = 13.124 cm c = 14.486 cm	
	$(z/c)_u$	$(z/c)_l$
0.0000	-0.0079	-0.0079
.0124	.0093	-.0144
.0251	.0188	-.0156
.0500	.0312	-.0158
.0750	.0395	-.0153
.0999	.0456	-.0146
.1499	.0556	-.0130
.1999	.0644	-.0117
.2998	.0772	-.0086
.3998	.0847	-.0039
.4997	.0866	.0037
.5997	.0838	.0128
.6996	.0773	.0221
.7996	.0670	.0298
.8995	.0528	.0340
1.0000	.0377	.0366
L.E. radius: 0.0054c		

$(x/c)_u$ and l	y = 28.468 cm c = 12.736 cm	
	$(z/c)_u$	$(z/c)_l$
0.0000	-0.0030	-0.0030
.0126	.0088	-.0070
.0249	.0150	-.0072
.0501	.0241	-.0064
.0750	.0307	-.0050
.0999	.0363	-.0036
.1500	.0459	-.0004
.2000	.0542	.0028
.3000	.0674	.0094
.3999	.0768	.0168
.4998	.0820	.0259
.5999	.0838	.0357
.6998	.0828	.0453
.7998	.0786	.0535
.8997	.0712	.0586
1.0000	.0636	.0624
L.E. radius: 0.0036c		

$(x/c)_u$ and l	y = 30.373 cm c = 12.144 cm	
	$(z/c)_u$	$(z/c)_l$
0.0000	-0.0031	-0.0031
.0230	.0117	-.0065
.0487	.0218	-.0056
.0759	.0297	-.0040
.1259	.0418	0
.1767	.0510	.0027
.2803	.0648	.0096
.3834	.0736	.0184
.4871	.0801	.0301
.5896	.0841	.0418
.6934	.0853	.0506
.7956	.0832	.0596
.8986	.0776	.0659
1.0000	.0694	.0682
L.E. radius: 0.0031c		

TABLE 4.- Concluded

$(x/c)_u$ and l	y = 32.278 cm c = 10.815 cm	
	$(z/c)_u$	$(z/c)_l$
0.0000	0.0099	0.0099
.0352	.0249	.0068
.0925	.0392	.0094
.2074	.0587	.0136
.3189	.0709	.0240
.4345	.0803	.0371
.5470	.0867	.0488
.6616	.0890	.0592
.7750	.0895	.0686
.8880	.0862	.0749
1.0000	.0810	.0796
L.E. radius: 0.0023c		

$(x/c)_u$ and l	y = 34.183 cm c = 8.466 cm	
	$(z/c)_u$	$(z/c)_l$
0.0000	0.0312	0.0312
.1470	.0582	.0381
.2895	.0780	.0501
.4326	.0918	.0657
.5752	.1014	.0780
.7189	.1080	.0912
.8608	.1107	.1011
1.0000	.1074	.1056
L.E. radius: 0.0012c		

TABLE 5.- AIRFOIL COORDINATES FOR WING W_{32}

$(x/c)_u$ and l	y = 7.440 cm c = 15.133 cm	
	$(z/c)_u$	$(z/c)_l$
0.0000	-0.0027	-0.0027
.0255	.0290	-.0233
.0500	.0433	-.0255
.0755	.0535	-.0248
.1004	.0613	-.0242
.1504	.0717	-.0232
.1997	.0762	-.0220
.3066	.0772	-.0217
.3990	.0772	-.0206
.4997	.0772	-.0106
.5994	.0772	.0052
.7004	.0772	.0252
.7998	.0769	.0448
.8996	.0733	.0556
.9508	.0671	.0549
1.0000	.0571	.0478
L.E. radius: 0.0171c		

$(x/c)_u$ and l	y = 9.314 cm c = 14.907 cm	
	$(z/c)_u$	$(z/c)_l$
0.0000	-0.0027	-0.0027
.0245	.0262	-.0239
.0491	.0397	-.0261
.0741	.0501	-.0259
.0990	.0576	-.0252
.1494	.0687	-.0239
.1992	.0746	-.0227
.2982	.0753	-.0213
.3994	.0767	-.0187
.4996	.0777	-.0094
.5993	.0789	.0068
.6999	.0799	.0269
.8001	.0803	.0462
.9005	.0750	.0564
.9513	.0685	.0557
1.0000	.0583	.0491
L.E. radius: 0.0174c		

$(x/c)_u$ and l	y = 11.219 cm c = 14.702 cm	
	$(z/c)_u$	$(z/c)_l$
0.0000	-0.0036	-0.0036
.0252	.0226	-.0242
.0498	.0339	-.0273
.0752	.0422	-.0287
.0997	.0489	-.0285
.1465	.0575	-.0287
.1997	.0639	-.0266
.2994	.0705	-.0242
.3998	.0745	-.0176
.4998	.0776	-.0074
.5997	.0803	.0079
.7001	.0828	.0290
.8001	.0826	.0475
.9001	.0765	.0574
.9509	.0695	.0568
1.0000	.0598	.0511
L.E. radius: 0.0174c		

TABLE 5.- Continued

y = 13.124 cm c = 14.506 cm			
$(x/c)_u$	$(z/c)_u$	$(x/c)_l$	$(z/c)_l$
0.0000	-0.0039	0.0000	-0.0039
.0040	.0075	.0060	-.0173
.0063	.0098	.0086	-.0194
.0110	.0133	.0138	-.0222
.0231	.0193	.0268	-.0263
.0476	.0273	.0522	-.0306
.0723	.0331	.0776	-.0327
.0970	.0380	.1026	-.0334
.1466	.0457	.1529	-.0331
.1963	.0520	.2029	-.0313
.2959	.0622	.3029	-.0252
.3957	.0702	.4027	-.0166
.4957	.0765	.5024	-.0060
.5957	.0814	.6016	.0086
.6960	.0840	.7002	.0306
.7965	.0832	.7992	.0492
.8976	.0762	.8990	.0585
.9228	.0735	.9240	.0585
.9482	.0697	.9492	.0574
.9737	.0644	.9746	.0546
.9993	.0597	1.0000	.0497
L.E. radius: 0.0182c			

y = 27.516 cm c = 12.893 cm			
$(x/c)_u$	$(z/c)_u$	$(x/c)_l$	$(z/c)_l$
0.0000	-0.0232	0.0000	-0.0232
.0039	-.0154	.0061	-.0325
.0063	-.0136	.0087	-.0337
.0110	-.0110	.0140	-.0353
.0230	-.0061	.0268	-.0372
.0475	.0008	.0522	-.0384
.0721	.0067	.0774	-.0382
.0967	.0120	.1026	-.0372
.1462	.0203	.1527	-.0341
.1958	.0280	.2027	-.0297
.2951	.0416	.3024	-.0191
.3948	.0540	.4021	-.0071
.4951	.0652	.5016	.0063
.5944	.0755	.6007	.0221
.6942	.0841	.6992	.0439
.7447	.0894	.7979	.0626
.8960	.0879	.8978	.0719
.9214	.0857	.9232	.0721
.9470	.0825	.9486	.0709
.9728	.0784	.9740	.0608
.9988	.0729	1.0000	.0630
L.E. radius: 0.0099c			

TABLE 5.- Continued

$(x/c)_u$ and l	y = 28.605 cm c = 12.642 cm	
	$(z/c)_u$	$(z/c)_l$
0.0000	-0.0239	-0.0239
.0191	-.0092	-.0368
.0442	-.0020	-.0392
.0695	.0040	-.0388
.0946	.0090	-.0380
.1449	.0179	-.0346
.1951	.0259	-.0299
.2958	.0400	-.0189
.3964	.0530	-.0064
.4971	.0645	.0074
.5975	.0753	.0233
.6982	.0848	.0454
.7989	.0906	.0643
.8995	.0896	.0737
.9498	.0842	.0725
1.0000	.0745	.0645
L.E. radius: 0.0090c		

$(x/c)_u$ and l	y = 29.695 cm c = 12.344 cm	
	$(z/c)_u$	$(z/c)_l$
0.0000	-0.0243	-0.0243
.0309	-.0064	-.0385
.0564	.0004	-.0387
.0819	.0060	-.0377
.1385	.0150	-.0342
.1840	.0235	-.0235
.2860	.0383	-.0179
.3879	.0521	-.0051
.4899	.0644	.0088
.5920	.0759	.0251
.6940	.0858	.0475
.7961	.0924	.0665
.8981	.0918	.0759
.9492	.0864	.0749
1.0000	.0765	.0677
L.E. radius: 0.0086c		

$(x/c)_u$ and l	y = 30.785 cm c = 11.902 cm	
	$(z/c)_u$	$(z/c)_l$
0.0000	-0.0245	-0.0245
.0307	-.0055	-.0365
.0570	.0011	-.0365
.1095	.0113	-.0337
.1618	.0207	-.0290
.2665	.0363	-.0171
.3713	.0508	-.0041
.4761	.0642	.0107
.5809	.0766	.0275
.6857	.0875	.0501
.7904	.0950	.0698
.8952	.0950	.0796
.9475	.0898	.0781
1.0000	.0798	.0700
L.E. radius: 0.0081c		

TABLE 5.- Continued

$(x/c)_u$ and l	y = 31.874 cm c = 11.270 cm	
	$(z/c)_u$	$(z/c)_l$
0.0000	-0.0216	-0.0216
.0140	-.0101	-.0295
.0687	.0061	-.0313
.1235	.0165	-.0275
.2330	.0345	-.0156
.3426	.0503	-.0016
.4521	.0649	.0135
.5616	.0787	.0313
.6714	.0906	.0543
.7809	.0994	.0746
.8905	.1005	.0845
.9452	.0949	.0834
1.0000	.0847	.0746
L.E. radius: 0.0068c		

$(x/c)_u$ and l	y = 32.956 cm c = 10.350 cm	
	$(z/c)_u$	$(z/c)_l$
0.0000	-0.0155	-0.0155
.0255	-.0010	-.0231
.0555	.0098	-.0236
.1735	.0317	-.0125
.2915	.0501	.0015
.4096	.0667	.0179
.5276	.0822	.0366
.6459	.0964	.0609
.7639	.1067	.0822
.8820	.1085	.0928
.9409	.1031	.0918
1.0000	.0923	.0825
L.E. radius: 0.0056c		

$(x/c)_u$ and l	y = 34.054 cm c = 9.042 cm	
	$(z/c)_u$	$(z/c)_l$
0.0000	-0.0037	0.0037
.0317	.0174	-.0053
.0635	.0258	-.0059
.1972	.0500	.0081
.3309	.0705	.0256
.4649	.0893	.0458
.5986	.1067	.0728
.7323	.1197	.0958
.8663	.1230	.1073
.9261	.1177	.1062
1.0000	.1056	.0955
L.E. radius: 0.0053c		

TABLE 5.- Concluded

$(x/c)_u$ and l	y = 35.141 cm c = 6.922 cm	
	$(z/c)_u$	$(z/c)_l$
0.0000	0.0466	0.0466
.0613	.0653	.0389
.1350	.0793	.0437
.3079	.1072	.0683
.4807	.1317	.0944
.6554	.1505	.1277
.8268	.1574	.1420
.9134	.1519	.1402
1.0000	.1369	.1266
L.E. radius: 0.0022c		

$(x/c)_u$ and l	y = 35.687 cm c = 4.953 cm	
	$(z/c)_u$	$(z/c)_l$
0.0000	0.1144	0.1144
.1164	.1503	.1210
.2785	.1759	.1446
.5190	.2046	.1810
.7595	.2169	.2000
.8795	.2113	.1985
1.0000	.1908	.1795
L.E. radius: 0.0000c		

TABLE 6.- AIRFOIL COORDINATES FOR WING W_{34}

$(x/c)_u$ and l	y = 7.440 cm c = 15.255 cm	
	$(z/c)_u$	$(z/c)_l$
0.0000	0.0070	0.0070
.0250	.0388	-.0153
.0500	.0541	-.0176
.1001	.0691	-.0201
.1500	.0756	-.0205
.2000	.0766	-.0211
.3000	.0771	-.0208
.3999	.0771	-.0201
.5000	.0766	-.0150
.6001	.0763	-.0035
.7000	.0759	.0170
.8000	.0721	.0346
.8999	.0638	.0438
.9500	.0548	.0430
.9650	.0509	.0410
L.E. radius:	0.0211c	

$(x/c)_u$ and l	y = 9.314 cm c = 14.864 cm	
	$(z/c)_u$	$(z/c)_l$
0.0000	0.0068	0.0068
.0249	.0342	-.0150
.0501	.0473	-.0181
.1001	.0641	-.0203
.1500	.0713	-.0220
.2001	.0737	-.0220
.3002	.0748	-.0220
.4002	.0752	-.0200
.5003	.0755	-.0138
.6003	.0766	-.0026
.7004	.0766	.0193
.8004	.0733	.0364
.9005	.0641	.0449
.9504	.0552	.0434
1.0000	.0427	.0345
L.E. radius:	0.0207c	

$(x/c)_u$ and l	y = 11.219 cm c = 14.483 cm	
	$(z/c)_u$	$(z/c)_l$
0.0000	0.0051	0.0051
.0251	.0310	-.0172
.0500	.0428	-.0209
.1000	.0556	-.0249
.1499	.0628	-.0263
.1999	.0665	-.0256
.3001	.0705	-.0233
.4000	.0735	-.0209
.5000	.0756	-.0128
.6000	.0775	-.0023
.6999	.0772	.0205
.8001	.0731	.0374
.9000	.0647	.0456
.9500	.0573	.0449
1.0000	.0449	.0367
L.E. radius:	0.0209c	

TABLE 6.- Concluded

$(x/c)_u$ and l	y = 13.124 cm c = 14.094 cm	
	$(z/c)_u$	$(z/c)_l$
0.0000	0.0034	0.0034
.0250	.0285	-.0195
.0499	.0375	-.0252
.1000	.0469	-.0297
.1499	.0533	-.0312
.2000	.0586	-.0308
.3001	.0669	-.0274
.4001	.0717	-.0214
.5001	.0766	-.0128
.5999	.0780	0
.6999	.0777	.0207
.8000	.0750	.0391
.9000	.0669	.0474
.9501	.0586	.0461
1.0000	.0474	.0389
L.E. radius: 0.0195c		

$(x/c)_u$ and l	y = 36.406 cm c = 9.340 cm	
	$(z/c)_u$	$(z/c)_l$
0.0000	-0.0454	-0.0454
.0250	-.0272	-.0555
.0500	-.0193	-.0549
.1001	-.0068	-.0517
.1501	.0022	-.0460
.1999	.0125	-.0403
.3000	.0299	-.0261
.3998	.0465	-.0120
.5001	.0623	.0052
.5999	.0759	.0261
.7000	.0895	.0511
.8001	.1009	.0737
.8999	.1042	.0868
.9500	.1004	.0884
1.0000	.0919	.0821
L.E. radius: 0.0063c		

TABLE 7.- AIRFOIL COORDINATES FOR WING W_{34e}

$(x/c)_u$ and l	y = 7.440 cm c = 15.255 cm	
	$(z/c)_u$	$(z/c)_l$
0.0000	0.0212	0.0212
.0250	.0396	-.0147
.0500	.0541	-.0176
.1001	.0691	-.0201
.1500	.0756	-.0205
.2000	.0766	-.0211
.3000	.0771	-.0208
.3999	.0771	-.0201
.5000	.0766	-.0150
.6001	.0763	-.0052
.7000	.0756	.0093
.8000	.0714	.0236
.8999	.0624	.0286
.9499	.0541	.0266
1.0000	.0400	.0201
L.E. radius:	0.0211c	

$(x/c)_u$ and l	y = 9.314 cm c = 14.864 cm	
	$(z/c)_u$	$(z/c)_l$
0.0000	0.0070	0.0070
.0249	.0367	-.0154
.0501	.0497	-.0185
.1001	.0644	-.0217
.1500	.0711	-.0220
.2001	.0743	-.0231
.3002	.0759	-.0227
.4002	.0772	-.0188
.5003	.0786	-.0128
.6003	.0791	-.0025
.7004	.0776	.0138
.8004	.0733	.0285
.9005	.0632	.0359
.9504	.0549	.0273
1.0000	.0427	.0270
L.E. radius:	0.0217c	

$(x/c)_u$ and l	y = 11.219 cm c = 14.483 cm	
	$(z/c)_u$	$(z/c)_l$
0.0000	0.0051	0.0051
.0251	.0337	-.0172
.0500	.0435	-.0216
.1000	.0552	-.0253
.1499	.0628	-.0256
.1999	.0675	-.0253
.3001	.0724	-.0242
.4000	.0763	-.0200
.5000	.0775	-.0135
.6000	.0779	.0011
.6999	.0775	.0191
.8001	.0744	.0340
.9000	.0656	.0414
.9500	.0572	.0400
1.0000	.0438	.0314
L.E. radius:	0.0202c	

TABLE 7.- Concluded

$(x/c)_u$ and l	y = 13.124 cm c = 14.094 cm	
	$(z/c)_u$	$(z/c)_l$
0.0000	0.0045	0.0045
.0250	.0301	-.0195
.0499	.0384	-.0263
.1000	.0481	-.0301
.1499	.0537	-.0305
.2000	.0596	-.0301
.3001	.0679	-.0263
.4001	.0732	-.0204
.5001	.0762	-.0117
.5999	.0780	.0018
.6999	.0783	.0213
.8000	.0762	.0398
.9000	.0672	.0470
.9501	.0586	.0440
1.0000	.0458	.0353
L.E. radius: 0.0187c		

$(x/c)_u$ and l	y = 36.406 cm c = 9.340 cm	
	$(z/c)_u$	$(z/c)_l$
0.0000	-0.0454	-0.0454
.0250	-.0272	-.0555
.0500	-.0193	-.0549
.1001	-.0068	-.0517
.1501	.0022	-.0460
.1999	.0125	-.0403
.3000	.0299	-.0261
.3998	.0465	-.0120
.5001	.0623	.0052
.6000	.0759	.0261
.7000	.0895	.0511
.8001	.1009	.0737
.8999	.1042	.0868
.9500	.1004	.0884
1.0000	.0919	.0821
L.E. radius: 0.0063c		

TABLE 8.- AIRFOIL COORDINATES FOR WING W_{35}

$(x/c)_u$ and l	y = 7.440 cm c = 15.306 cm	
	$(z/c)_u$	$(z/c)_l$
0.0000	0.0080	0.0080
.0259	.0398	-.0141
.0495	.0528	-.0179
.1009	.0705	-.0197
.2005	.0772	-.0197
.3015	.0772	-.0197
.4014	.0772	-.0197
.5003	.0768	-.0124
.5999	.0768	-.0005
.7001	.0768	.0183
.8000	.0747	.0348
.8999	.0651	.0418
1.0000	.0445	.0355
L.E. radius: 0.0481c		

$(x/c)_u$ and l	y = 9.314 cm c = 14.834 cm	
	$(z/c)_u$	$(z/c)_l$
0.0000	0.0068	0.0068
.0260	.0368	-.0146
.0507	.0497	-.0178
.1014	.0652	-.0204
.2012	.0741	-.0217
.3026	.0760	-.0224
.4021	.0774	-.0207
.5005	.0788	-.0132
.6003	.0800	.0010
.7010	.0788	.0193
.8009	.0745	.0356
.9007	.0656	.0438
1.0000	.0464	.0372
L.E. radius: 0.0221c		

$(x/c)_u$ and l	y = 11.219 cm c = 14.351 cm	
	$(z/c)_u$	$(z/c)_l$
0.0000	0.0062	0.0062
.0262	.0381	-.0159
.0504	.0513	-.0188
.1007	.0572	-.0255
.2005	.0653	-.0262
.3019	.0708	-.0235
.4009	.0749	-.0214
.4996	.0775	-.0129
.5996	.0796	.0014
.6998	.0800	.0211
.7995	.0766	.0381
.8993	.0681	.0476
1.0000	.0481	.0389
L.E. radius: 0.0214c		

TABLE 8.- Concluded

$(x/c)_u$ and l	y = 13.124 cm c = 13.871 cm	
	$(z/c)_u$	$(z/c)_l$
0.0000	0.0049	0.0049
.0256	.0309	-.0190
.0504	.0390	-.0247
.1007	.0500	-.0293
.2011	.0623	-.0298
.3018	.0690	-.0264
.4018	.0751	-.0211
.4997	.0793	-.0123
.5997	.0817	.0024
.7001	.0806	.0222
.7997	.0775	.0397
.8991	.0687	.0476
1.0000	.0500	.0408
L.E. radius: 0.0203c		

$(x/c)_u$ and l	y = 37.148 cm c = 7.800 cm	
	$(z/c)_u$	$(z/c)_l$
0.0000	-0.0570	-0.0570
.0264	-.0387	-.0700
.0495	-.0306	-.0720
.1003	-.0163	-.0694
.1986	.0055	-.0583
.3006	.0251	-.0433
.3989	.0427	-.0257
.4992	.0589	-.0062
.5969	.0752	.0169
.6939	.0882	.0427
.7952	.1019	.0700
.8968	.1084	.0908
1.0000	.0922	.0847
L.E. radius: 0.0094c		

TABLE 9.- AIRFOIL COORDINATES FOR WING W_{36}

$(x/c)_u$ and l	y = 7.440 cm c = 15.255 cm	
	$(z/c)_u$	$(z/c)_l$
0.0000	0.0073	0.0073
.0250	.0340	-.0093
.0500	.0493	-.0153
.0999	.0673	-.0198
.1500	.0749	-.0205
.2000	.0763	-.0205
.3000	.0763	-.0205
.4001	.0771	-.0170
.5000	.0778	-.0080
.5999	.0781	.0022
.7000	.0778	.0170
.8000	.0701	.0301
.8999	.0576	.0371
.9109	.0558	.0378
L.E. radius: 0.0055c		

$(x/c)_u$ and l	y = 9.314 cm c = 14.872 cm	
	$(z/c)_u$	$(z/c)_l$
0.0000	0.0075	0.0075
.0249	.0295	-.0072
.0500	.0427	-.0132
.0999	.0601	-.0184
.1500	.0709	-.0203
.2000	.0758	-.0200
.3001	.0779	-.0174
.4000	.0794	-.0128
.5001	.0804	-.0060
.6000	.0811	.0060
.7001	.0791	.0188
.8000	.0705	.0299
.9001	.0572	.0374
.9501	.0502	.0391
1.0000	.0425	.0415
L.E. radius: 0.0056c		

$(x/c)_u$ and l	y = 11.219 cm c = 14.483 cm	
	$(z/c)_u$	$(z/c)_l$
0.0000	0.0070	0.0070
.0251	.0277	-.0070
.0500	.0395	-.0114
.1000	.0559	-.0154
.1499	.0668	-.0154
.2000	.0731	-.0142
.3039	.0800	-.0128
.4000	.0840	-.0077
.5000	.0859	0
.6000	.0847	.0110
.7001	.0803	.0224
.8001	.0702	.0307
.9000	.0566	.0365
.9500	.0489	.0384
1.0000	.0431	.0421
L.E. radius: 0.0058c		

TABLE 9.- Concluded

$(x/c)_u$ and l	y = 13.124 cm c = 14.094 cm	
	$(z/c)_u$	$(z/c)_l$
0.0000	0.0056	0.0056
.0250	.0256	-.0063
.0501	.0357	-.0087
.1000	.0575	-.0101
.1501	.0609	-.0101
.2000	.0703	-.0090
.3001	.0825	-.0059
.4001	.0894	0
.5001	.0912	.0059
.6001	.0890	.0159
.7001	.0829	.0260
.8000	.0721	.0339
.9000	.0582	.0395
.9501	.0503	.0405
1.0000	.0438	.0427
L.E. radius: 0.0059c		

$(x/c)_u$ and l	y = 36.406 cm c = 9.340 cm	
	$(z/c)_u$	$(z/c)_l$
0.0000	-0.0215	-0.0215
.0250	-.0063	-.0256
.0500	.0041	-.0250
.1001	.0147	-.0231
.1501	.0239	-.0204
.1999	.0324	-.0158
.3000	.0449	-.0095
.4001	.0555	-.0011
.4999	.0623	.0109
.5999	.0674	.0226
.7000	.0685	.0335
.8001	.0664	.0408
.8999	.0623	.0487
.9500	.0601	.0522
1.0000	.0568	.0552
L.E. radius: 0.0041c		

TABLE 10.- AIRFOIL COORDINATES FOR WING W_{37}

$(x/c)_u$ and l	y = 7.440 cm c = 15.133 cm	
	$(z/c)_u$	$(z/c)_l$
0.0000	0.0070	0.0070
.0258	.0394	-.0154
.0514	.0539	-.0190
.0723	.0633	-.0213
.1000	.0697	-.0220
.1994	.0759	-.0227
.2472	.0759	-.0225
.2996	.0759	-.0217
.3996	.0765	-.0196
.4997	.0769	-.0116
.6000	.0769	.0056
.6991	.0765	.0248
.7989	.0762	.0436
.8986	.0727	.0545
.9267	.0700	.0549
L.E. radius: 0.0191c		

$(x/c)_u$ and l	y = 9.314 cm c = 14.902 cm	
	$(z/c)_u$	$(z/c)_l$
0.0000	0.0072	0.0072
.0256	.0344	-.0167
.0508	.0469	-.0206
.0764	.0557	-.0220
.1022	.0619	-.0227
.1993	.0656	-.0245
.3000	.0682	-.0245
.4002	.0704	-.0213
.5003	.0731	-.0131
.6005	.0750	.0039
.7002	.0760	.0239
.7997	.0757	.0409
.8994	.0728	.0525
.9542	.0653	.0511
1.0000	.0547	.0443
L.E. radius: 0.0194c		

$(x/c)_u$ and l	y = 11.219 cm c = 14.694 cm	
	$(z/c)_u$	$(z/c)_l$
0.0000	0.0000	0.0000
.0256	.0245	-.0245
.0512	.0322	-.0296
.0757	.0396	-.0328
.0997	.0446	-.0328
.1995	.0551	-.0325
.2996	.0608	-.0303
.3998	.0671	-.0245
.5006	.0714	-.0133
.6003	.0735	.0036
.6997	.0742	.0220
.7995	.0735	.0396
.8996	.0698	.0519
.9525	.0638	.0508
1.0000	.0529	.0429
L.E. radius: 0.0190c		

TABLE 10.- Concluded

$(x/c)_u$ and l	y = 13.124 cm c = 14.493 cm	
	$(z/c)_u$	$(z/c)_l$
0.0000	-0.0142	-0.0142
.0251	.0114	-.0351
.0499	.0198	-.0394
.0750	.0259	-.0417
.0999	.0303	-.0424
.1998	.0442	-.0401
.2999	.0543	-.0343
.3998	.0627	-.0256
.4996	.0687	-.0142
.5997	.0734	.0023
.6996	.0755	.0212
.7995	.0745	.0398
.8994	.0680	.0505
.9497	.0613	.0485
1.0000	.0519	.0412
L.E. radius: 0.0186c		

$(x/c)_u$ and l	y = 34.925 cm c = 11.999 cm	
	$(z/c)_u$	$(z/c)_l$
0.0000	-0.0724	-0.0724
.0250	-.0595	-.0826
.0500	-.0533	-.0834
.0749	-.0481	-.0838
.1001	-.0432	-.0821
.2000	-.0260	-.0696
.3000	-.0114	-.0565
.4001	.0036	-.0415
.5000	.0171	-.0260
.5999	.0301	-.0097
.7000	.0423	.0123
.8000	.0521	.0330
.8999	.0542	.0428
.9500	.0504	.0419
1.0000	.0415	.0362
L.E. radius: 0.0057c		

TABLE 11.- AIRFOIL COORDINATES FOR WING W_{38}

$(x/c)_u$ and l	y = 7.440 cm c = 15.133 cm	
	$(z/c)_u$	$(z/c)_l$
0.0000	0.0067	0.0067
.0245	.0322	-.0101
.0493	.0490	-.0171
.0994	.0685	-.0206
.1479	.0762	-.0210
.1994	.0772	-.0210
.2989	.0772	-.0210
.3990	.0772	-.0171
.4997	.0772	-.0070
.5997	.0772	.0074
.5997	.0742	.0206
.7998	.0661	.0287
.8996	.0535	.0339
.9272	.0493	.0349
L.E. radius: 0.0055c		

$(x/c)_u$ and l	y = 9.314 cm c = 14.920 cm	
	$(z/c)_u$	$(z/c)_l$
0.0000	0.0068	0.0068
.0245	.0288	-.0075
.0494	.0422	-.0134
.1001	.0599	-.0184
.1486	.0698	-.0196
.1994	.0749	-.0203
.2996	.0773	-.0180
.4001	.0780	-.0128
.5001	.0783	-.0043
.6001	.0783	.0089
.7005	.0749	.0203
.8001	.0655	.0277
.9006	.0528	.0337
1.0000	.0388	.0378
L.E. radius: 0.0056c		

$(x/c)_u$ and l	y = 11.219 cm c = 14.702 cm	
	$(z/c)_u$	$(z/c)_l$
0.0000	0.0054	0.0054
.0245	.0252	-.0076
.0498	.0371	-.0123
.1004	.0541	-.0152
.1491	.0641	-.0155
.2001	.0705	-.0147
.3010	.0764	-.0126
.4003	.0817	-.0060
.5007	.0828	.0017
.6011	.0814	.0112
.7008	.0757	.0216
.8008	.0658	.0295
.9001	.0532	.0352
1.0000	.0397	.0387
L.E. radius: 0.0055c		

TABLE 11.- Concluded

$(x/c)_u$ and l	y = 13.124 cm c = 14.483 cm	
	$(z/c)_u$	$(z/c)_l$
0.0000	0.0026	0.0026
.0246	.0256	-.0077
.0496	.0321	-.0102
.1001	.0461	-.0105
.1491	.0570	-.0098
.2003	.0658	-.0088
.2999	.0786	-.0051
.4000	.0851	0
.5009	.0880	.0070
.6010	.0847	.0154
.7012	.0779	.0237
.8009	.0668	.0303
.9002	.0537	.0358
1.0000	.0407	.0396
L.E. radius: 0.0054c		

$(x/c)_u$ and l	y = 34.925 cm c = 11.999 cm	
	$(z/c)_u$	$(z/c)_l$
0.0000	-0.0243	-0.0243
.0248	-.0146	-.0277
.0493	-.0080	-.0277
.0997	.0036	-.0252
.1503	.0142	-.0216
.2003	.0224	-.0171
.3008	.0366	-.0089
.4014	.0466	0
.5019	.0538	.0102
.6012	.0582	.0216
.7013	.0599	.0305
.7995	.0610	.0379
.9001	.0578	.0451
1.0000	.0519	.0506
L.E. radius: 0.0028c		

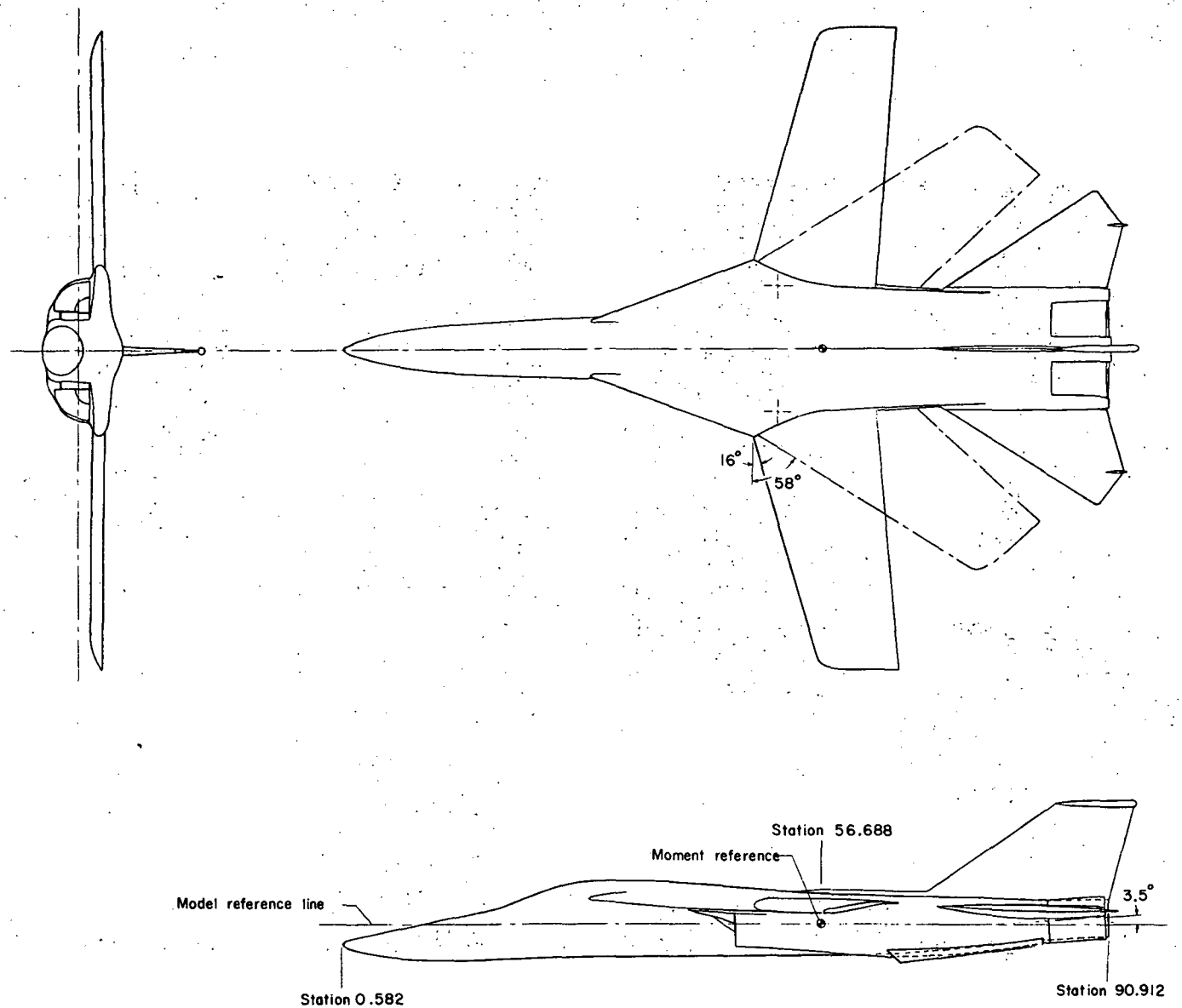

Figure 1.- General arrangement of 1/24-scale model variable-sweep fighter airplane shown with wing W_{34e} (planform B). All linear dimensions in cm unless otherwise noted.

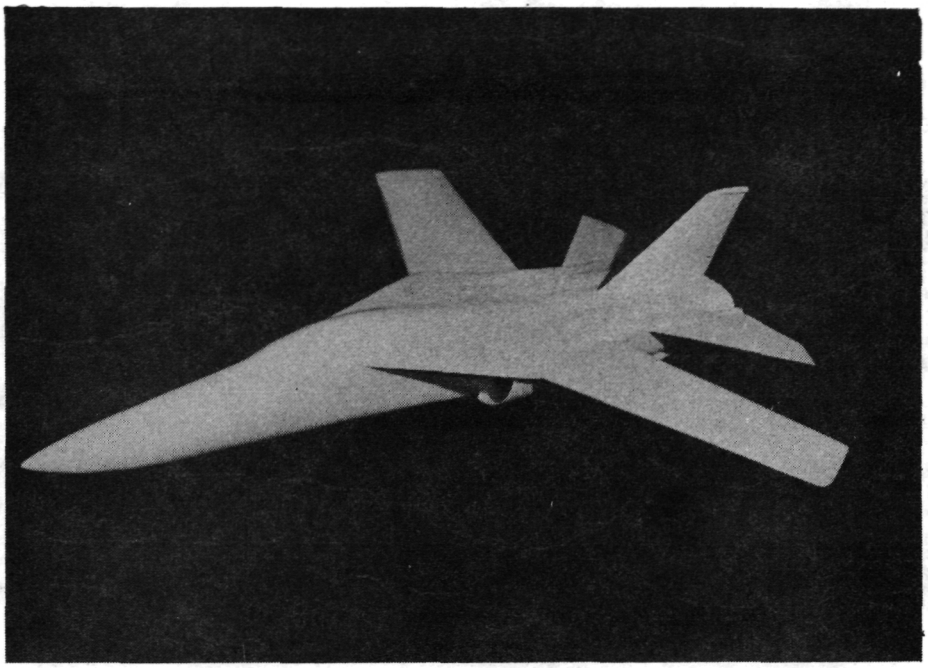

L-70-1212

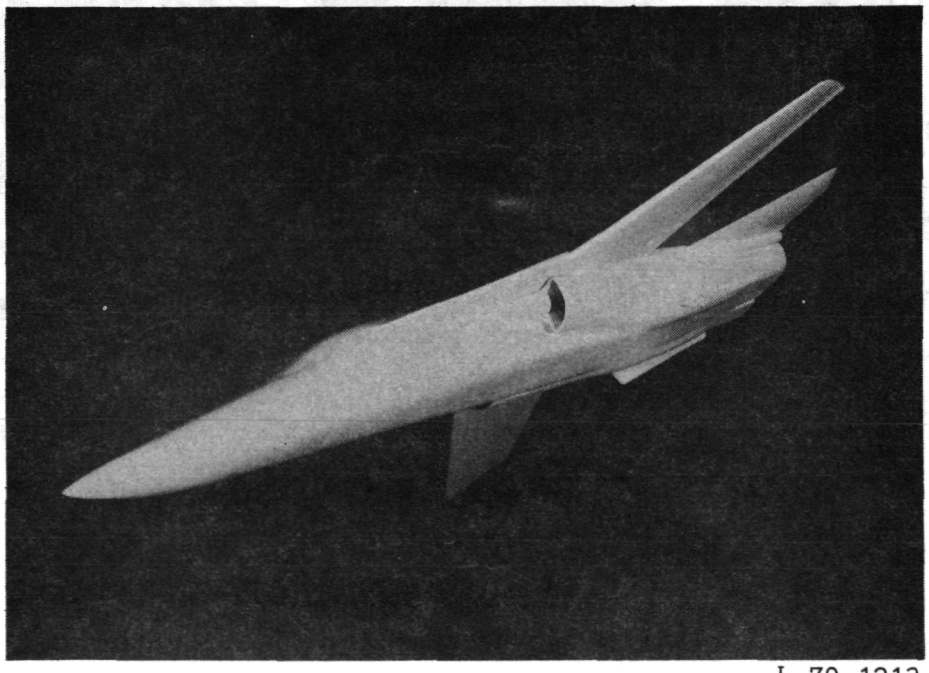

L-70-1213

Figure 2.- Photographs of model with wing W_{34e}.

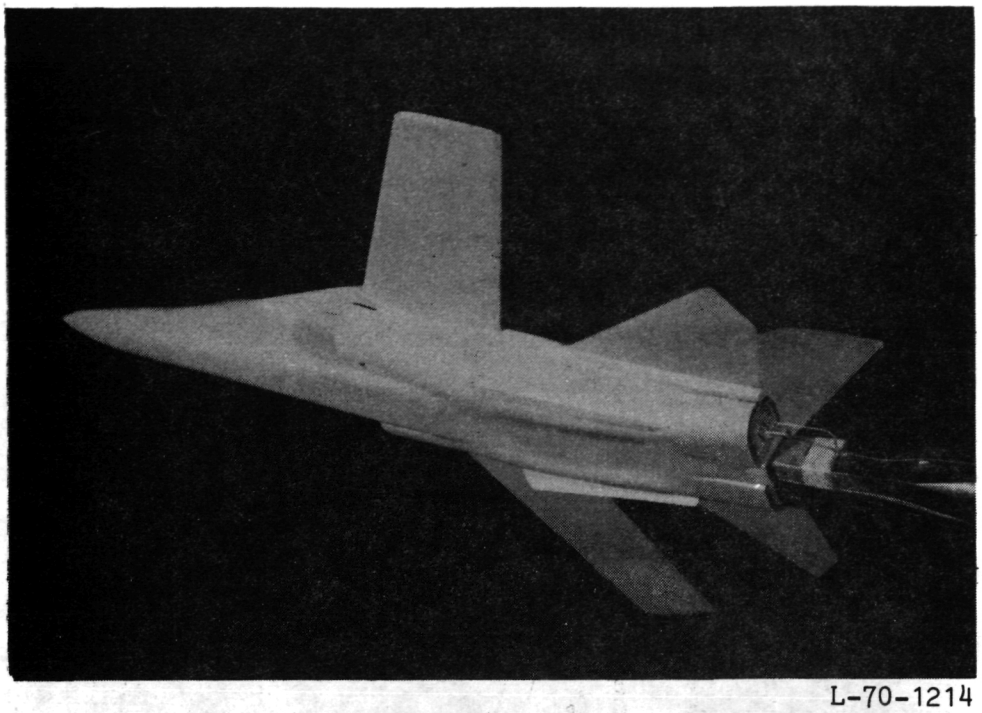

L-70-1214

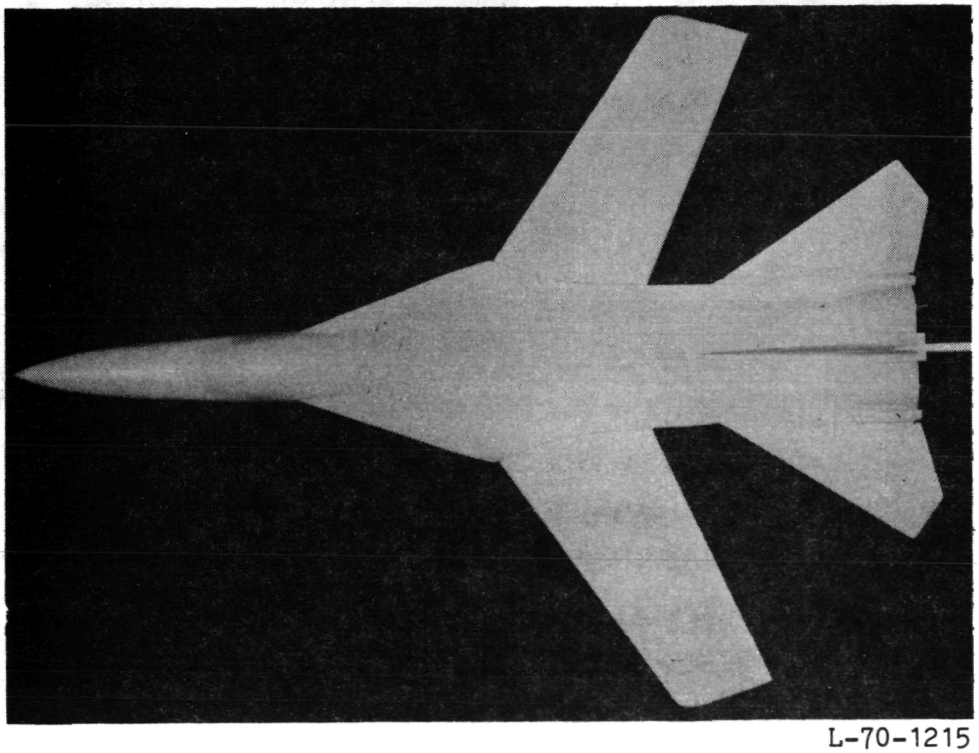

L-70-1215

Figure 2.- Concluded.

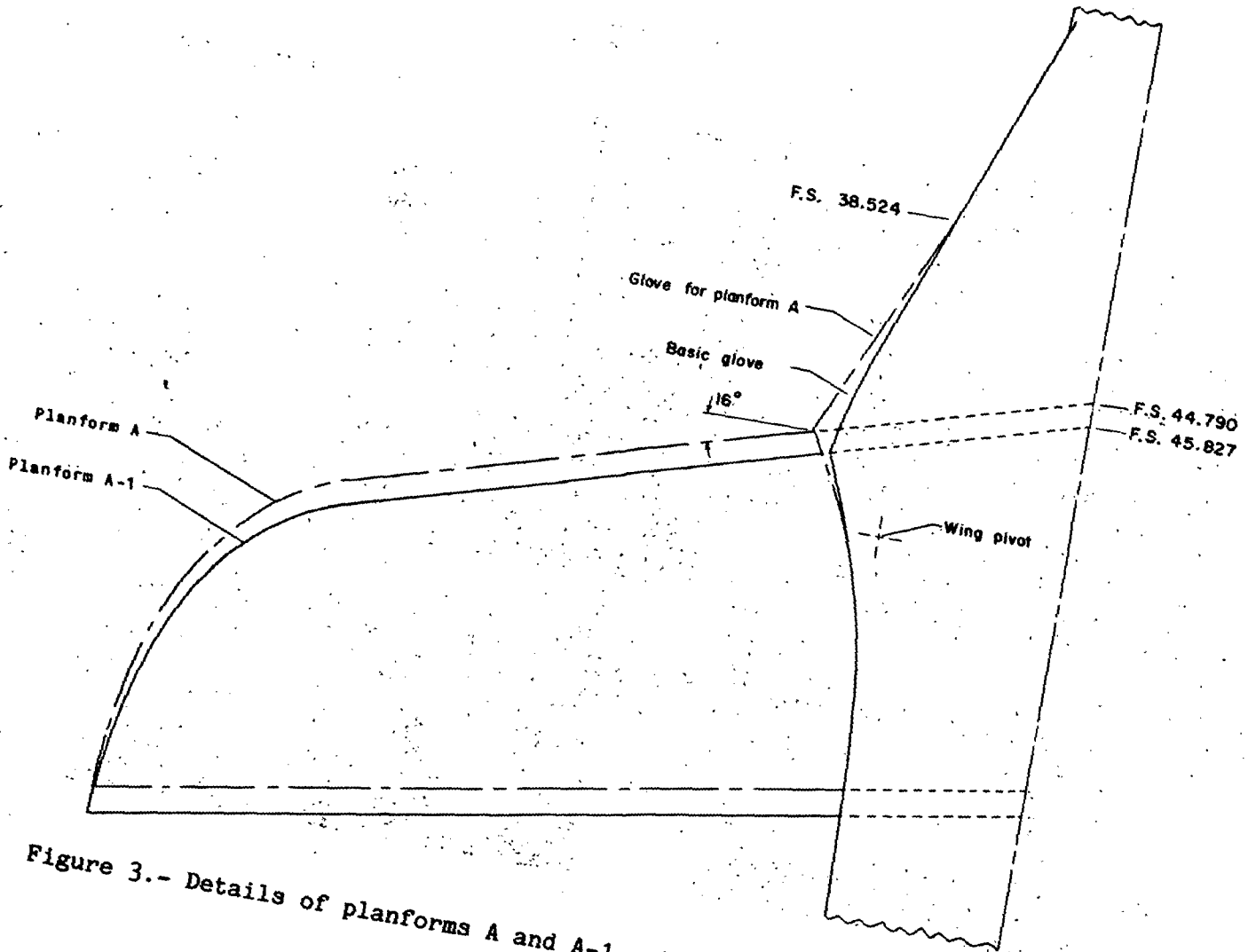

Figure 3.- Details of planforms A and A-1. All linear dimensions in cm.

PLANFORM	c_r	c_t	b	S	$\bar{c}$	TAPER RATIO	ASPECT RATIO
F-111	15.964	5.187	80.010	846.77	11.483	0.325	7.56
A, A-1	15.982	11.854	72.390	1008.06	14.019	.742	5.20
B	16.774	9.080	75.353	974.03*	13.310*	.541	5.83
C	17.188	7.478	76.835	947.58	12.969	.435	6.23

*Reference constants used for all data computation.

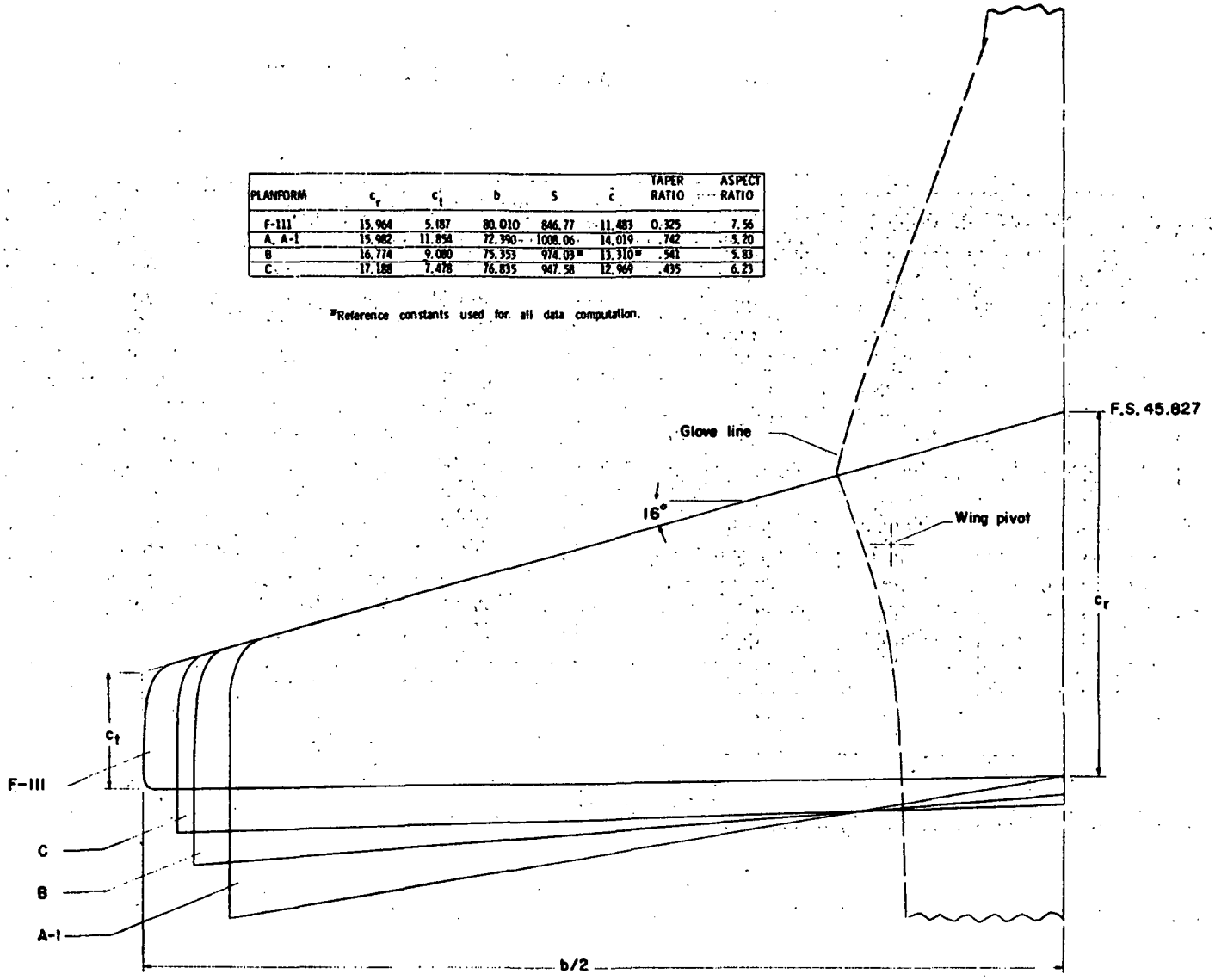

Figure 4.- Details of planforms A, B, and C and basic planform F-111. All linear dimensions in cm.

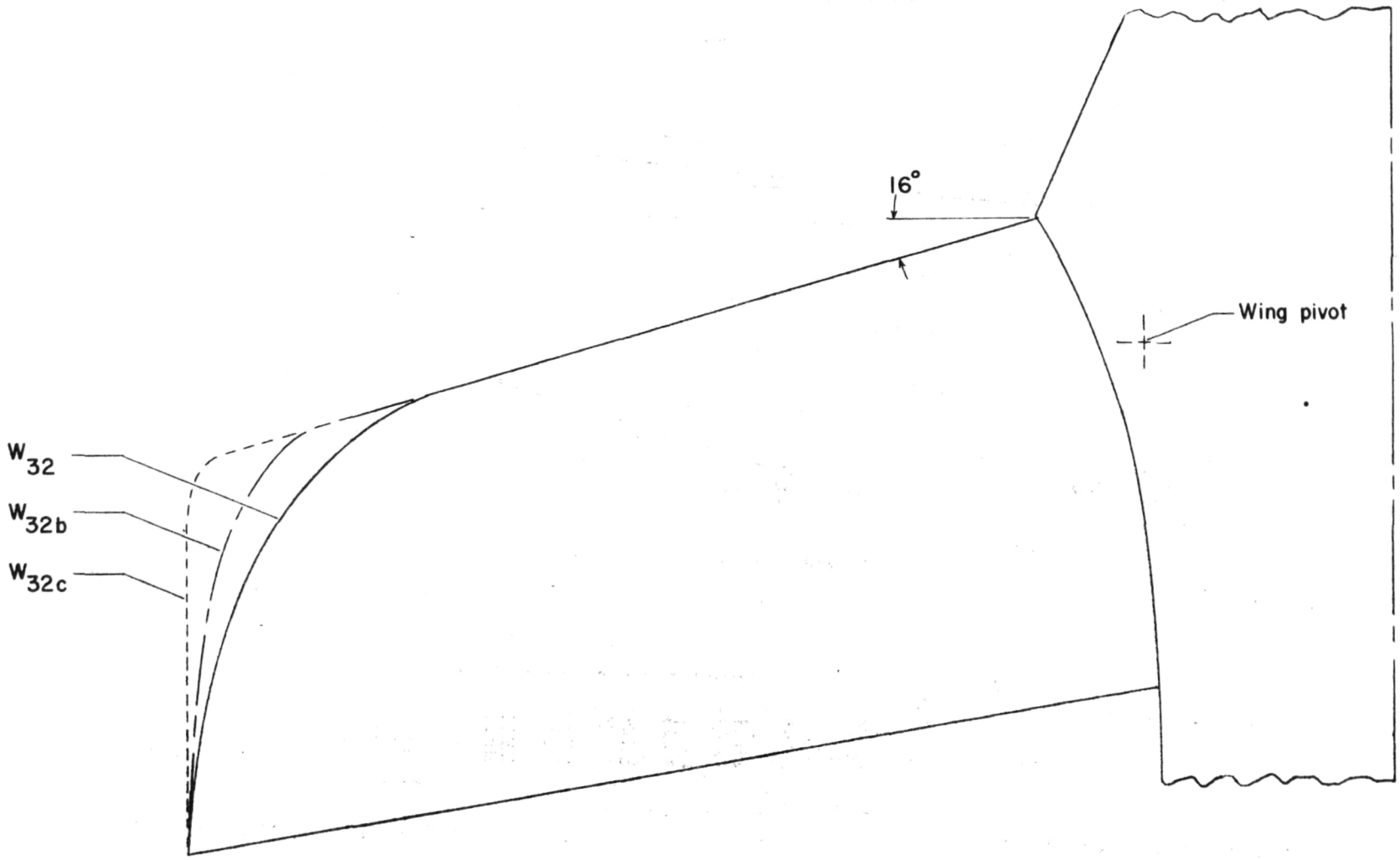

Figure 5.- Tip planform shape comparison for wing W_{32}.

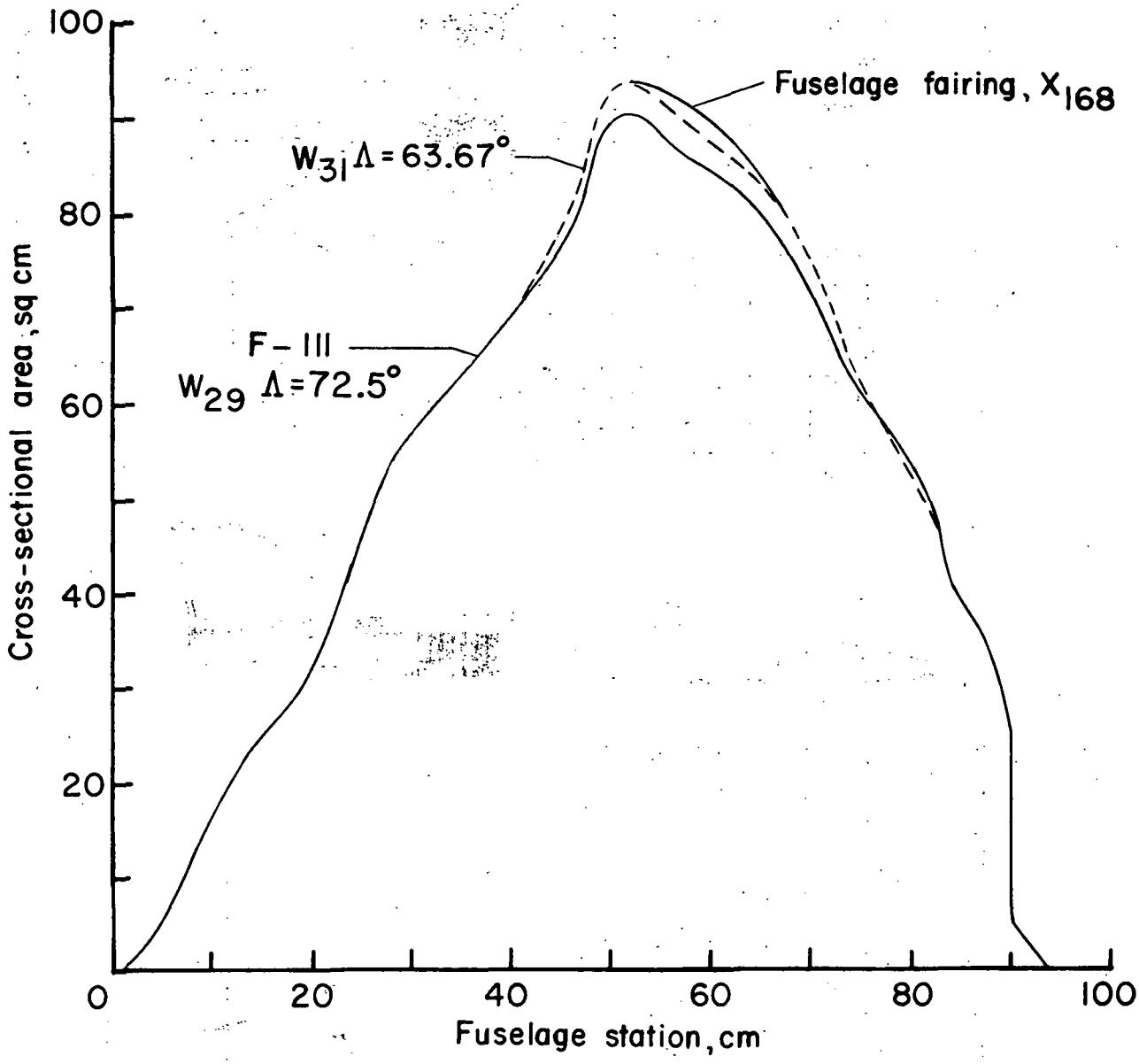

Figure 6.- Cross-sectional area distribution of model with 100-percent-capture-ratio area removed.

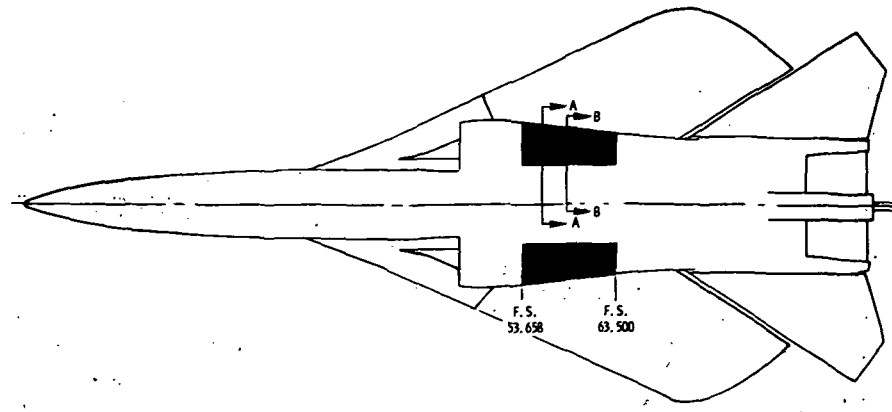

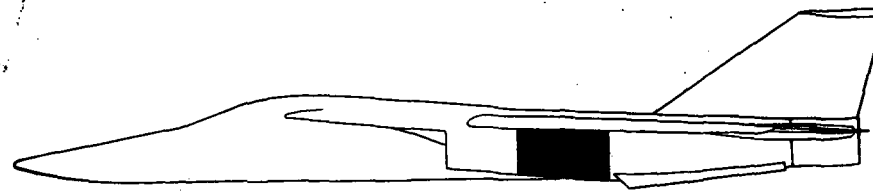

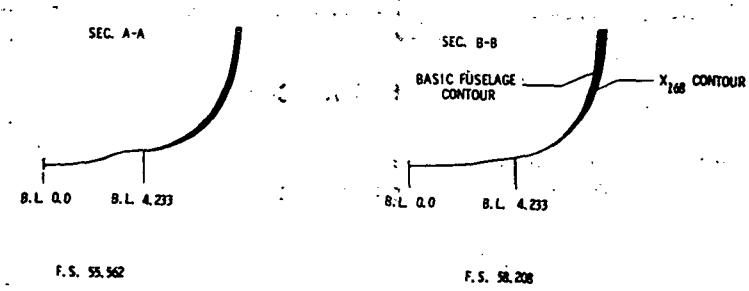

Figure 7.- Details of fuselage fairing X_{168}. All linear dimensions in cm.

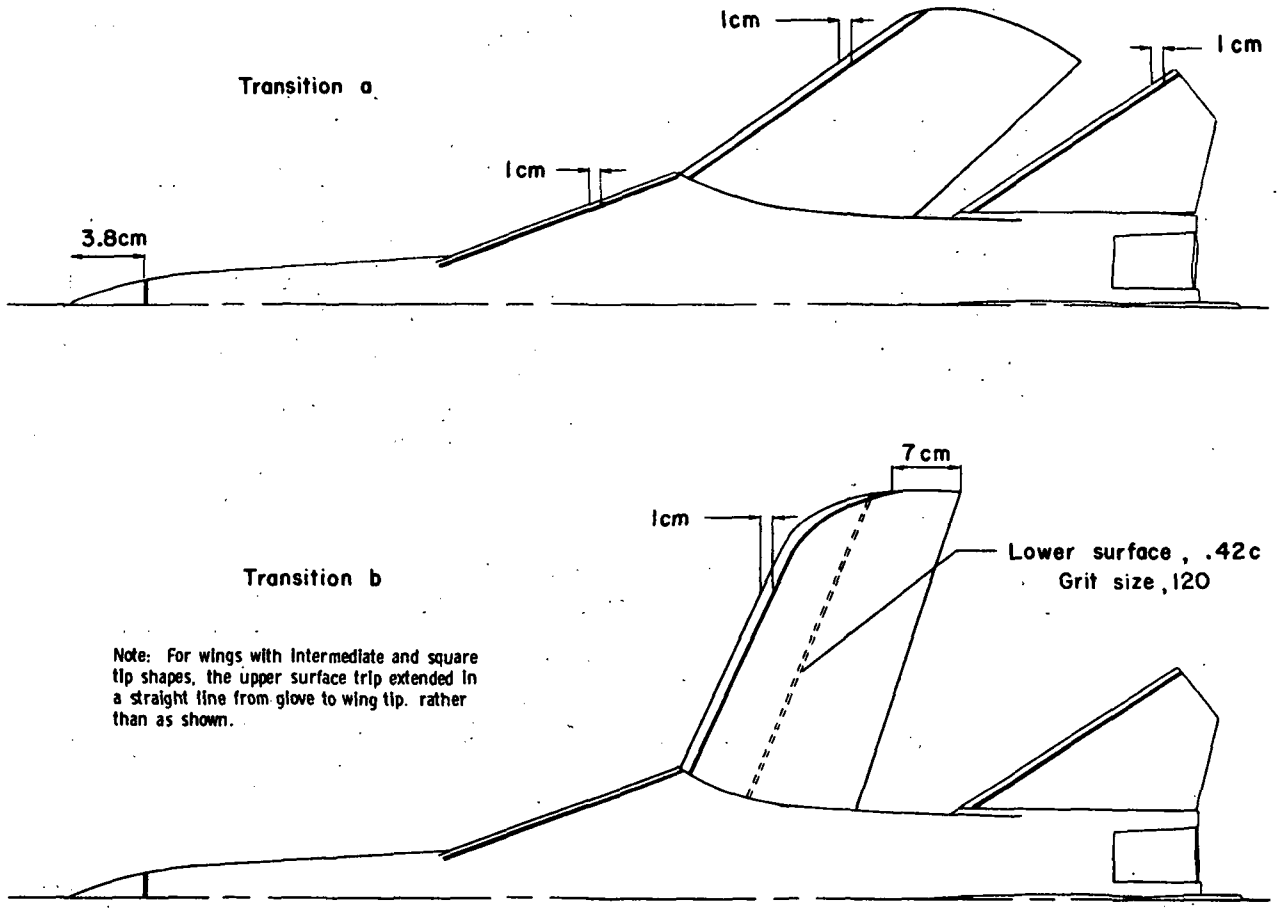

Figure 8.- Model boundary-layer transition arrangements. Grit size 150 except where noted otherwise.

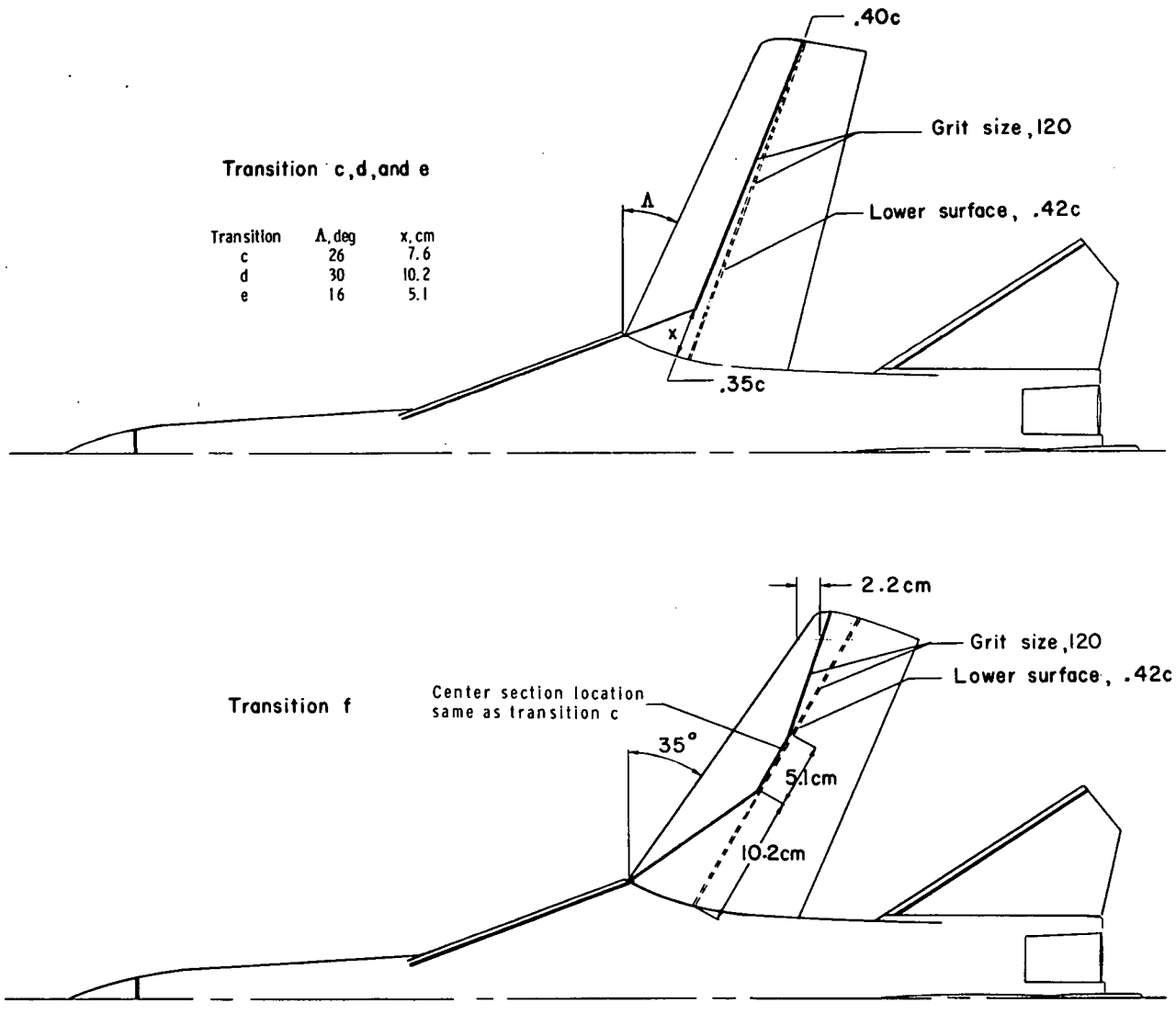

Figure 8.- Concluded.

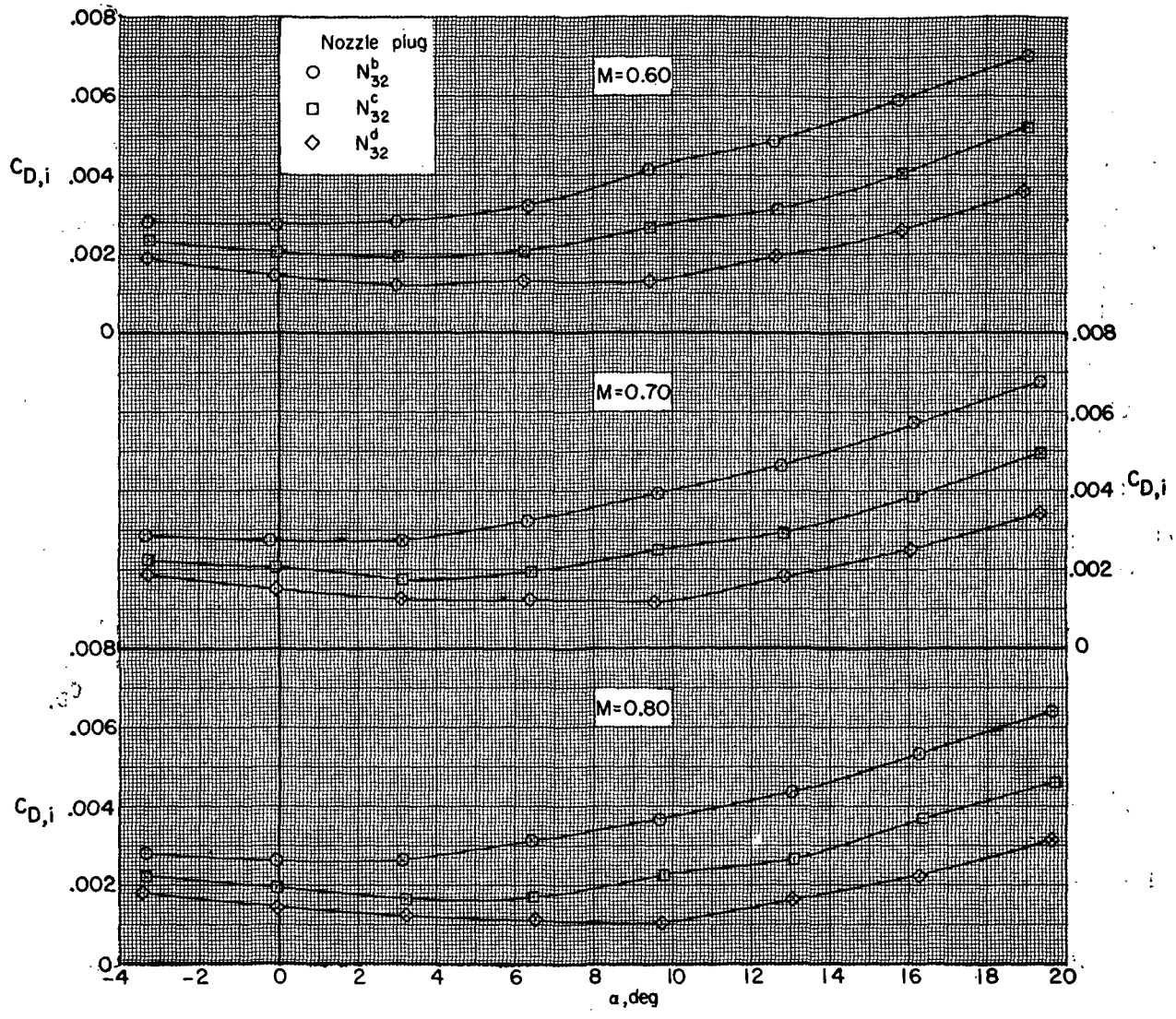

(a) Internal drag.

Figure 9.- Model internal drag and mass-flow characteristics.

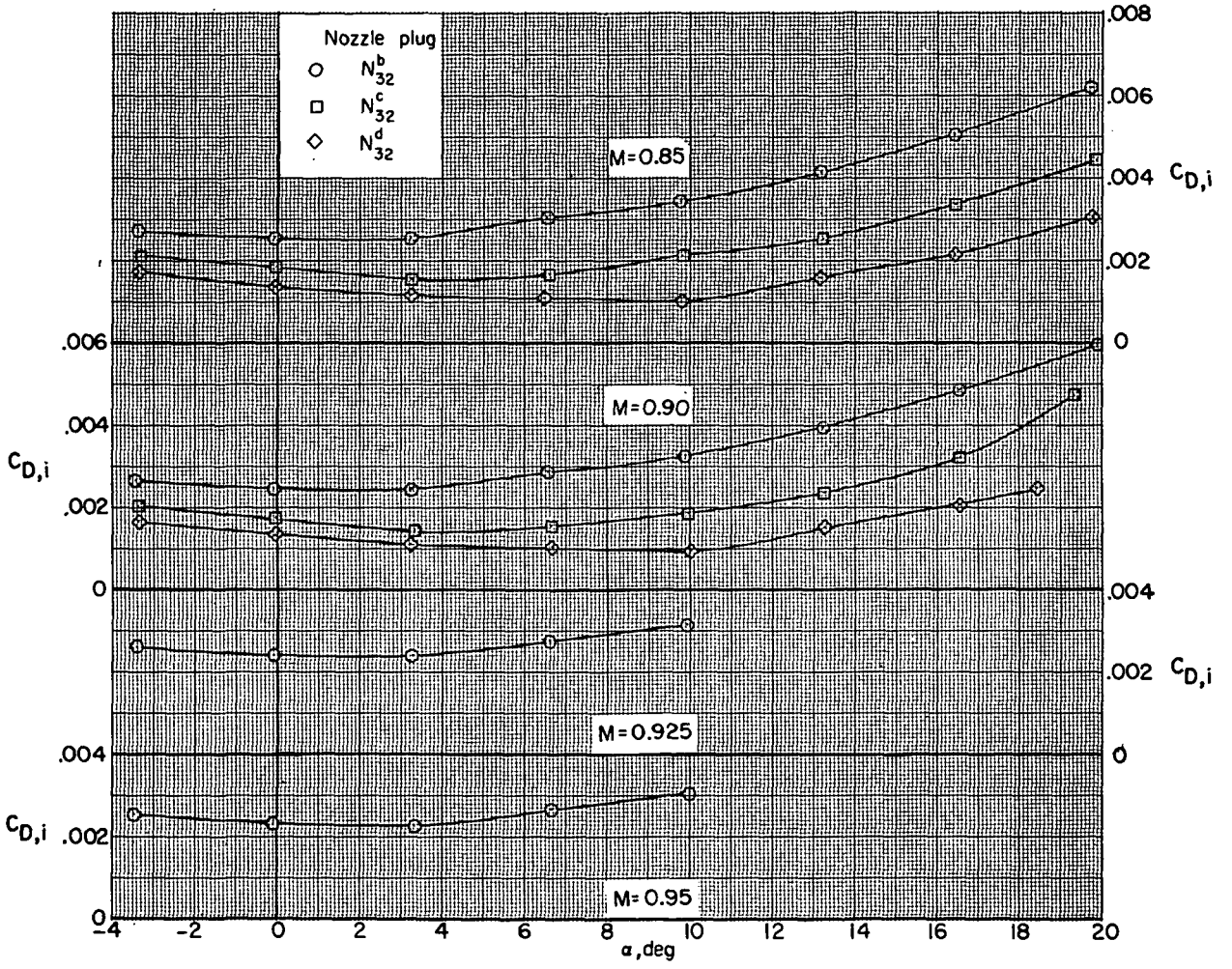

(a) Concluded.

Figure 9.- Continued.

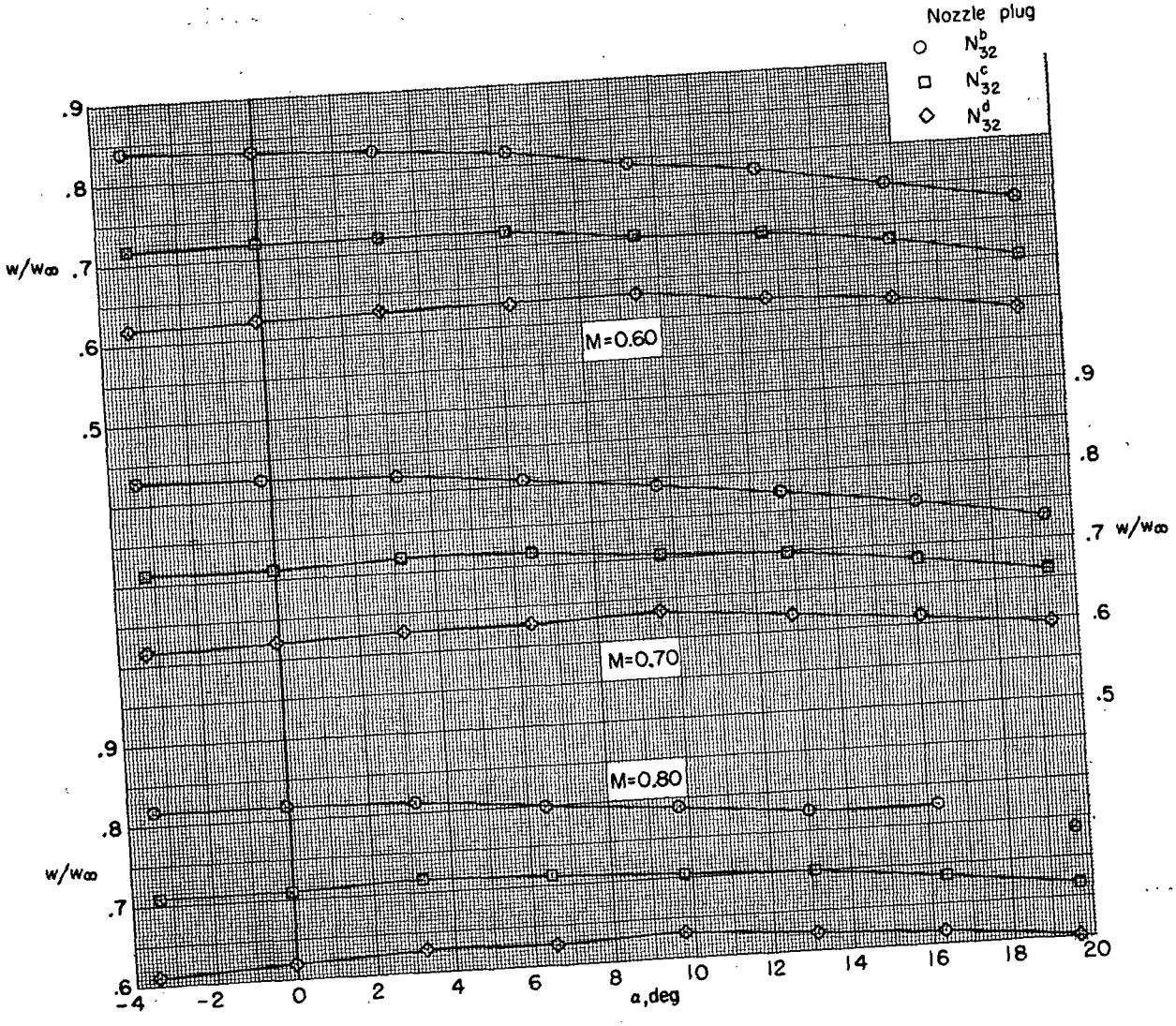

(b) Mass-flow ratio.

Figure 9.- Continued.

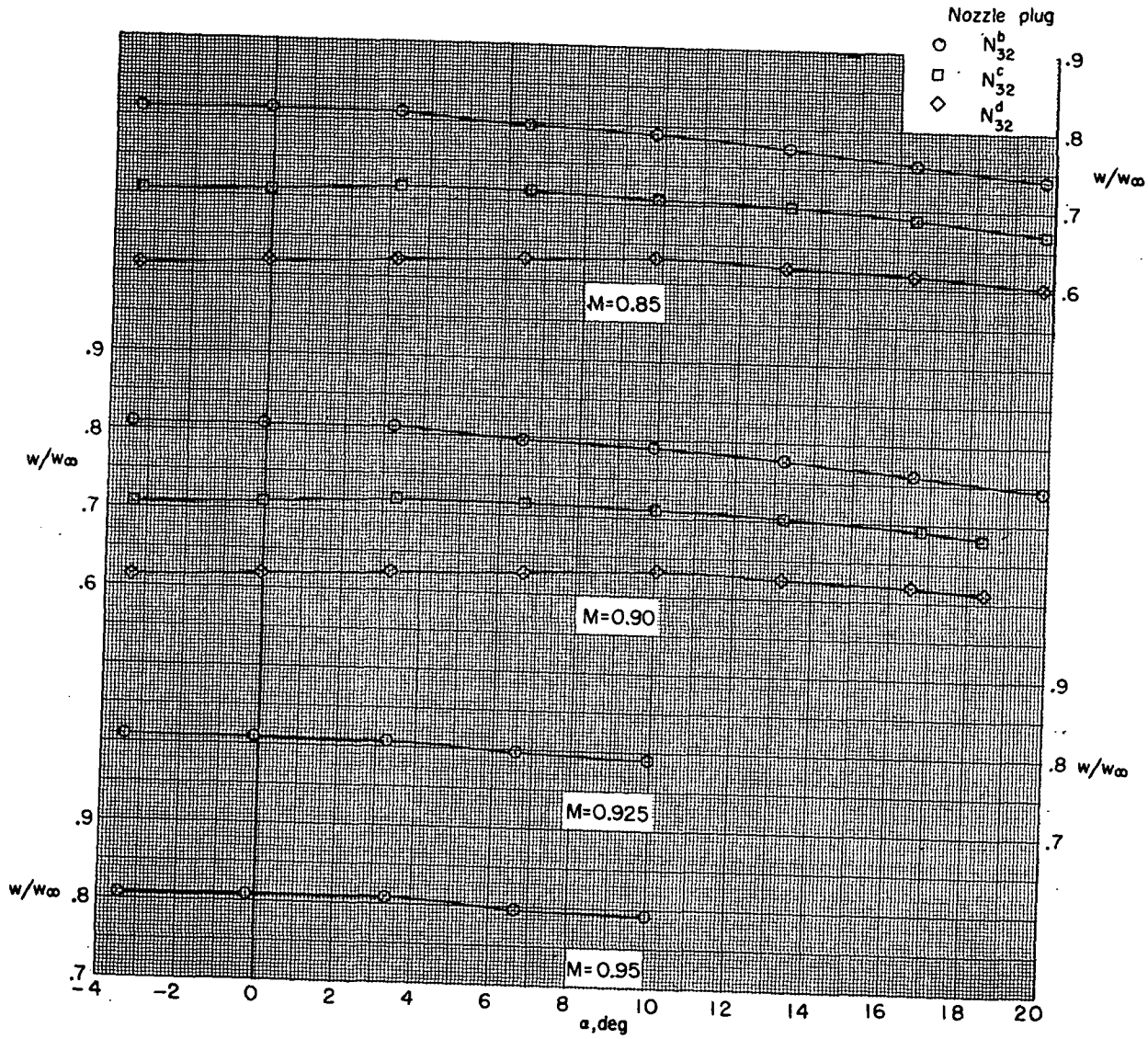

(b) Concluded.

Figure 9.- Concluded.

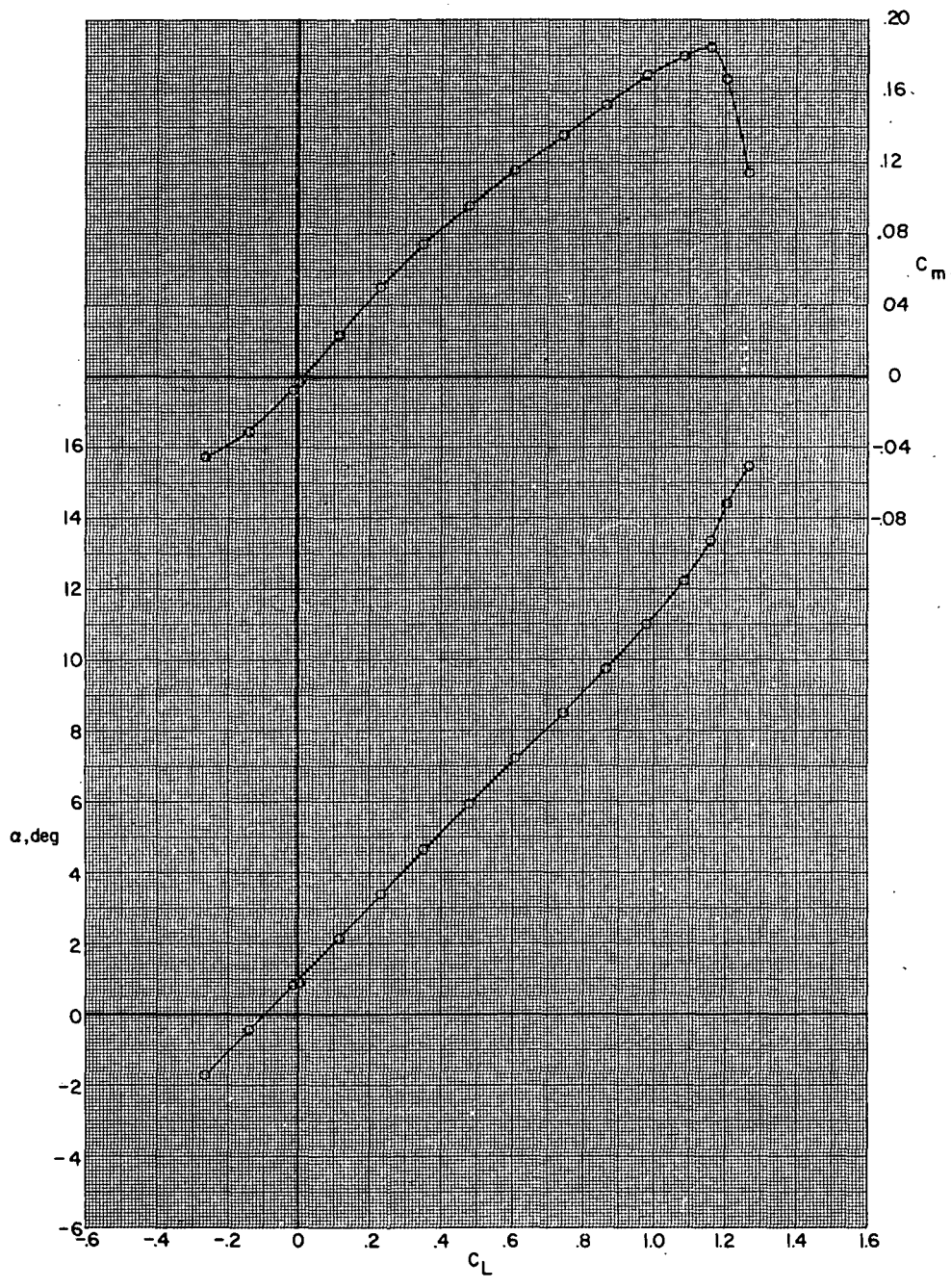

(a) M = 0.60.

Figure 10.- Aerodynamic characteristics for configuration $B_{80}G_{43}H_{13}I_{71}N_{32}^{b}V_{29}V_{38}W_{31}X_{24}X_{168}$ with wing swept 16.0°.

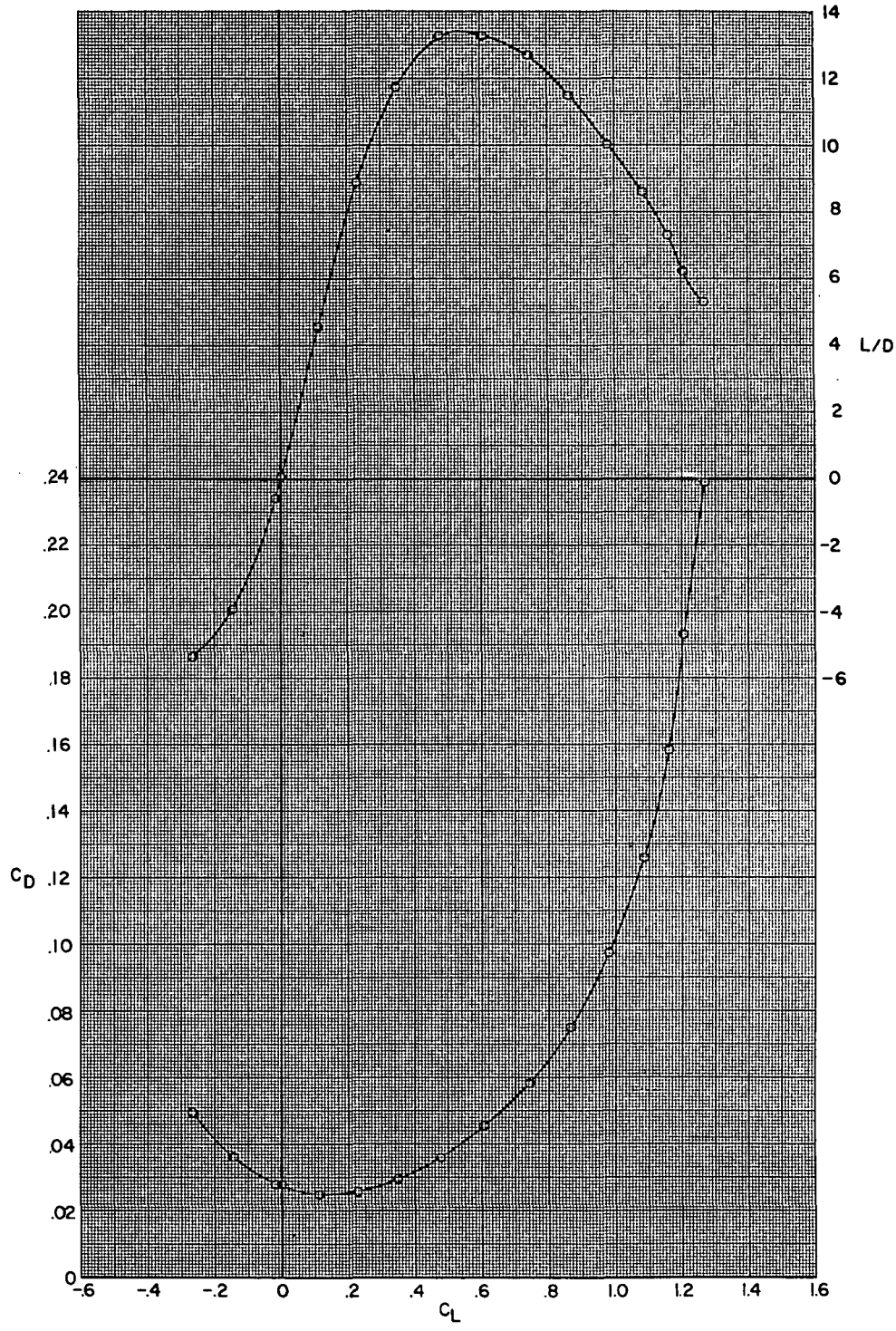

(a) Concluded.

Figure 10.- Continued.

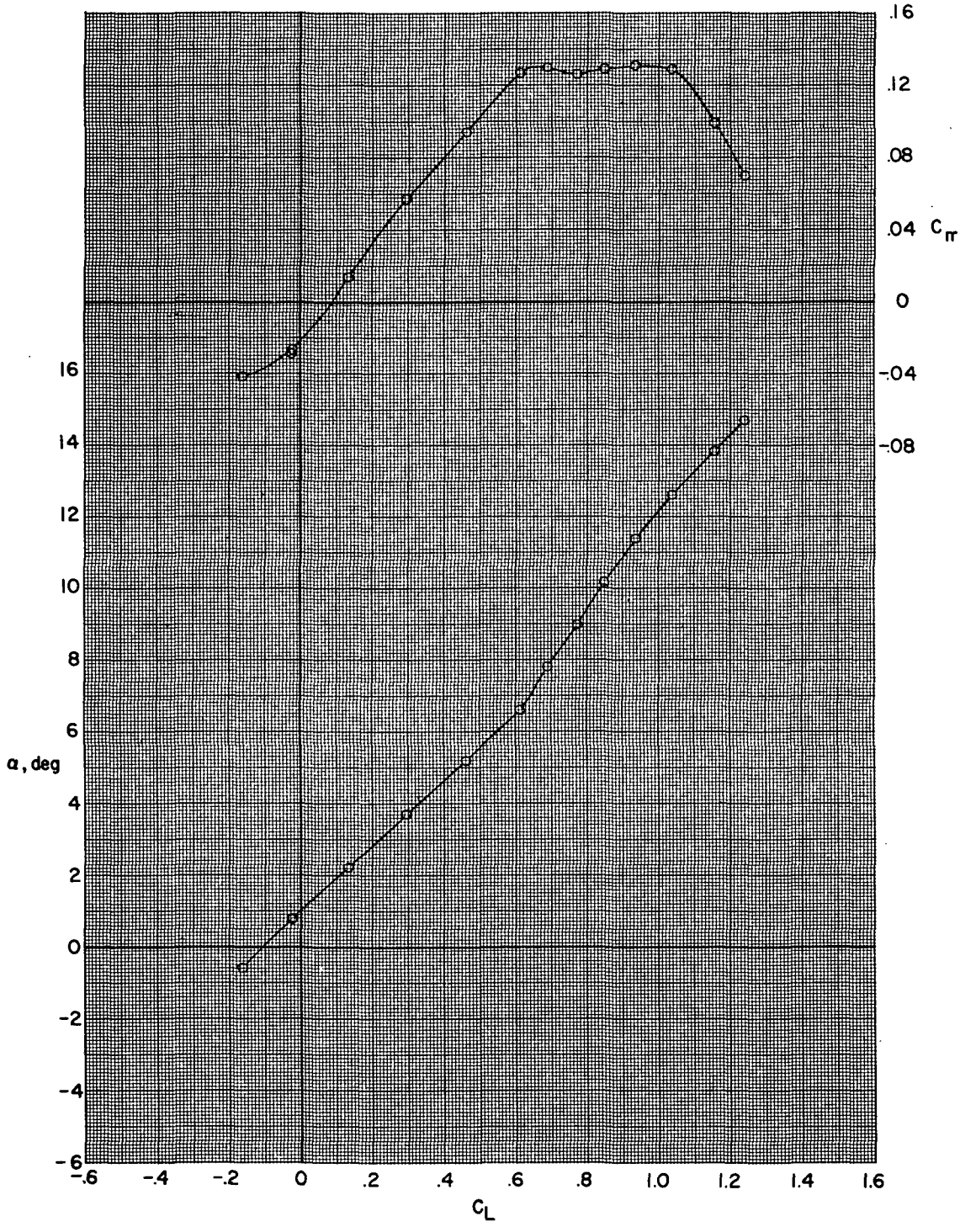

(b) M = 0.80.

Figure 10.- Continued.

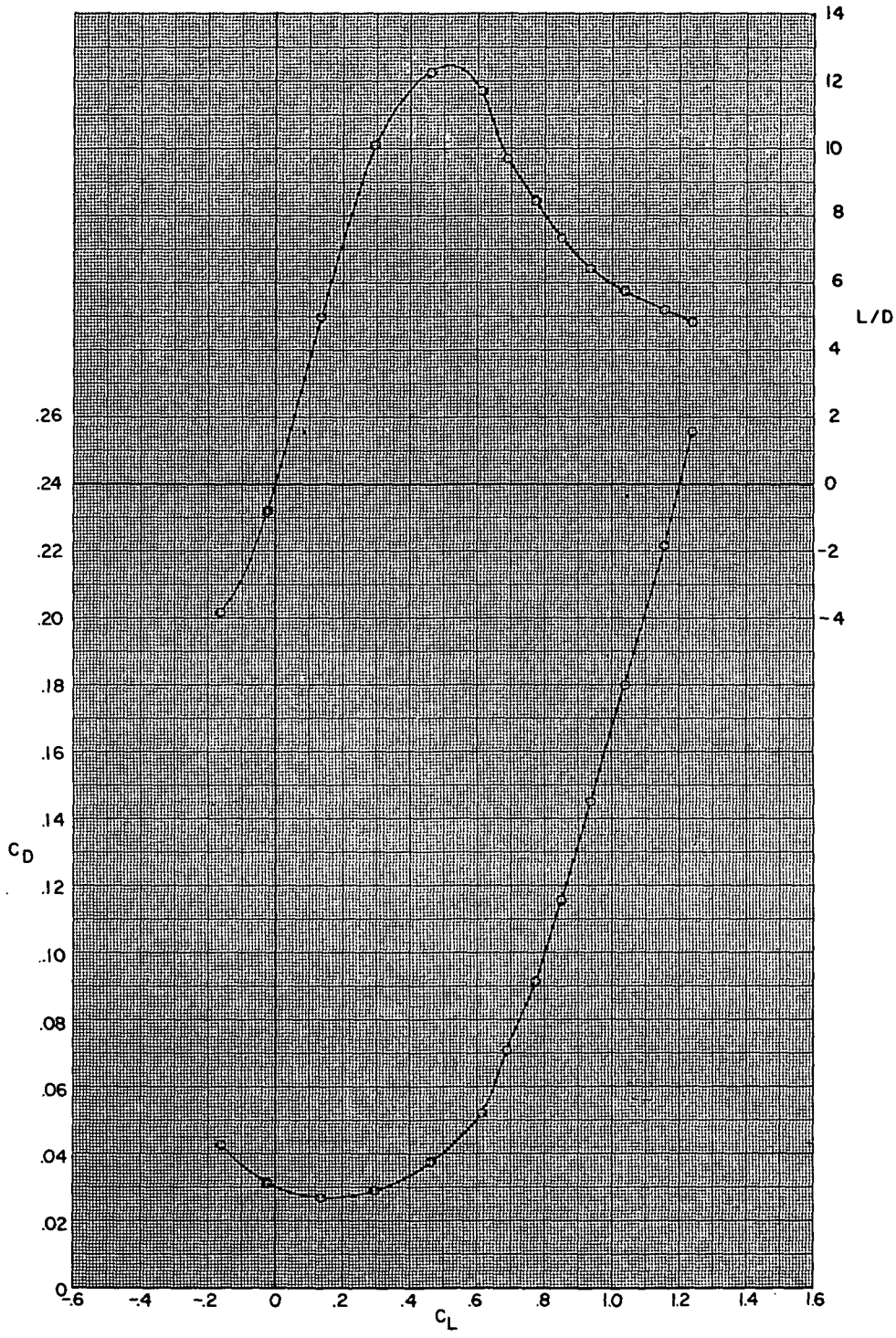

(b) Concluded.

Figure 10.- Continued.

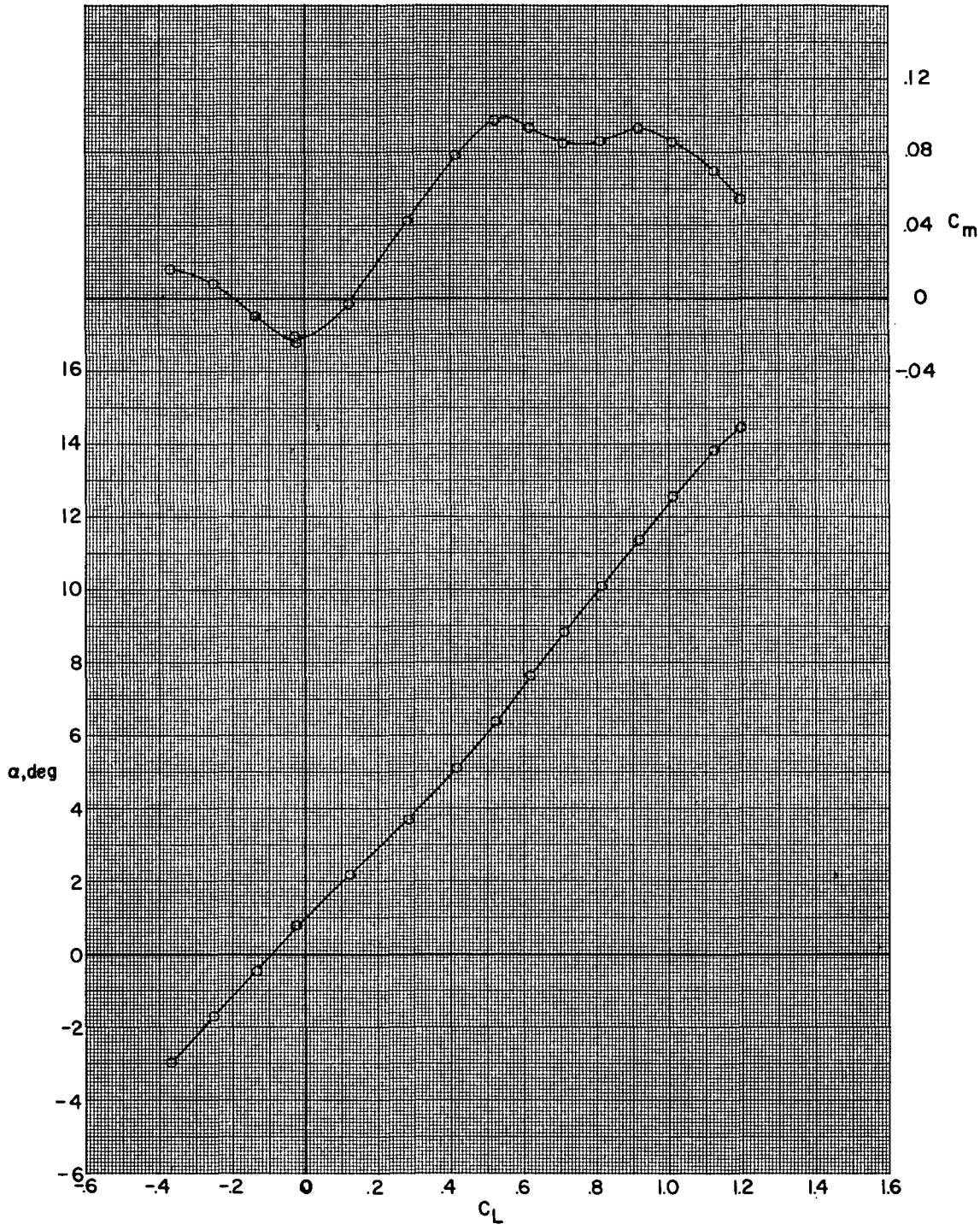

(c) M = 0.85.

Figure 10.- Continued.

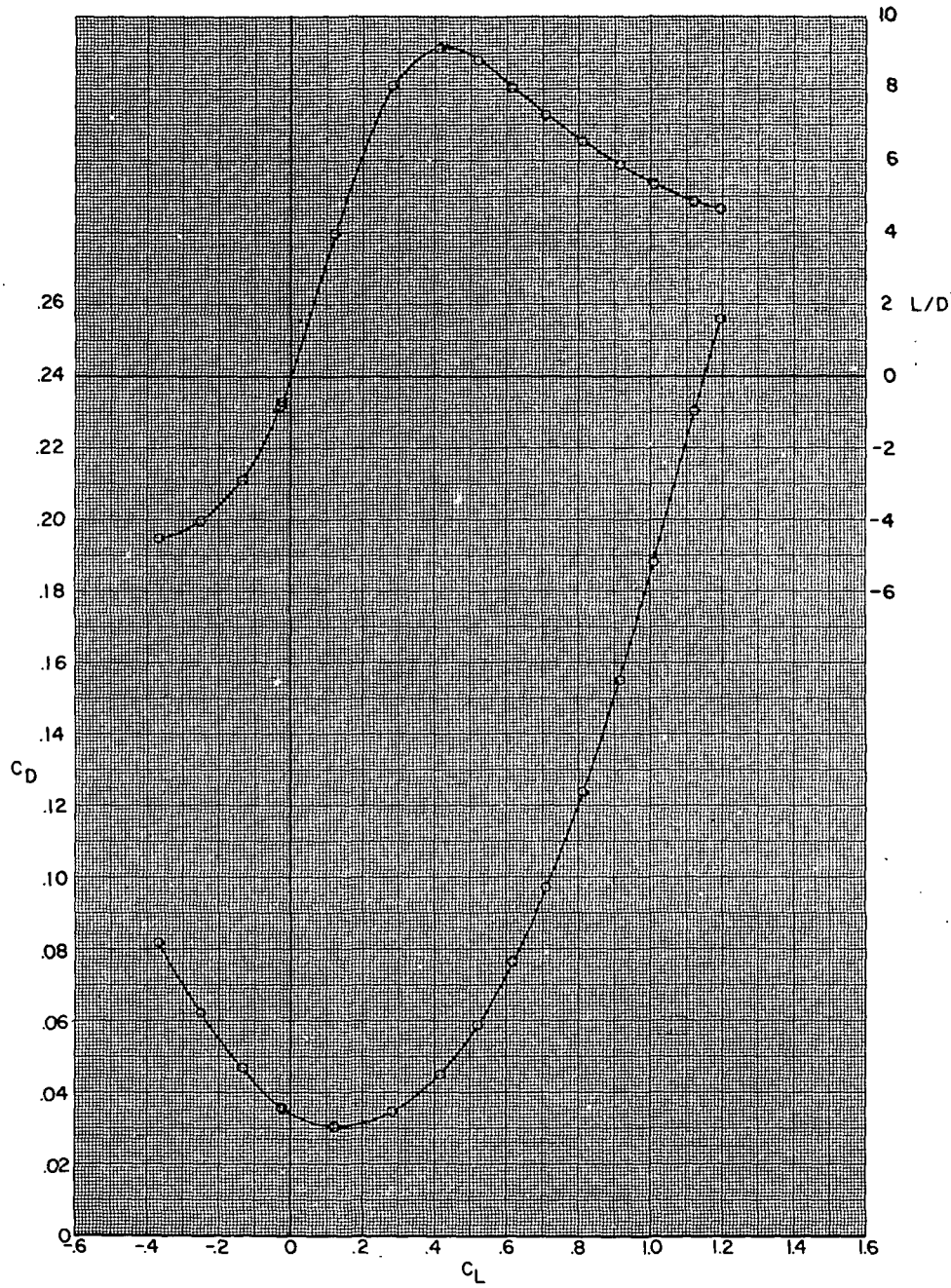

(c) Concluded.

Figure 10.- Continued.

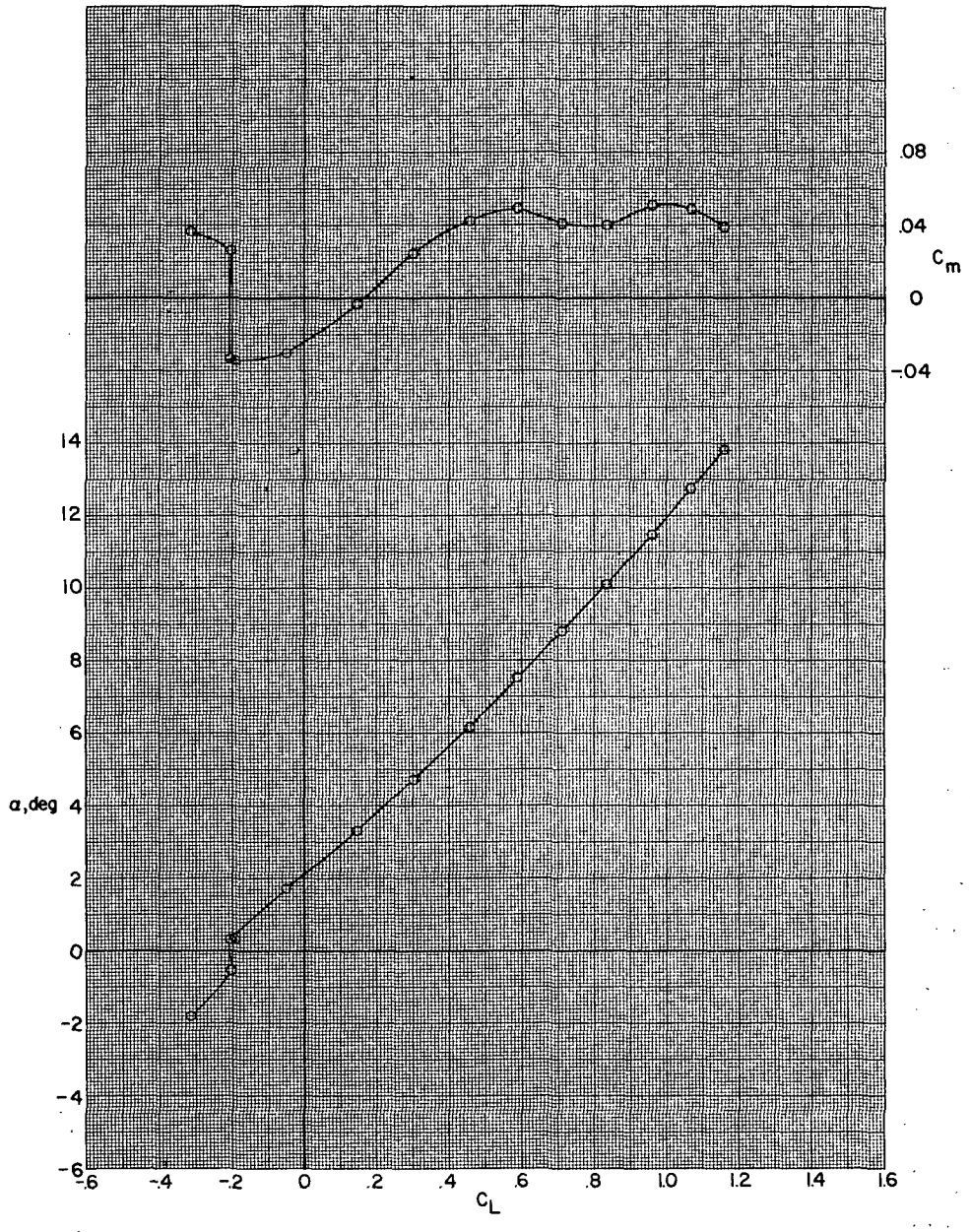

(d) M = 0.90.

Figure 10.- Continued.

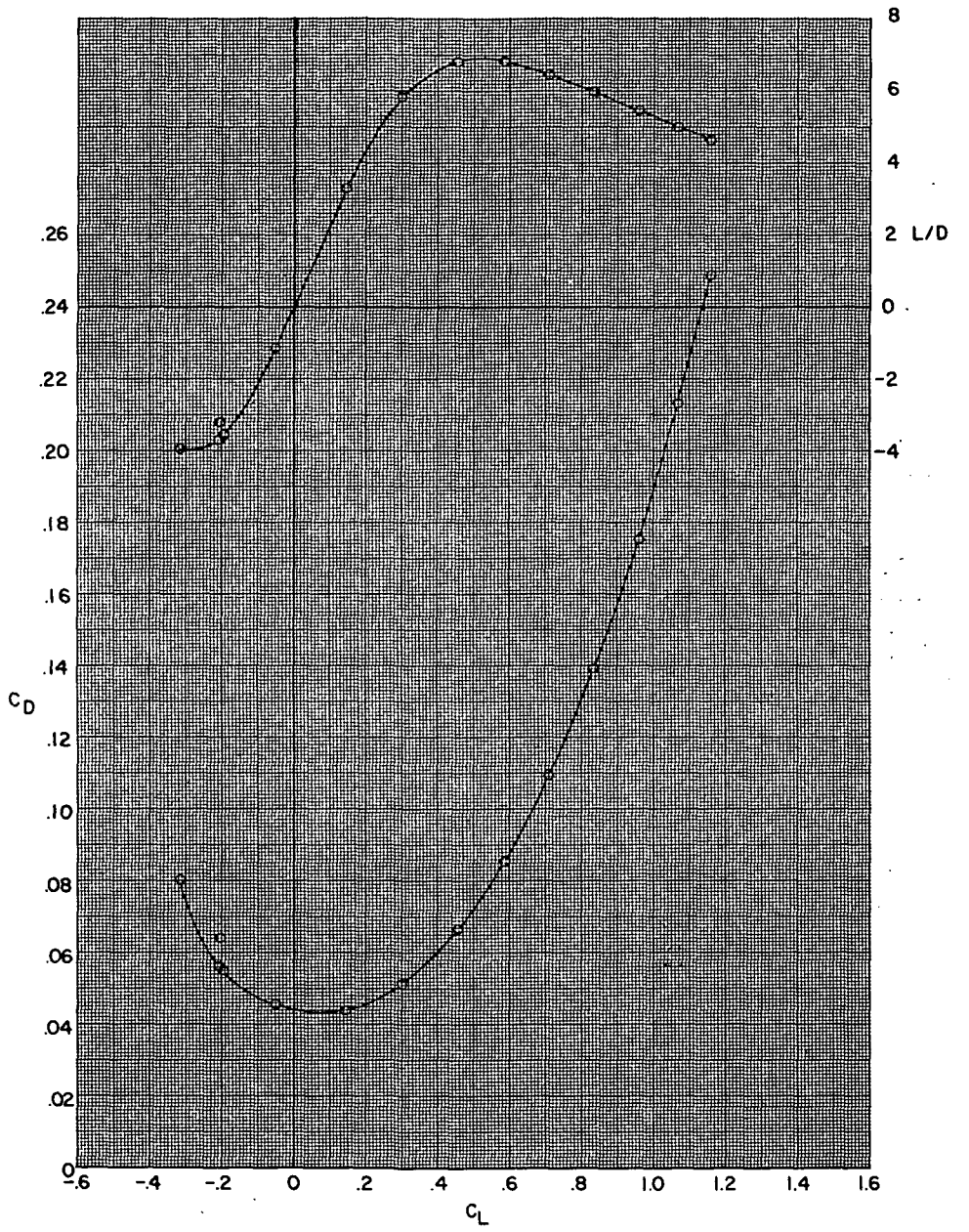

(d) Concluded.

Figure 10.- Concluded.

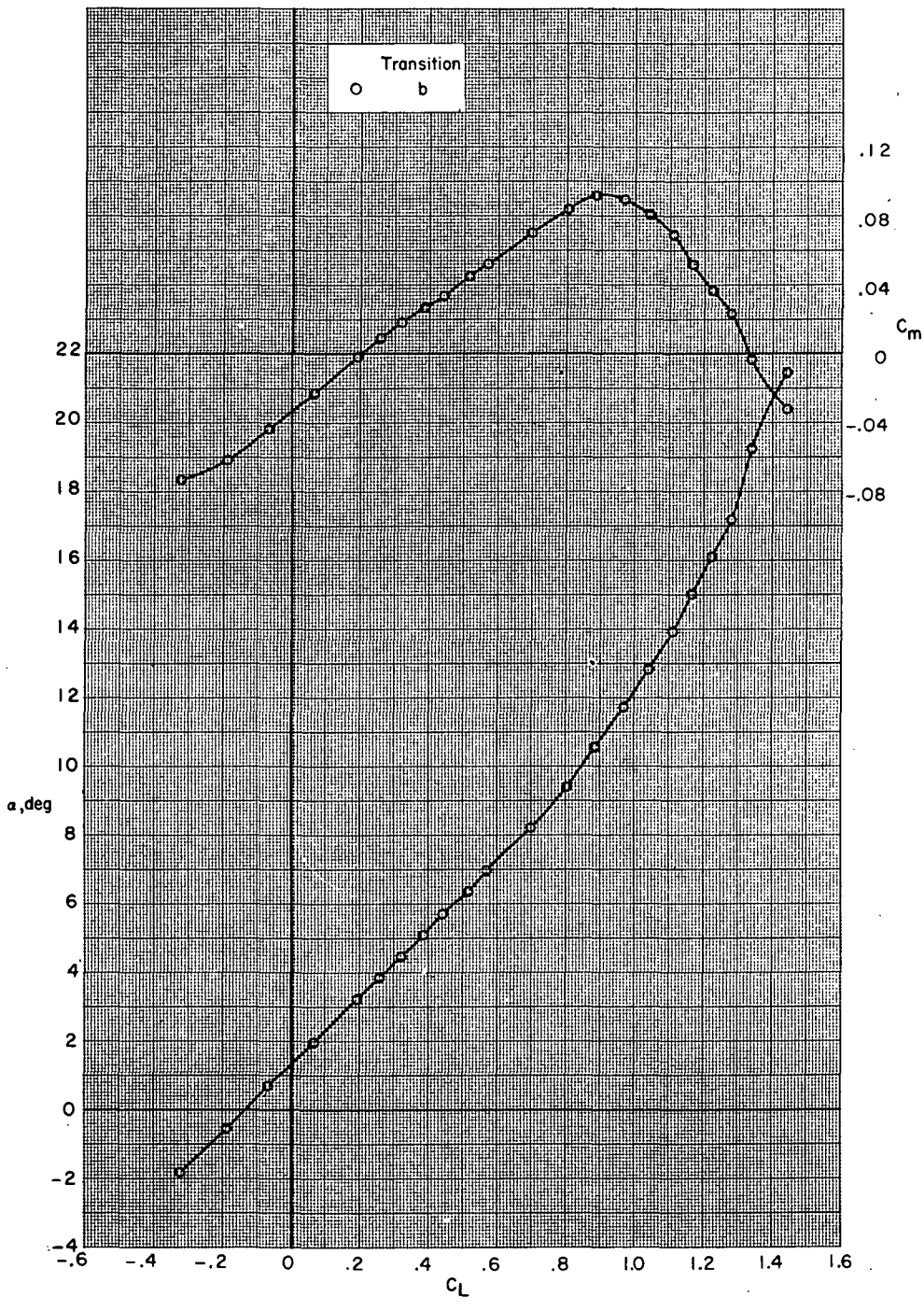

(a) M = 0.60.

Figure 11.- Aerodynamic characteristics for configuration $B_{80}G_{49}H_{13}I_{71}N_{32}^{b}V_{29}V_{38}W_{34e}X_{24}$ with wing swept 16.0°.

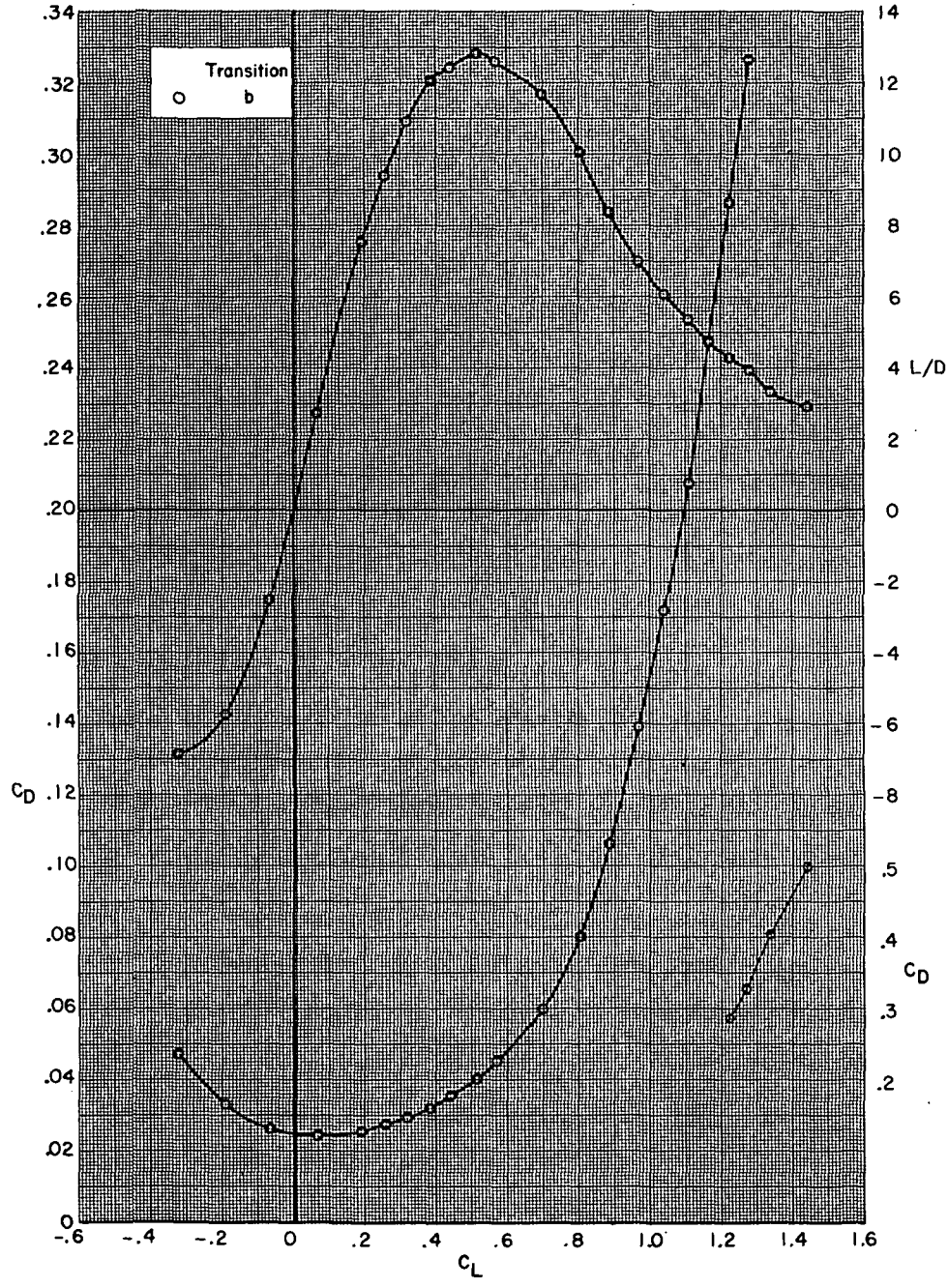

(a) Concluded.

Figure 11.- Continued.

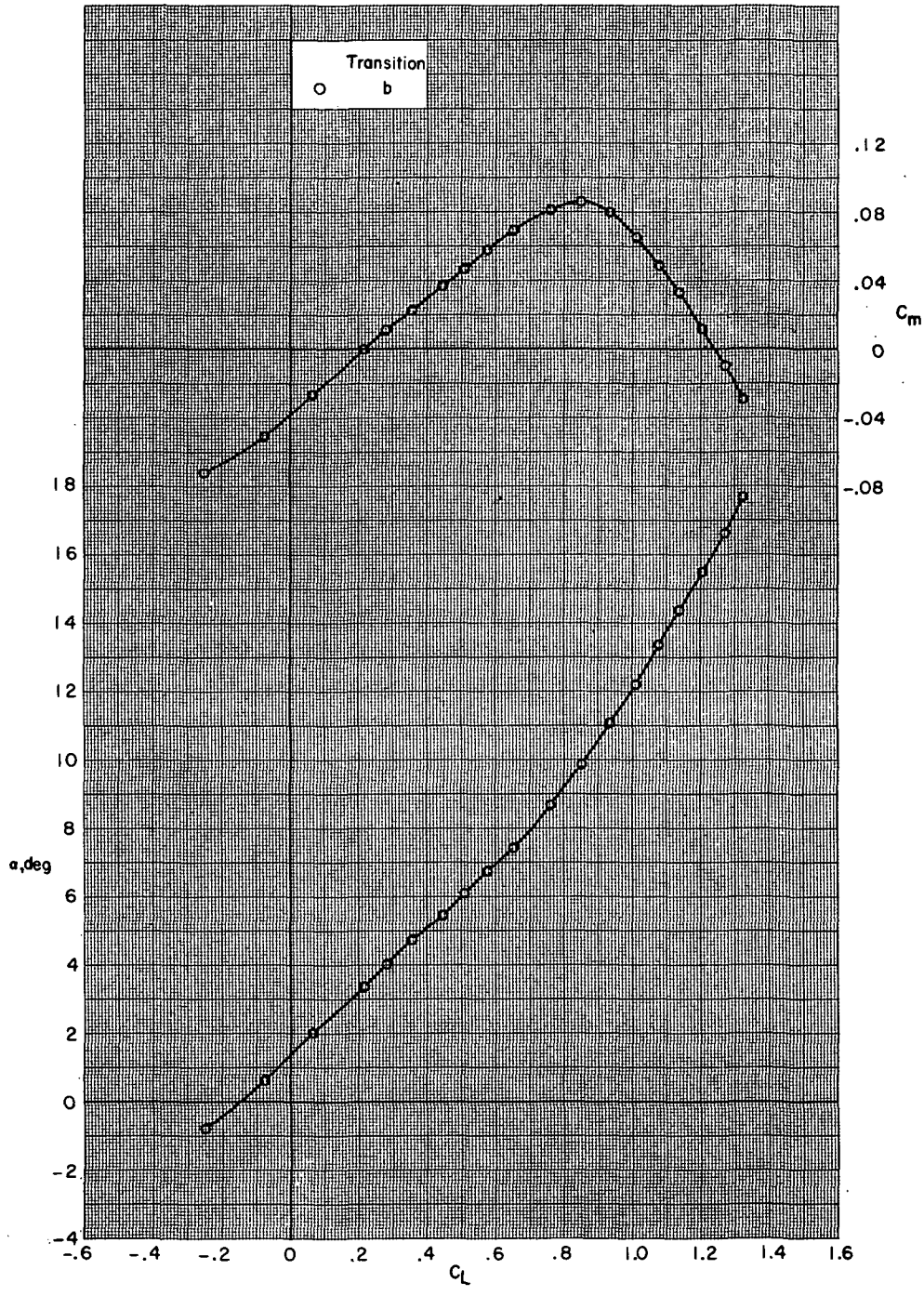

(b) M = 0.70.

Figure 11.- Continued.

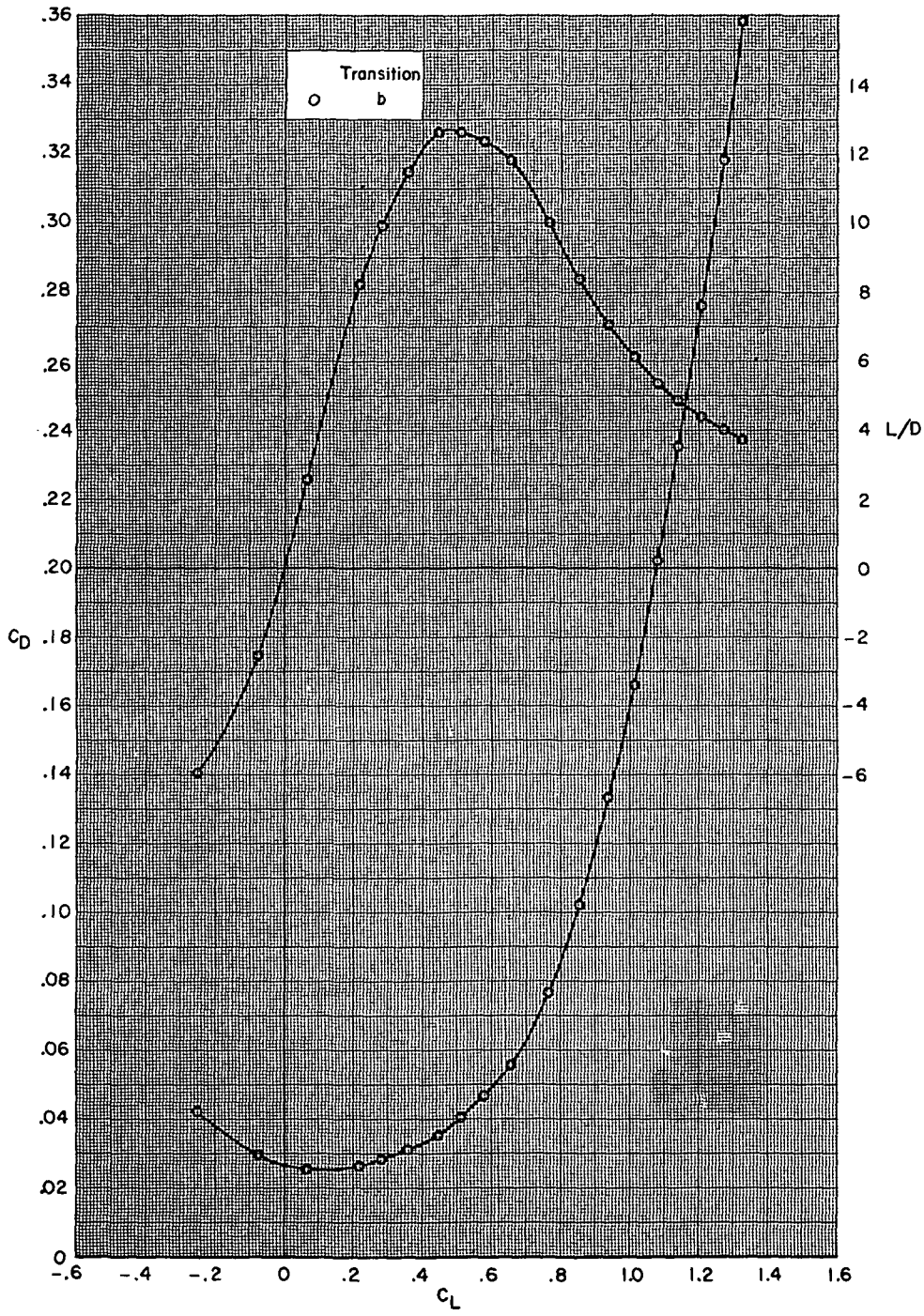

(b) Concluded.

Figure 11.- Continued.

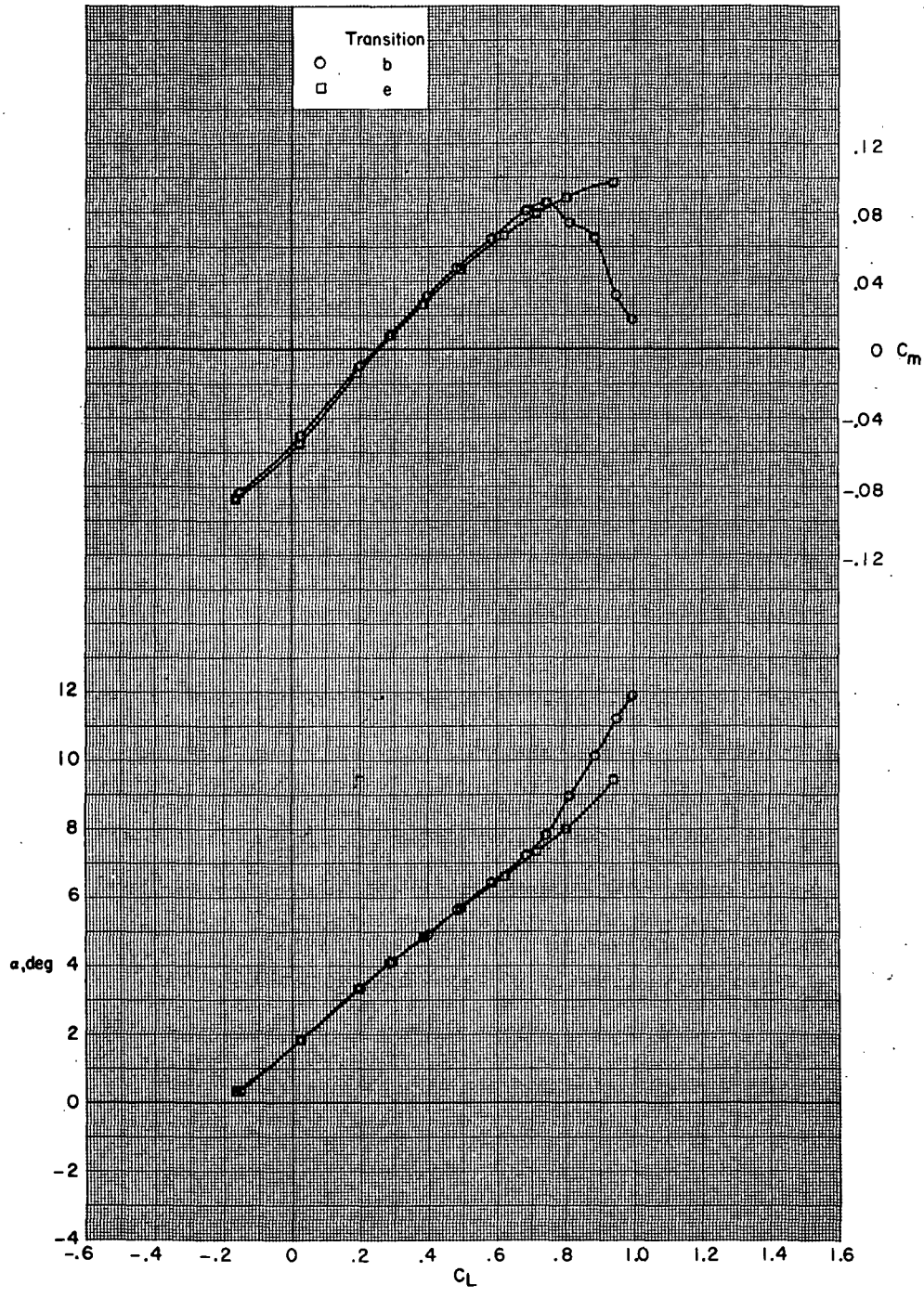

(c) M = 0.80.

Figure 11.- Continued.

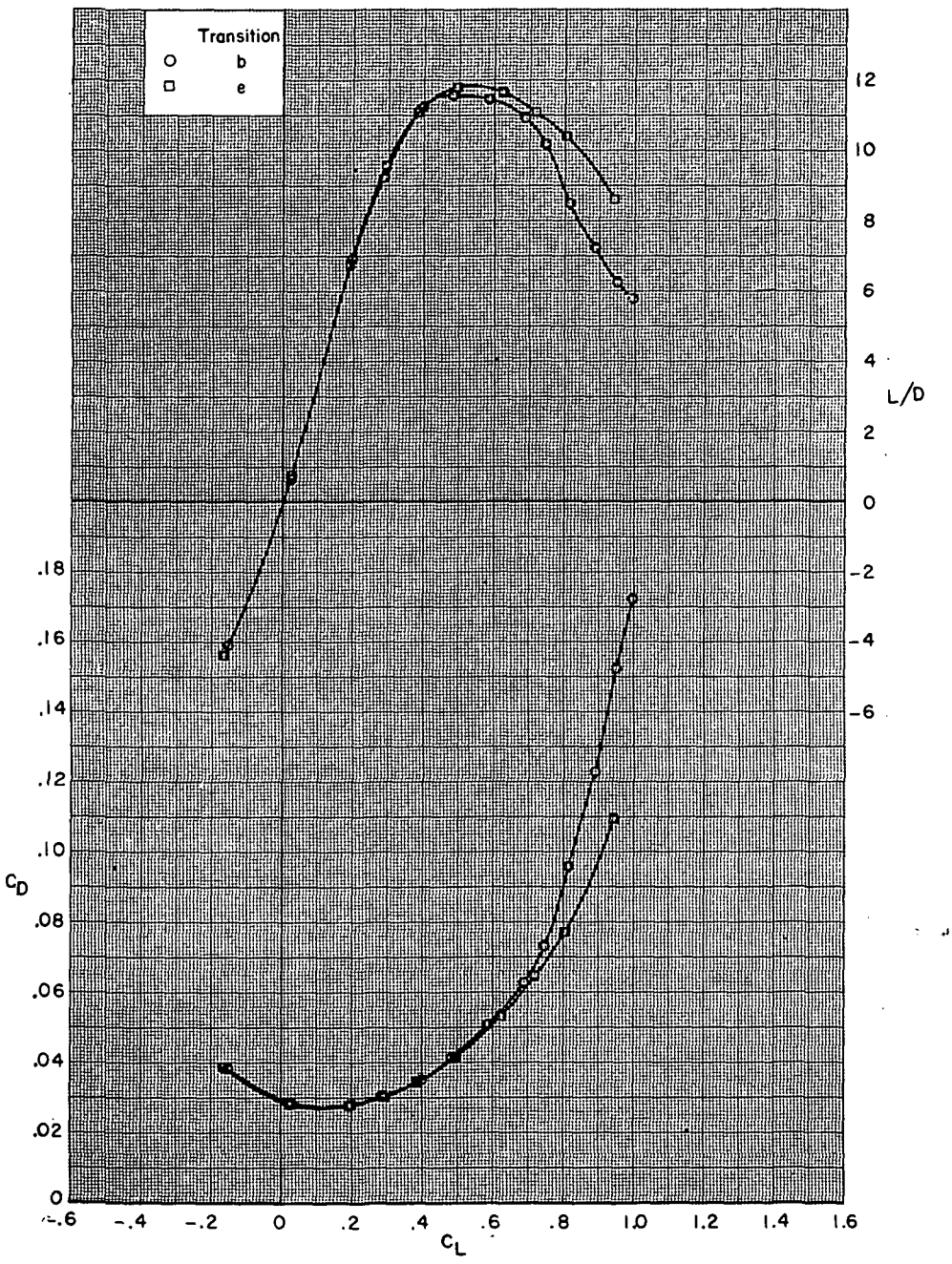

(c) Concluded.

Figure 11.- Continued.

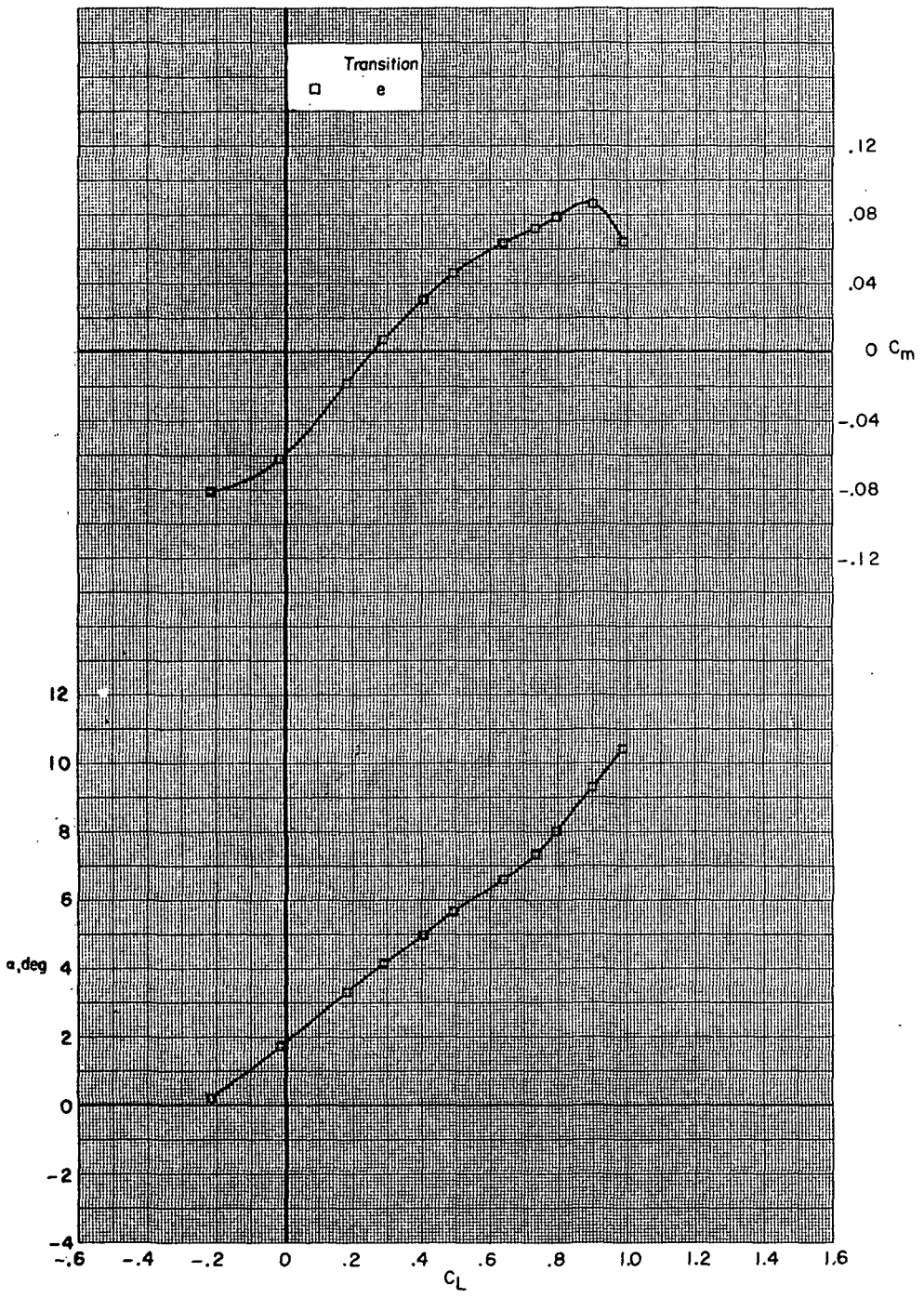

(d) M = 0.825.

Figure 11.- Continued.

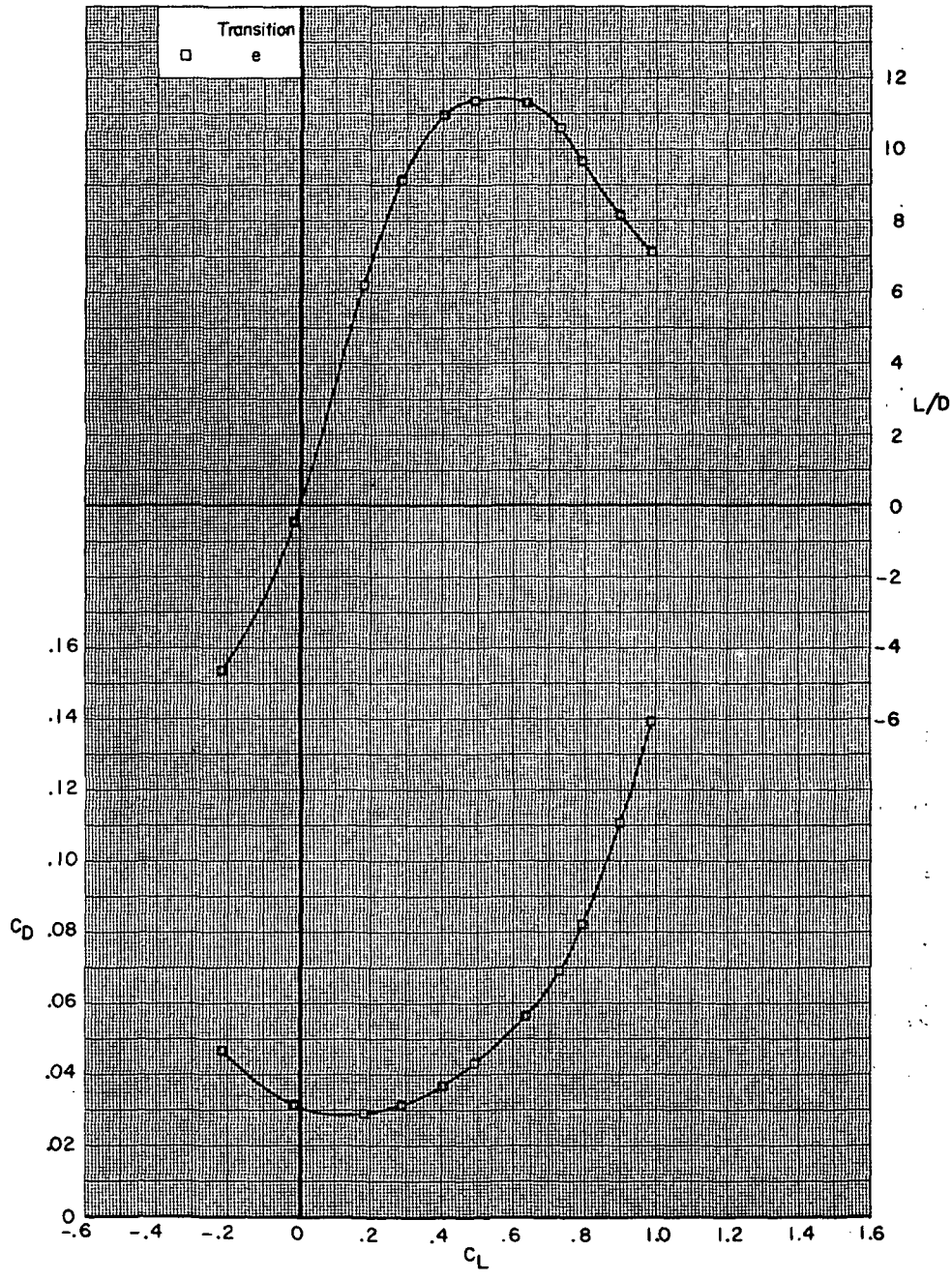

(d) Concluded.

Figure 11.- Continued.

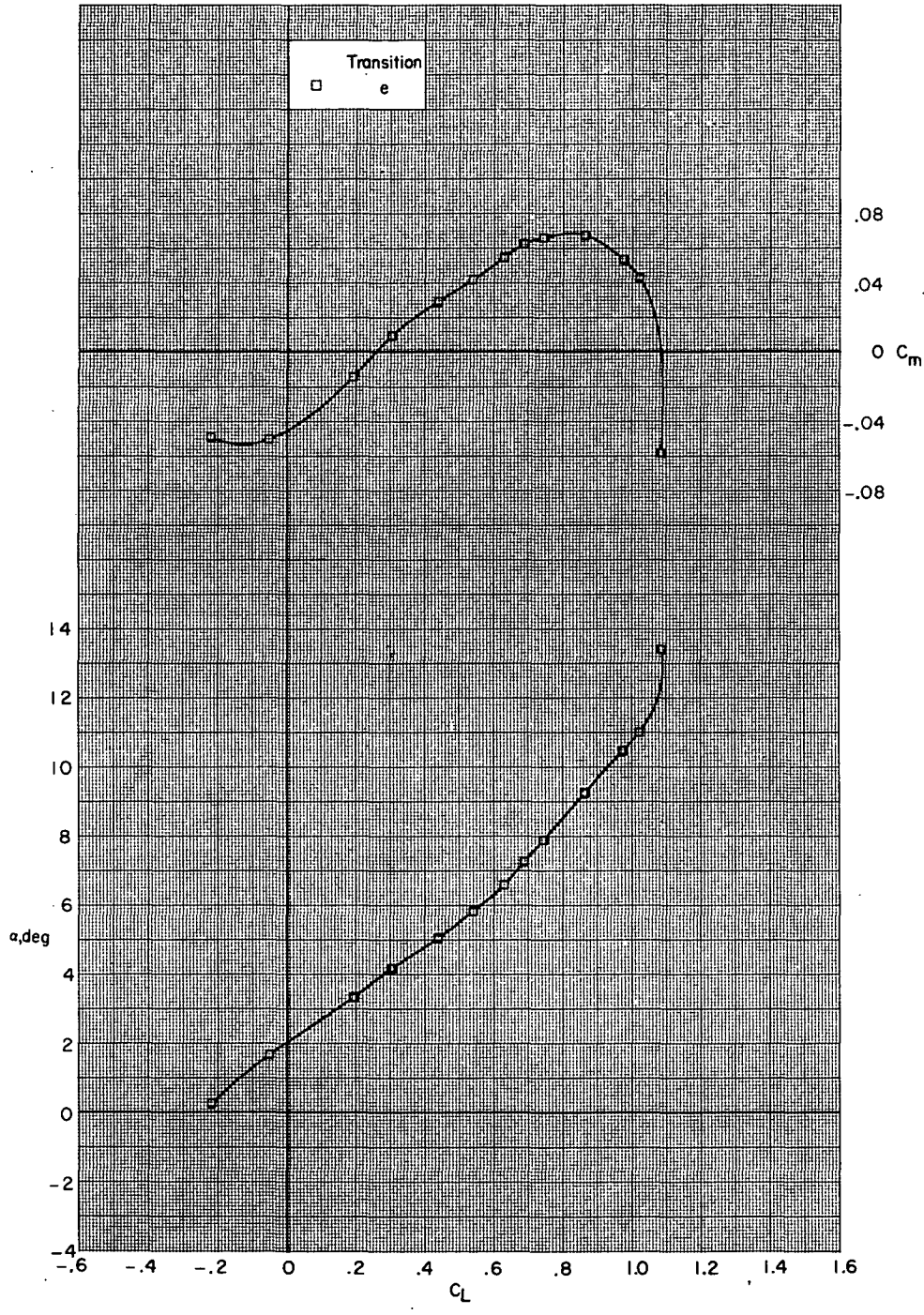

(e) M = 0.85.

Figure 11.- Continued.

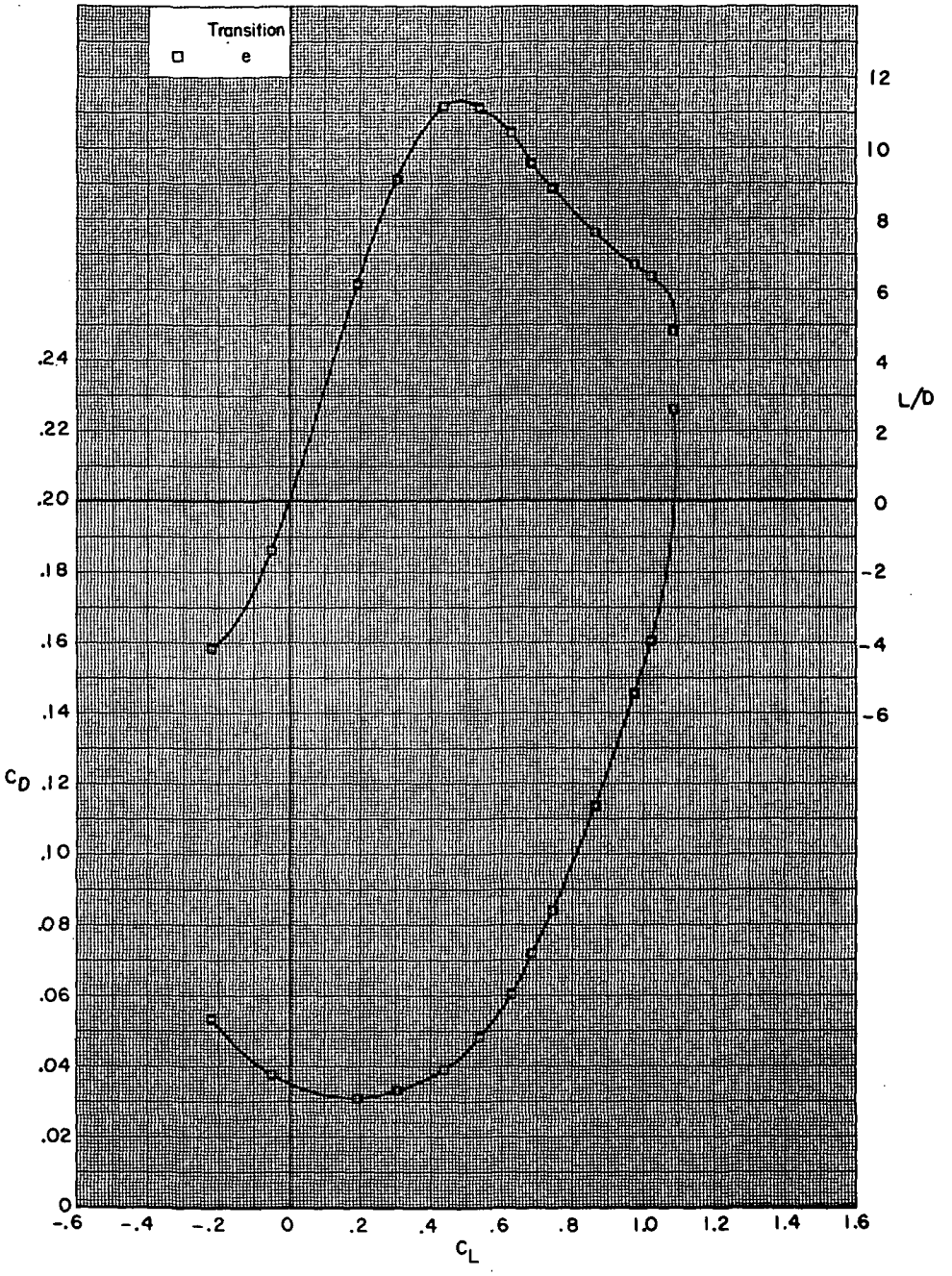

(e) Concluded.

Figure 11.- Concluded.

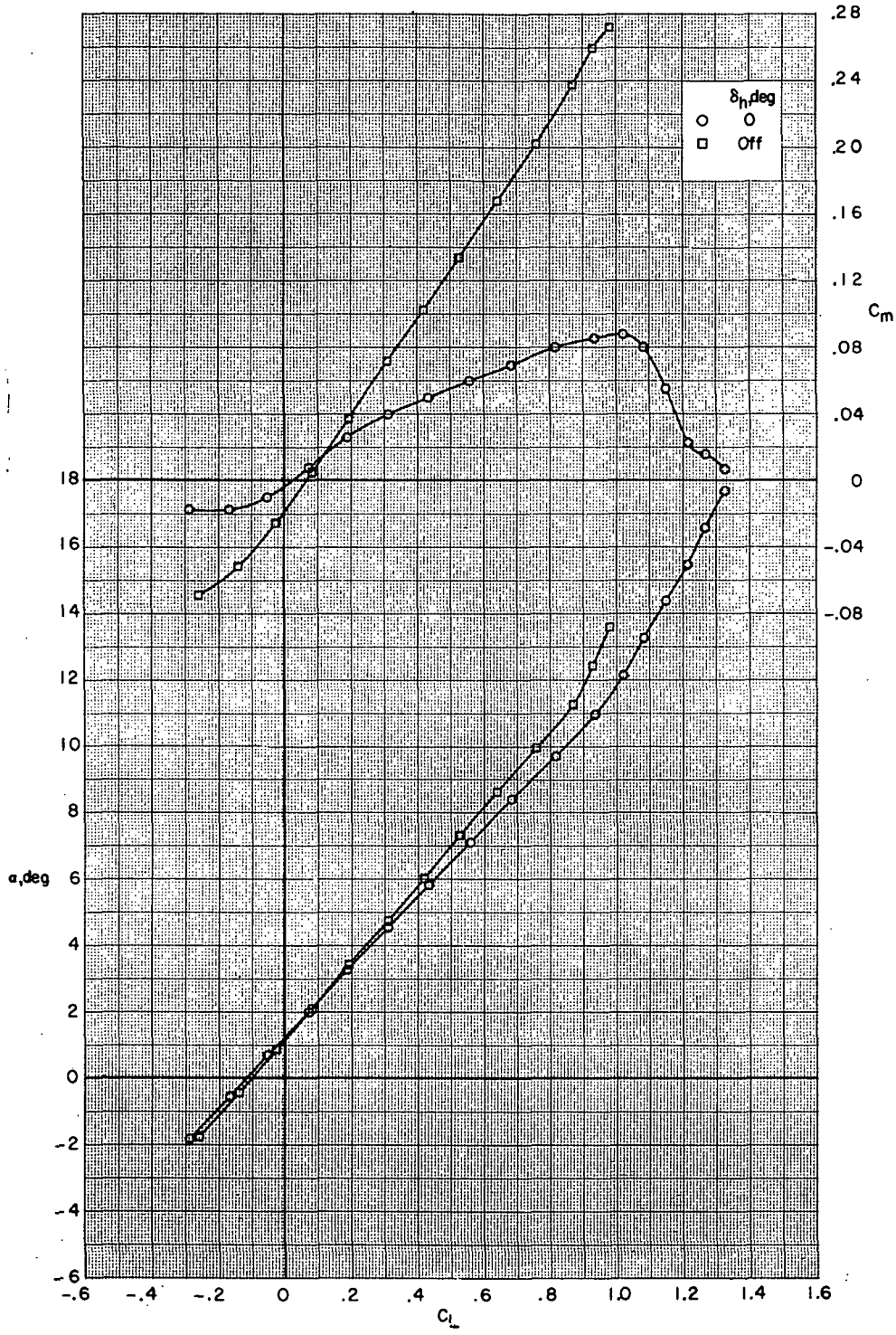

(a) M = 0.70.

Figure 12.- Aerodynamic characteristics for configuration $B_{80}G_{43}H_{13}I_{71}N^{b}_{32}V_{29}V_{38}W_{31}X_{24}X_{168}$ with wing swept 26.0°.

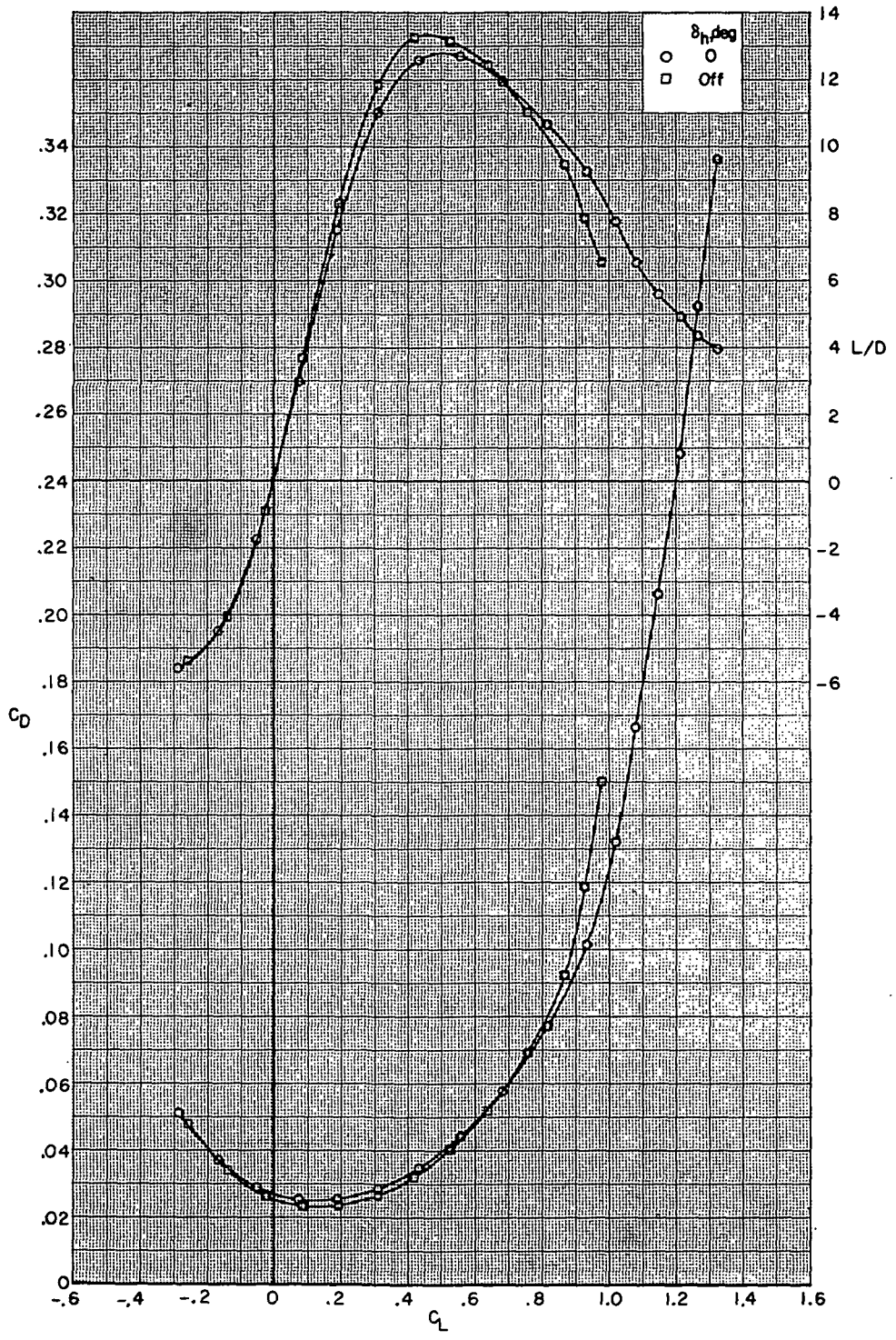

(a) Concluded.

Figure 12.- Continued.

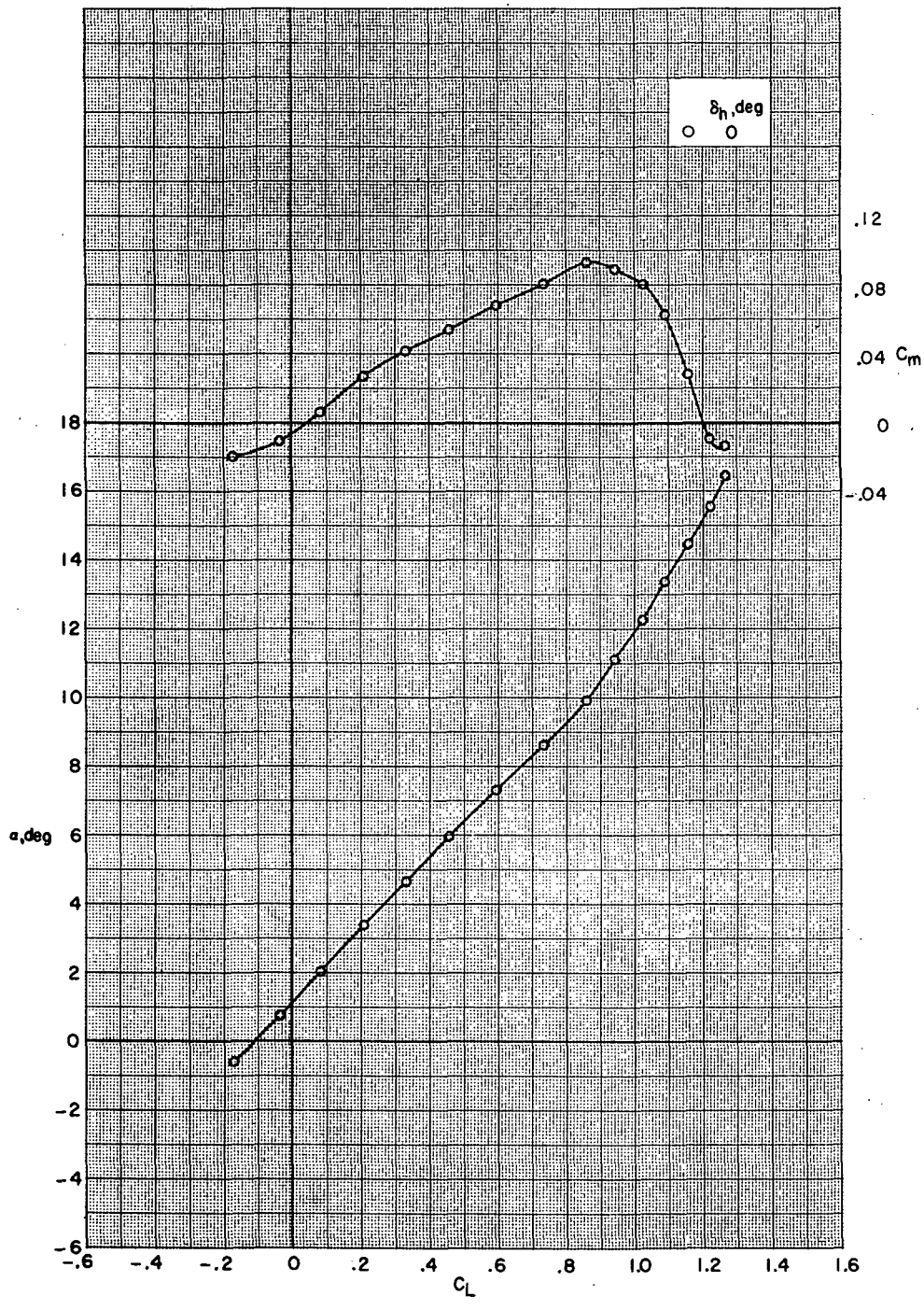

(b) M = 0.75.

Figure 12.- Continued.

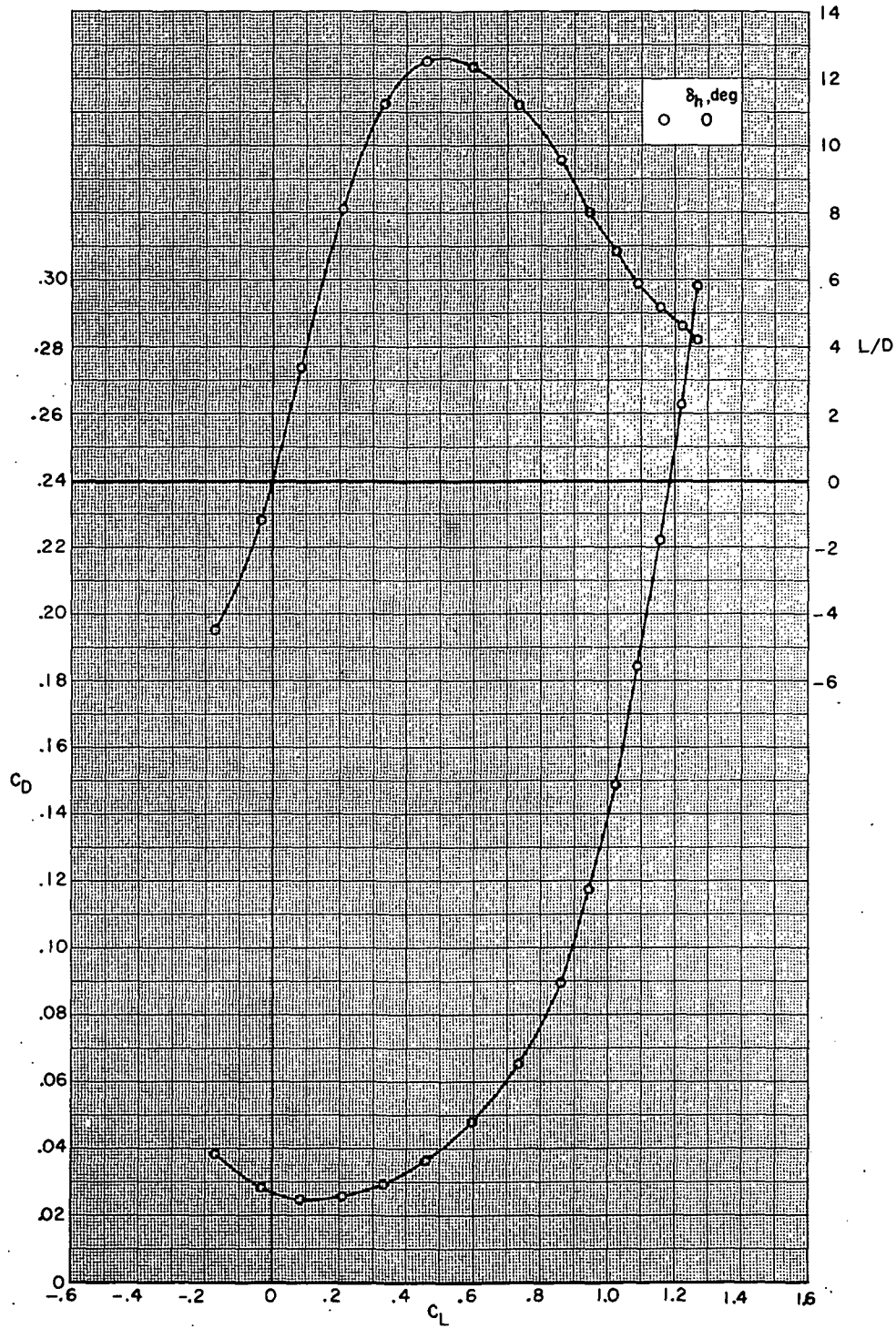

(b) Concluded.

Figure 12.- Continued.

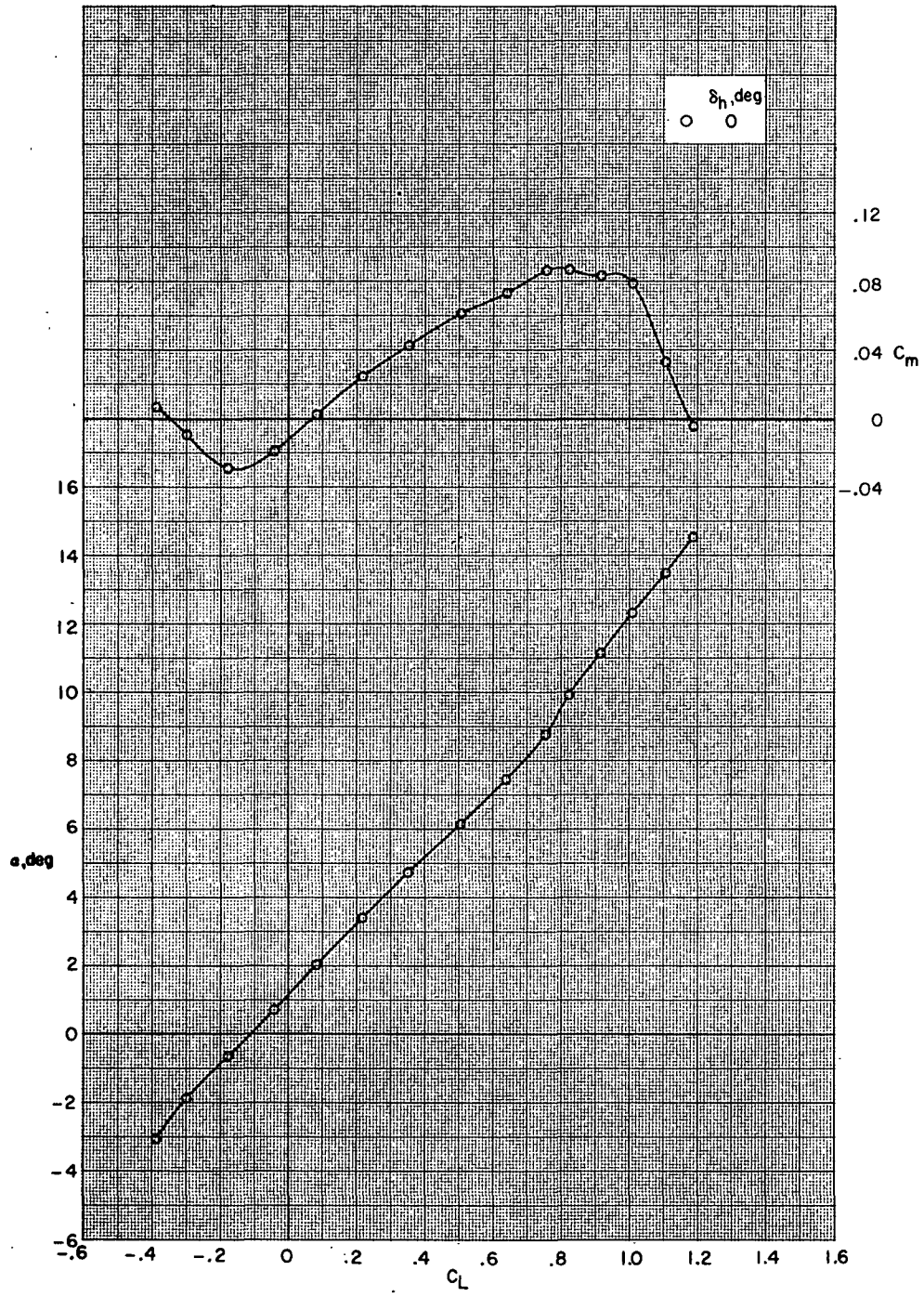

(c) M = 0.80.

Figure 12.- Continued.

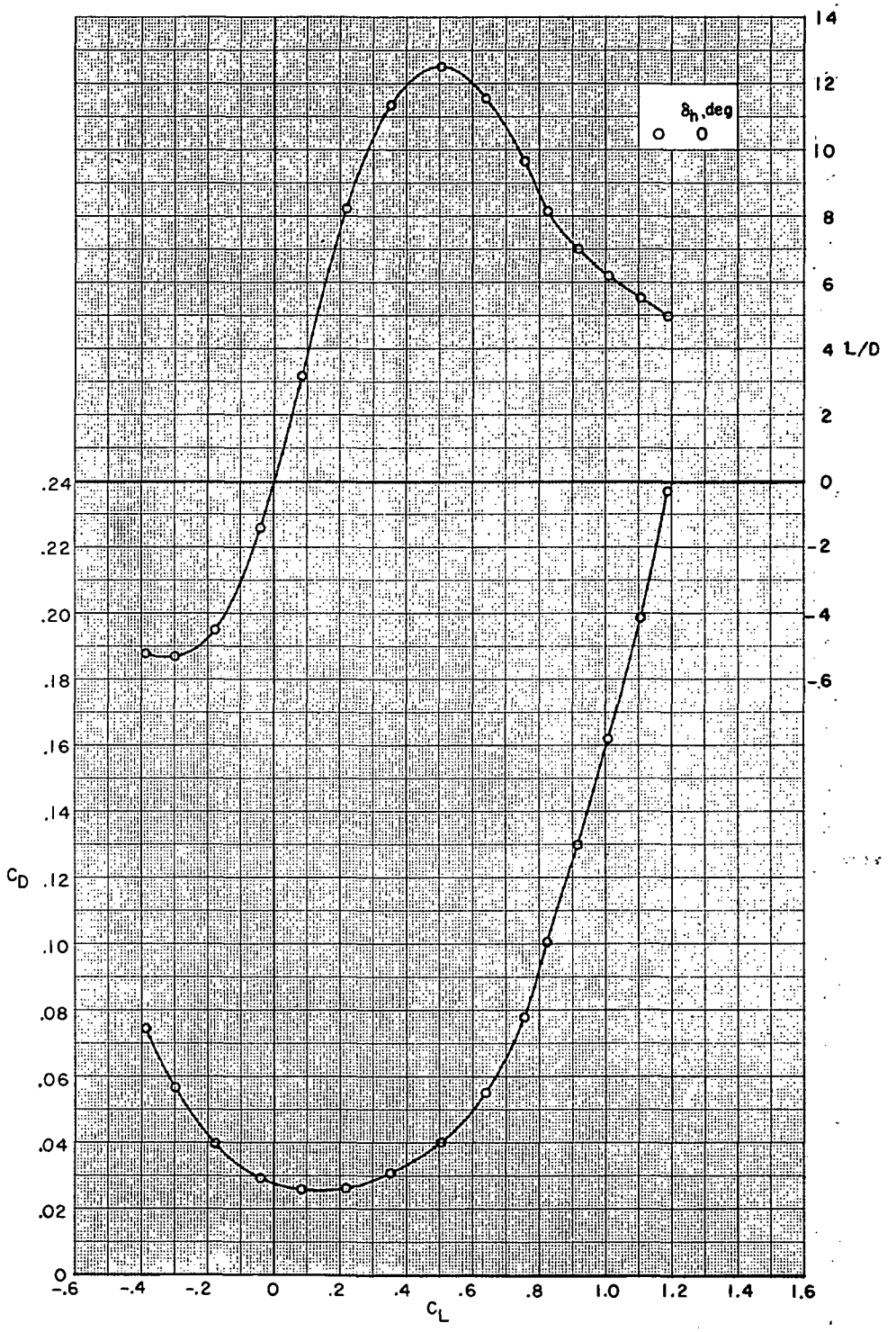

(c) Concluded.

Figure 12.- Continued.

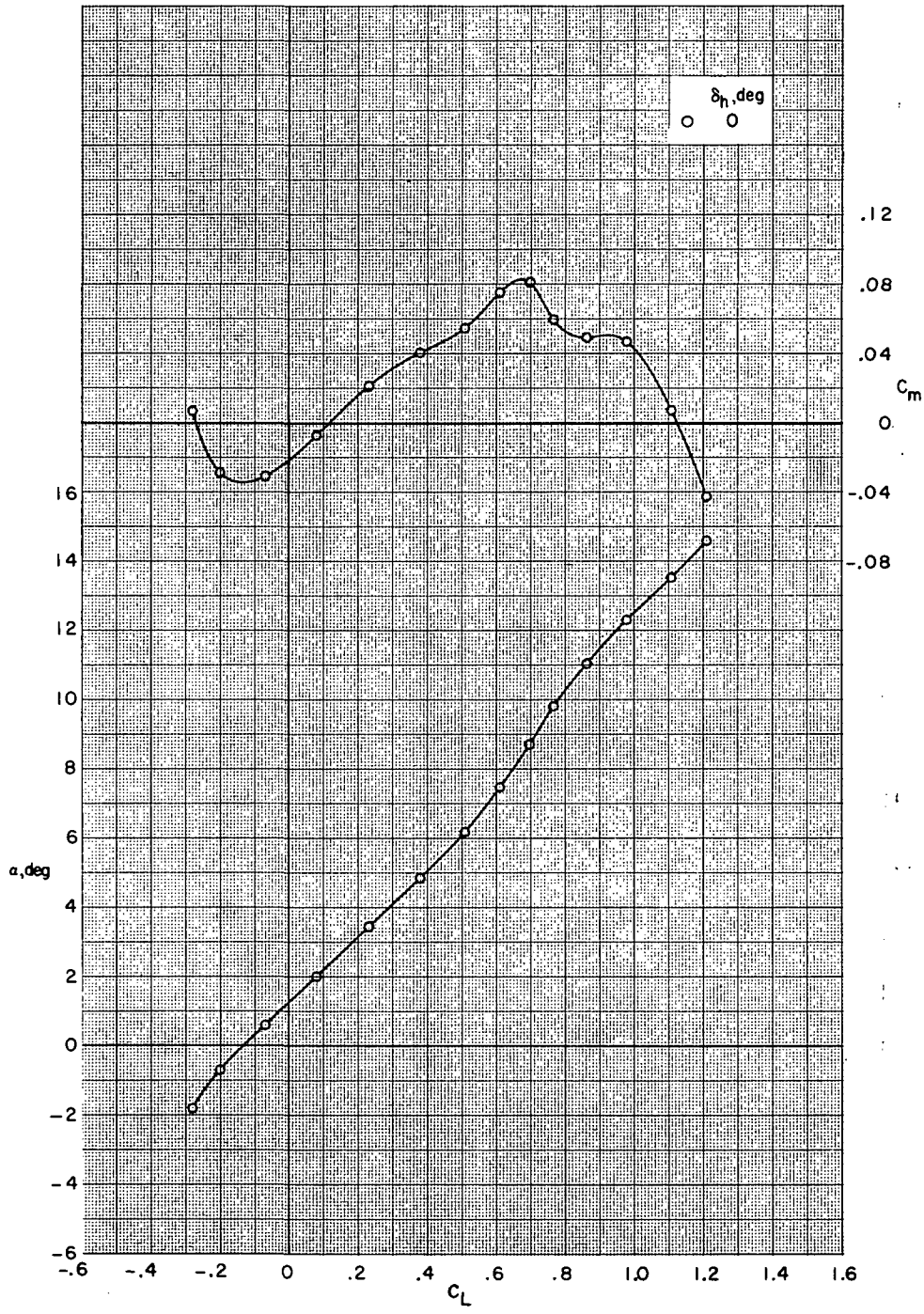

(d) M = 0.85.

Figure 12.- Continued.

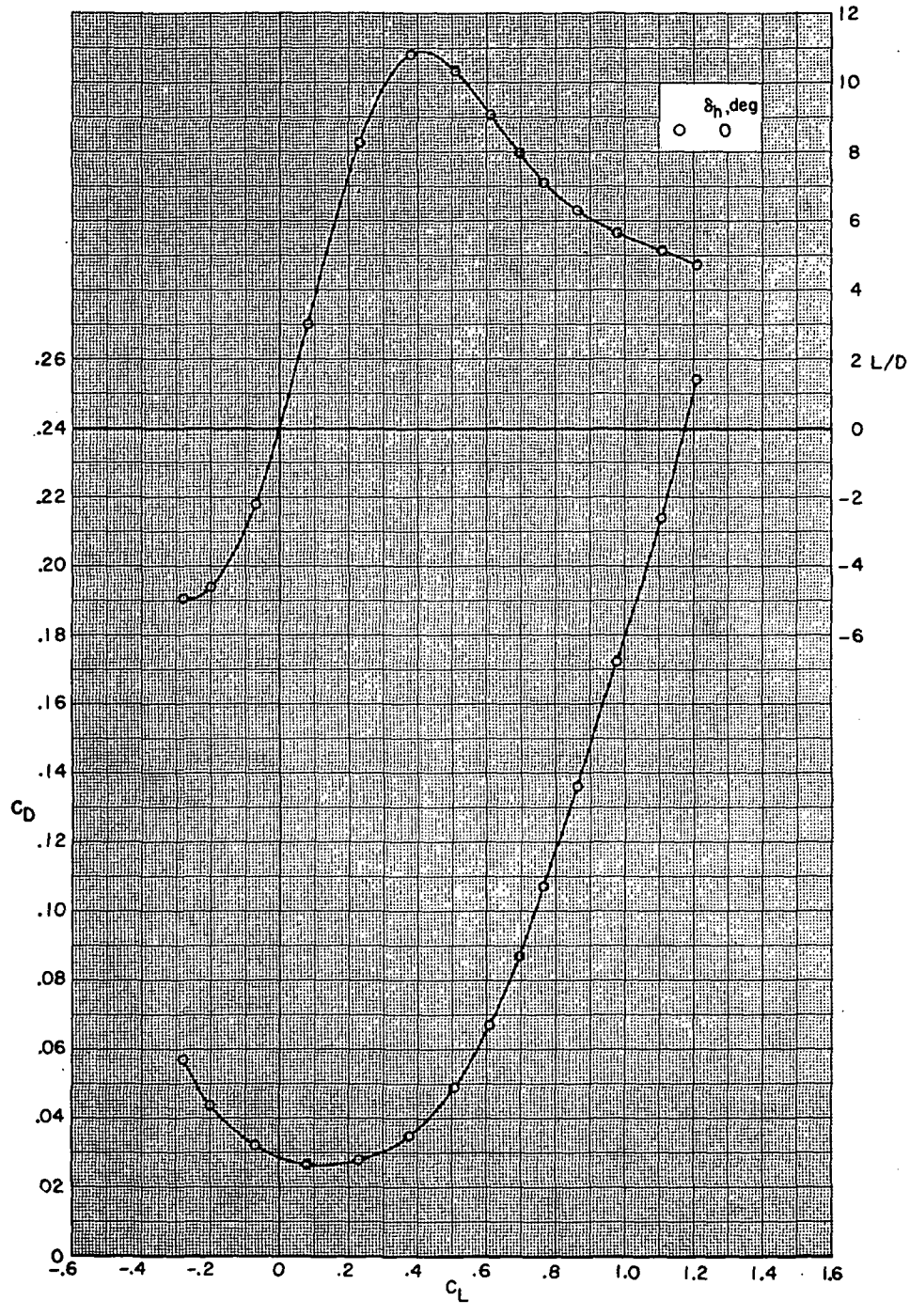

(d) Concluded.

Figure 12.- Continued.

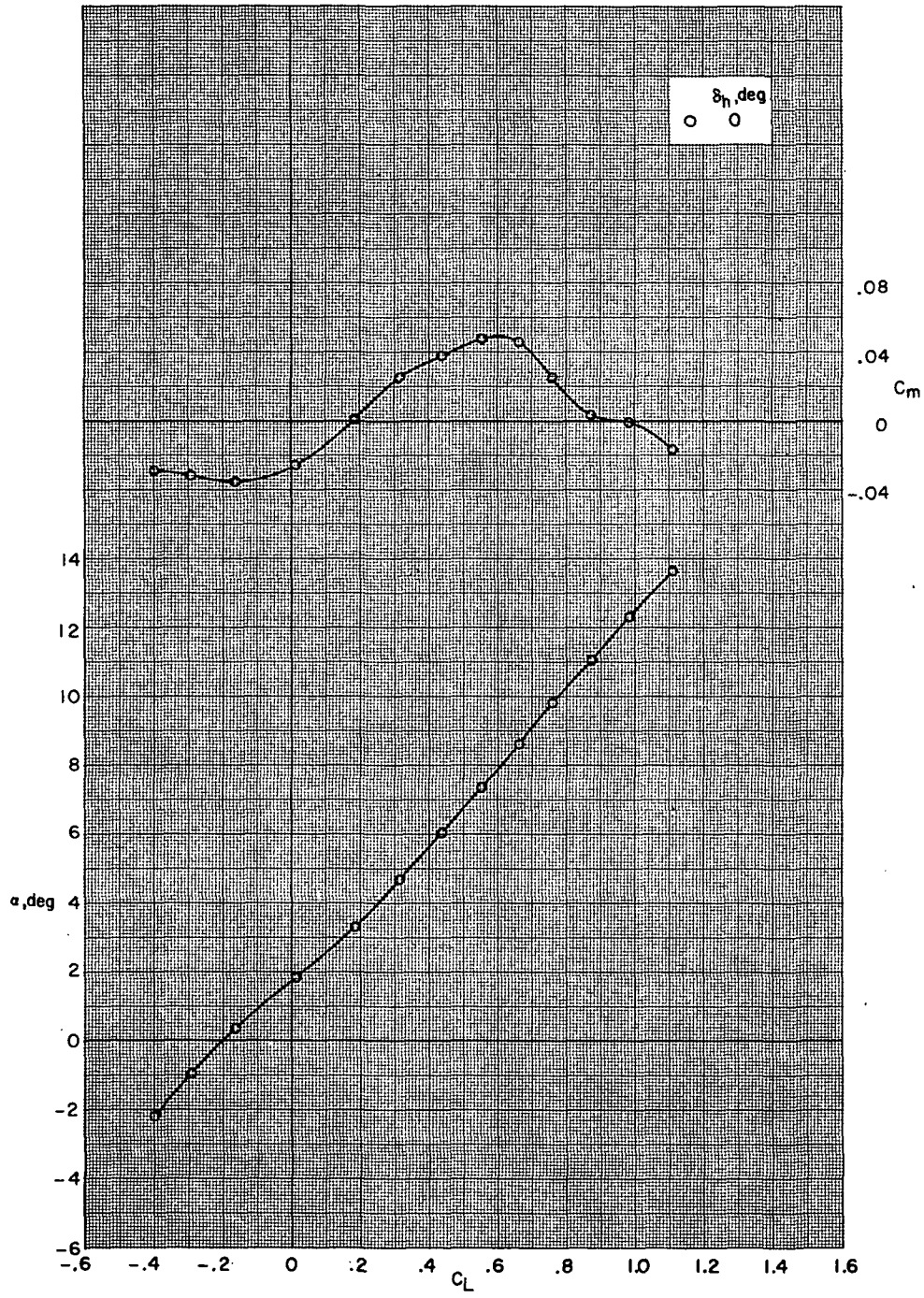

(e) M = 0.90.

Figure 12.- Continued.

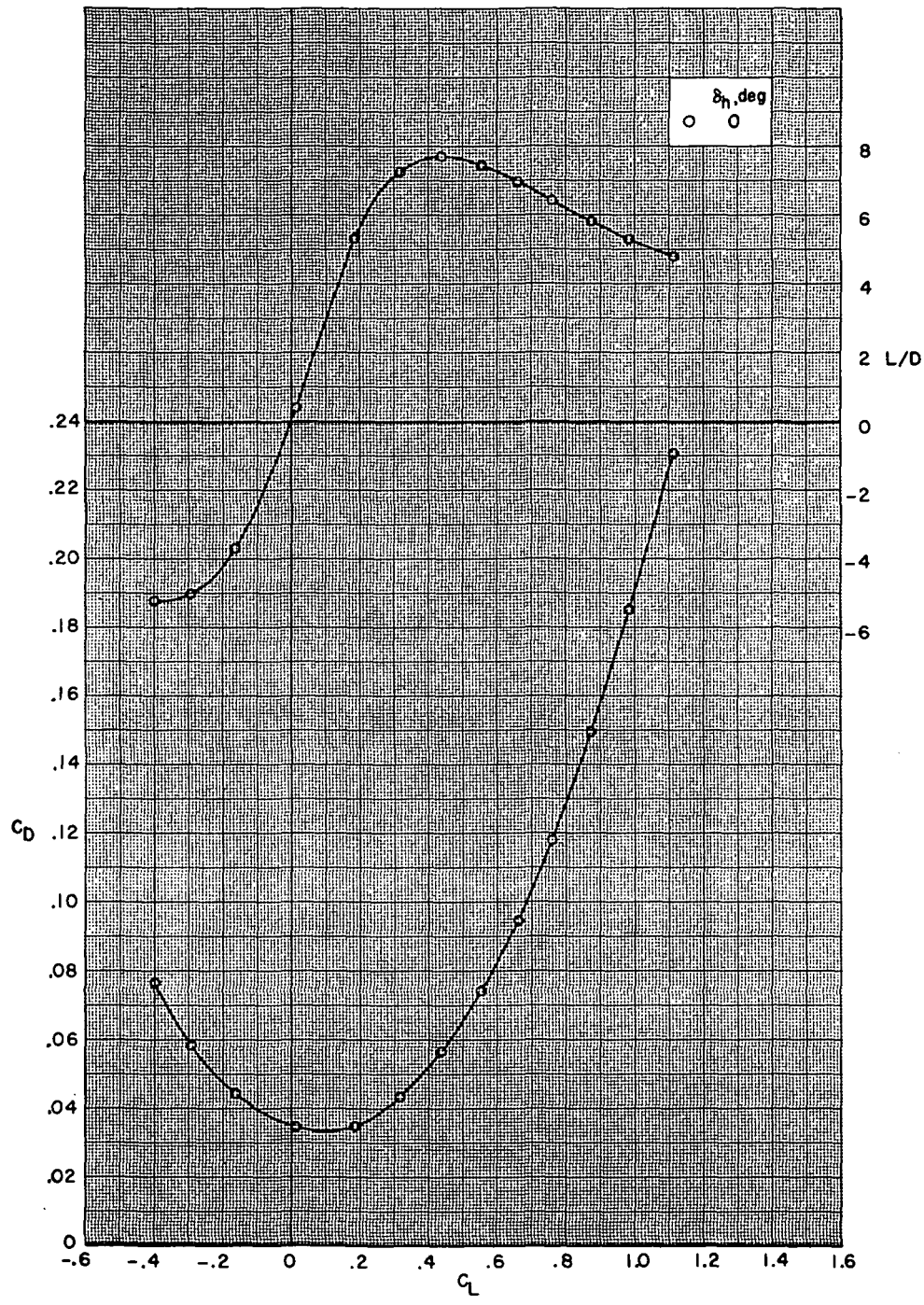

(e) Concluded.

Figure 12.- Concluded.

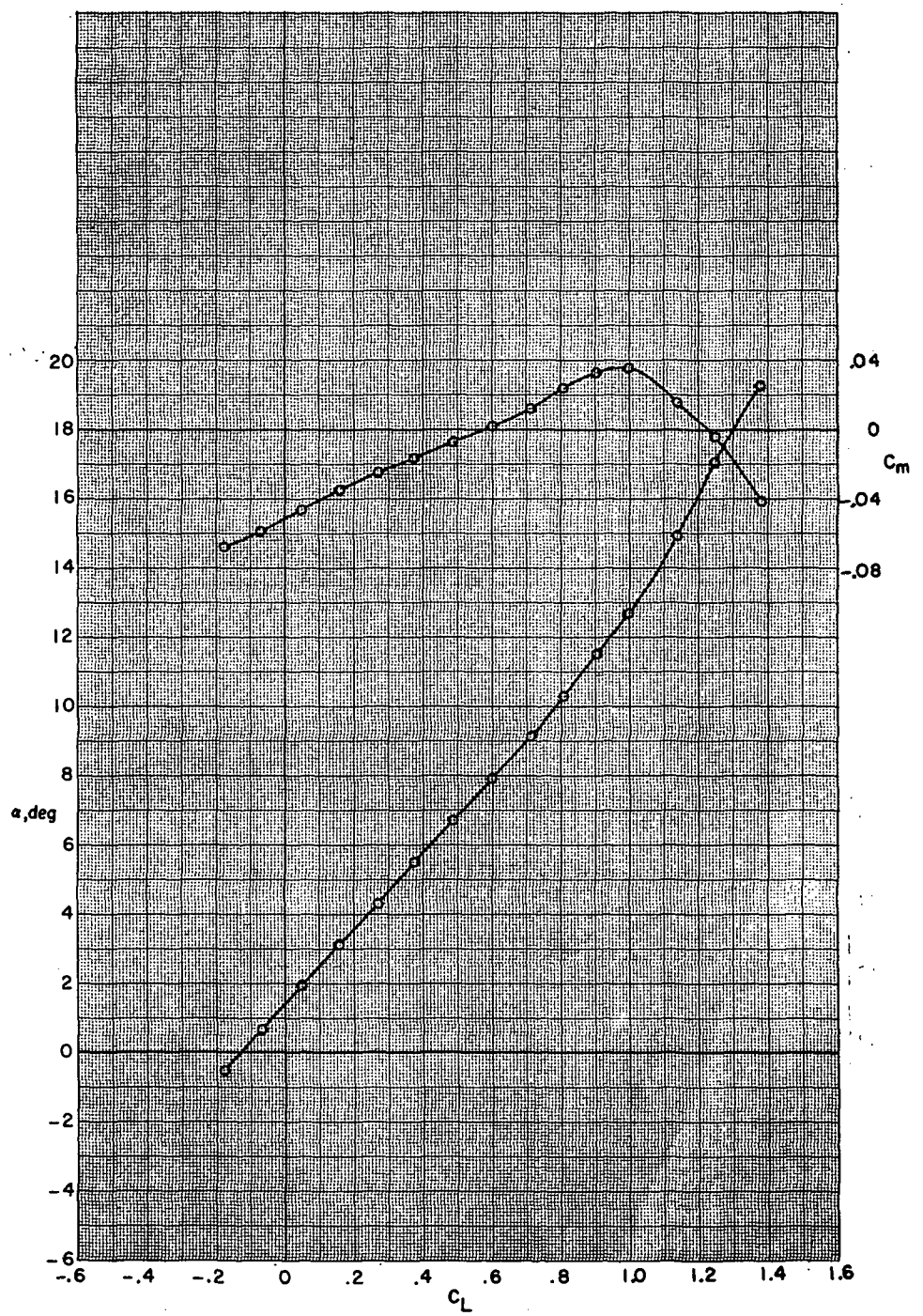

(a) M = 0.60.

Figure 13.- Aerodynamic characteristics for configuration $B_{80}G_{47}H_{13}I_{71}N_{32}^{b}V_{29}V_{38}W_{32}X_{24}X_{168}$ with wing swept 26.0°.

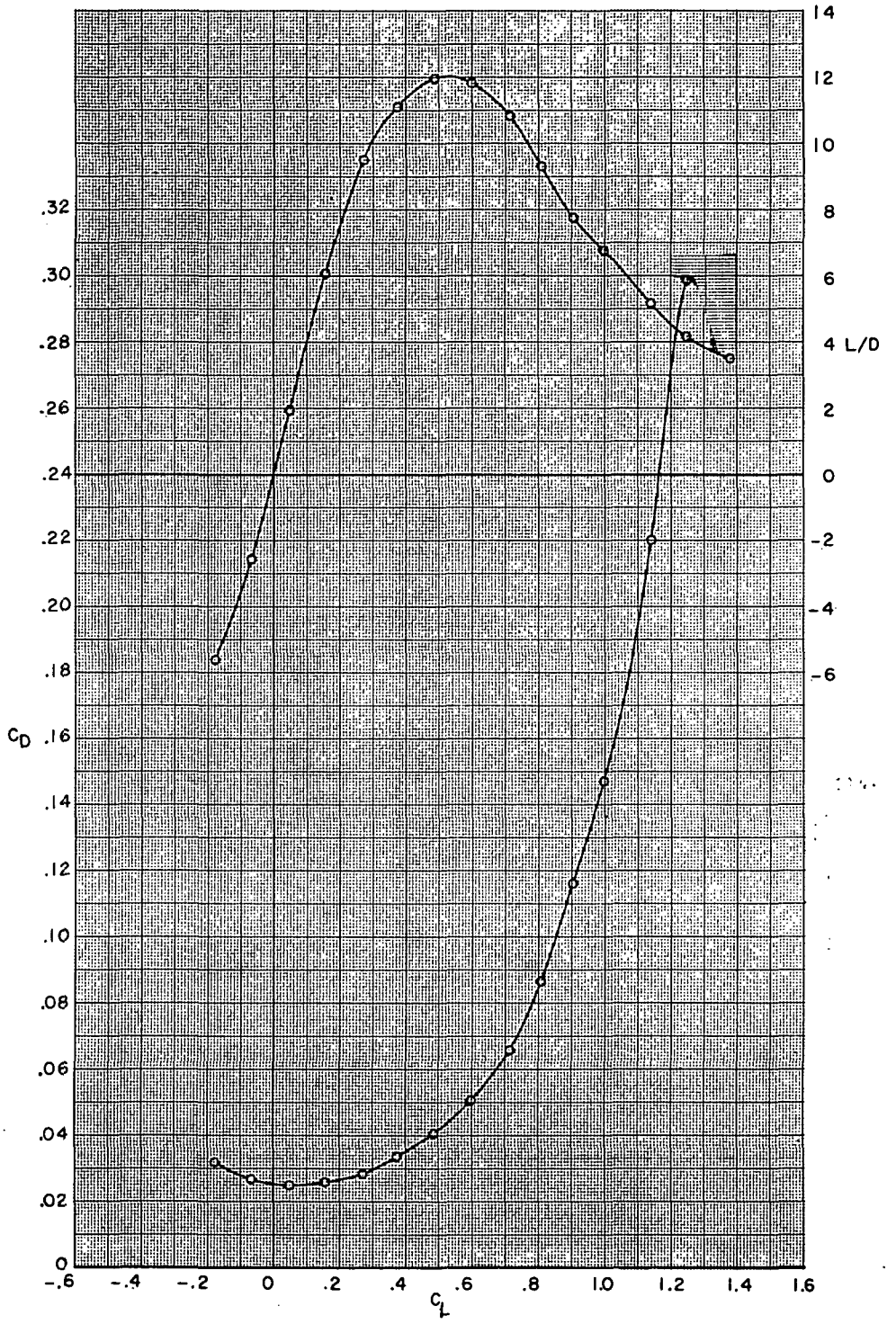

(a) Concluded.

Figure 13.- Continued.

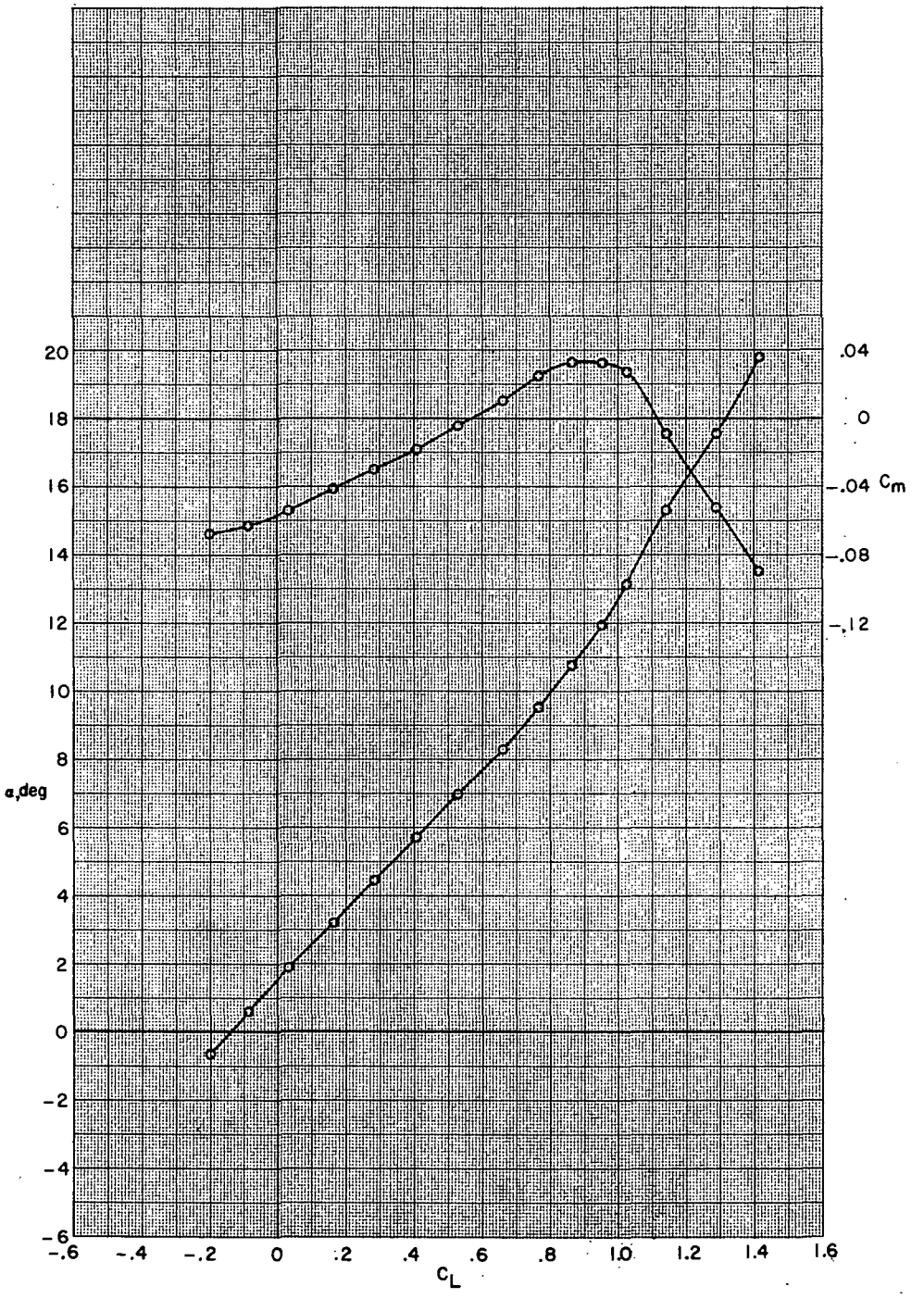

(b) M = 0.70.

Figure 13.- Continued.

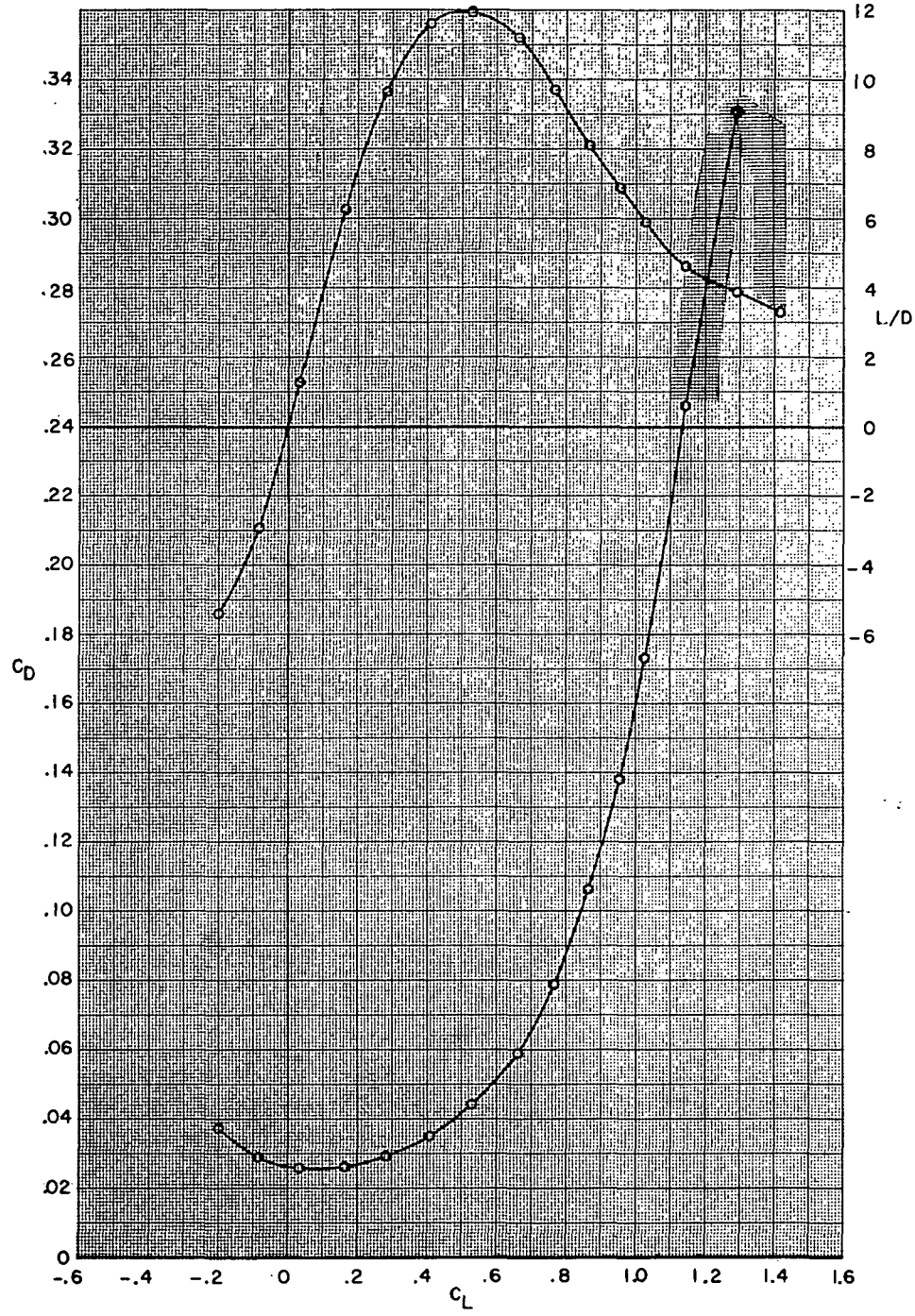

(b) Concluded.

Figure 13.- Continued.

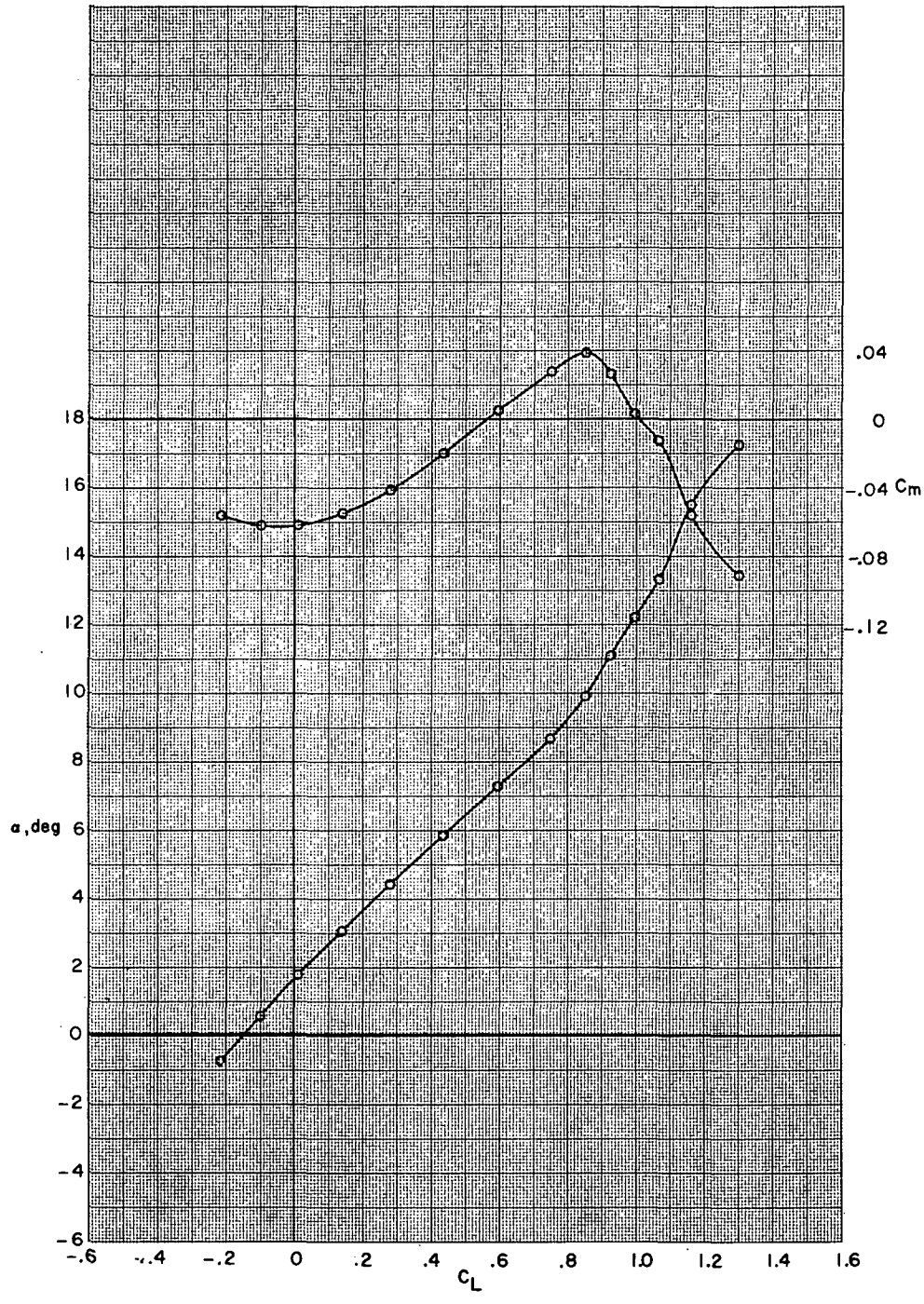

(c) M = 0.80.

Figure 13.- Continued.

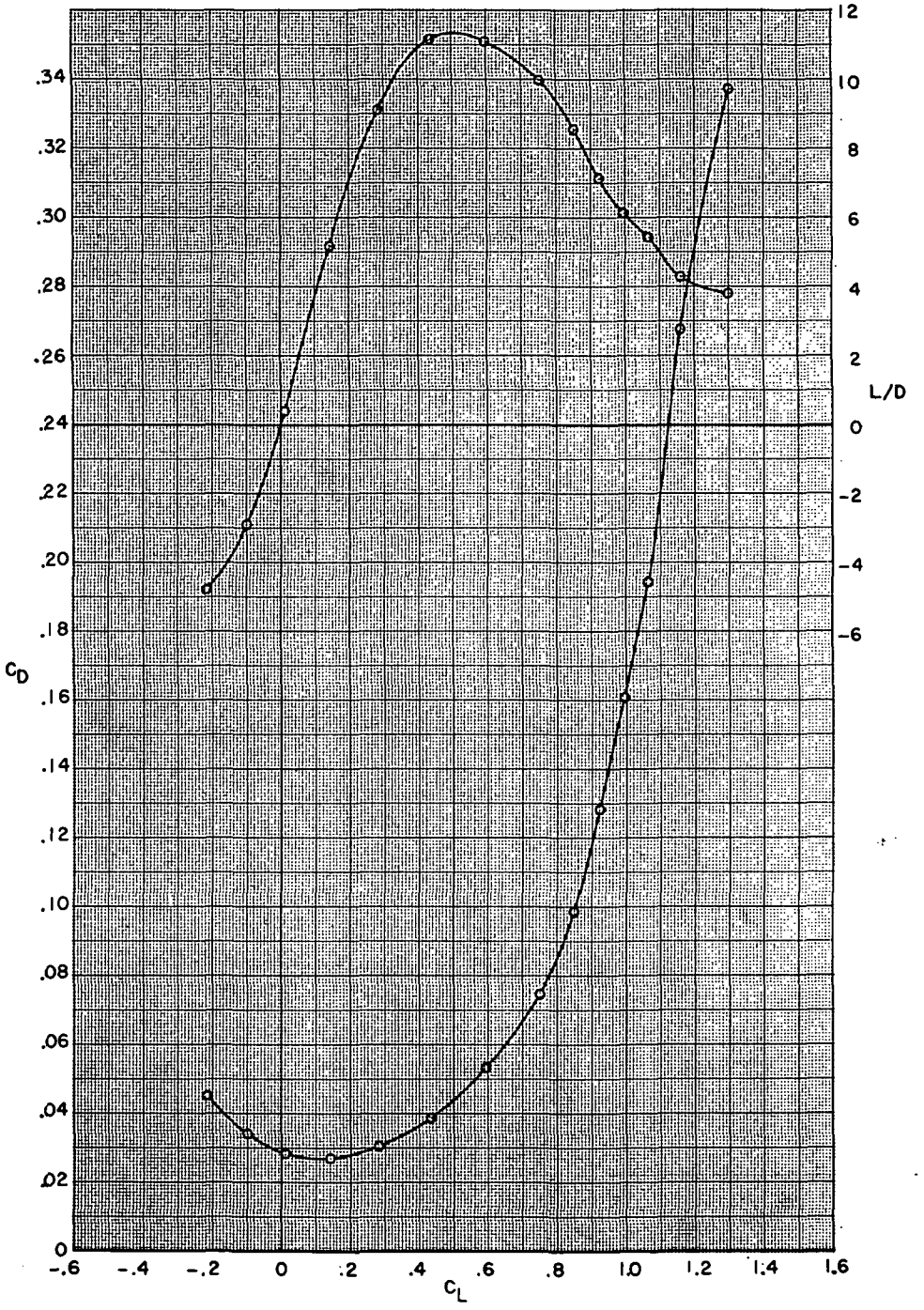

(c) Concluded.

Figure 13.- Continued.

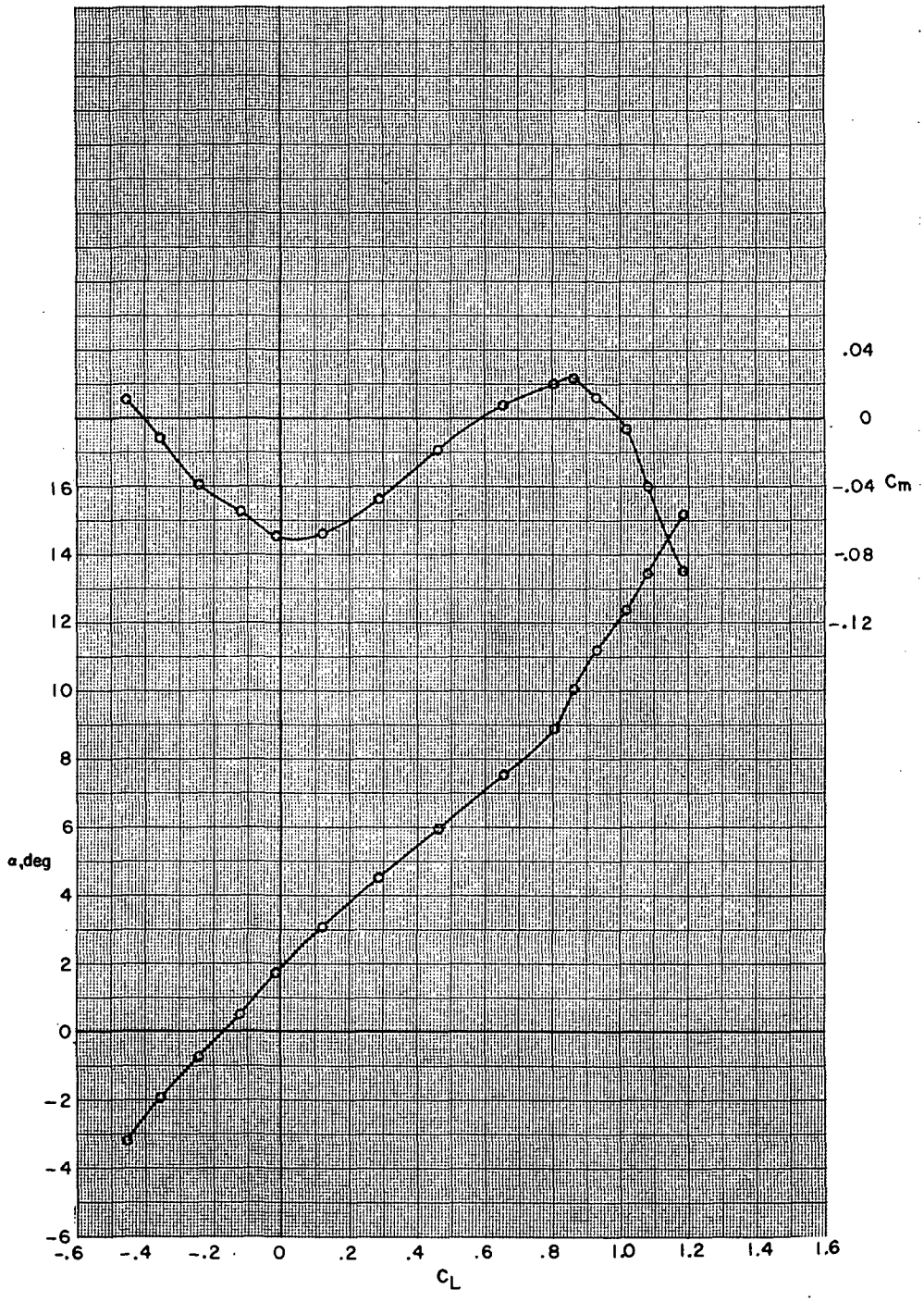

(d) M = 0.85.

Figure 13.- Continued.

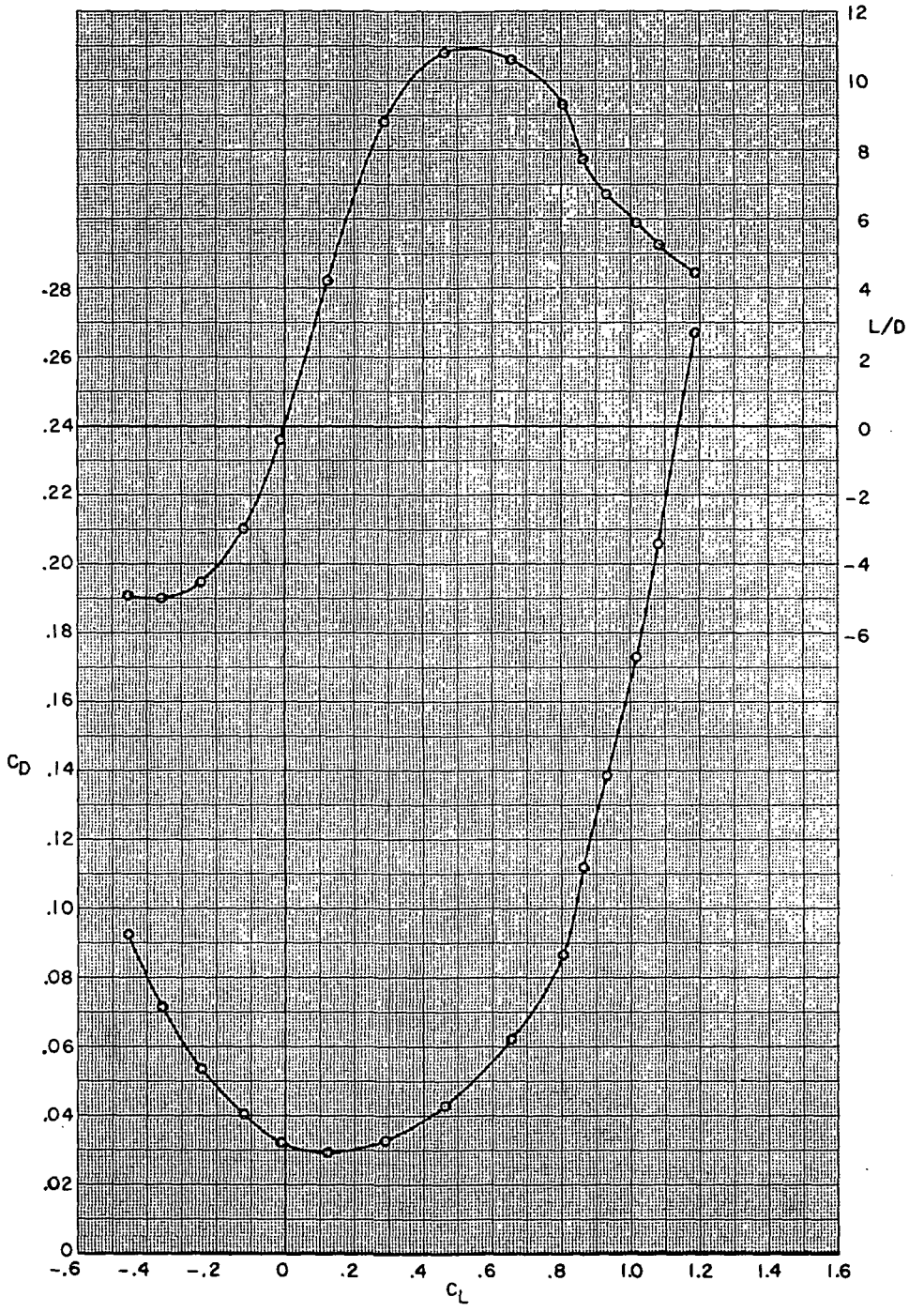

(d) Concluded.

Figure 13.- Continued.

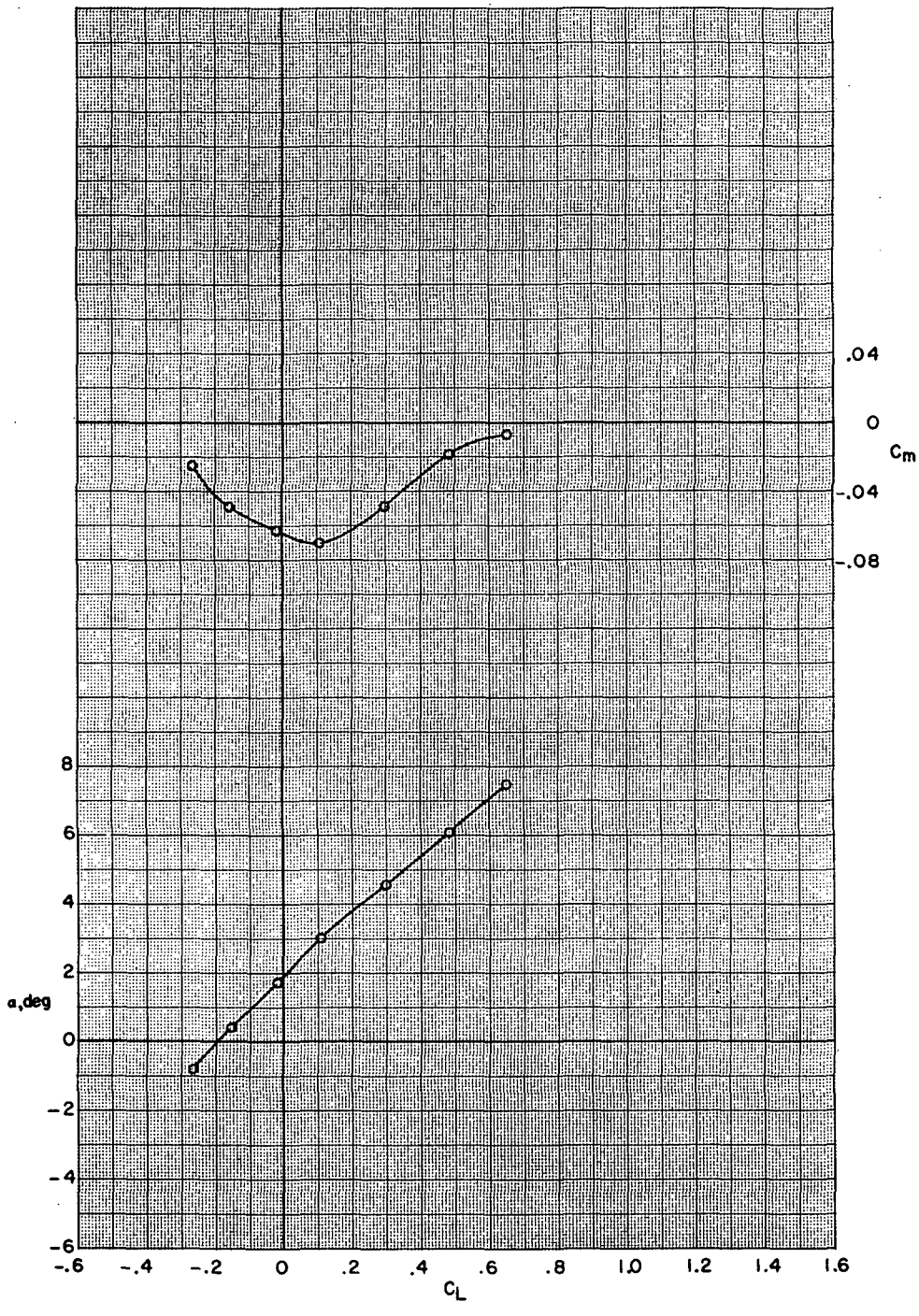

(e) M = 0.875.

Figure 13.- Continued.

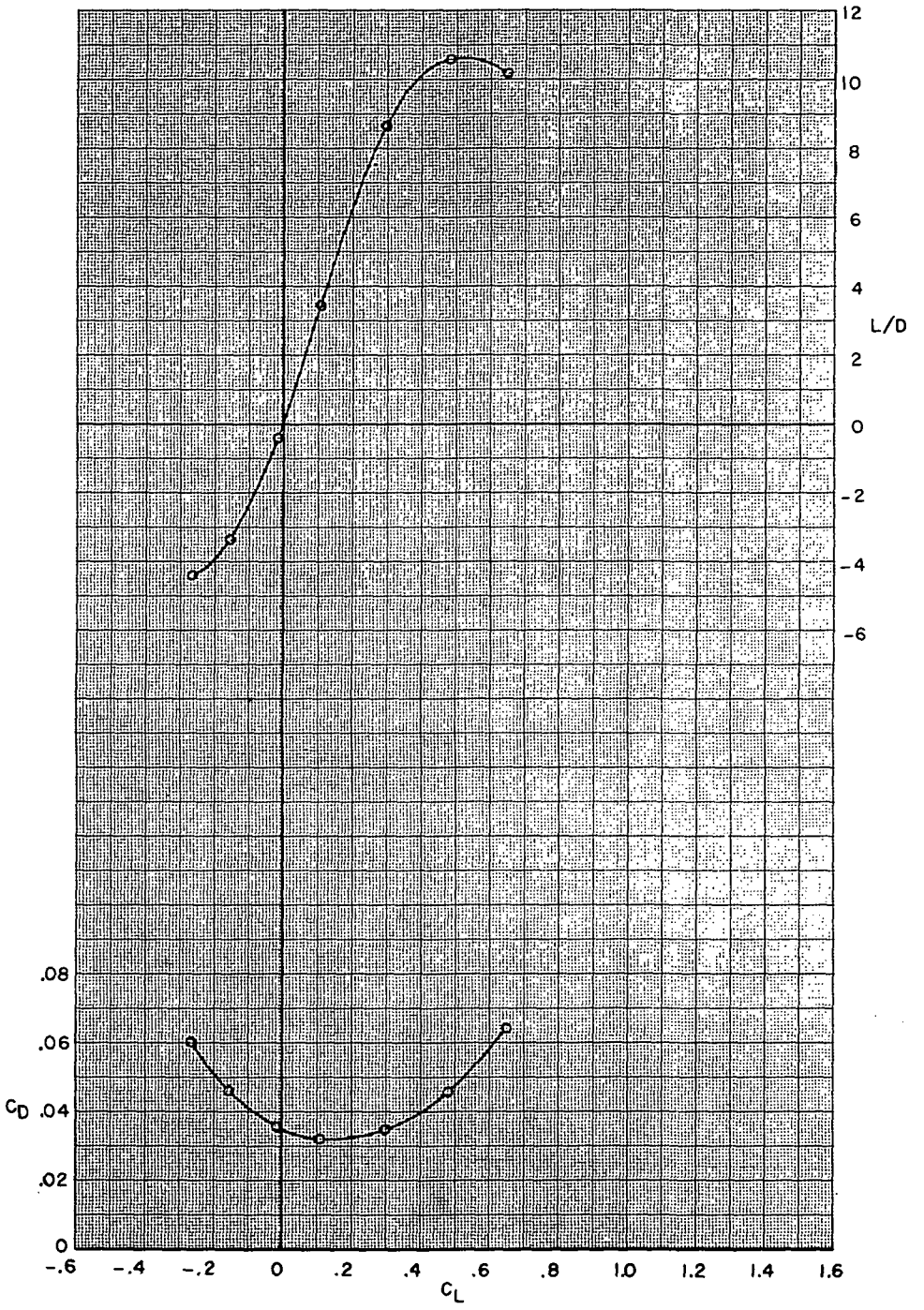

(e) Concluded.

Figure 13.- Continued.

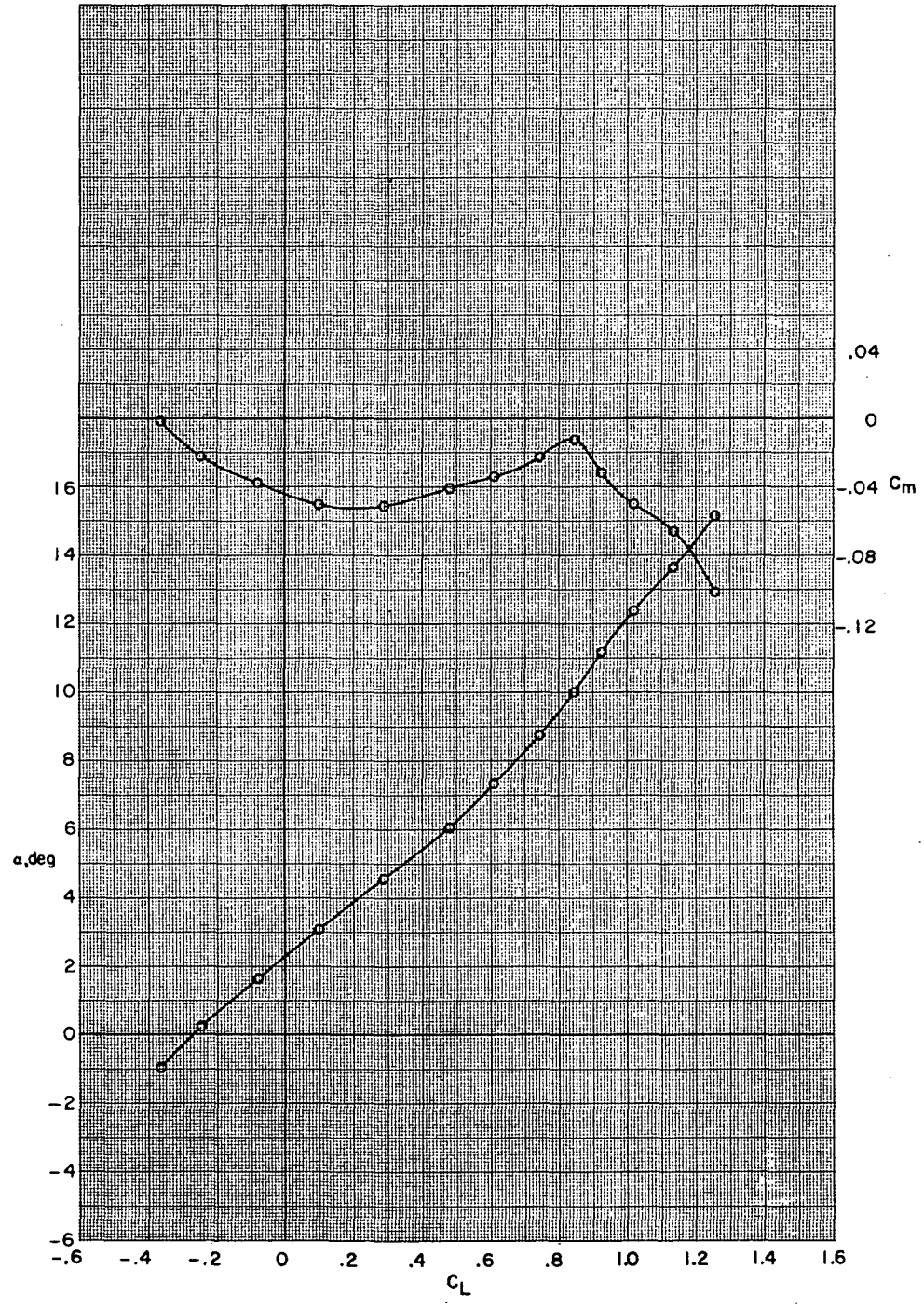

(f) M = 0.90.

Figure 13.- Continued.

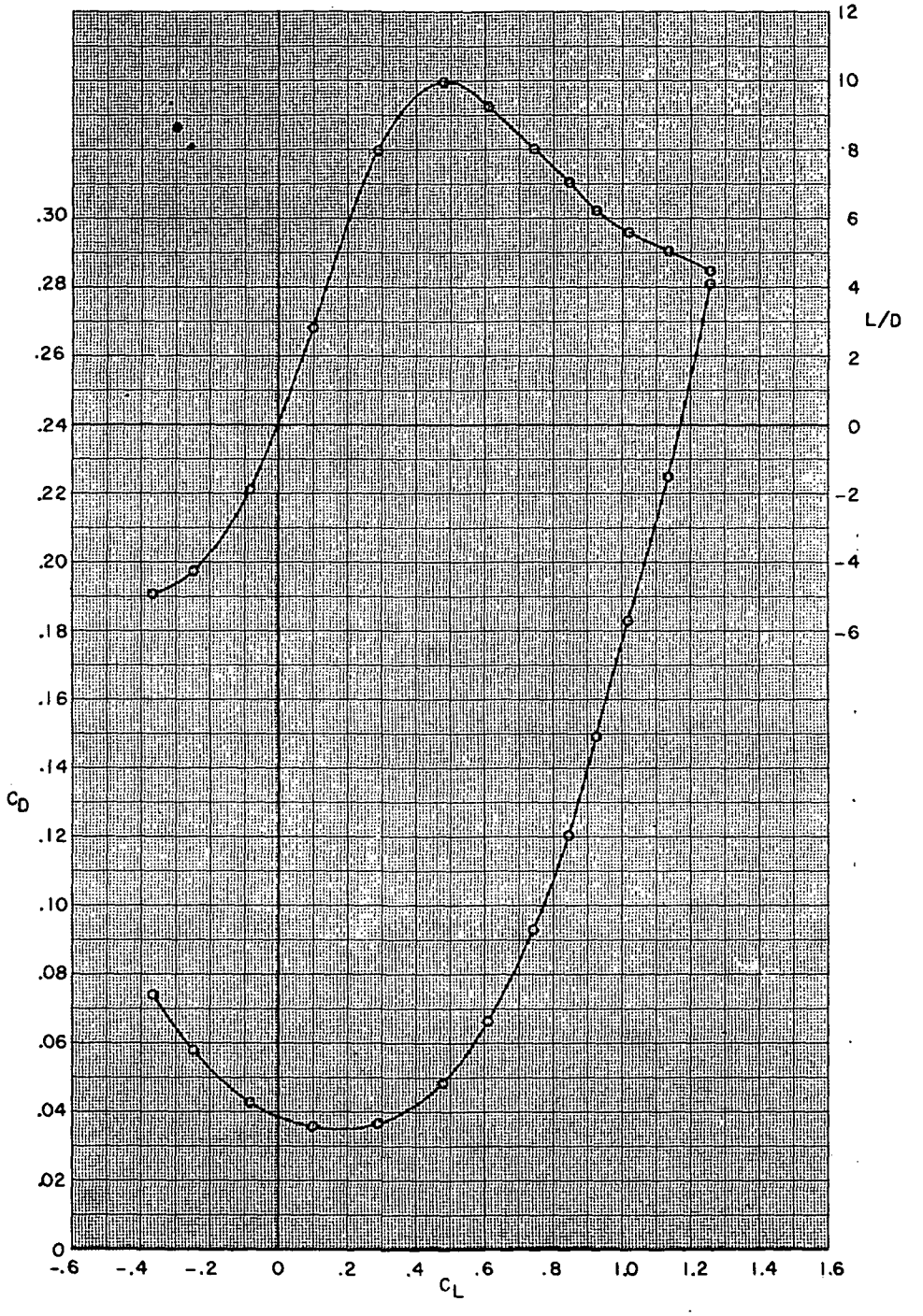

(f) Concluded.

Figure 13.- Continued.

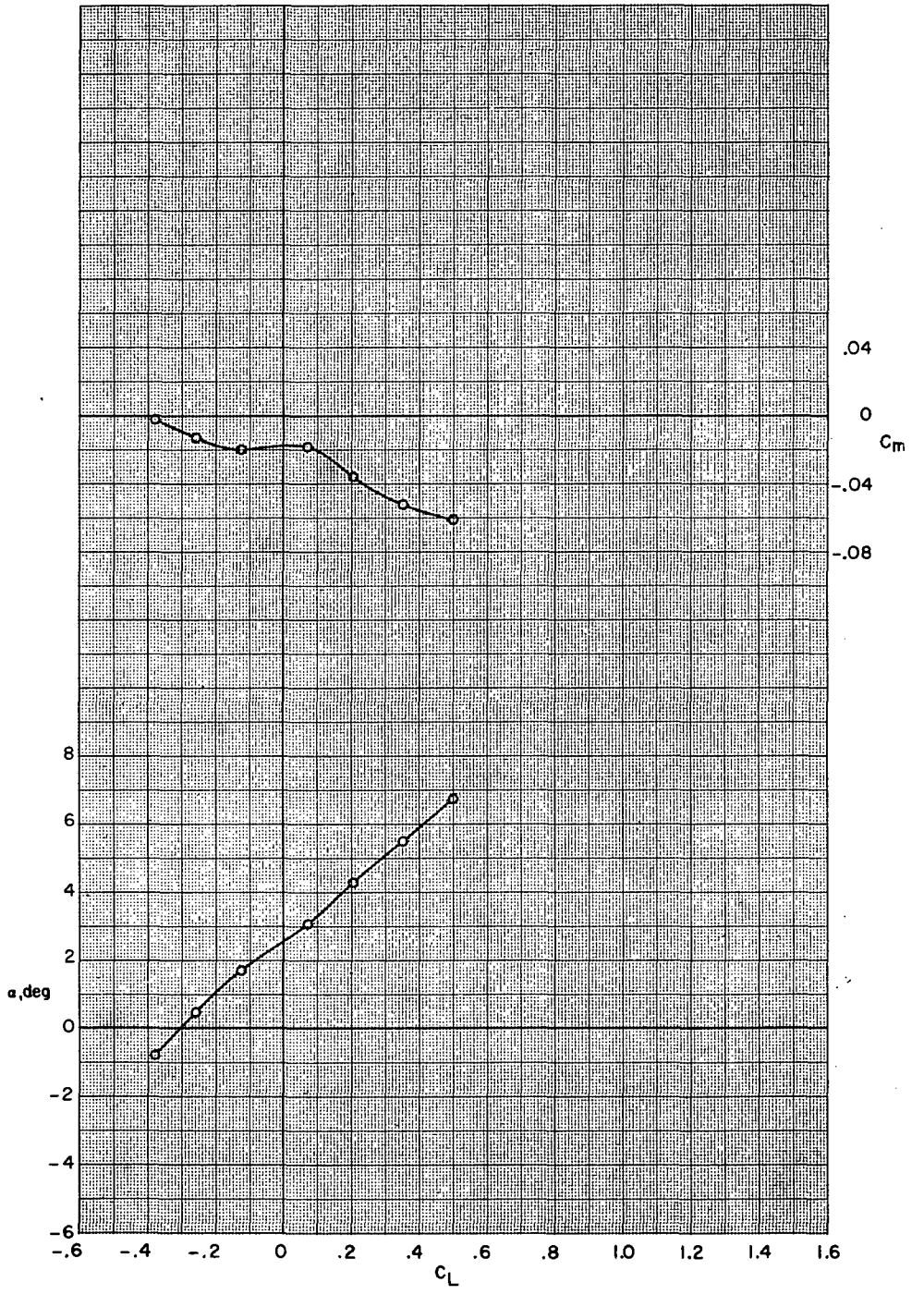

(g) M = 0.925.

Figure 13.- Continued.

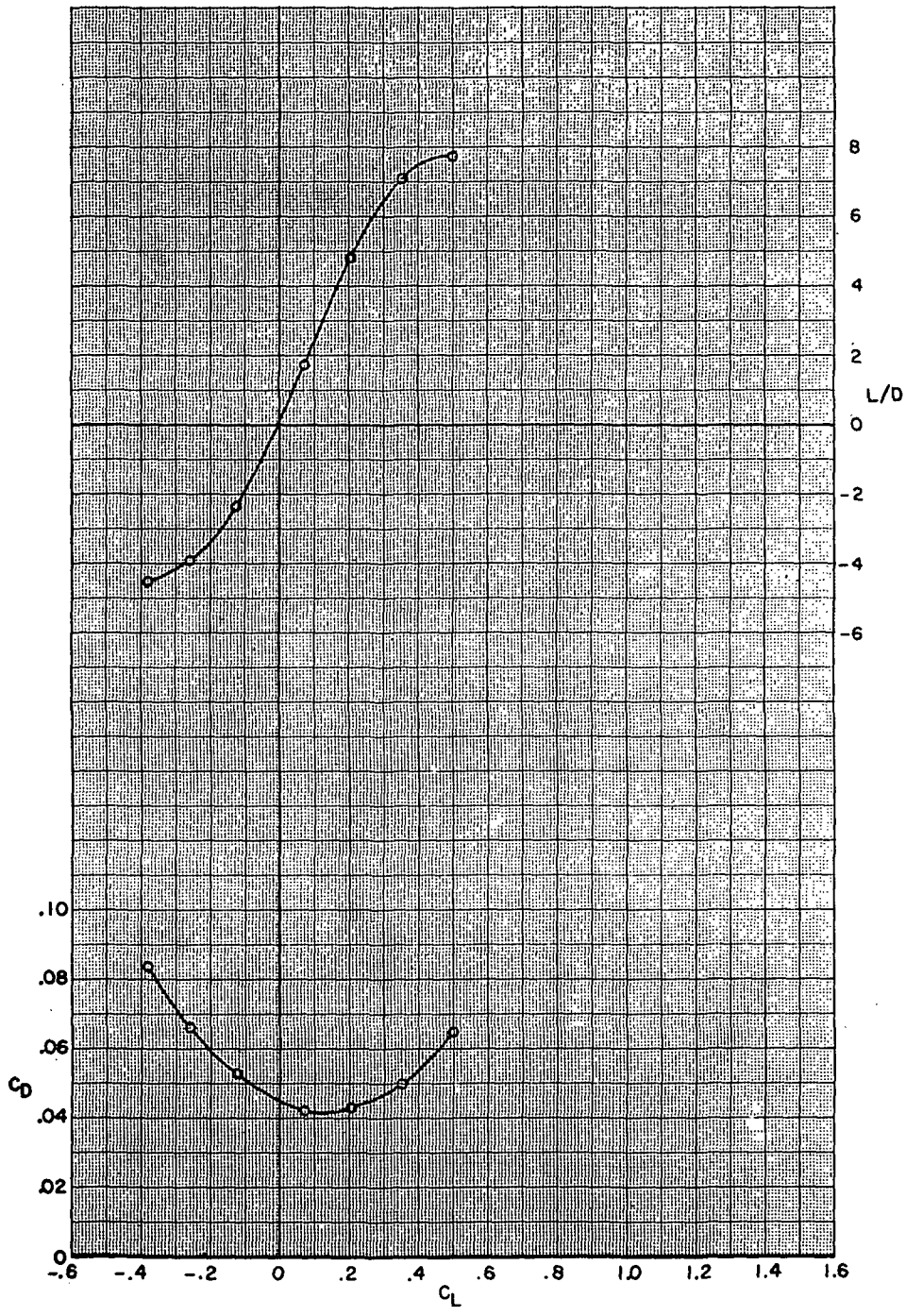

(g) Concluded.

Figure 13.- Continued.

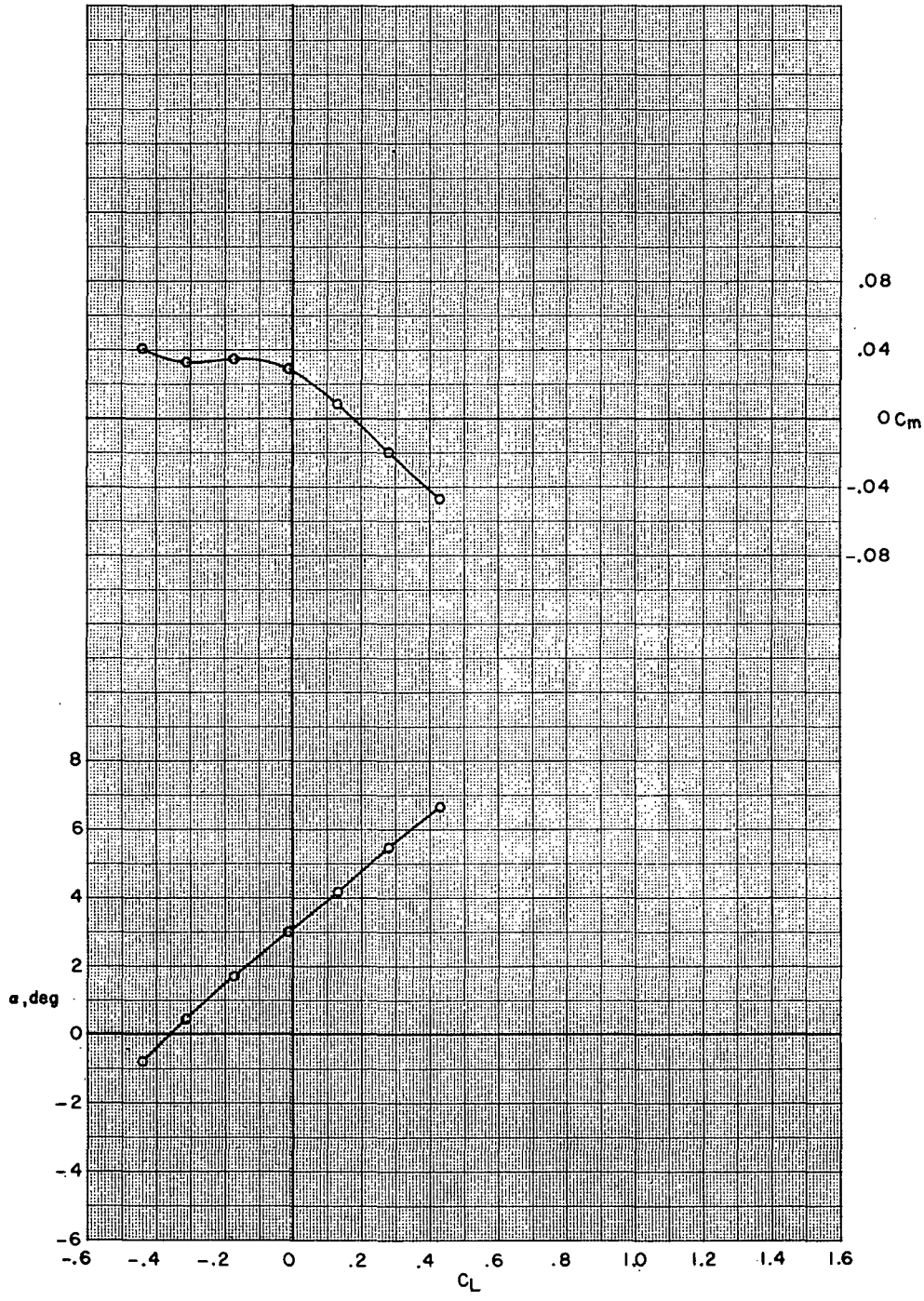

(h) M = 0.95.

Figure 13.- Continued.

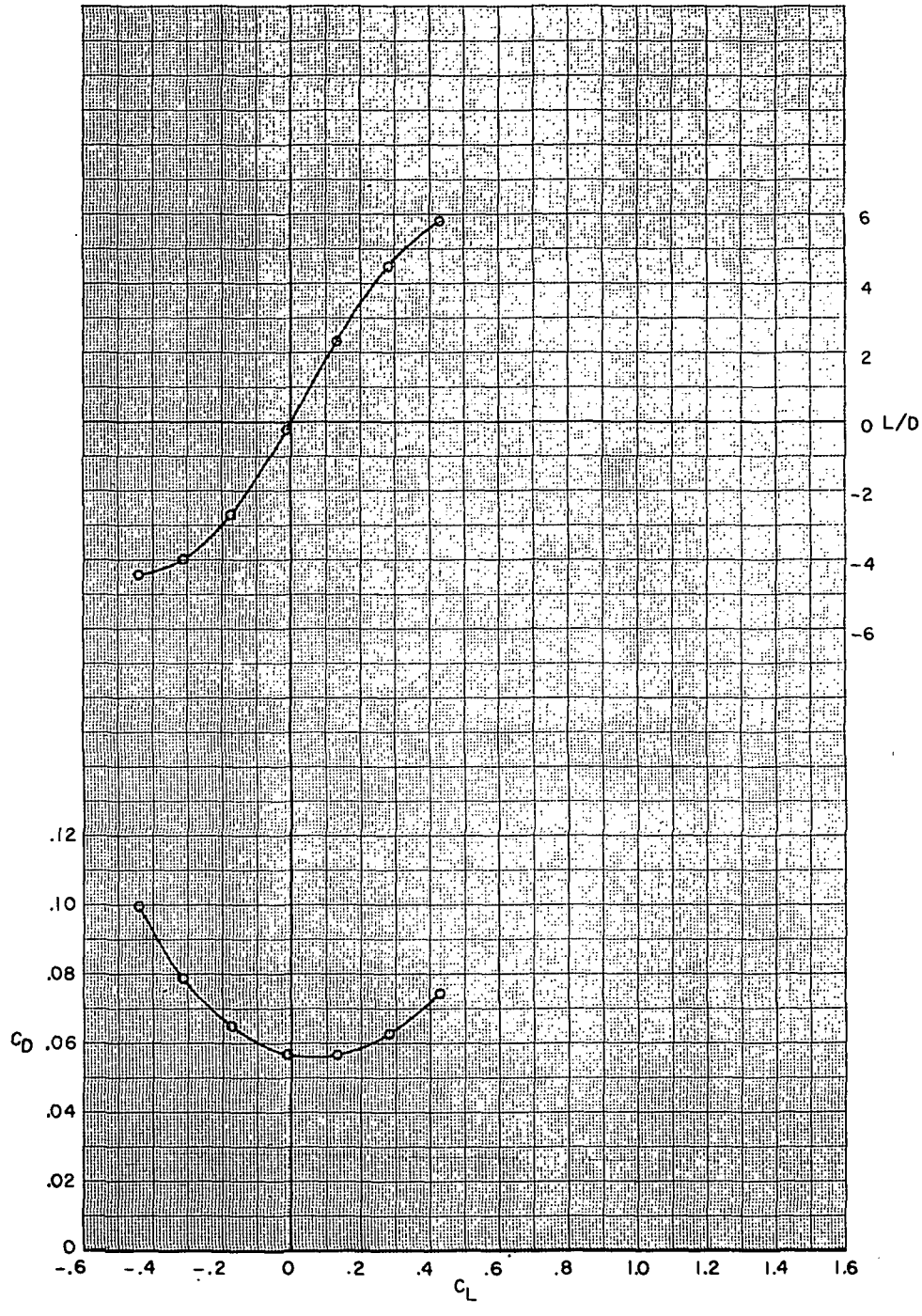

(h) Concluded.

Figure 13.- Concluded.

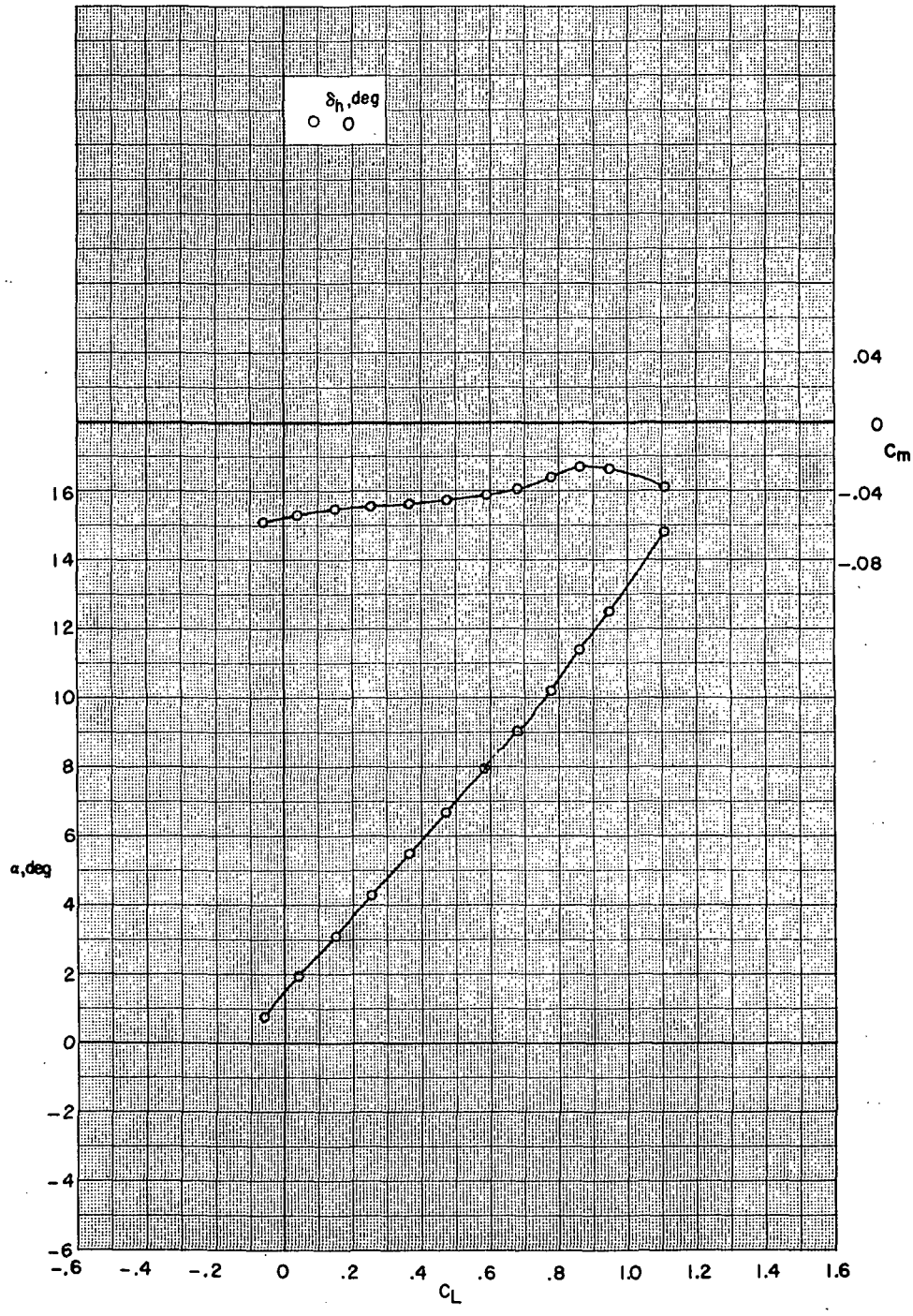

(a) M = 0.60.

Figure 14.- Aerodynamic characteristics for configuration $B_{80}G_{17}H_{13}I_{71}N^{b}_{32}V_{29}V_{38}W_{32a}X_{24}X_{168}$ with wing swept 26.0°.

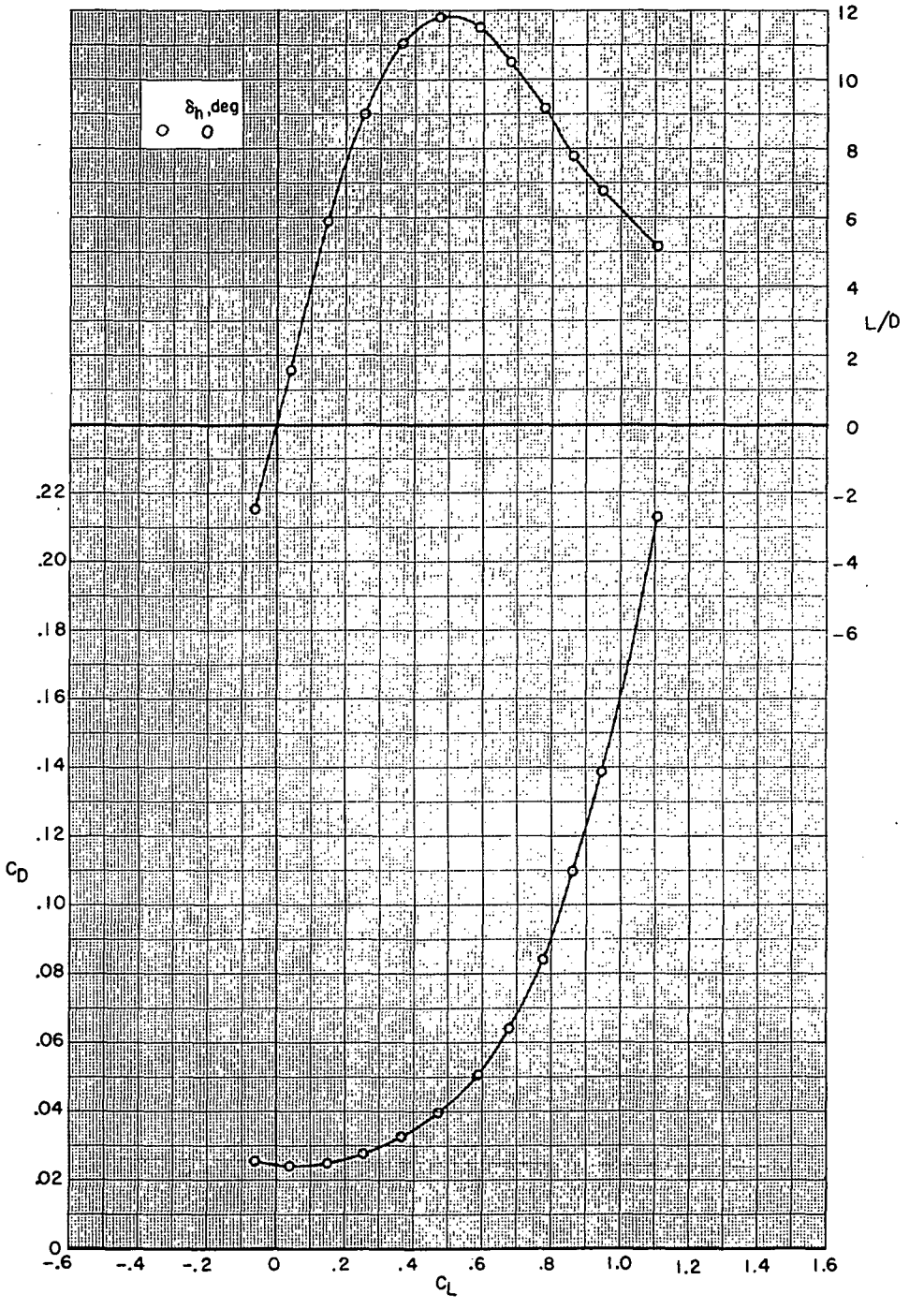

(a) Concluded.

Figure 14.- Continued.

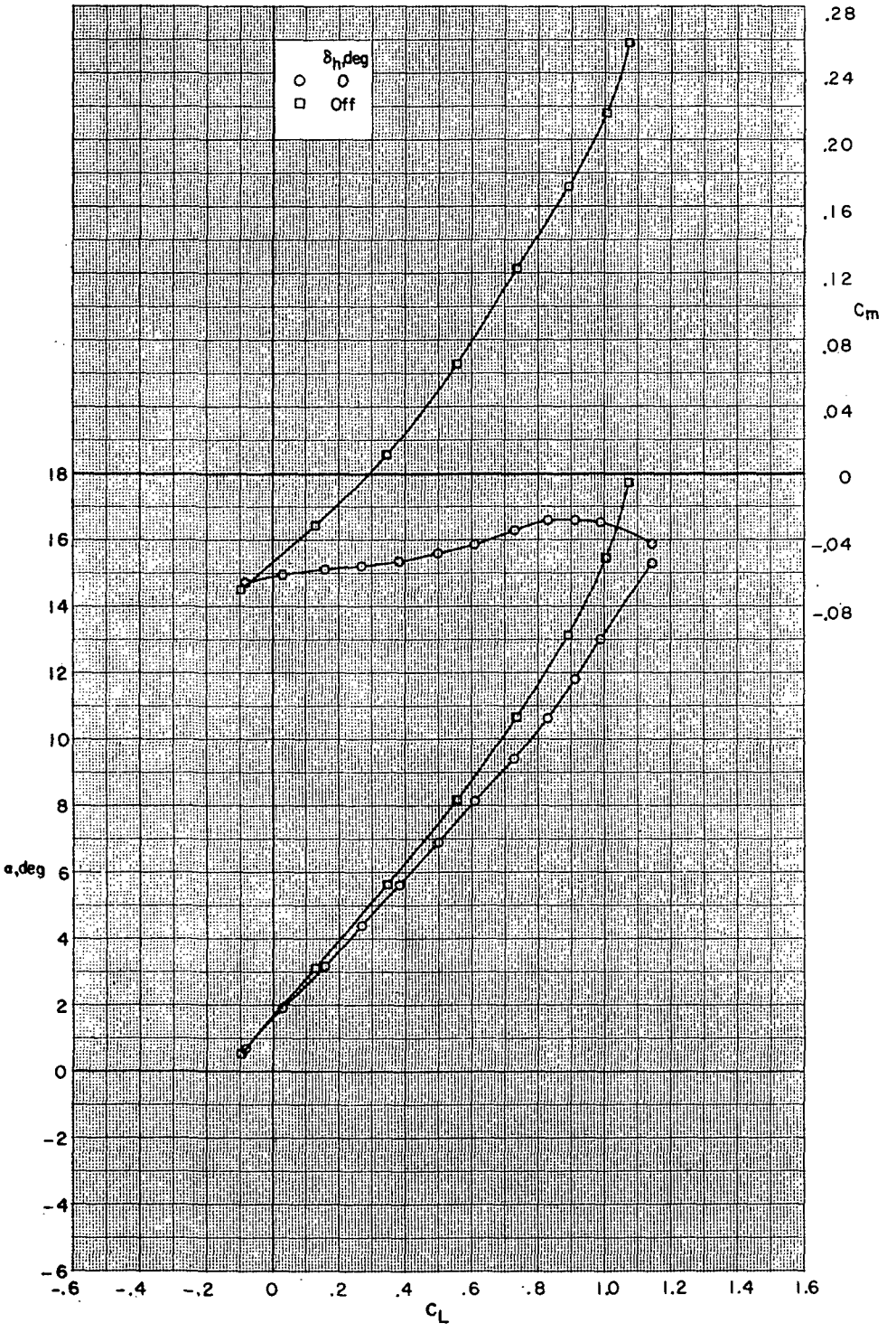

(b) M = 0.70.

Figure 14.- Continued.

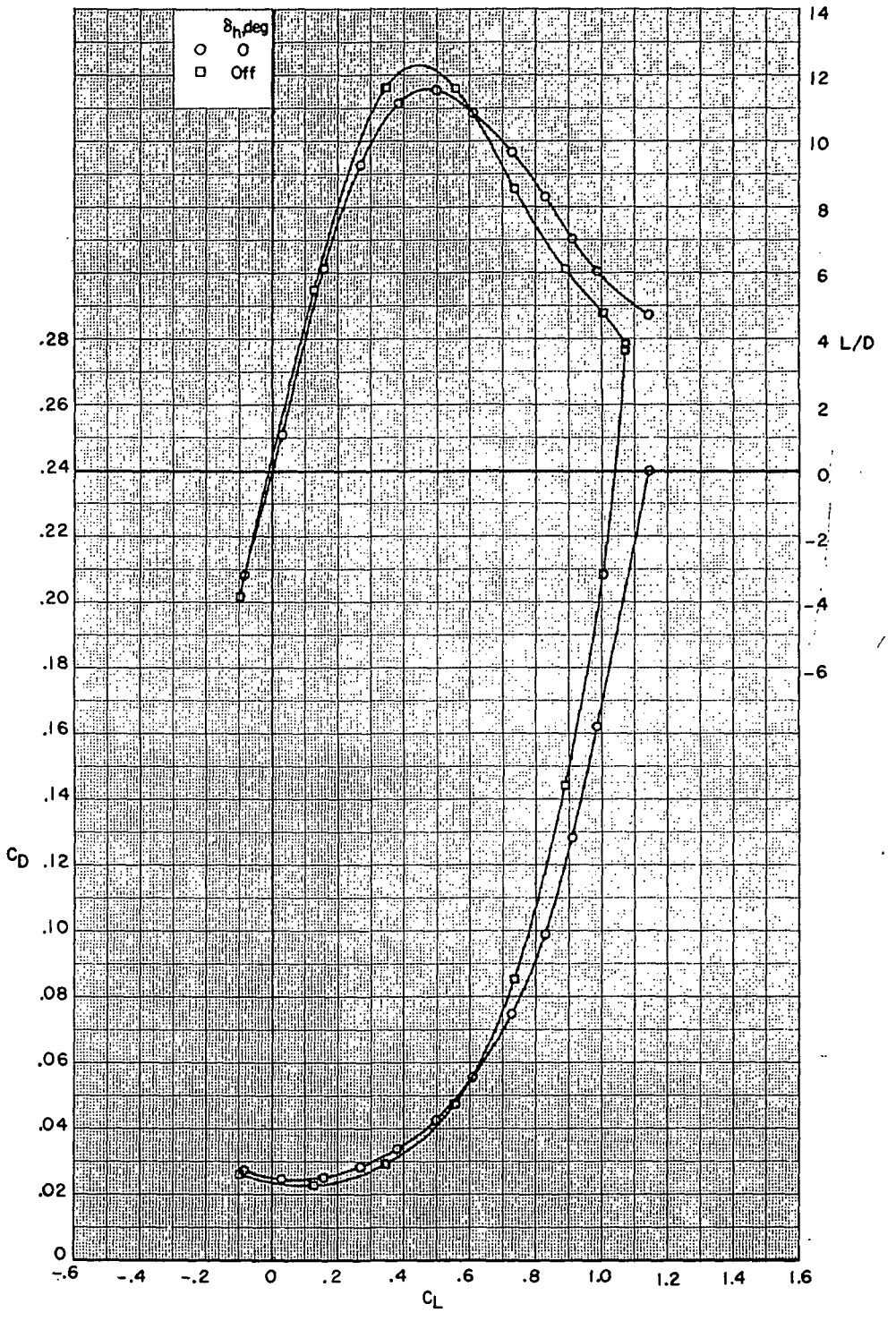

(b) Concluded.

Figure 14.- Continued.

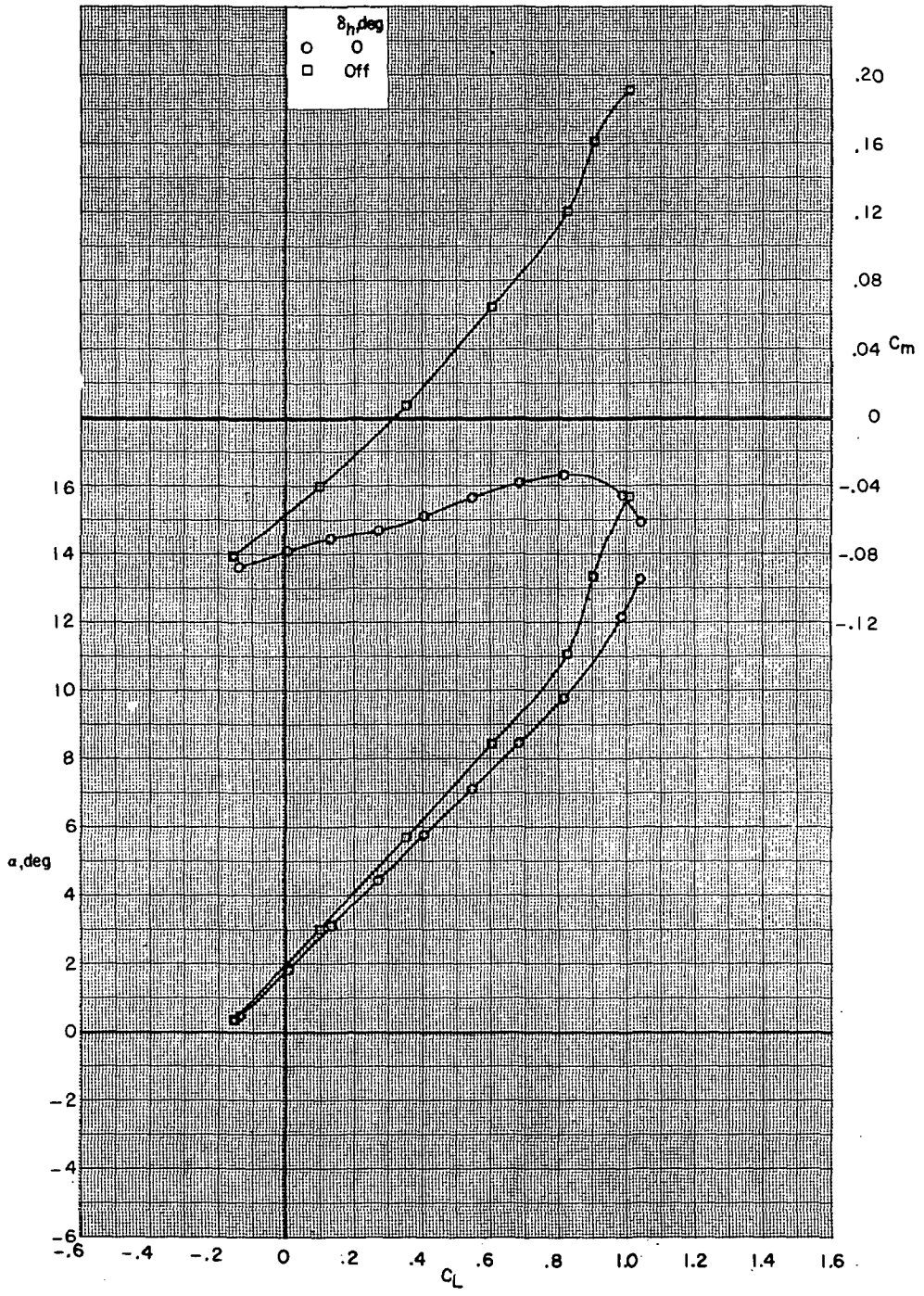

(c) M = 0.80.

Figure 14.- Continued.

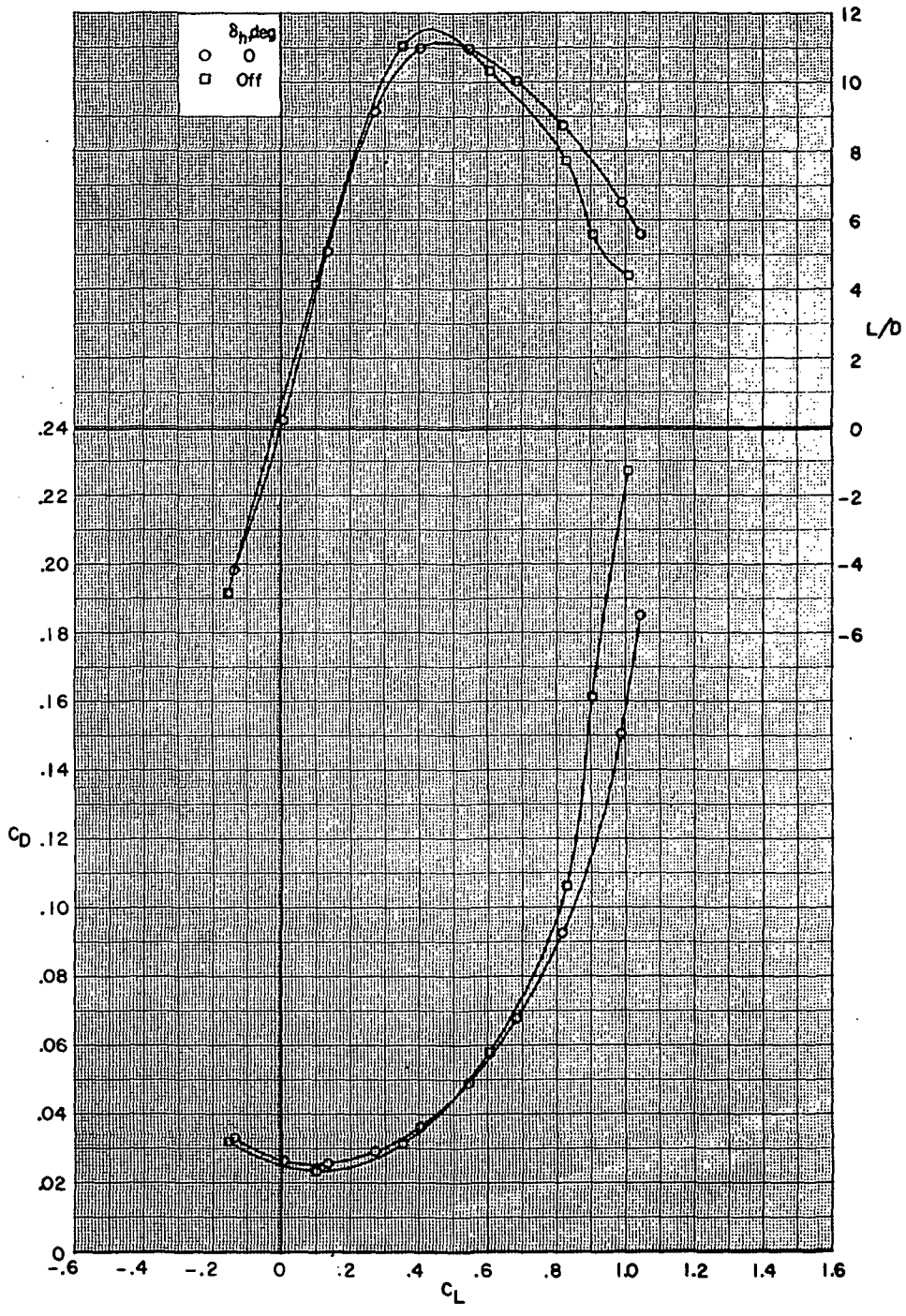

(c) Concluded.

Figure 14.- Continued.

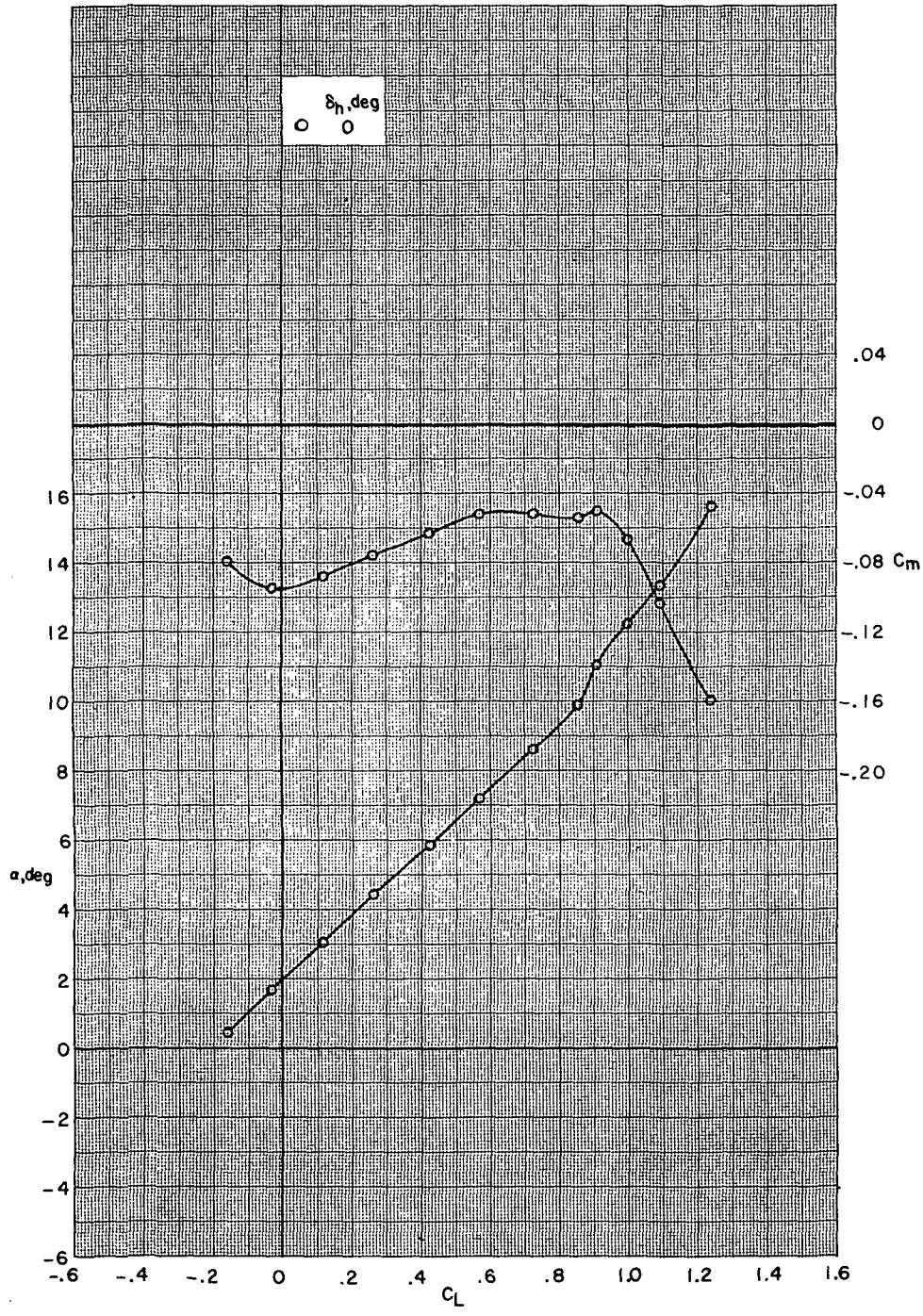

(d) M = 0.85.

Figure 14.- Continued.

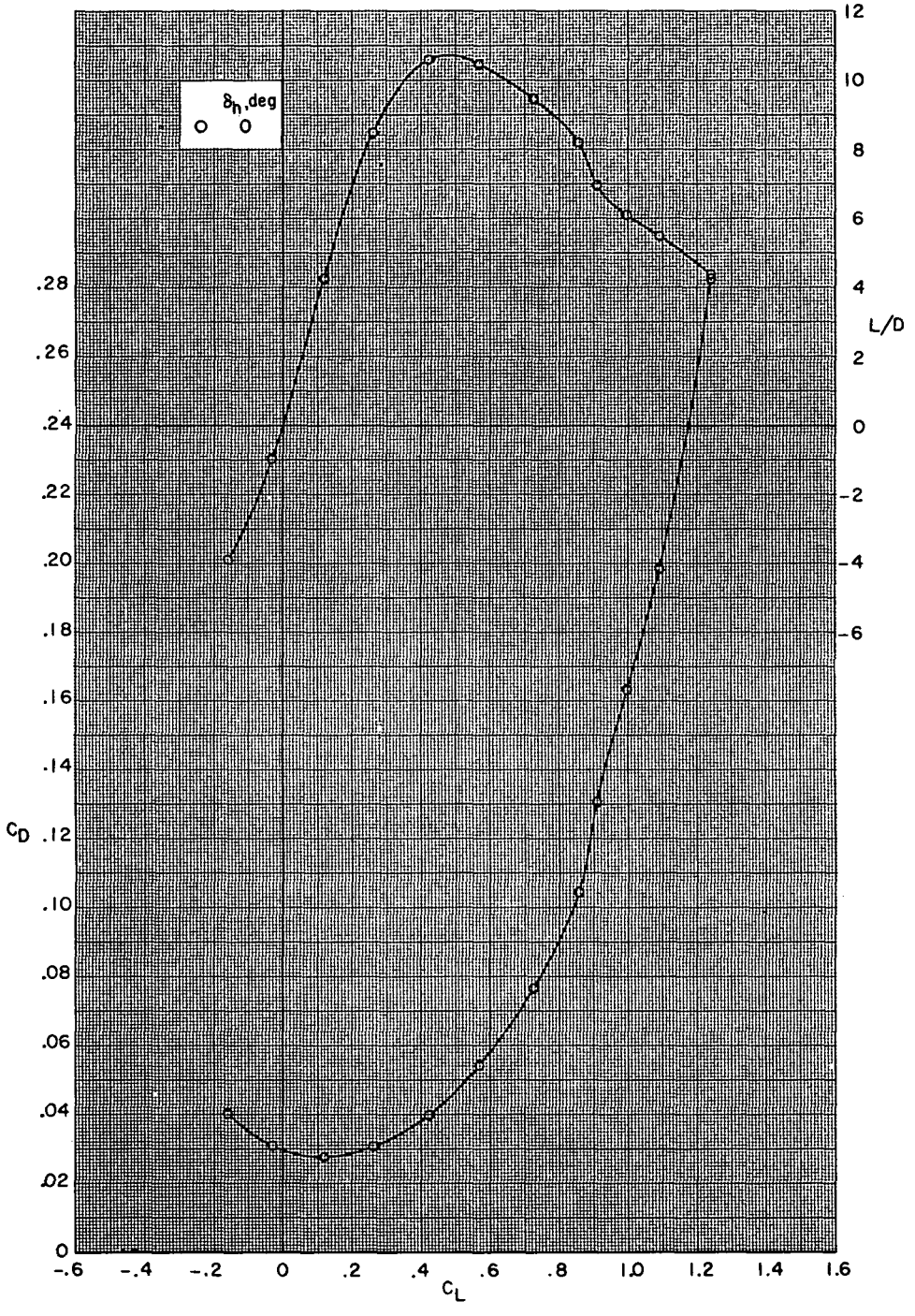

(d) Concluded.

Figure 14.- Continued.

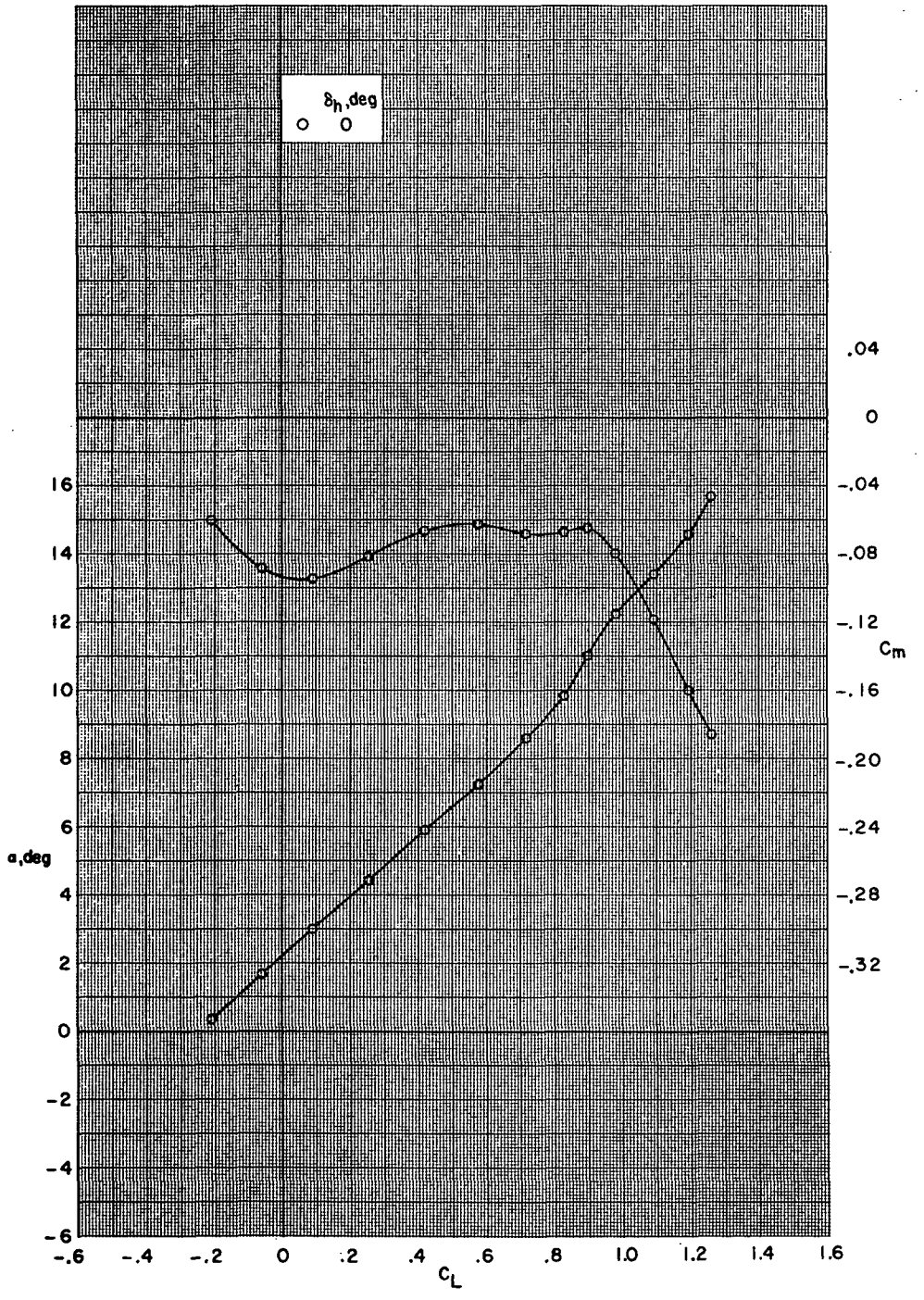

(e) M = 0.875.

Figure 14.- Continued.

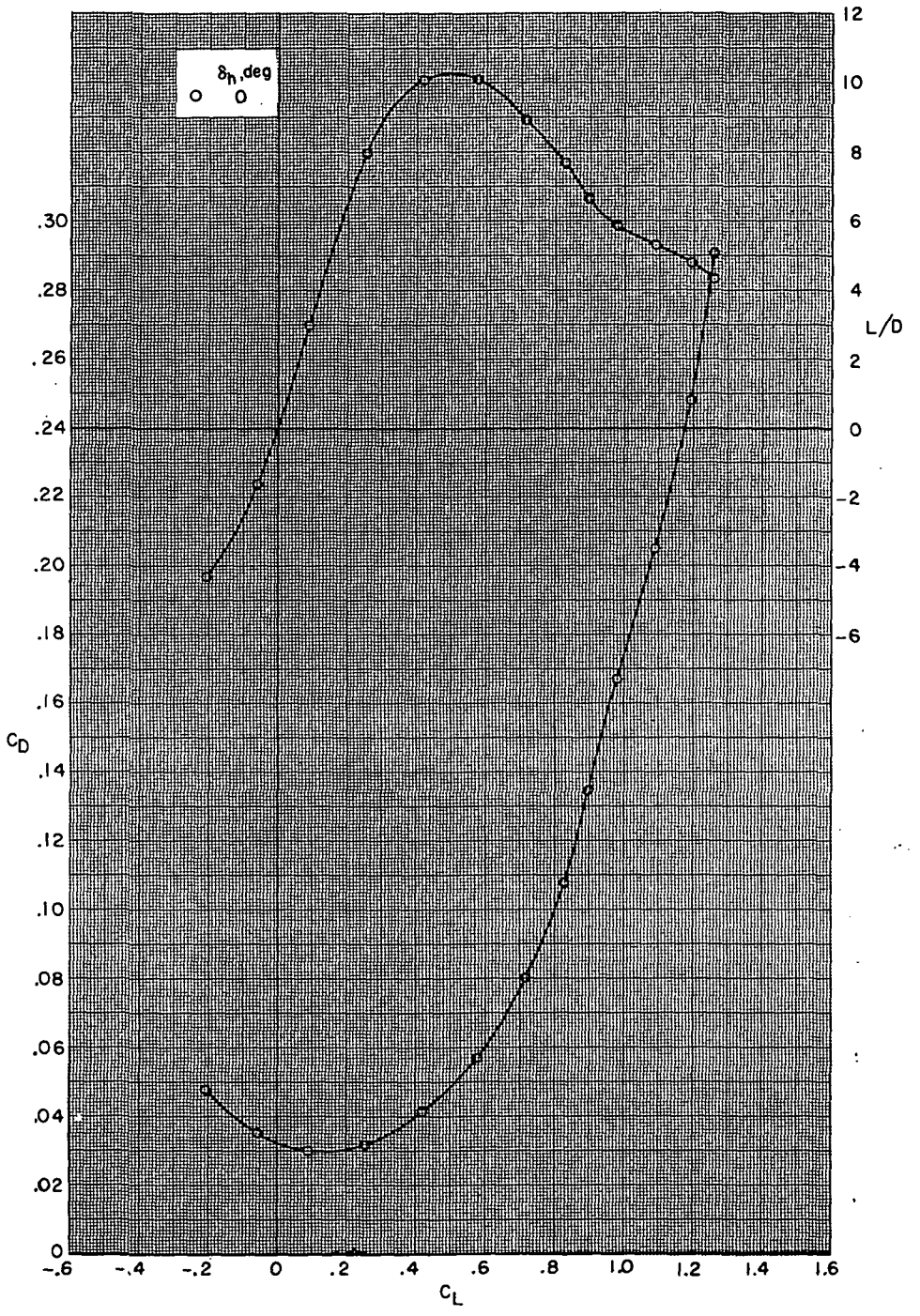

(e) Concluded.

Figure 14.- Continued.

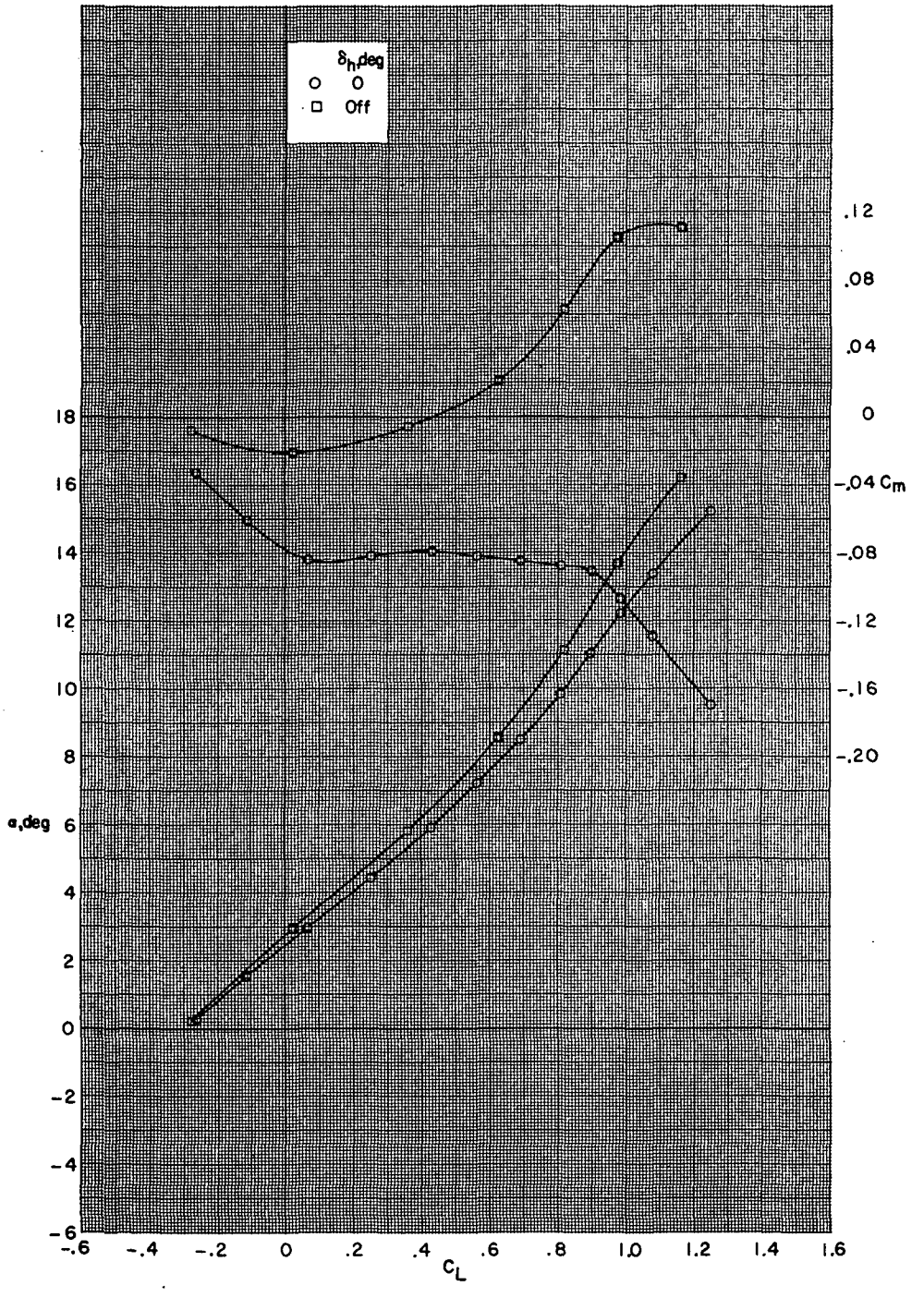

(f) M = 0.90.

Figure 14.- Continued.

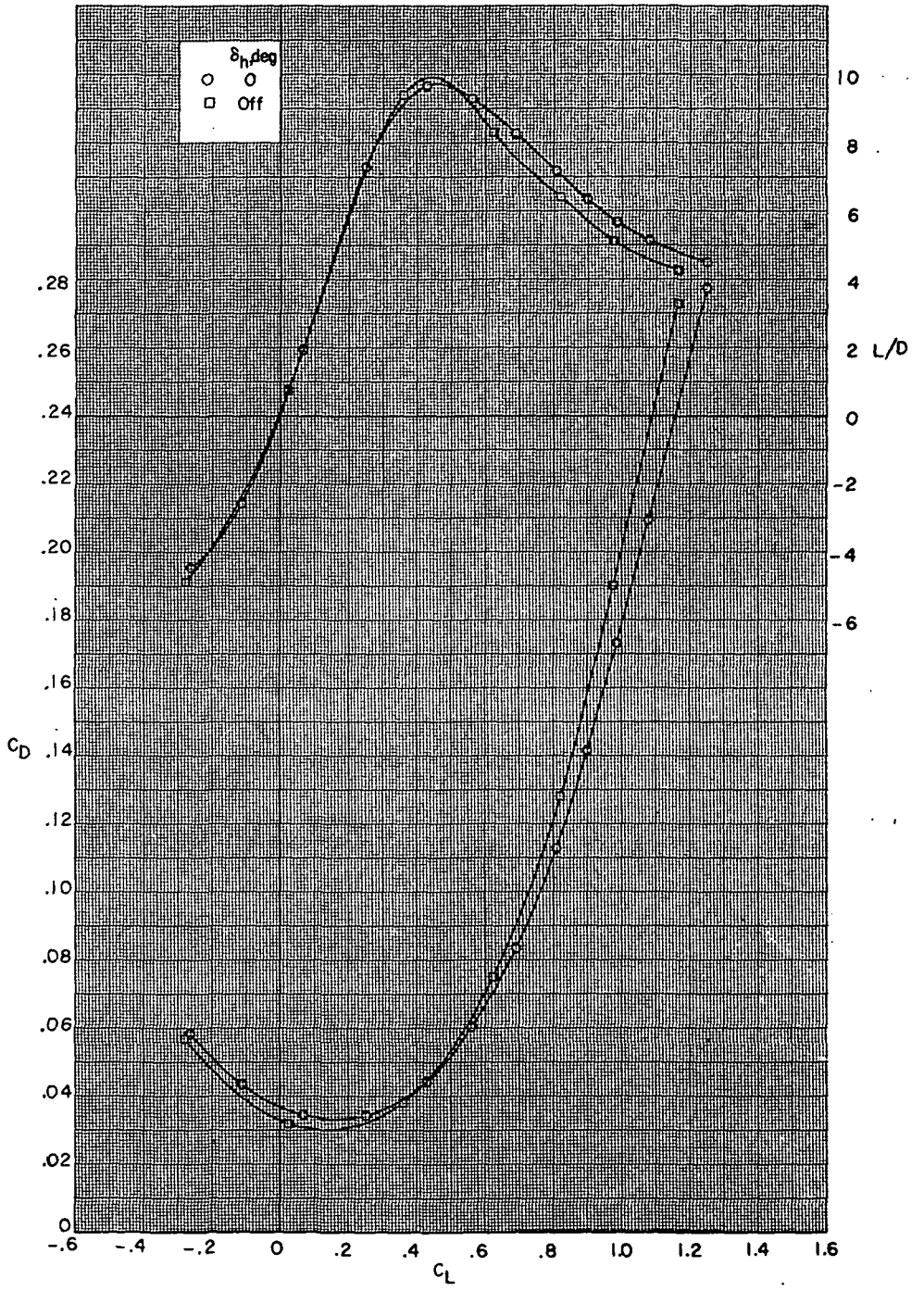

(f) Concluded.

Figure 14.- Concluded.

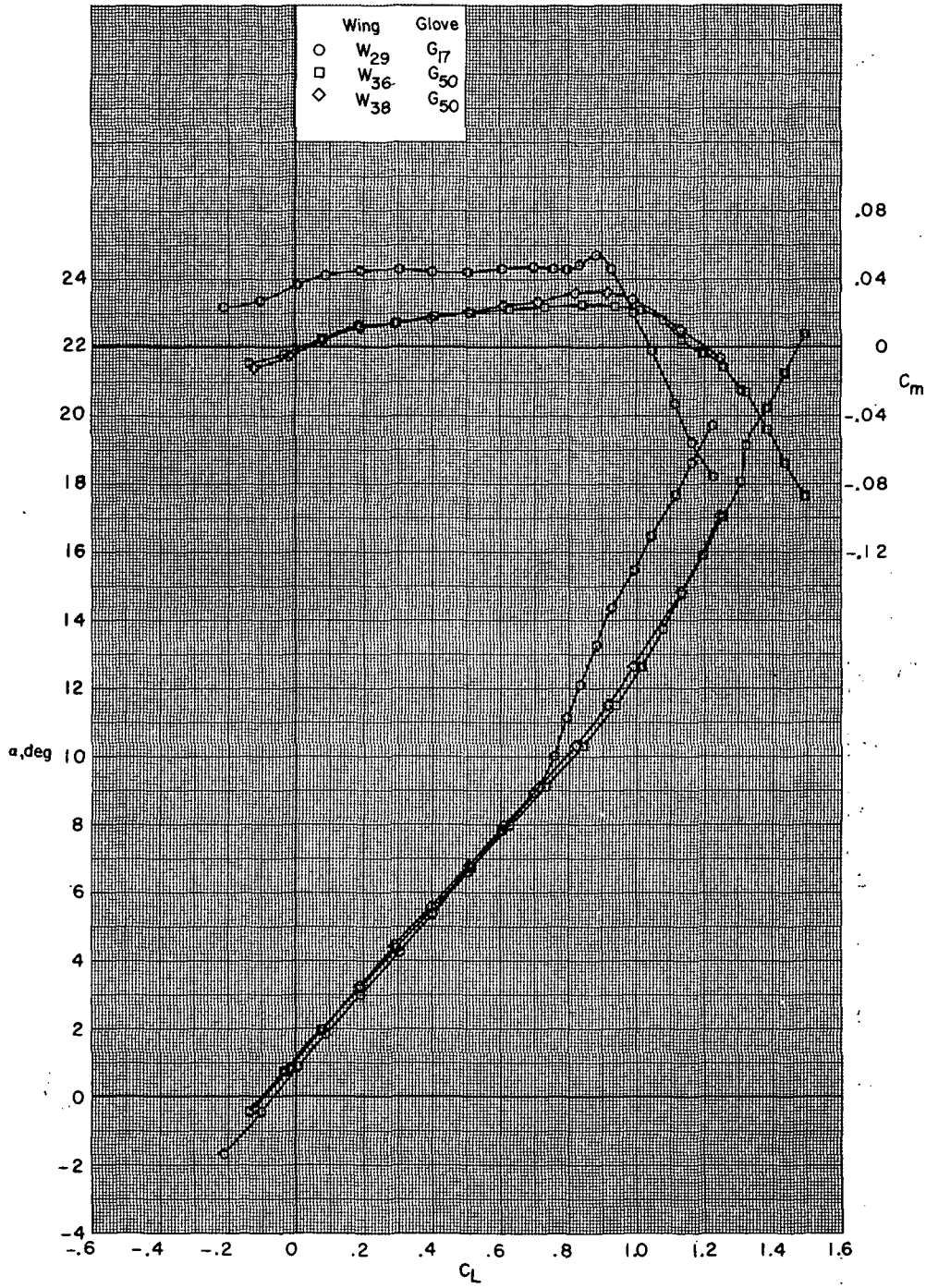

(a) M = 0.60.

Figure 15.- Effect of wing planform on aerodynamic characteristics for conventional wing configurations $B_{80}G_xH_{13}I_{71}N^b_{32}V_{29}V_{38}W_xX_{24}$ with wing swept 26.0°.

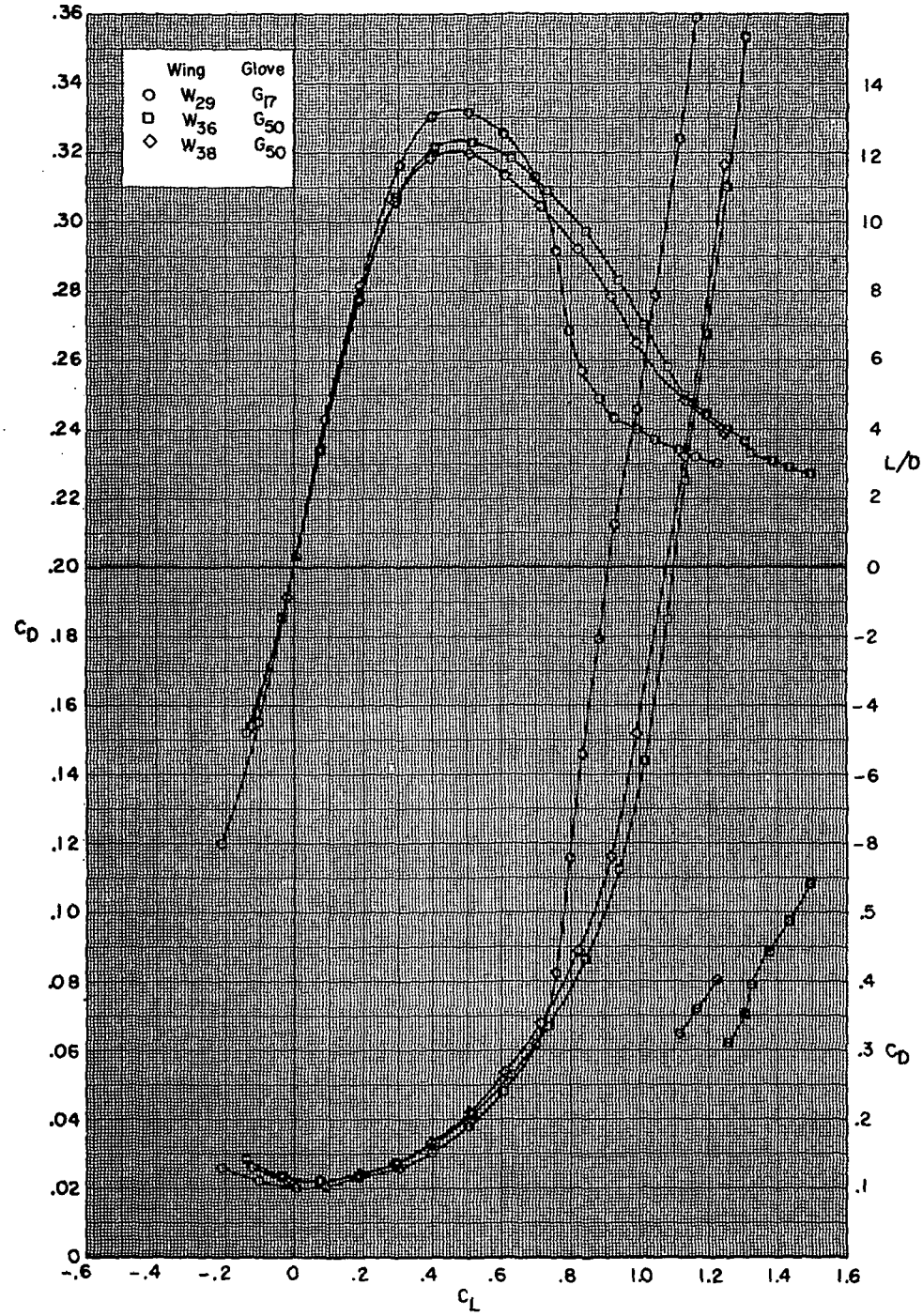

(a) Concluded.

Figure 15.- Continued.

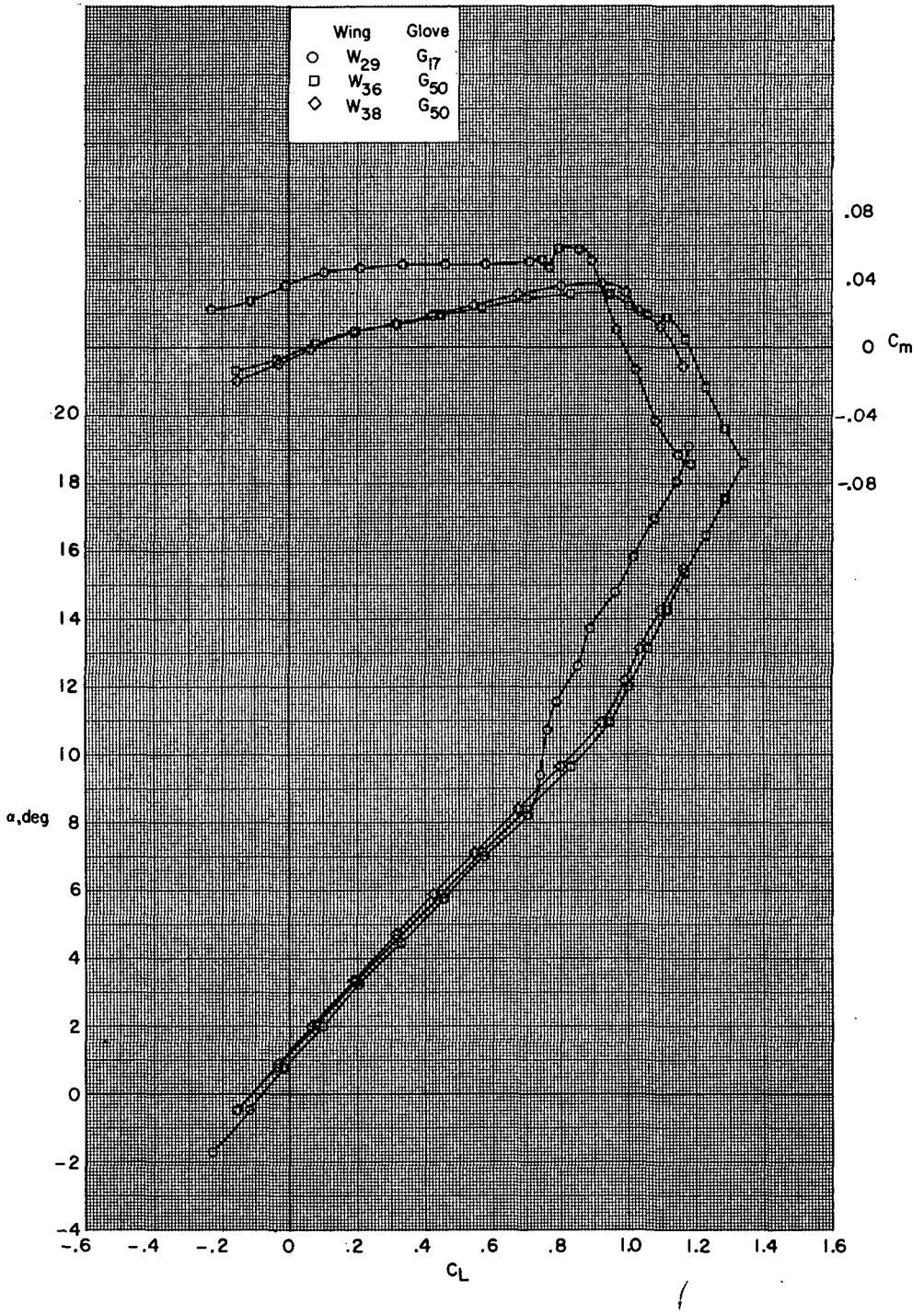

(b) M = 0.70.

Figure 15.- Continued.

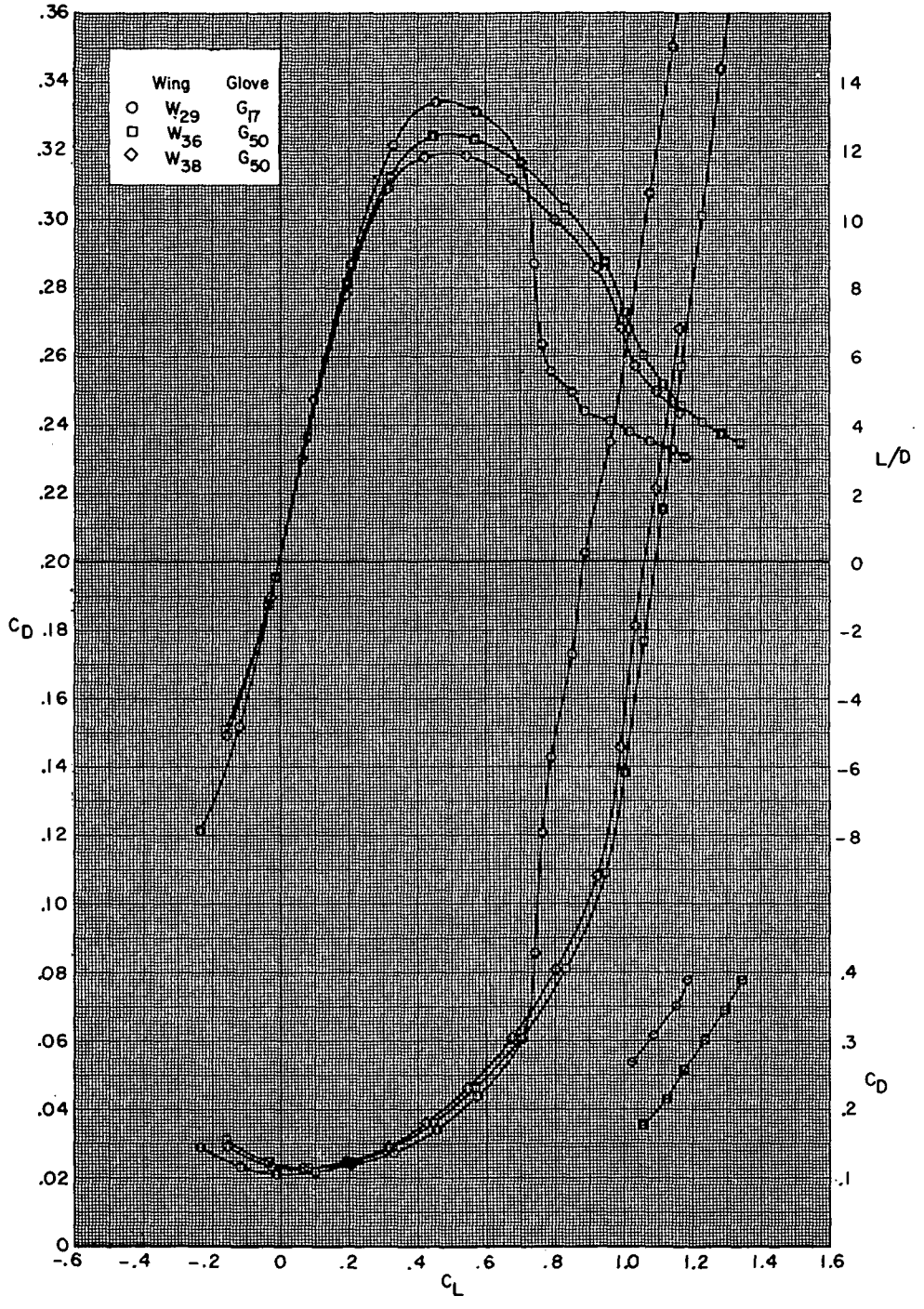

(b) Concluded.

Figure 15.- Continued.

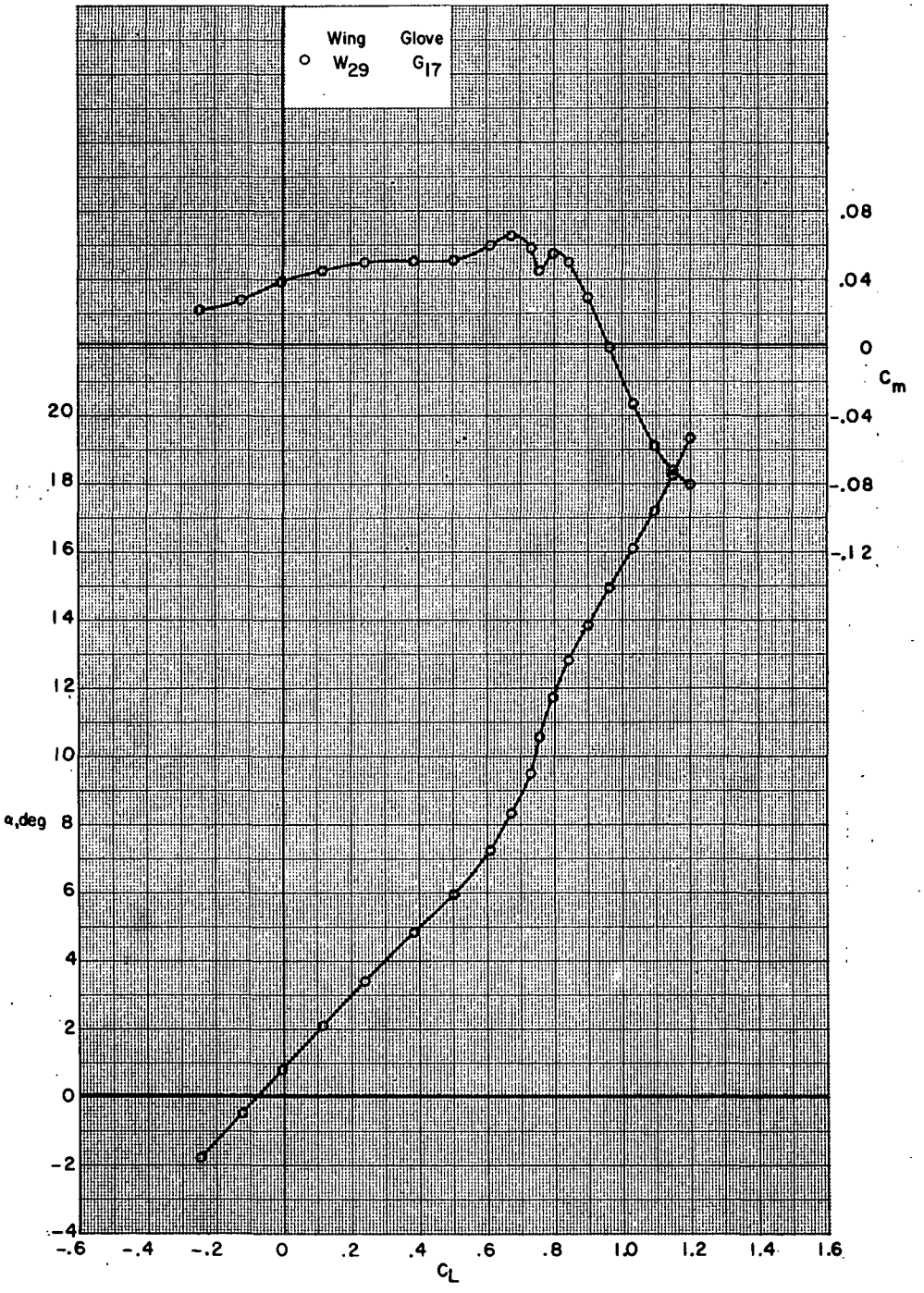

(c) M = 0.75.

Figure 15.- Continued.

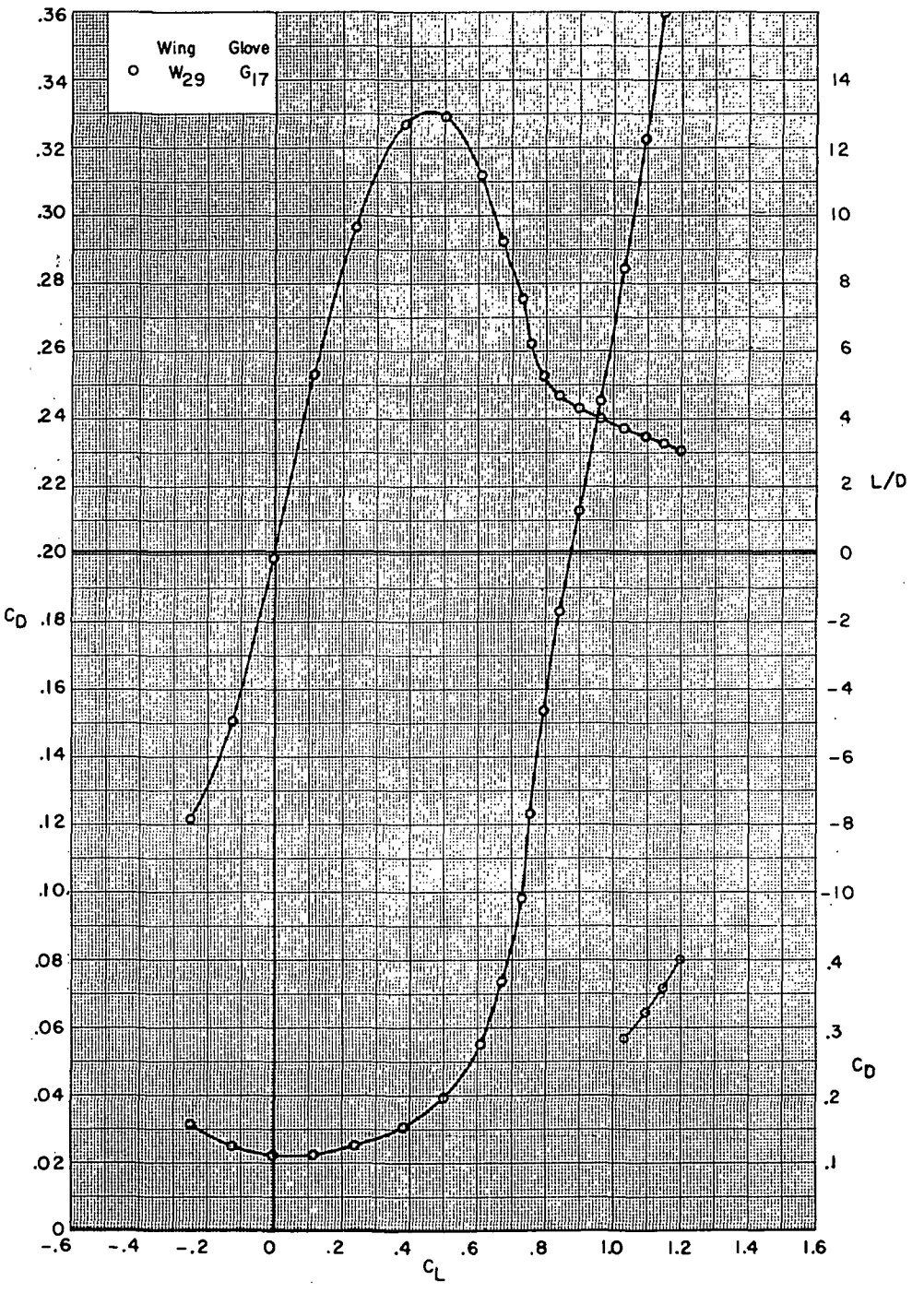

(c) Concluded.

Figure 15.- Continued.

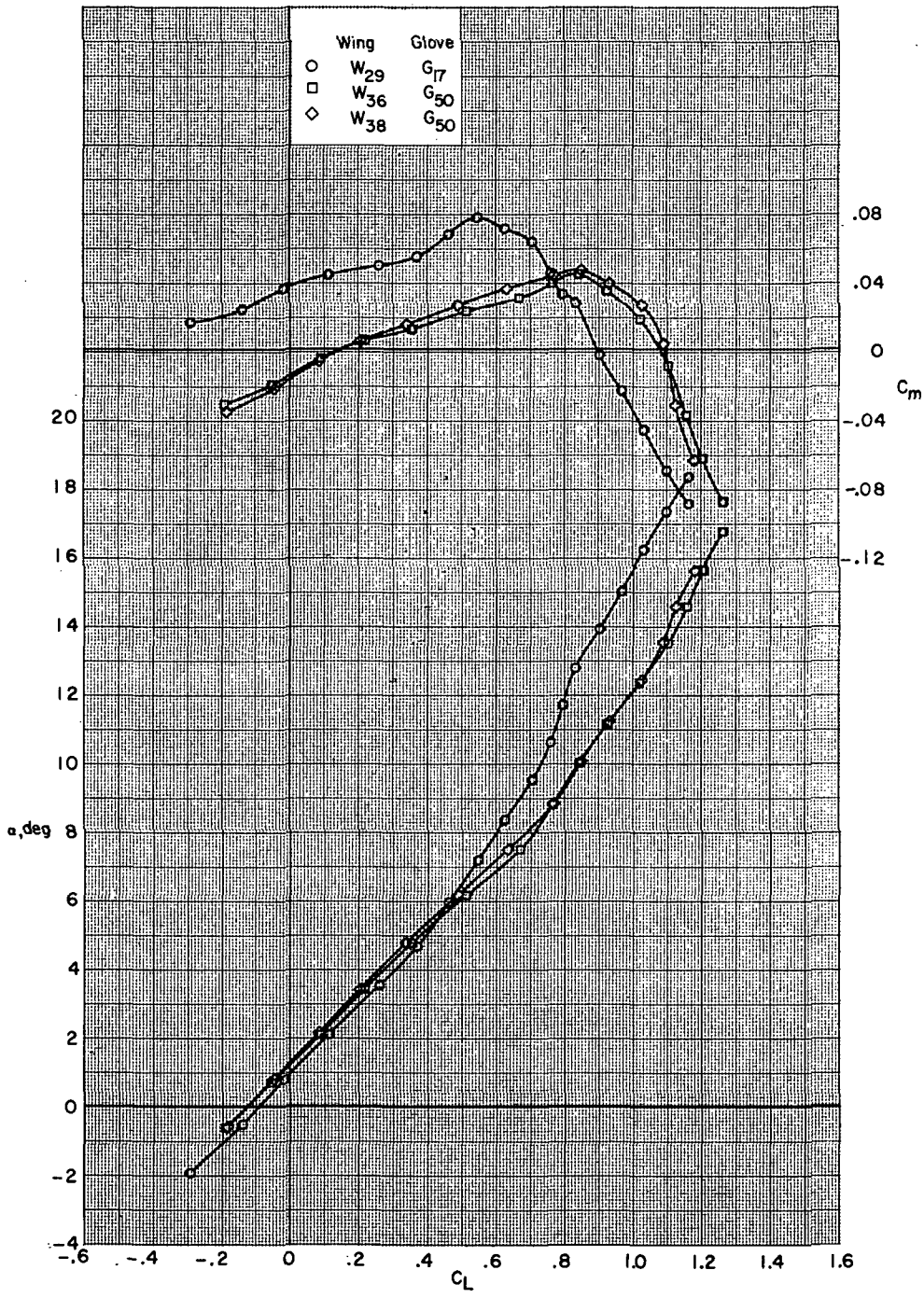

(d) M = 0.80.

Figure 15.- Continued.

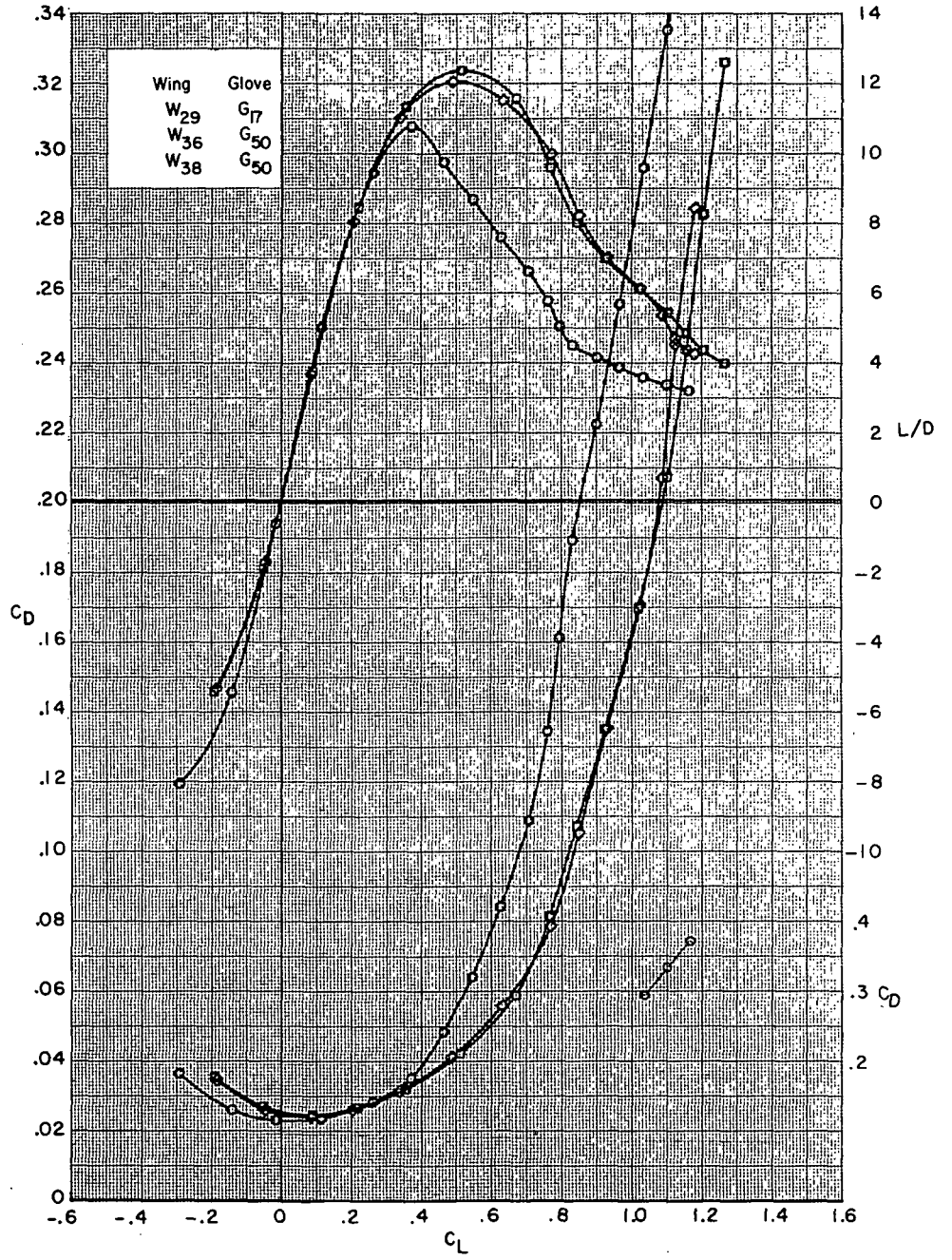

(d) Concluded.

Figure 15.- Continued.

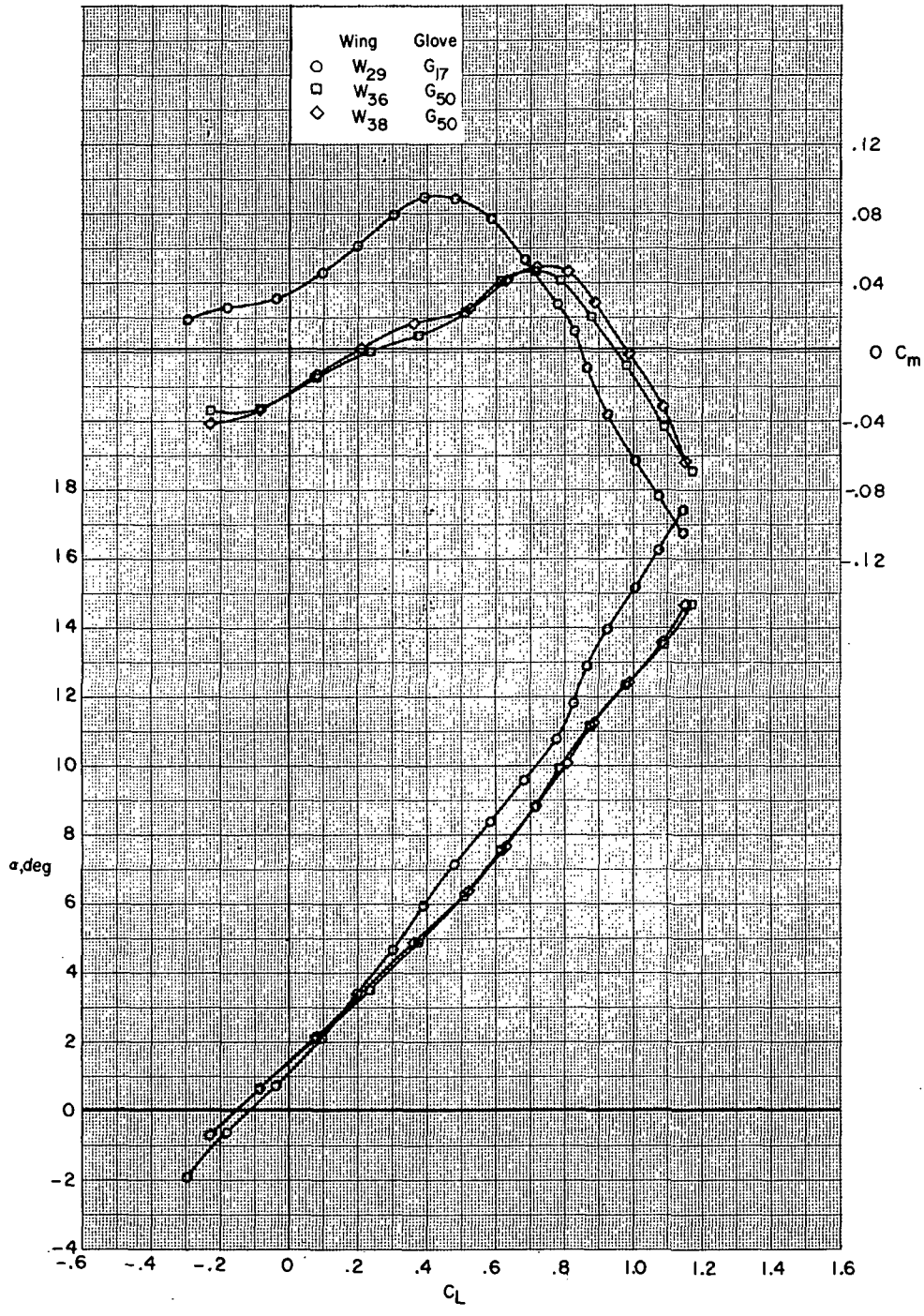

(e) M = 0.85.

Figure 15.- Continued.

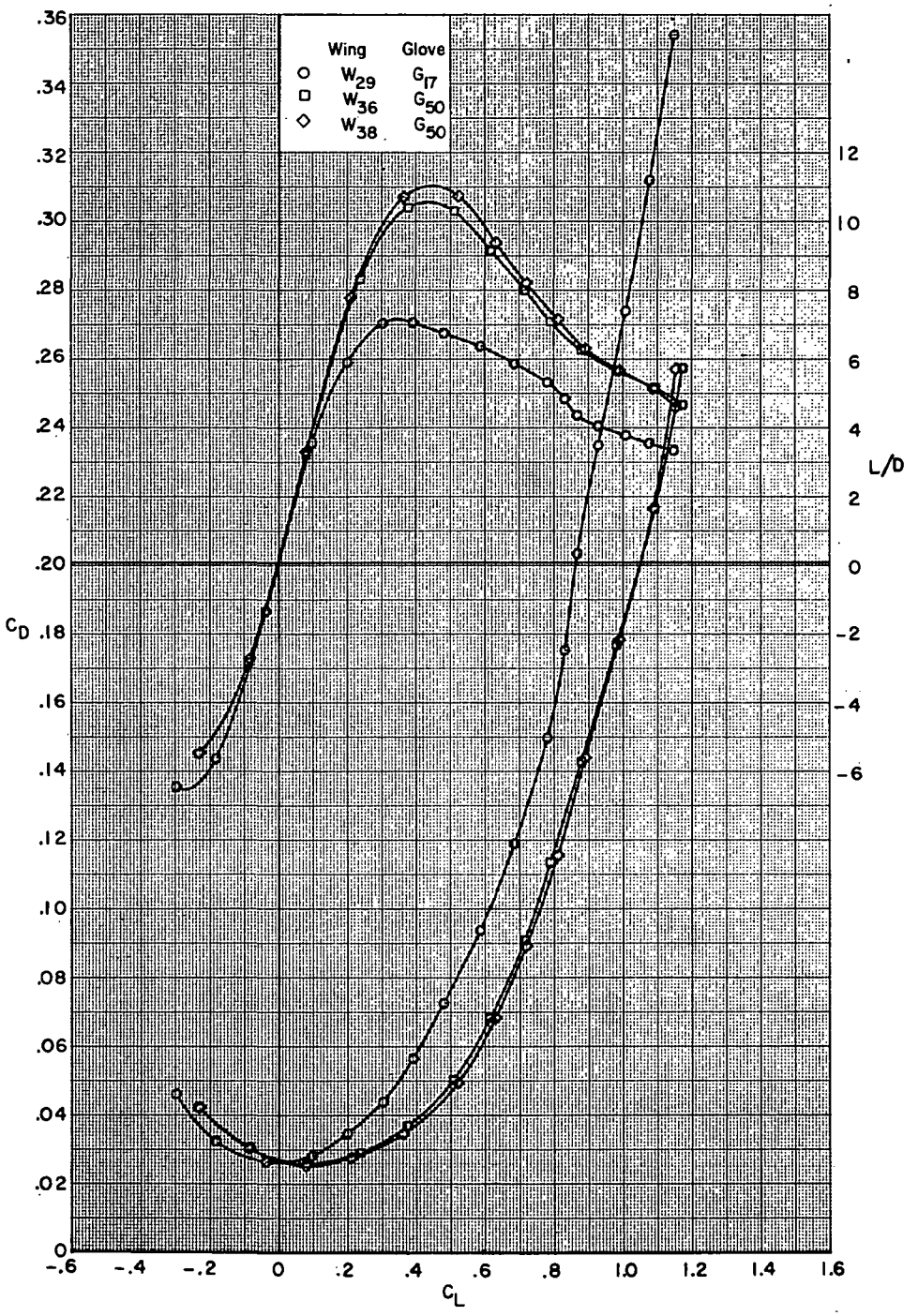

(e) Concluded.

Figure 15.- Continued.

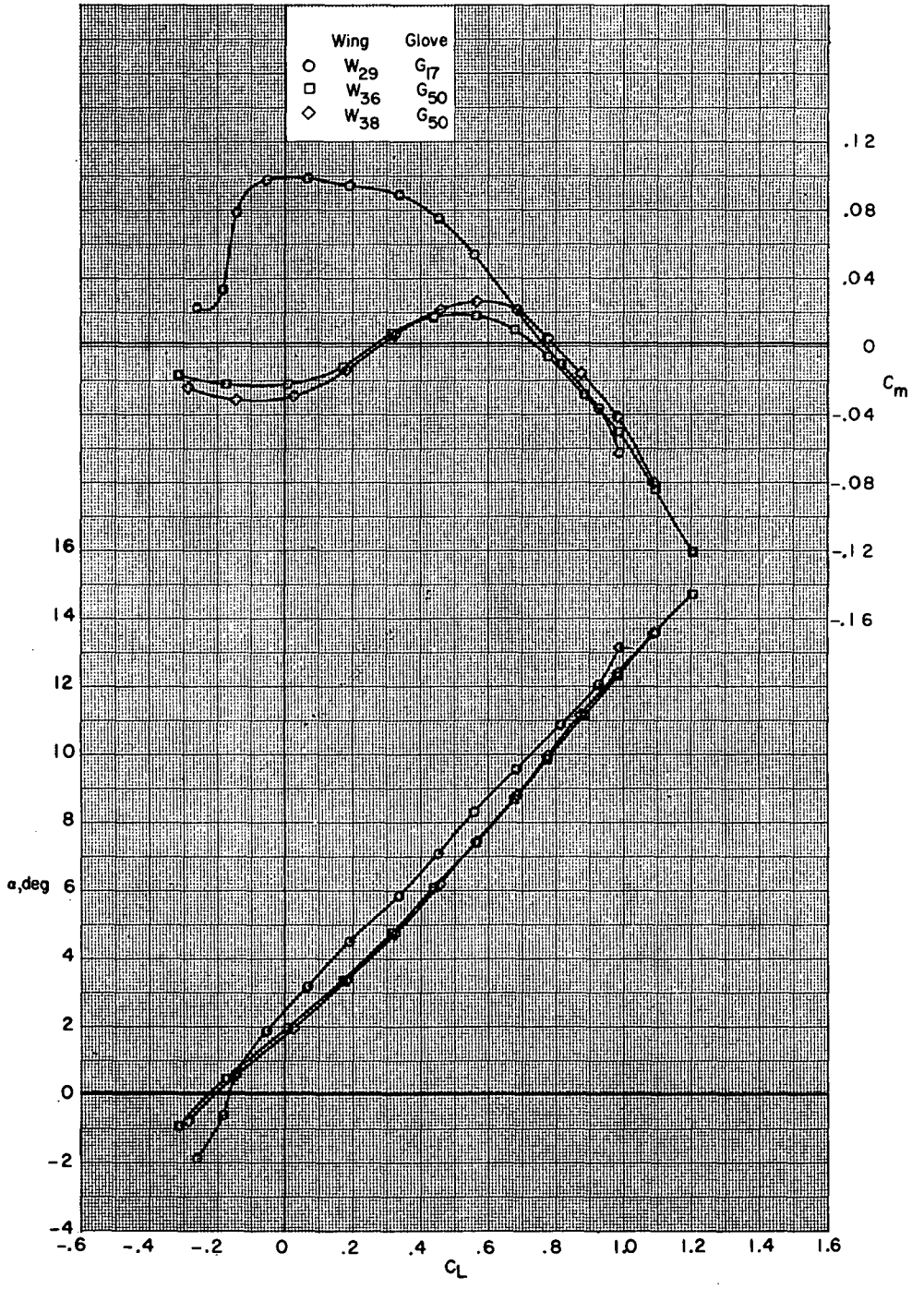

(f) M = 0.90.

Figure 15.- Continued.

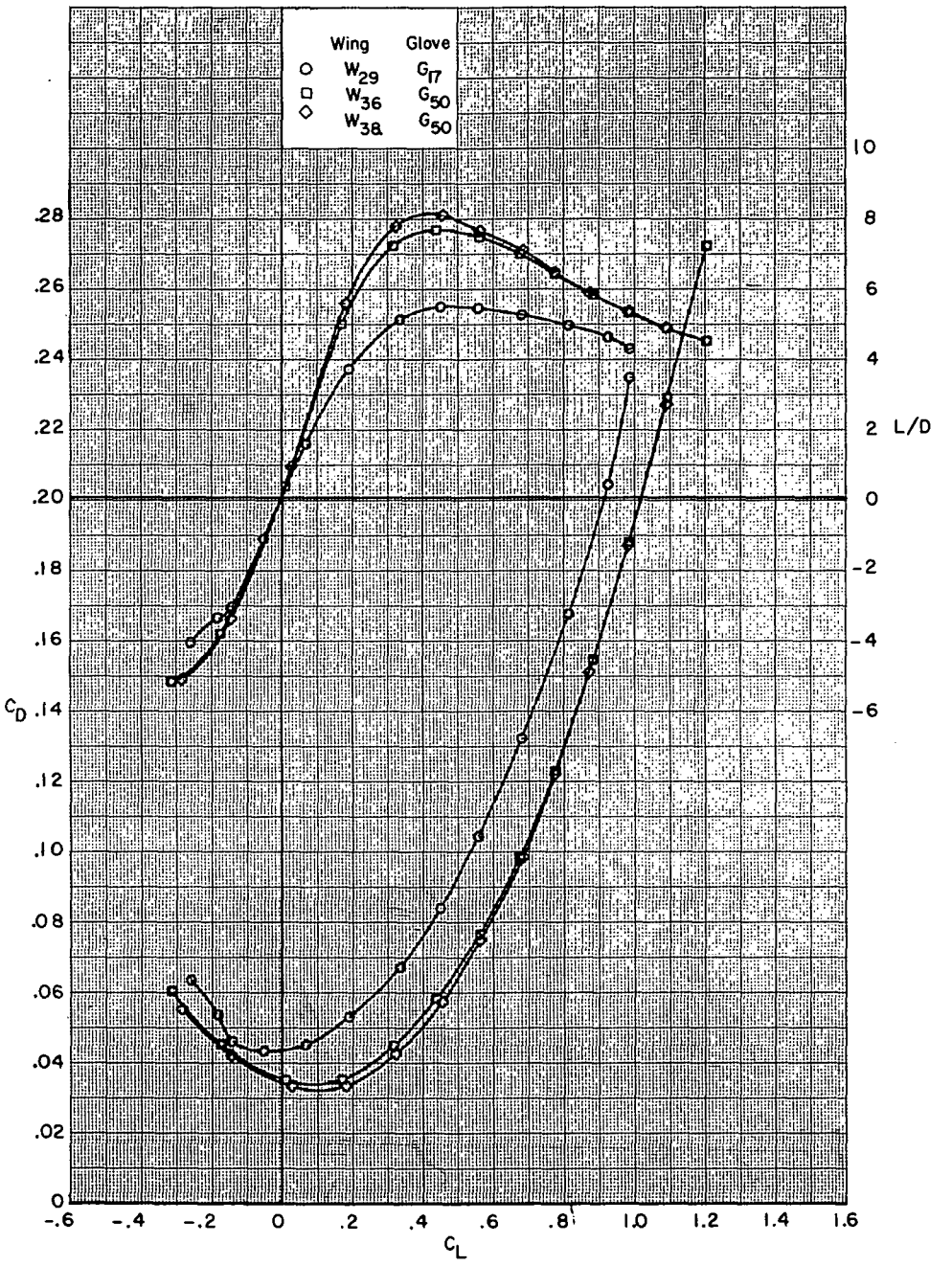

(f) Concluded.

Figure 15.- Concluded.

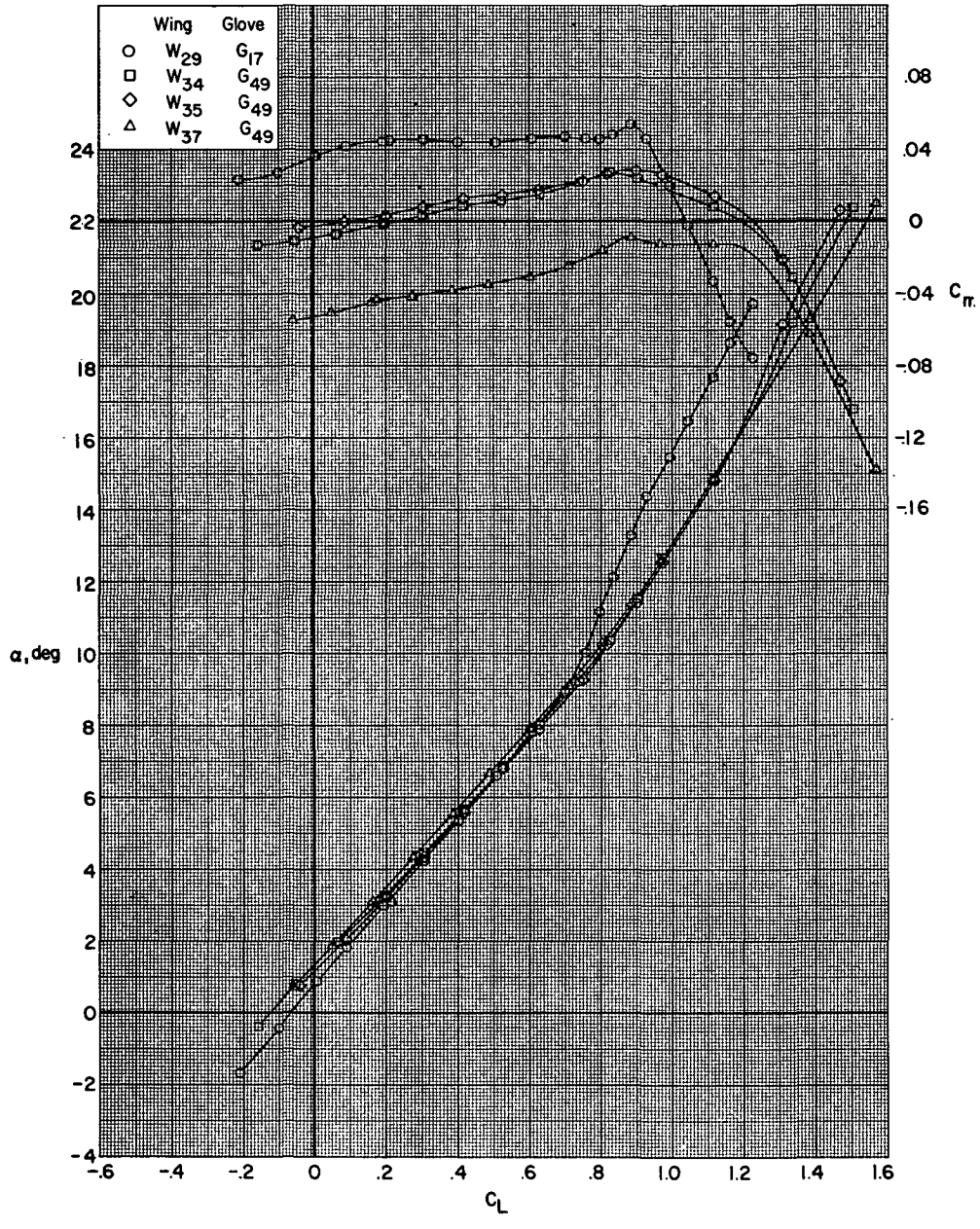

(a) M = 0.60.

Figure 16.- Effect of wing planform and airfoil on aerodynamic characteristics for configurations $B_{80}G_xH_{13}I_{71}N^b_{32}V_{29}V_{38}W_xX_{24}$ with wing swept 26.0°.

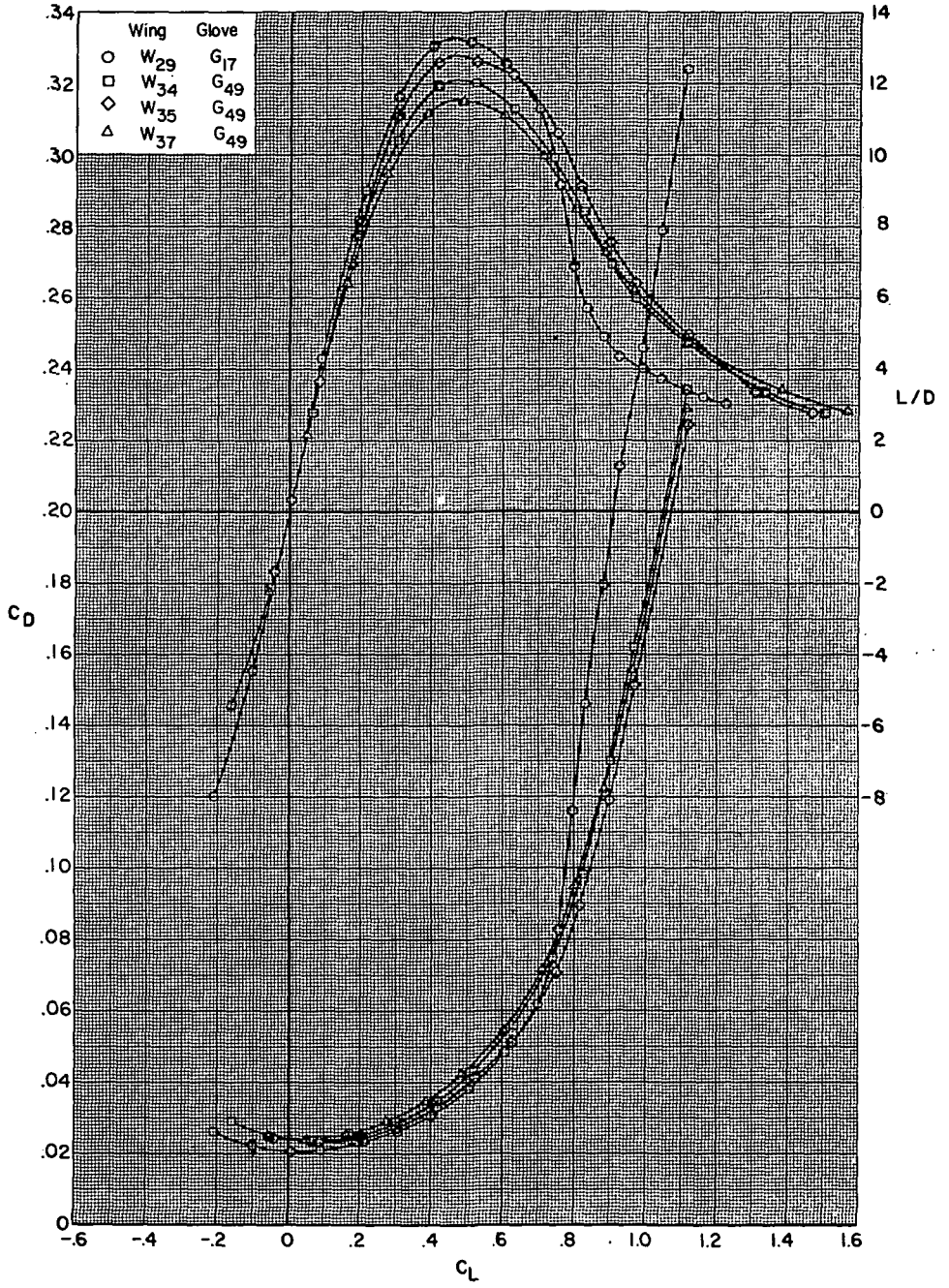

(a) Concluded.

Figure 16.- Continued.

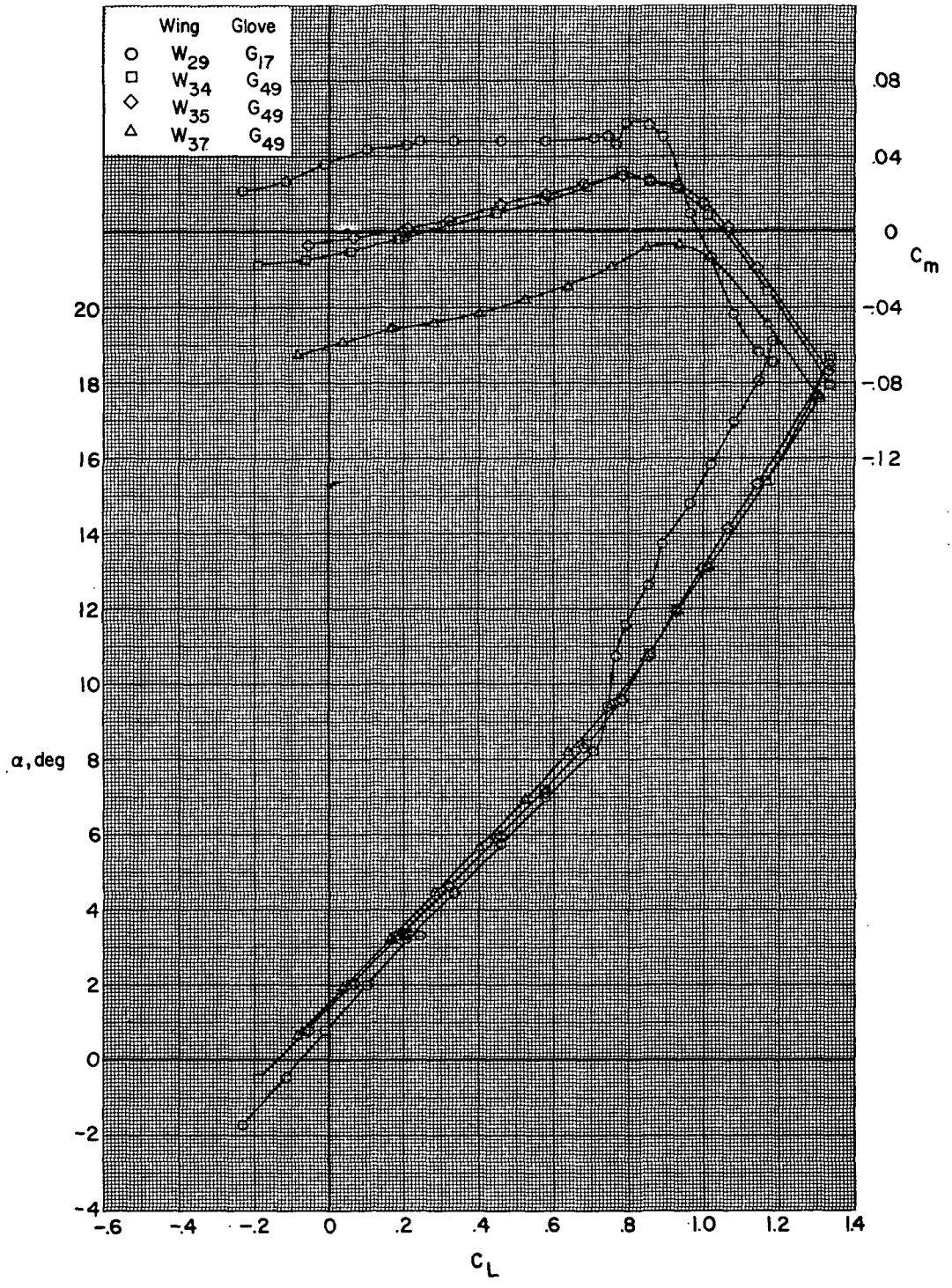

(b) M = 0.70.

Figure 16.- Continued.

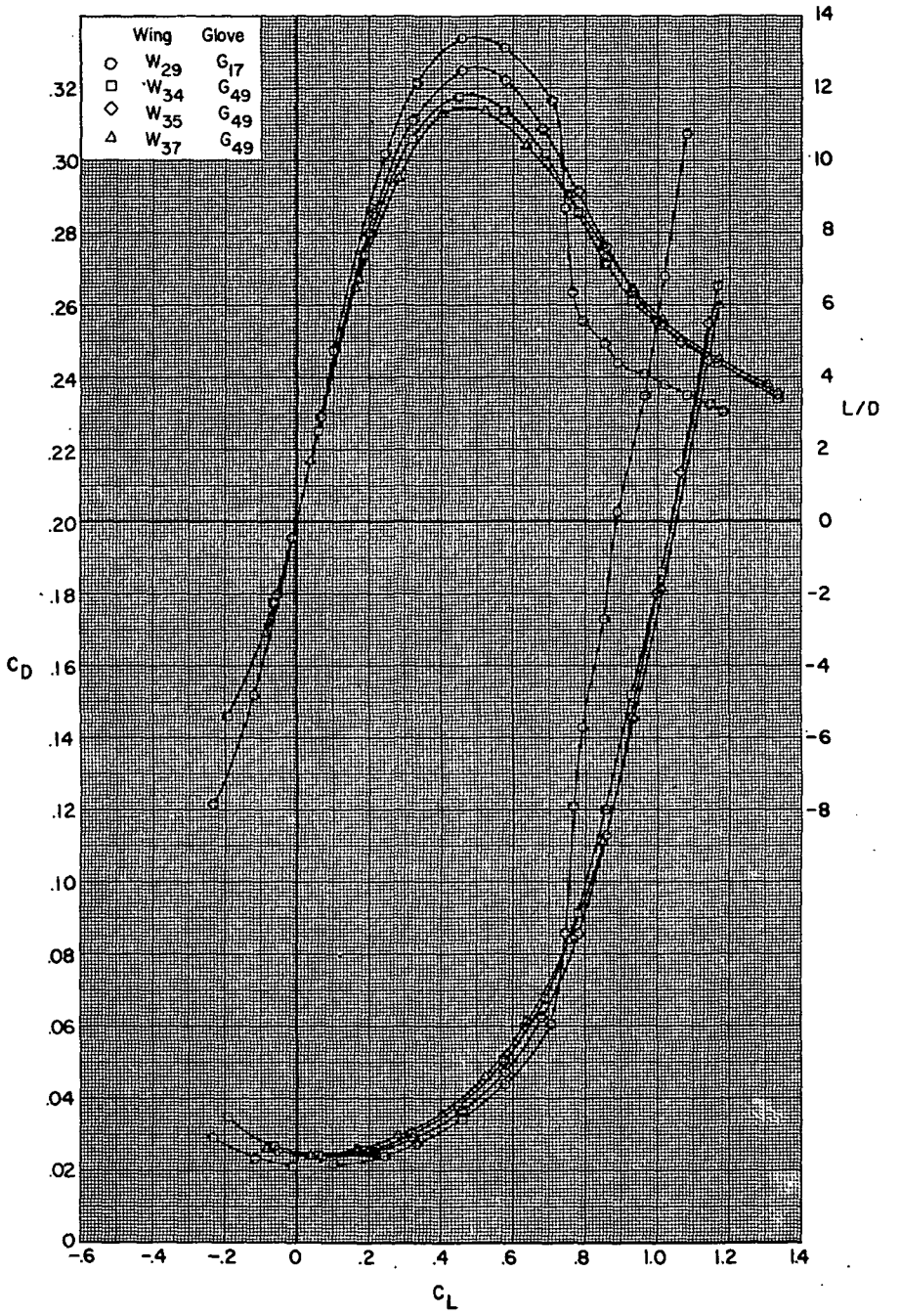

(b) Concluded.

Figure 16.- Continued.

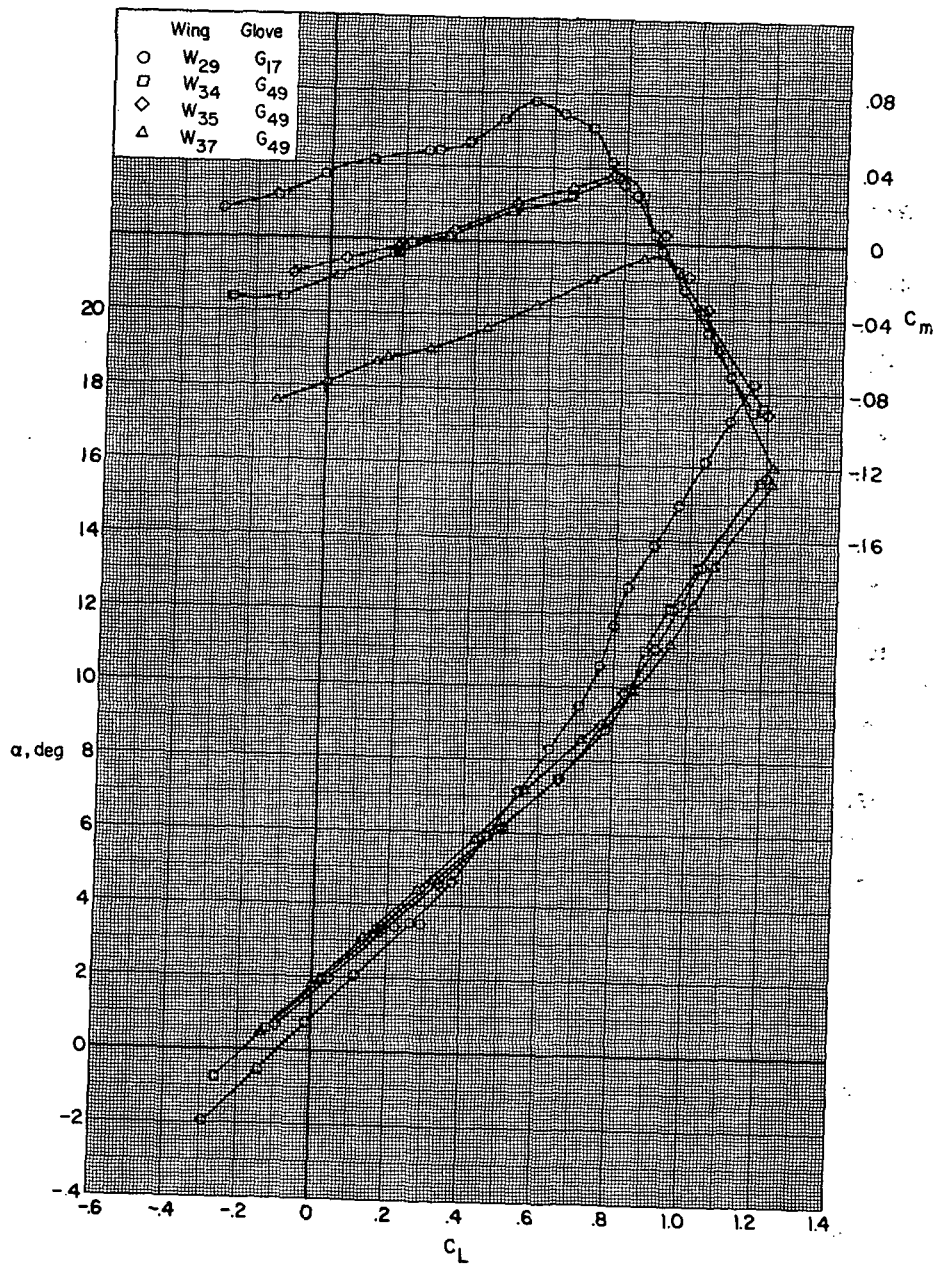

(c) M = 0.80.

Figure 16.- Continued.

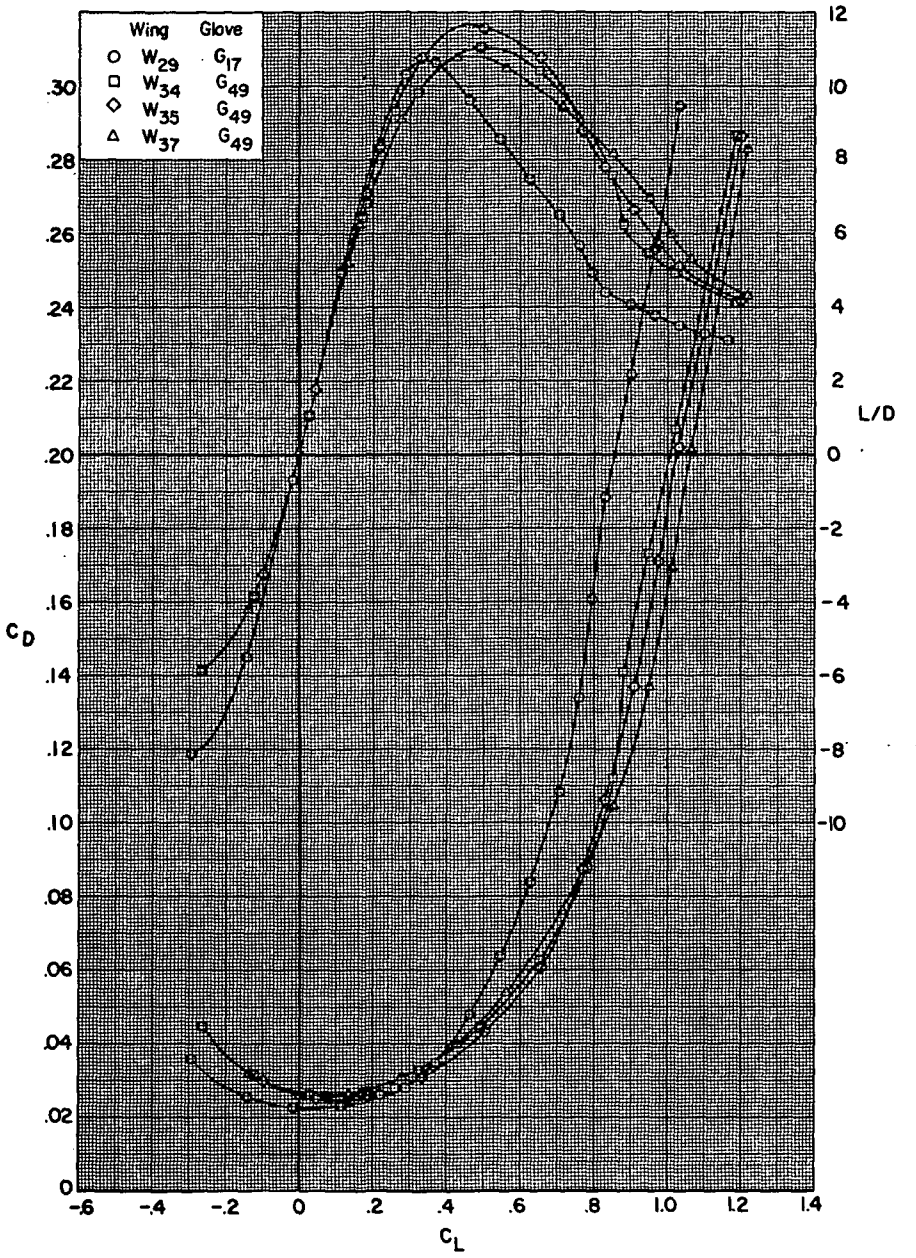

(c) Concluded.

Figure 16.- Continued.

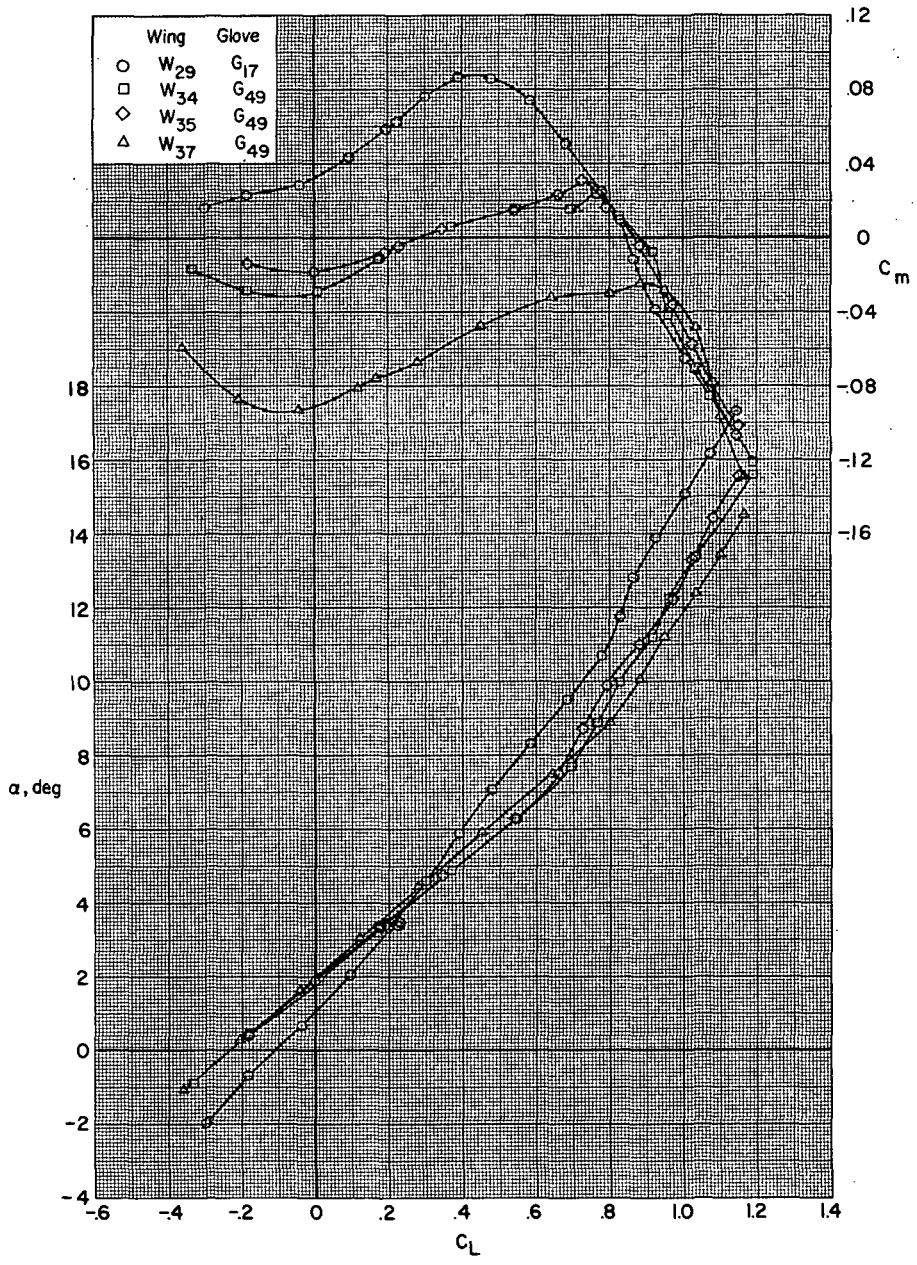

(d) M = 0.85.

Figure 16.- Continued.

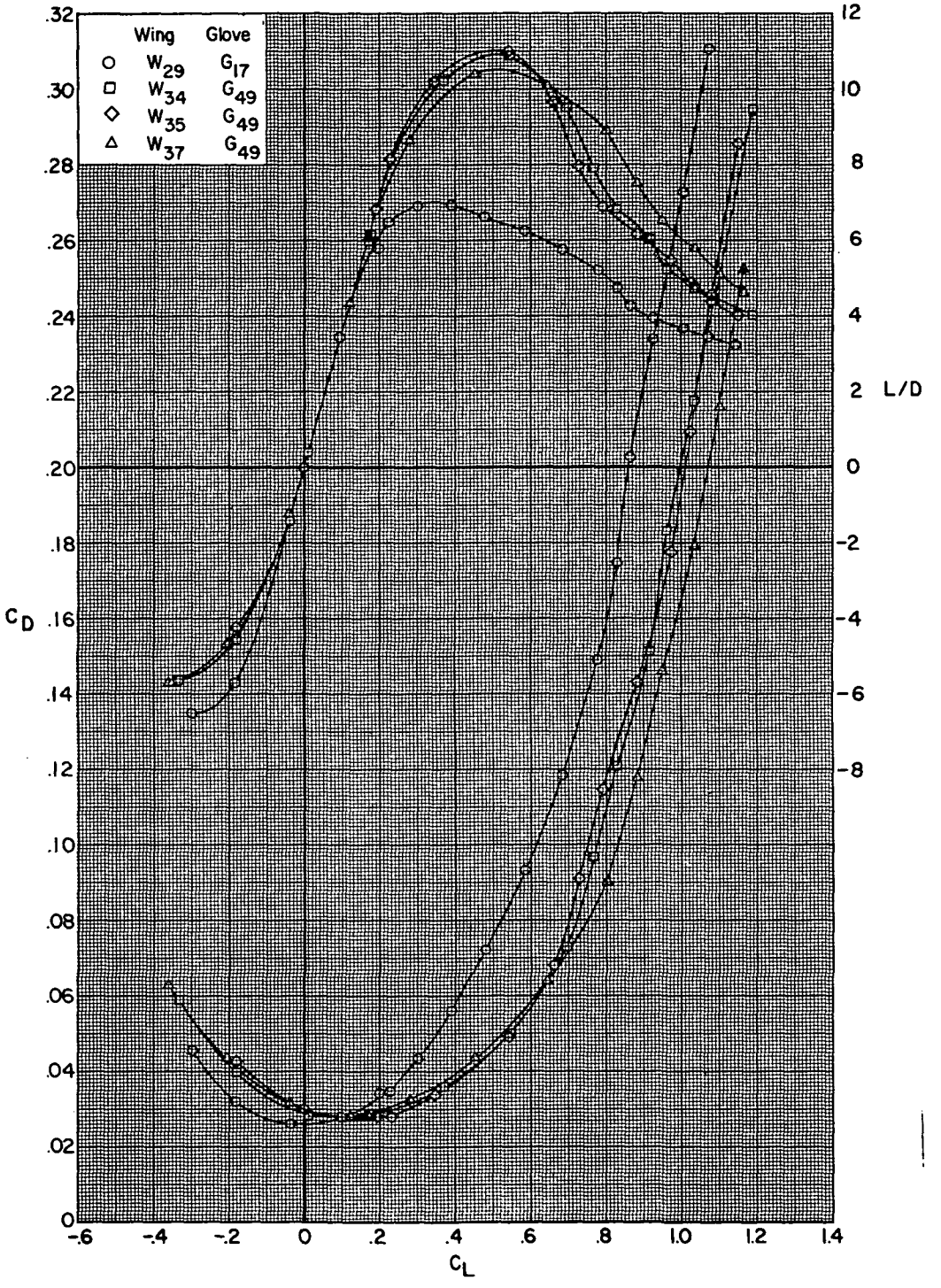

(d) Concluded.

Figure 16.- Continued.

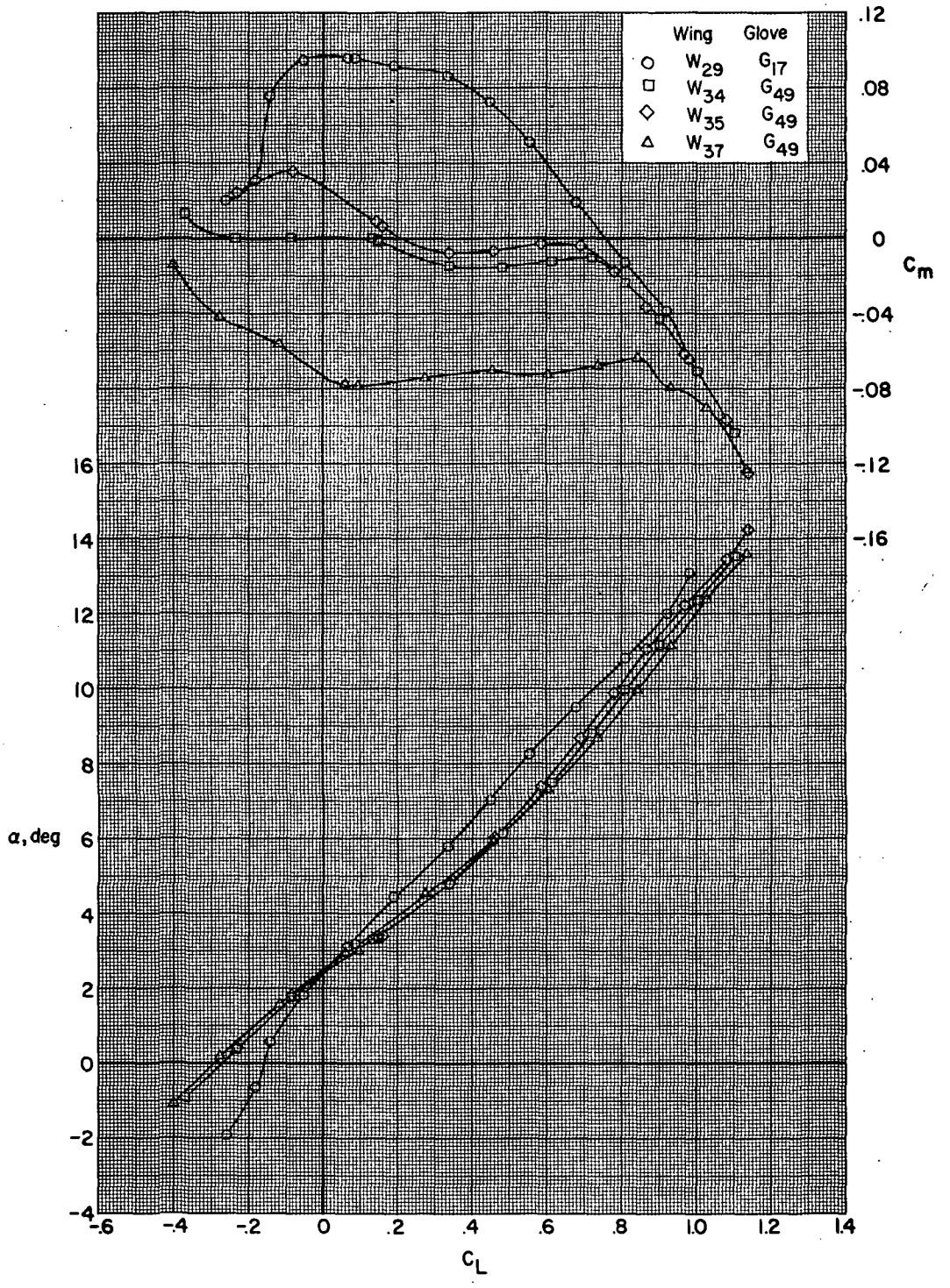

(e) M = 0.90.

Figure 16.- Continued.

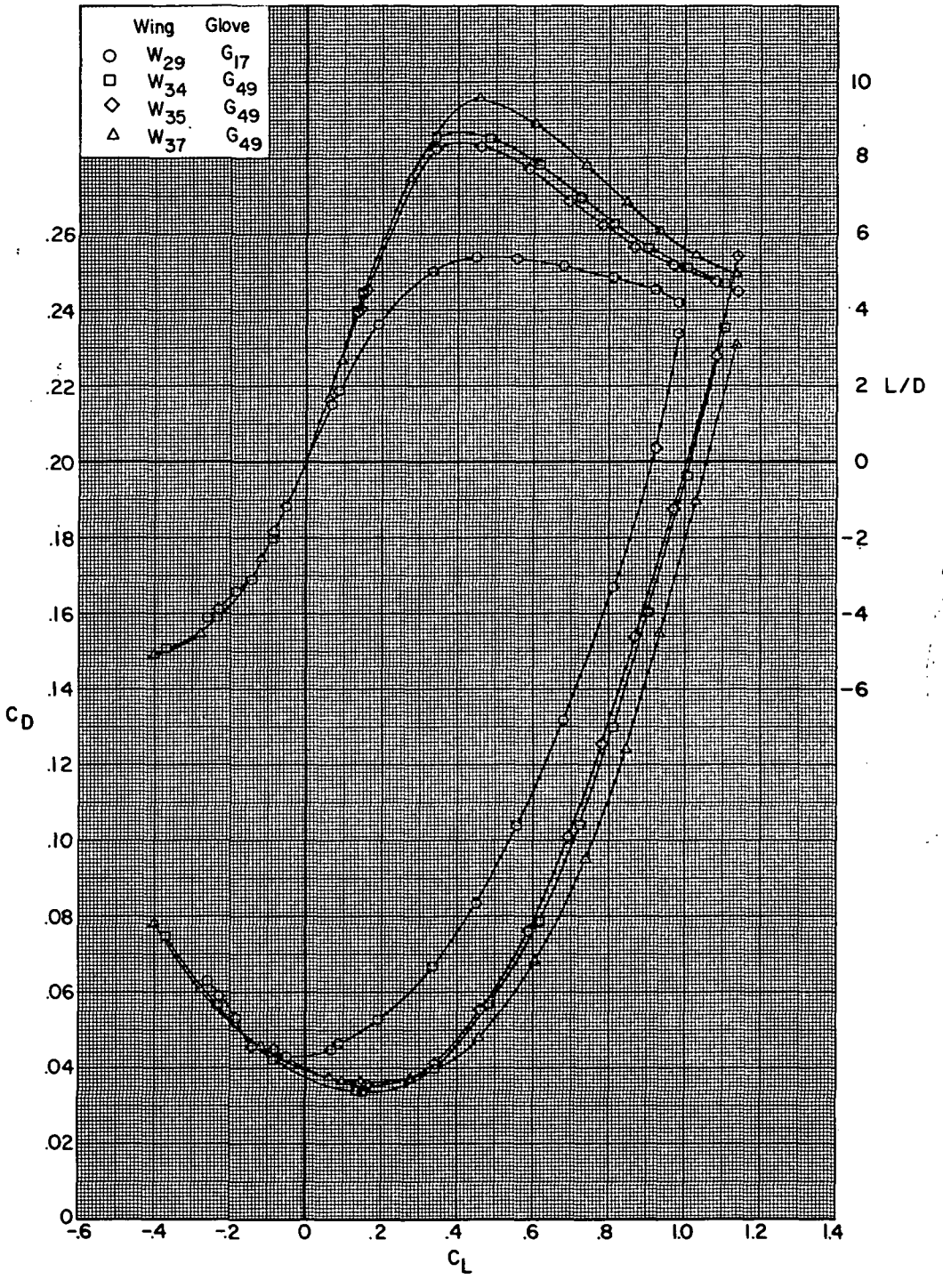

(e) Concluded.

Figure 16.- Concluded.

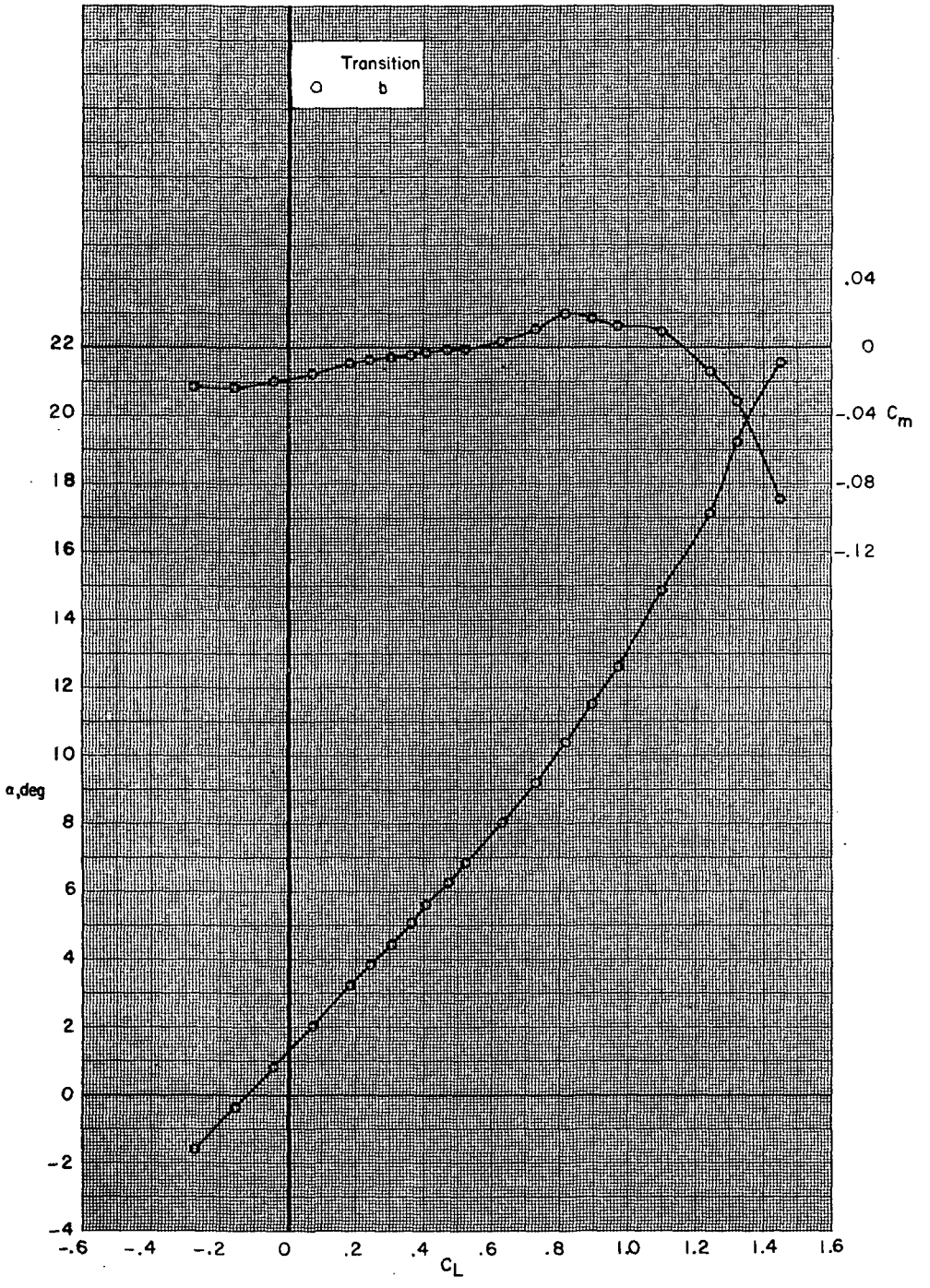

(a) M = 0.60.

Figure 17.- Aerodynamic characteristics for configuration $B_{80}G_{49}H_{13}I_{71}N_{32}^{b}V_{29}V_{38}W_{34e}X_{24}$ with wing swept 26.0°.

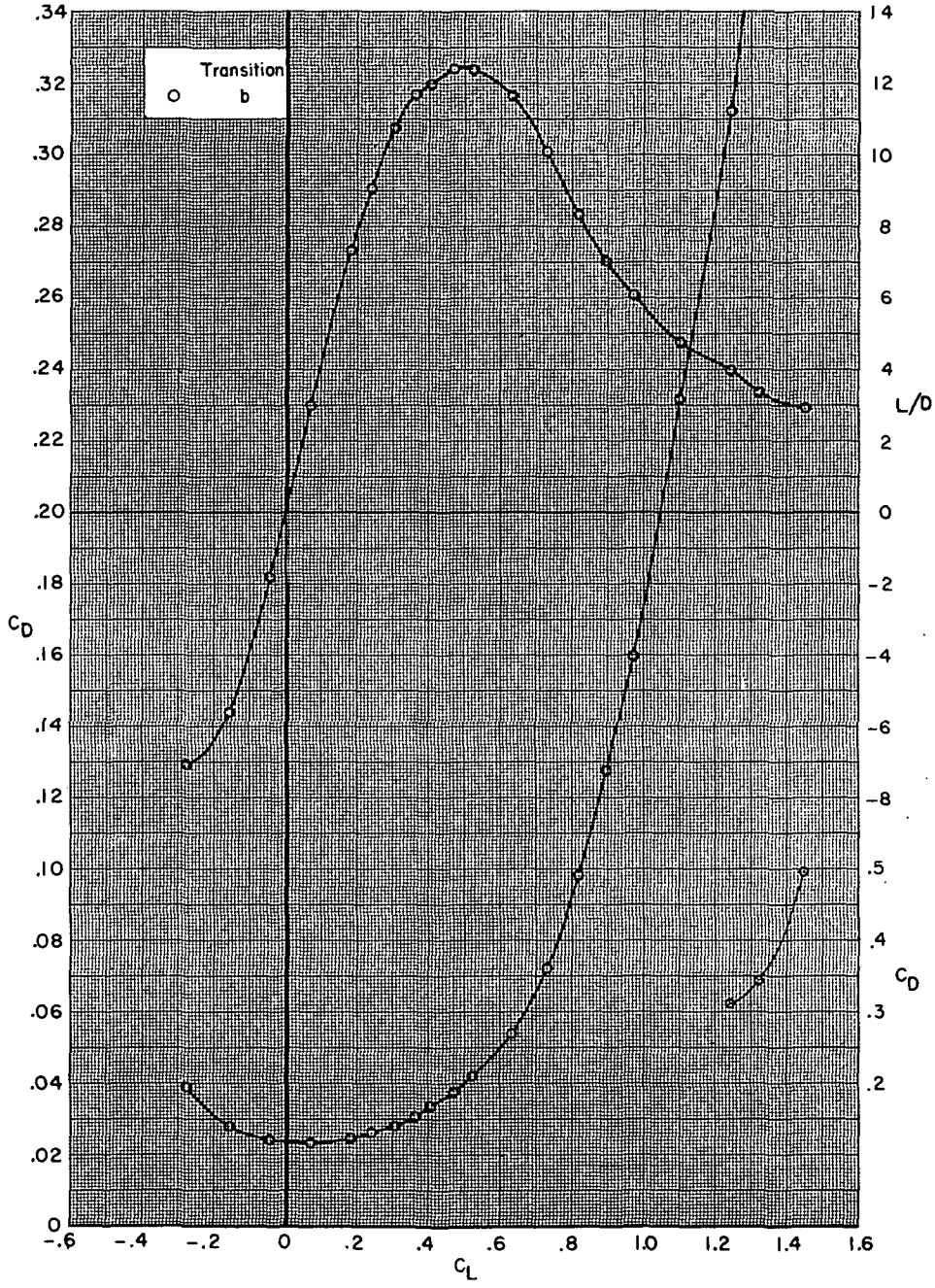

(a) Concluded.

Figure 17.- Continued.

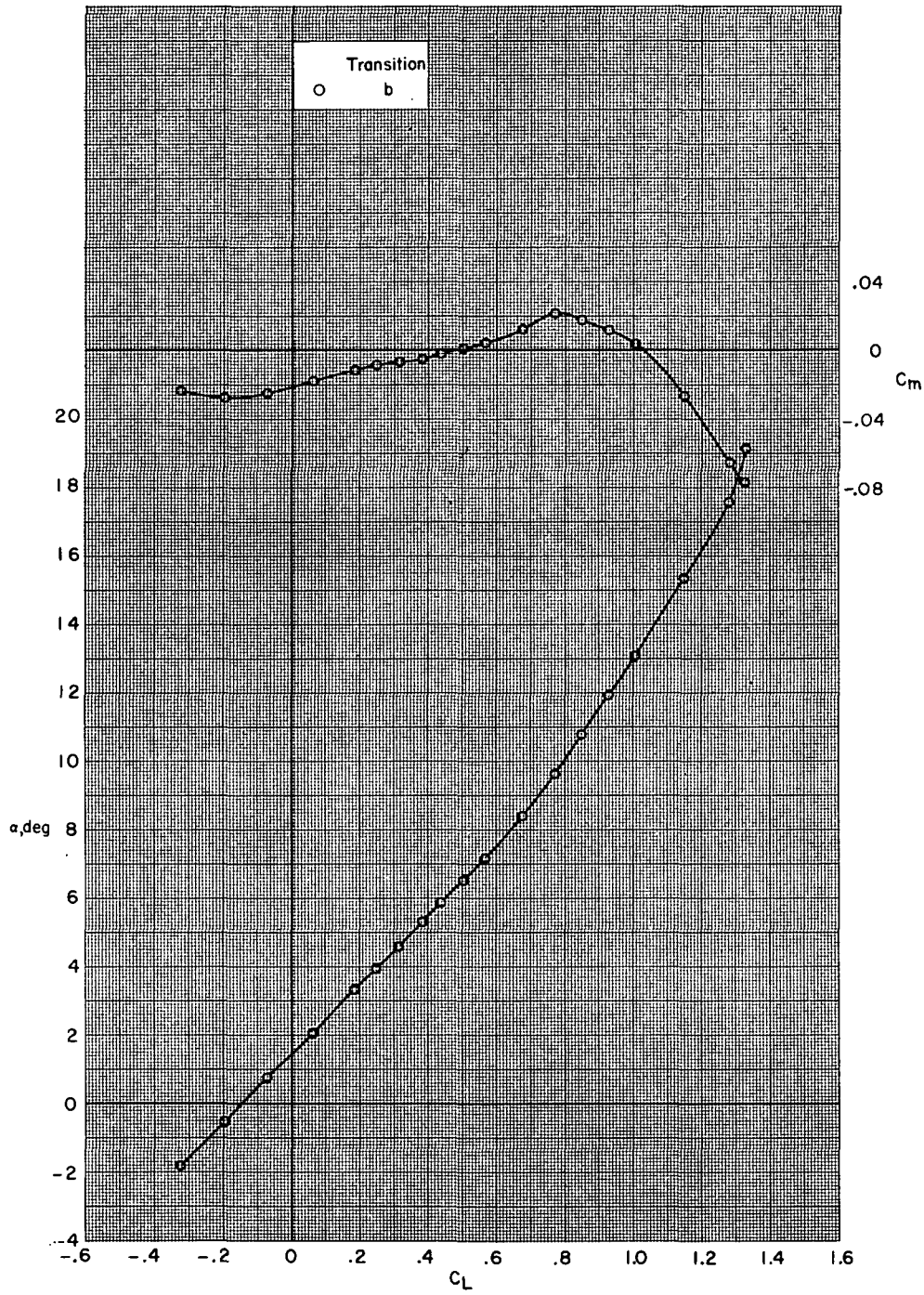

(b) M = 0.70.

Figure 17.- Continued.

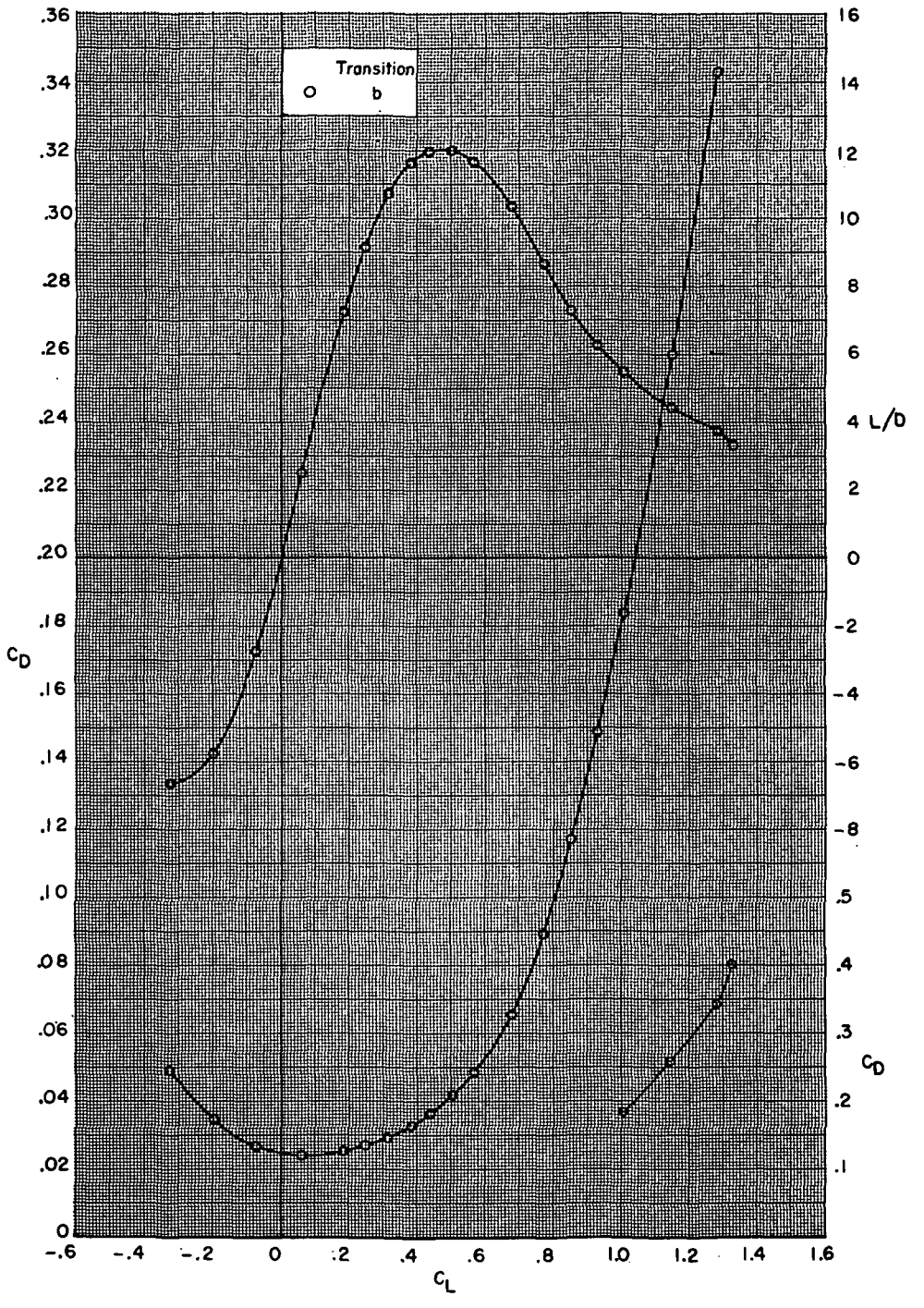

(b) Concluded.

Figure 17.- Continued.

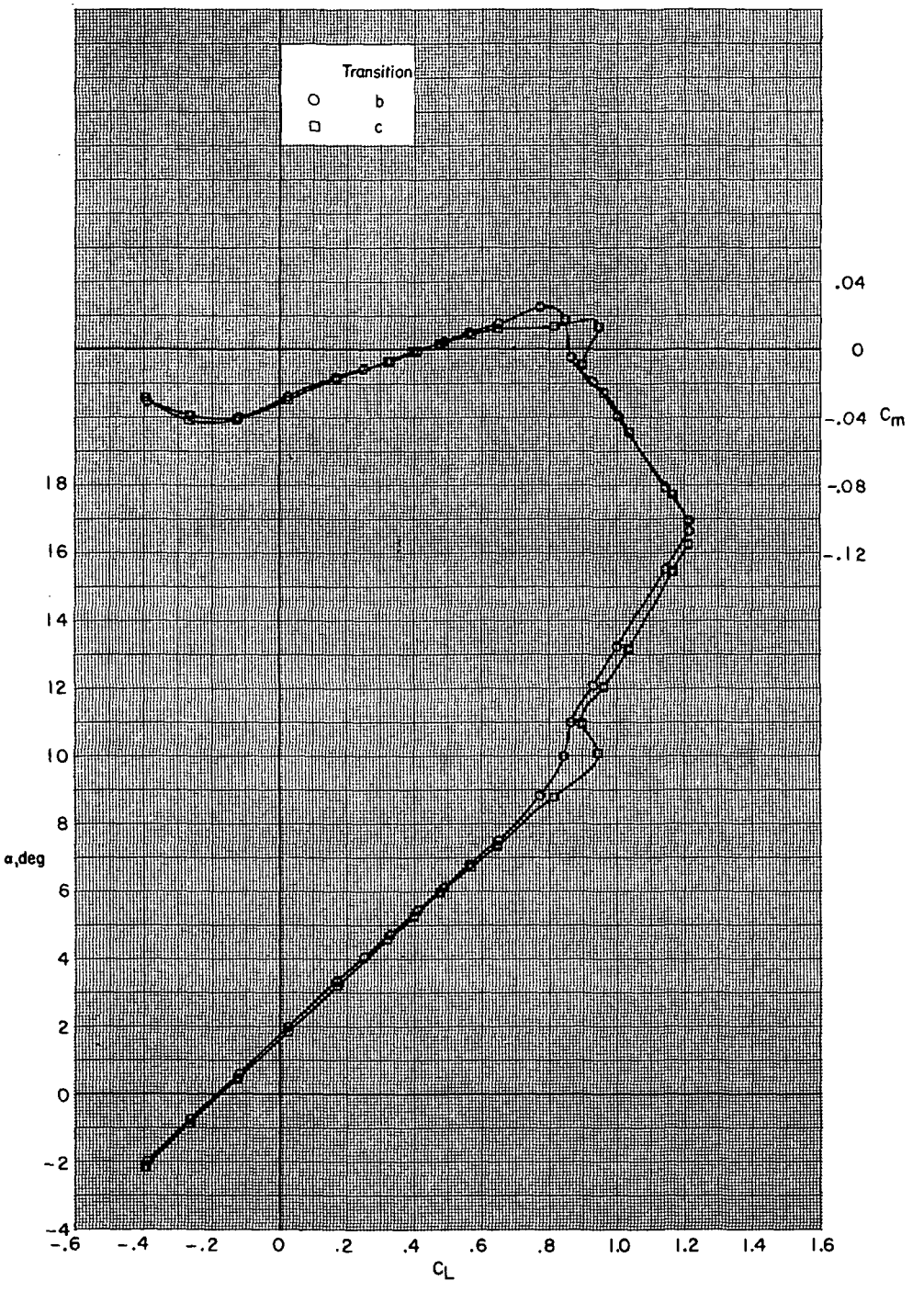

(c) M = 0.80.

Figure 17.- Continued.

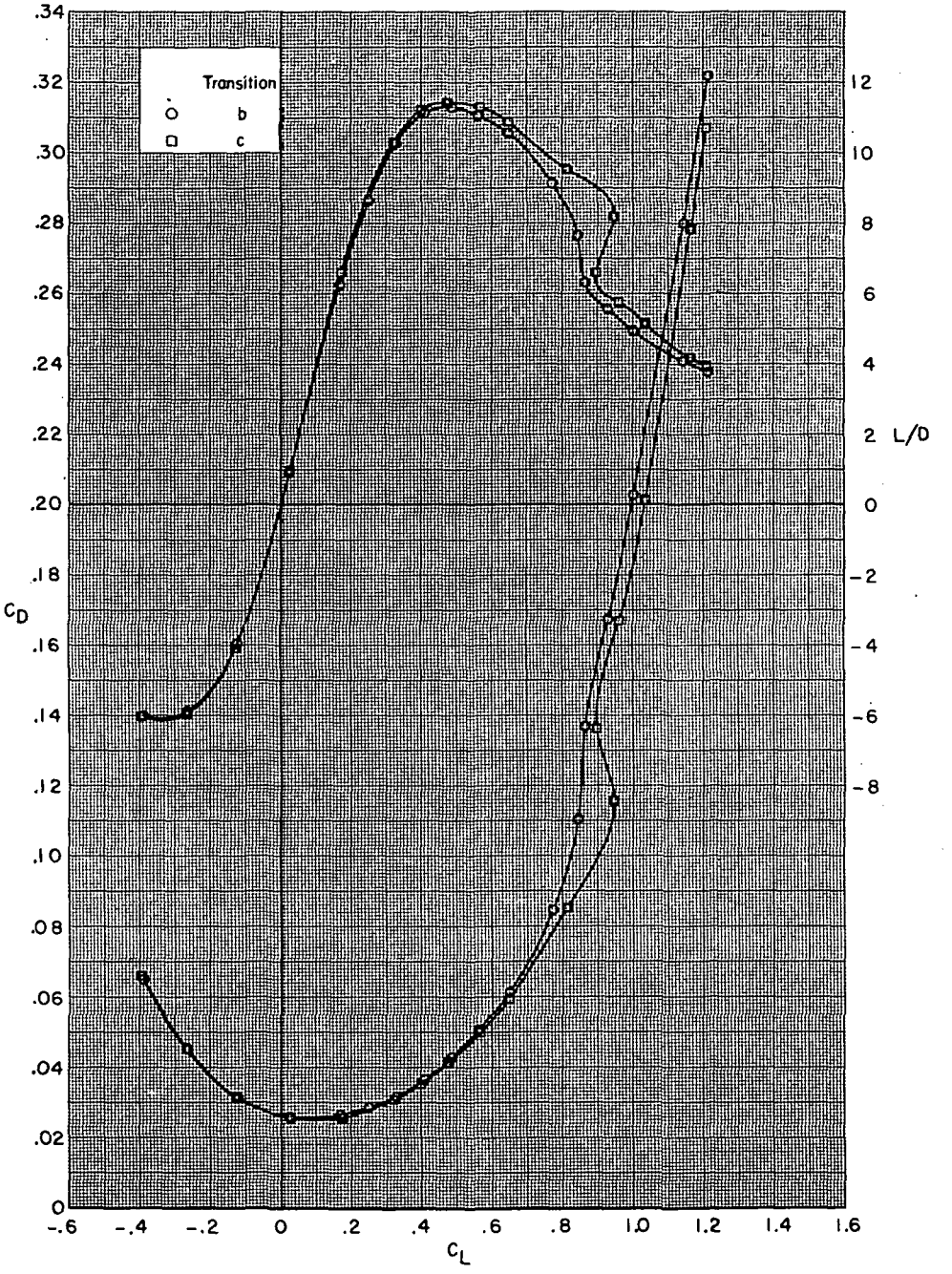

(c) Concluded.

Figure 17.- Continued.

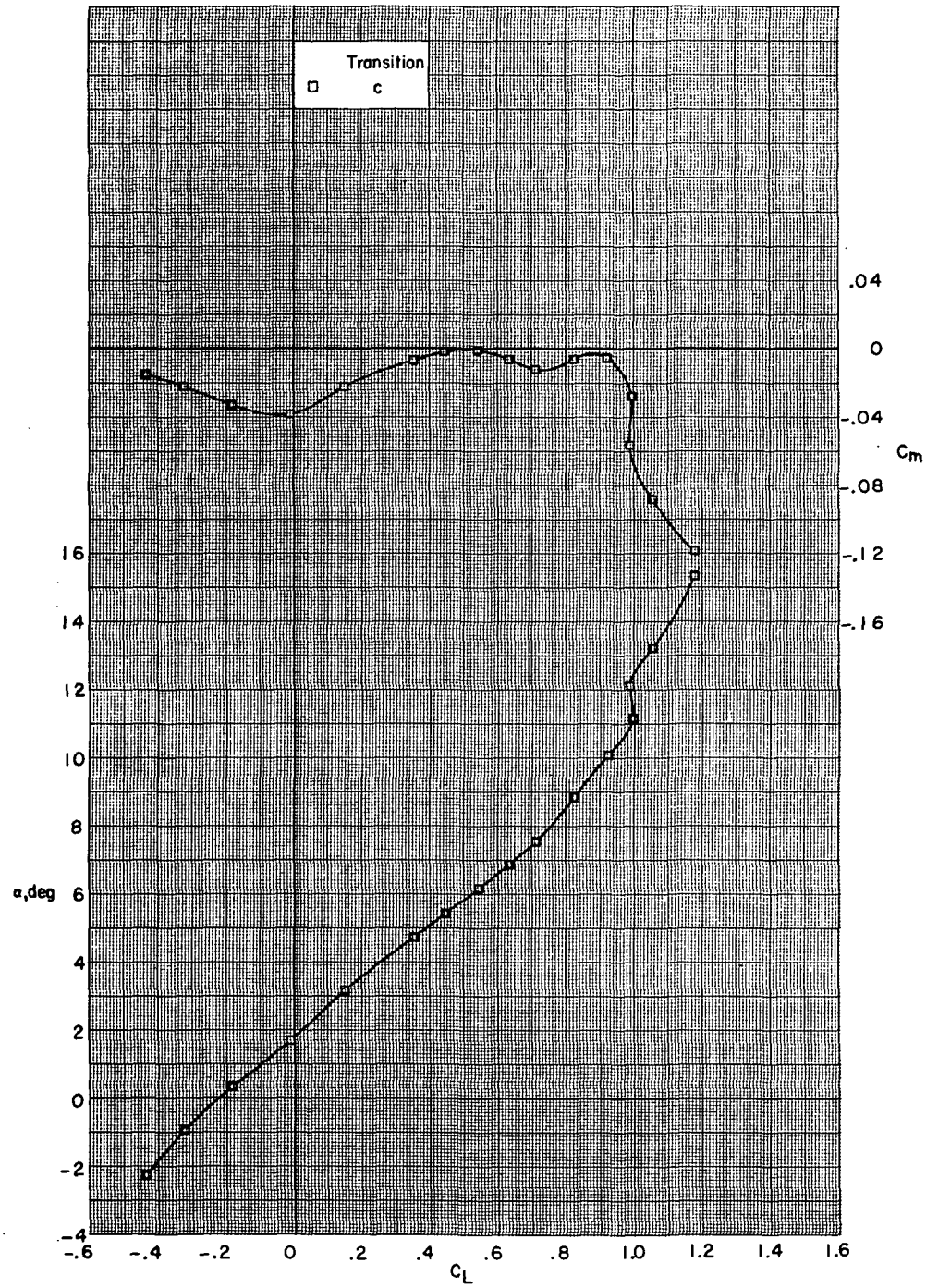

(d) M = 0.85.

Figure 17.- Continued.

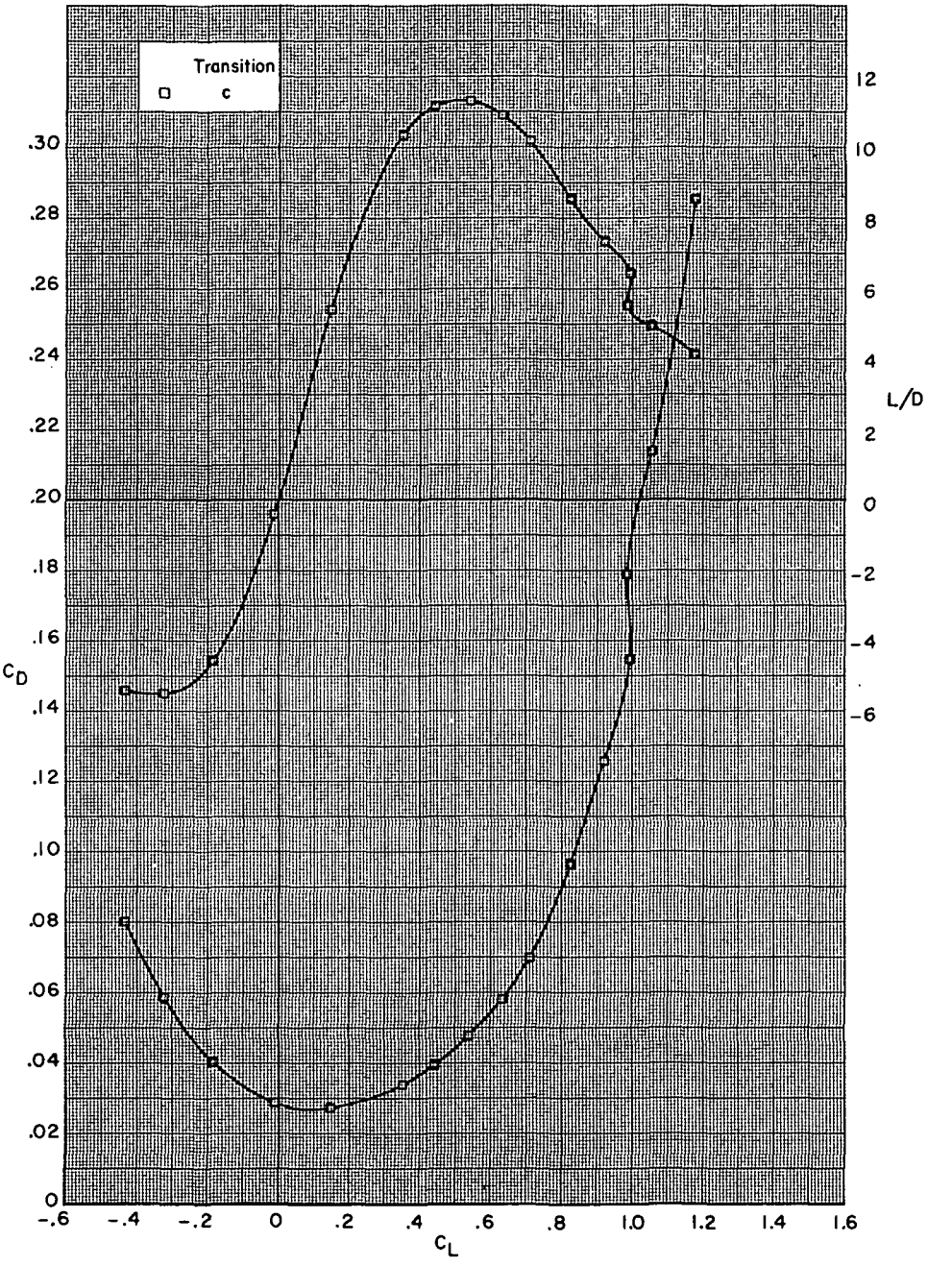

(d) Concluded.

Figure 17.- Continued.

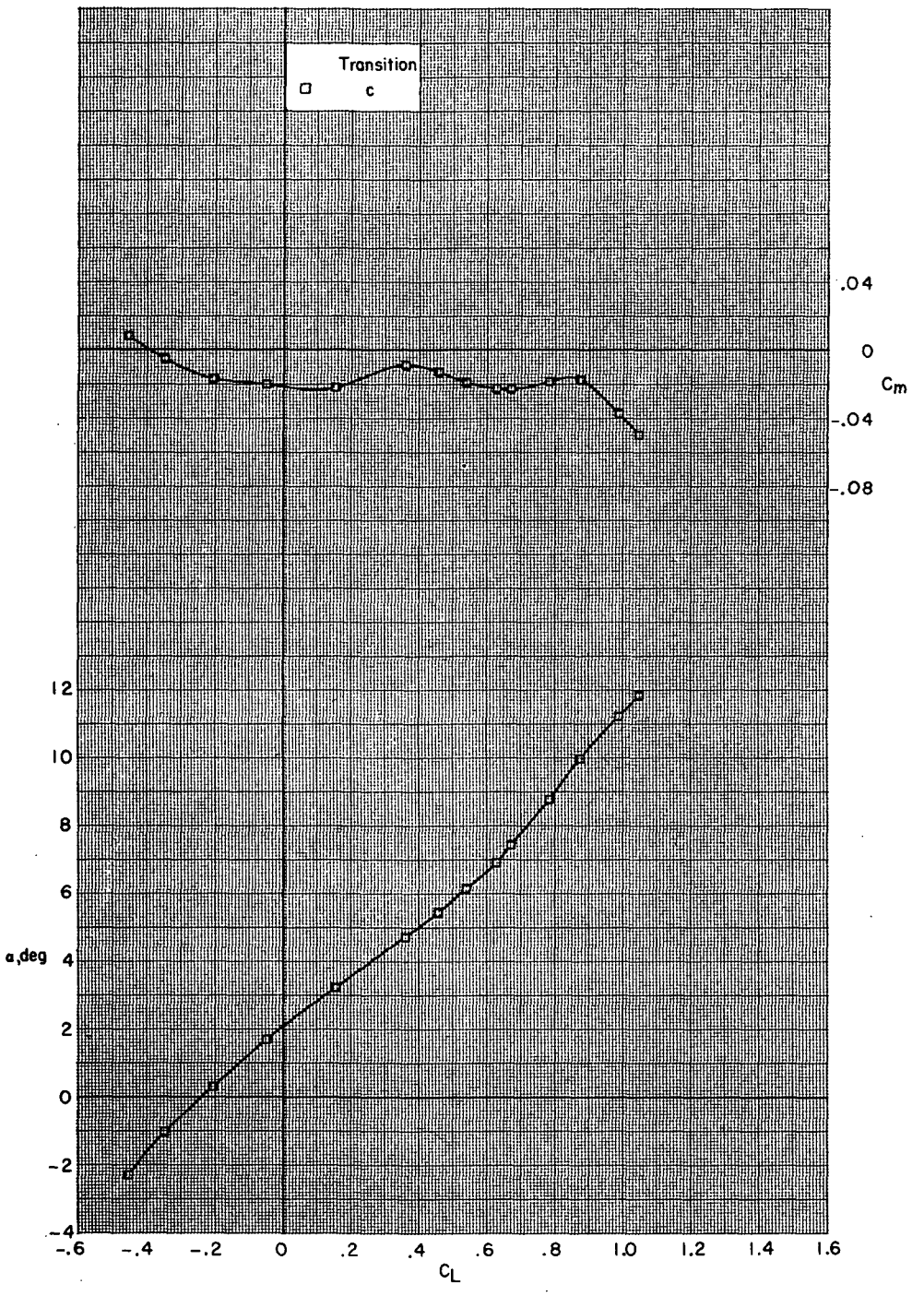

(e) M = 0.875.

Figure 17.- Continued.

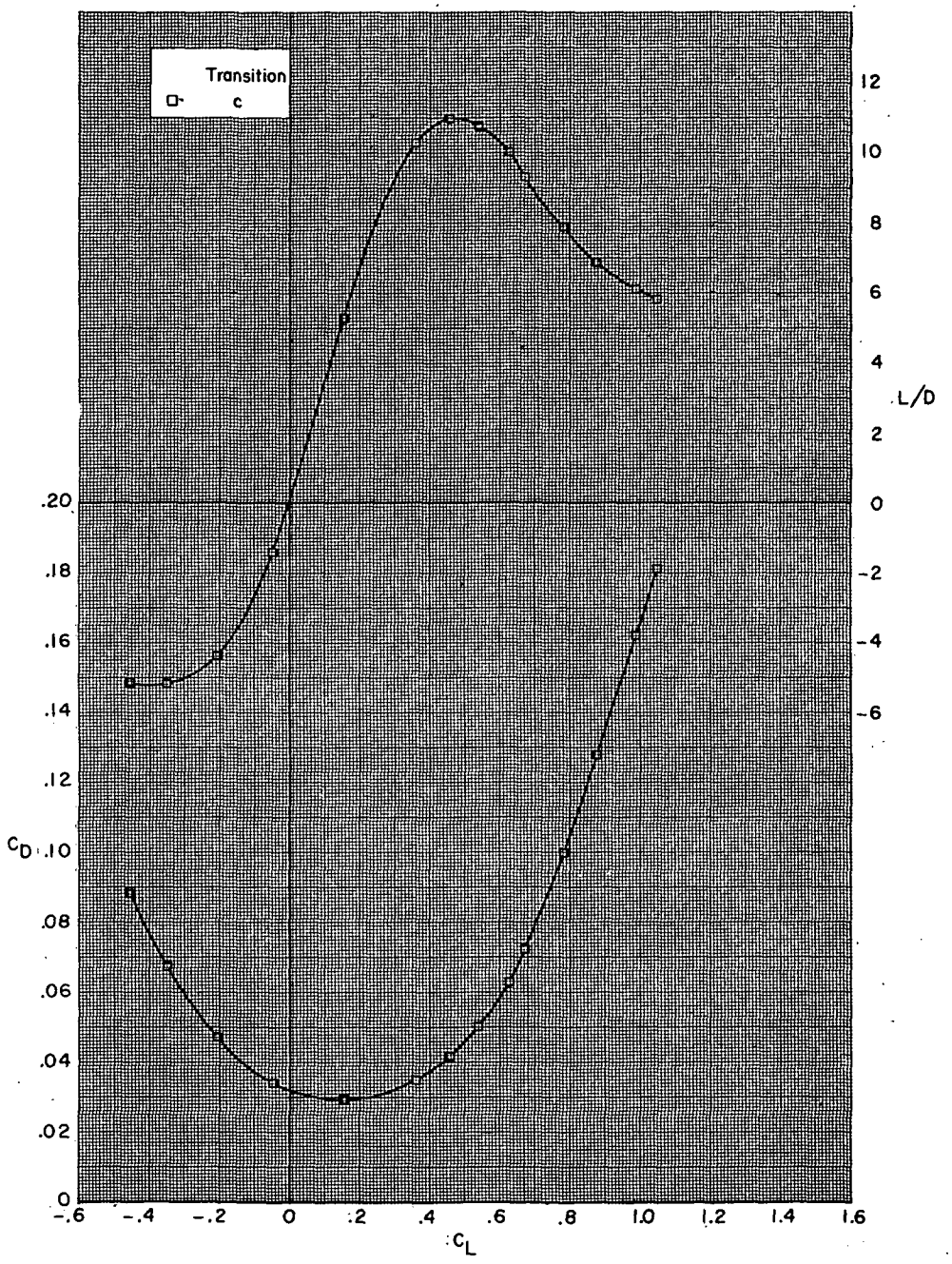

(e) Concluded.

Figure 17.- Continued.

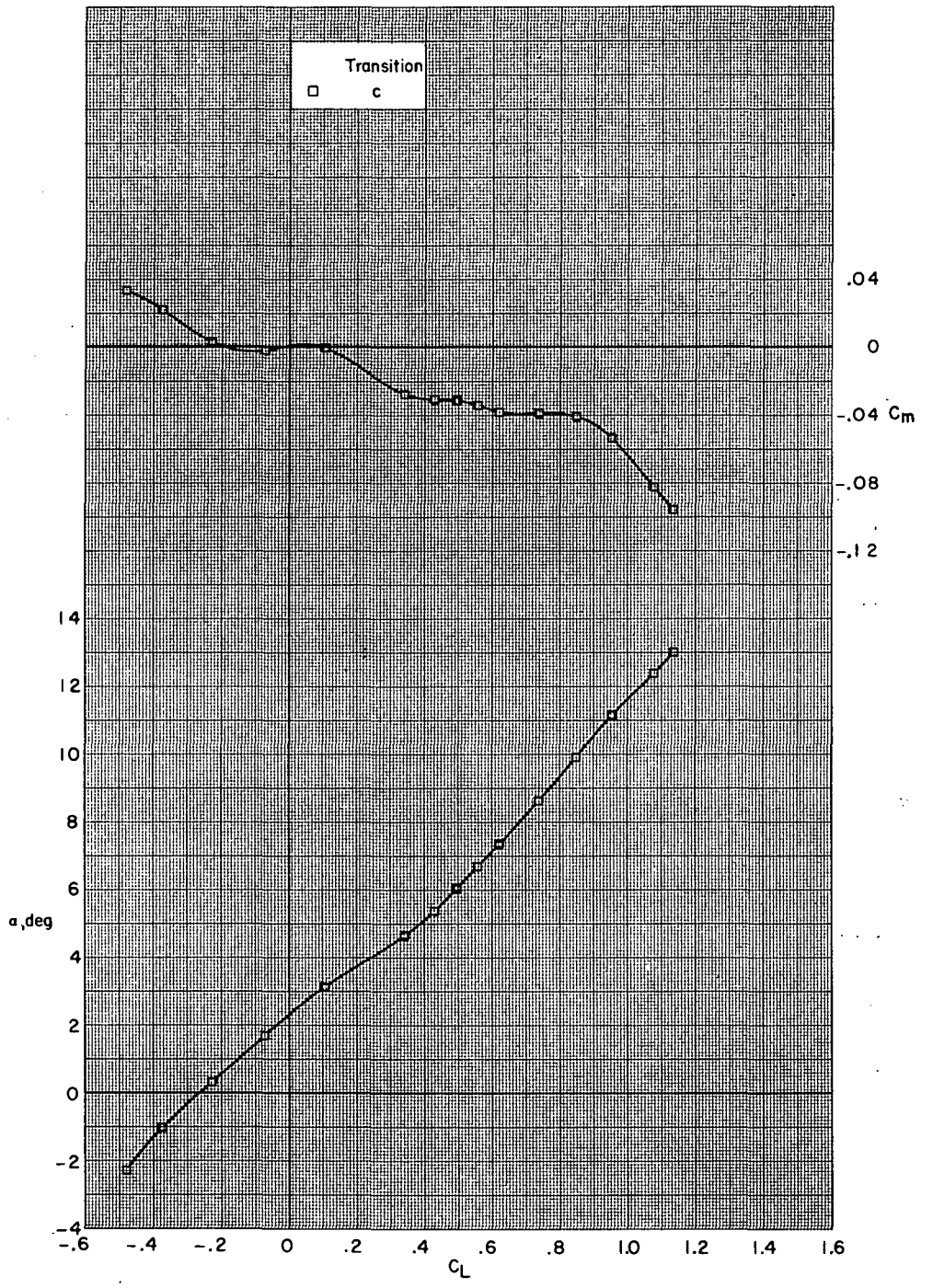

(f) M = 0.90.

Figure 17.- Continued.

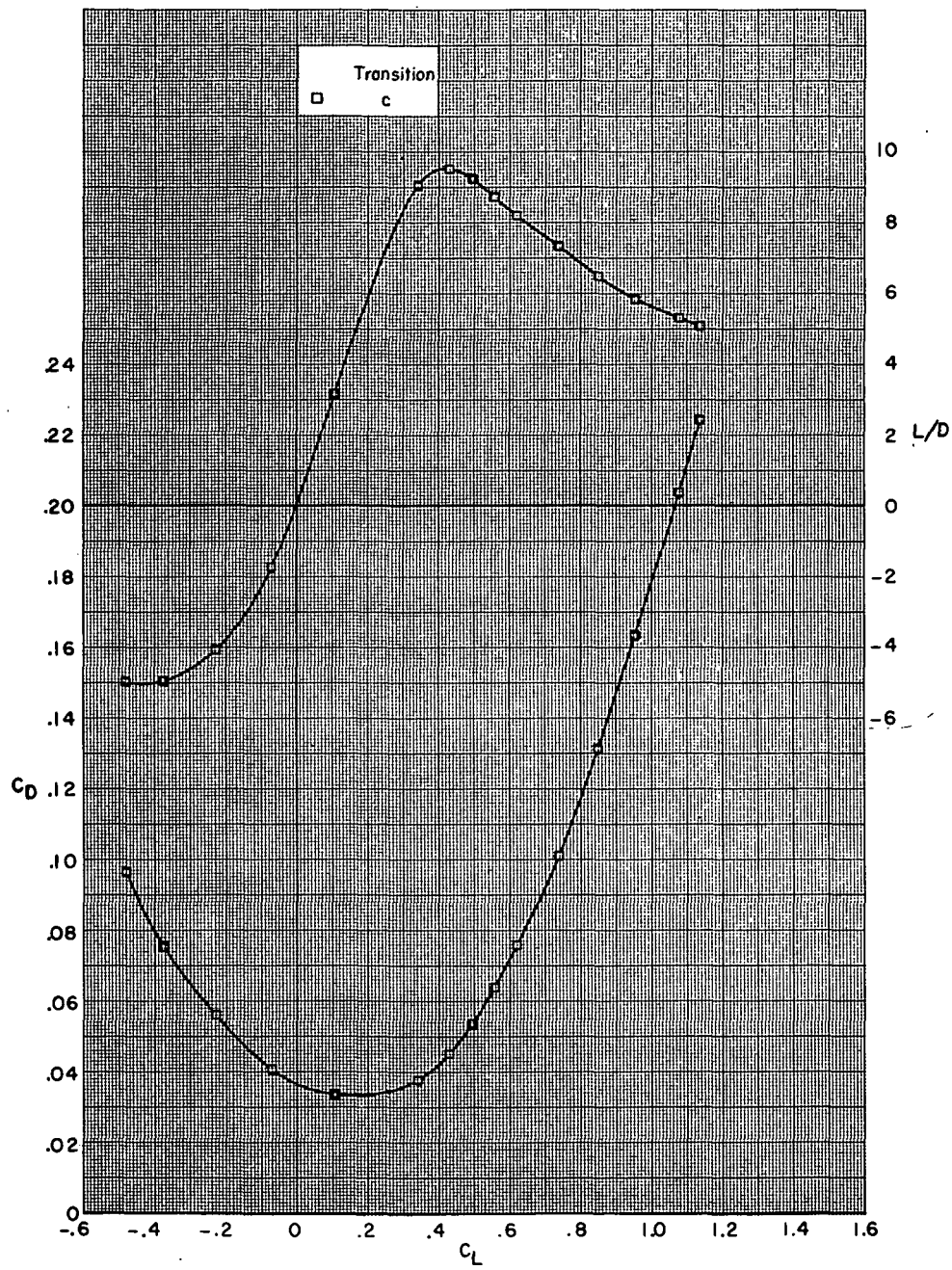

(f) Concluded.

Figure 17.- Concluded.

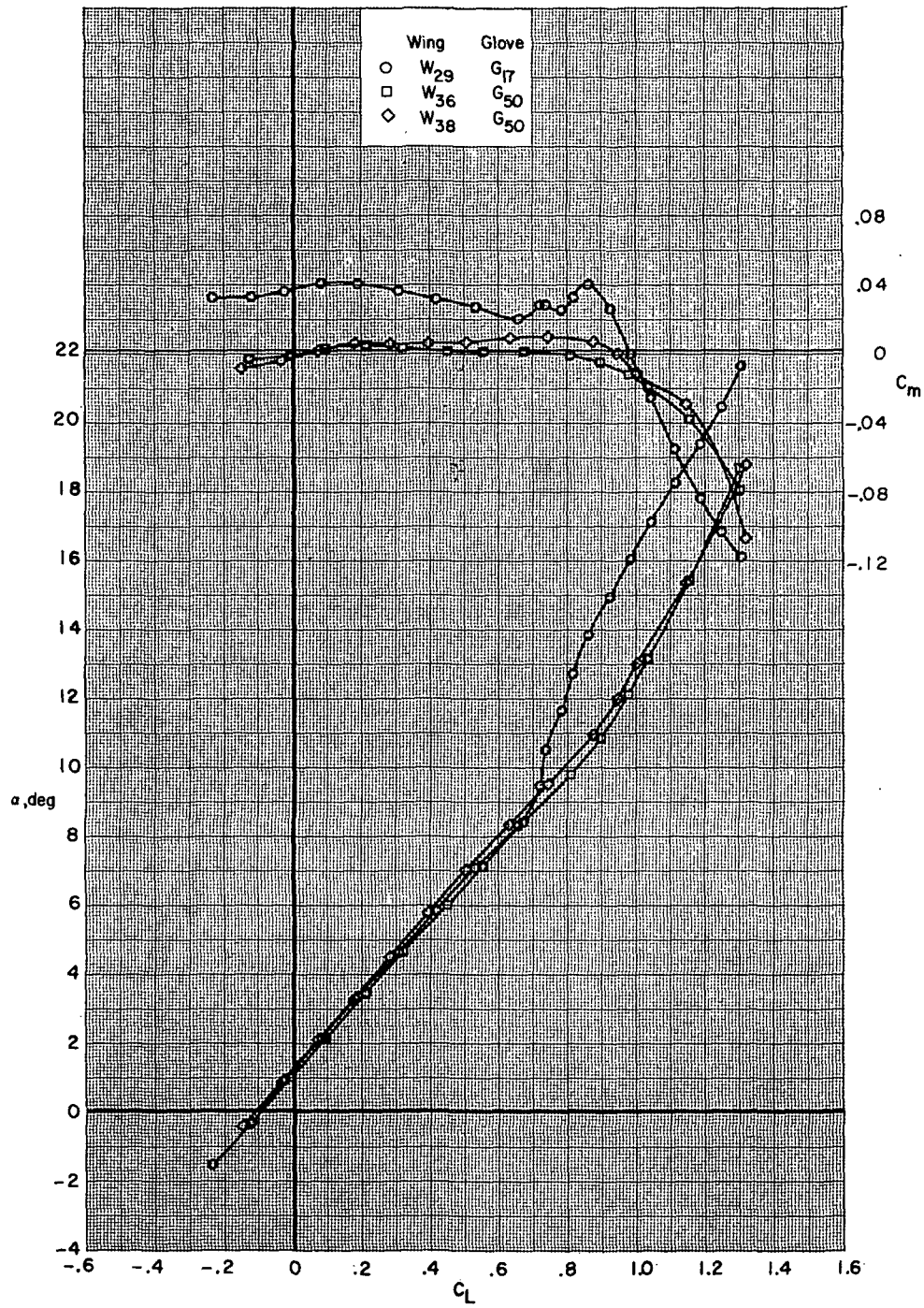

(a) M = 0.70.

Figure 18.- Effect of wing planform on aerodynamic characteristics for conventional wing configurations $B_{80}G_xH_{13}I_{71}N^b_{32}V_{29}V_{38}W_xX_{24}$ with wing swept 30.0°.

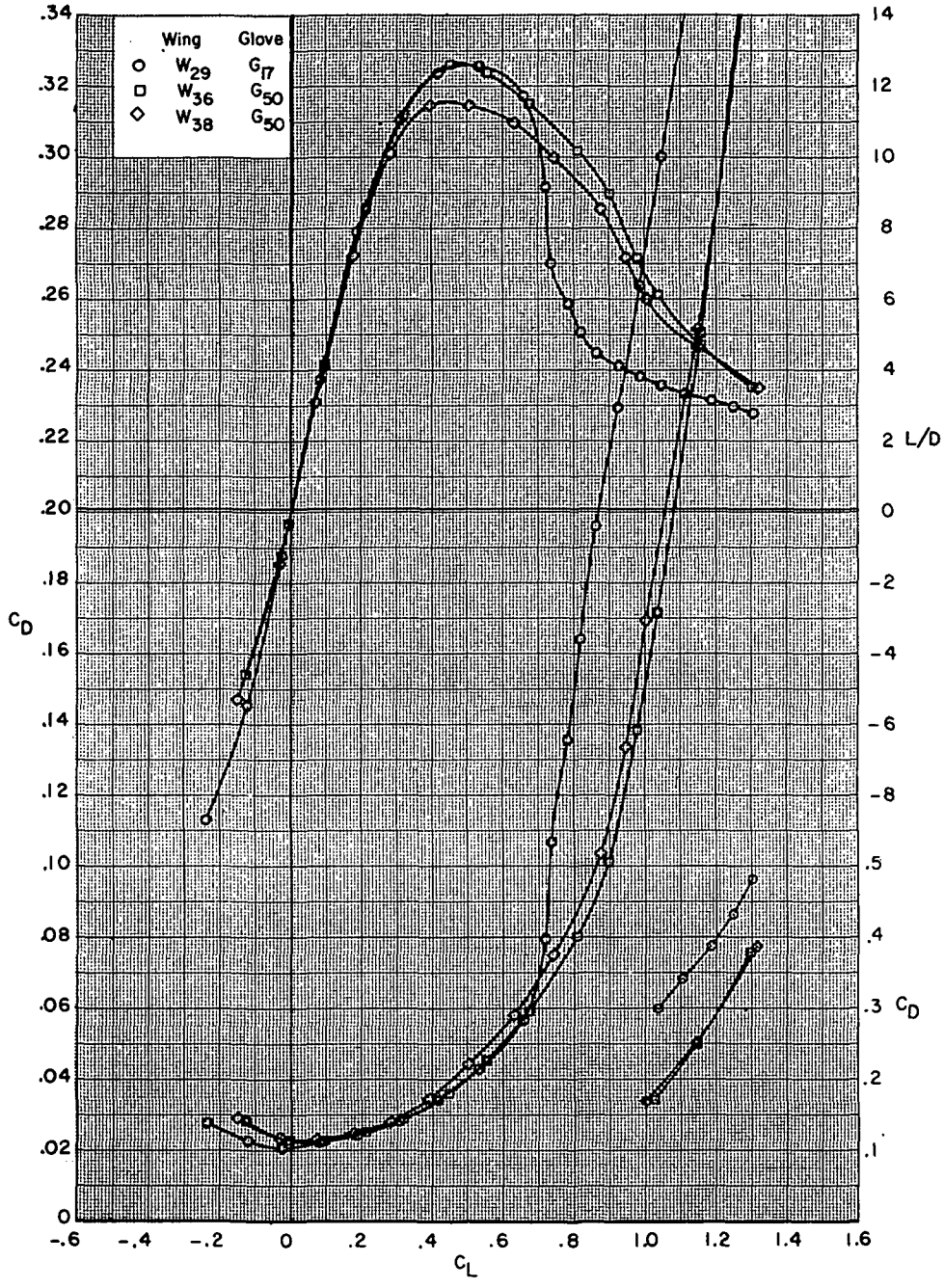

(a) Concluded.

Figure 18.- Continued.

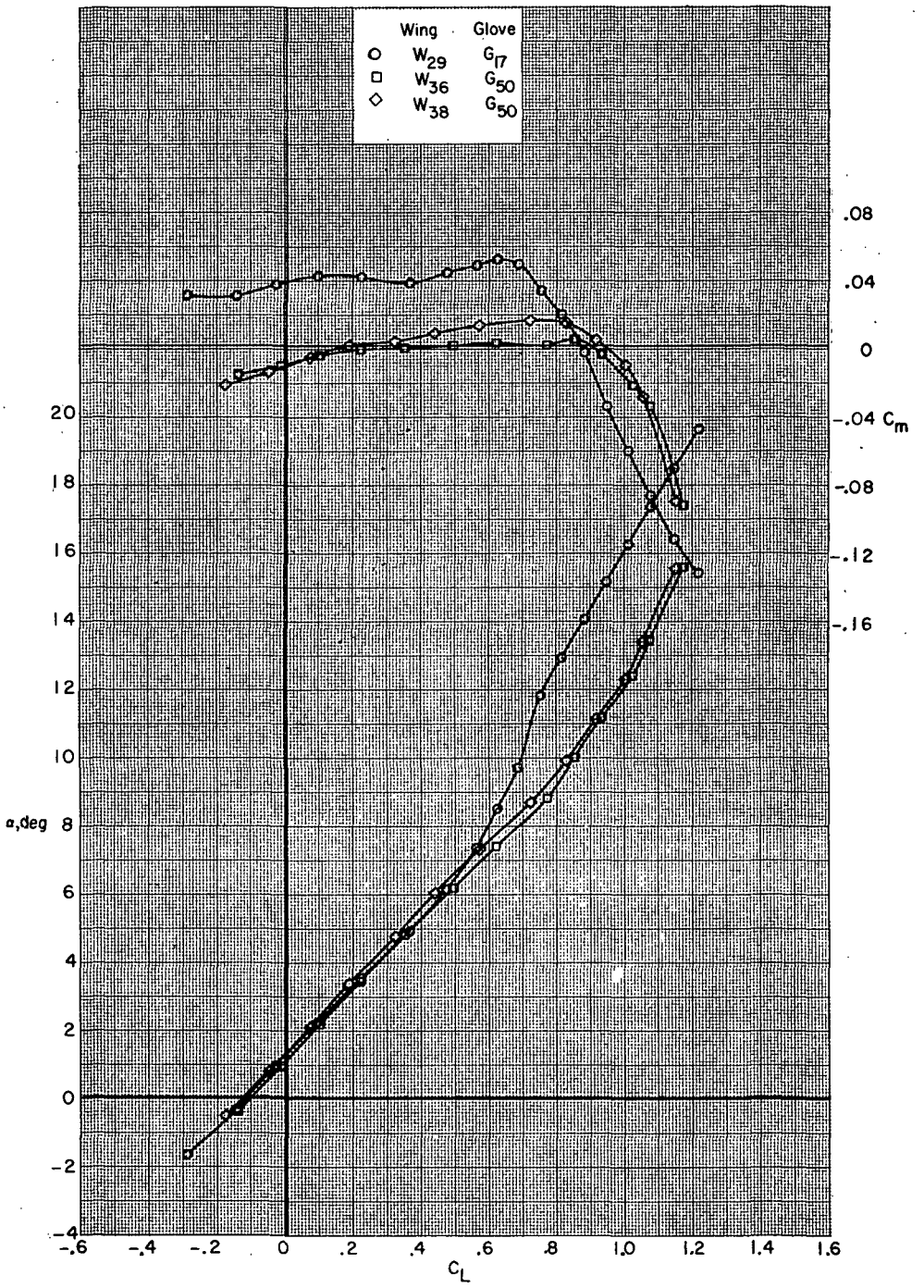

(b) M = 0.80.

Figure 18.- Continued.

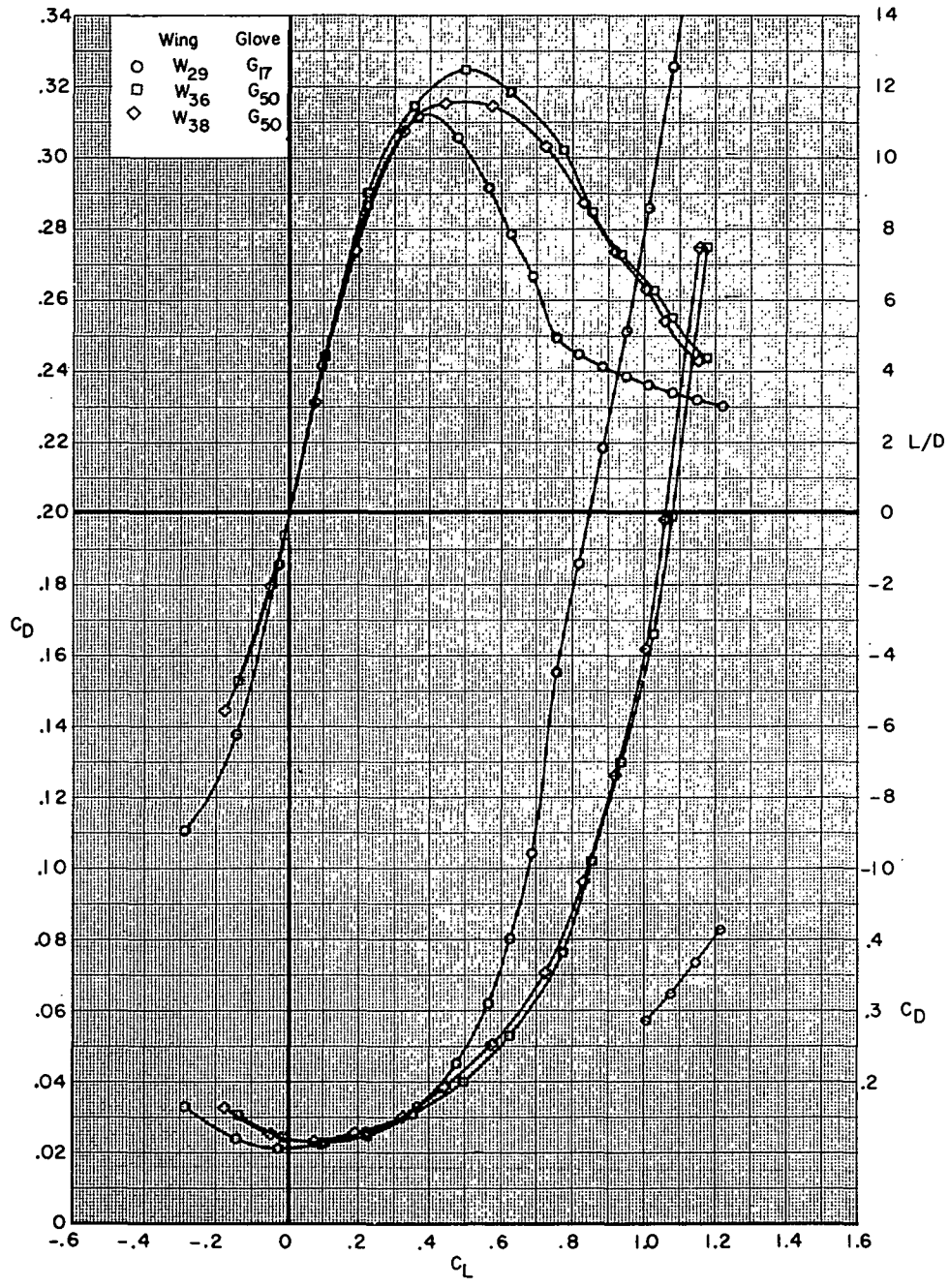

(b) Concluded.

Figure 18.- Continued.

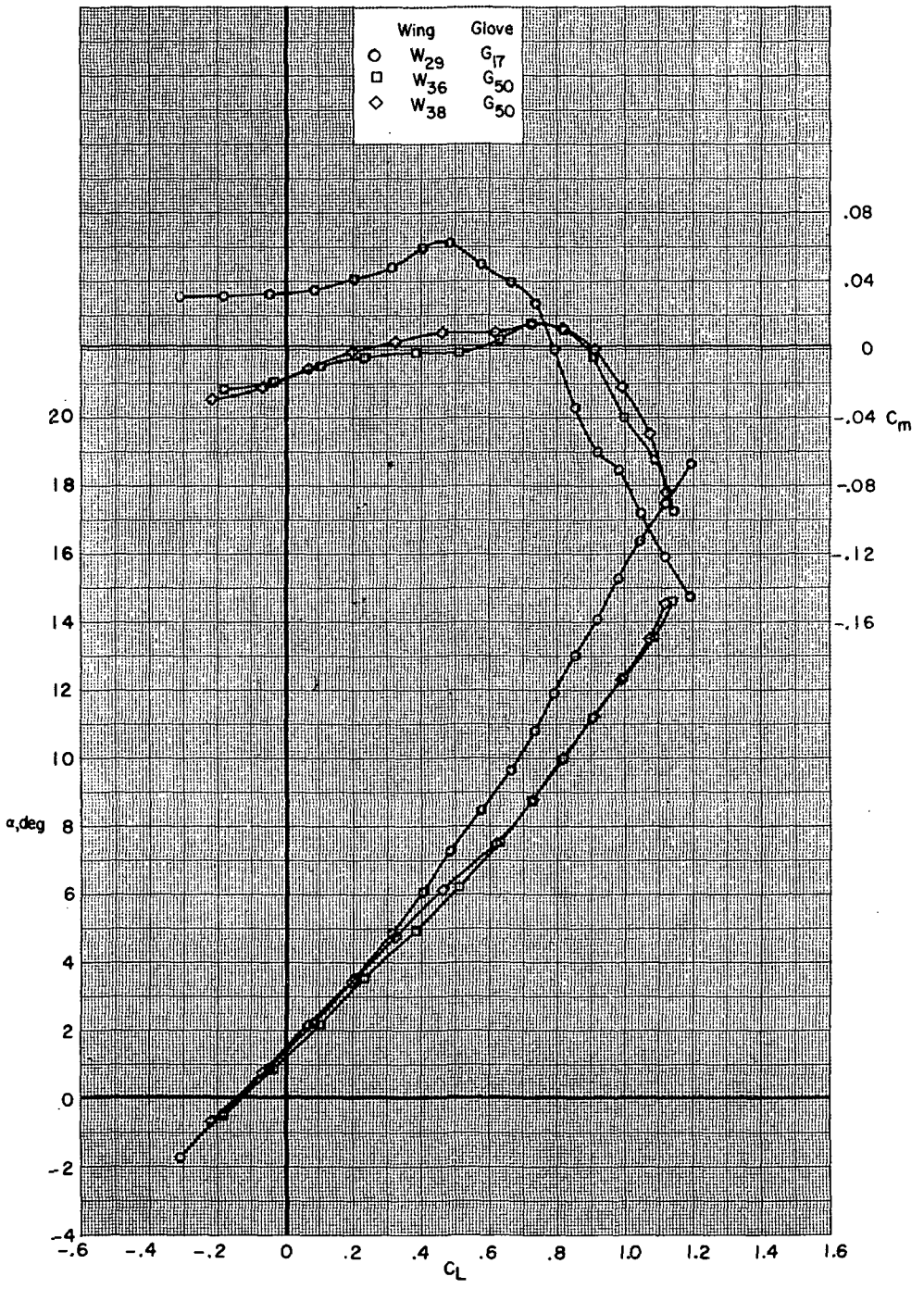

(c) M = 0.85.

Figure 18.- Continued.

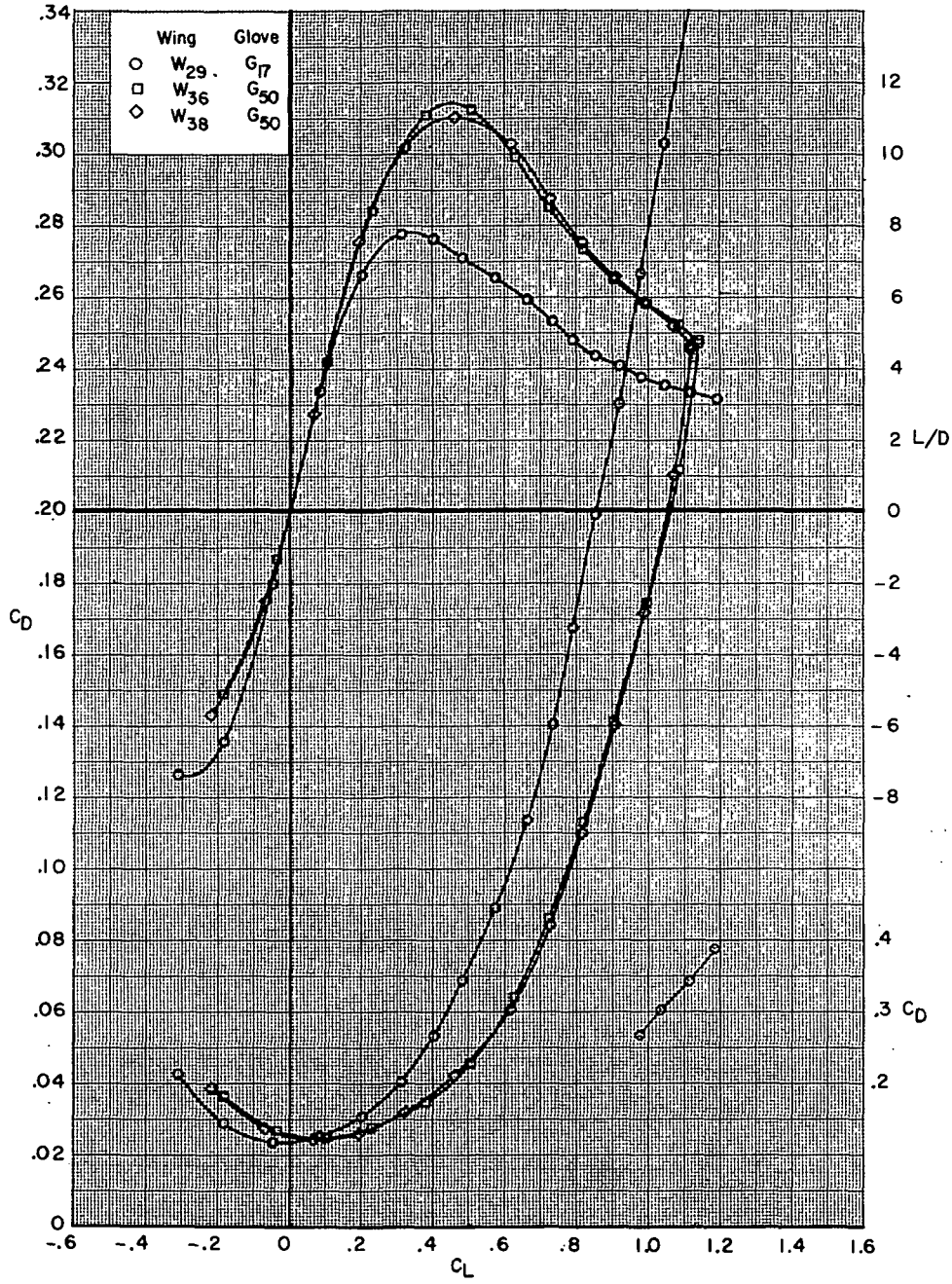

(c) Concluded.

Figure 18.- Continued.

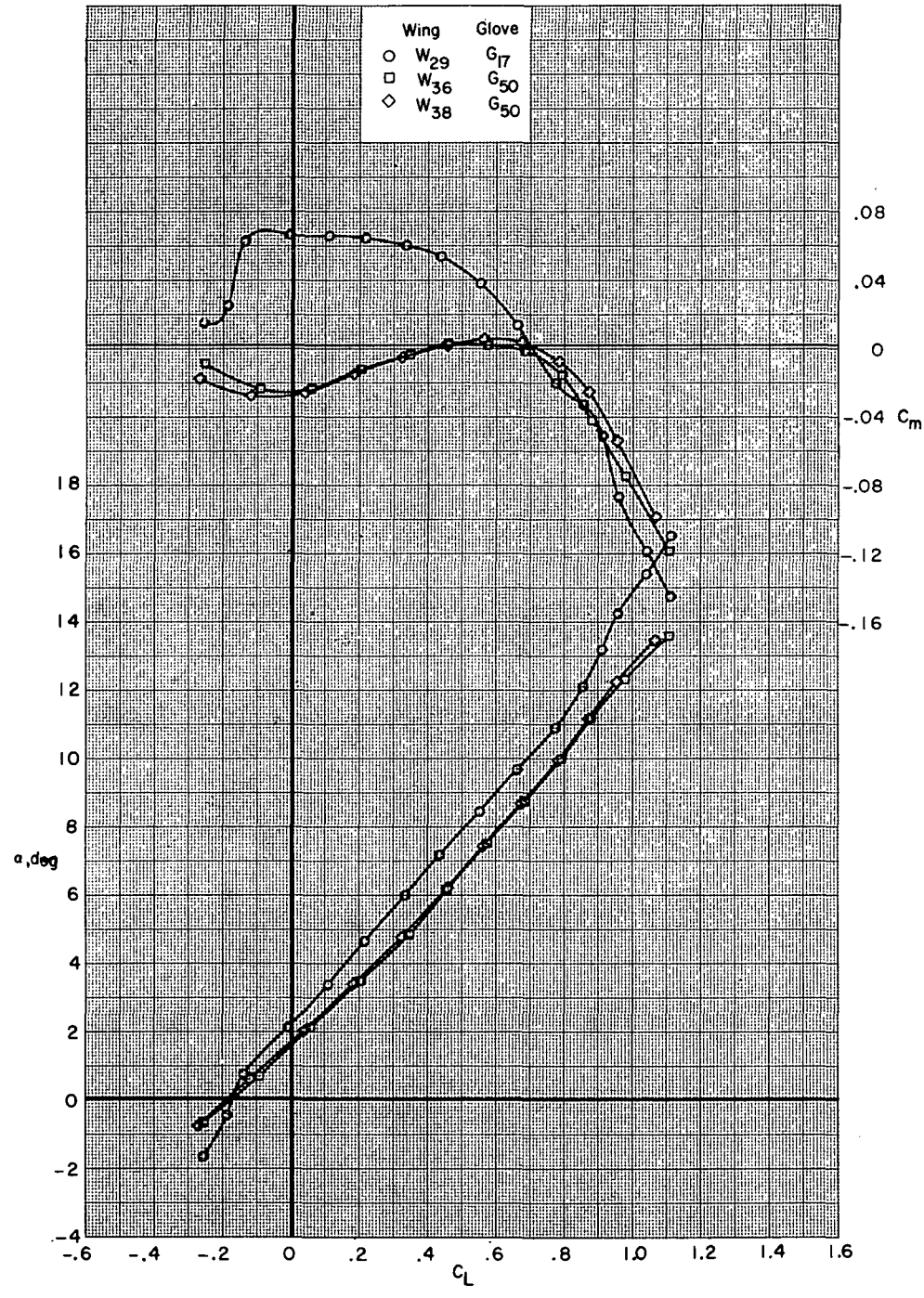

(d) M = 0.90.

Figure 18.- Continued.

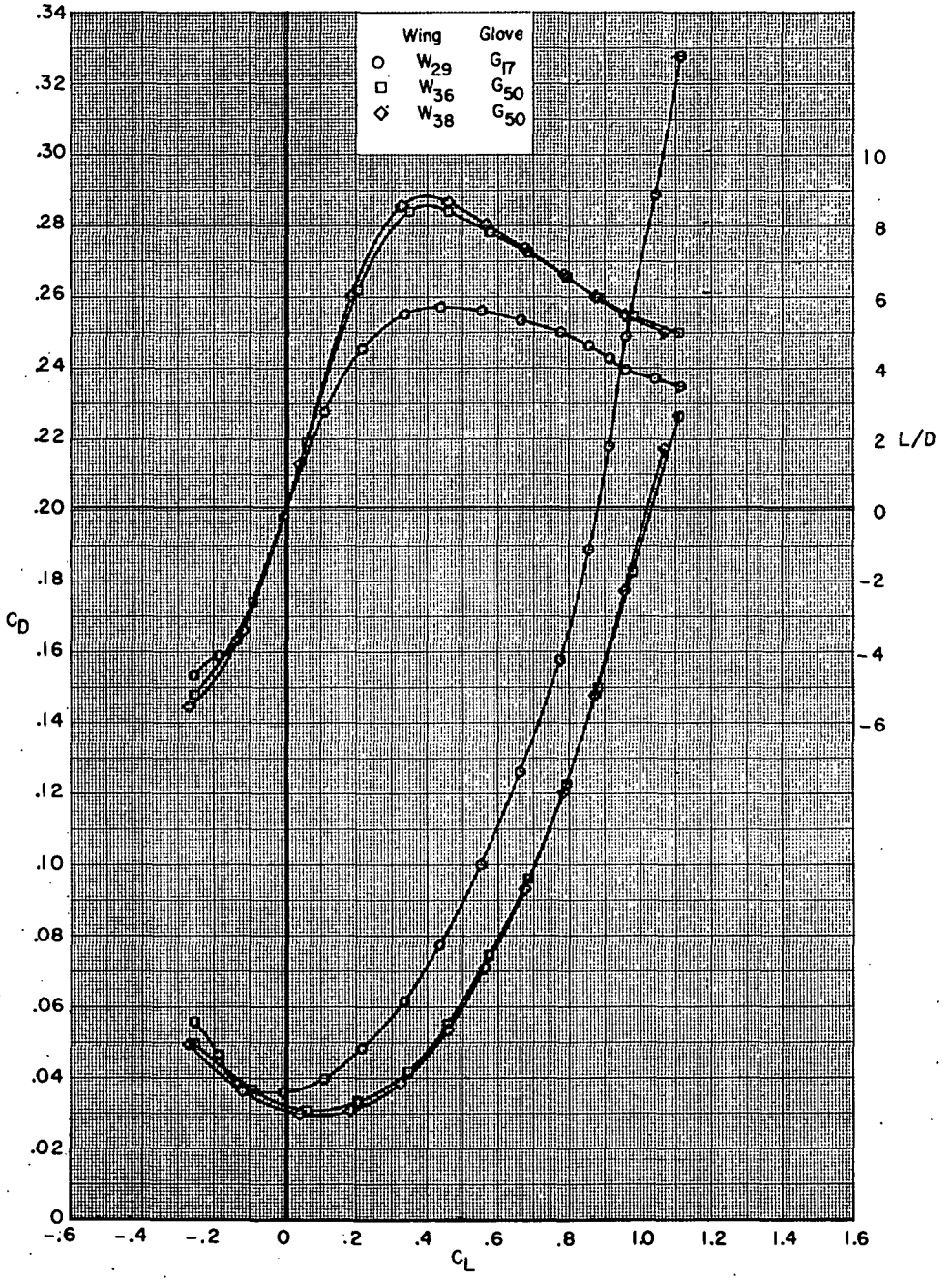

(d) Concluded.

Figure 18.- Concluded.

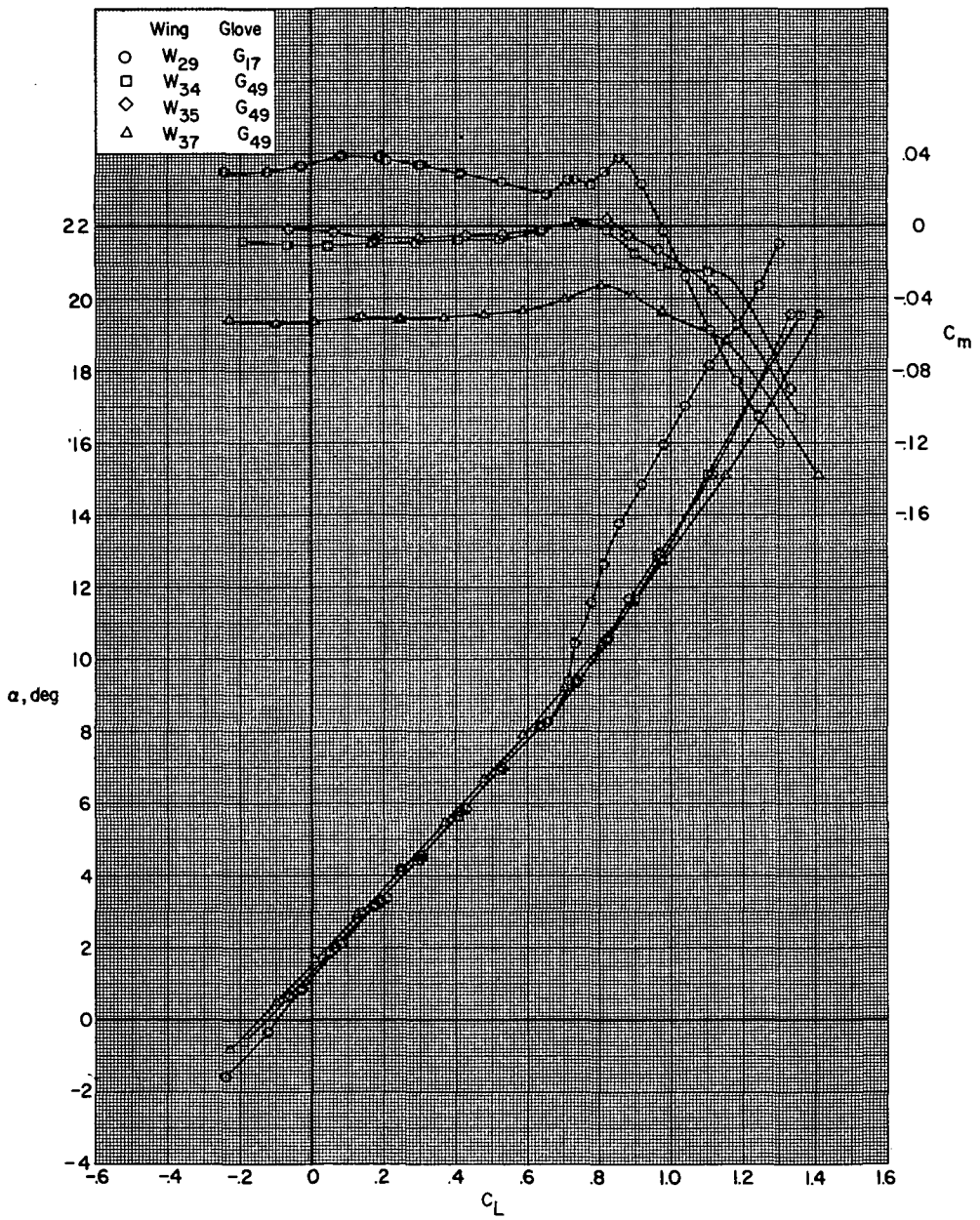

(a) M = 0.70.

Figure 19.- Effect of wing planform and airfoil on aerodynamic characteristics for configurations $B_{80}G_xH_{13}I_{71}N^b_{32}V_{29}V_{38}W_xX_{24}$ with wing swept 30.0°.

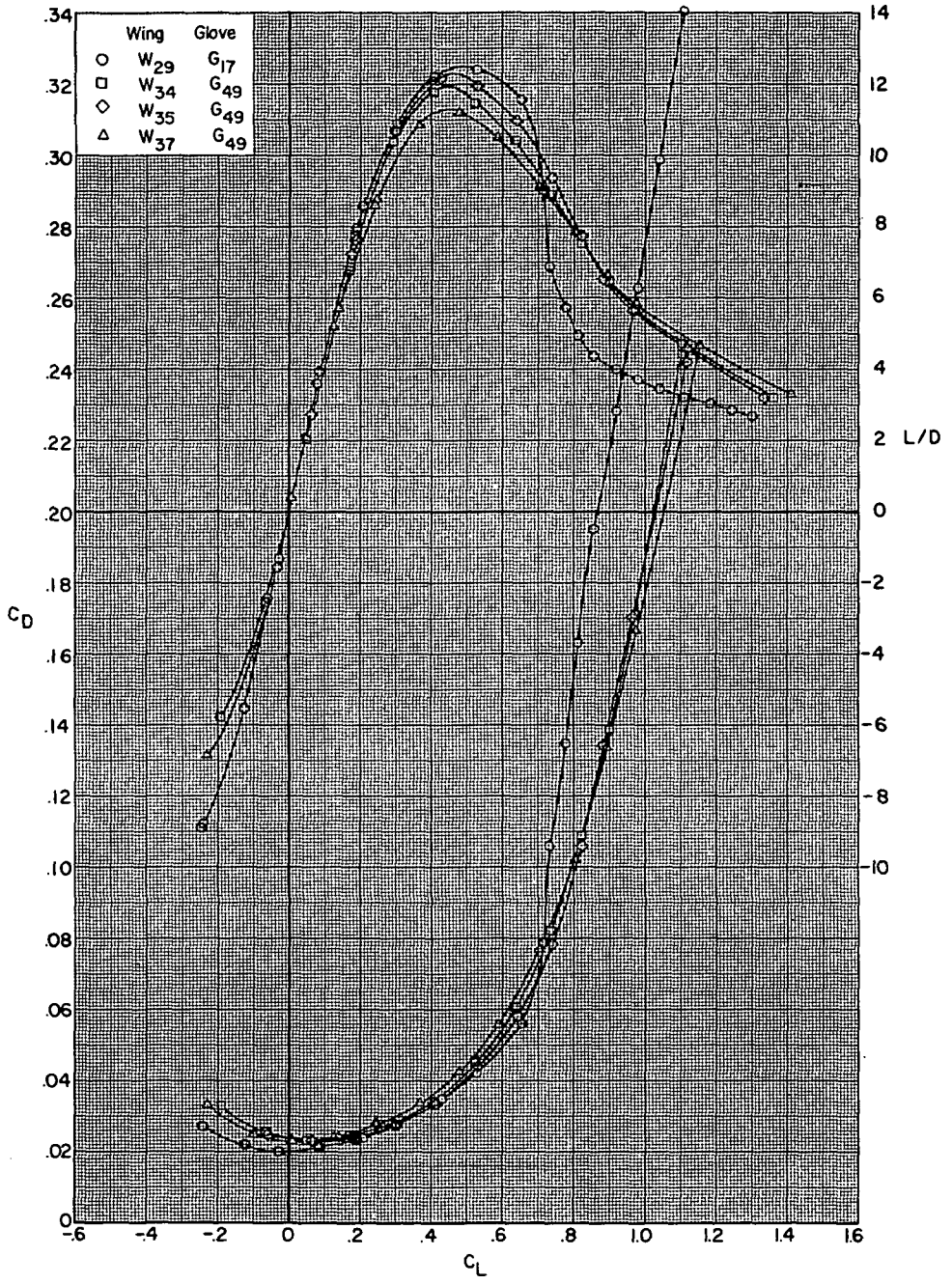

(a) Concluded.

Figure 19.- Continued.

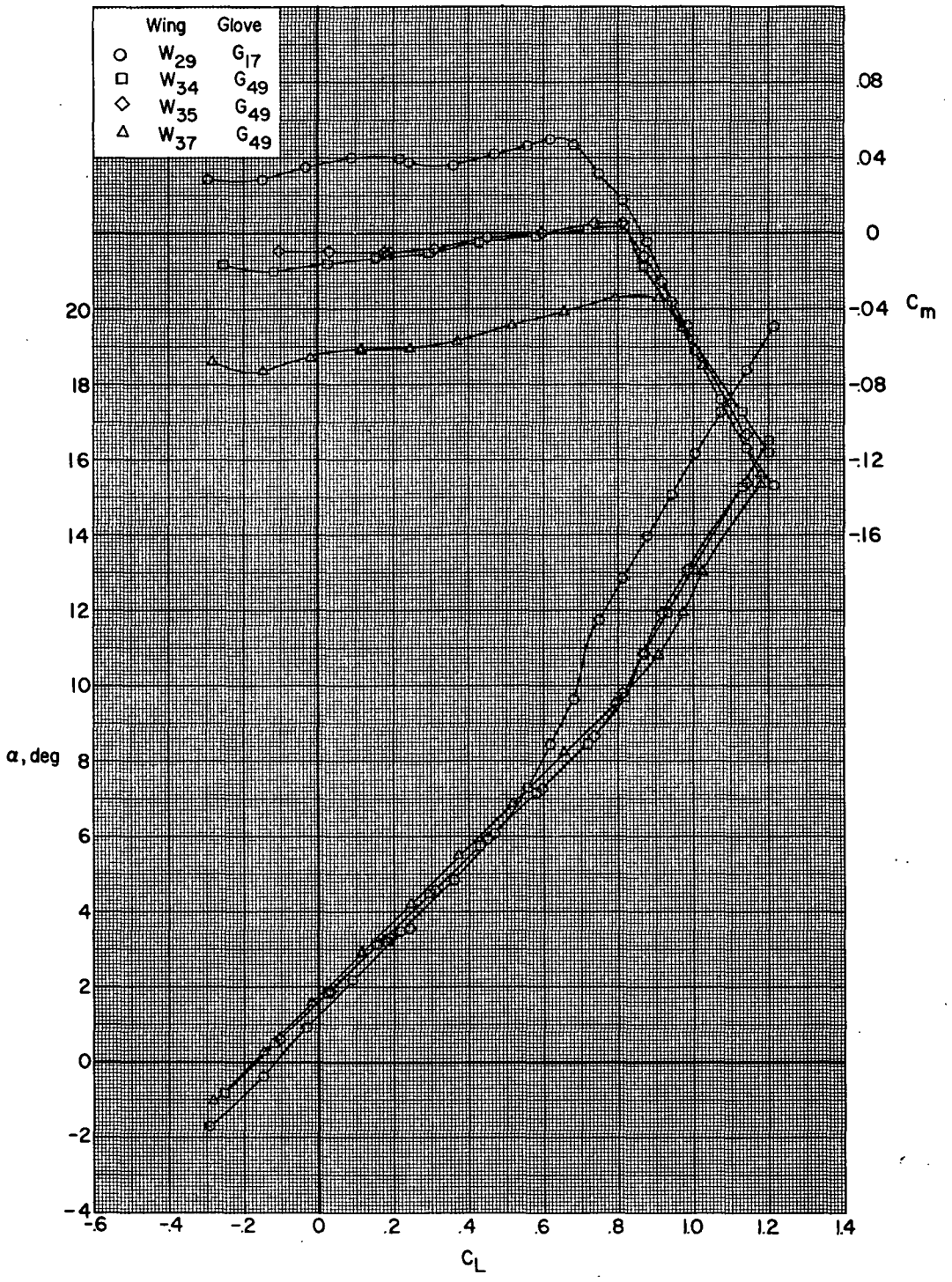

(b) M = 0.80.

Figure 19.- Continued.

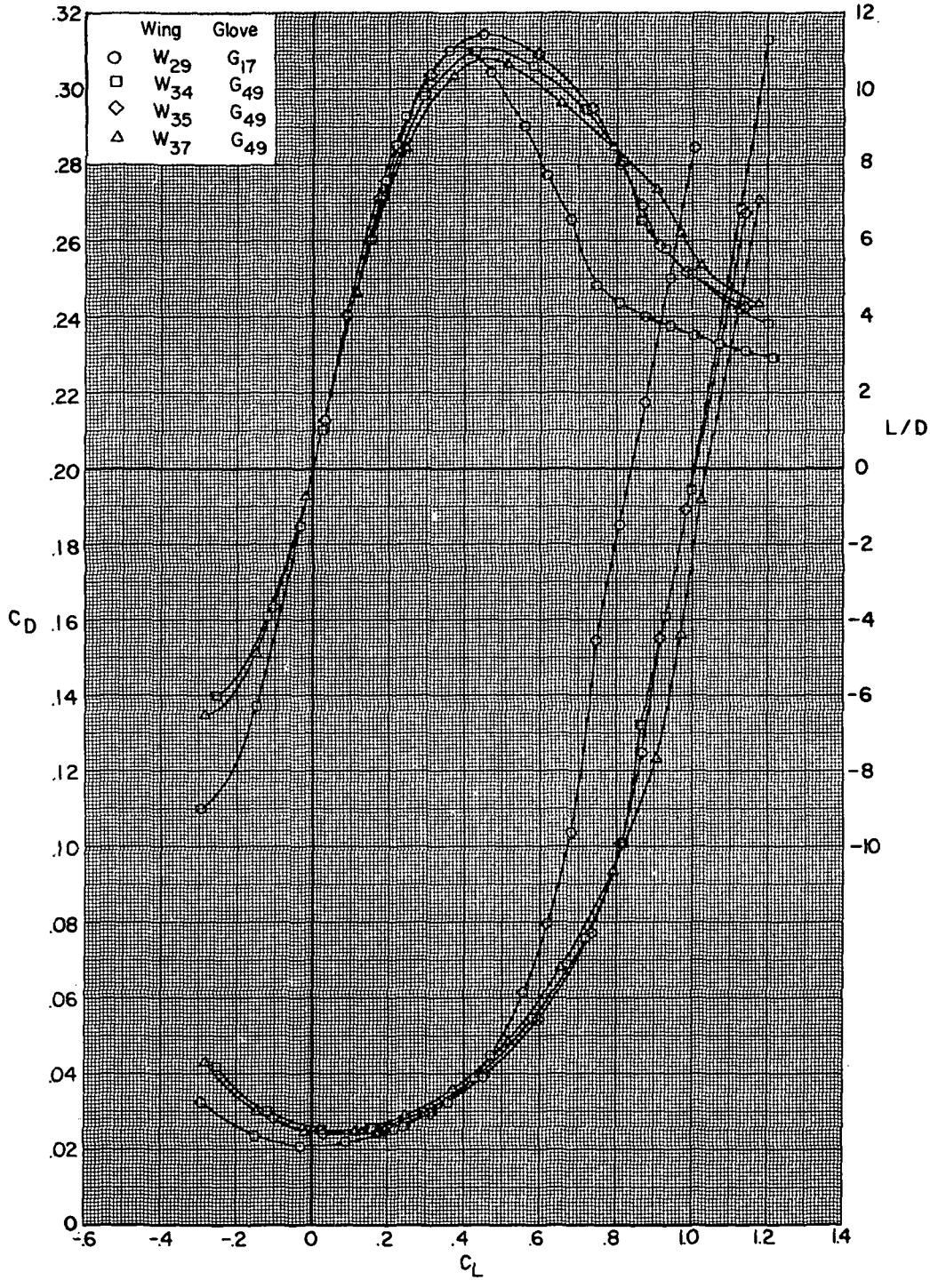

(b) Concluded.

Figure 19.- Continued.

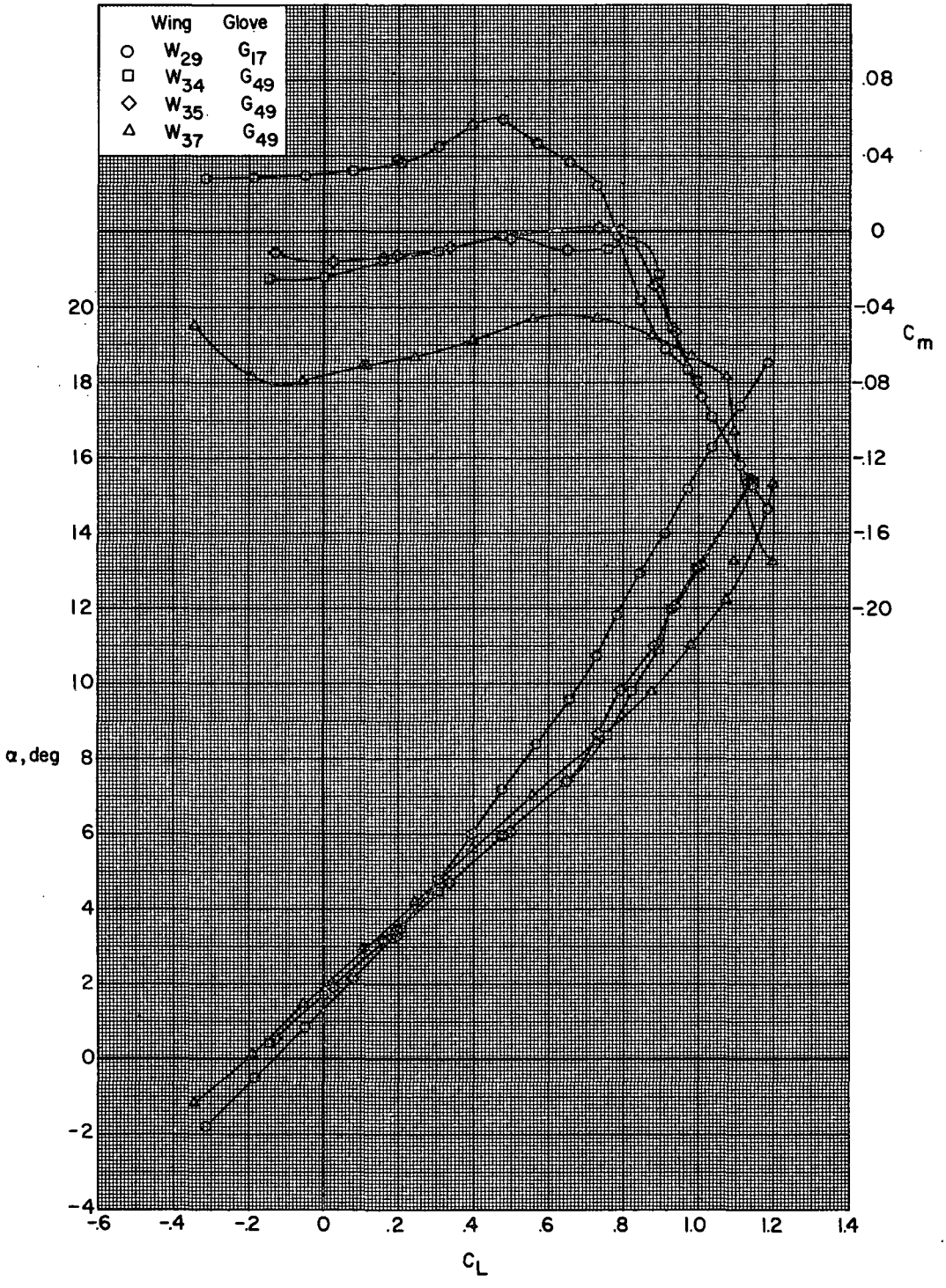

(c) M = 0.85.

Figure 19.- Continued.

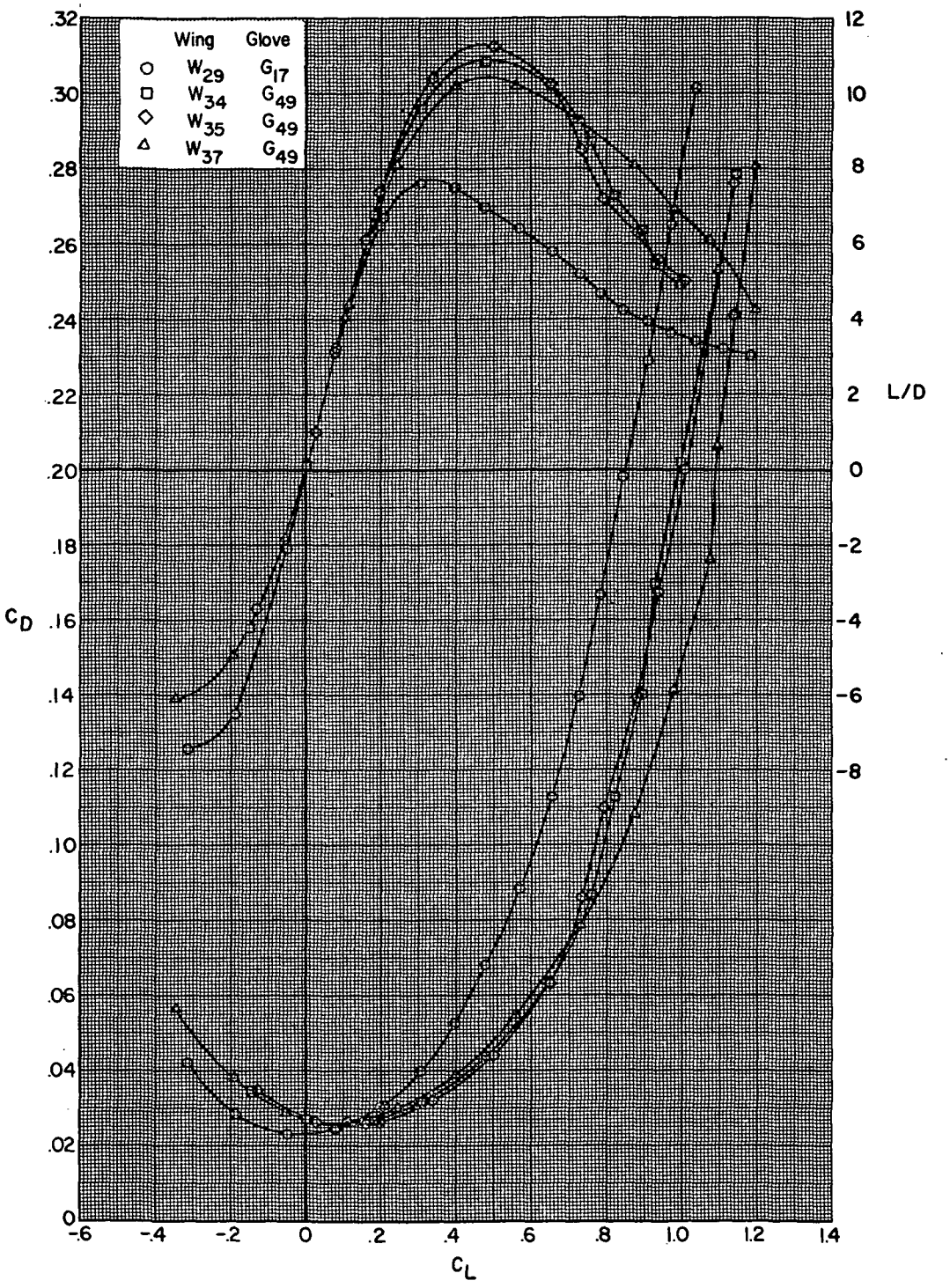

(c) Concluded.

Figure 19.- Continued.

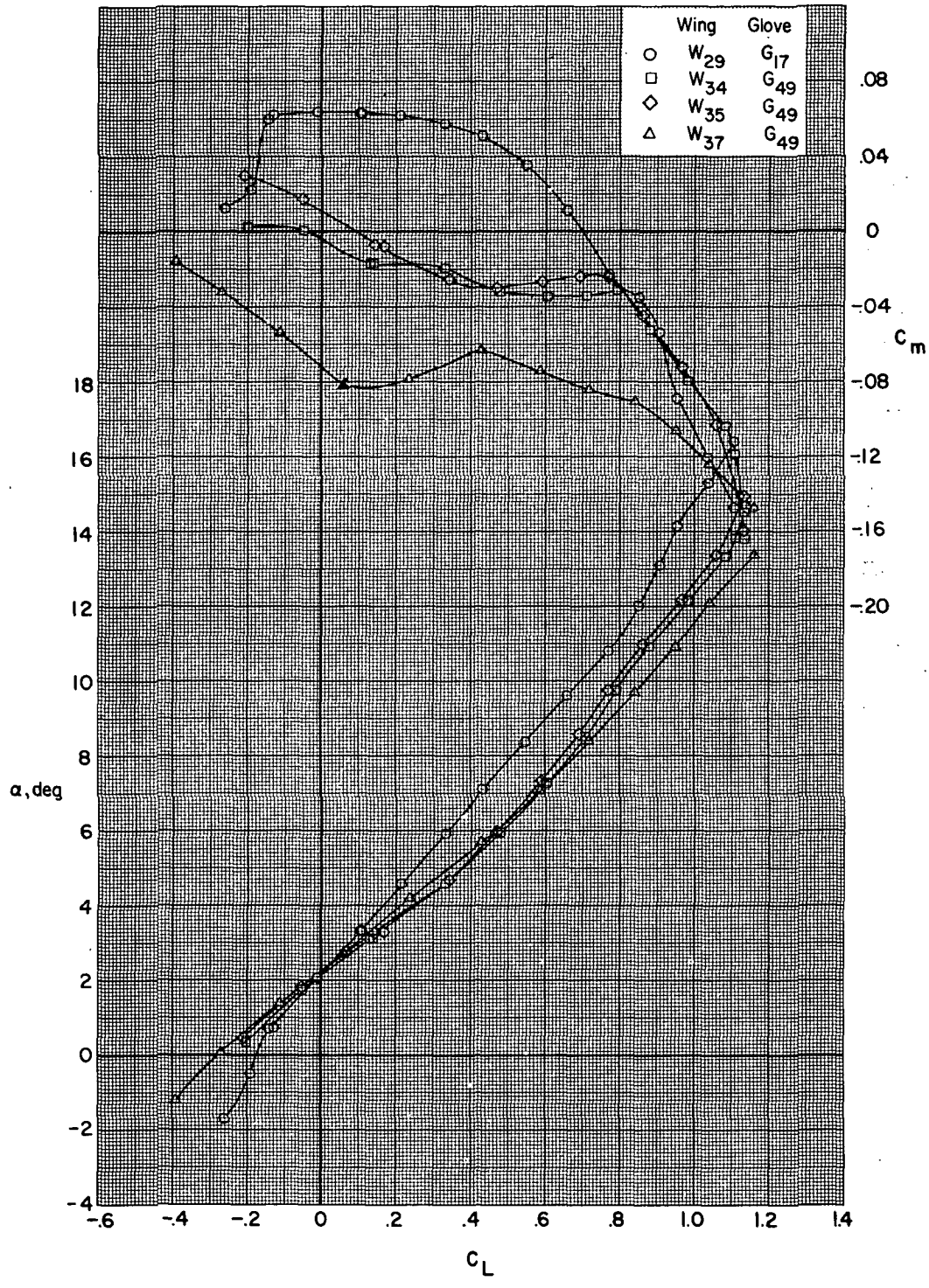

(d) M = 0.90.

Figure 19.- Continued.

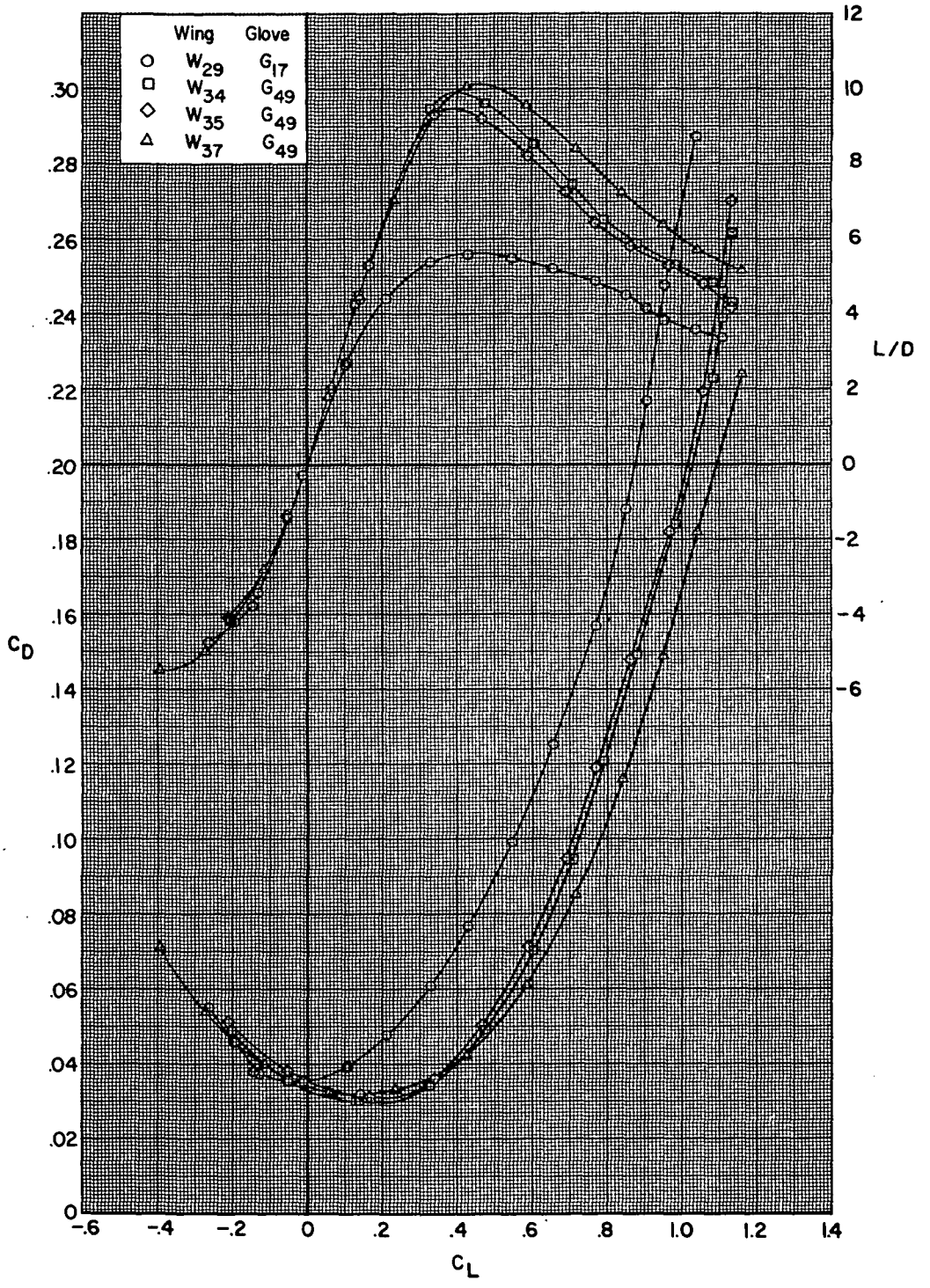

(d) Concluded.

Figure 19.- Concluded.

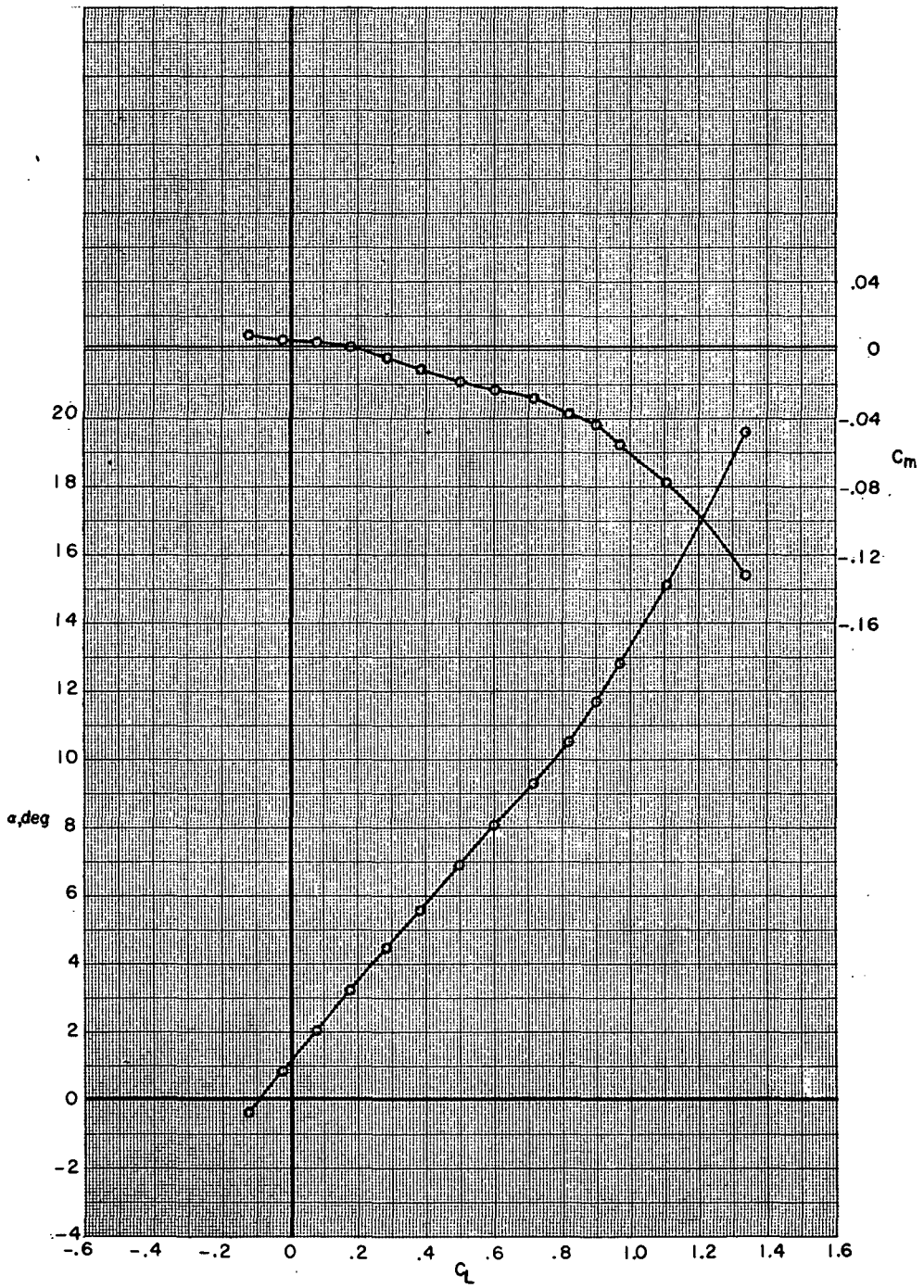

(a) M = 0.70.

Figure 20.- Aerodynamic characteristics for configuration $B_{80}G_{50}H_{13}I_{71}N^{b}_{32}V_{29}V_{38}W_{36}X_{24}$ with wing swept 35.0°.

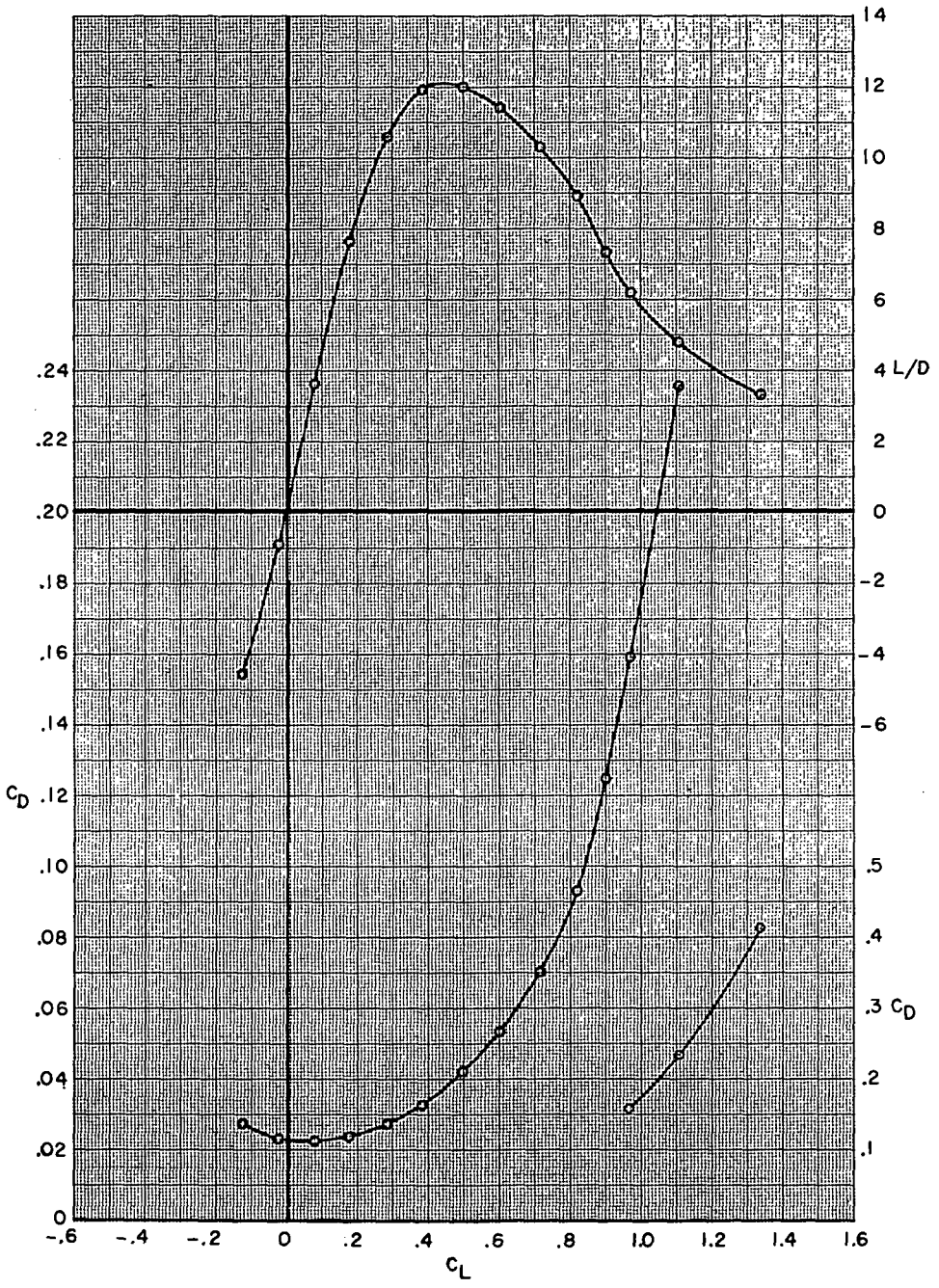

(a) Concluded.

Figure 20.- Continued.

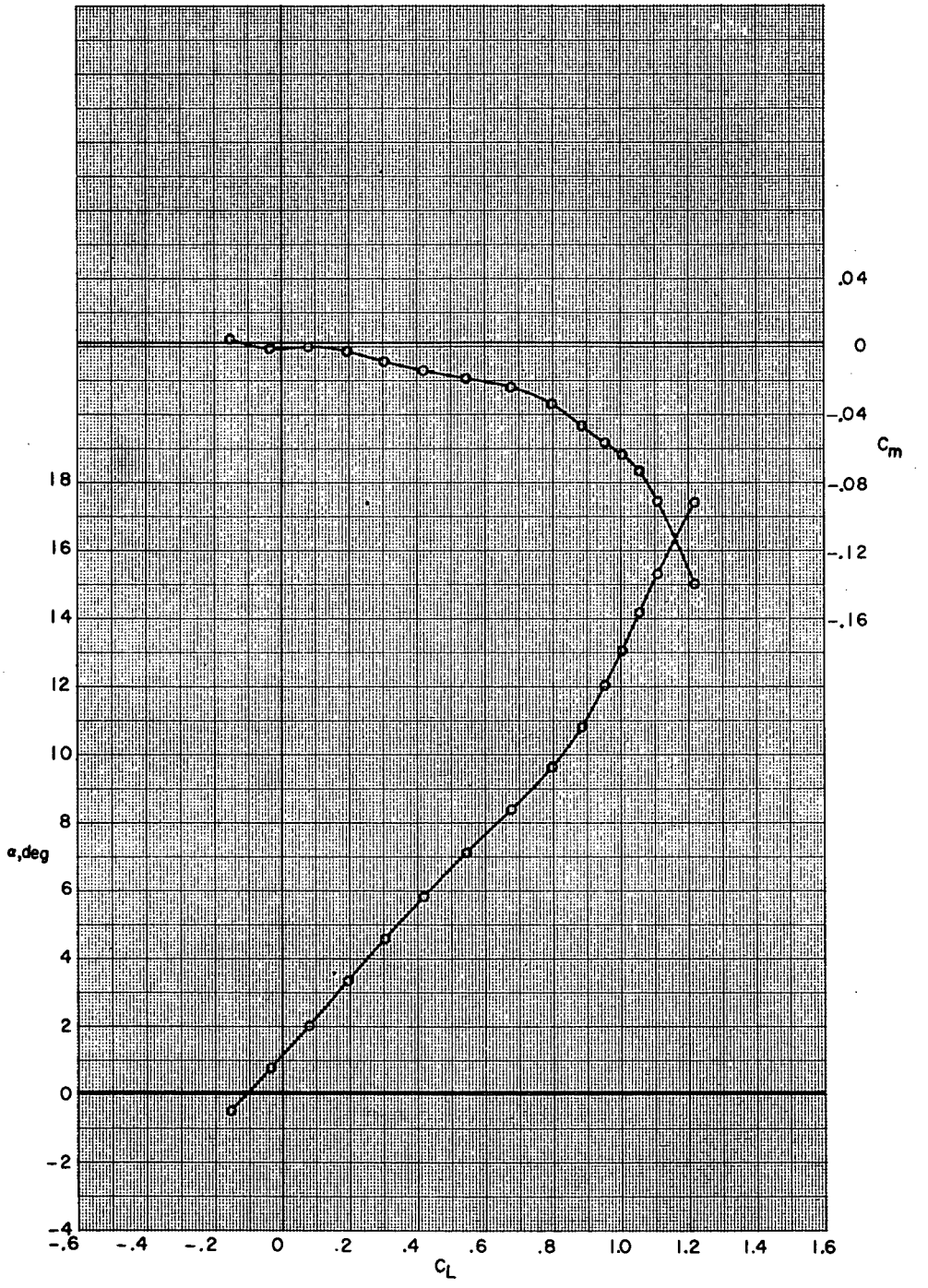

(b) M = 0.80.

Figure 20.- Continued.

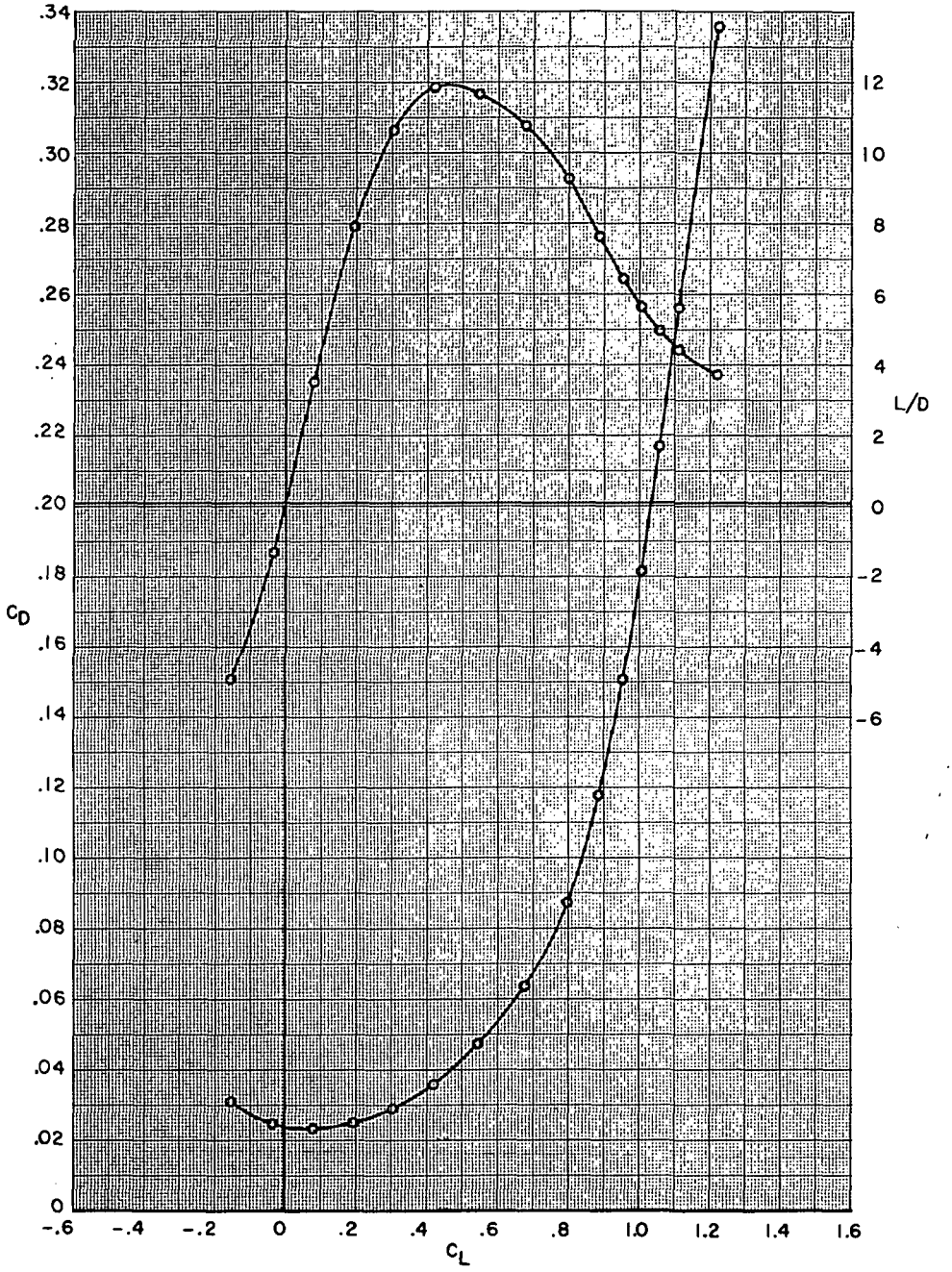

(b) Concluded.

Figure 20.- Continued.

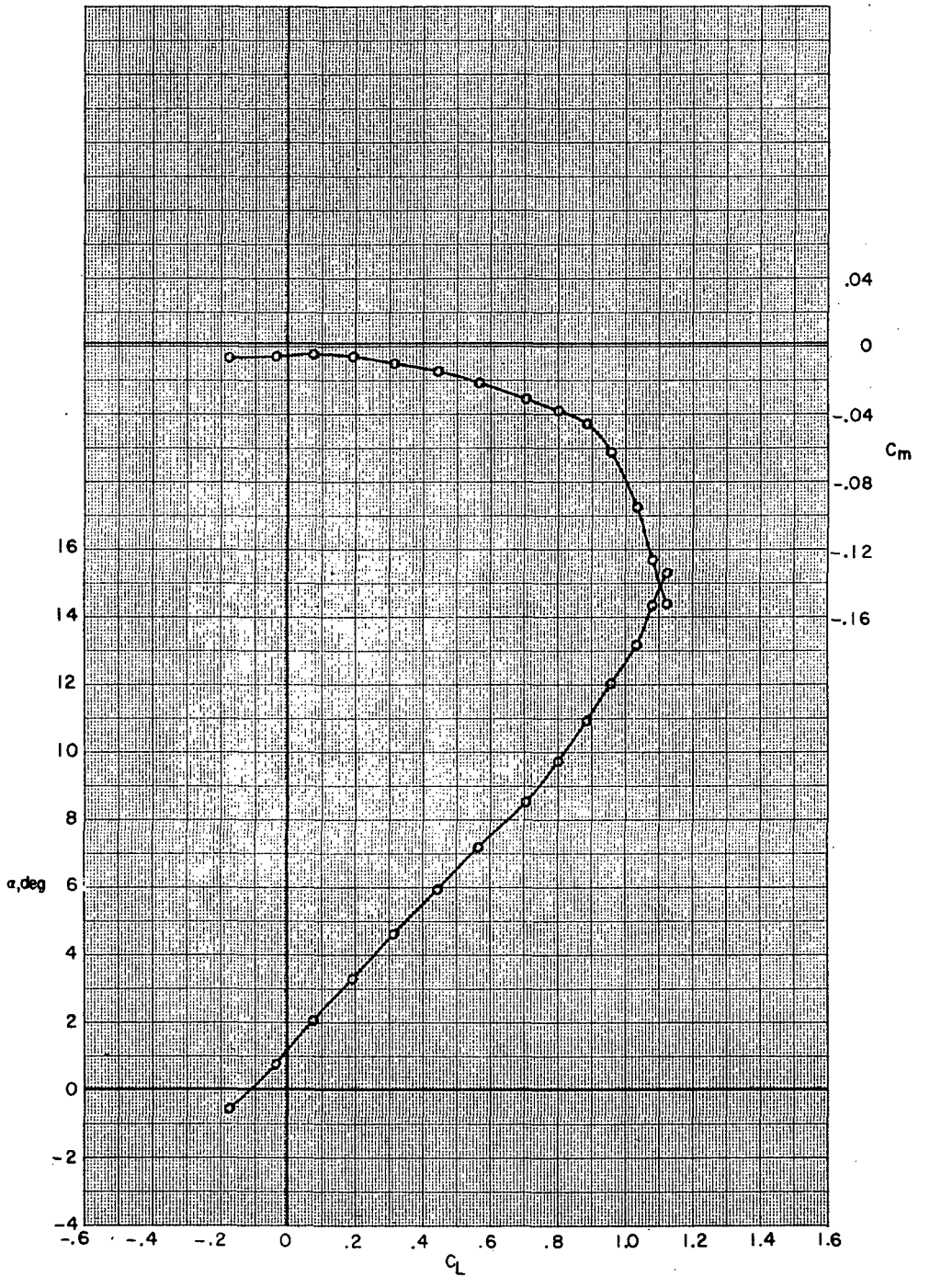

(c) M = 0.85.

Figure 20.- Continued.

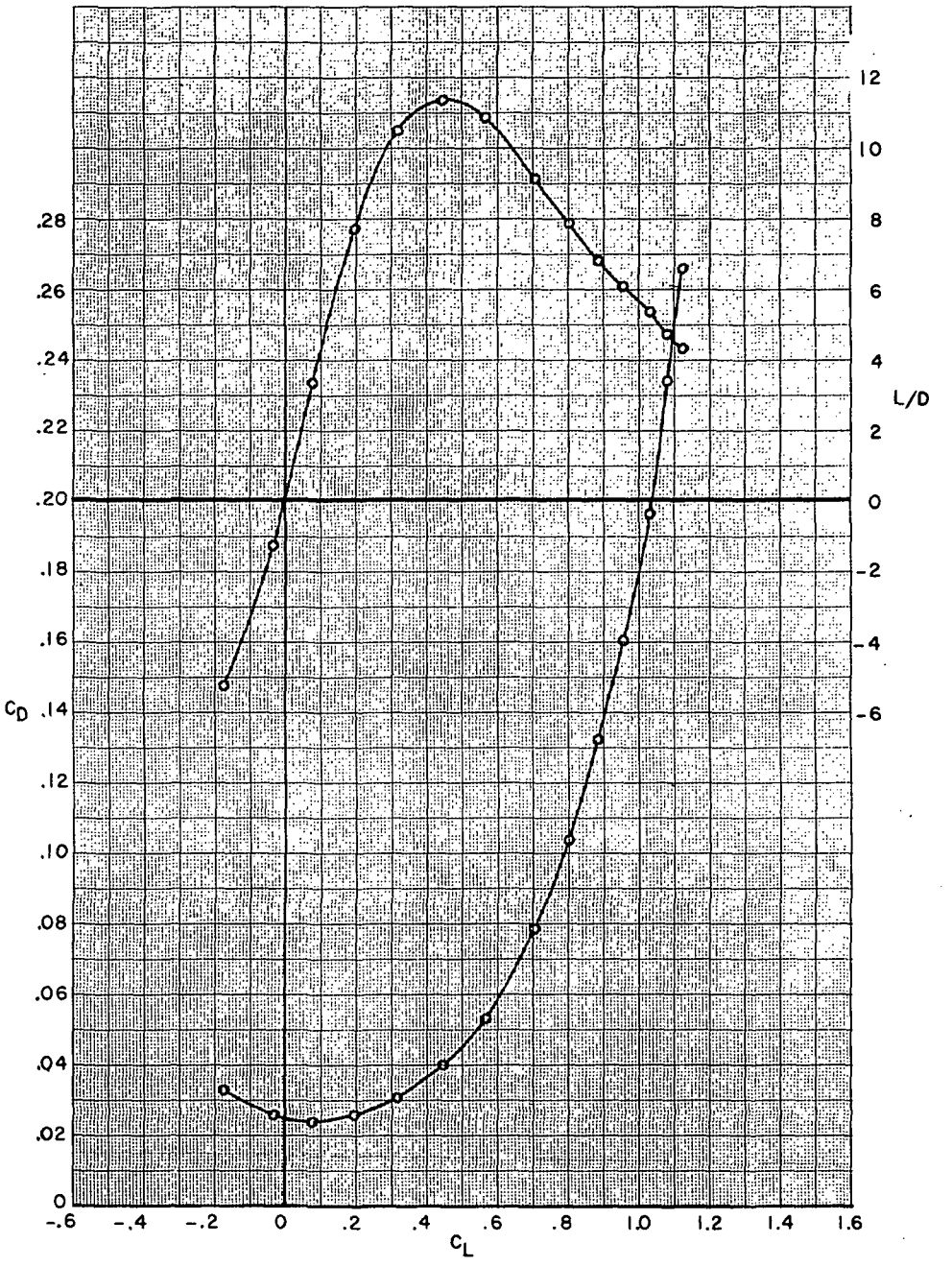

(c) Concluded.

Figure 20.- Continued.

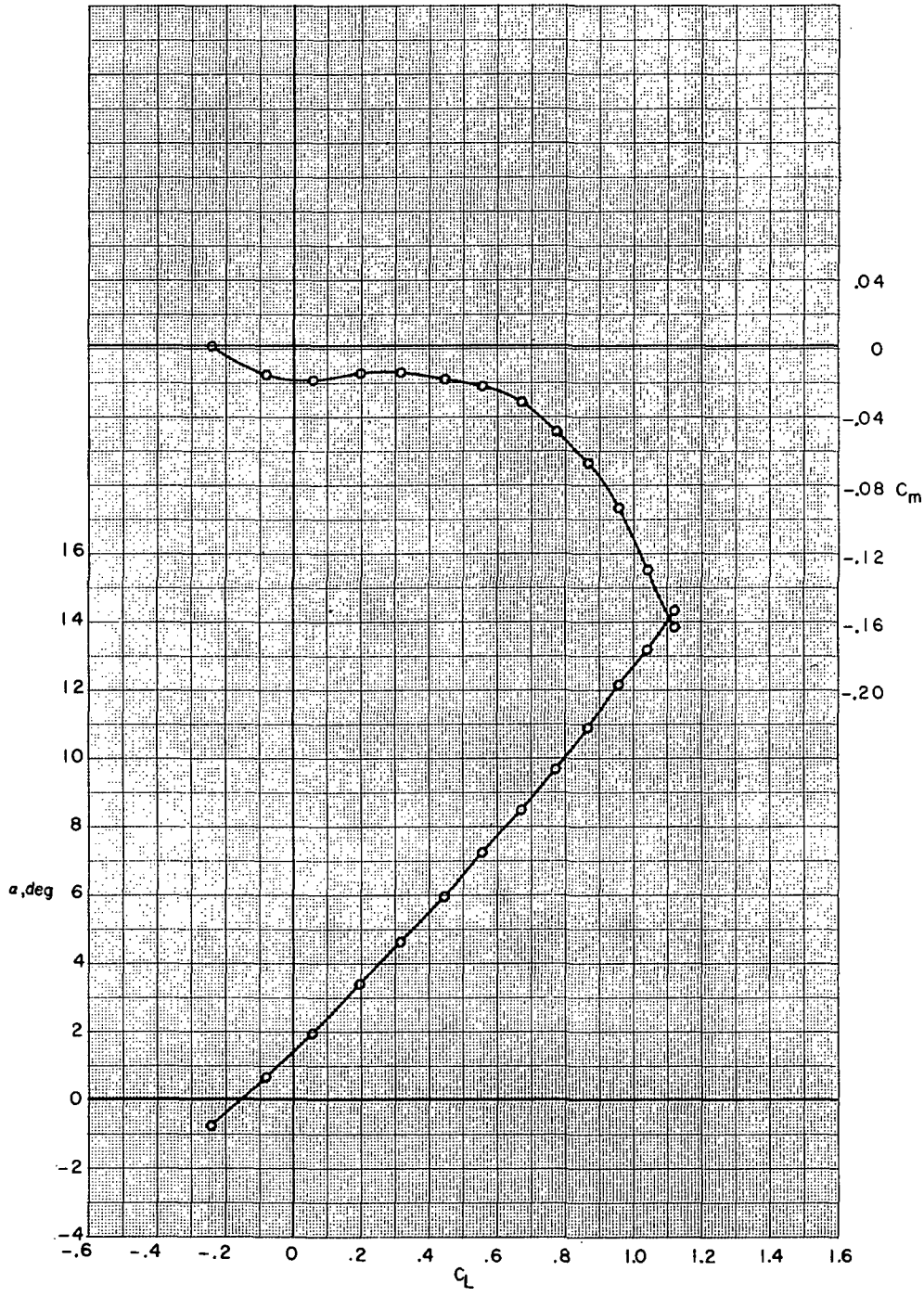

(d) M = 0.90.

Figure 20.- Continued.

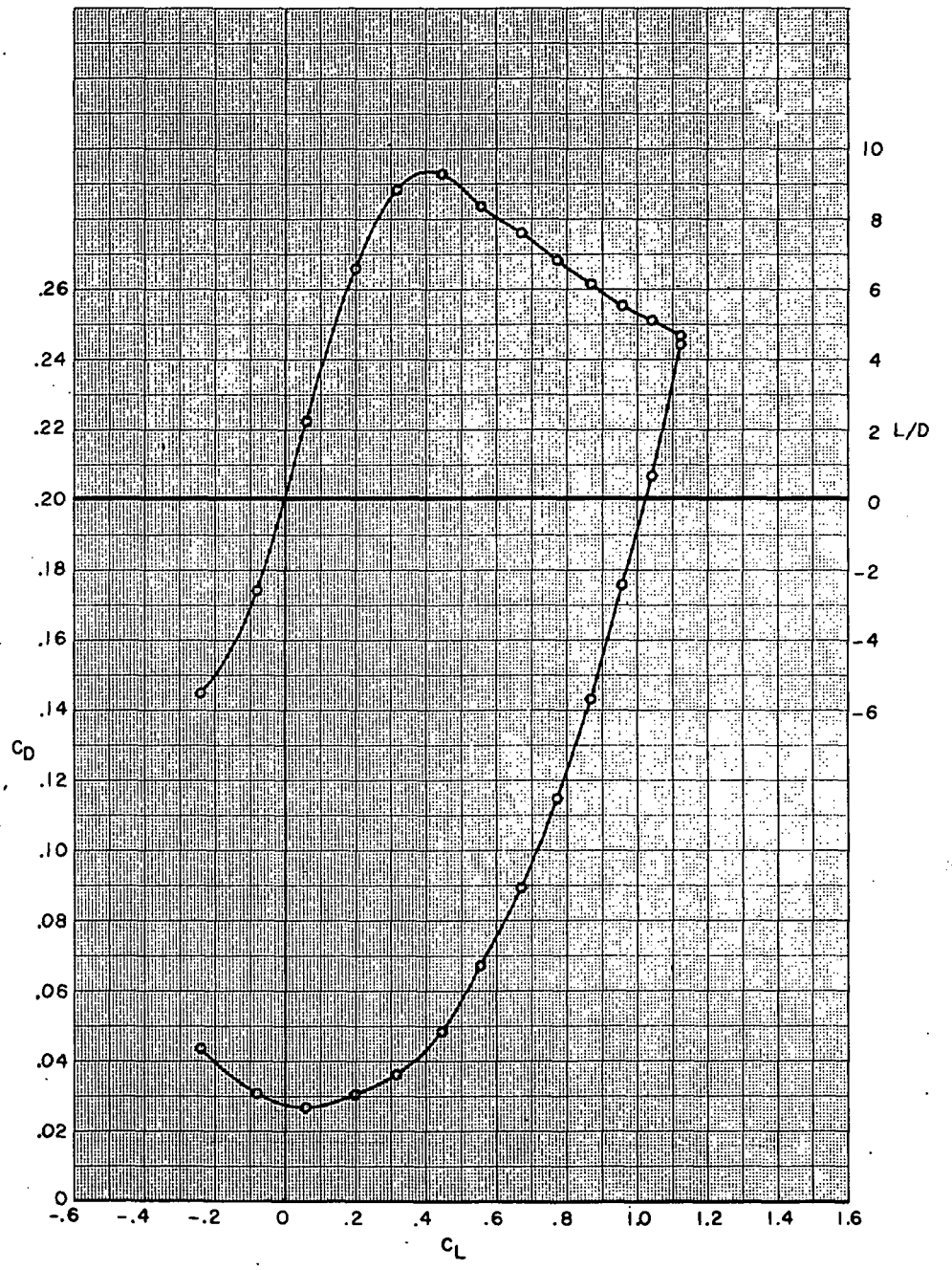

(d) Concluded.

Figure 20.- Continued.

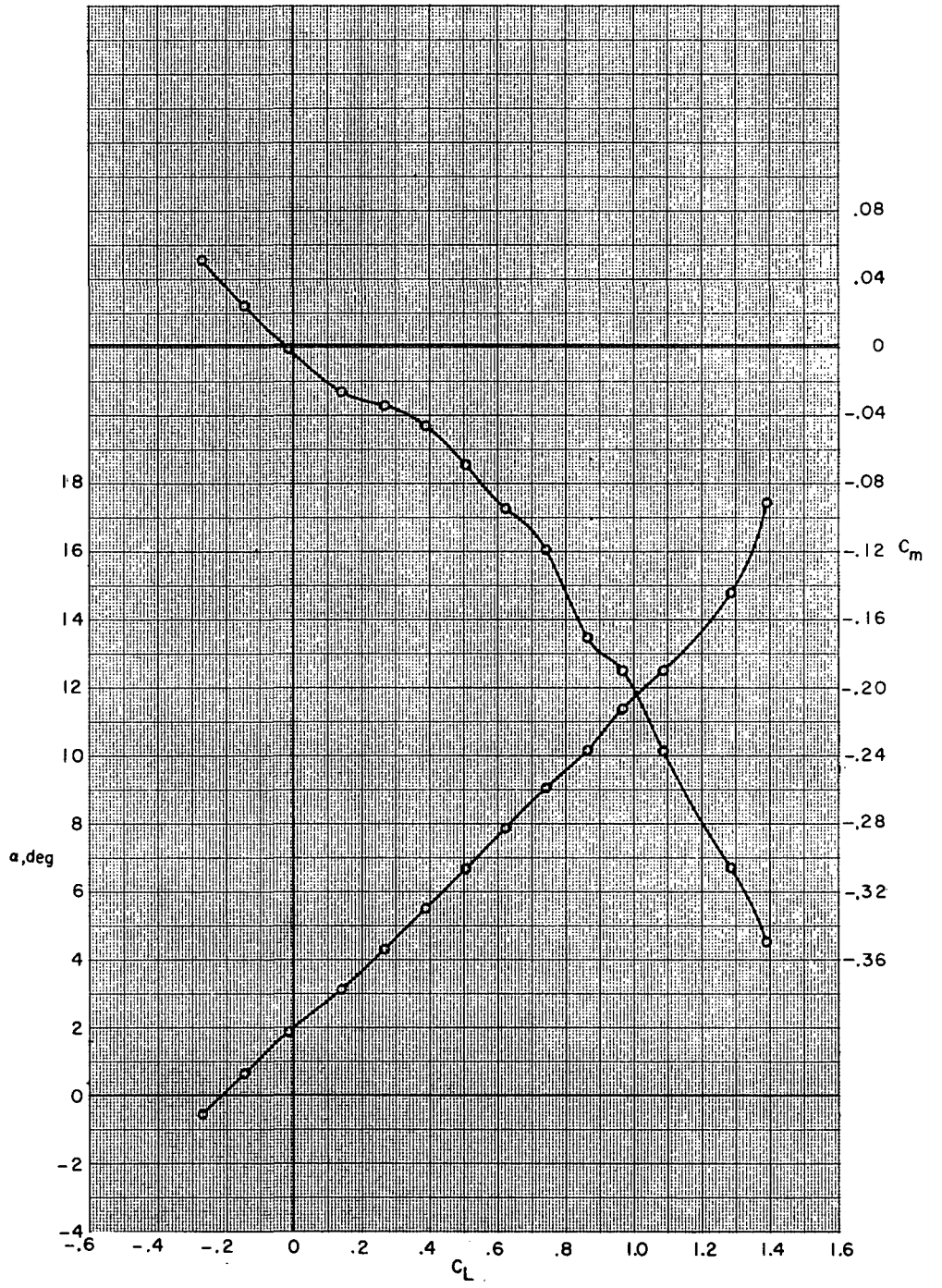

(e) M = 0.95.

Figure 20.- Continued.

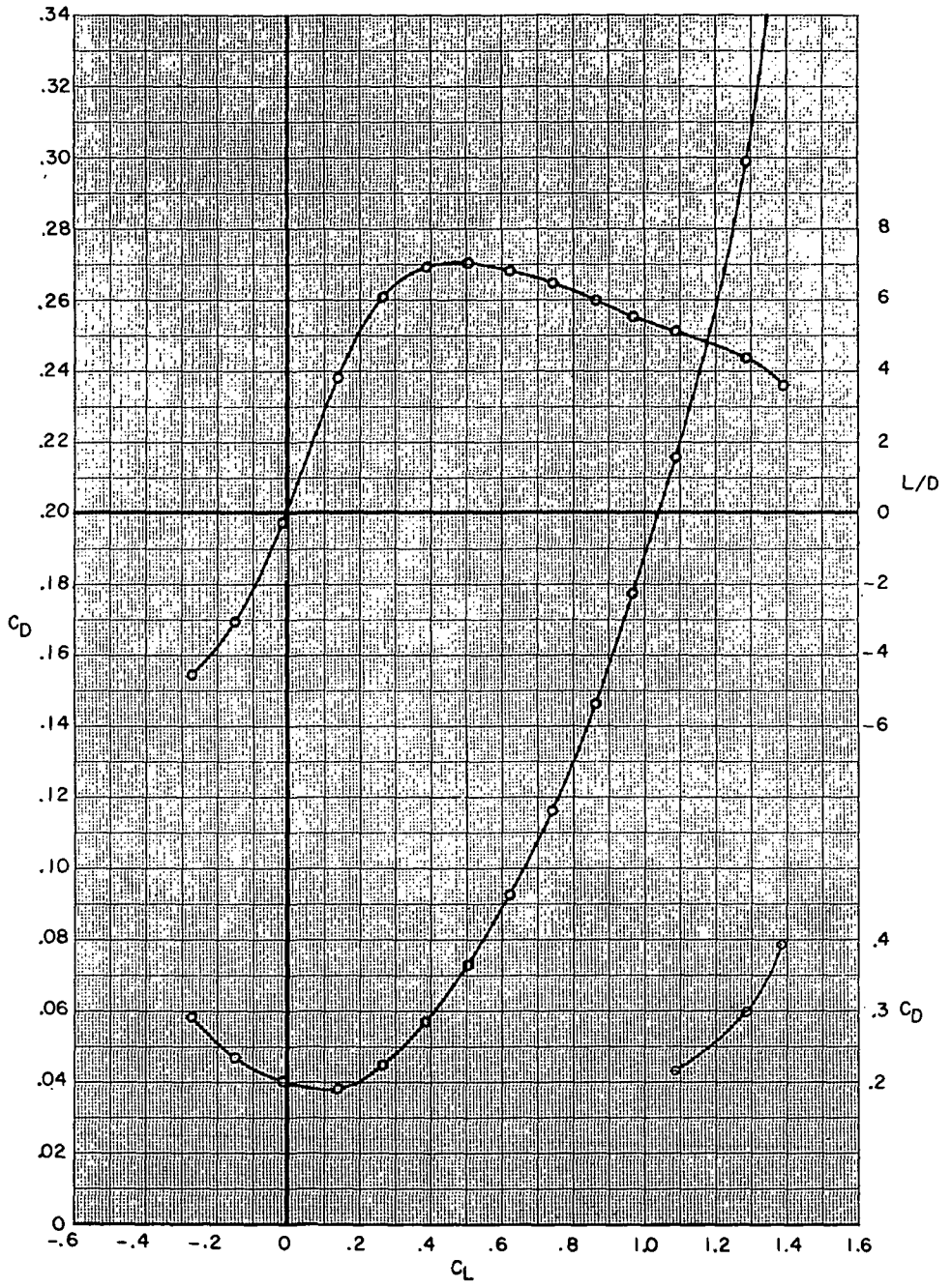

(e) Concluded.

Figure 20.- Concluded.

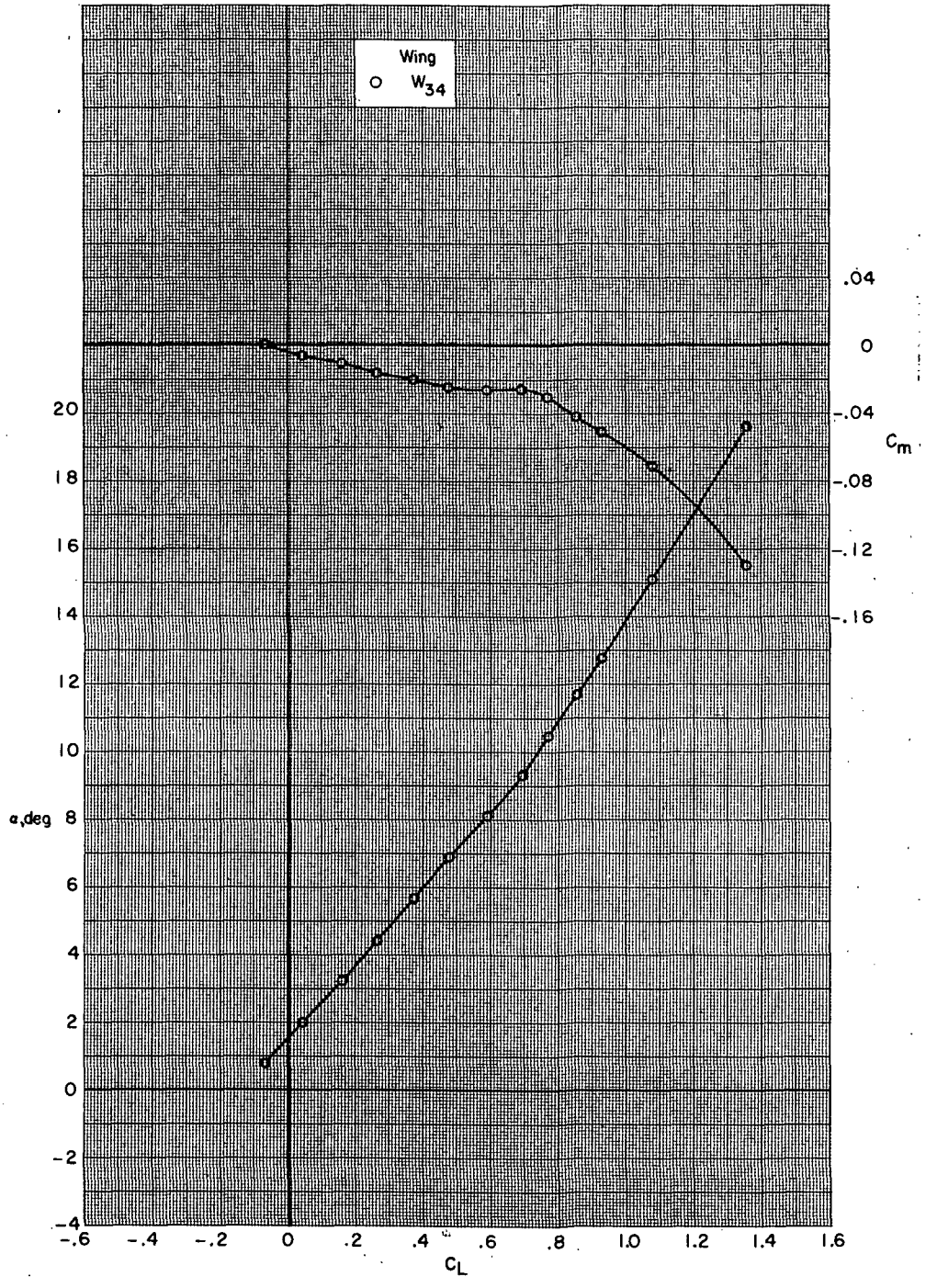

(a) M = 0.70.

Figure 21.- Effect of wing planform on aerodynamic characteristics for supercritical wing configurations $B_{80}G_{49}H_{13}I_{71}N^{b}_{32}V_{29}V_{38}W_{x}X_{24}$ with wing swept 35.0°.

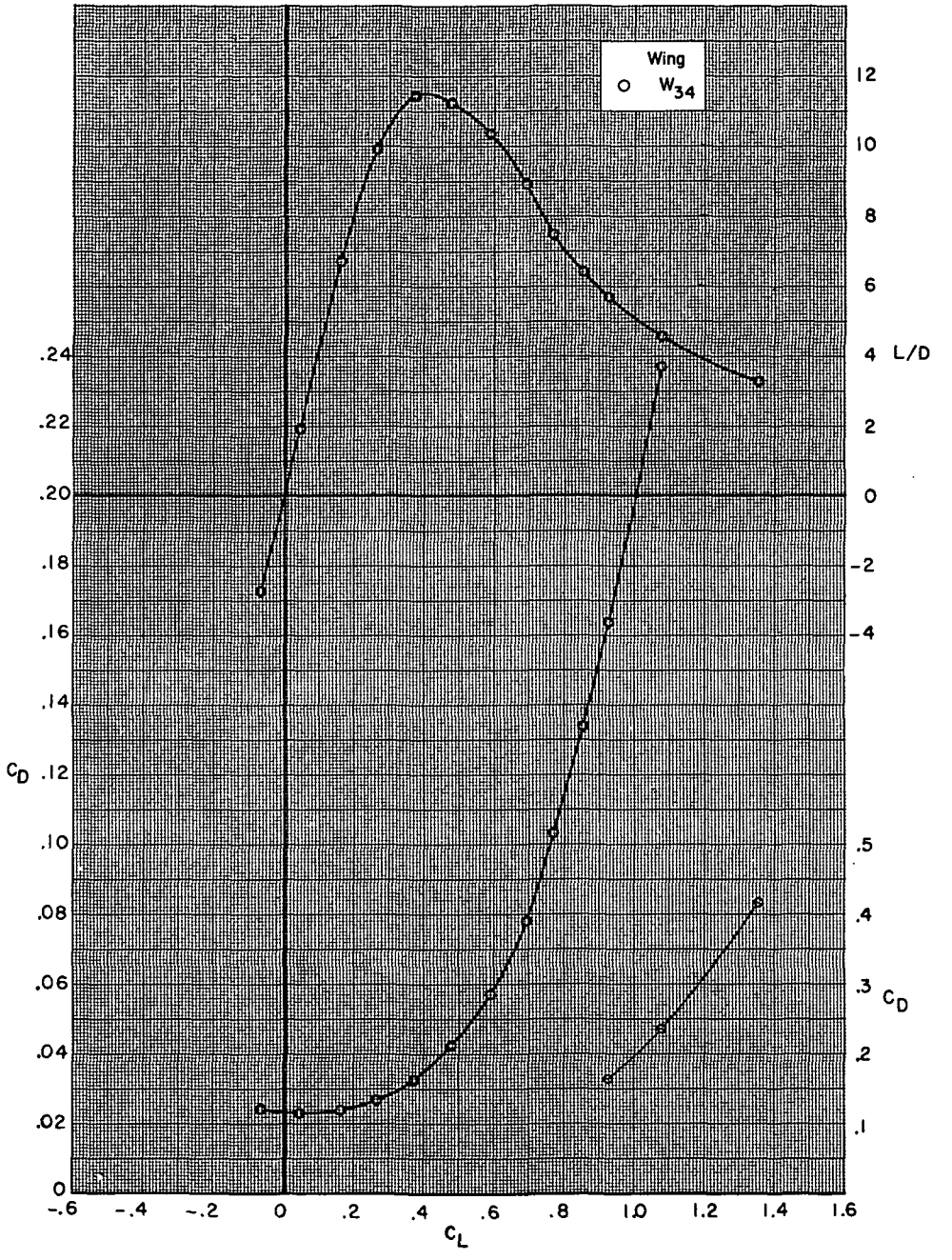

(a) Concluded.

Figure 21.- Continued.

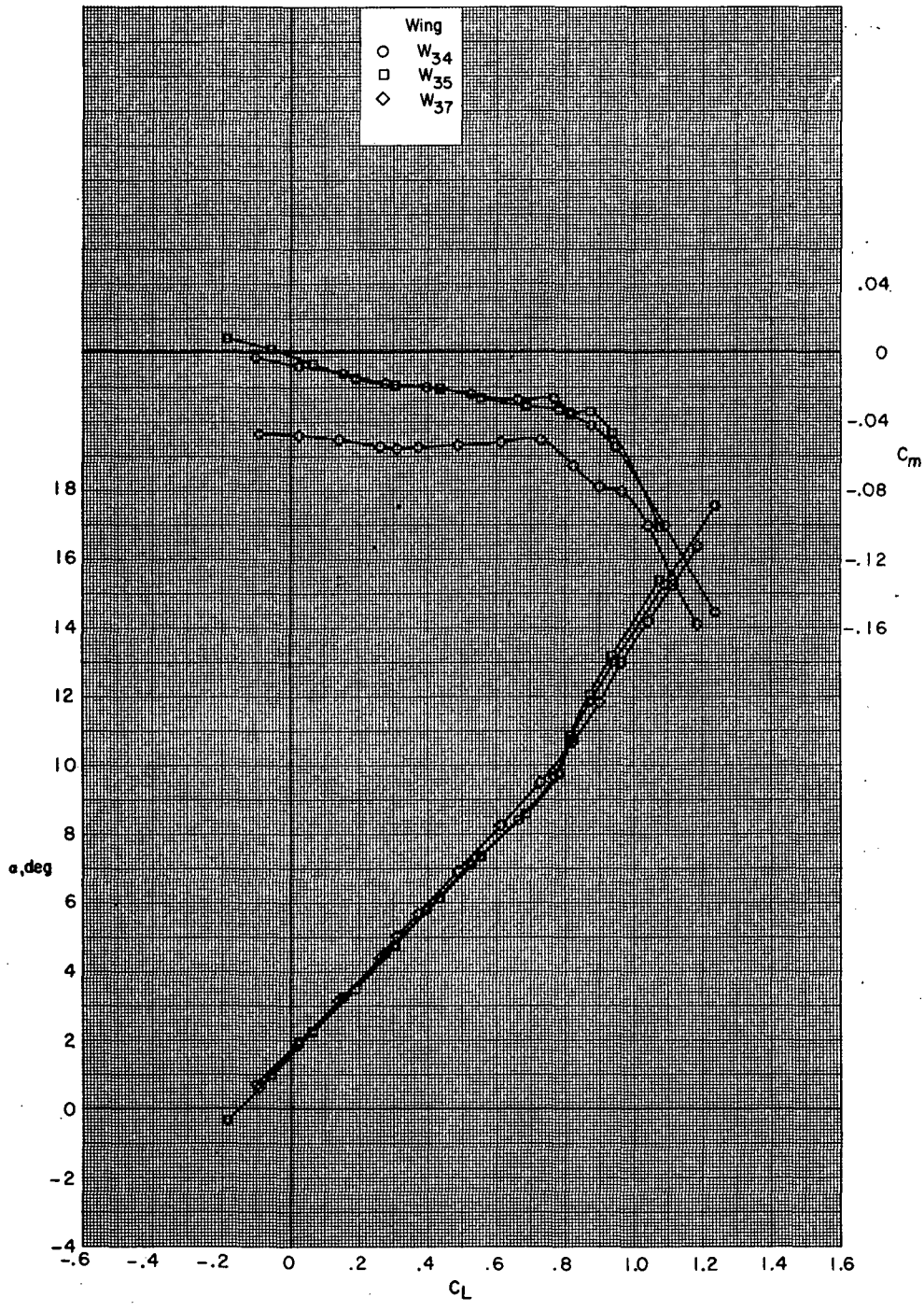

(b) M = 0.80.

Figure 21.- Continued.

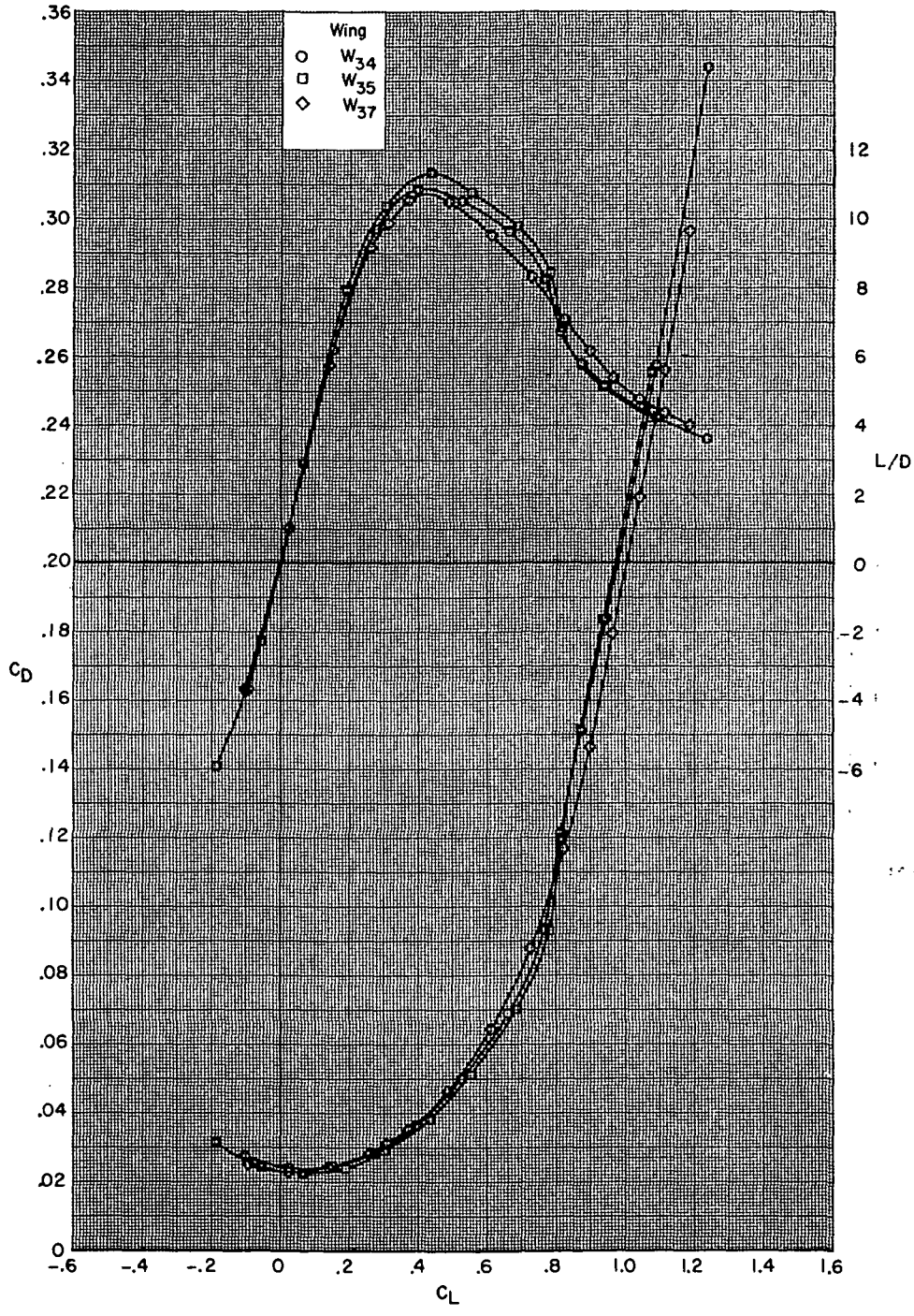

(b) Concluded.

Figure 21.- Continued.

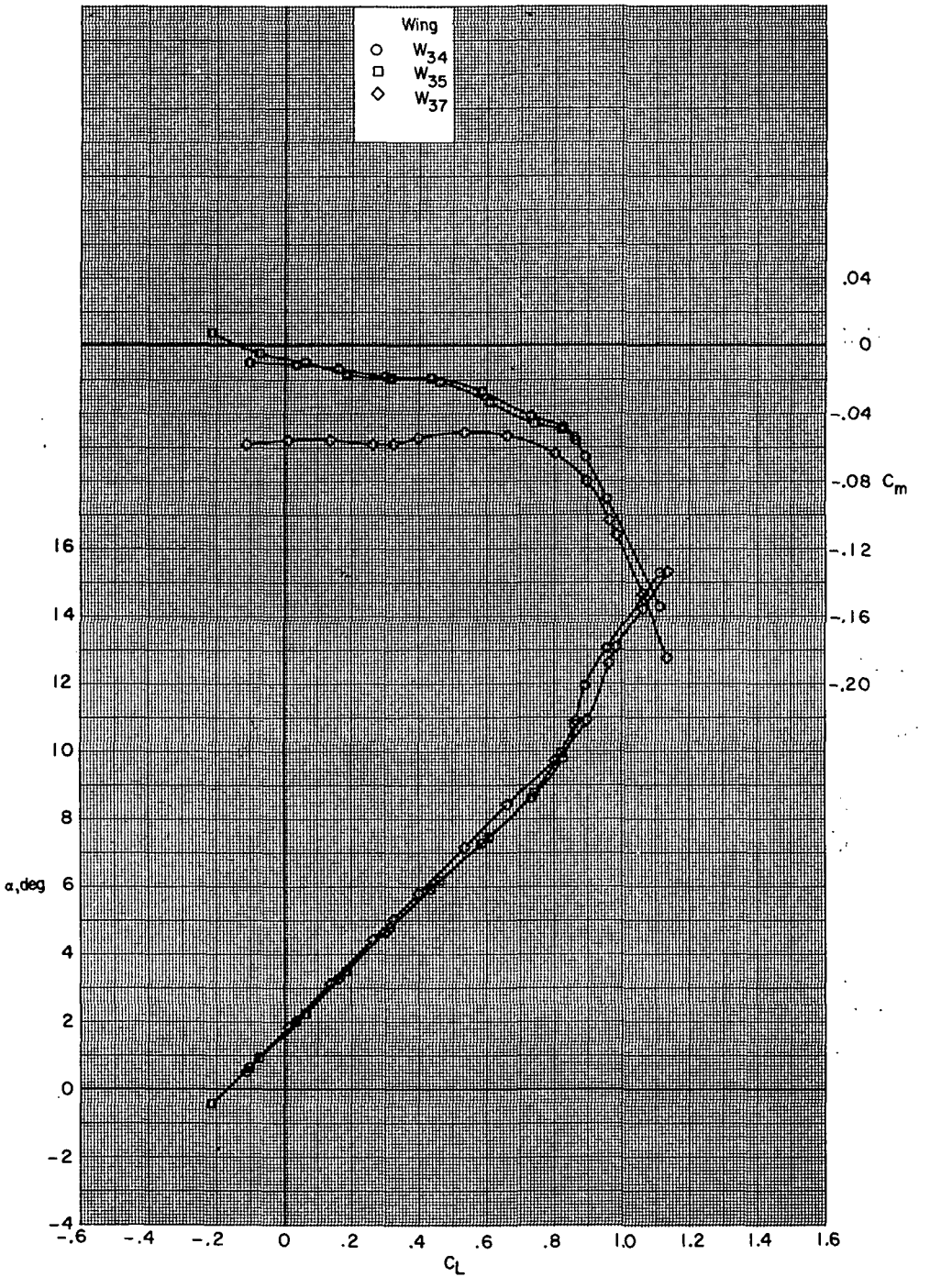

(c) M = 0.85.

Figure 21.- Continued.

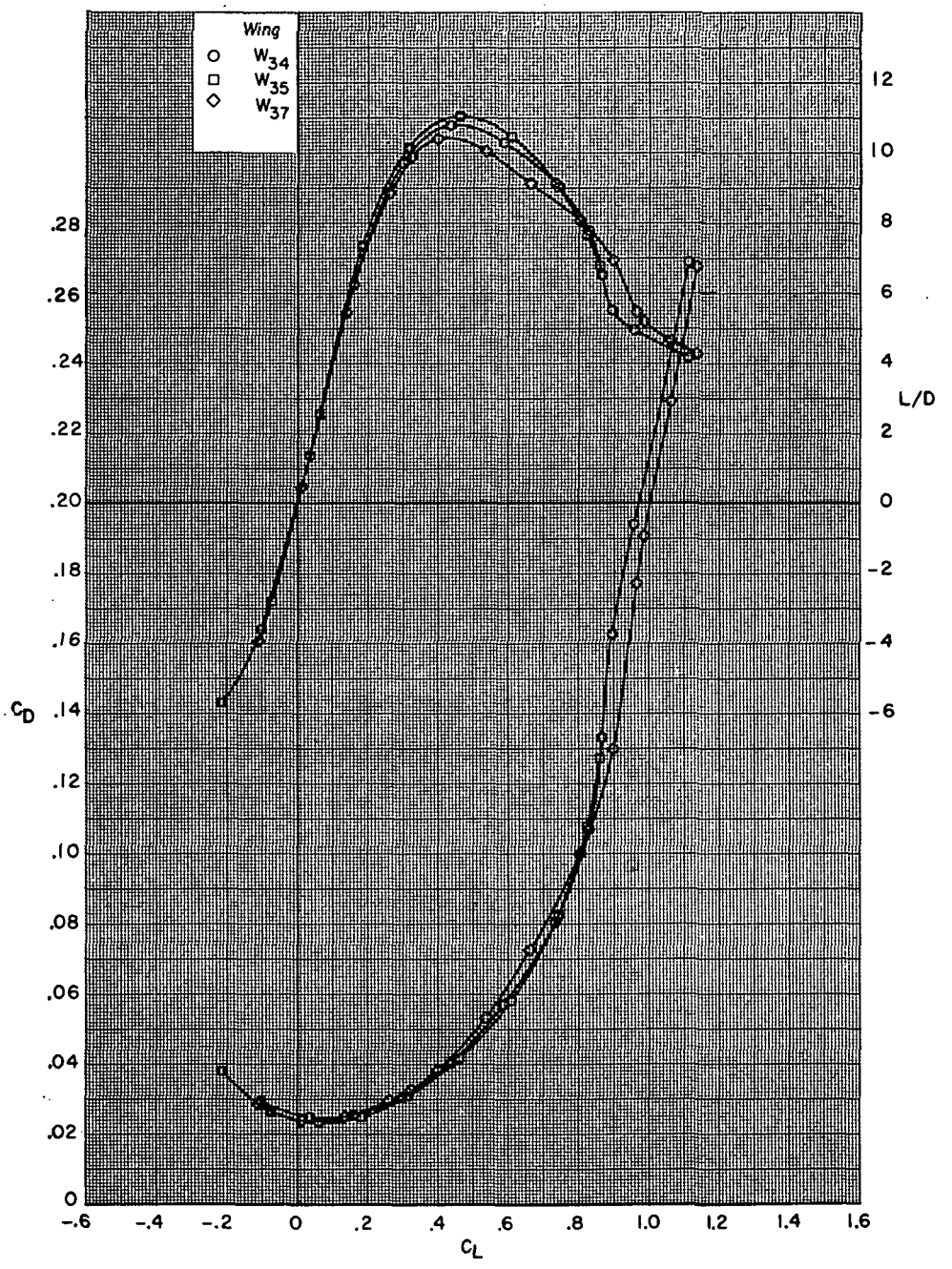

(c) Concluded.

Figure 21.- Continued.

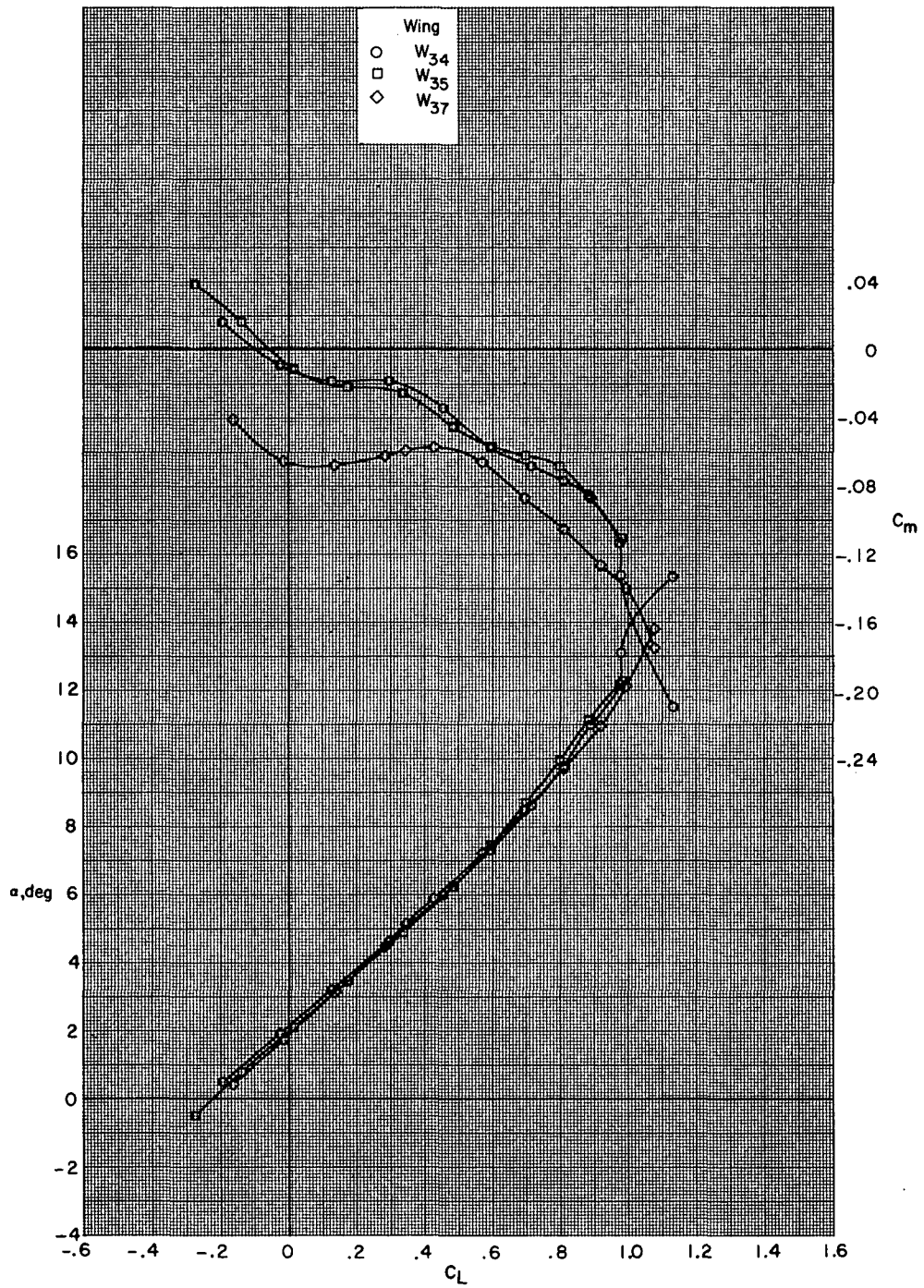

(d) M = 0.90.

Figure 21.- Continued.

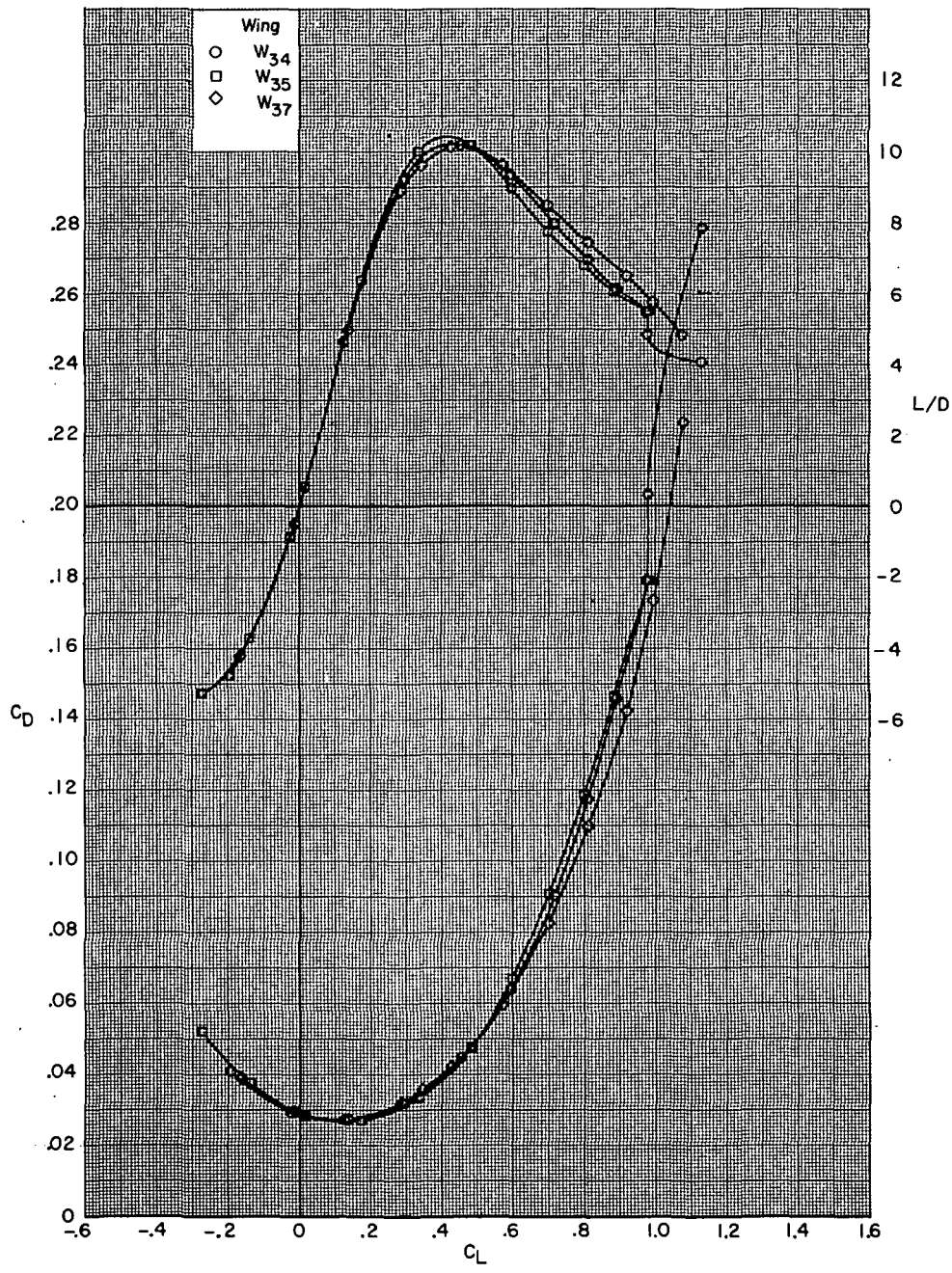

(d) Concluded.

Figure 21.- Continued.

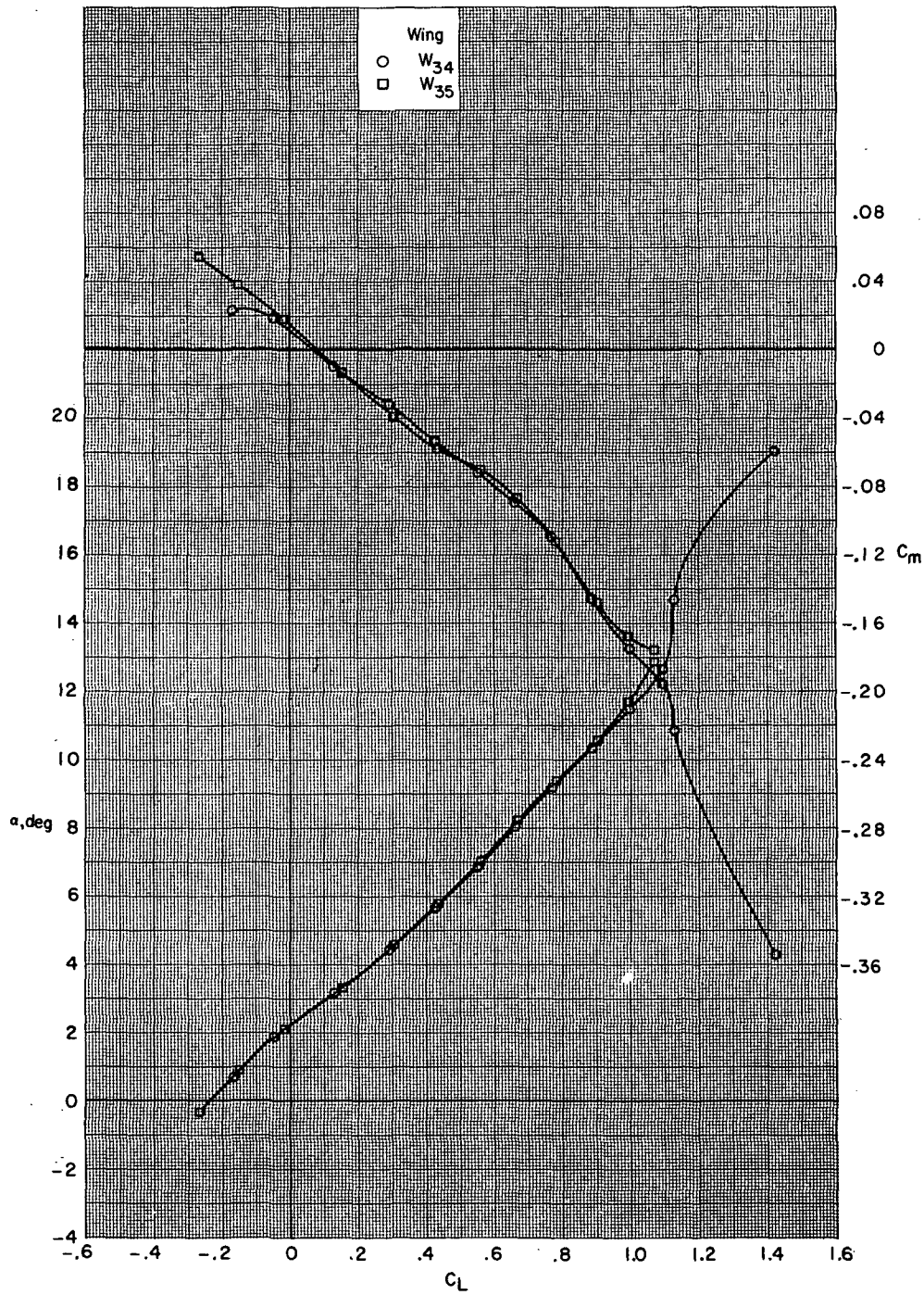

(e) M = 0.925.

Figure 21.- Continued.

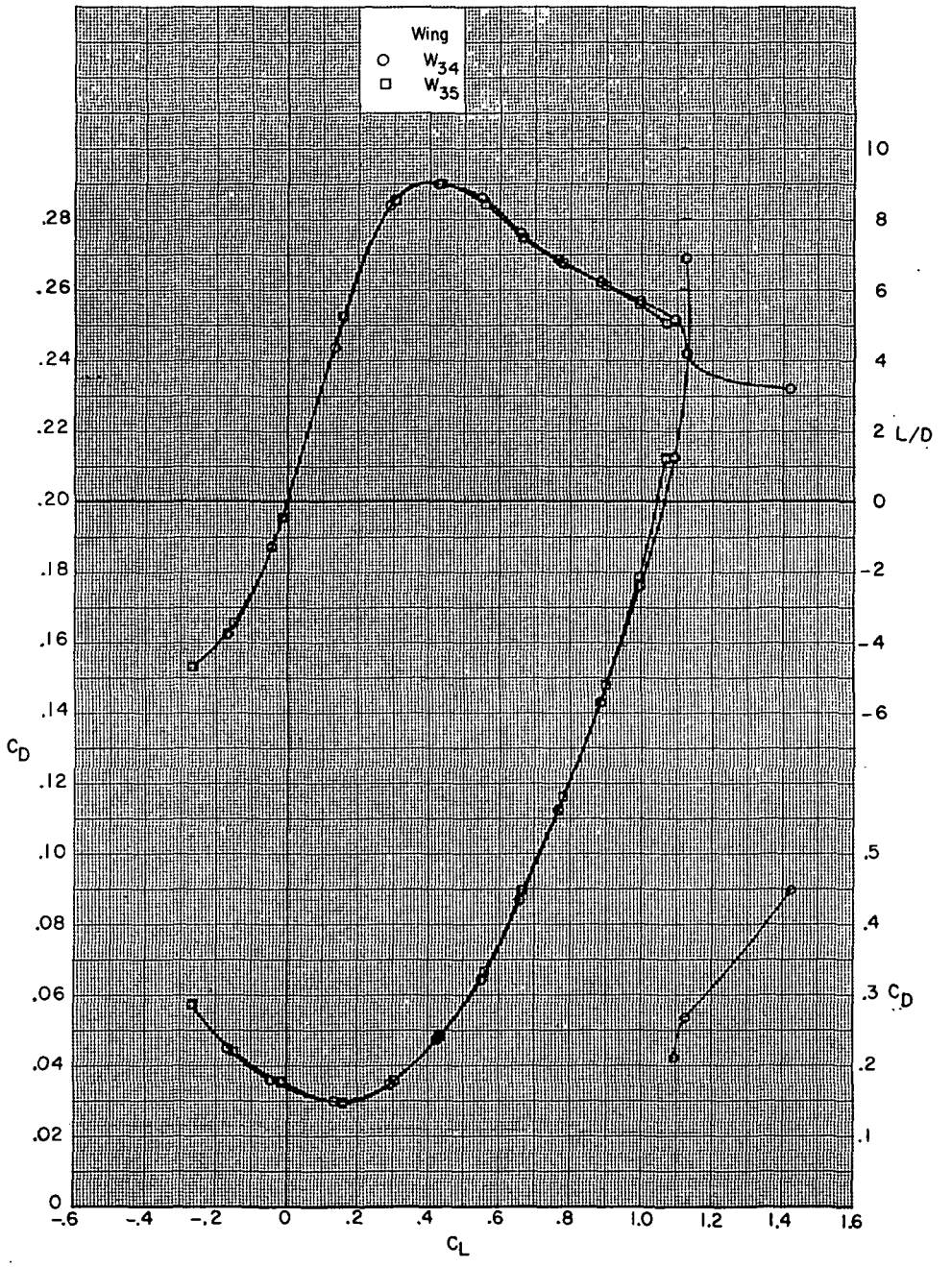

(e) Concluded.

Figure 21.- Continued.

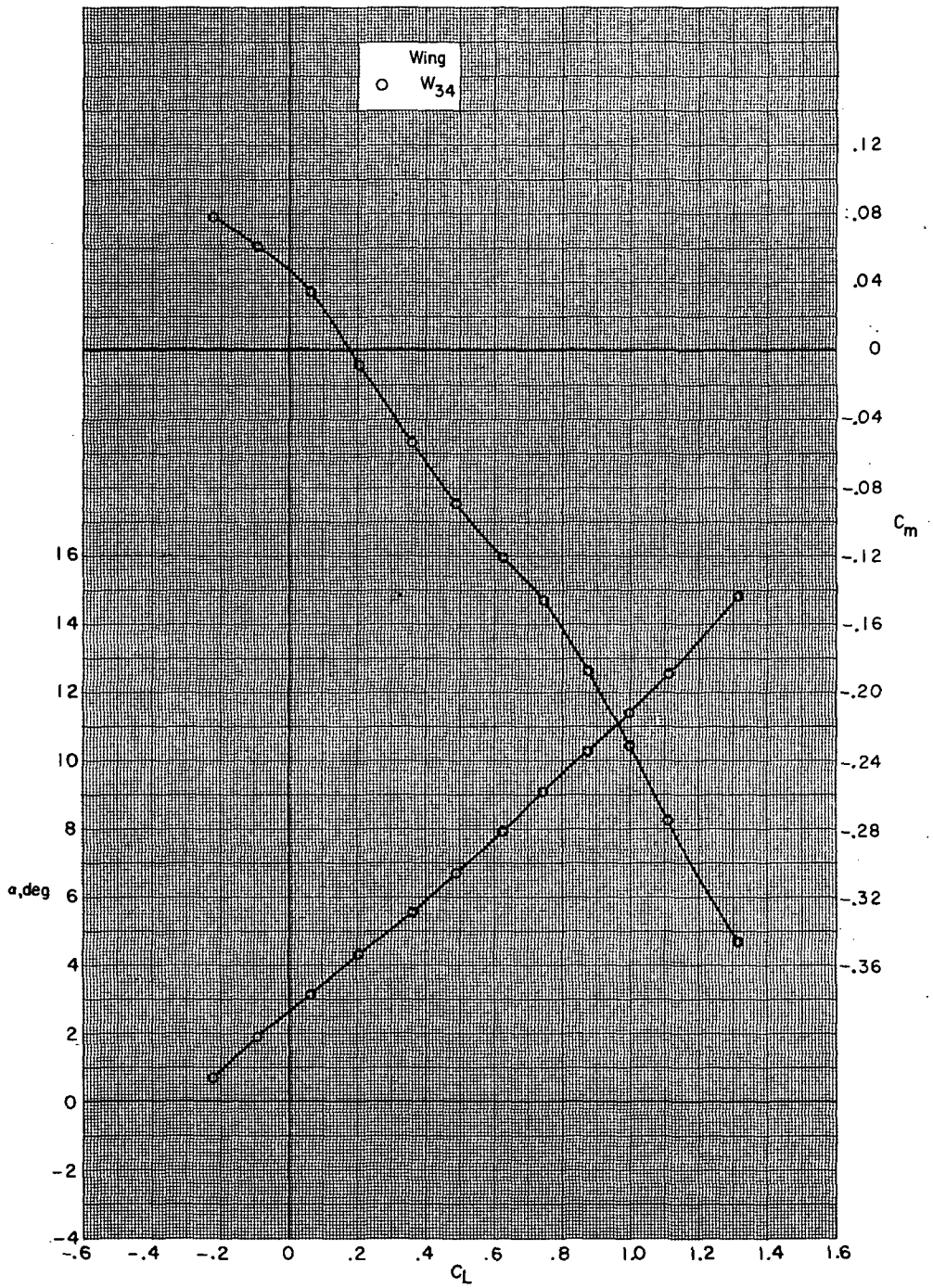

(f) M = 0.95.

Figure 21.- Continued.

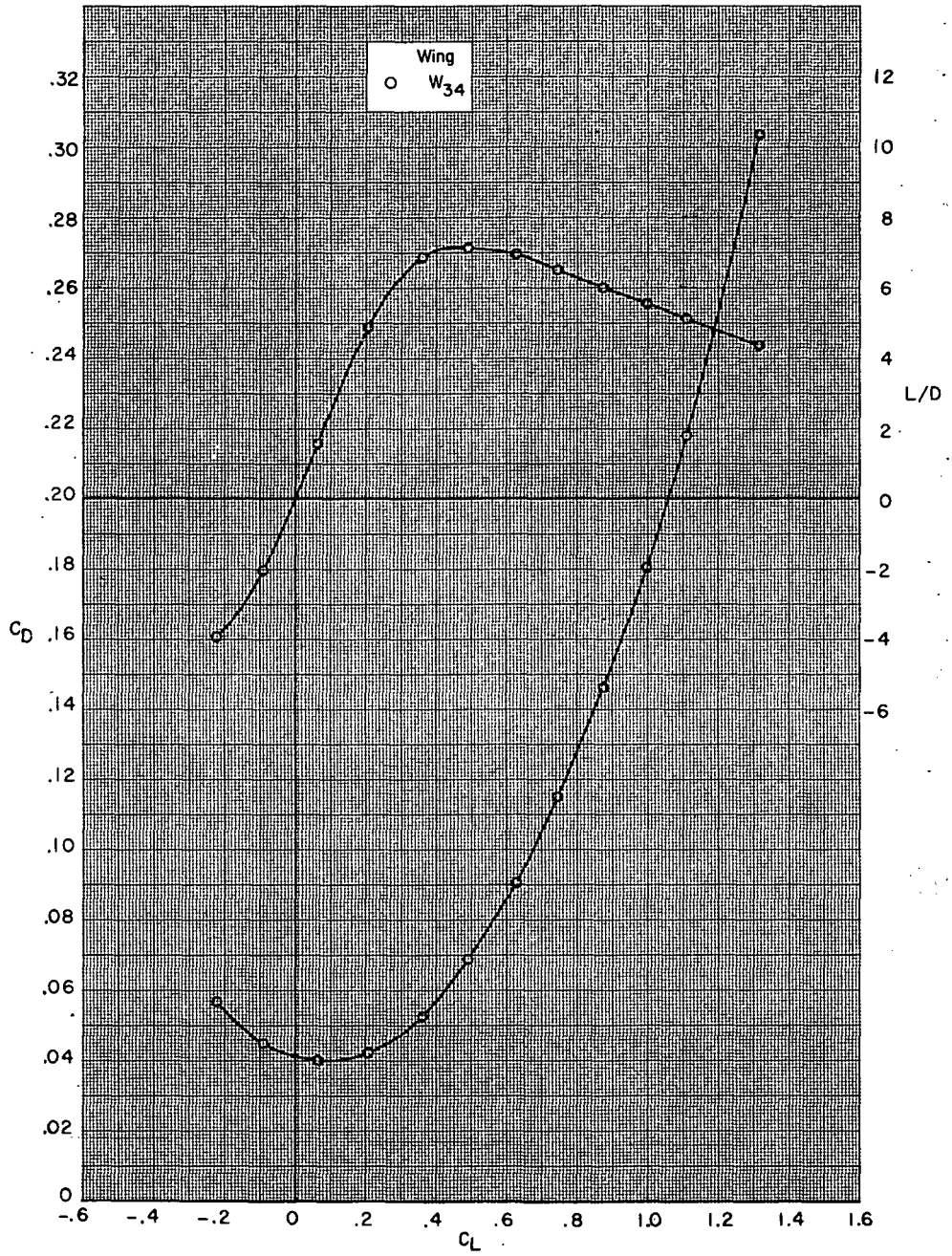

(f) Concluded.

Figure 21.- Concluded.

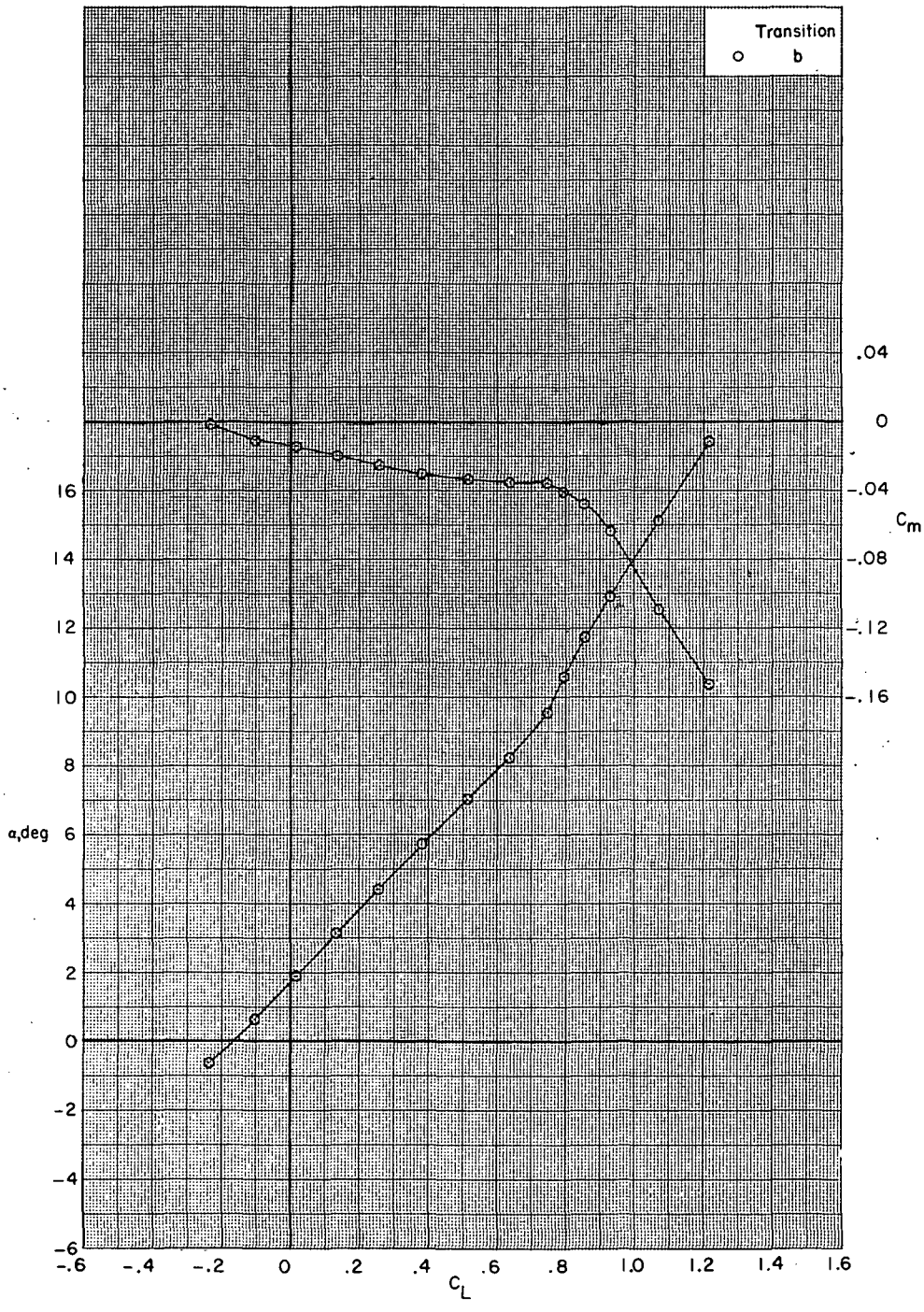

(a) M = 0.80.

Figure 22.- Aerodynamic characteristics for configuration $B_{80}G_{49}H_{13}I_{71}N^{b}_{32}V_{29}V_{38}W_{34e}X_{24}$ with wing swept 35.0°.

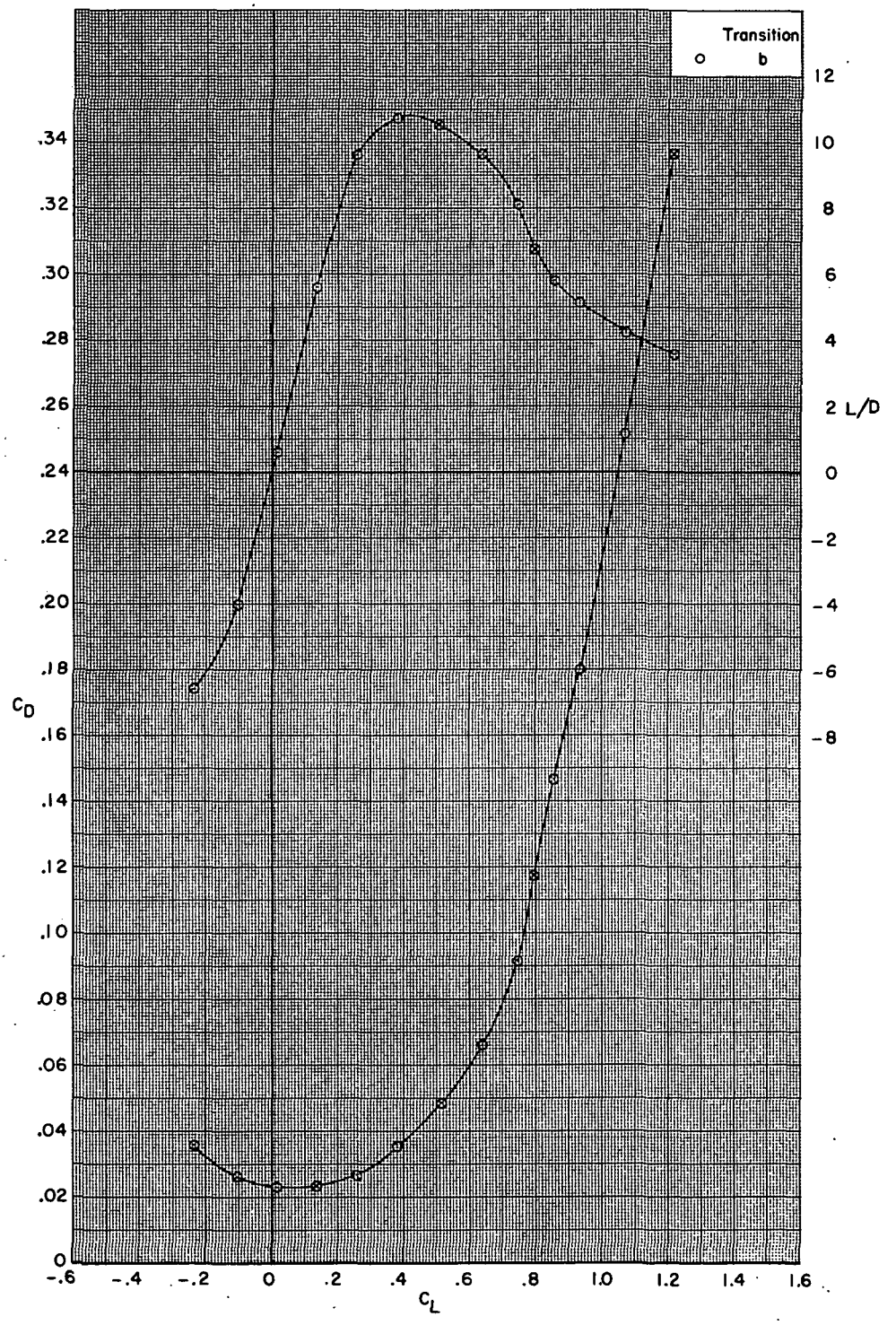

(a) Concluded.

Figure 22.- Continued.

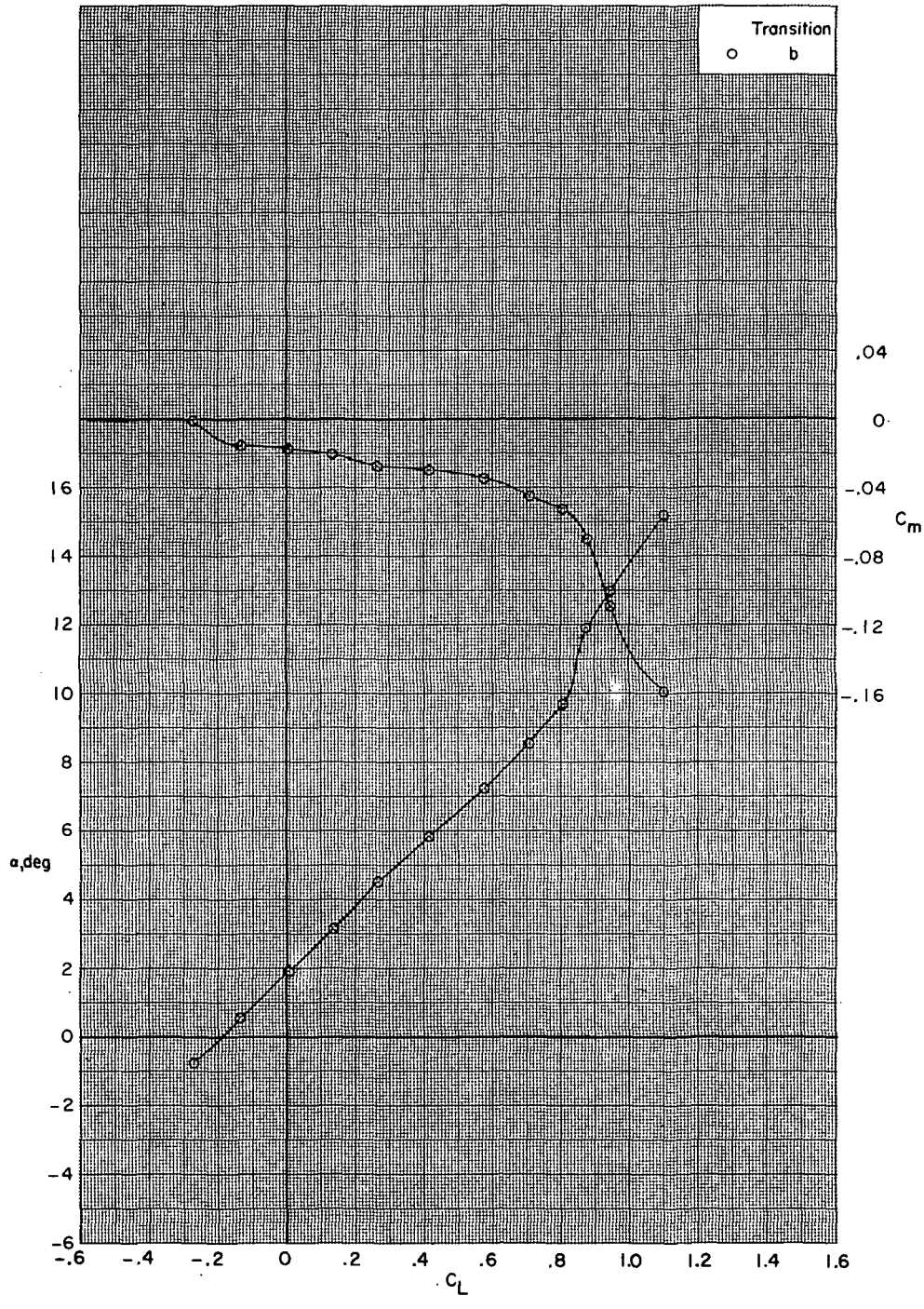

(b) M = 0.85.

Figure 22.- Continued.

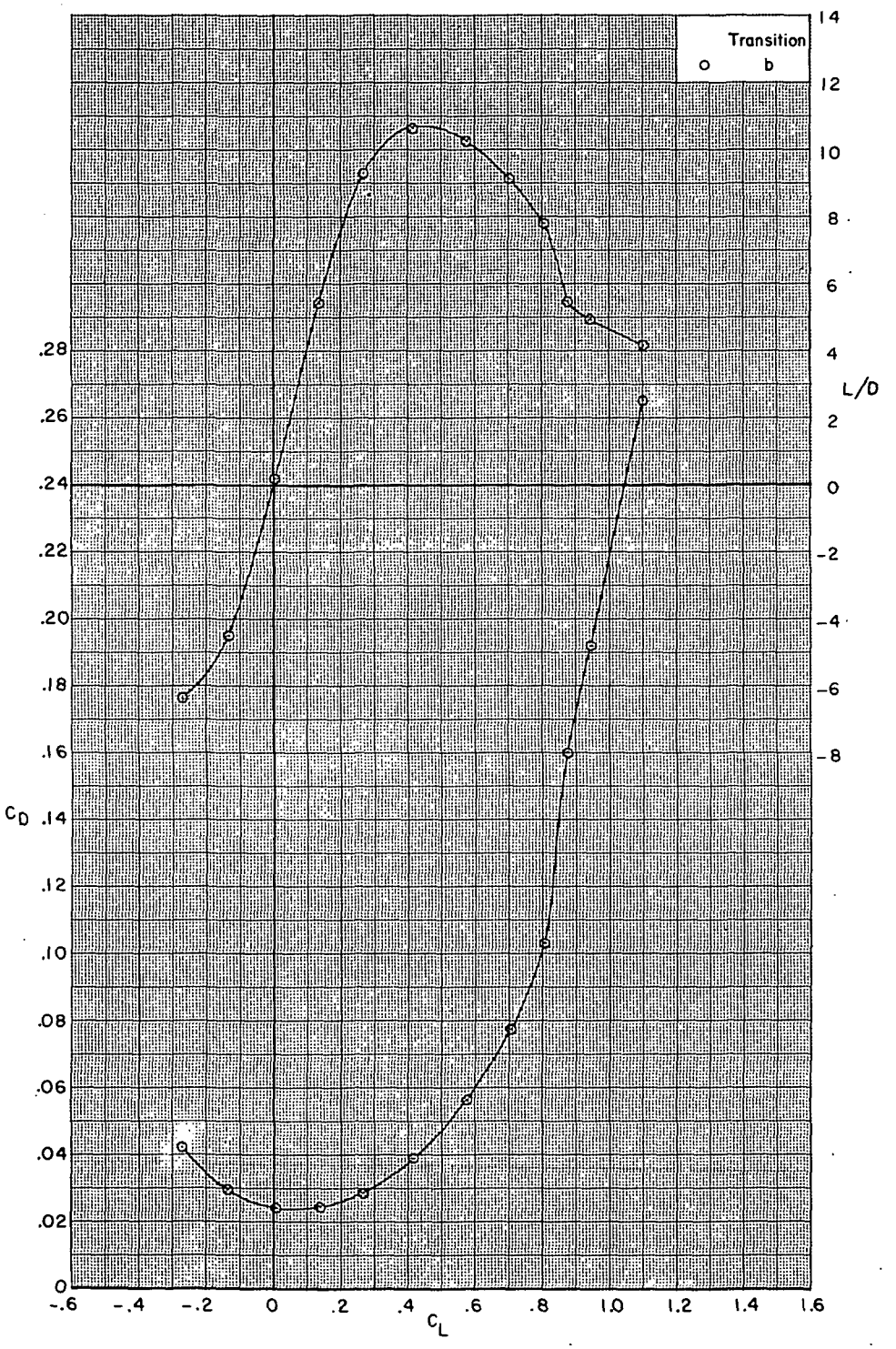

(b) Concluded.

Figure 22.- Continued.

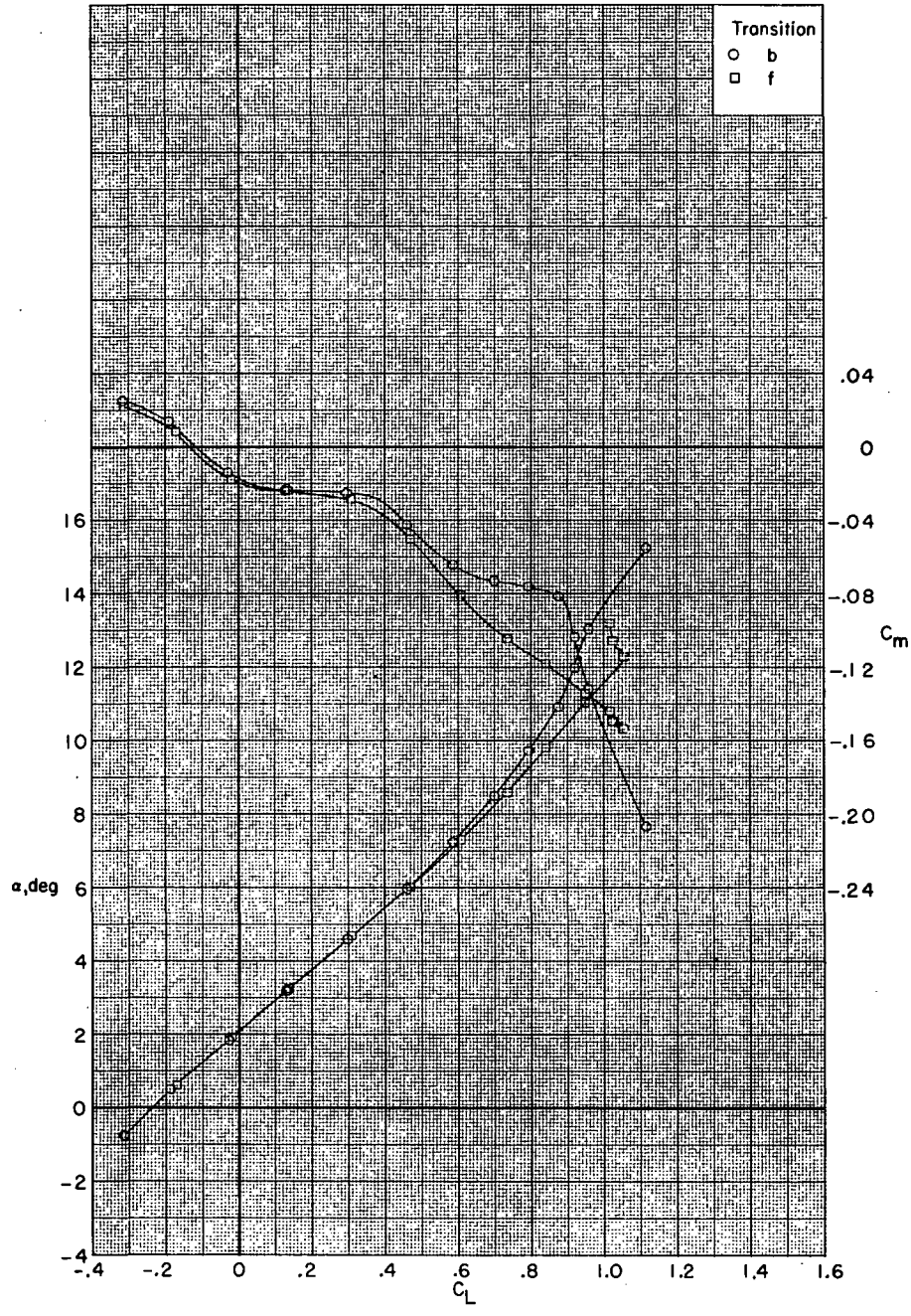

(c) M = 0.90.

Figure 22.- Continued.

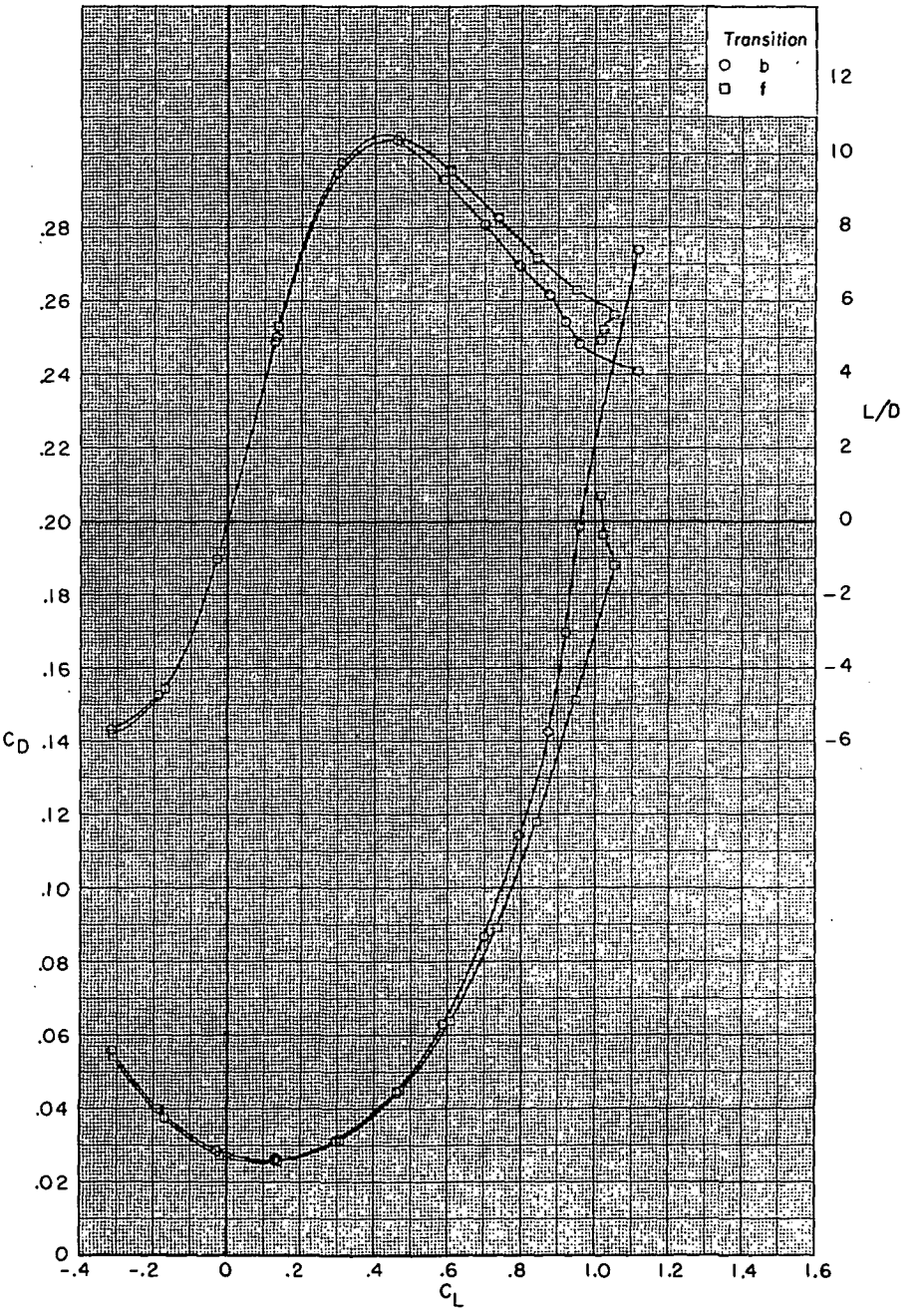

(c) Concluded.

Figure 22.- Concluded.

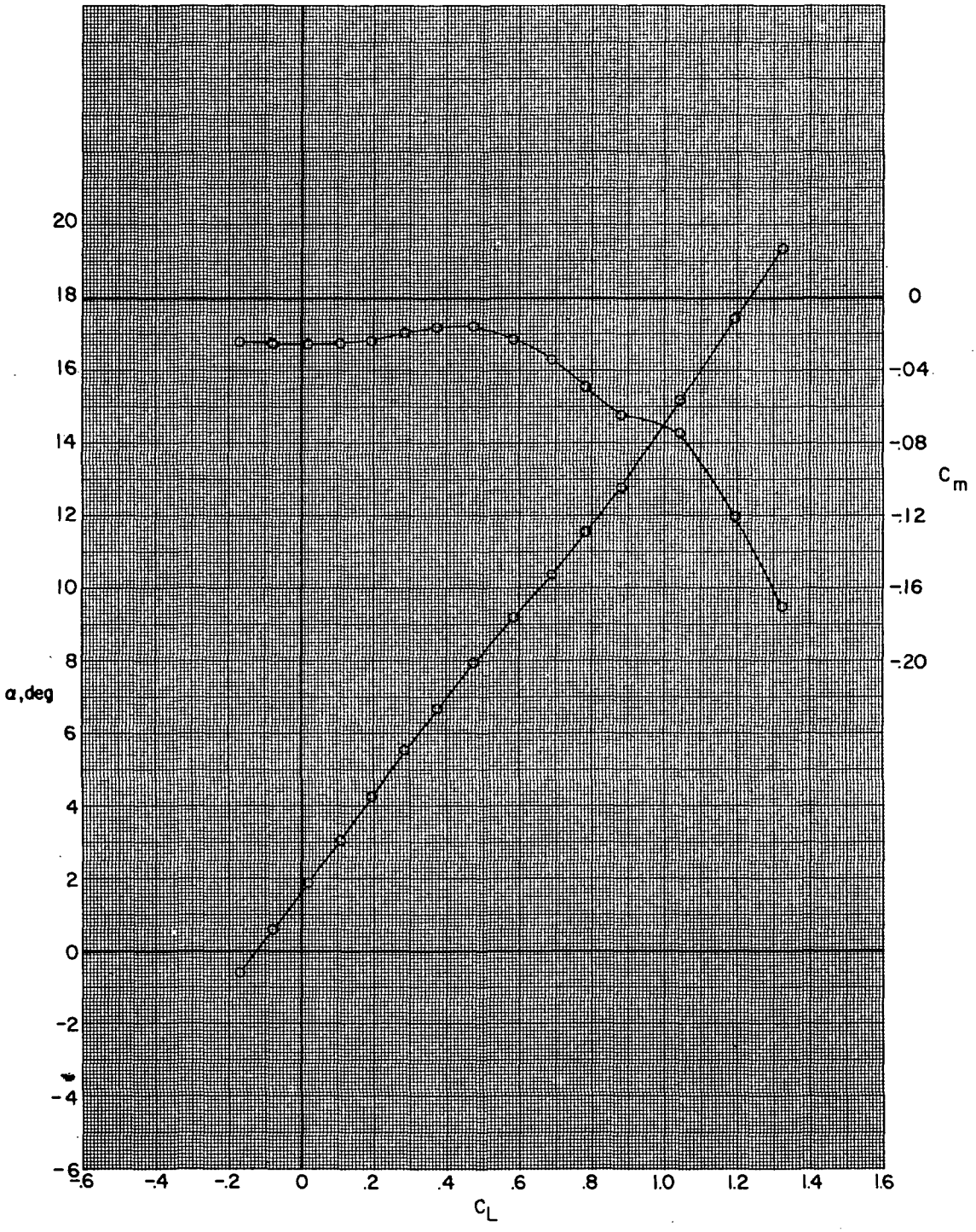

(a) M = 0.80.

Figure 23.- Aerodynamic characteristics for configuration $B_{80}G_{47}H_{13}I_{71}N^{b}_{32}V_{29}V_{38}W_{32}X_{24}X_{168}$ with wing swept 45.0°.

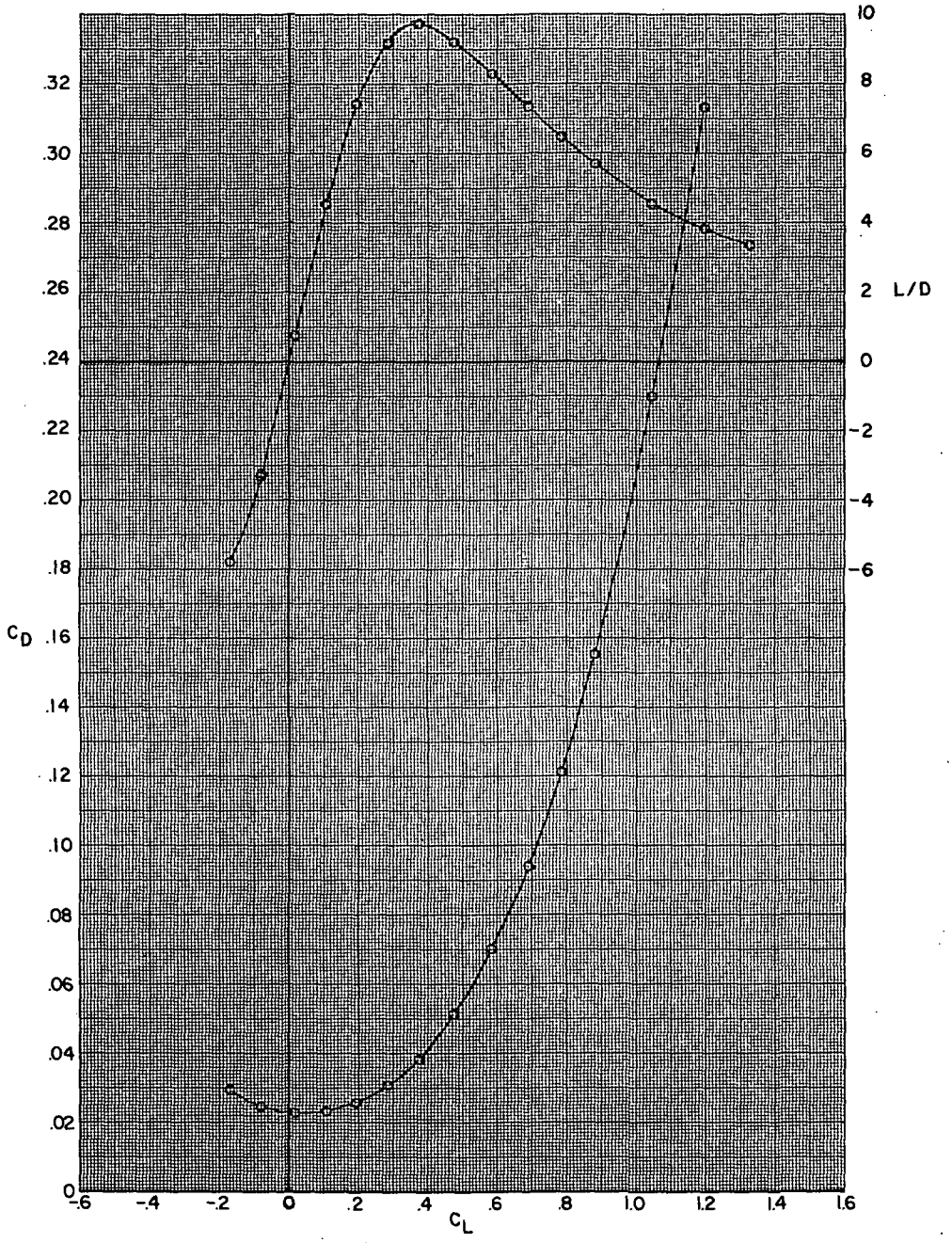

(a) Concluded.

Figure 23.- Continued.

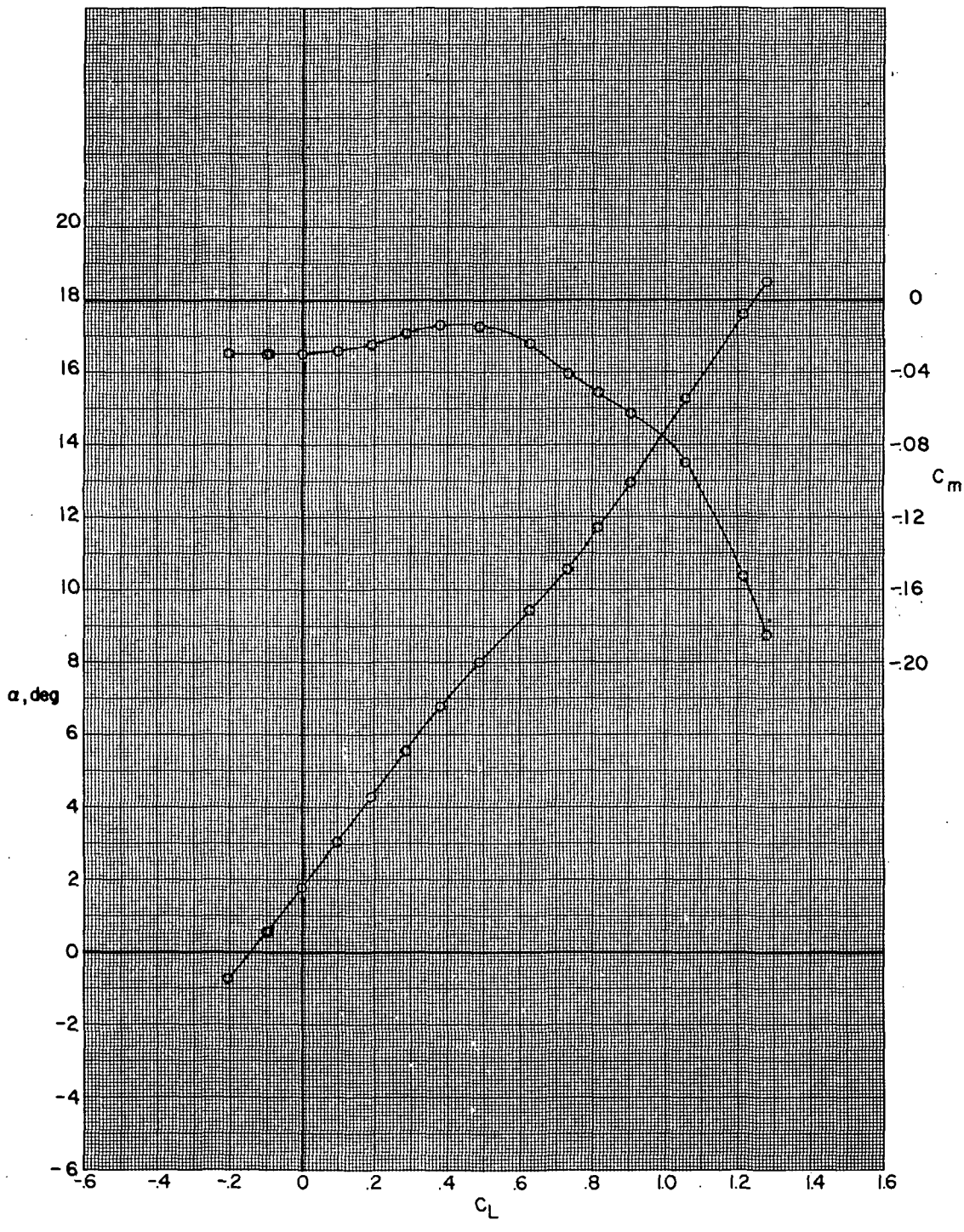

(b) M = 0.85.

Figure 23.- Continued.

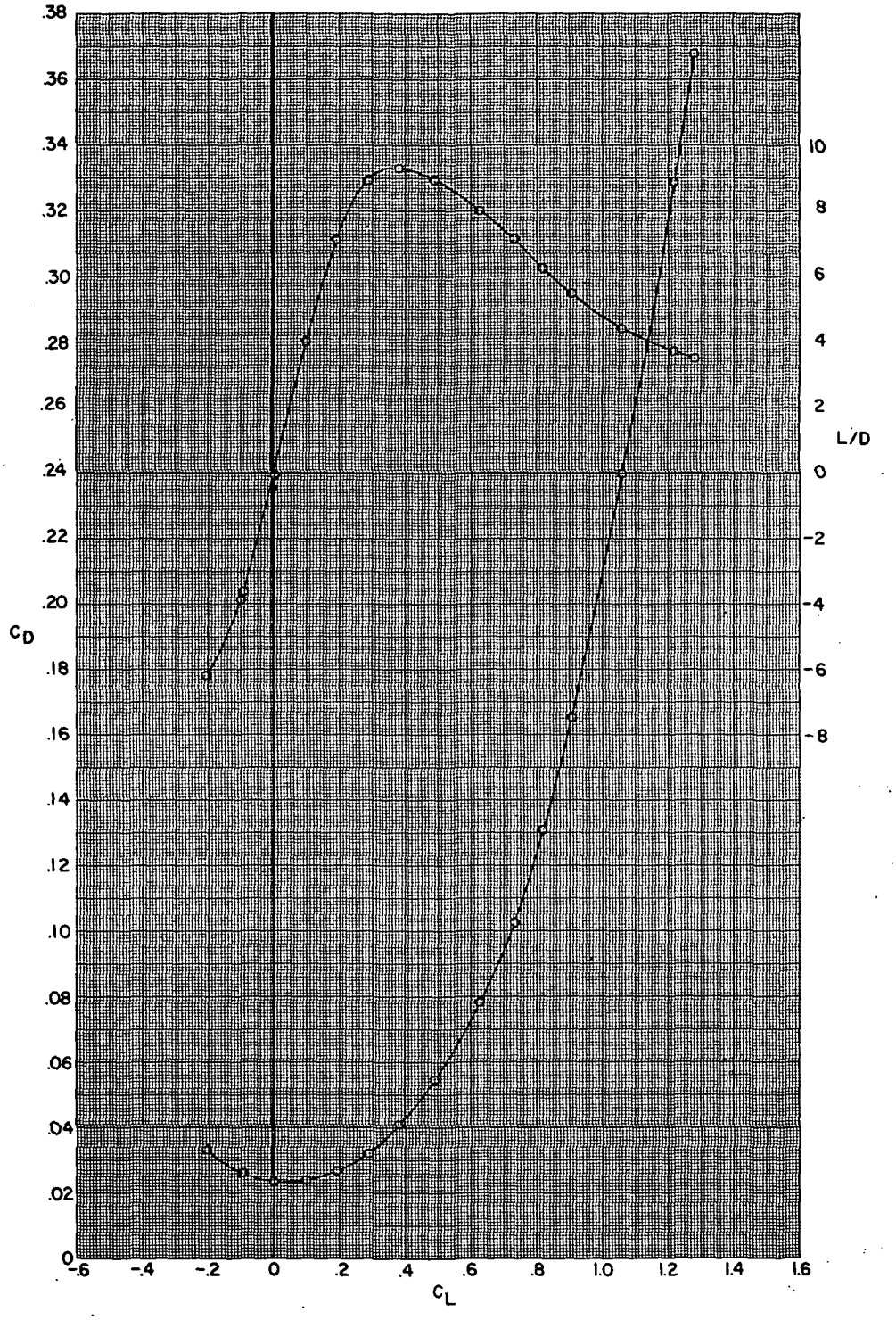

(b) Concluded.

Figure 23.- Continued.

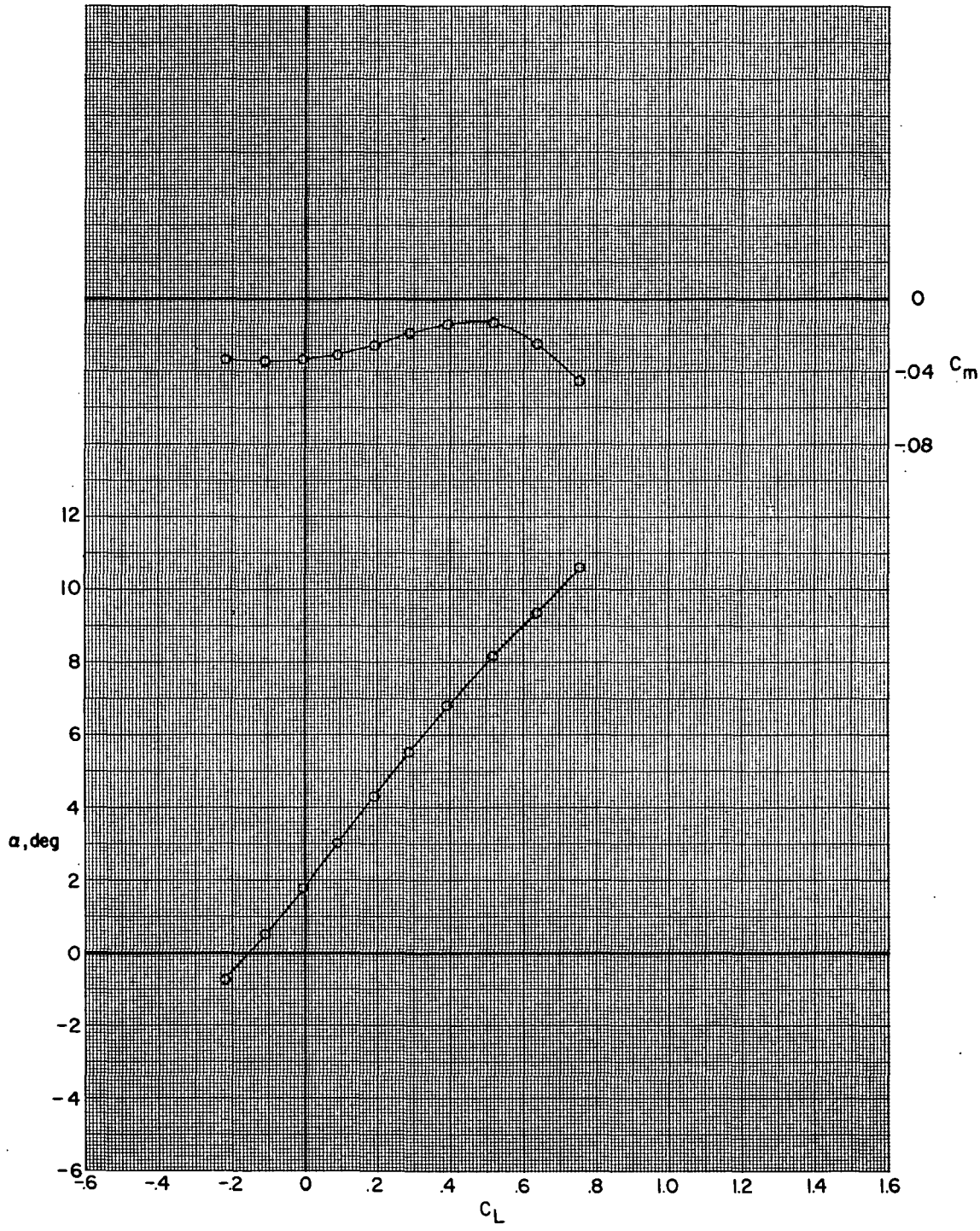

(c) M = 0.875.

Figure 23.- Continued.

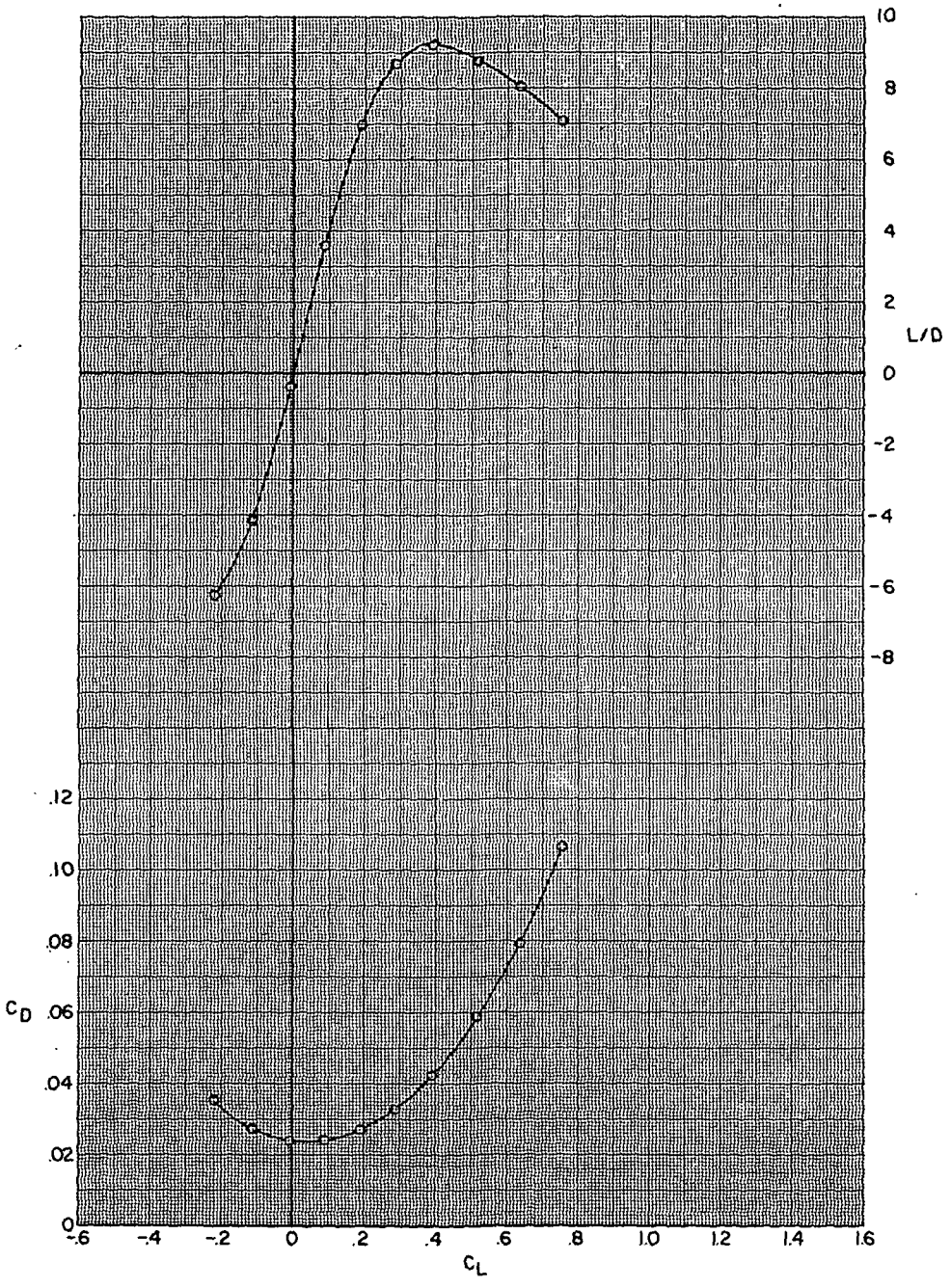

(c) Concluded.

Figure 23.- Continued.

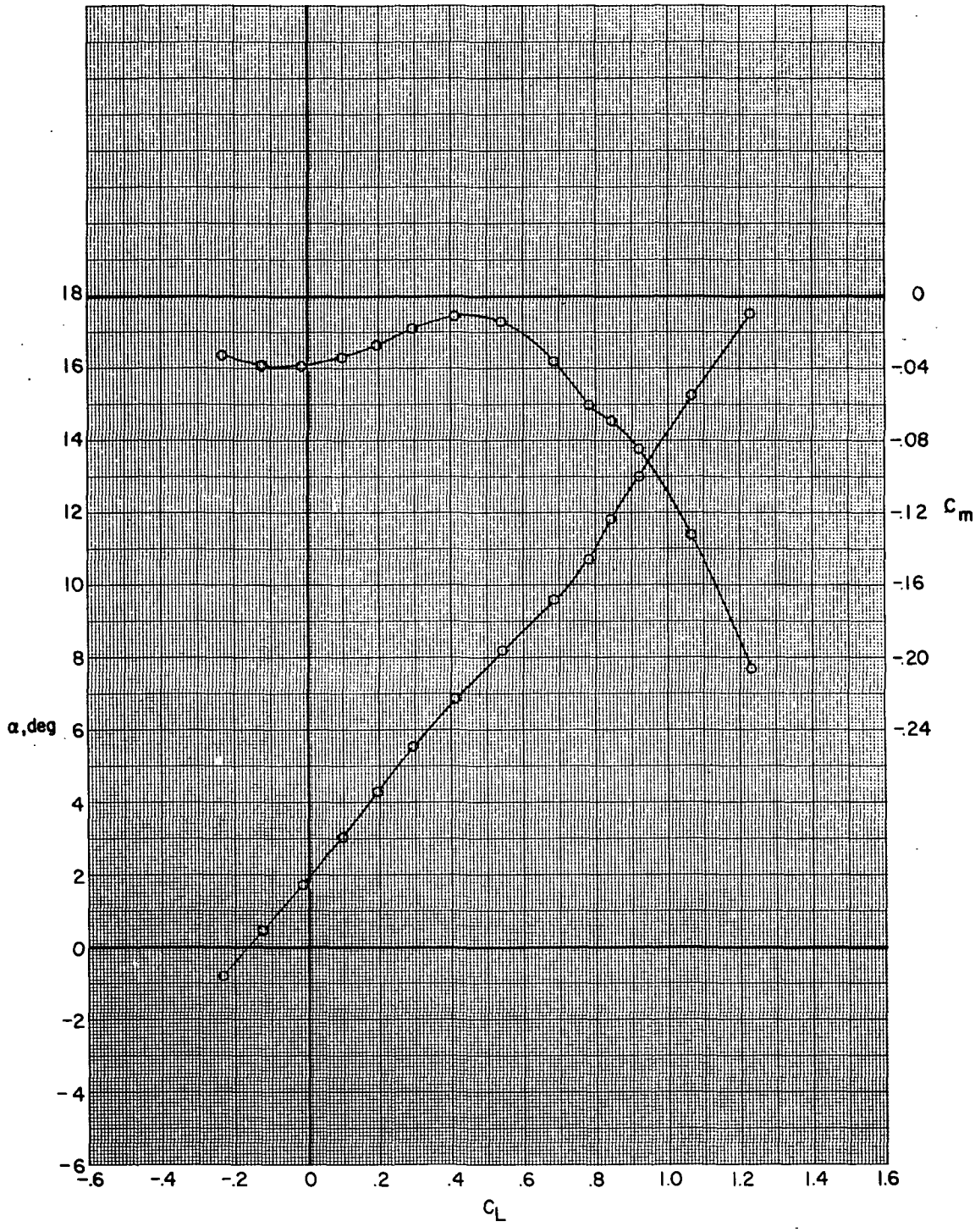

(d) M = 0.90.

Figure 23.- Continued.

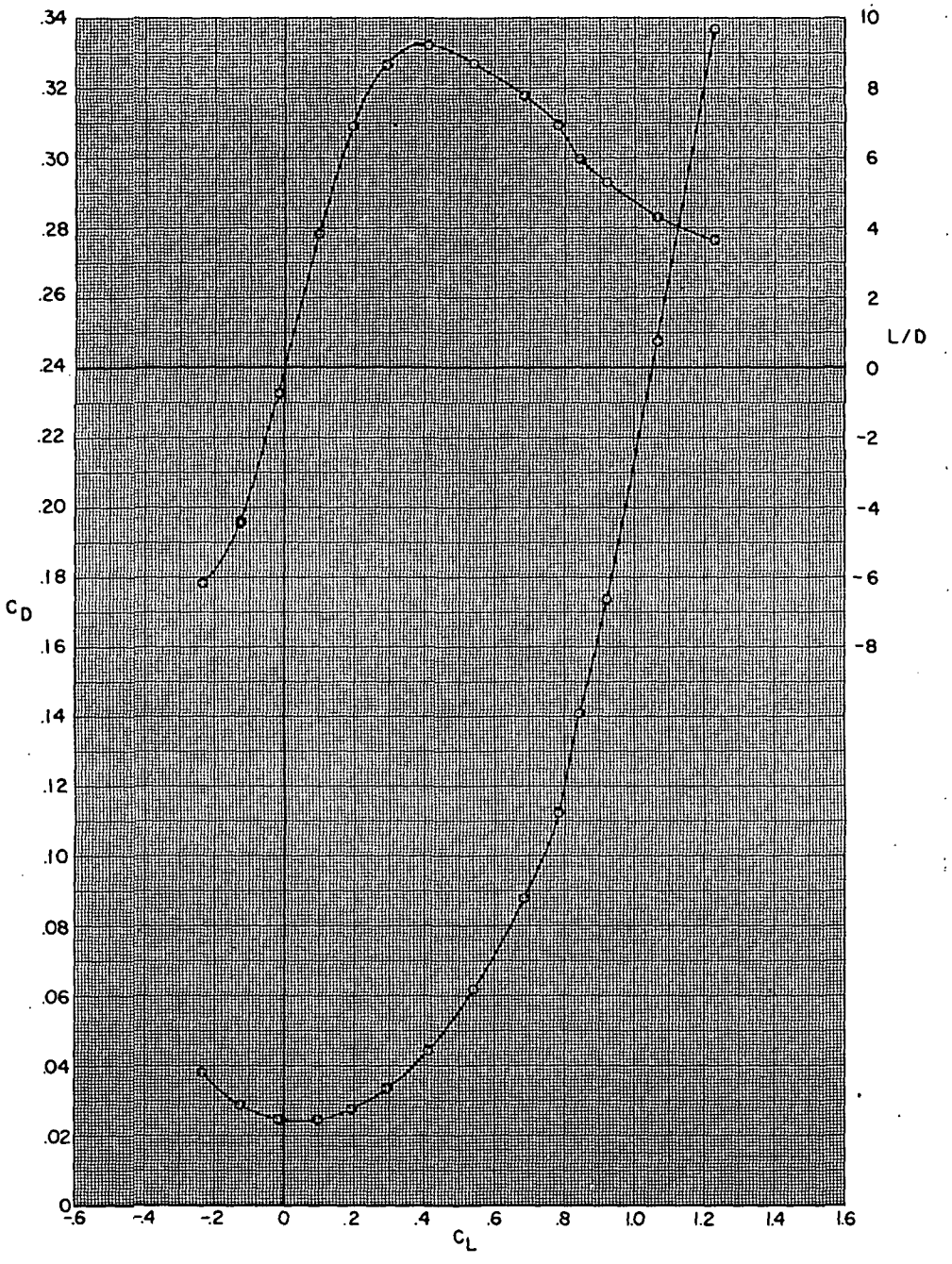

(d) Concluded.

Figure 23.- Continued.

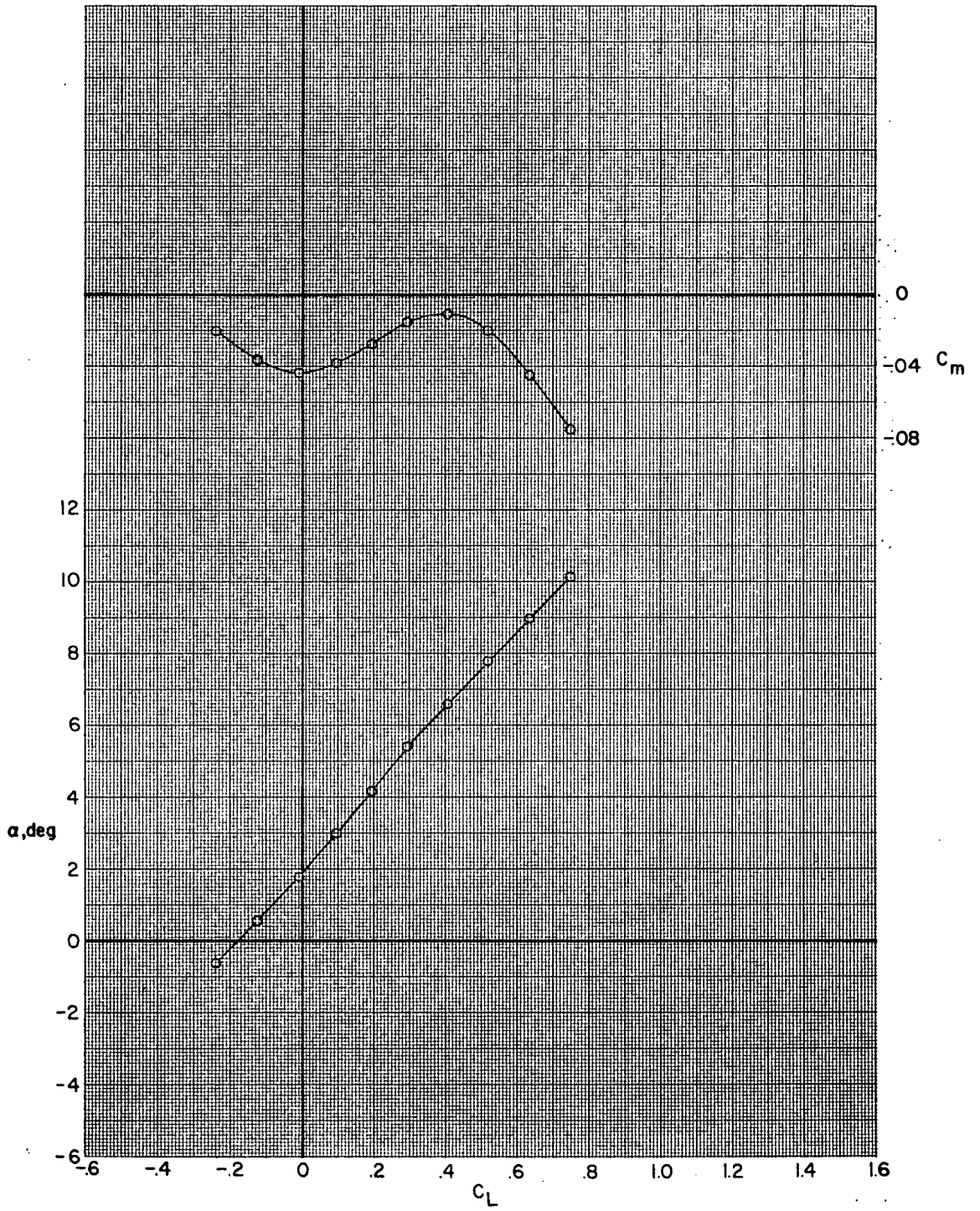

(e) M = 0.925.

Figure 23.- Continued.

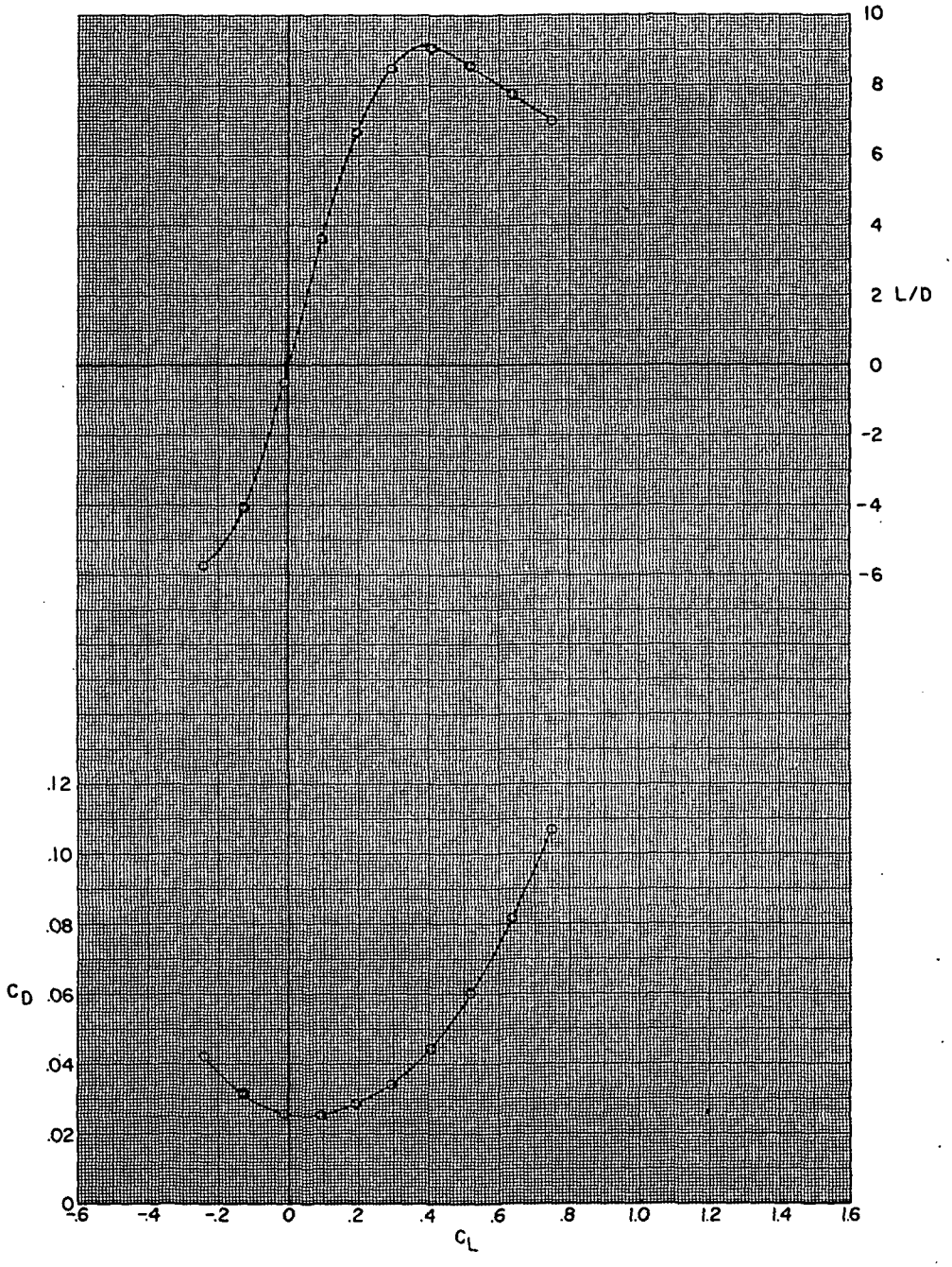

(e) Concluded.

Figure 23.- Continued.

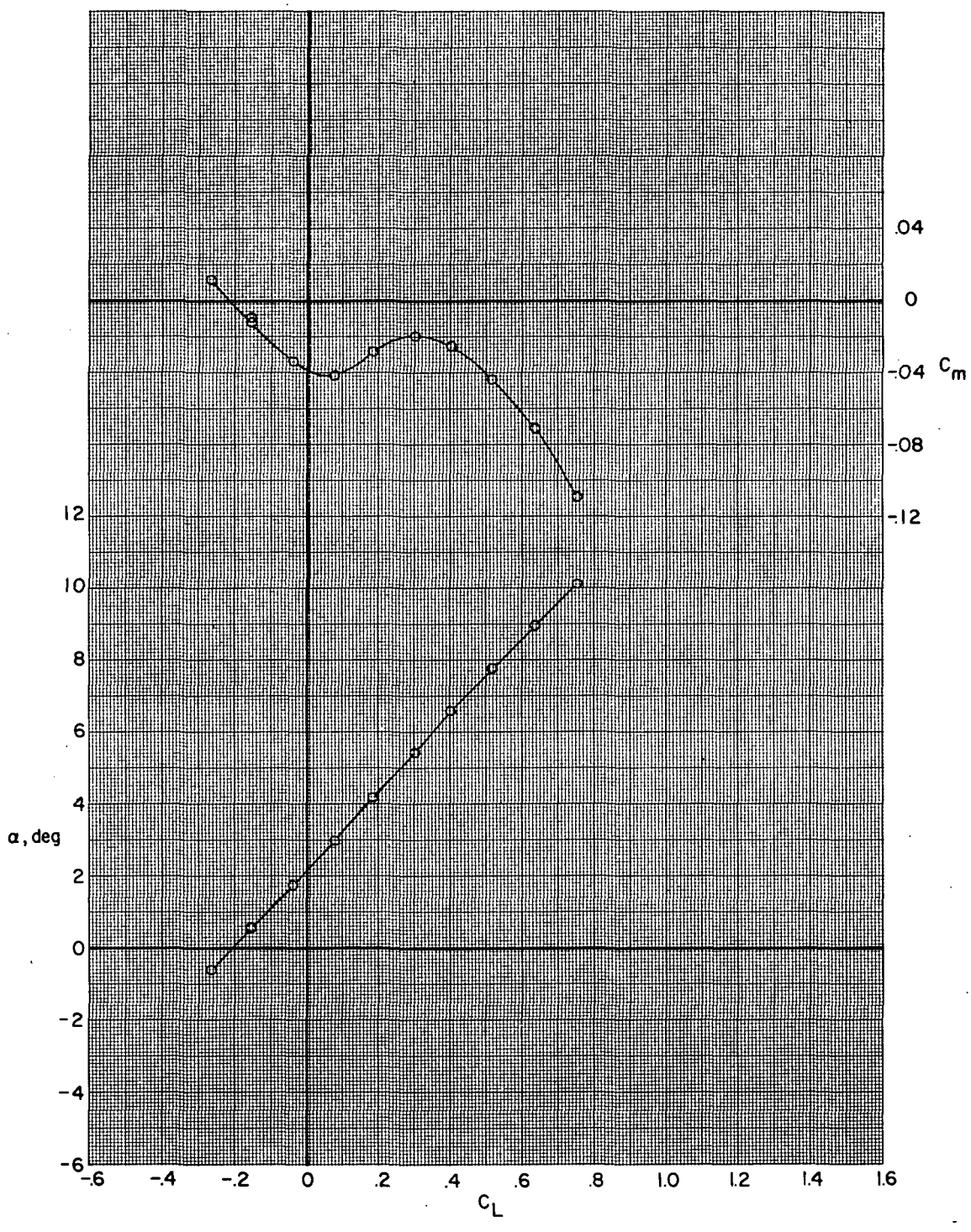

(f) M = 0.95.

Figure 23.- Continued.

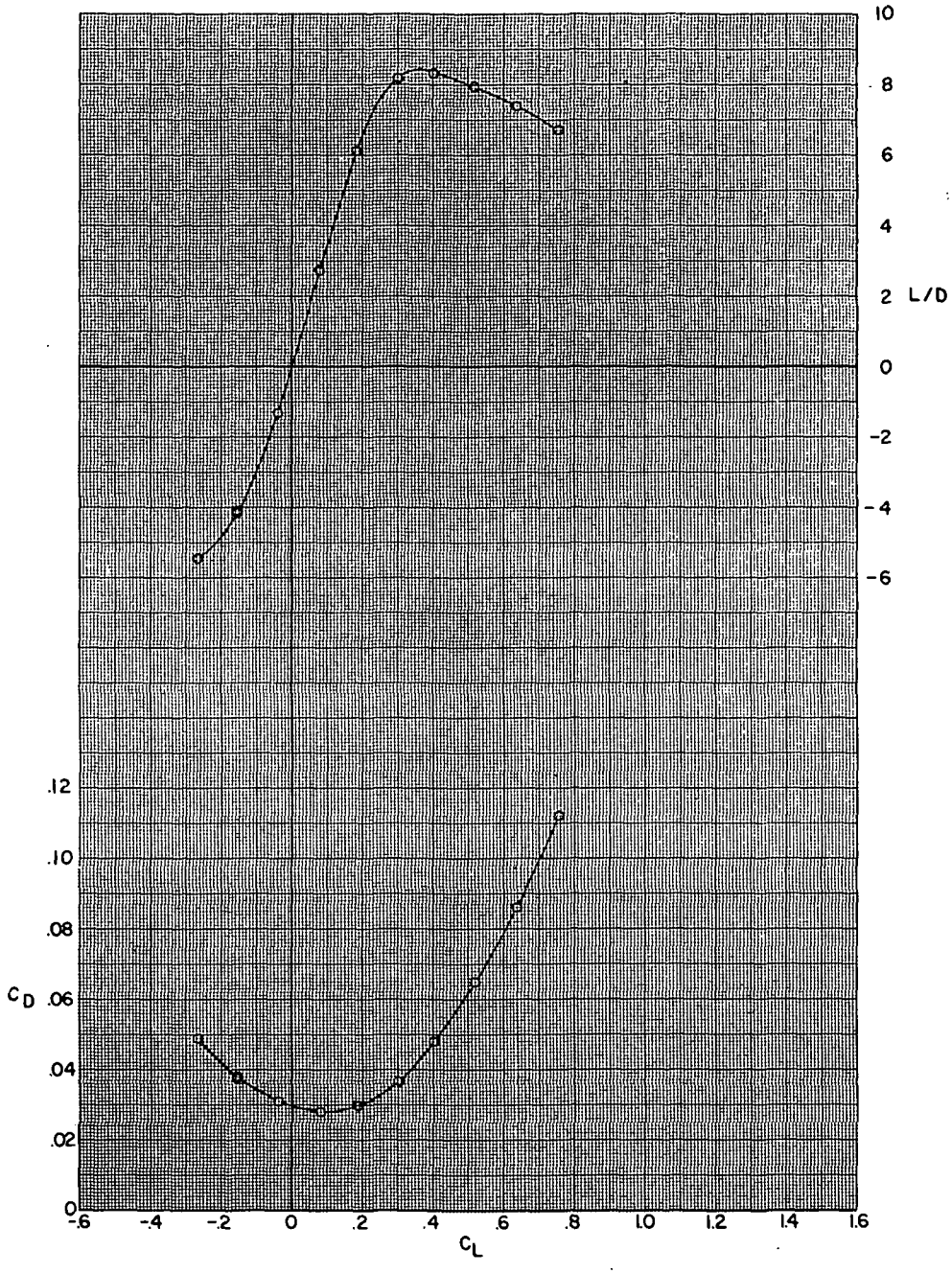

(f) Concluded.

Figure 23.- Concluded.

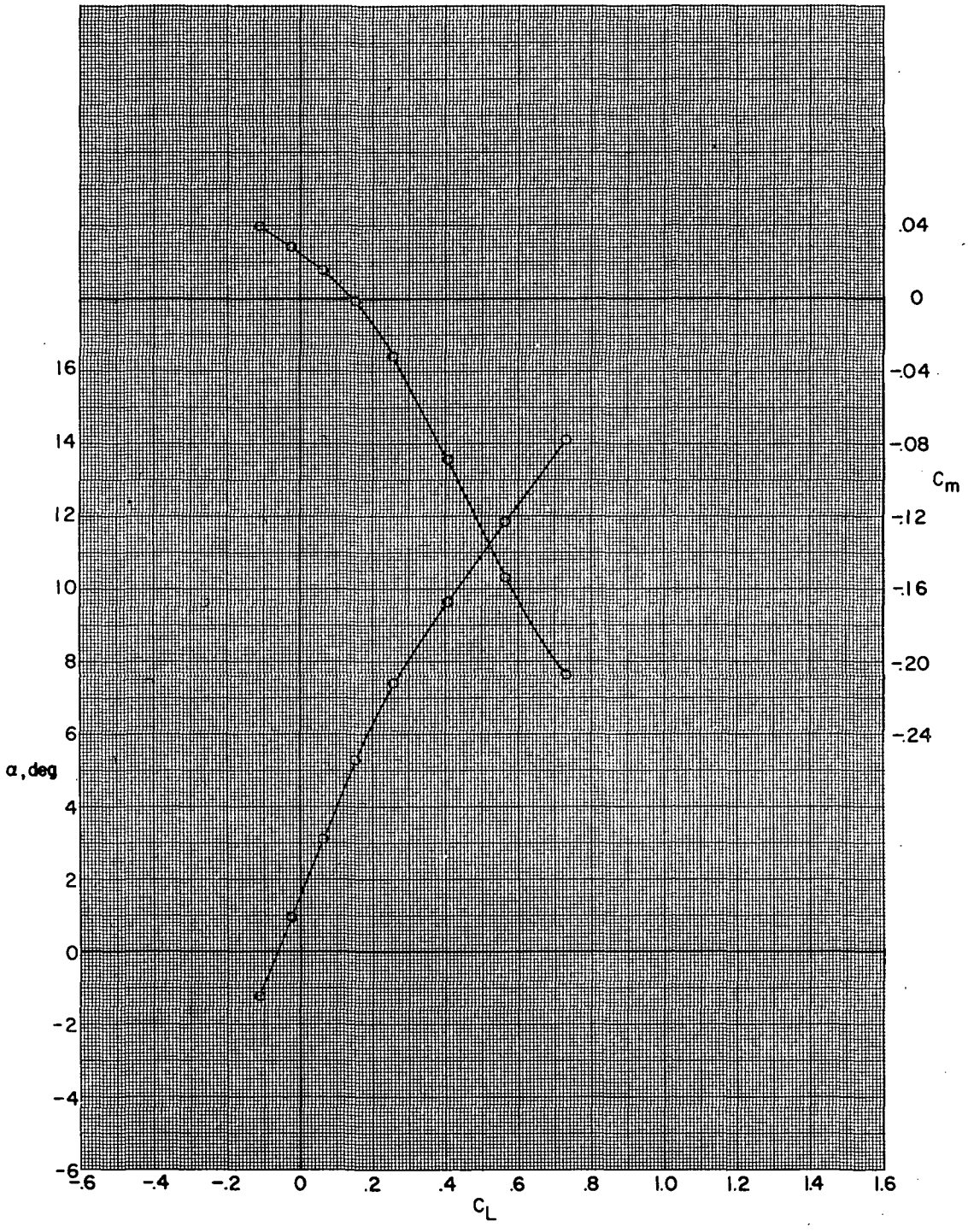

(a) M = 0.70.

Figure 24.- Aerodynamic characteristics for configuration $B_{80}G_{17}H_{13}I_{71}N^{b}_{32}V_{29}V_{38}W_{29}X_{24}X_{25}$ with wing swept 72.5°.

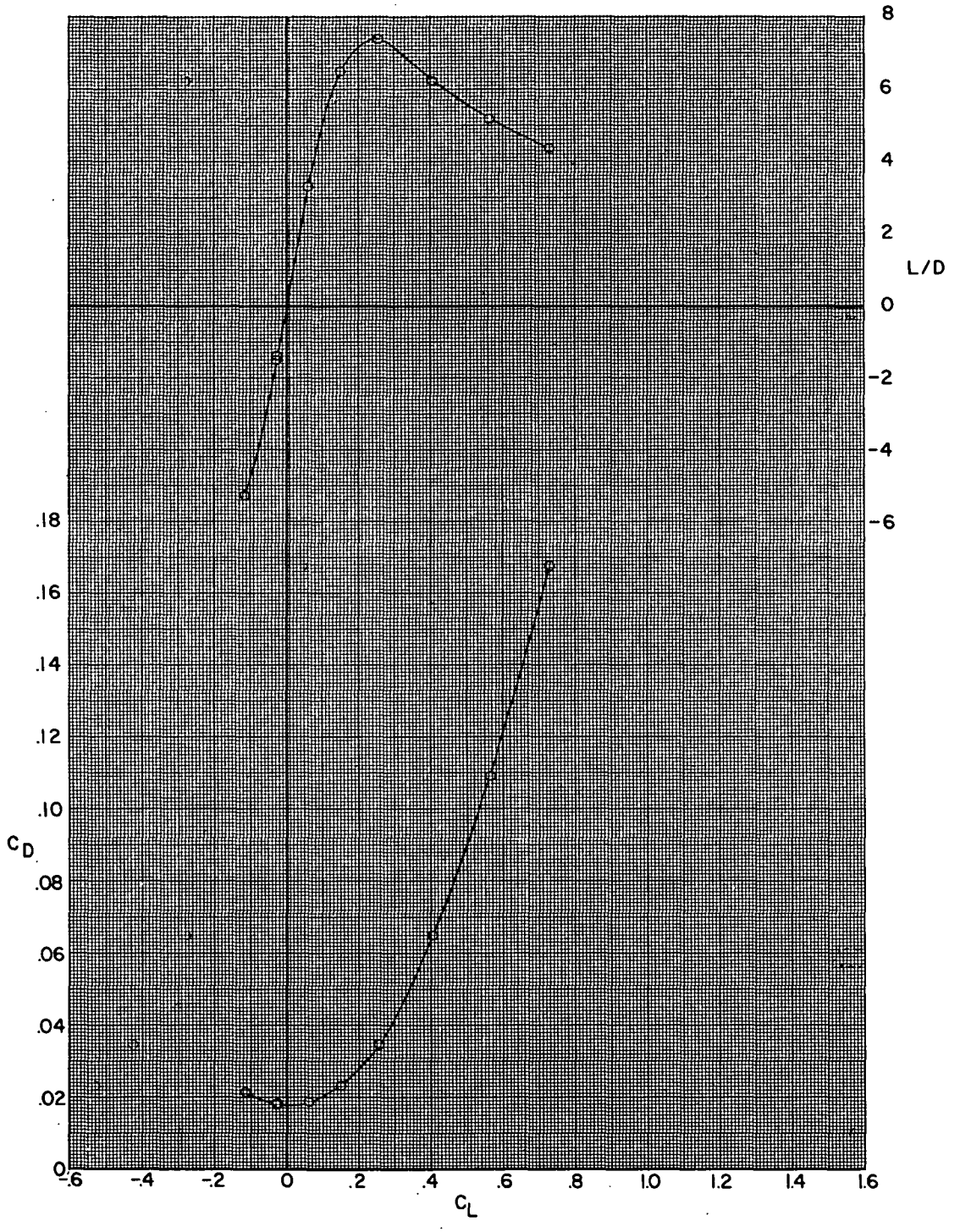

(a) Concluded.

Figure 24.- Continued.

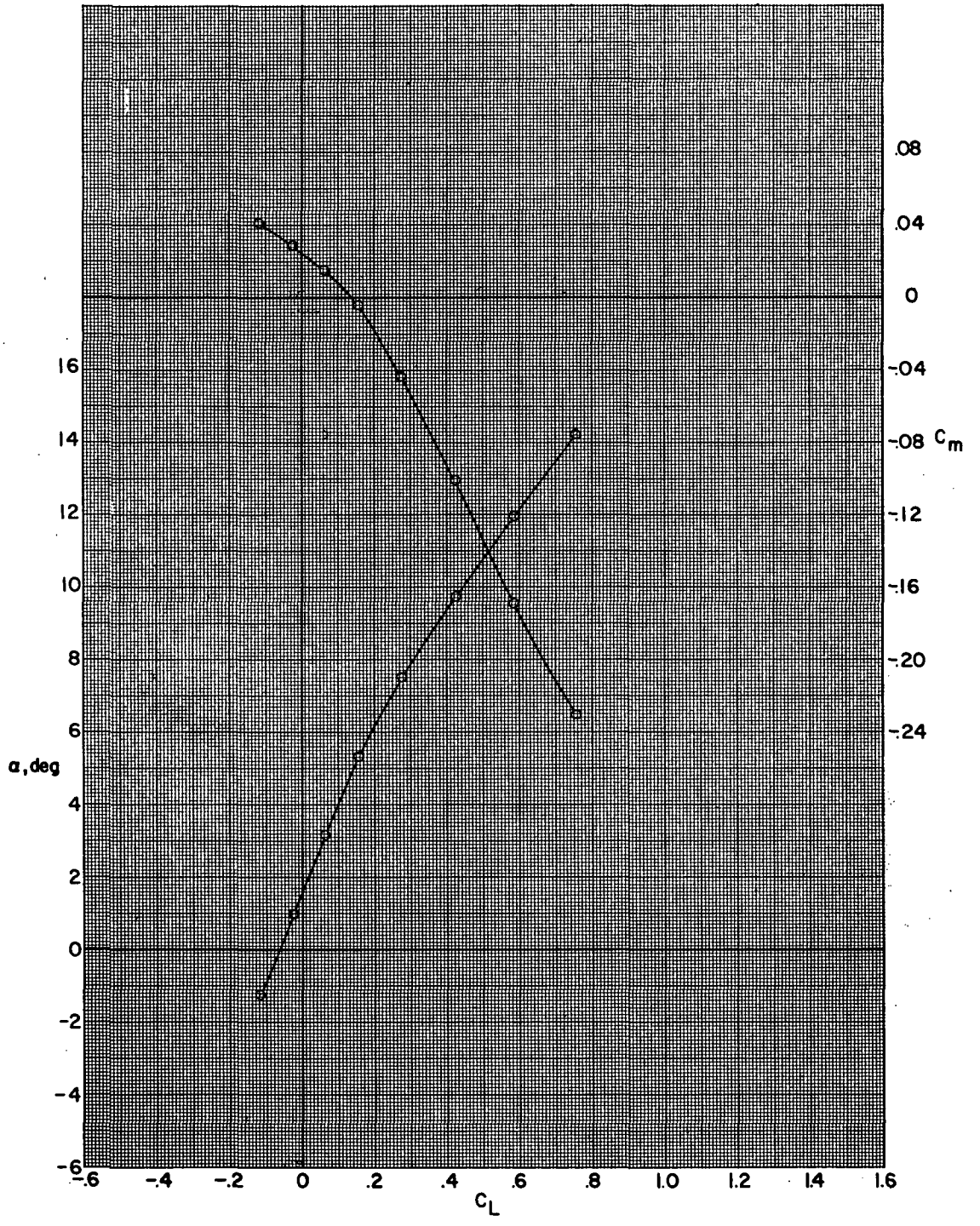

(b) M = 0.80.

Figure 24.- Continued.

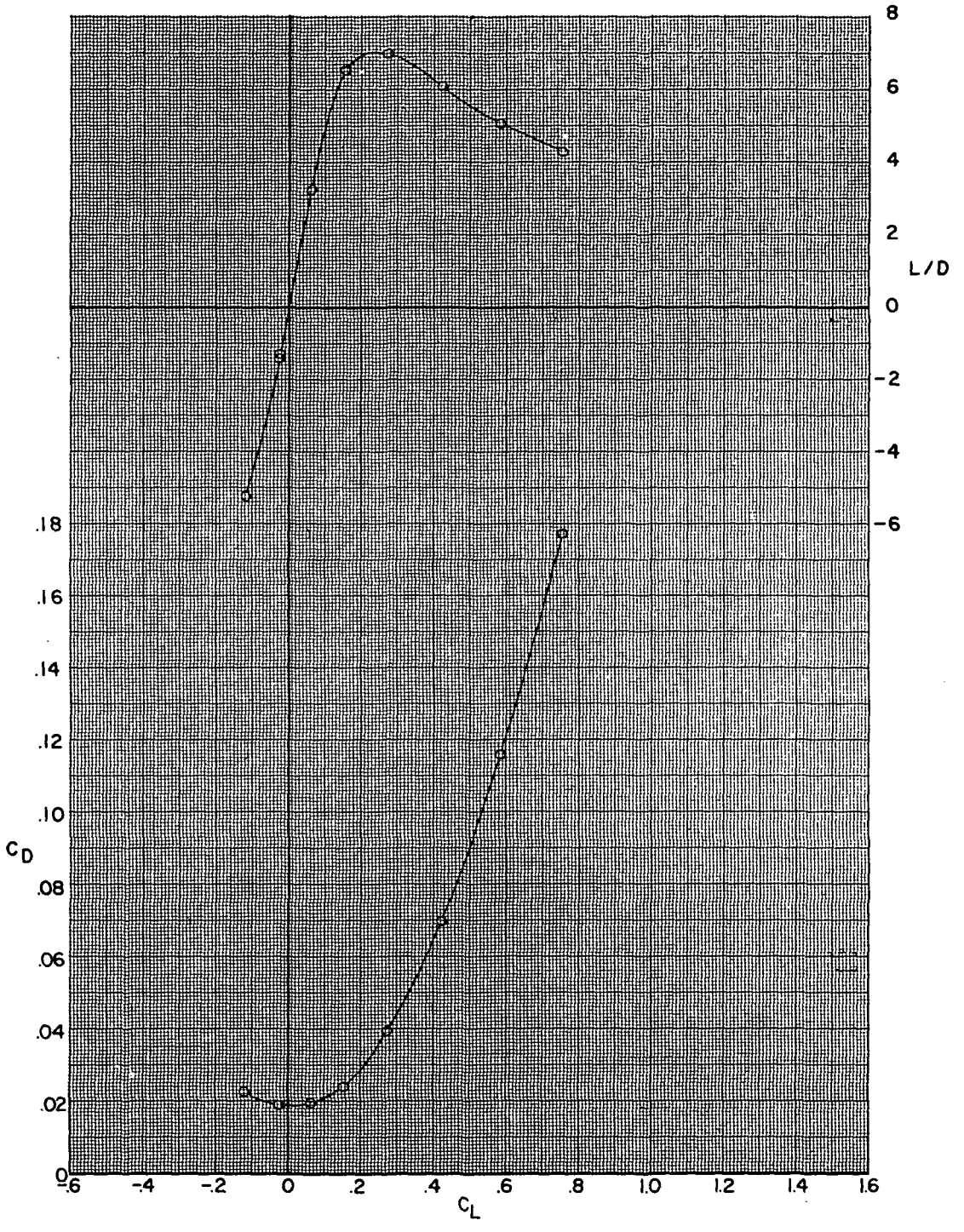

(b) Concluded.

Figure 24.- Continued.

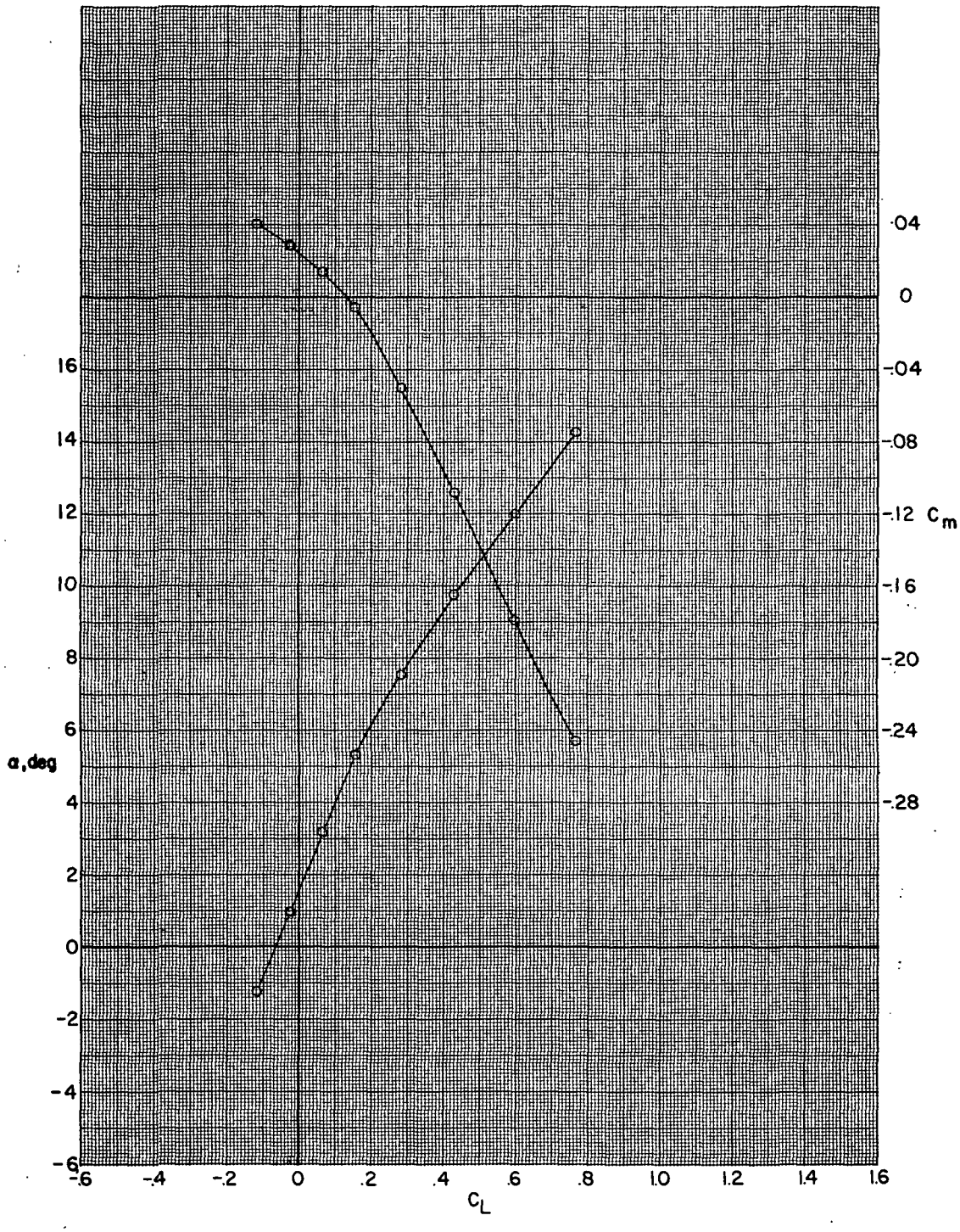

(c) M = 0.85.

Figure 24.- Continued.

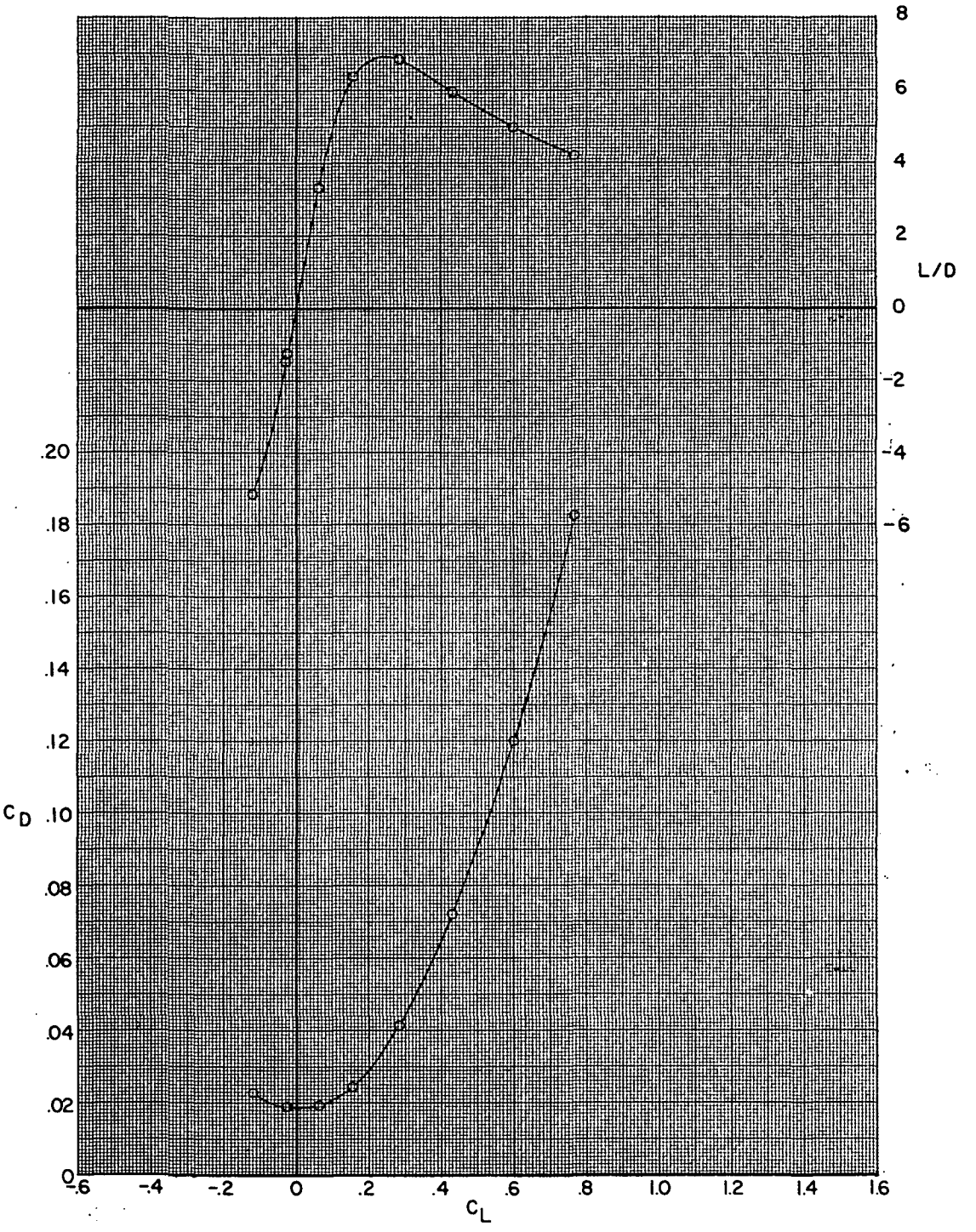

(c) Concluded.

Figure 24.- Continued.

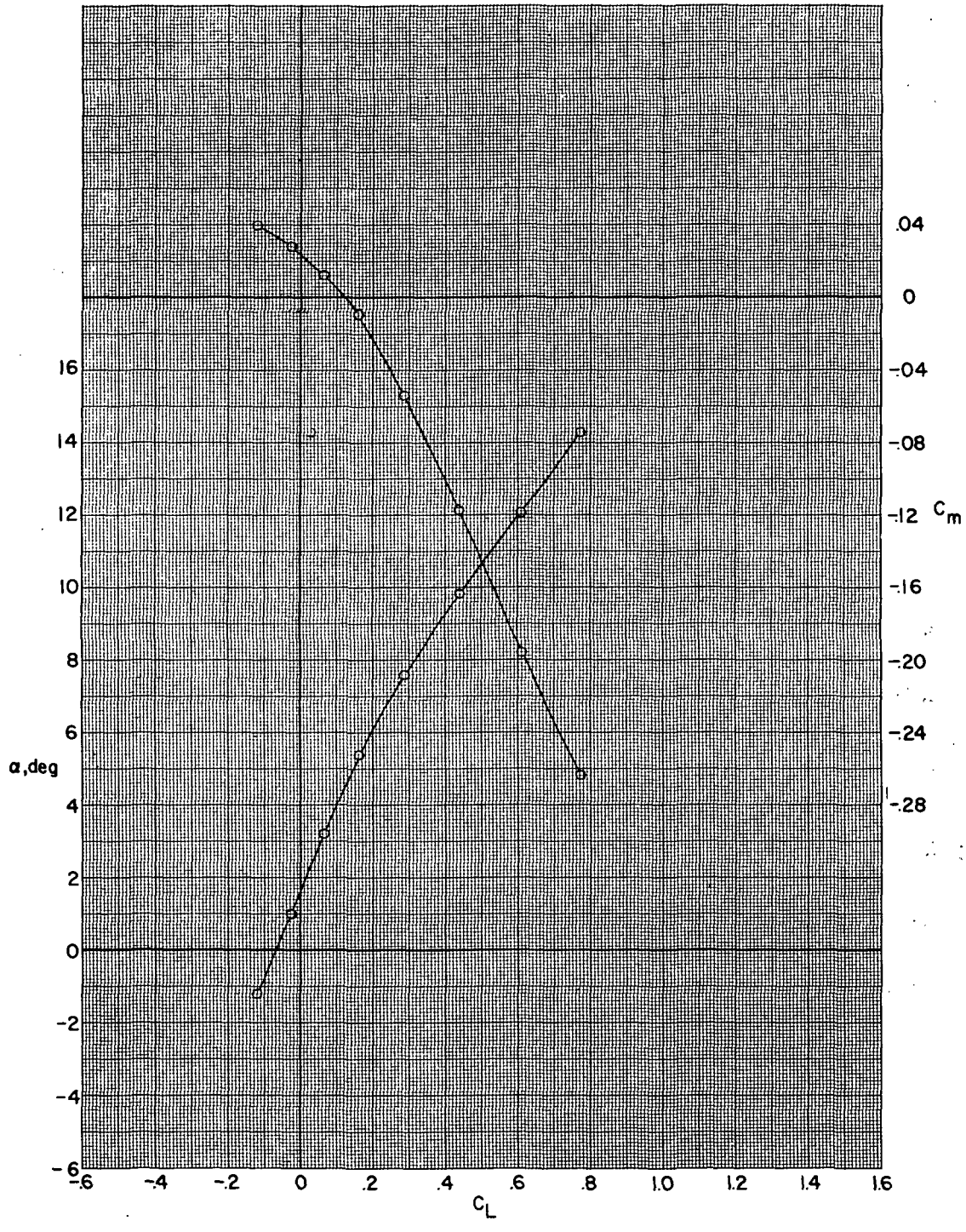

(d) M = 0.90.

Figure 24.- Continued.

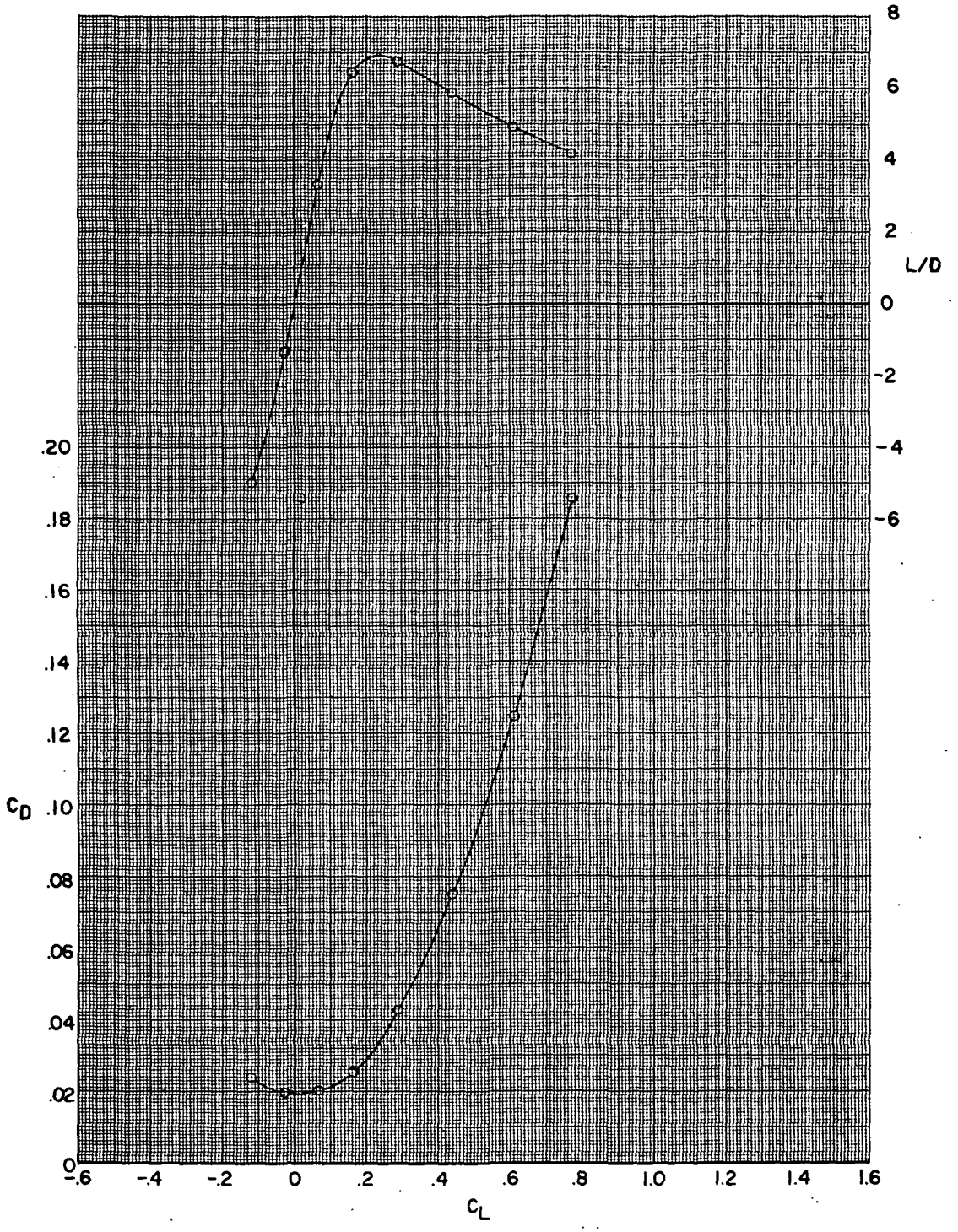

(d) Concluded.

Figure 24.- Continued.

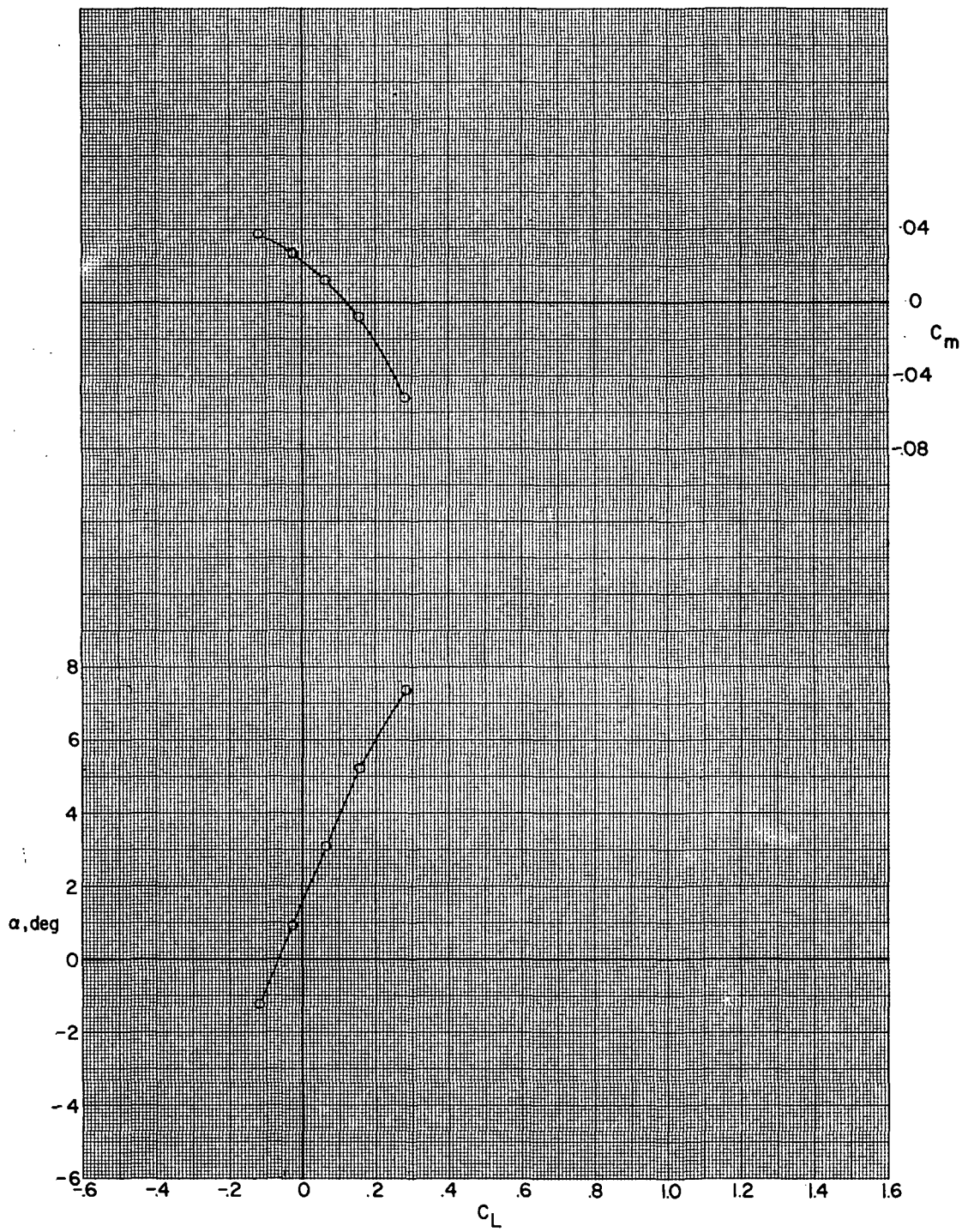

(e) M = 0.925.

Figure 24.- Continued.

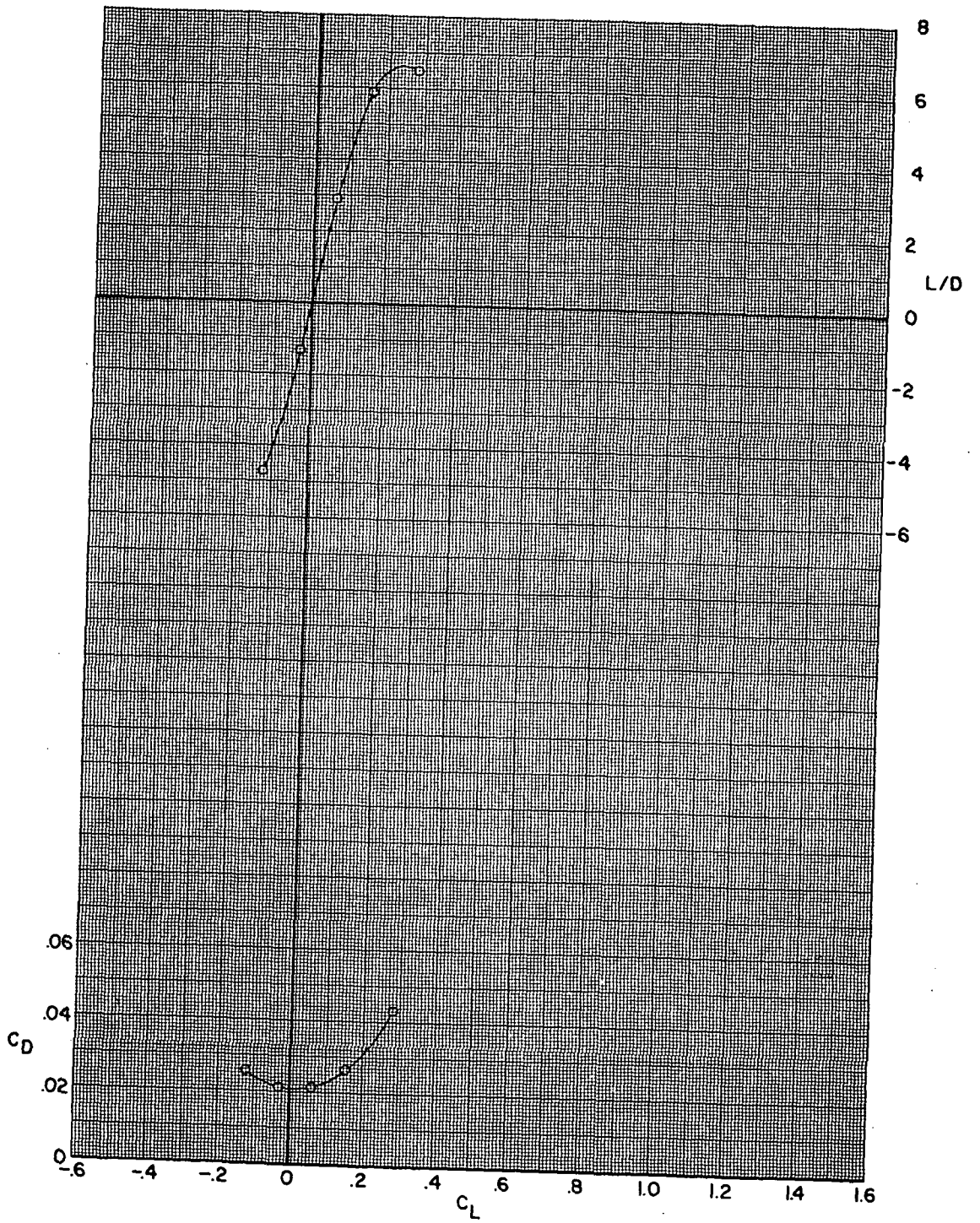

(e) Concluded.

Figure 24.- Continued.

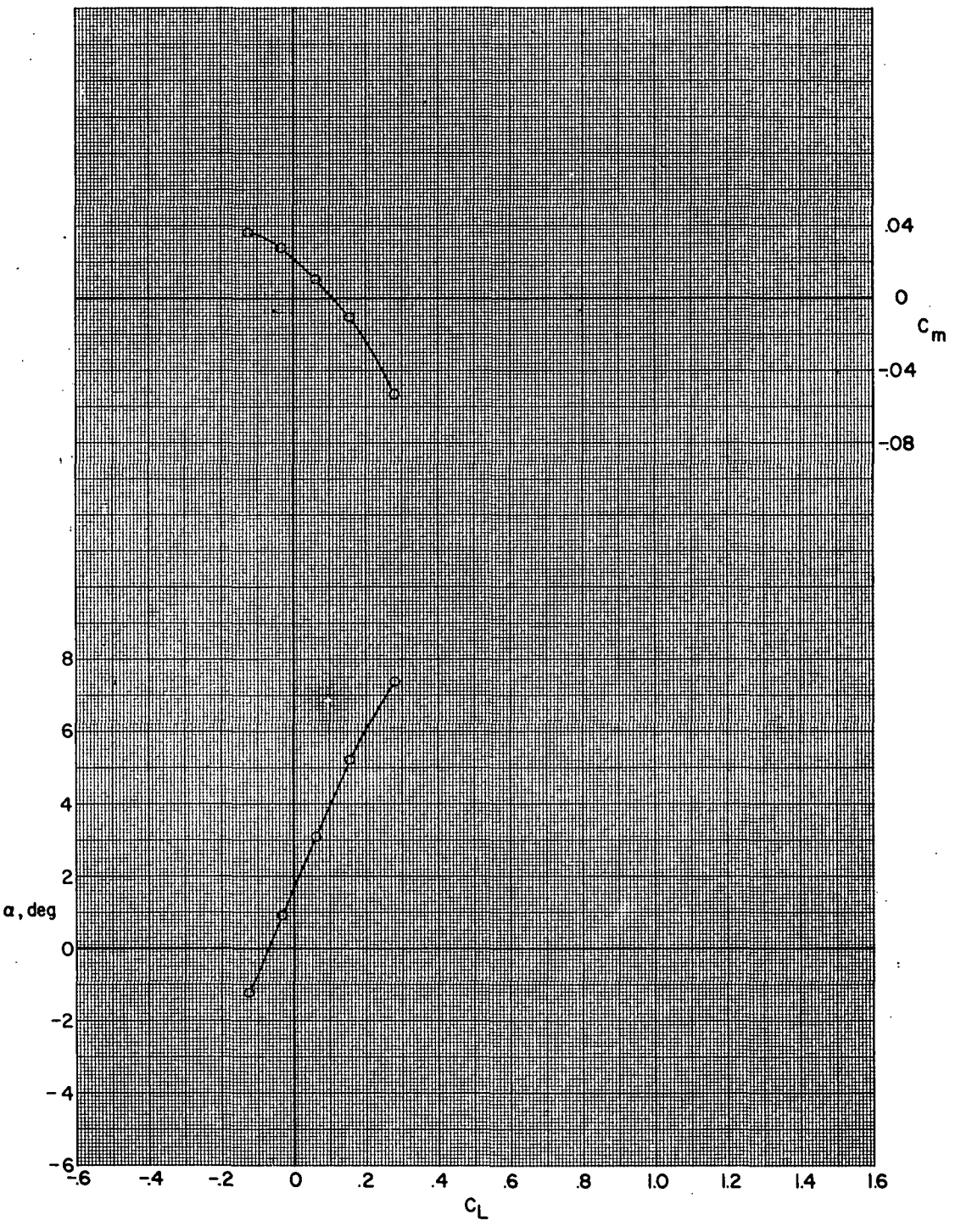

(f) M = 0.95.

Figure 24.- Continued.

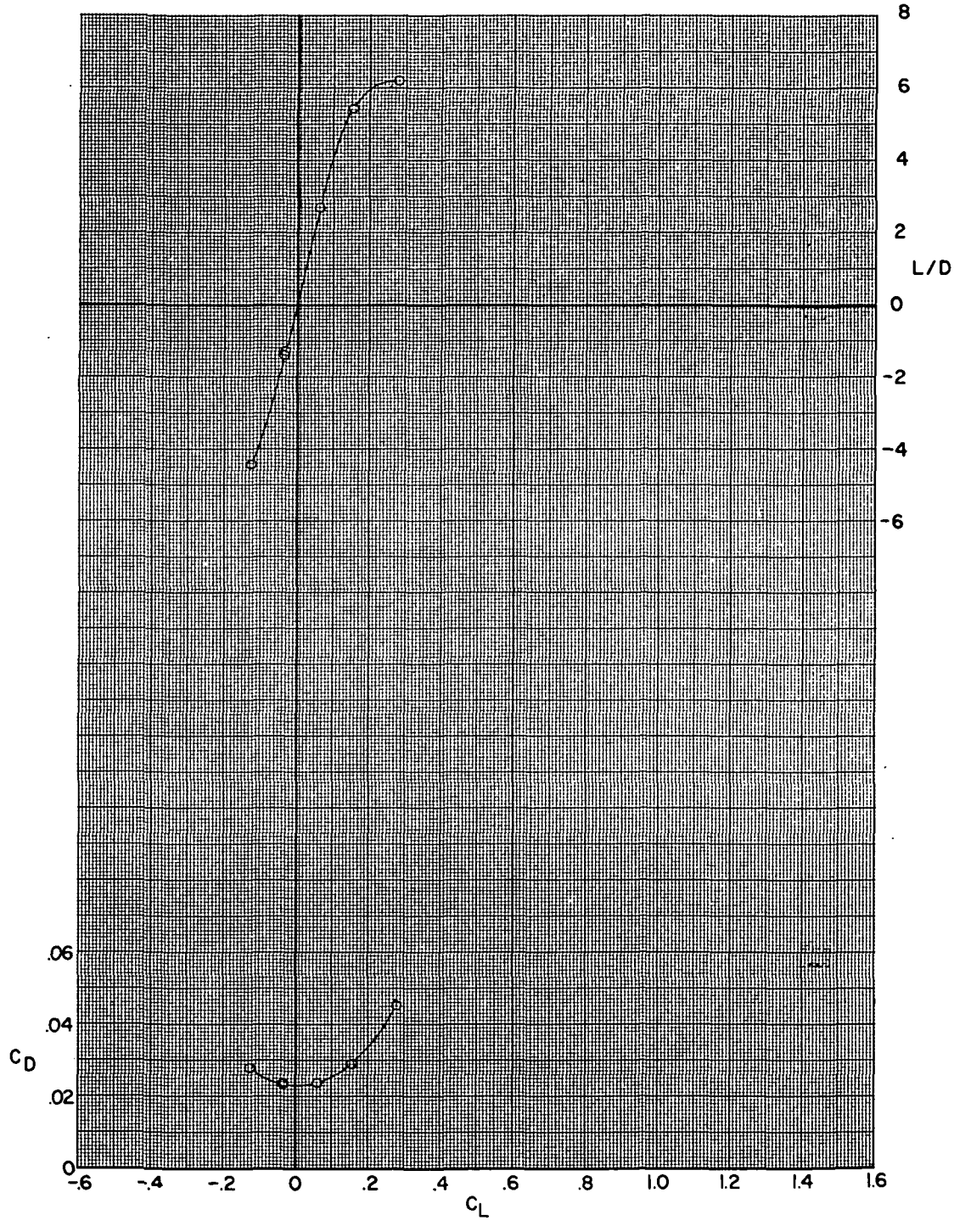

(f) Concluded.

Figure 24.- Continued.

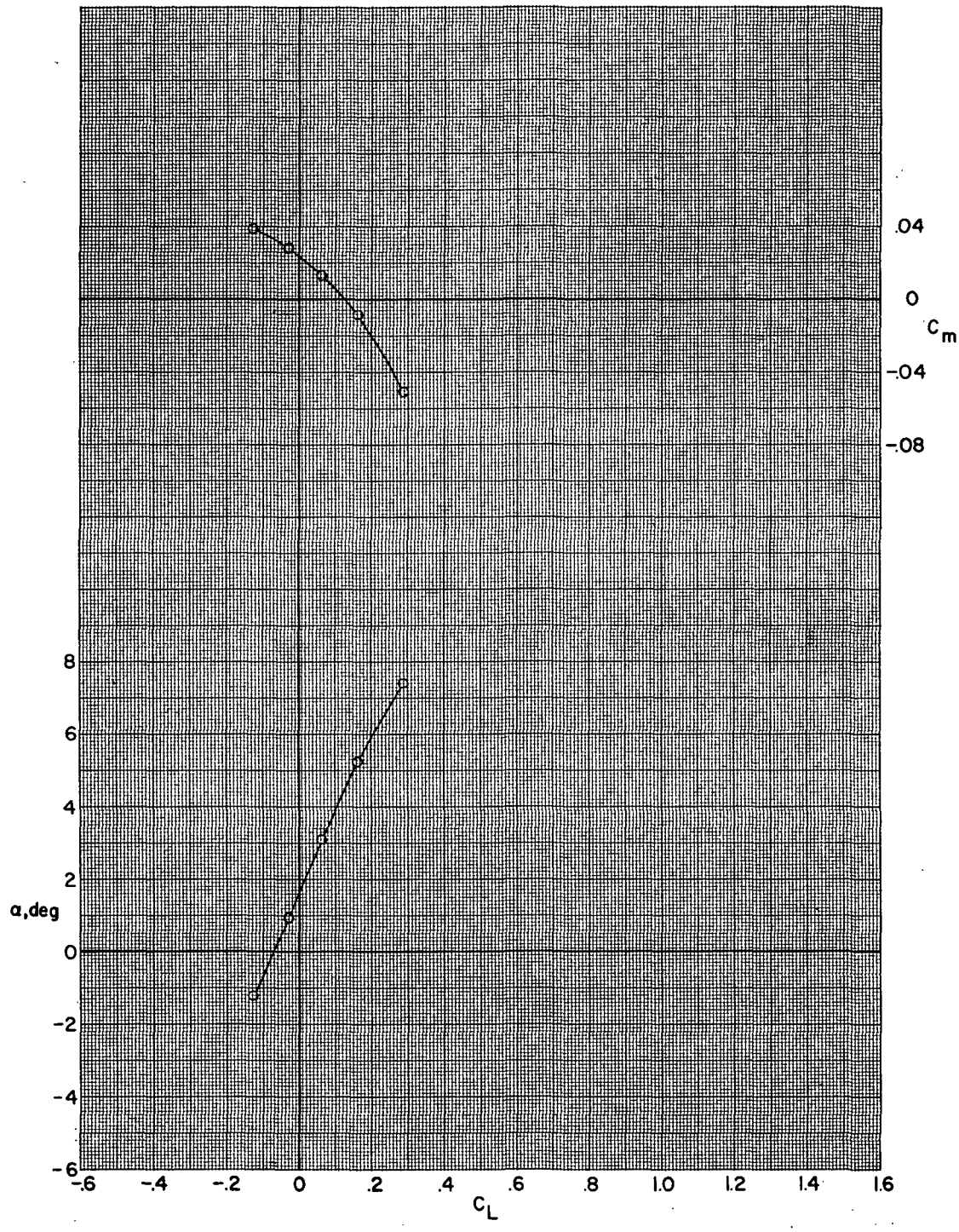

(g) M = 0.975.

Figure 24.- Continued.

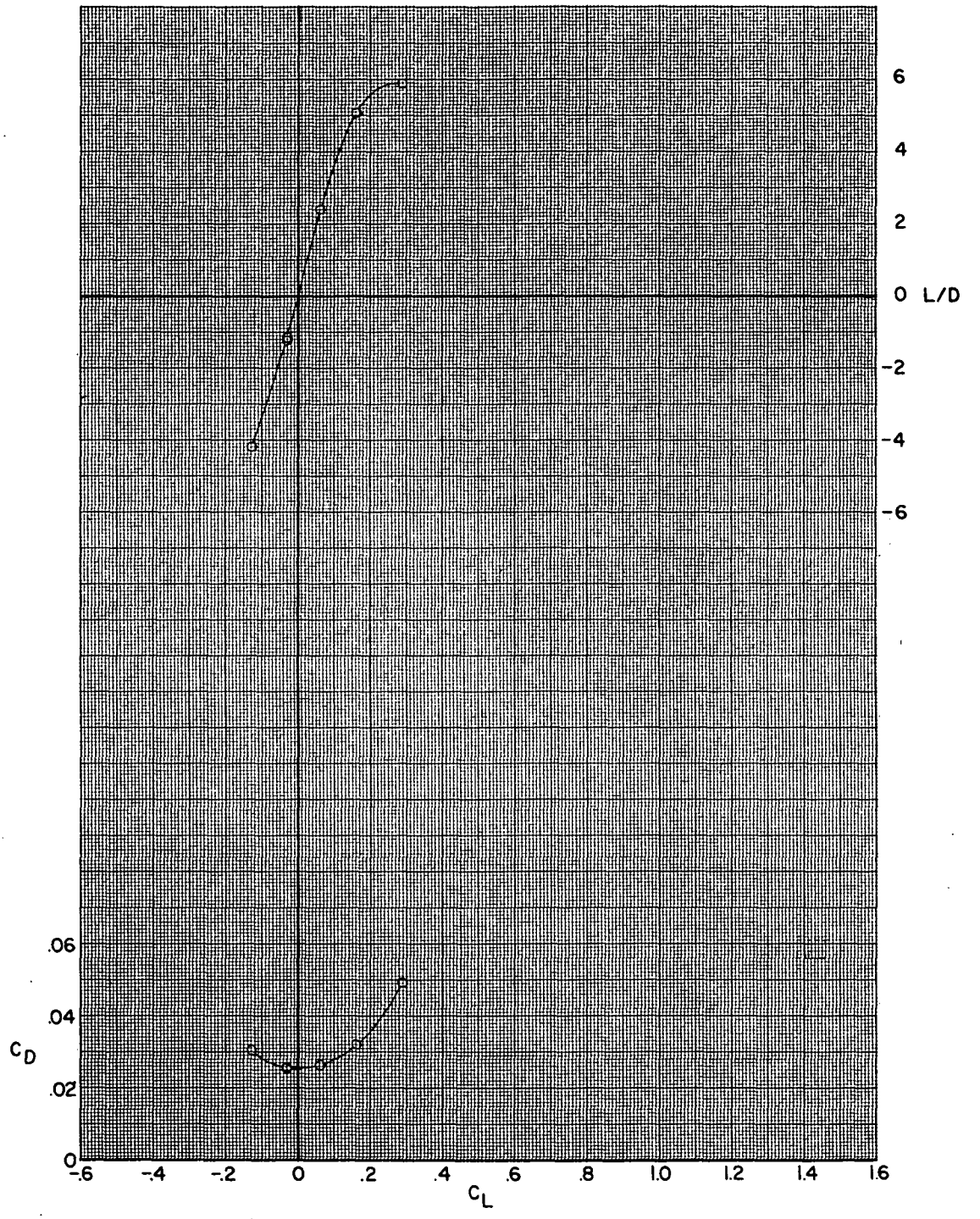

(g) Concluded.

Figure 24.- Concluded.

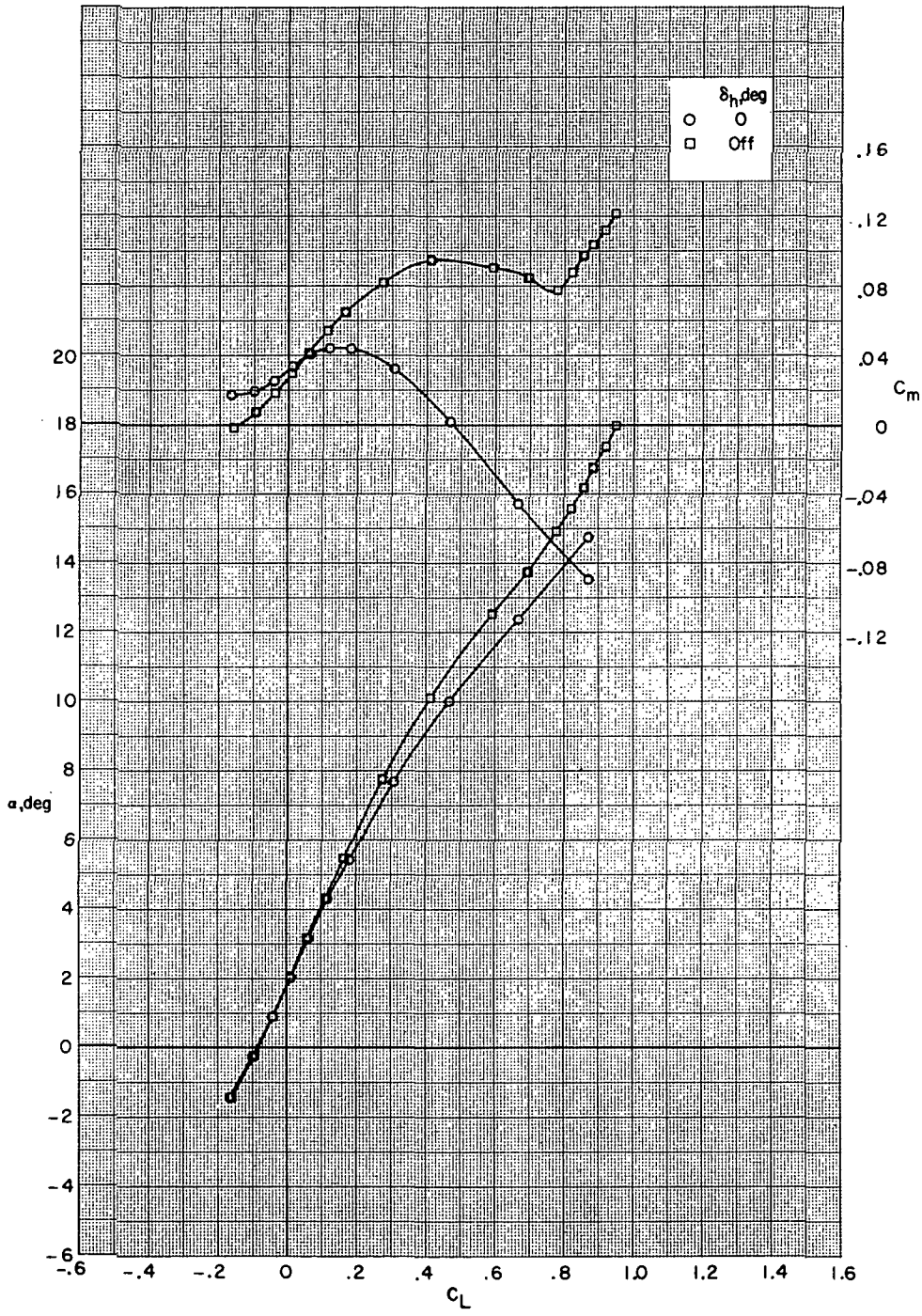

(a) M = 0.80.

Figure 25.- Aerodynamic characteristics for configuration $B_{80}G_{43}H_{13}I_{71}N^{b}_{32}V_{29}V_{38}W_{31}X_{24}X_{168}$ with wing swept 63.7°.

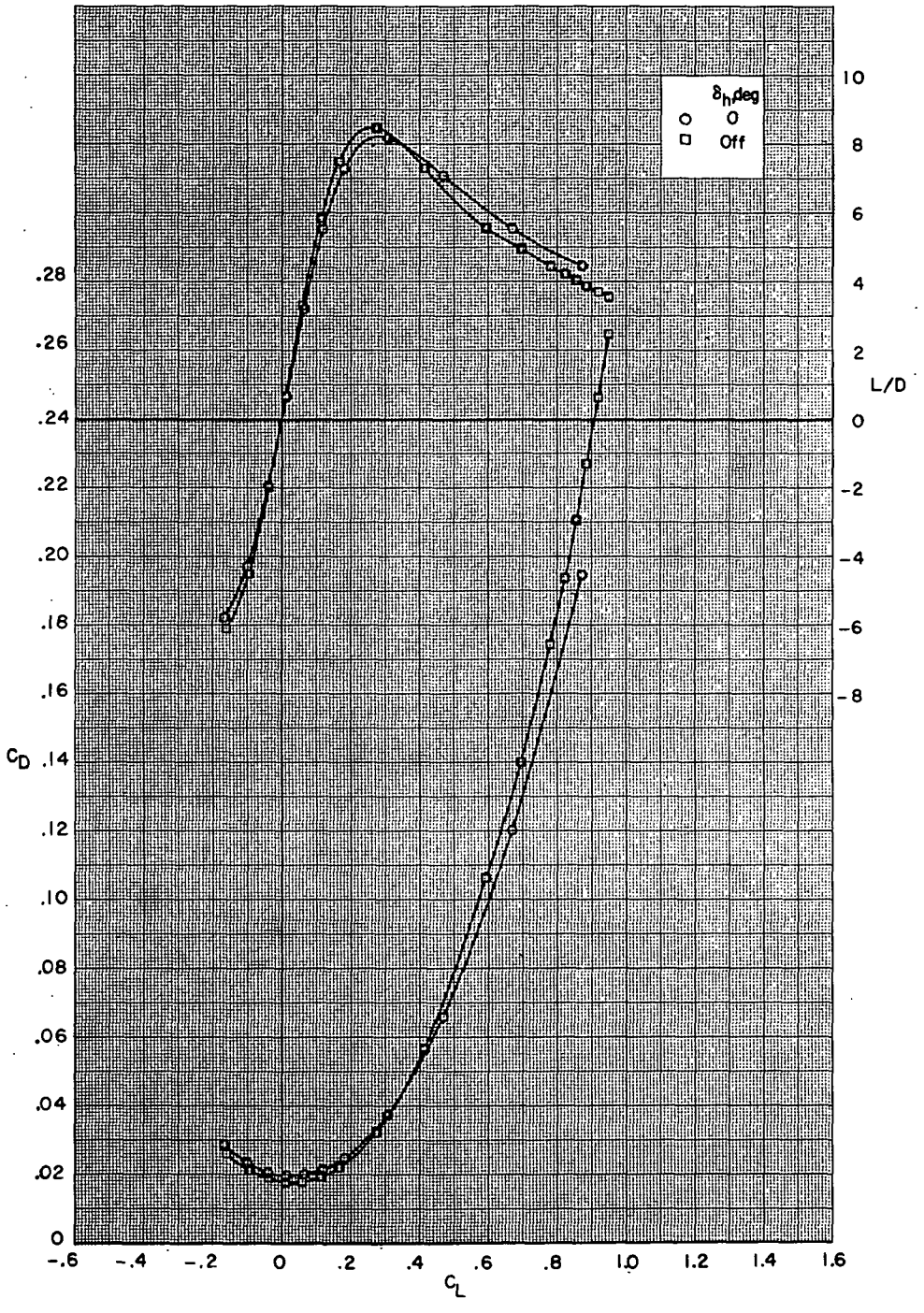

(a) Concluded.

Figure 25.- Continued.

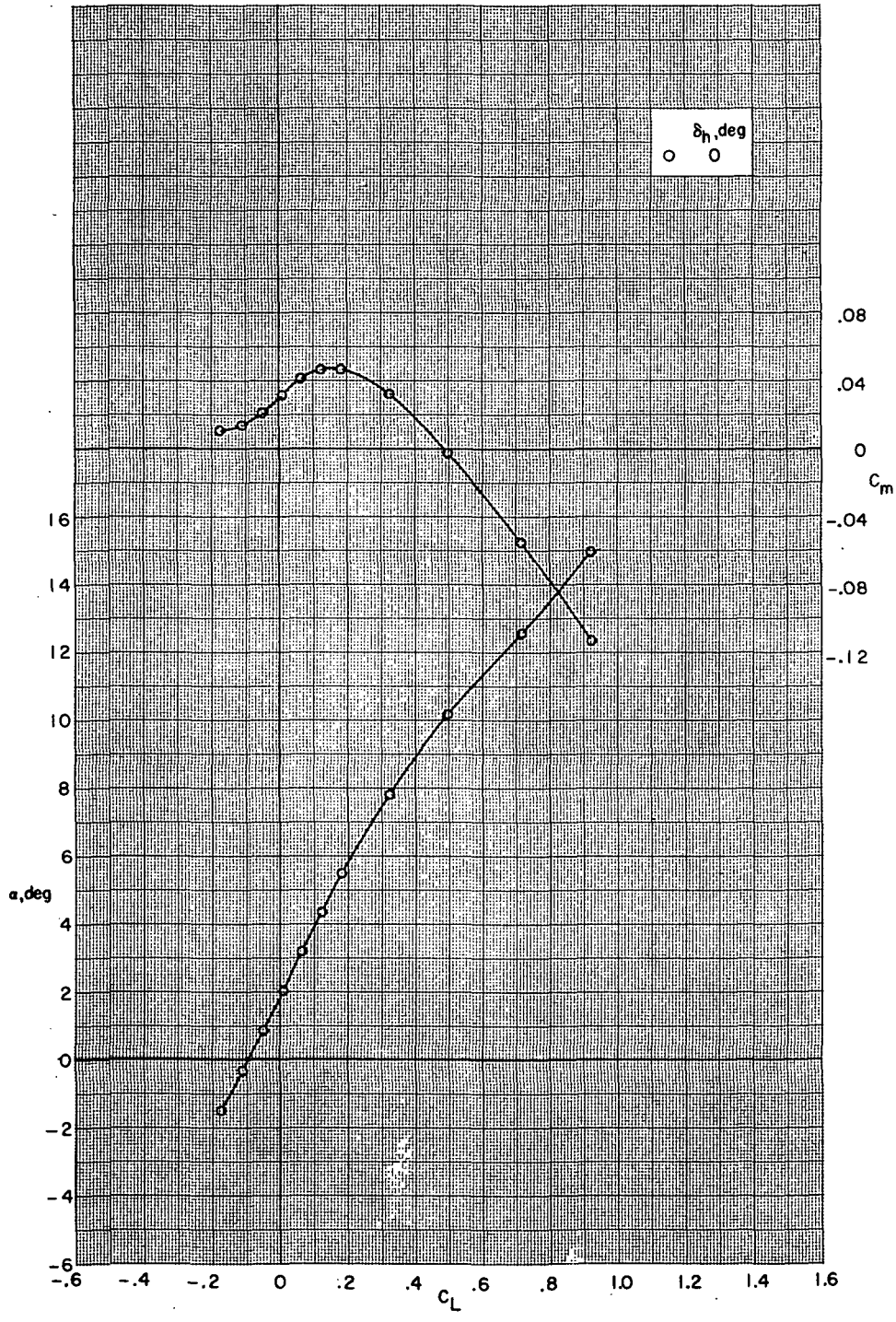

(b) M = 0.90.

Figure 25.- Continued.

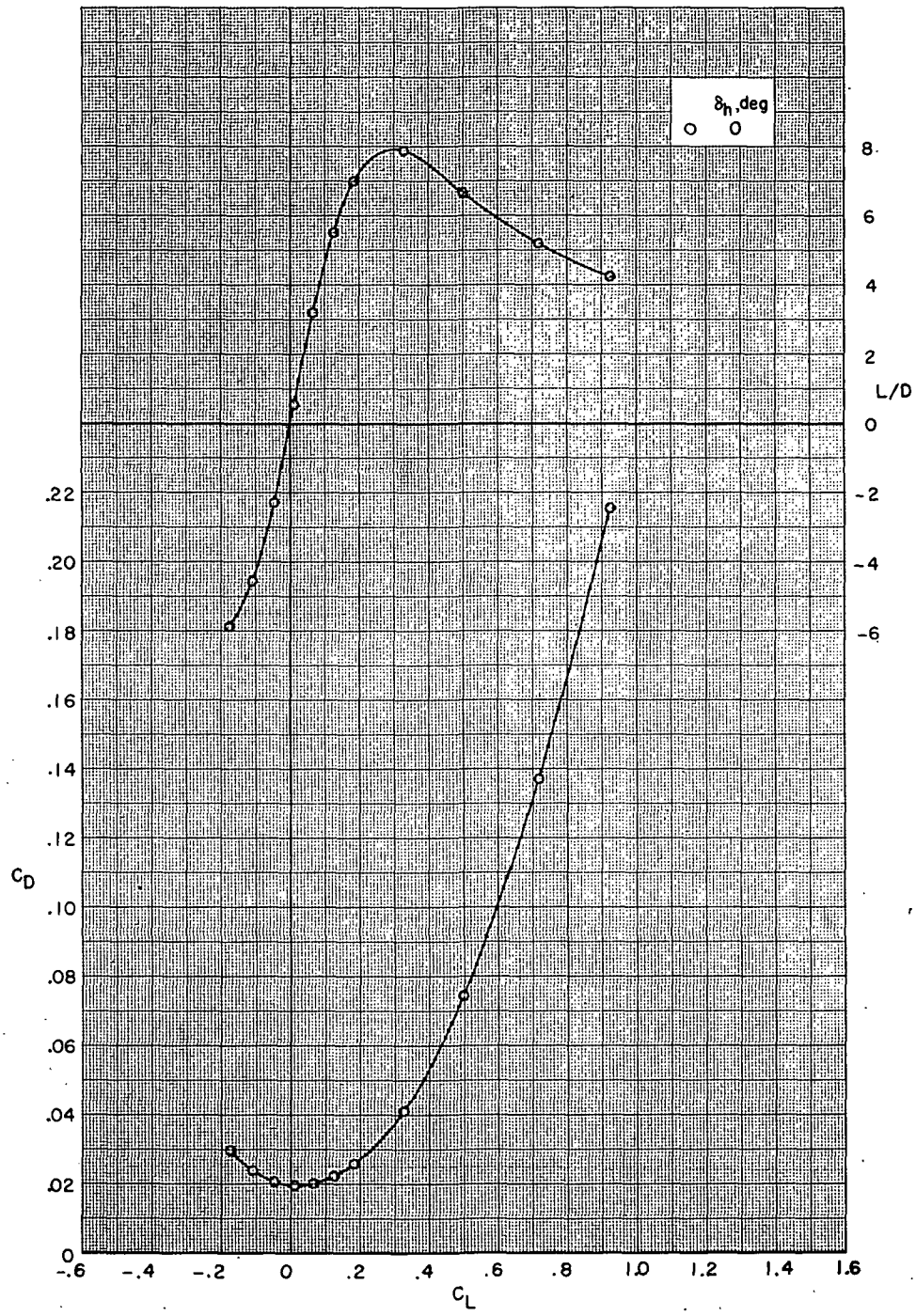

(b) Concluded.

Figure 25.- Continued.

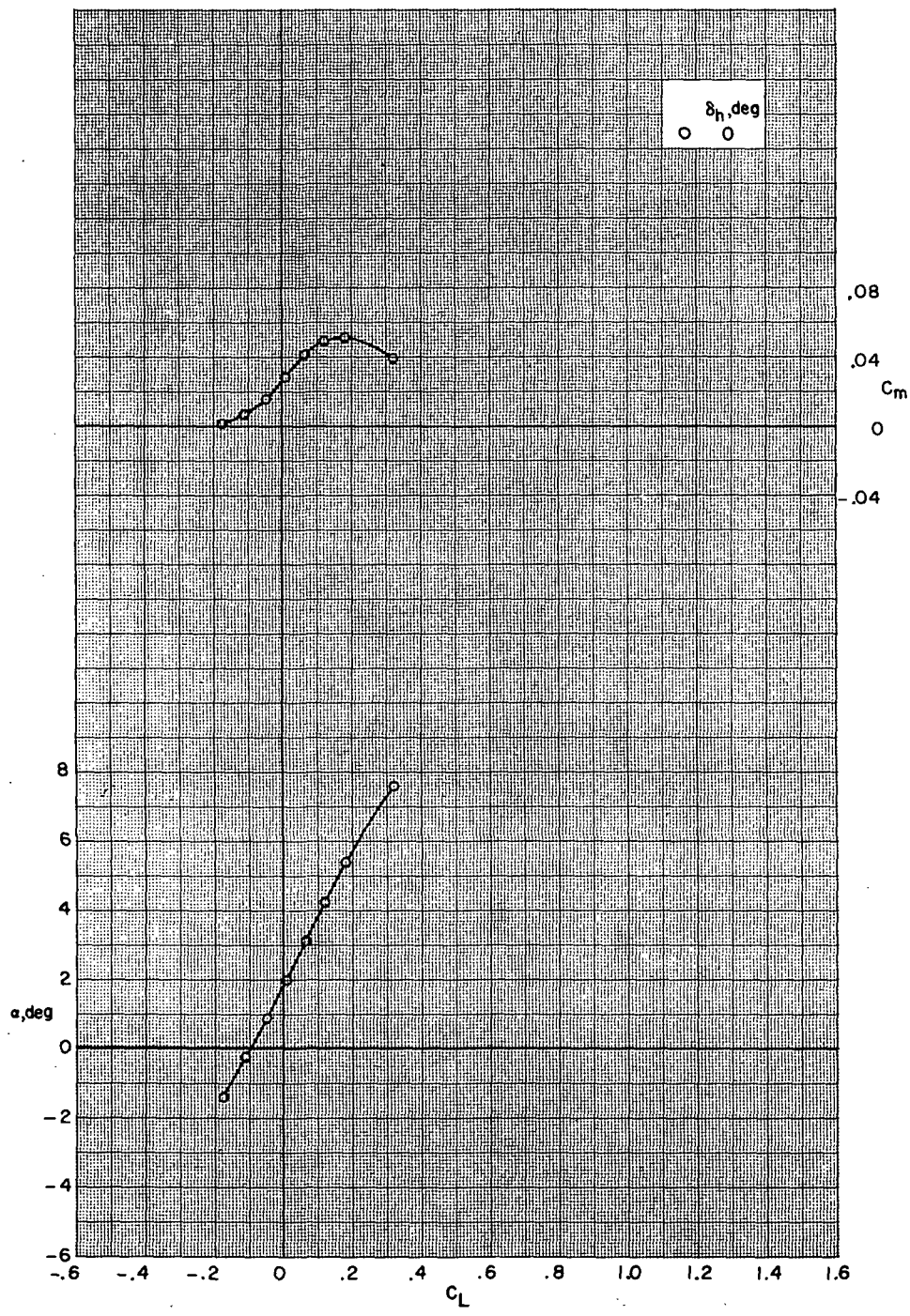

(c) M = 0.95.

Figure 25.- Continued.

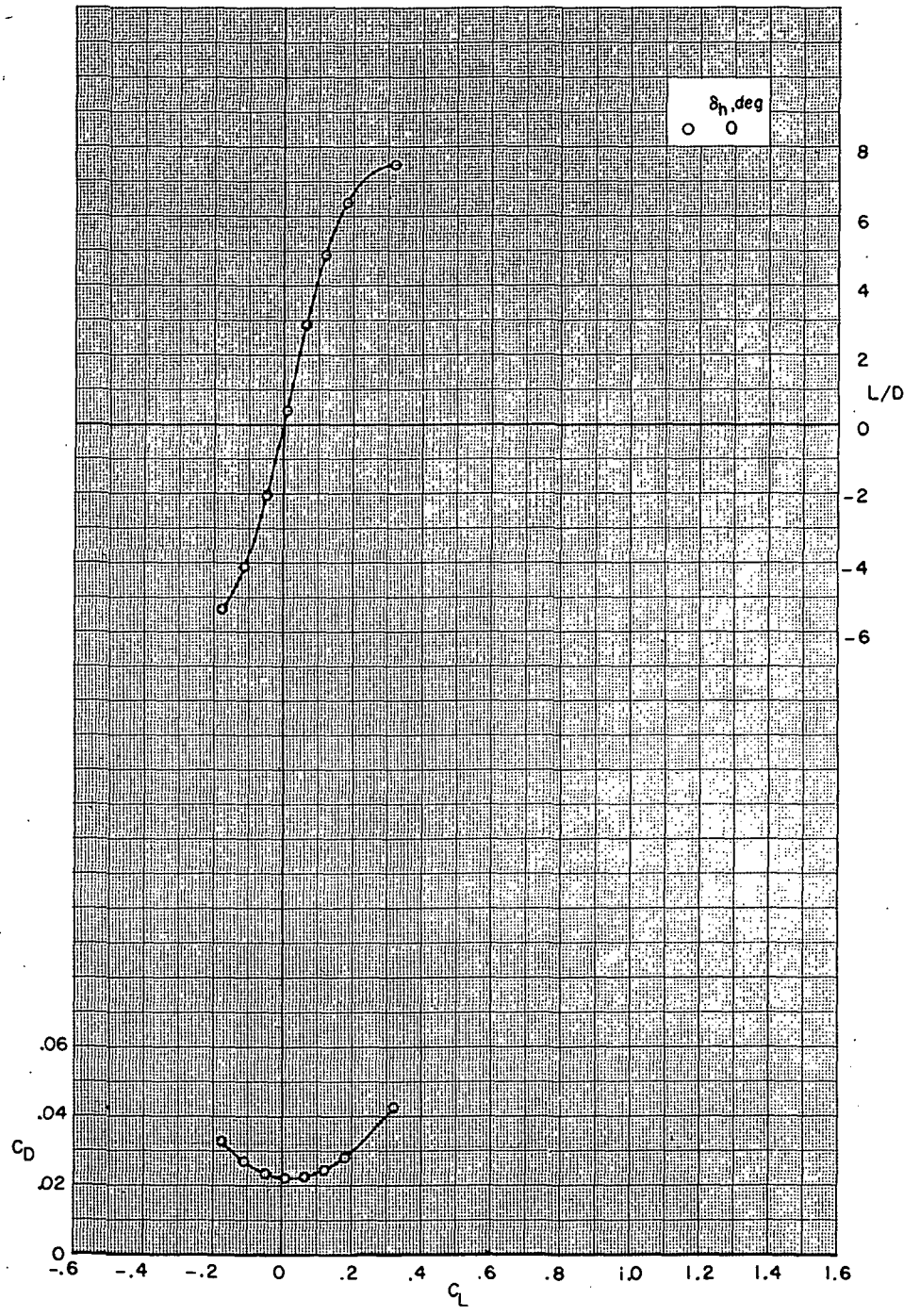

(c) Concluded.

Figure 25.- Concluded.

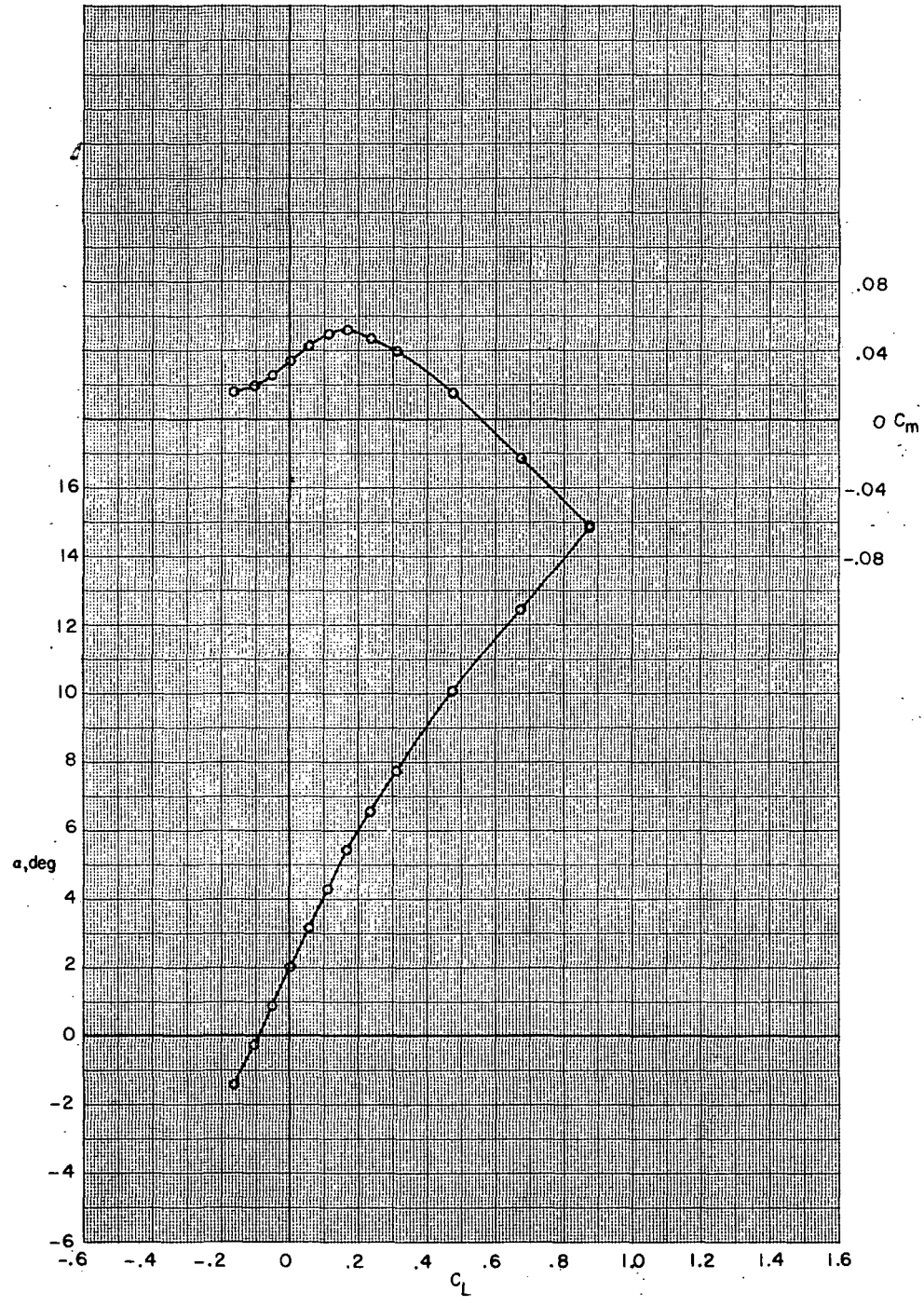

(a) M = 0.80.

Figure 26.- Aerodynamic characteristics for configuration $B_{80}G_{47}H_{13}I_{71}N^{b}_{32}V_{29}V_{38}W_{32}X_{24}X_{168}$ with wing swept 63.7°.

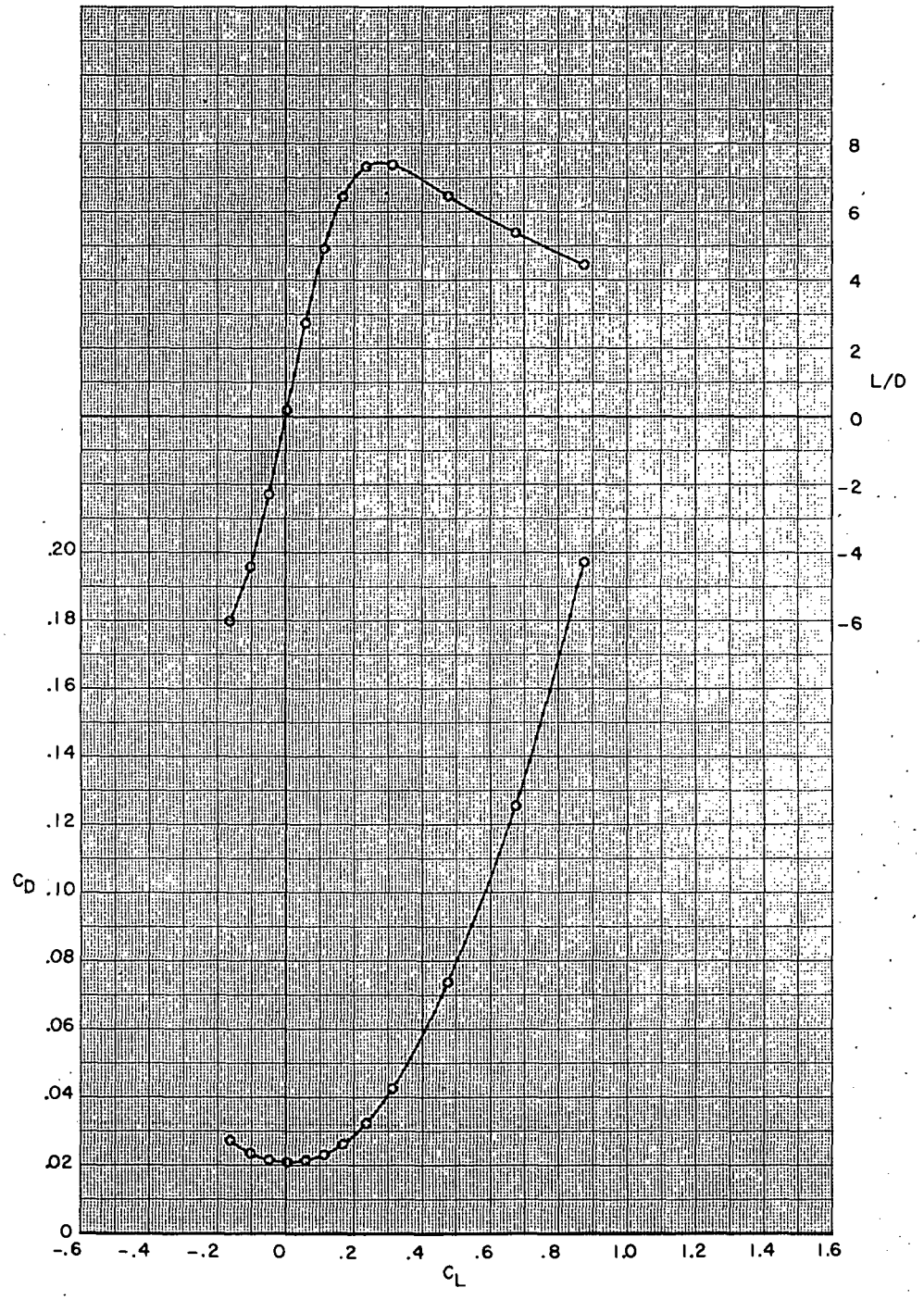

(a) Concluded.

Figure 26.- Continued.

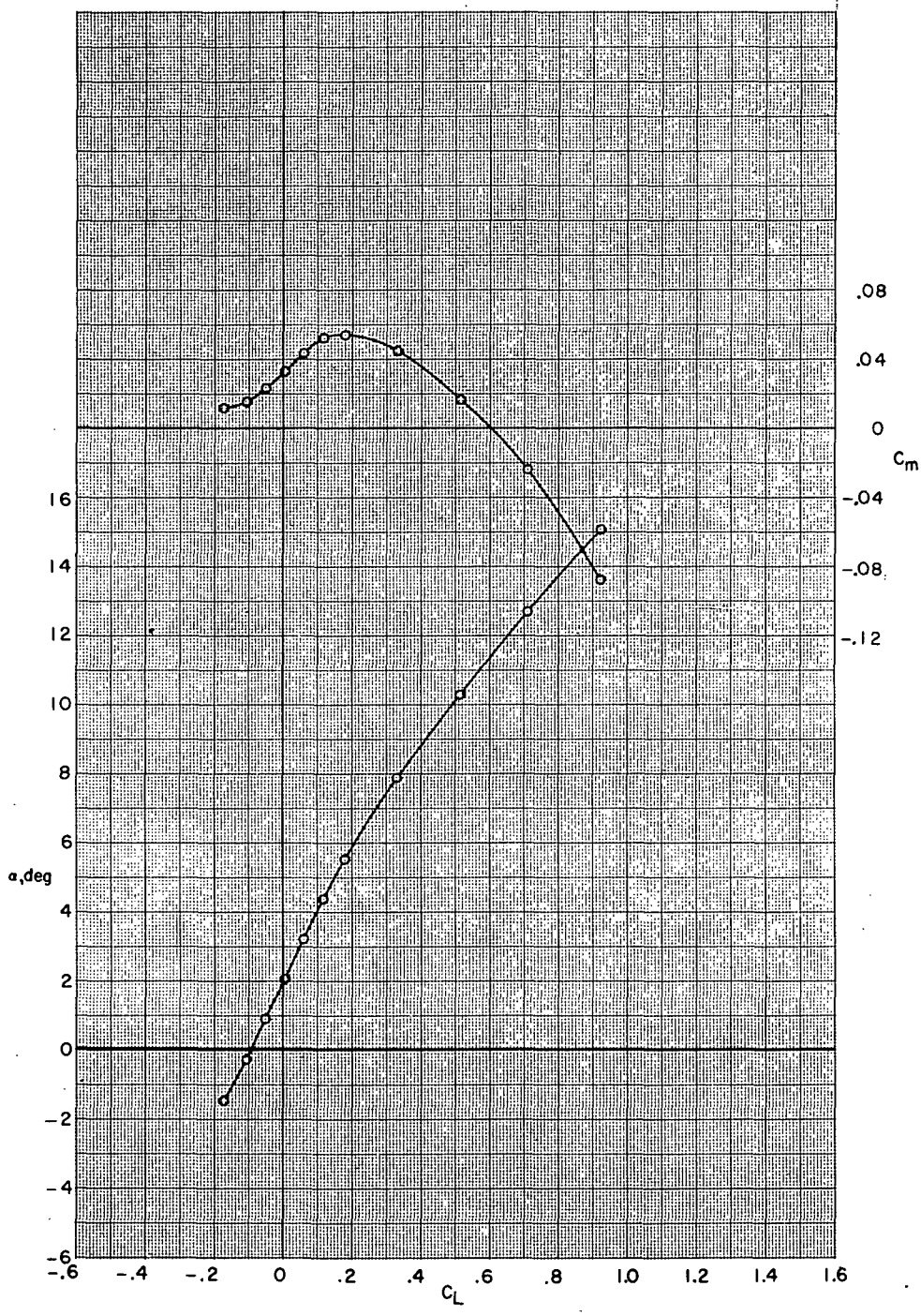

(b) M = 0.90.

Figure 26.- Continued.

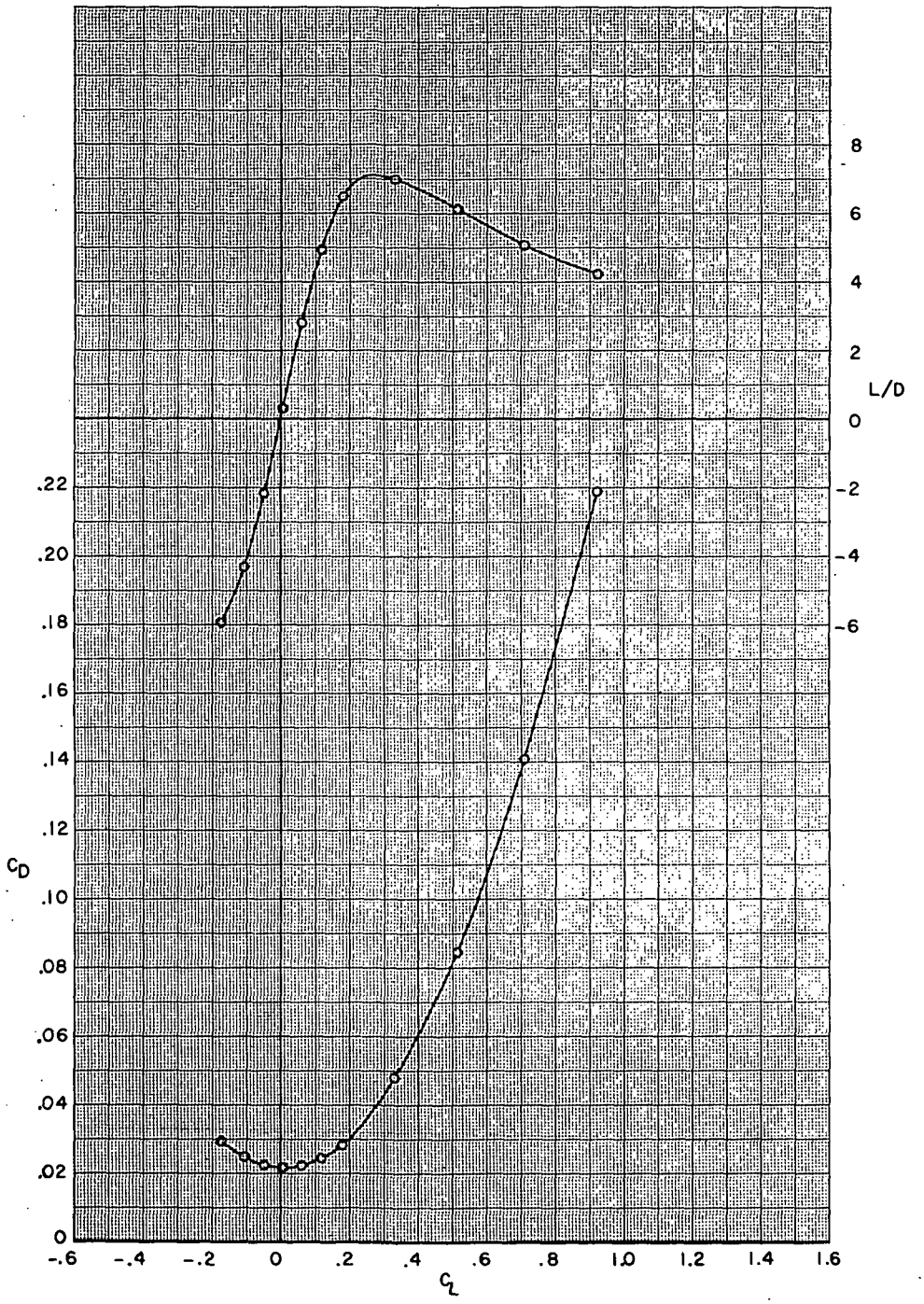

(b) Concluded.

Figure 26.- Continued.

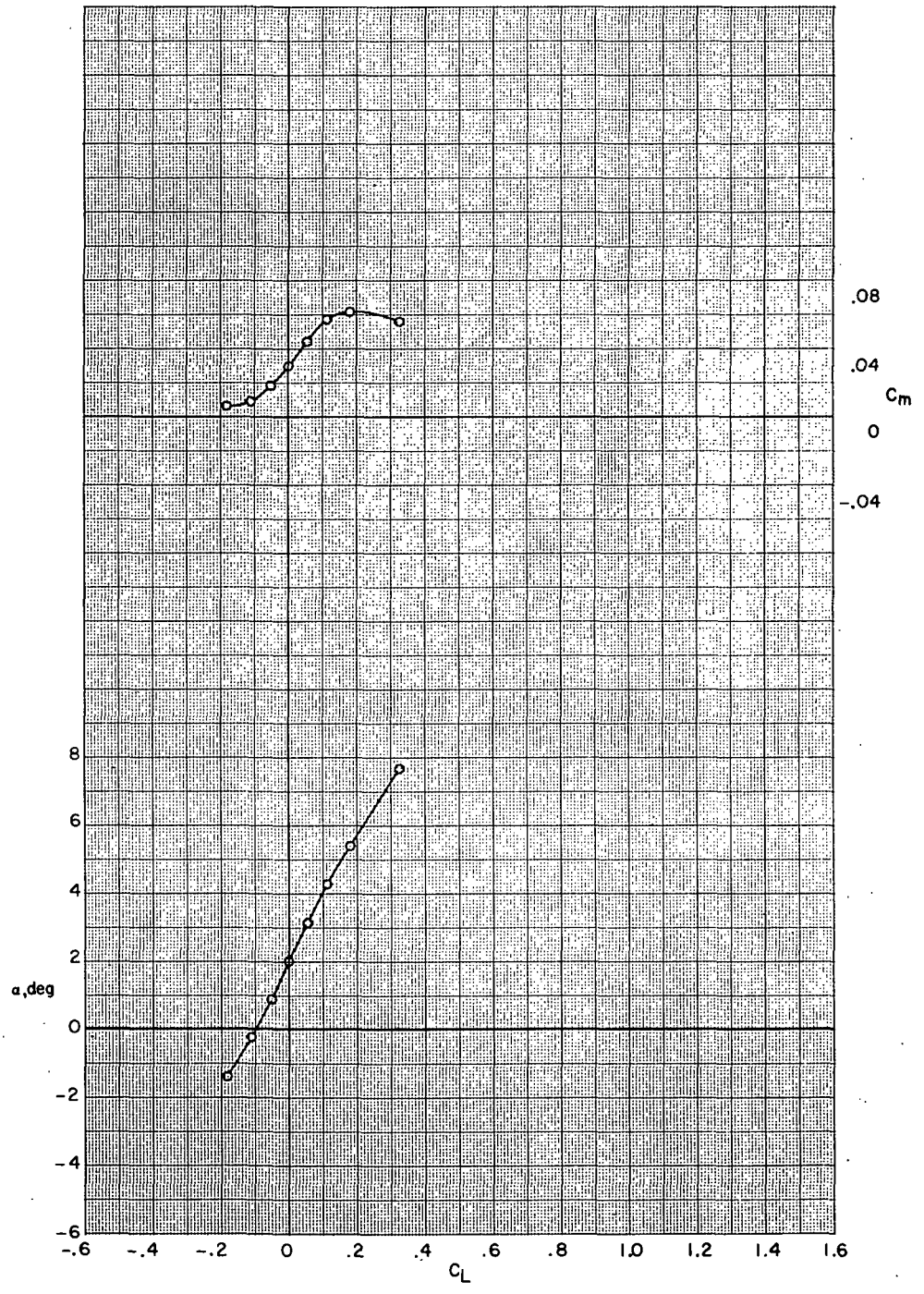

(c) M = 0.95.

Figure 26.- Continued.

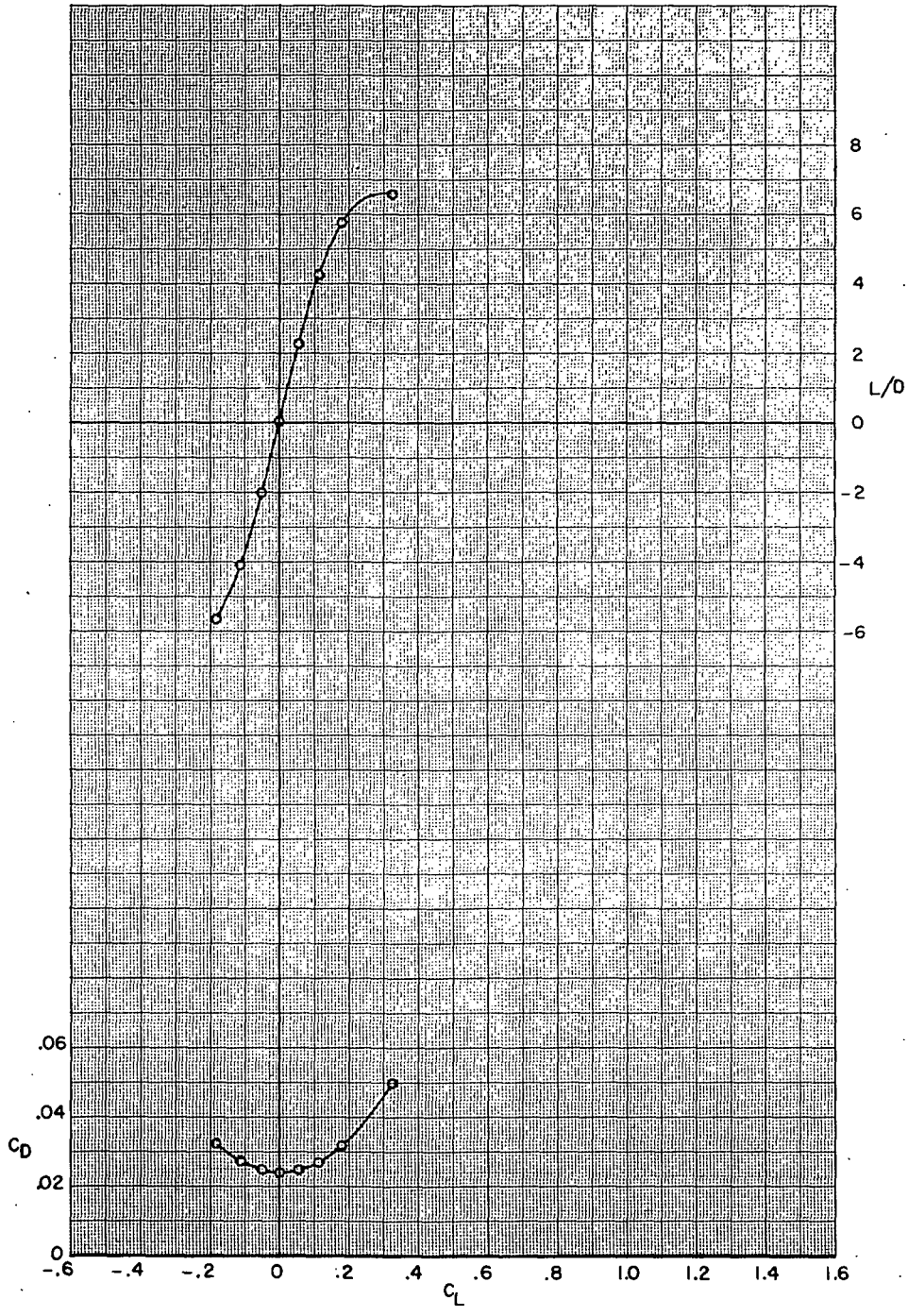

(c) Concluded.

Figure 26.- Concluded.

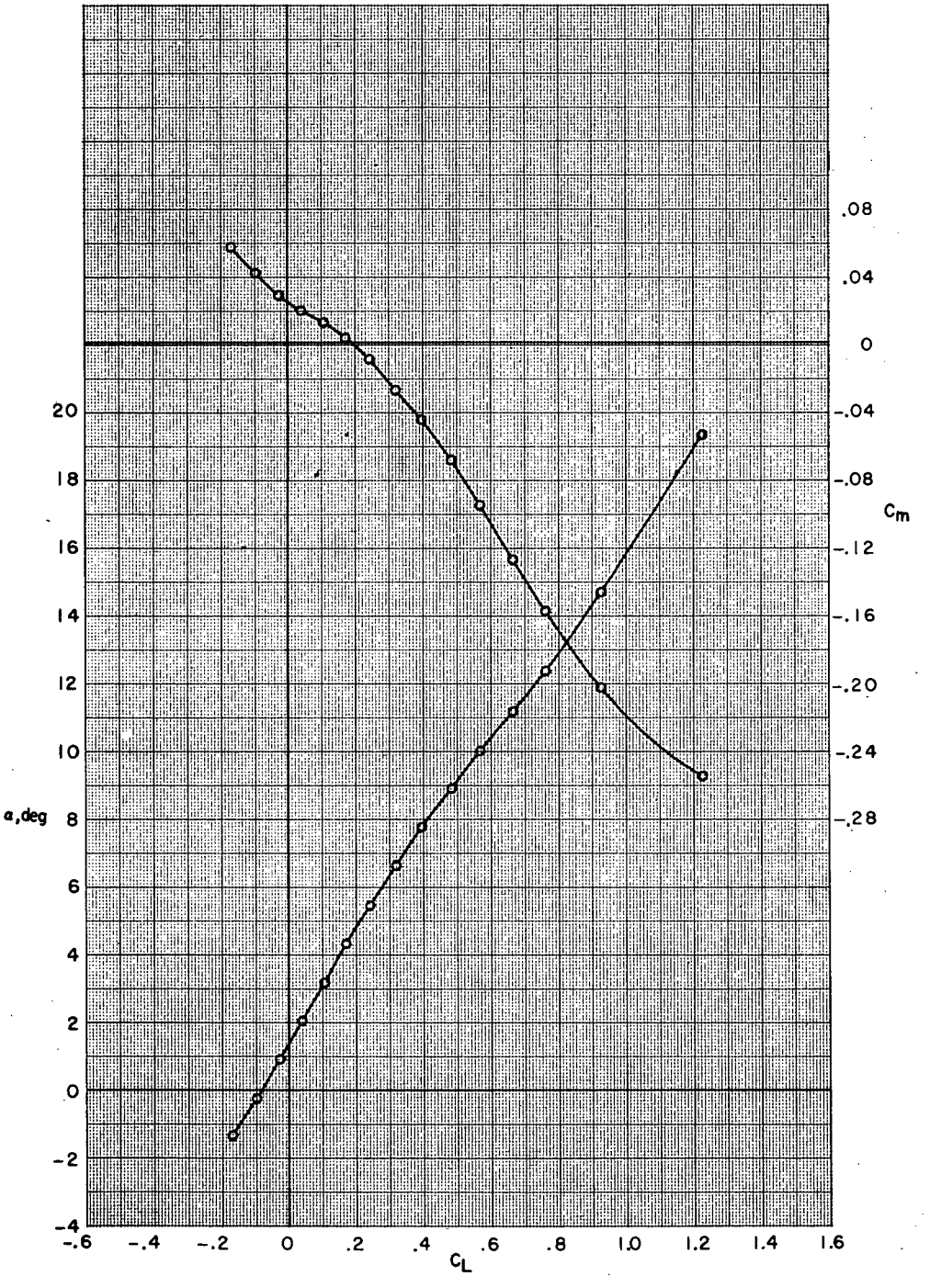

(a) M = 0.80.

Figure 27.- Aerodynamic characteristics for configuration $B_{80}G_{50}I_{71}N^{b}_{32}V_{29}V_{38}W_{36}X_{24}$ with wing swept 58.0°.

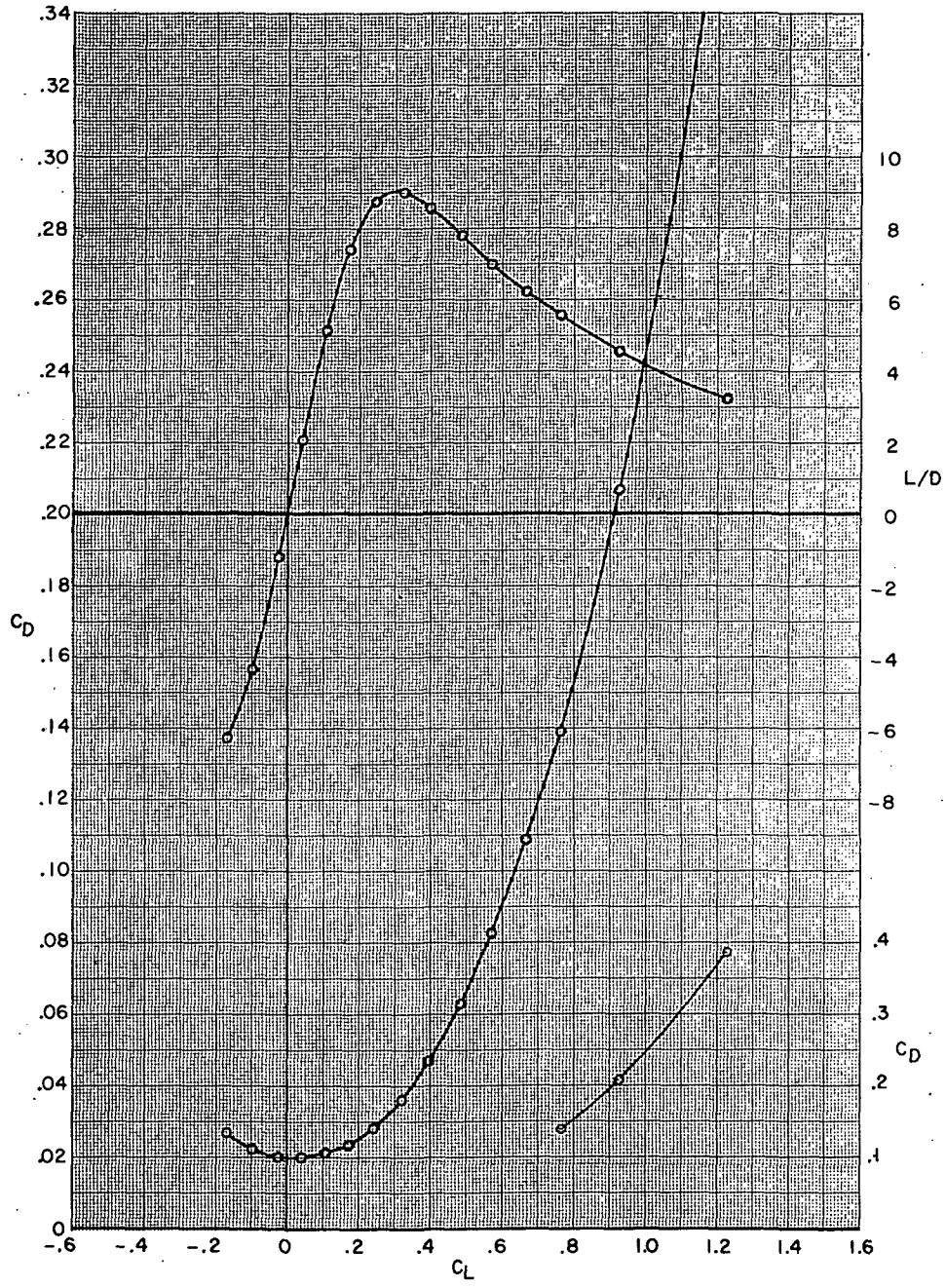

(a) Concluded.

Figure 27.- Continued.

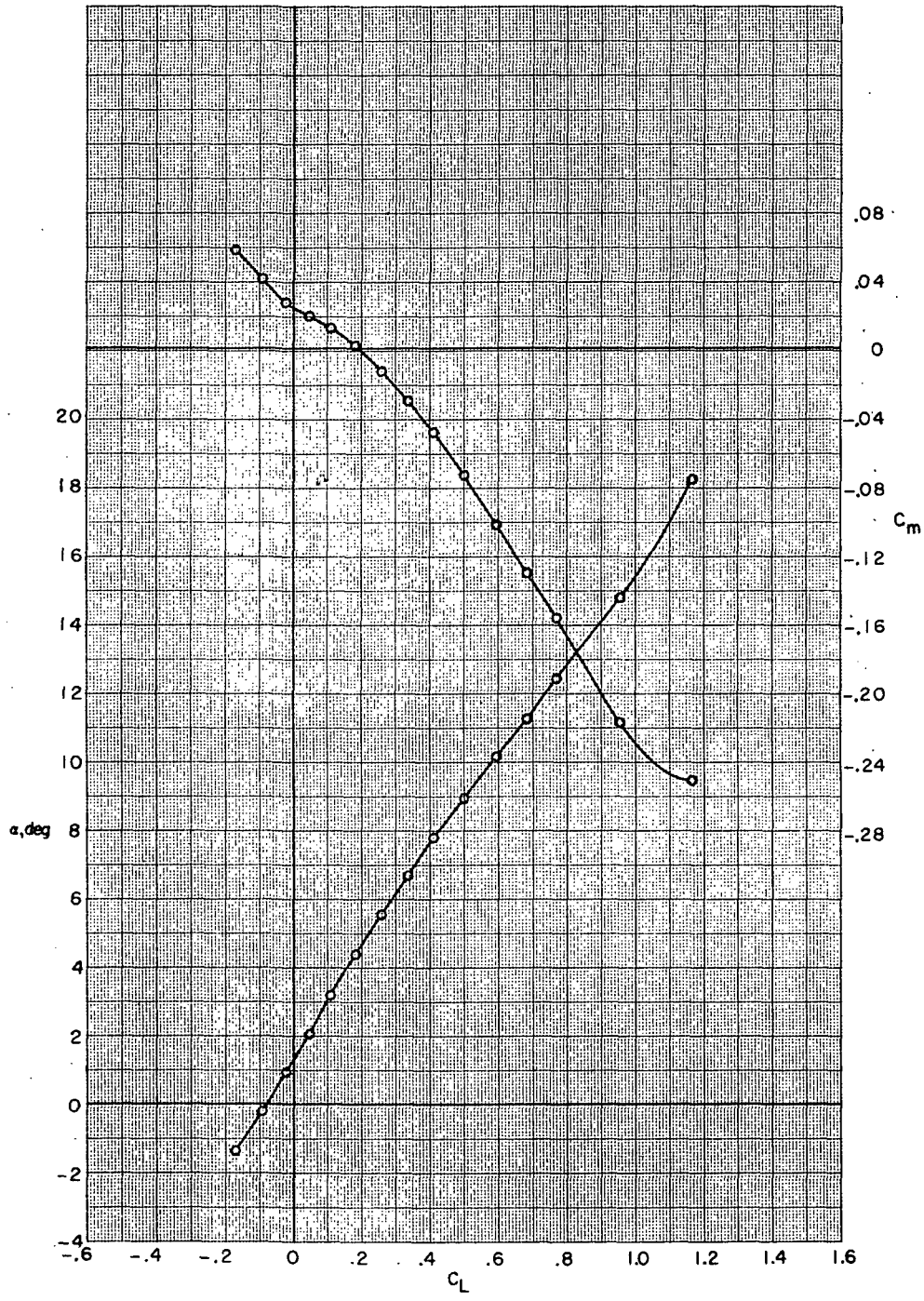

(b) M = 0.85.

Figure 27.- Continued.

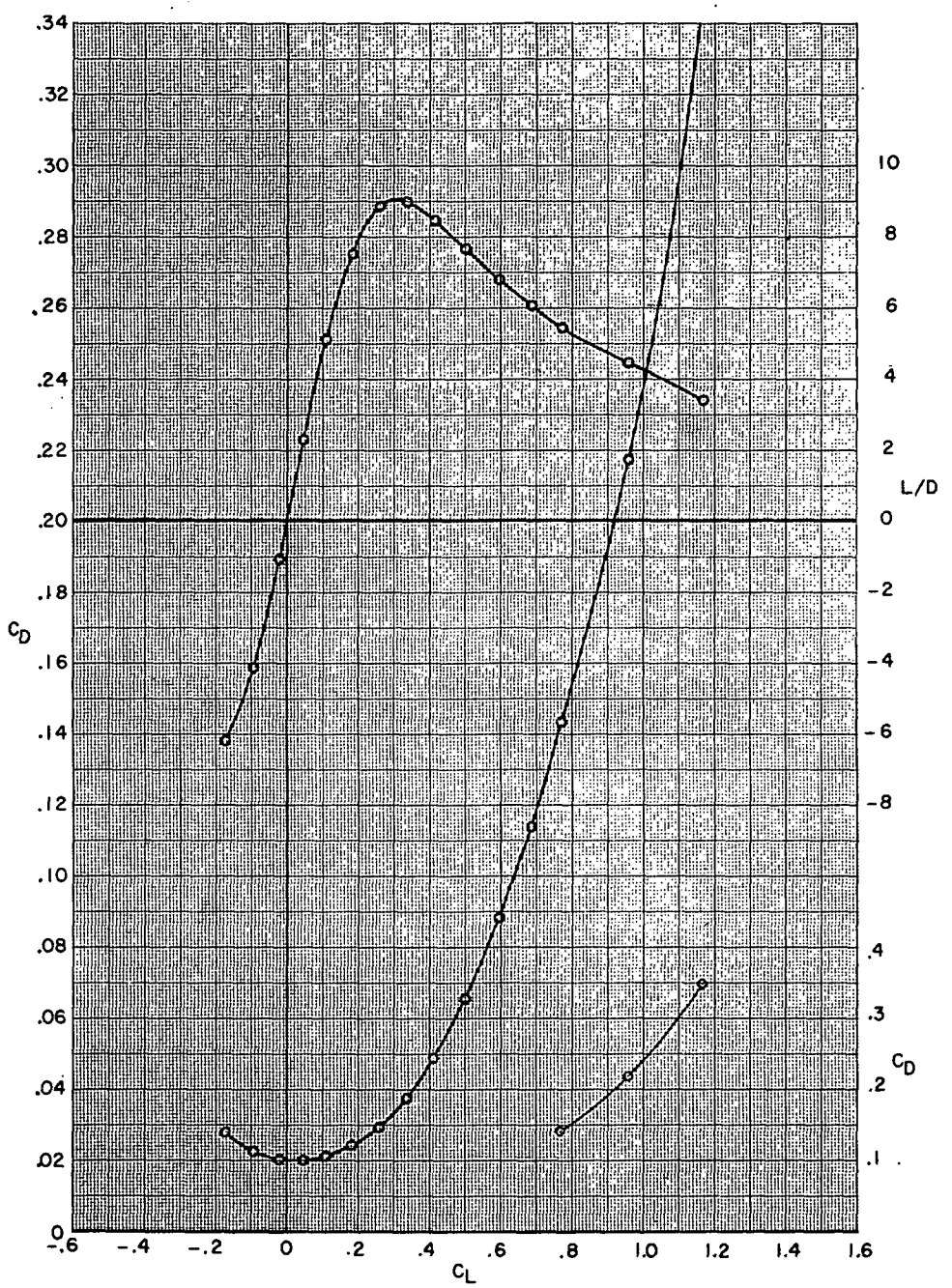

(b) Concluded.

Figure 27.- Continued.

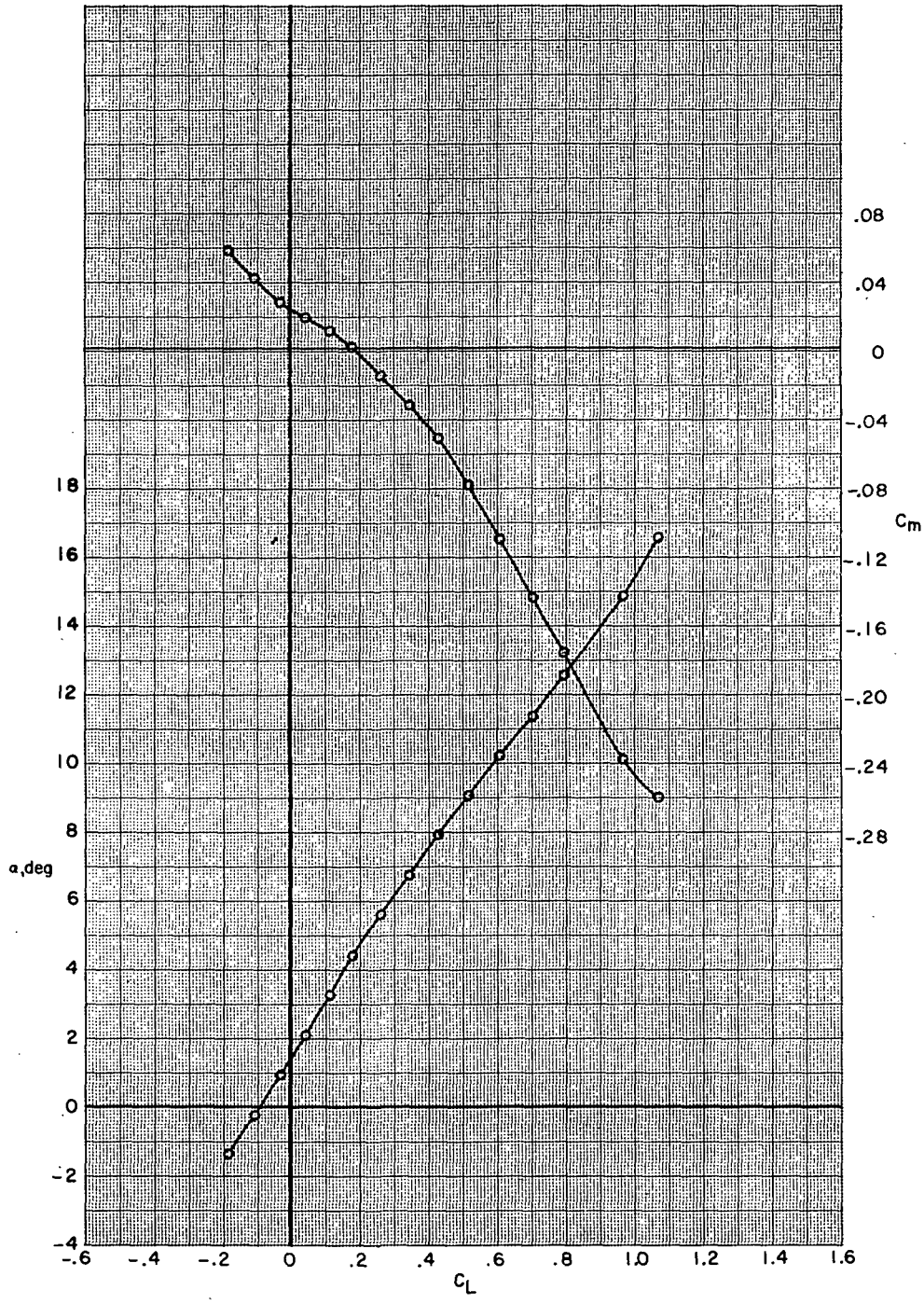

(c) M = 0.90.

Figure 27.- Continued.

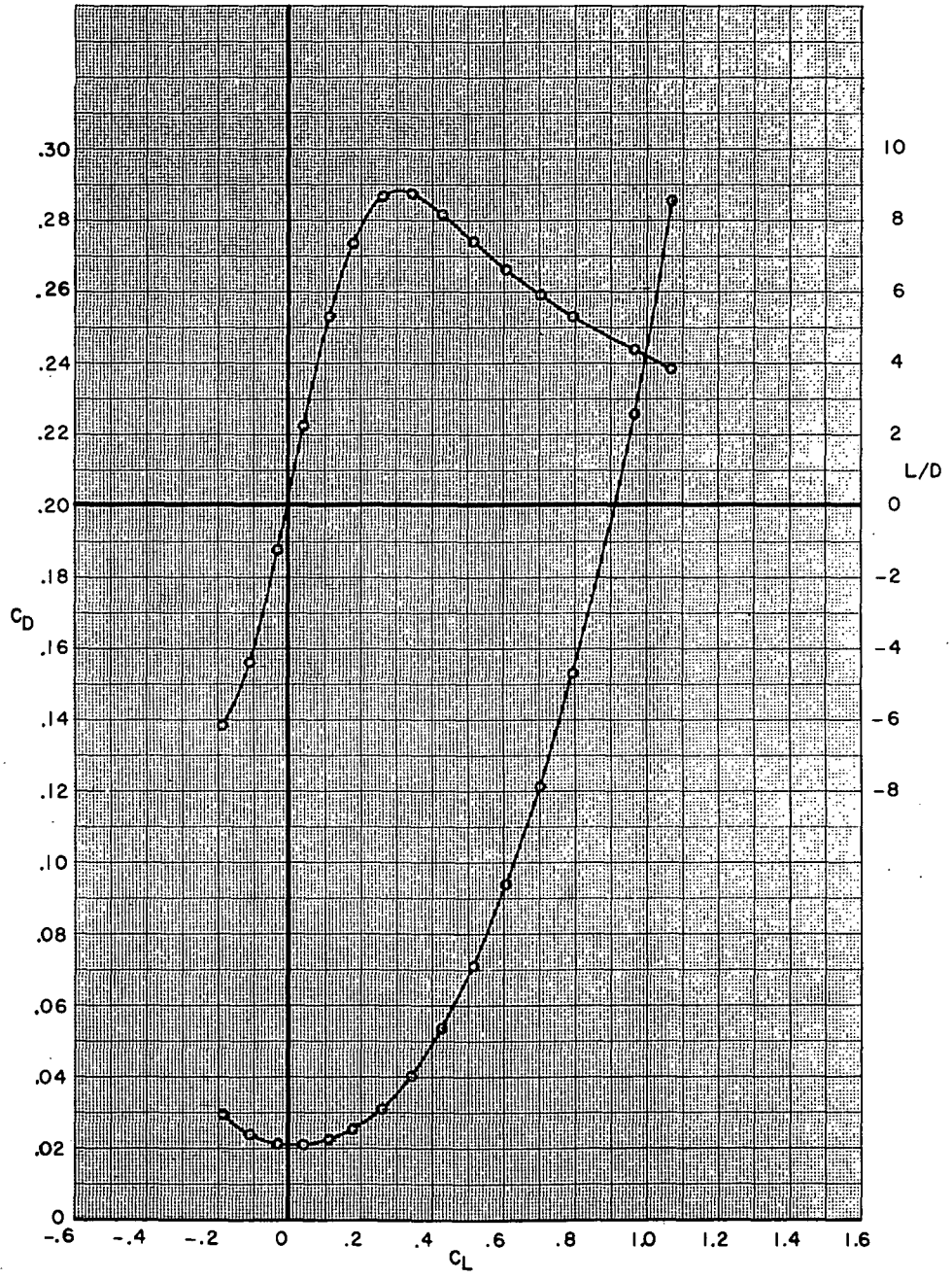

(c) Concluded.

Figure 27.- Continued.

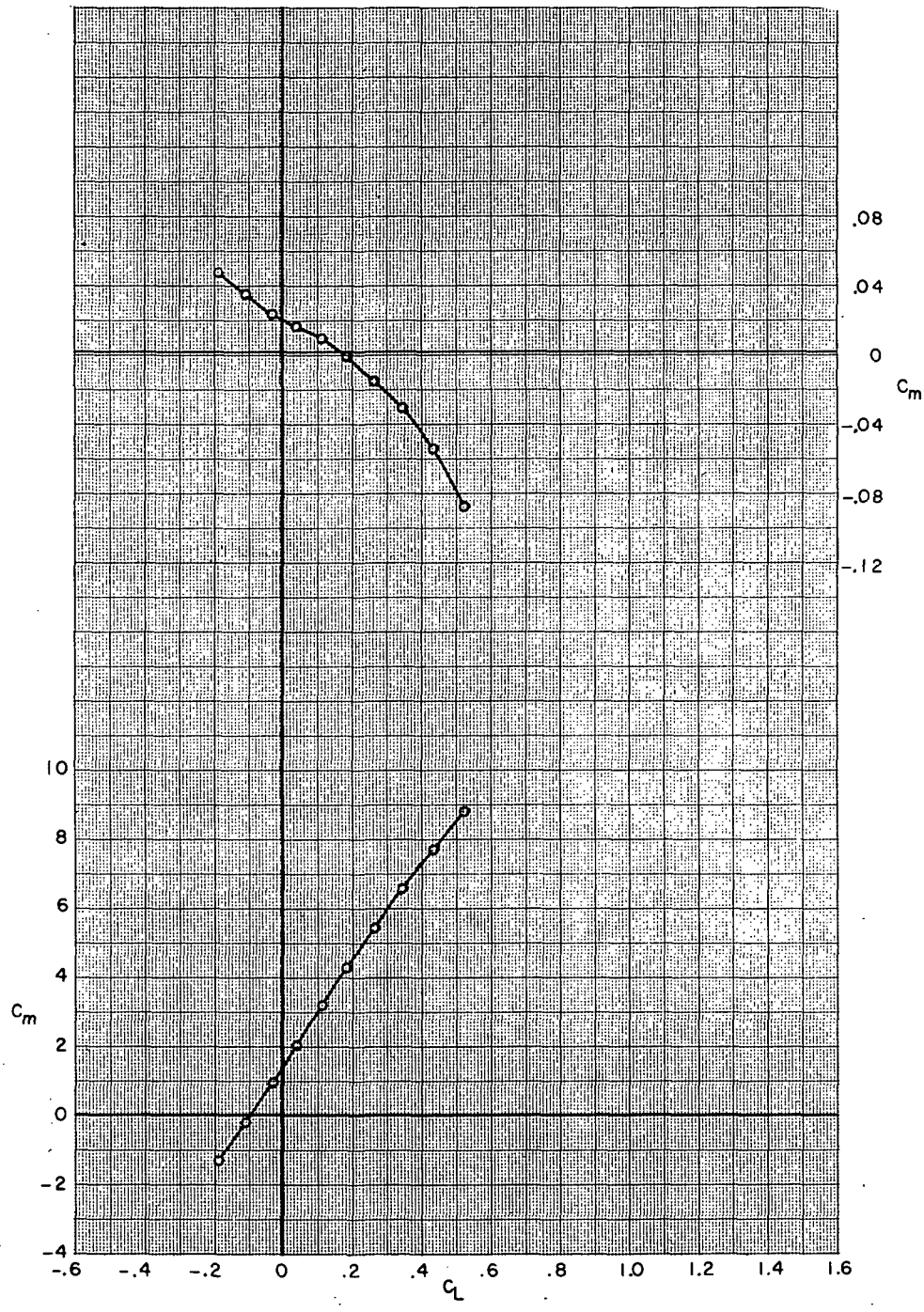

(d) M = 0.95.

Figure 27.- Continued.

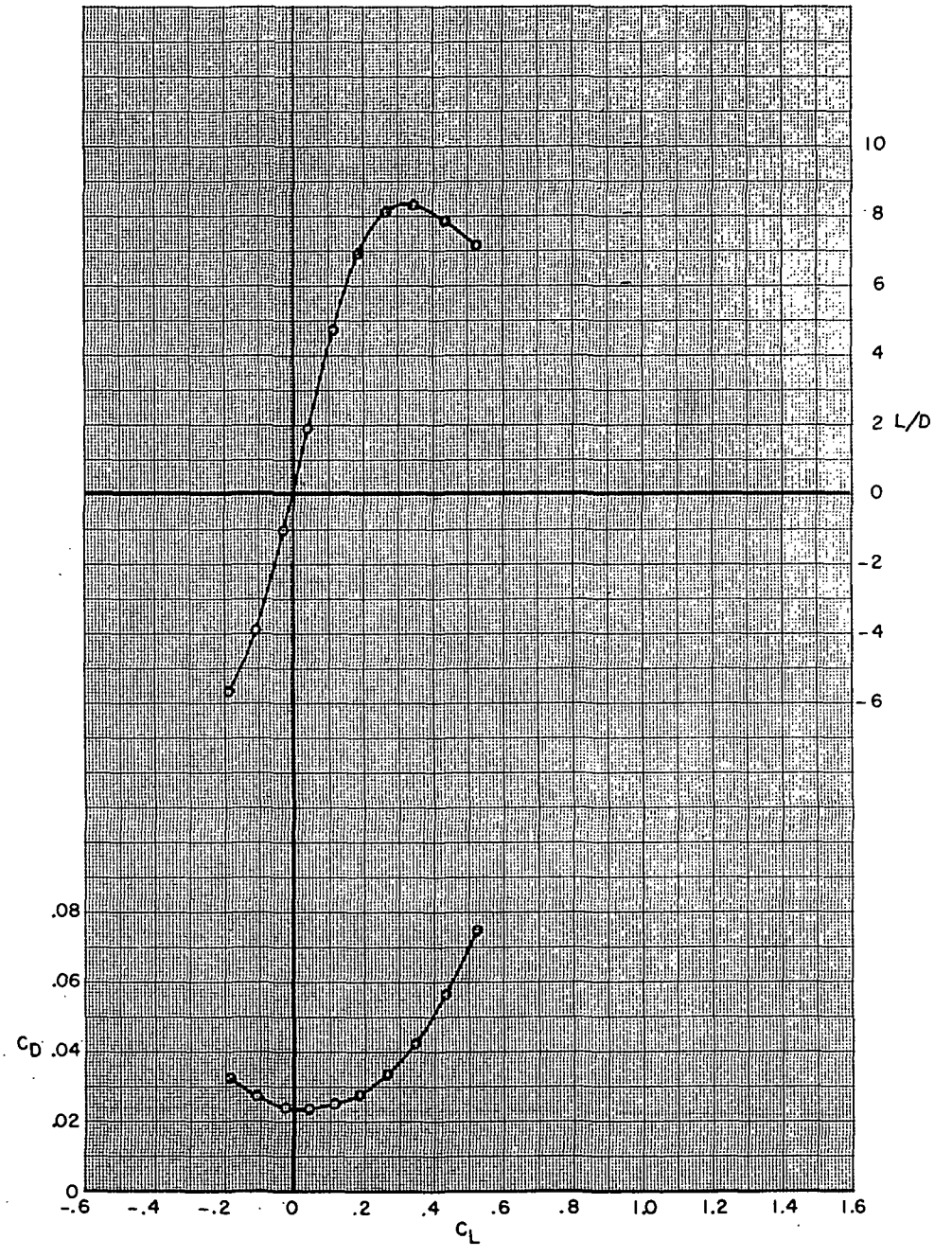

(d) Concluded.

Figure 27.- Concluded.

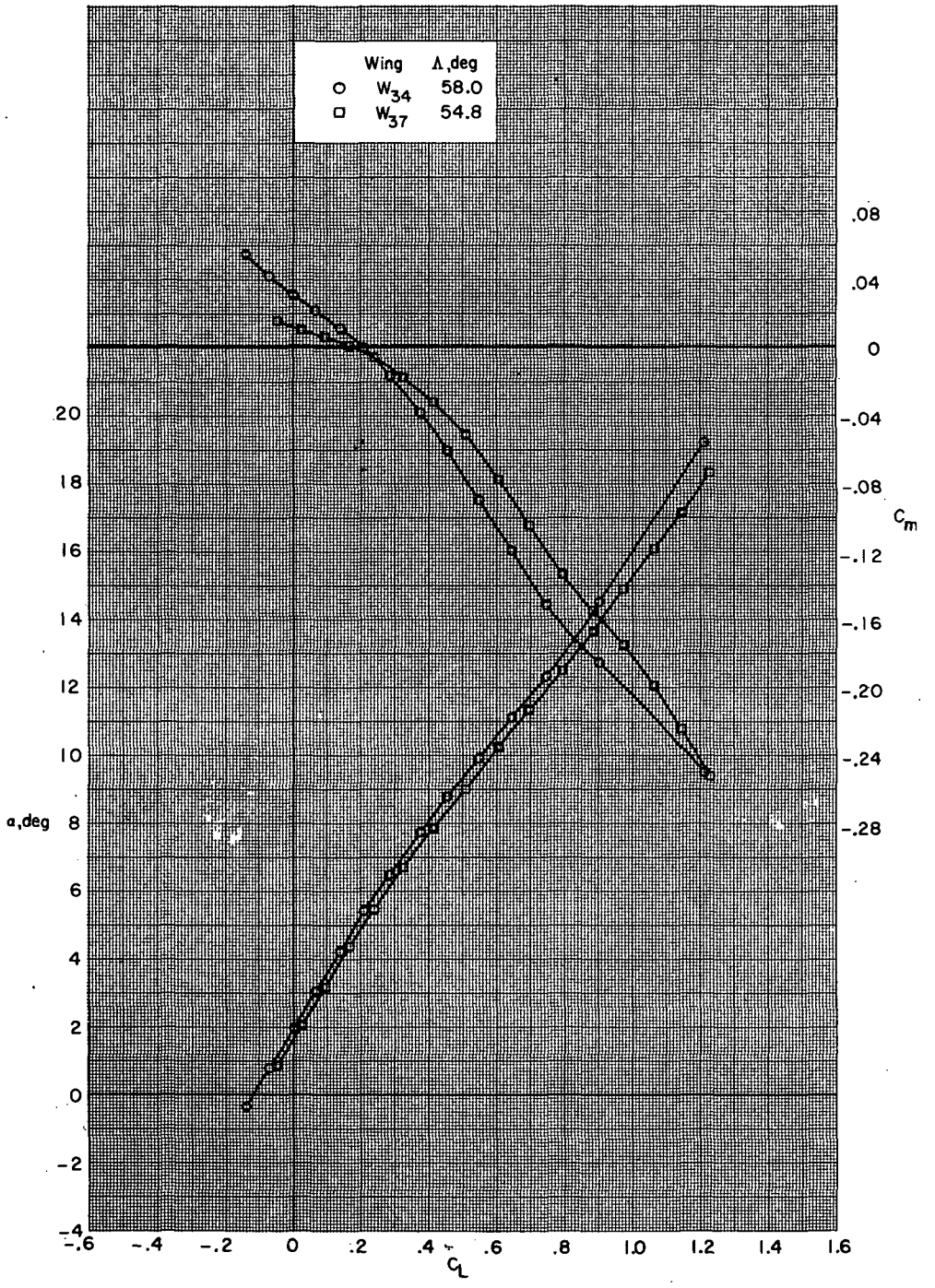

(a) M = 0.80.

Figure 28.- Effect of wing planform on aerodynamic characteristics for supercritical wing configurations $B_{80}G_{49}H_{13}I_{71}N^{b}_{32}V_{29}V_{38}W_{x}X_{24}$ with maximum wing sweep angle.

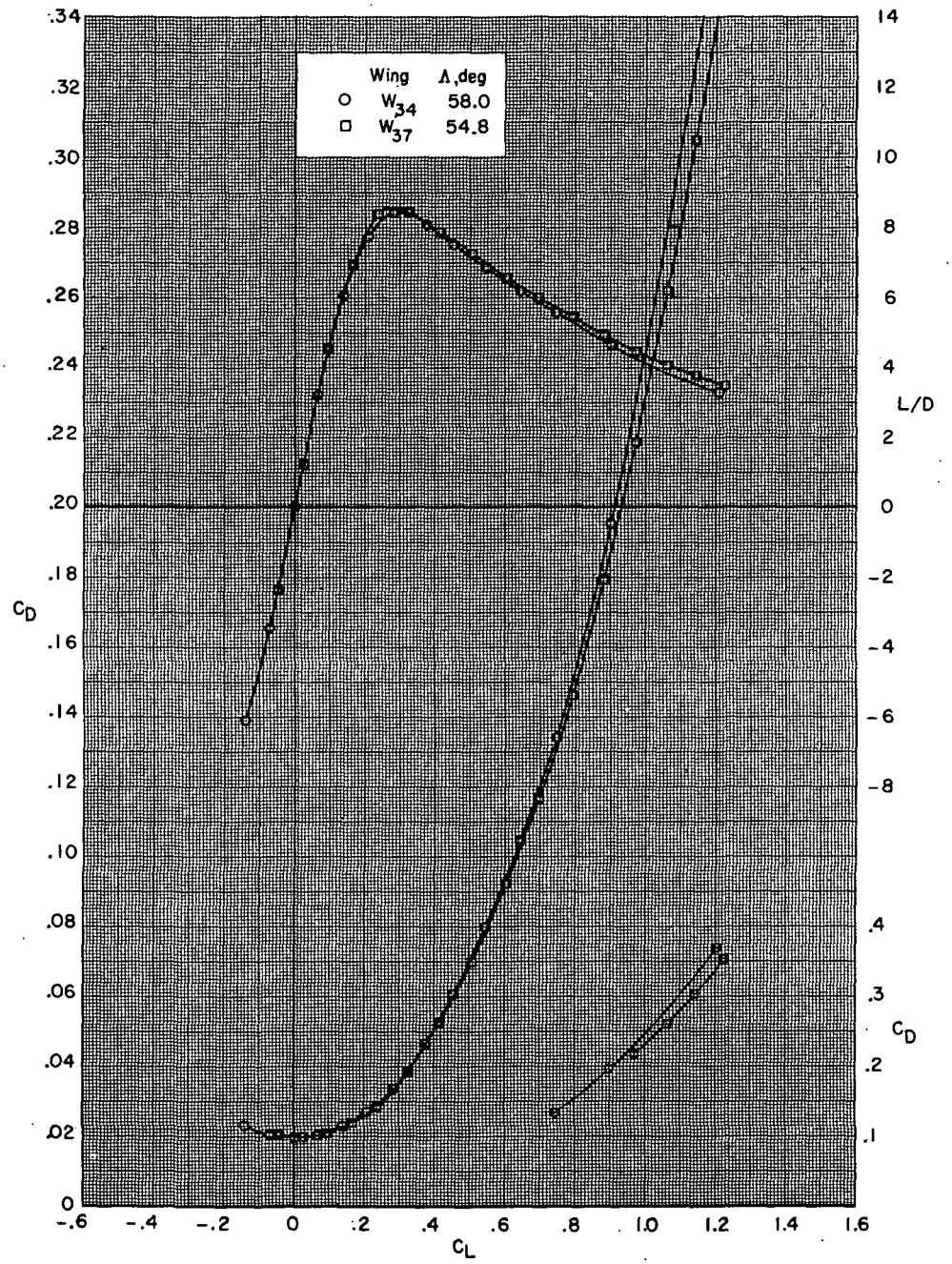

(a) Concluded.

Figure 28.- Continued.

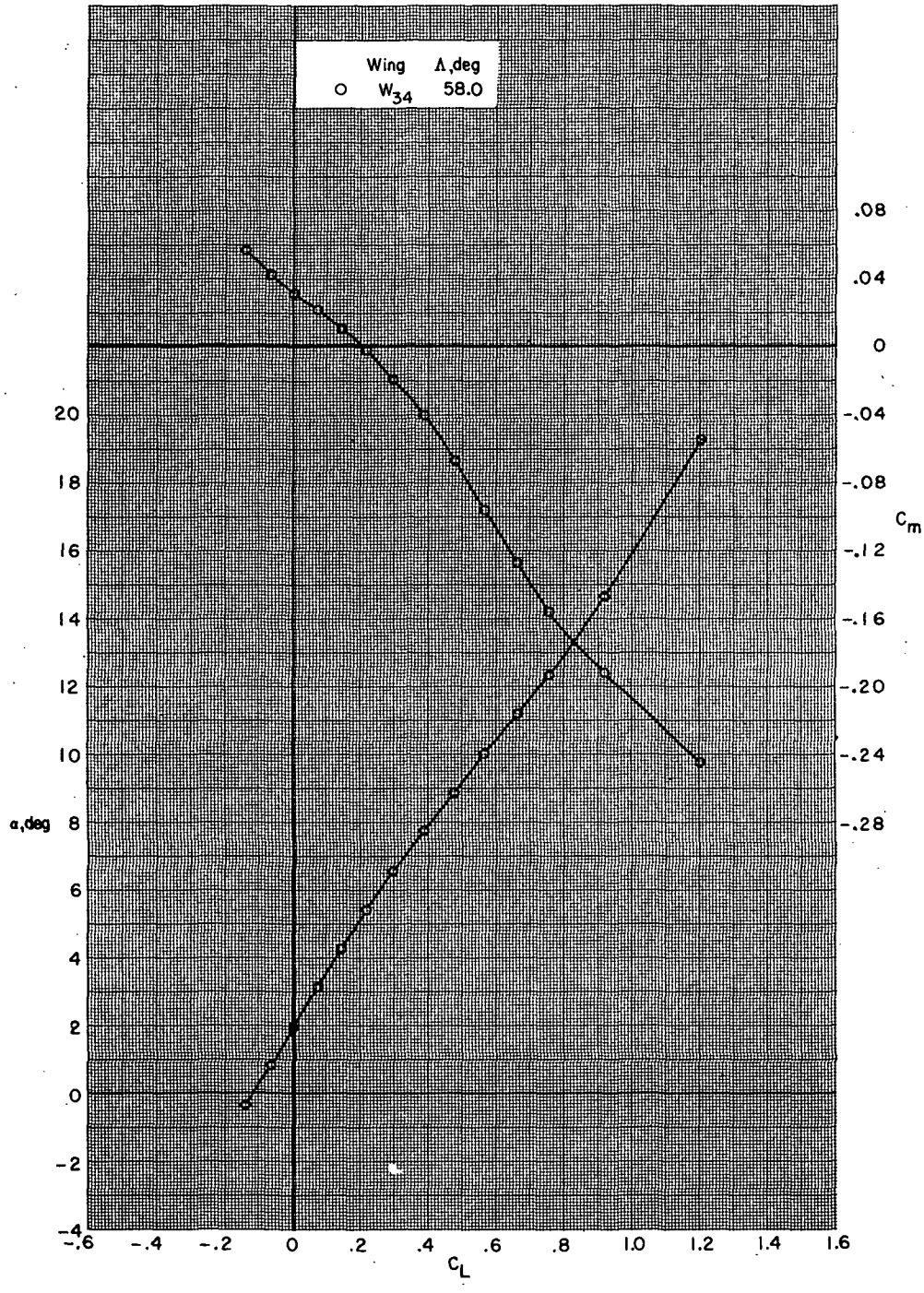

(b) M = 0.85.

Figure 28.- Continued.

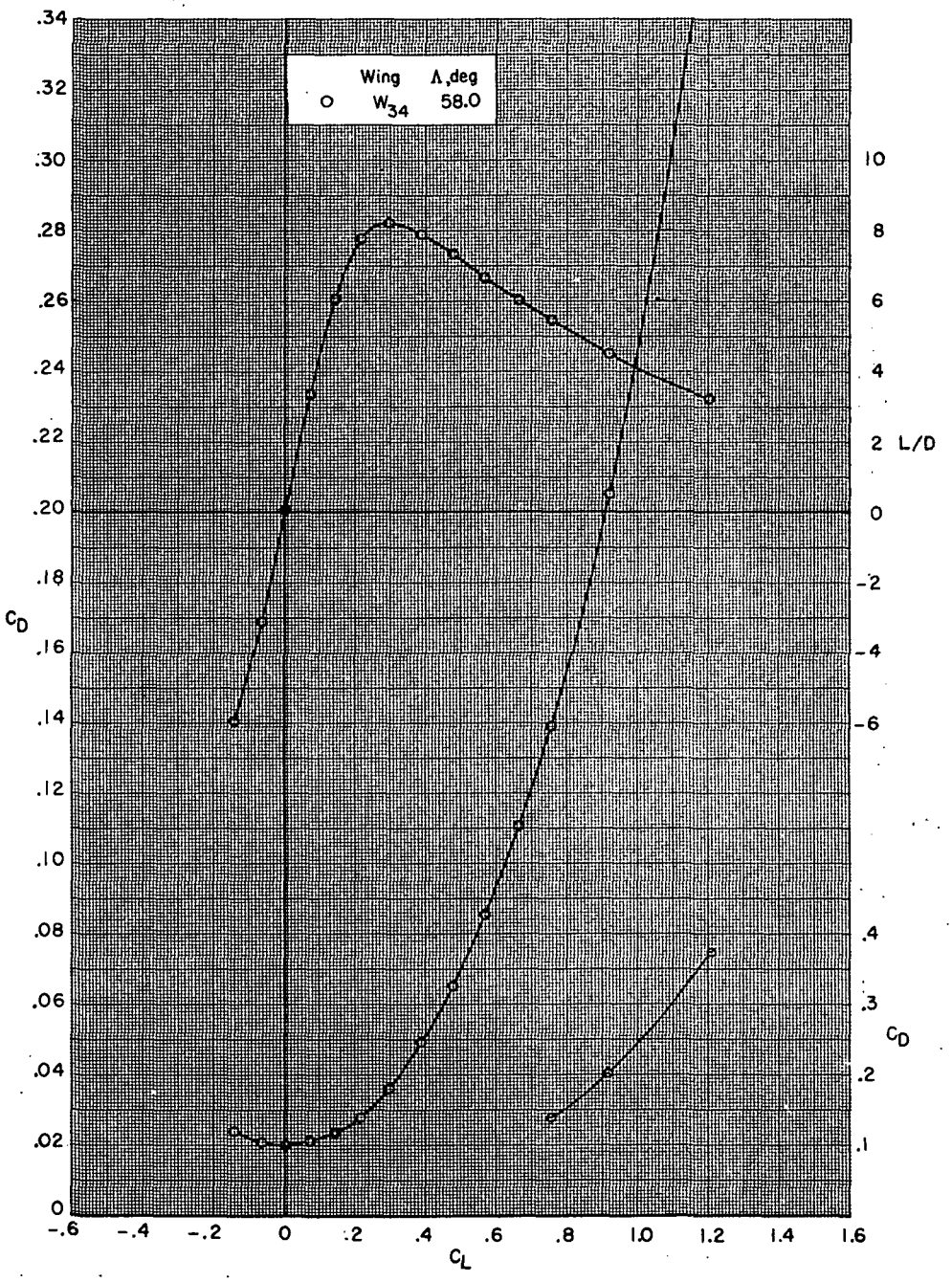

(b) Concluded.

Figure 28.- Continued.

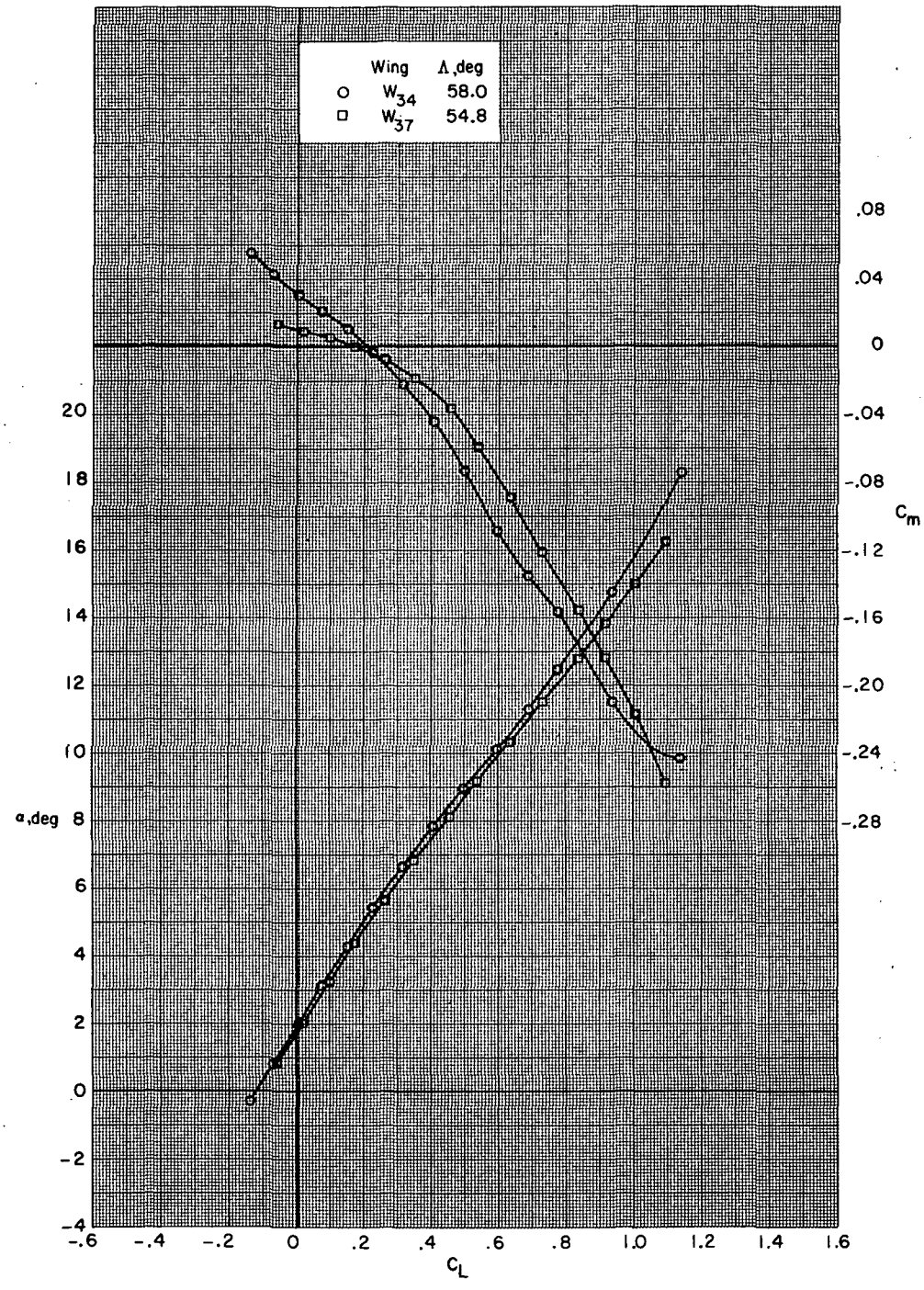

(c) M = 0.90.

Figure 28.- Continued.

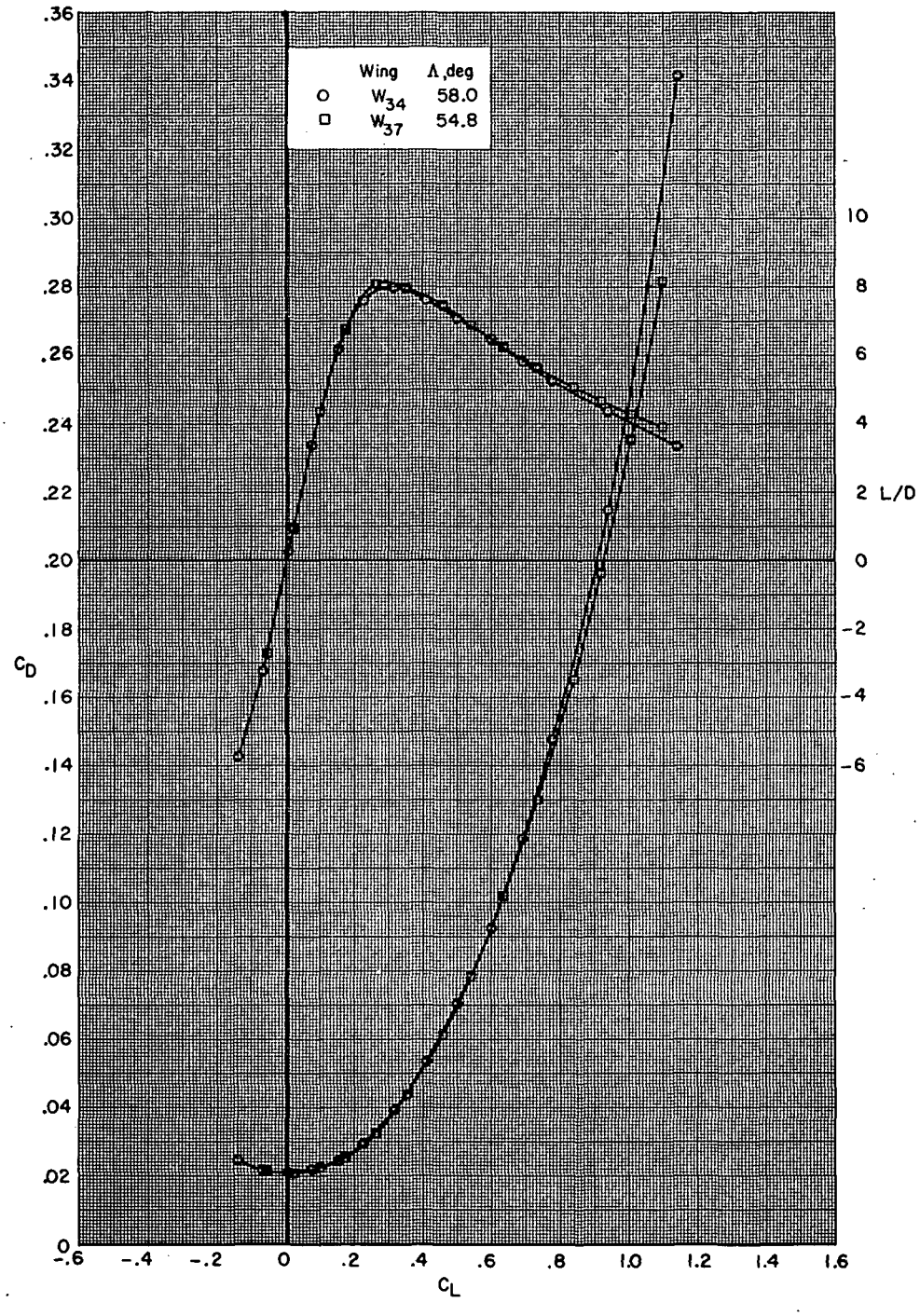

(c) Concluded.

Figure 28.- Continued.

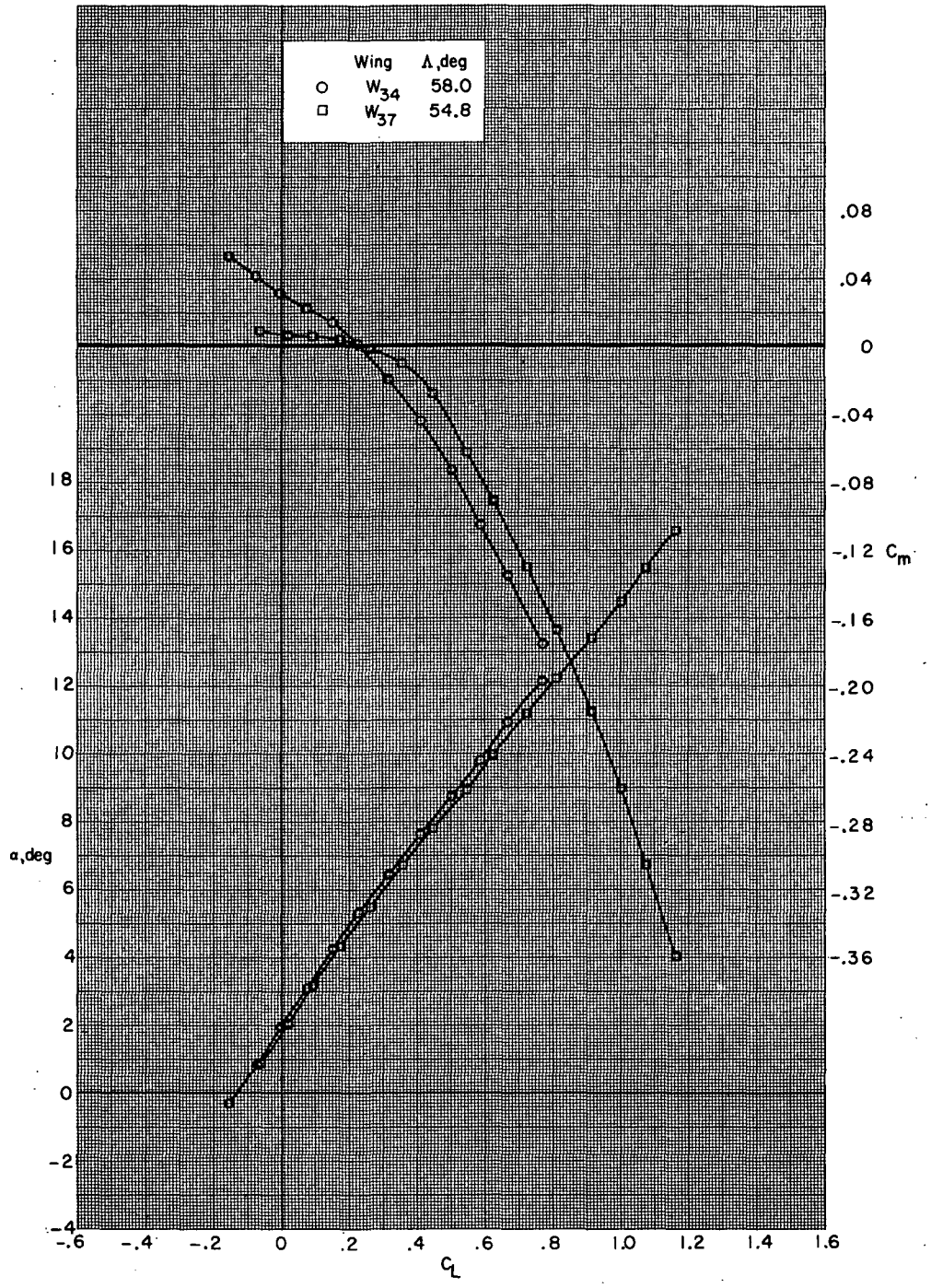

(d) M = 0.95.

Figure 28.- Continued.

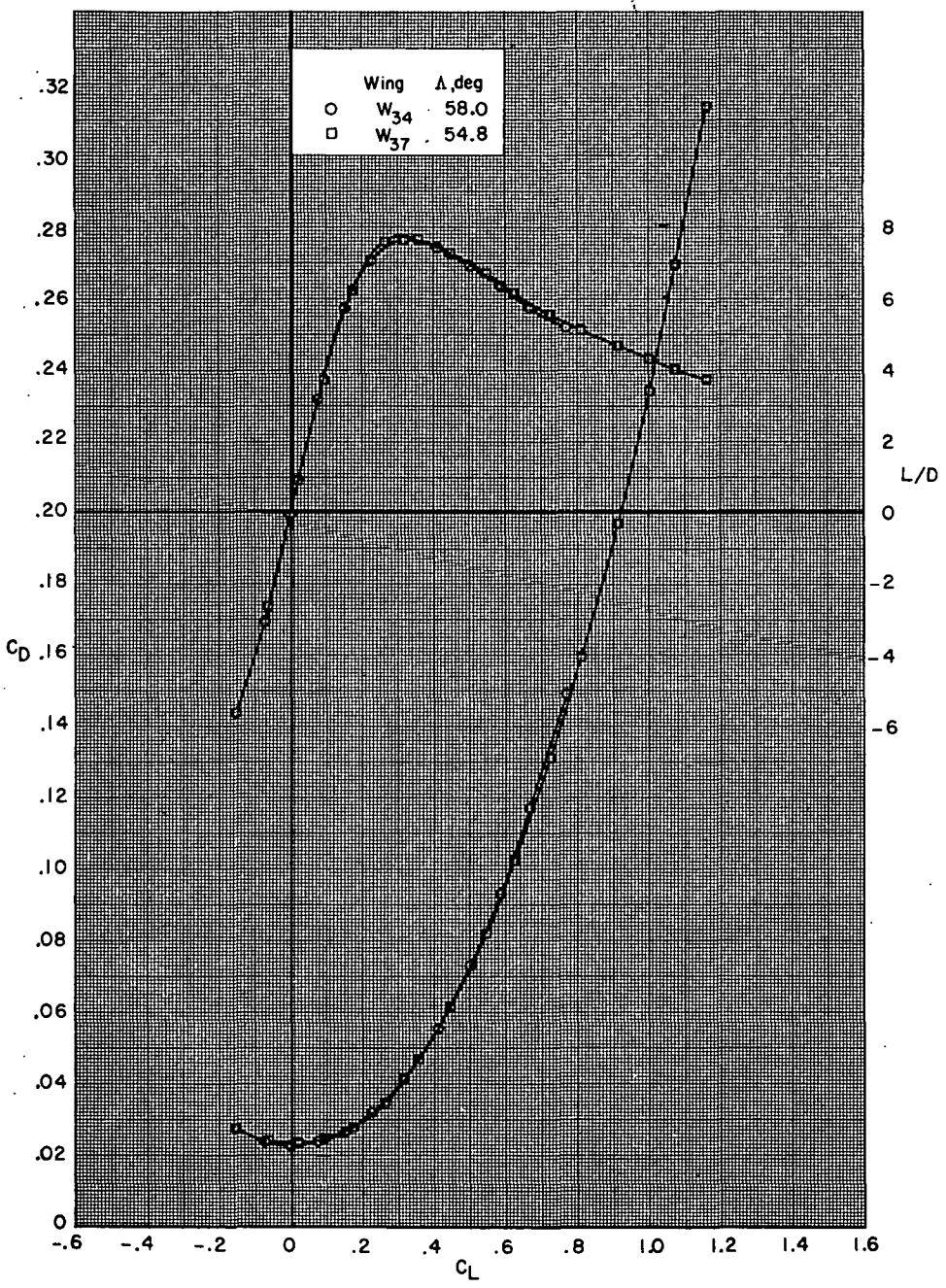

(d) Concluded.

Figure 28.- Concluded.

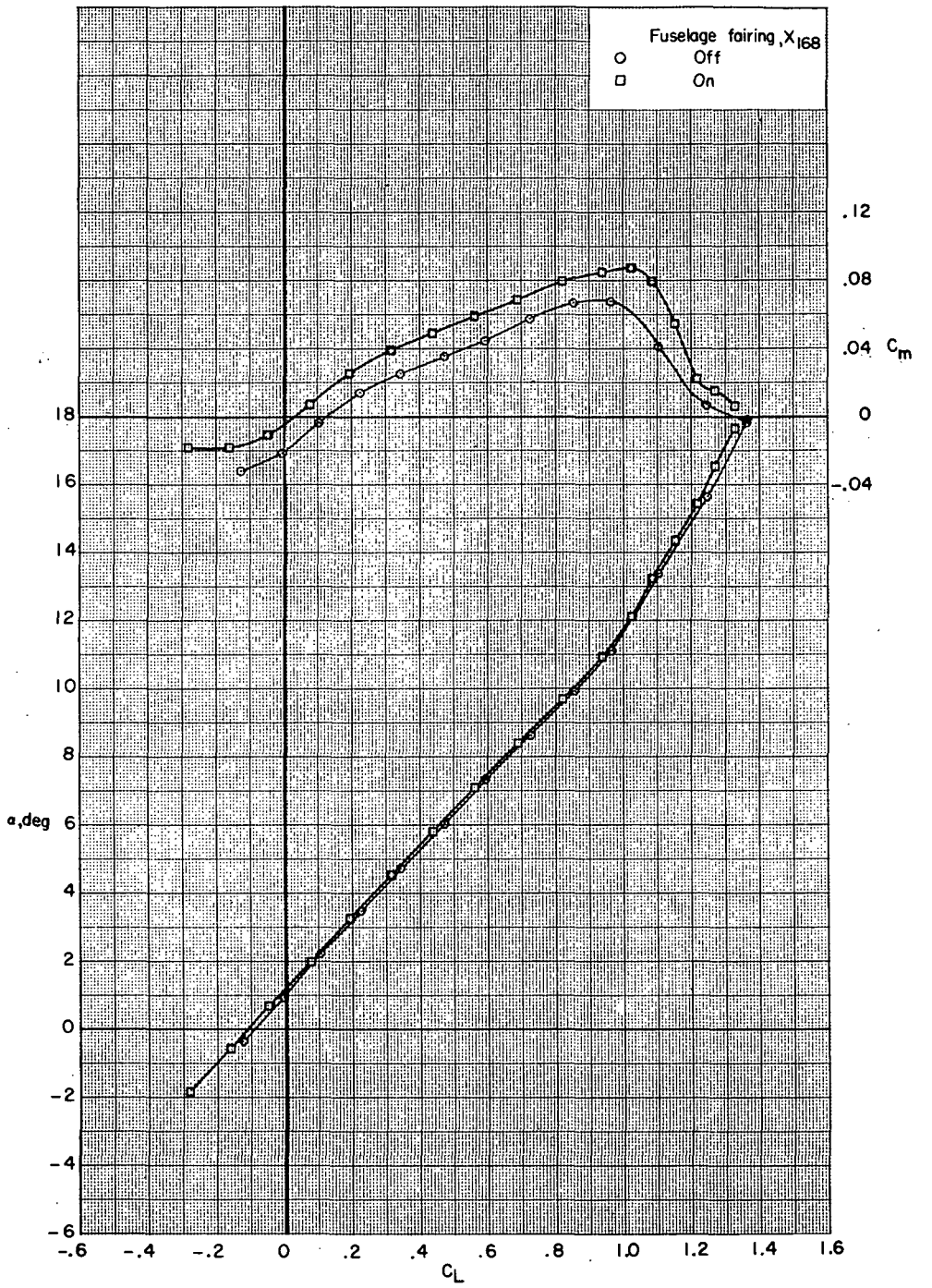

(a) M = 0.70.

Figure 29.- Effect of fuselage fairing X_{168} on aerodynamic characteristics for configuration $B_{80}G_{43}H_{13}I_{71}N^{b}_{32}V_{29}V_{38}W_{31}X_{24}$ with wing swept 26.0°.

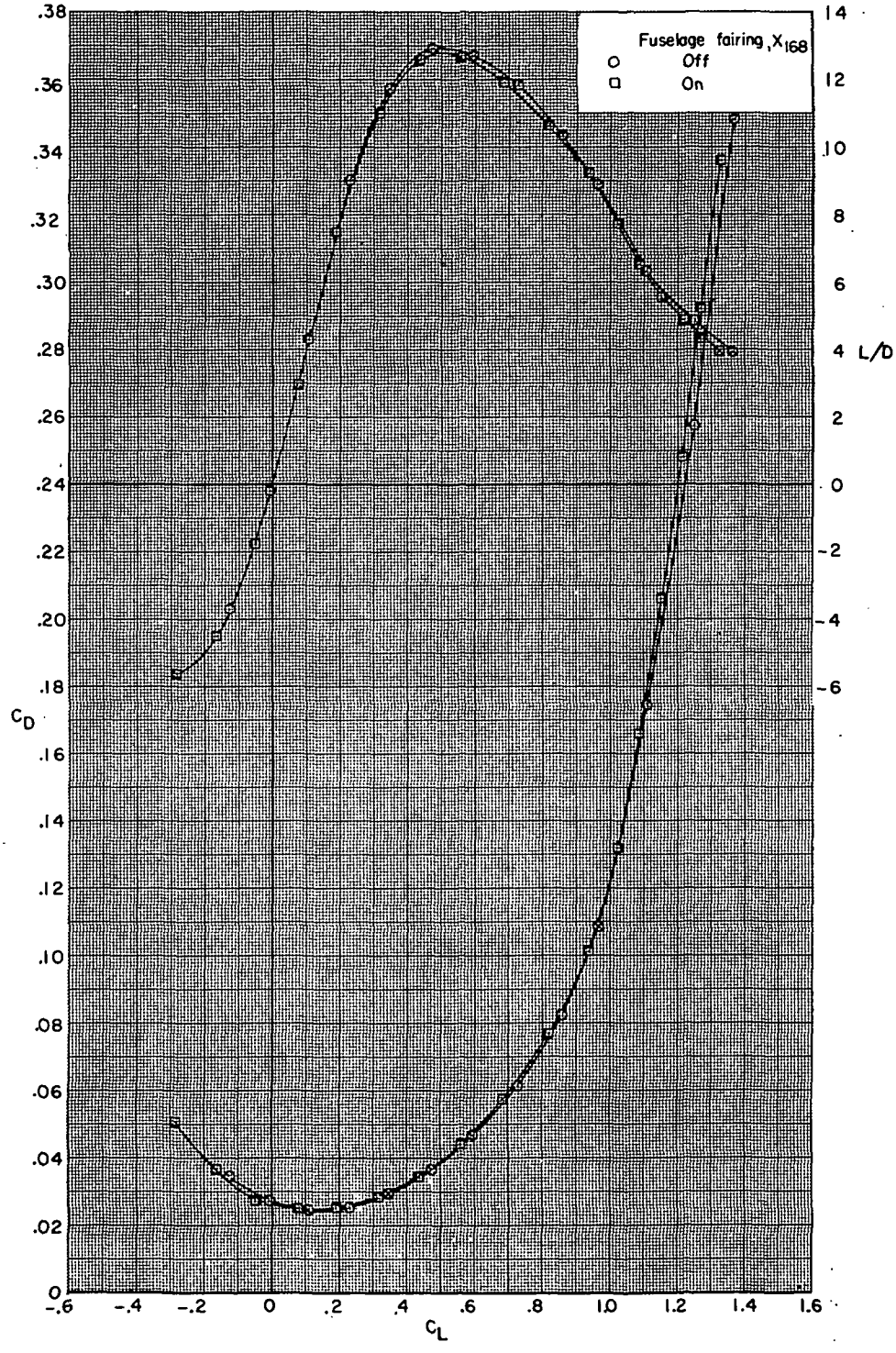

(a) Concluded.

Figure 29.- Continued.

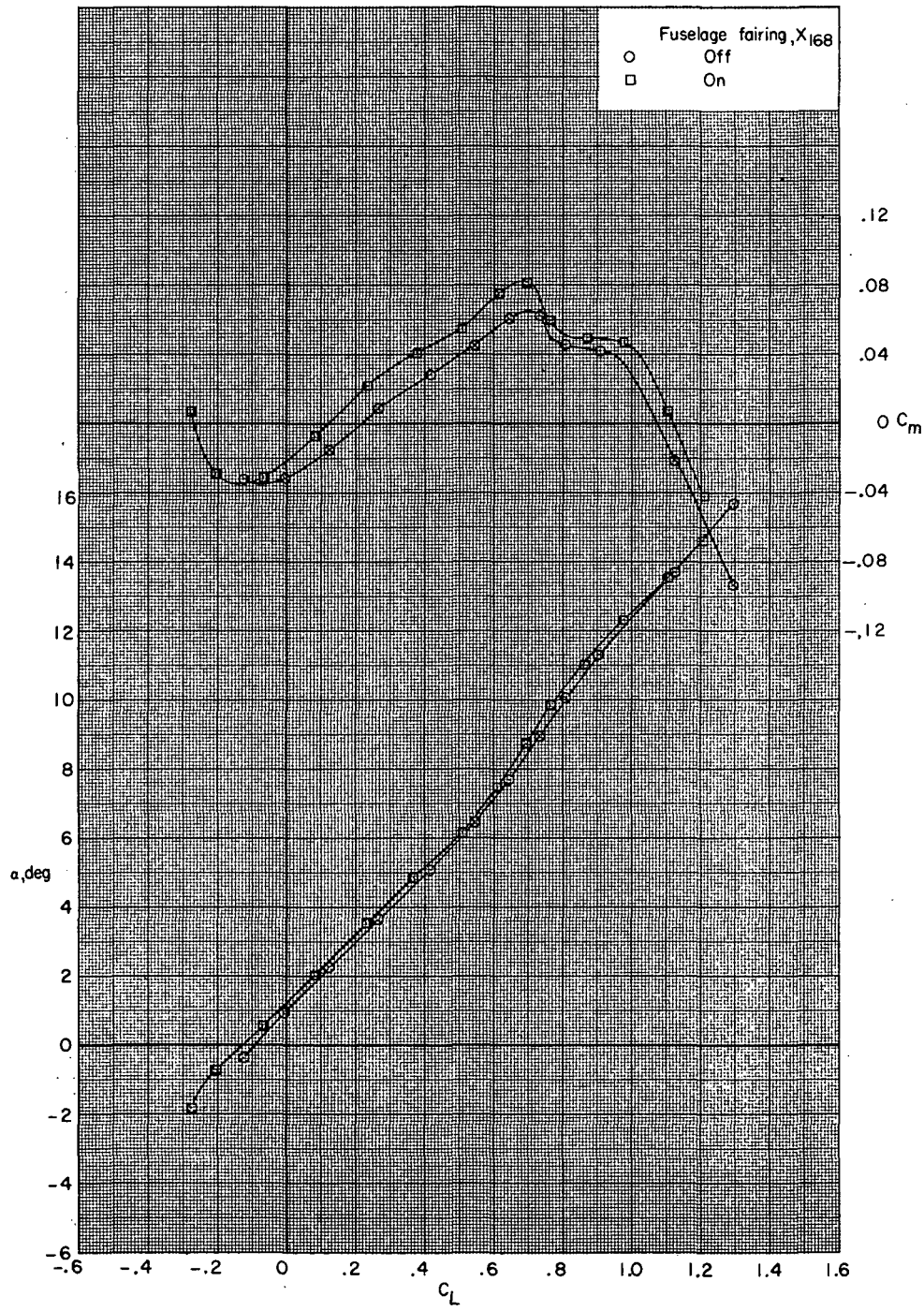

(b) M = 0.85.

Figure 29.- Continued.

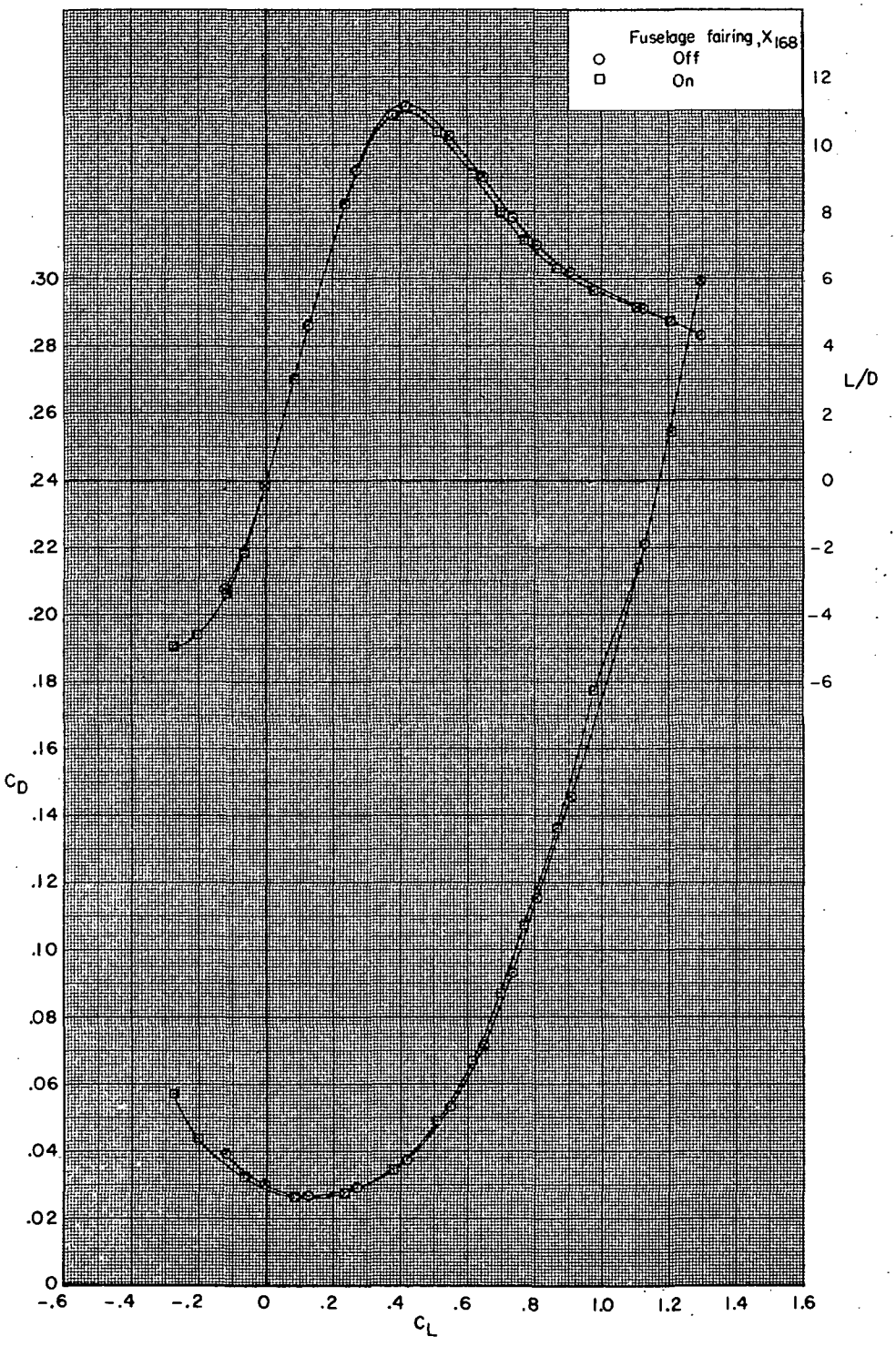

(b) Concluded.

Figure 29.- Continued.

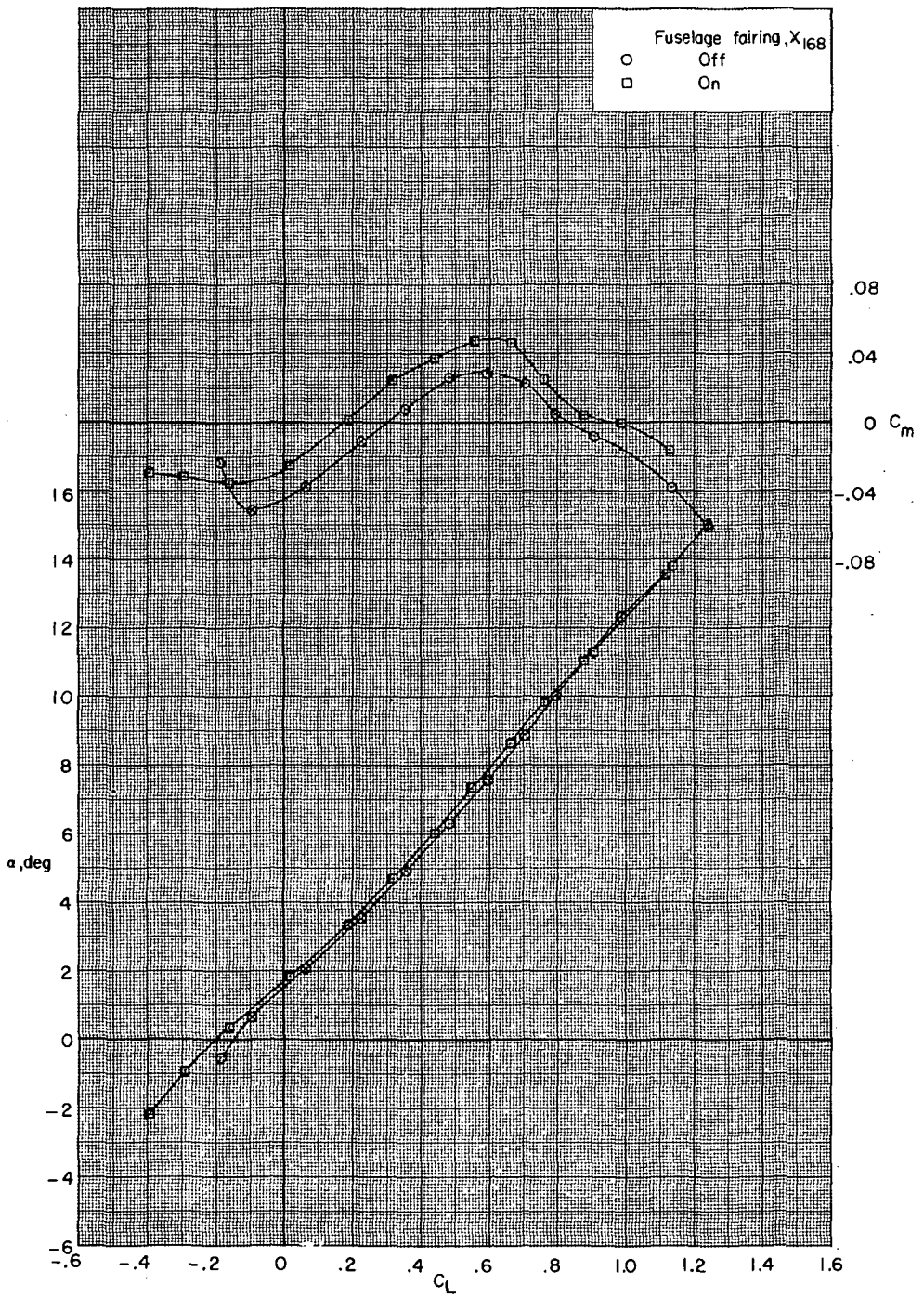

(c) M = 0.90.

Figure 29.- Continued.

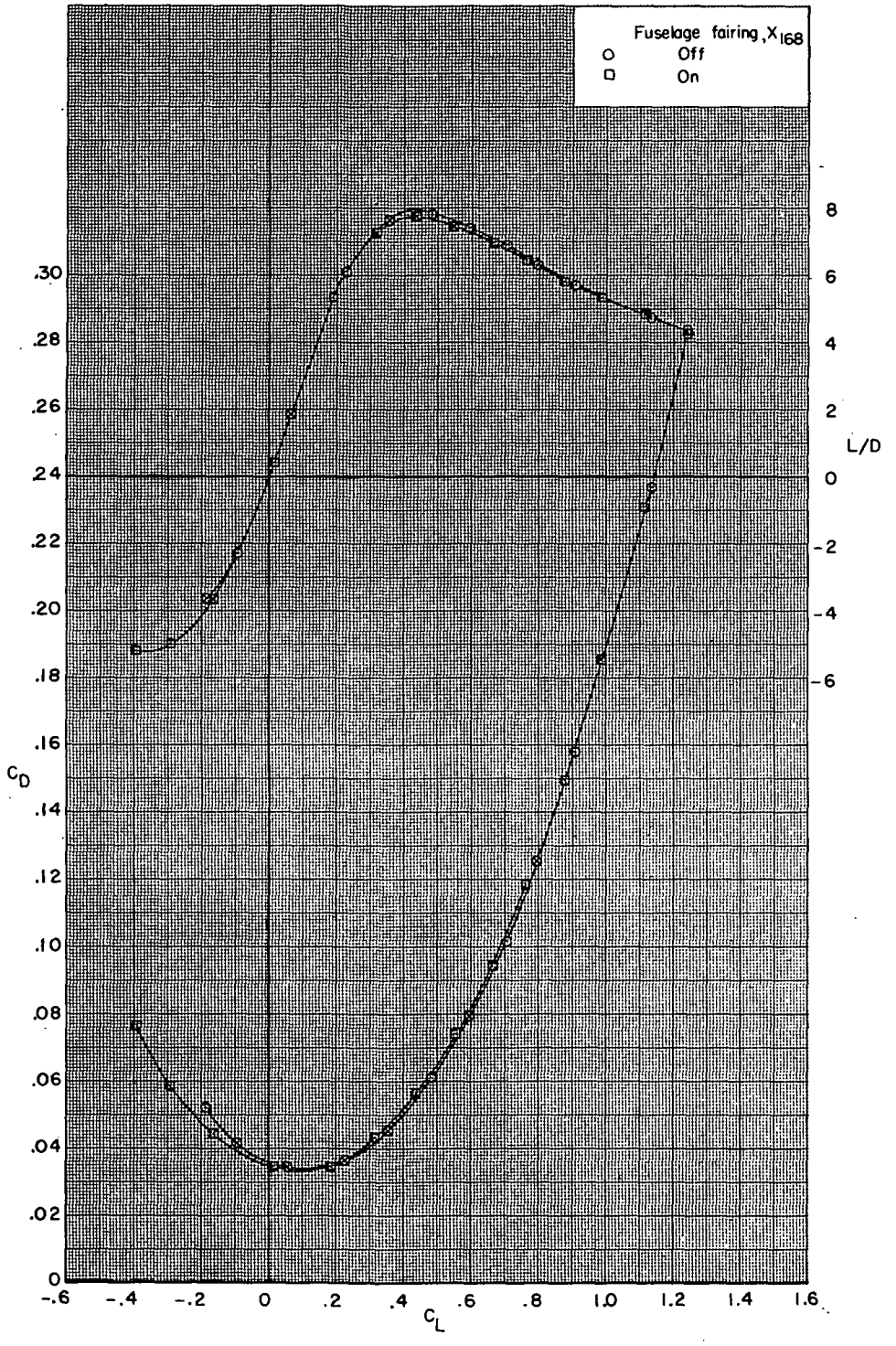

(c) Concluded.

Figure 29.- Concluded.

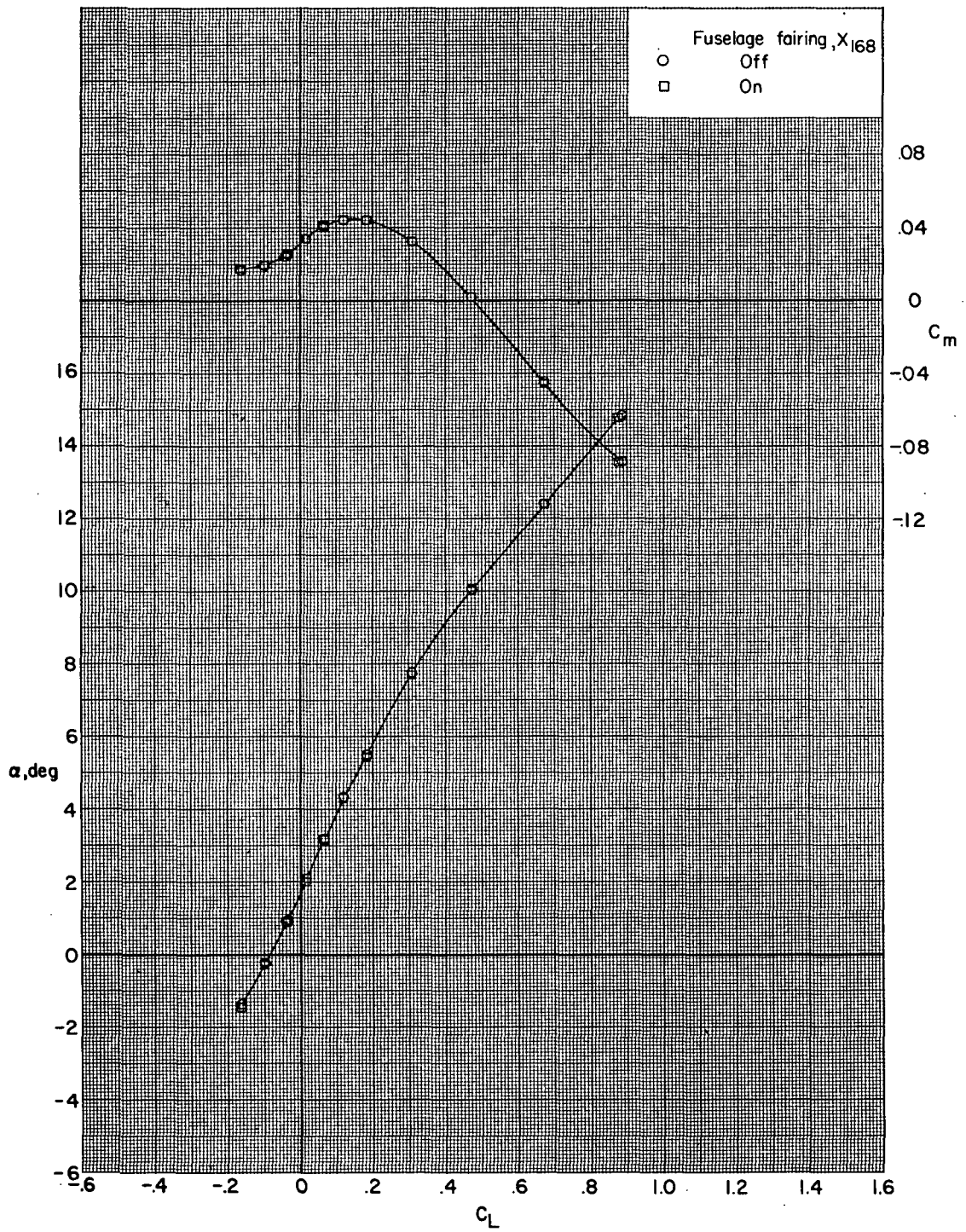

(a) M = 0.80.

Figure 30.- Effect of fuselage fairing X_{168} on aerodynamic characteristics for configuration $B_{80}G_{43}H_{13}I_{71}N^{b}_{32}V_{29}V_{38}W_{31}X_{24}$ with wing swept 63.7°.

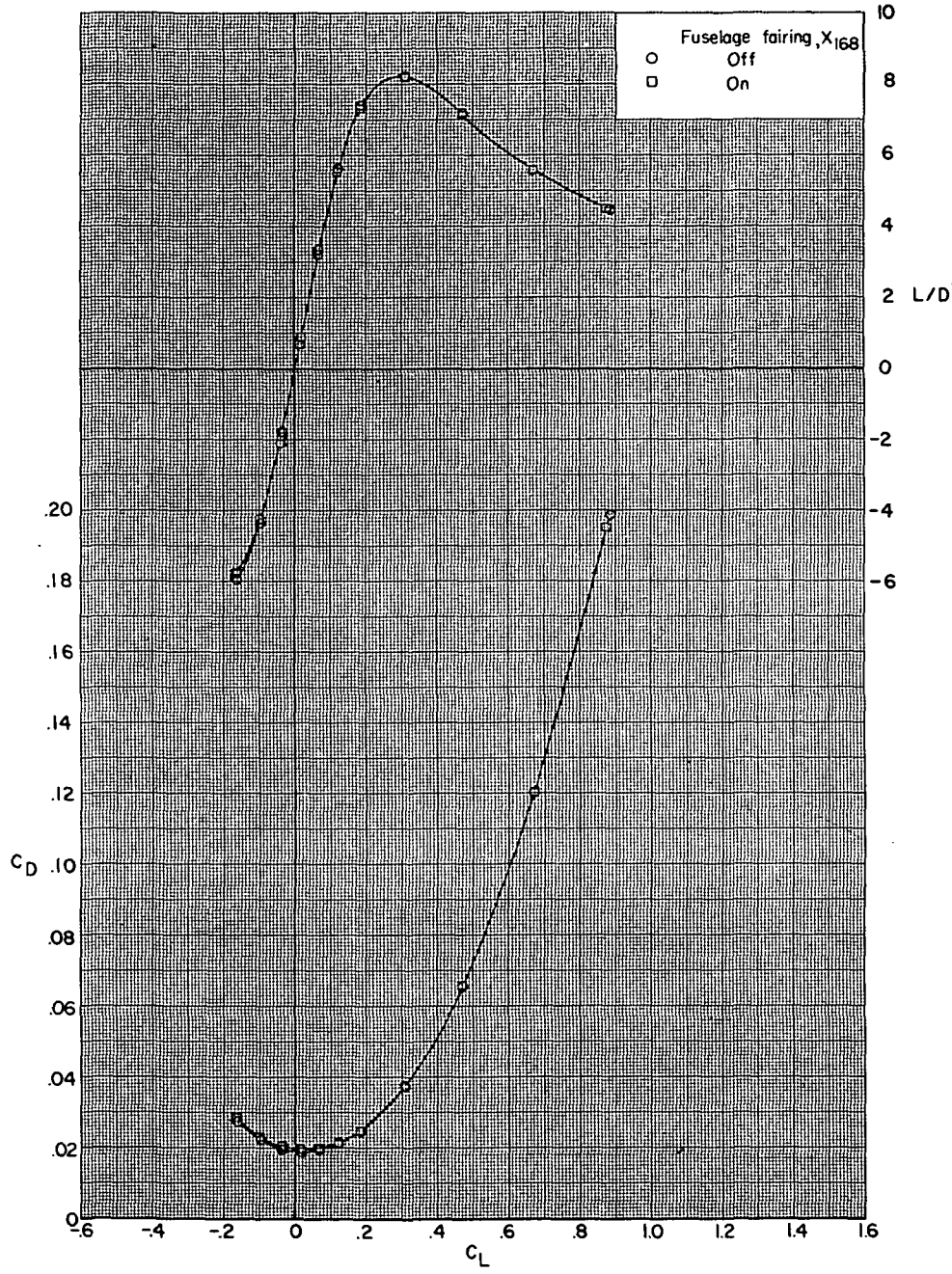

(a) Concluded.

Figure 30.- Continued.

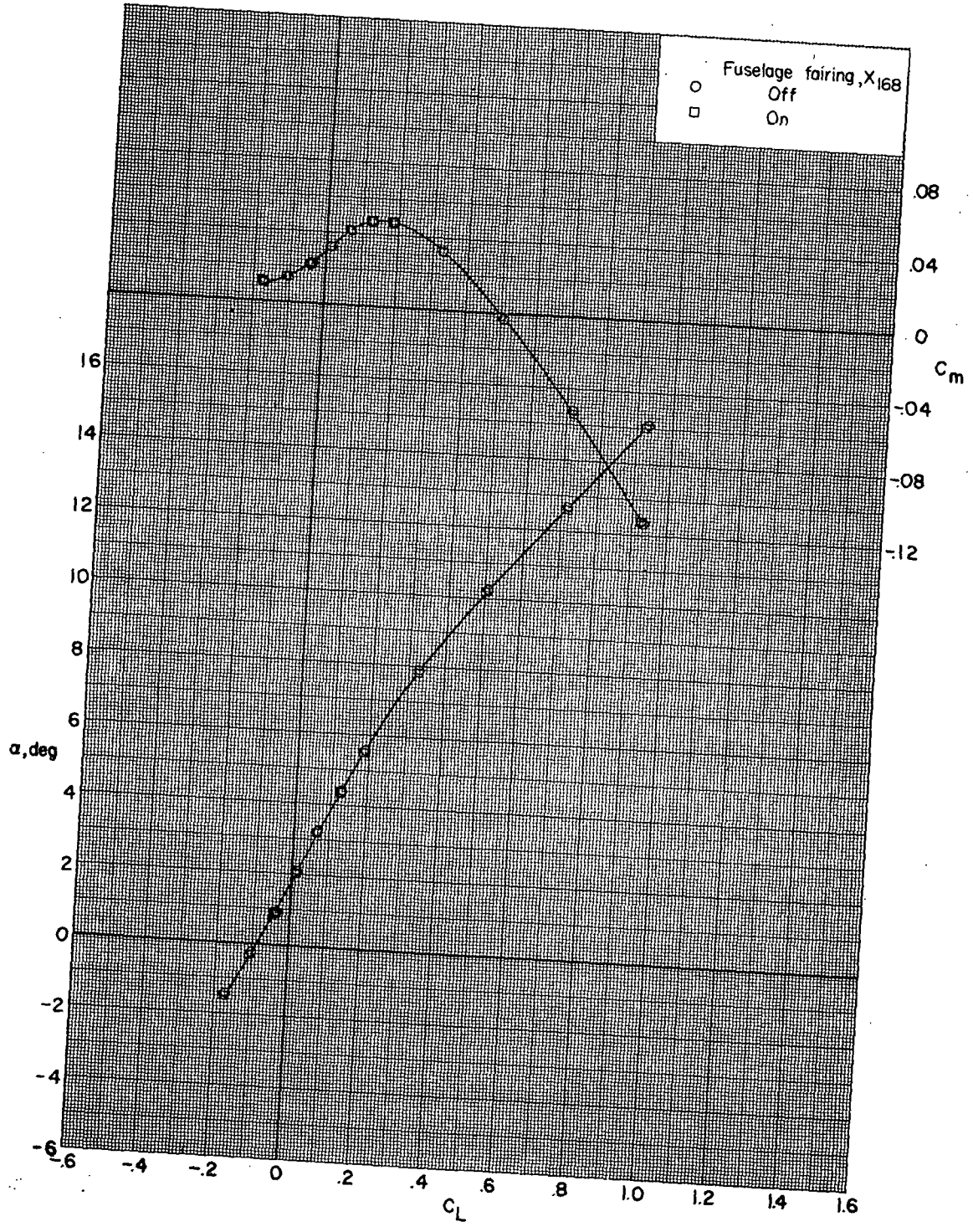

(b) M = 0.90.

Figure 30.- Continued.

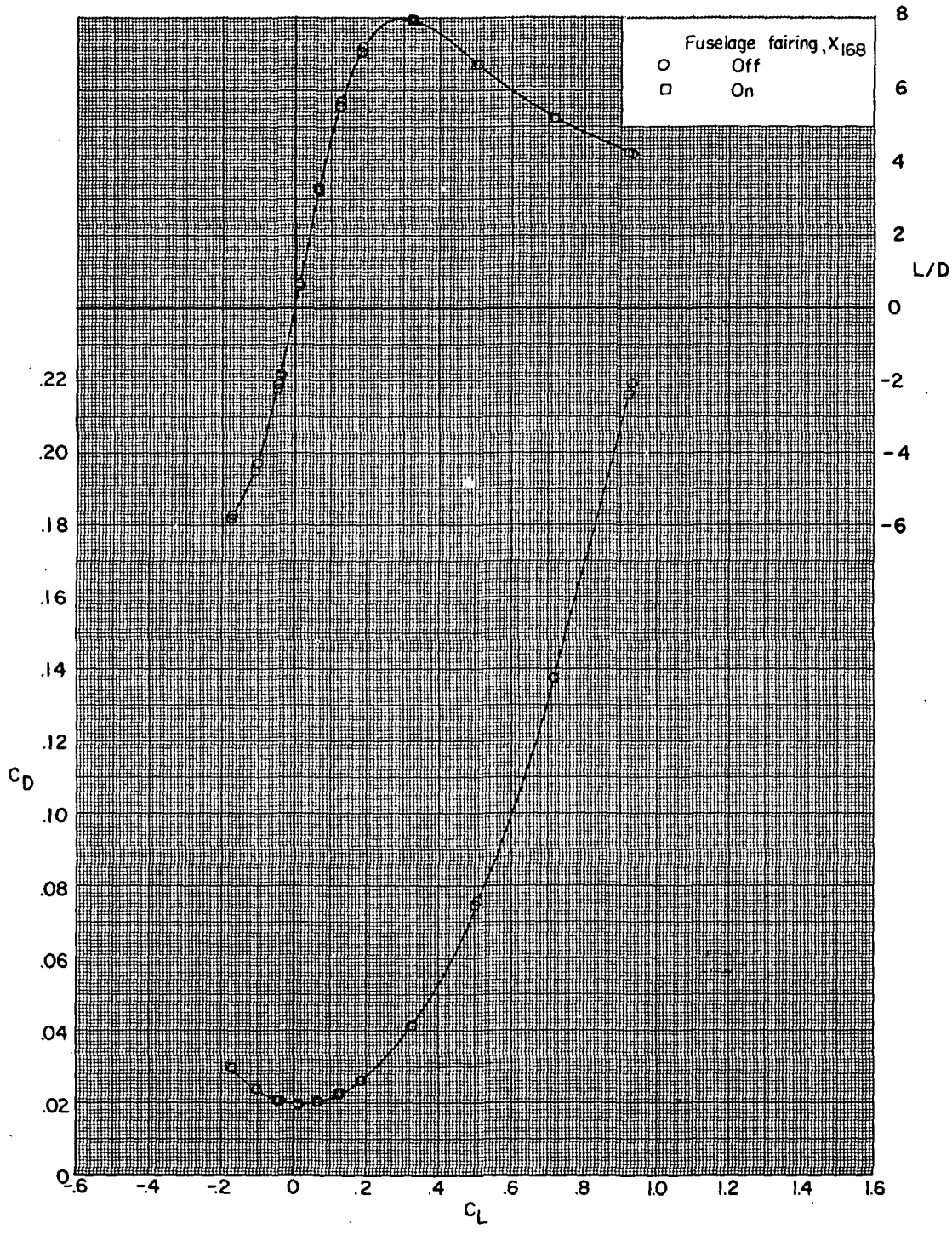

(b) Concluded.

Figure 30.- Continued.

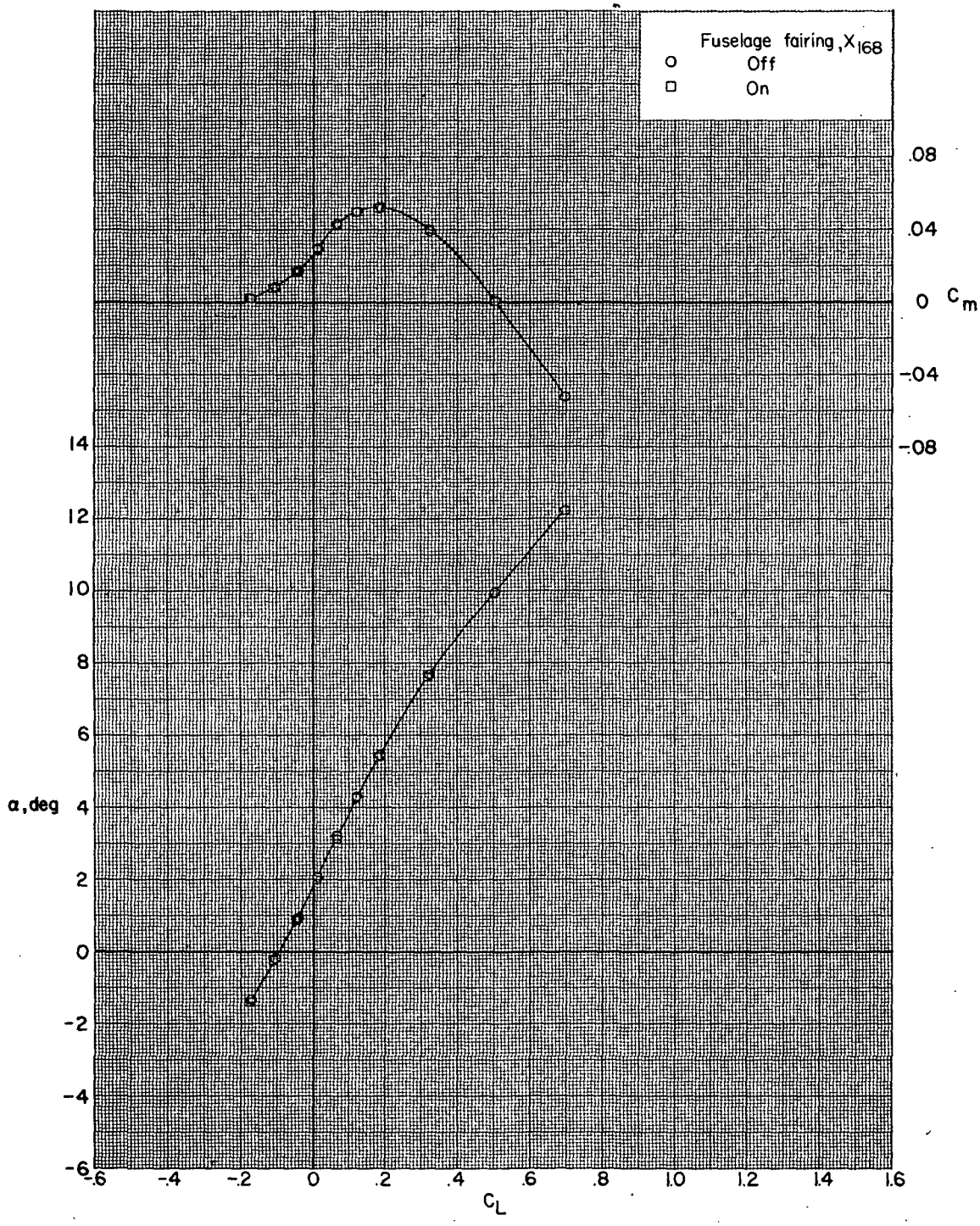

(c) M = 0.95.

Figure 30.- Continued.

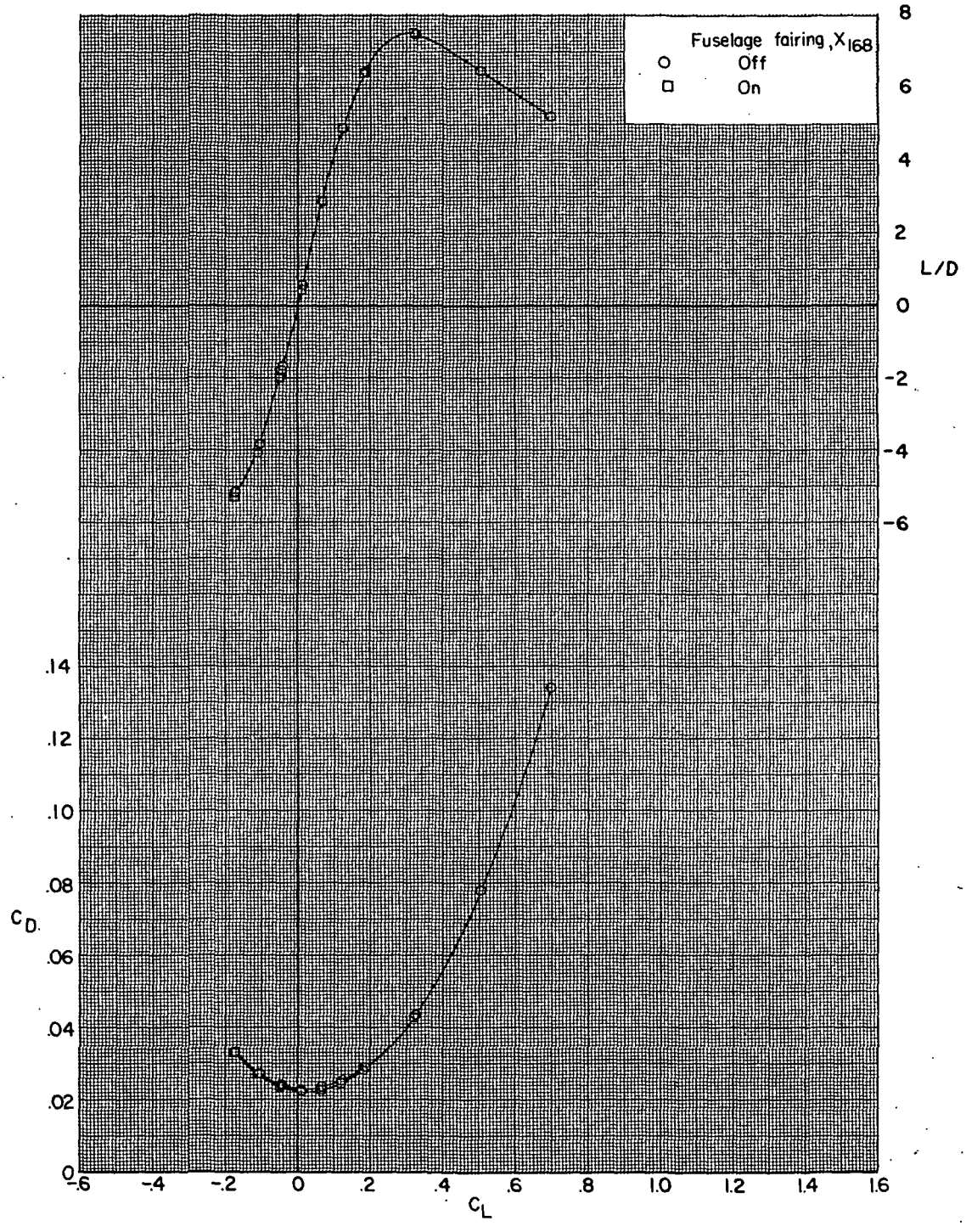

(c) Concluded.

Figure 30.- Concluded.

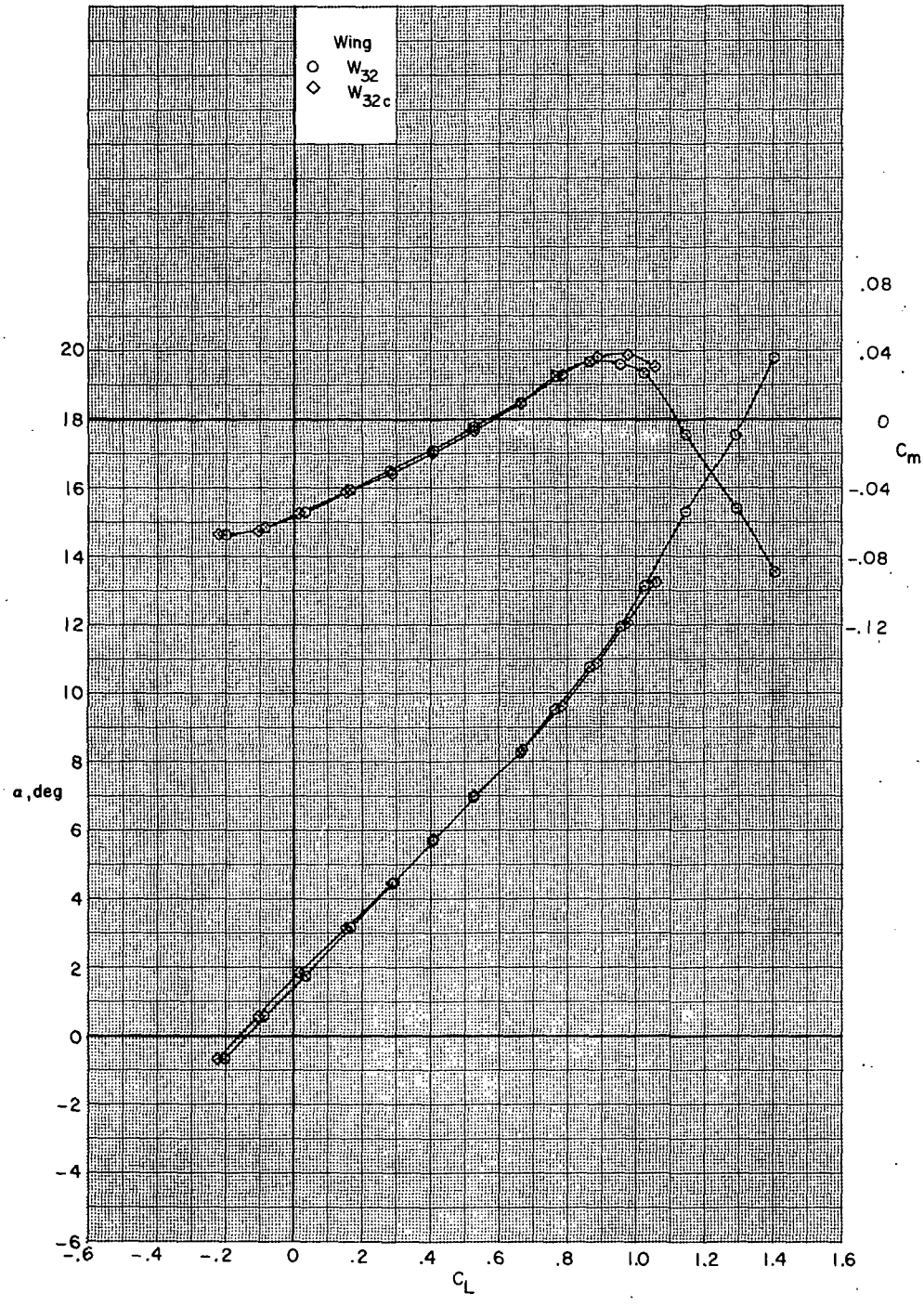

(a) M = 0.70.

Figure 31.- Effect of wing-tip planform shape on aerodynamic characteristics for configurations $B_{80}G_{47}H_{13}I_{71}N^{b}_{32}V_{29}V_{38}W_{x}X_{24}X_{168}$ with wing swept 26.0°.

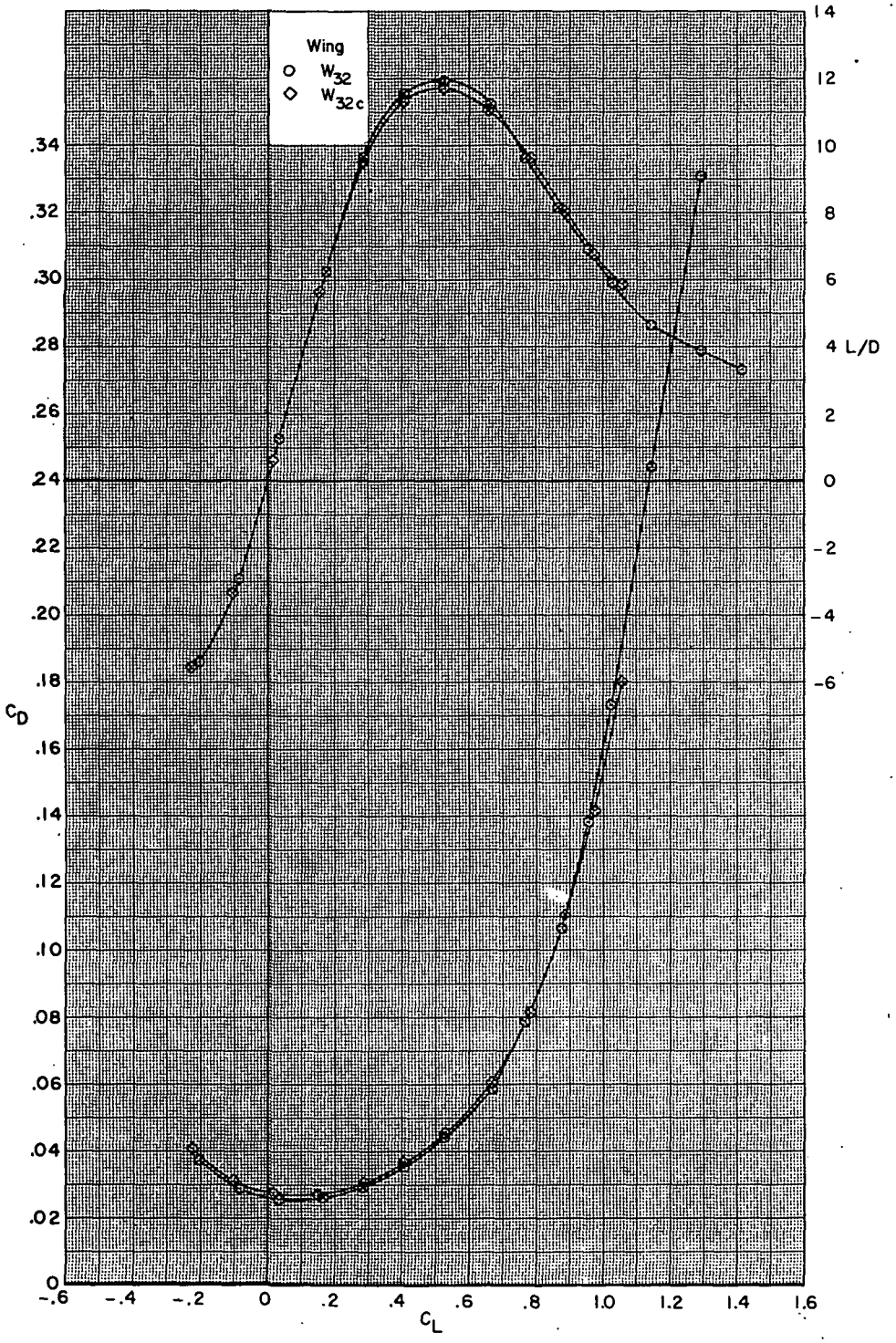

(a) Concluded.

Figure 31.- Continued.

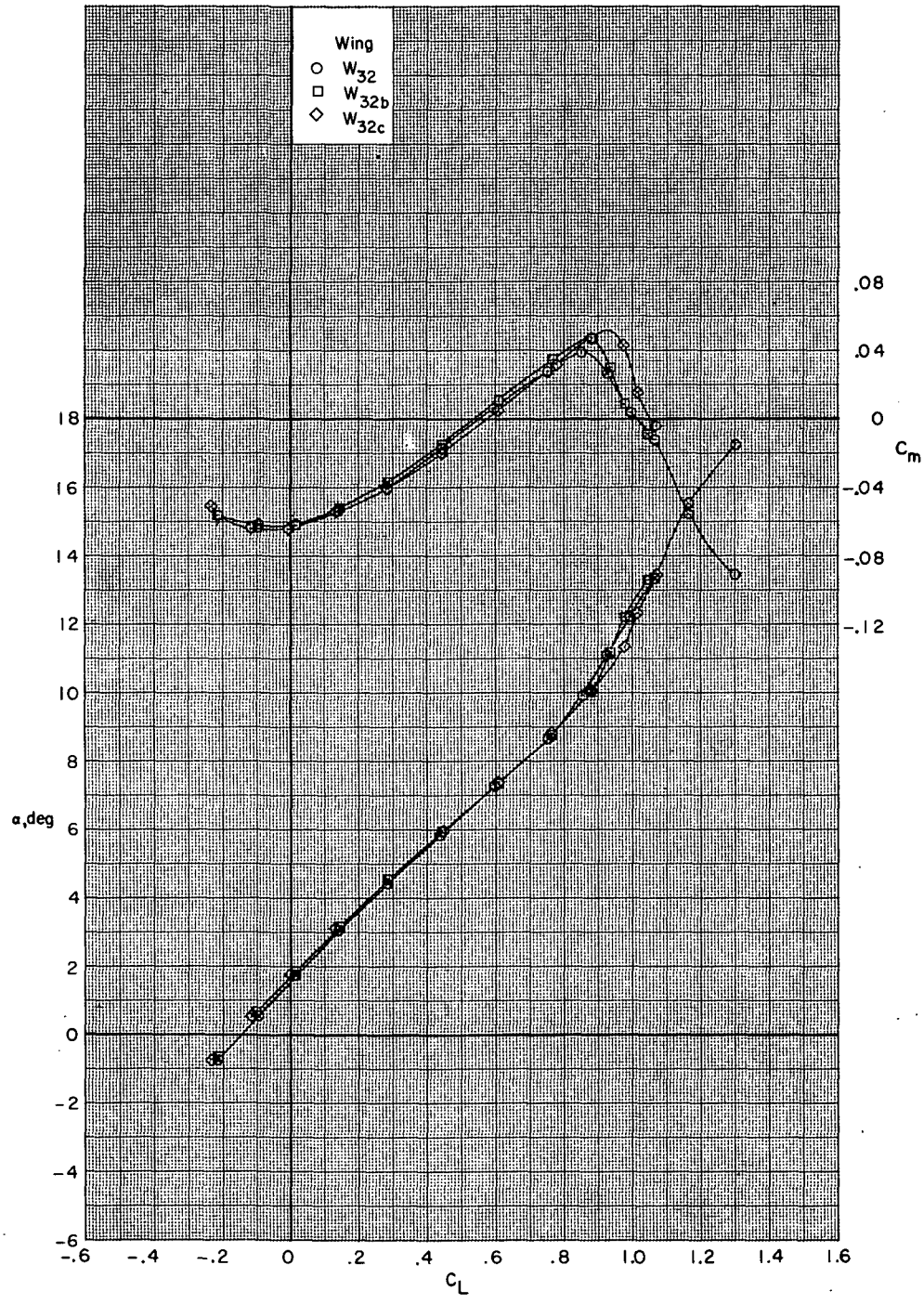

(b) M = 0.80.

Figure 31.- Continued.

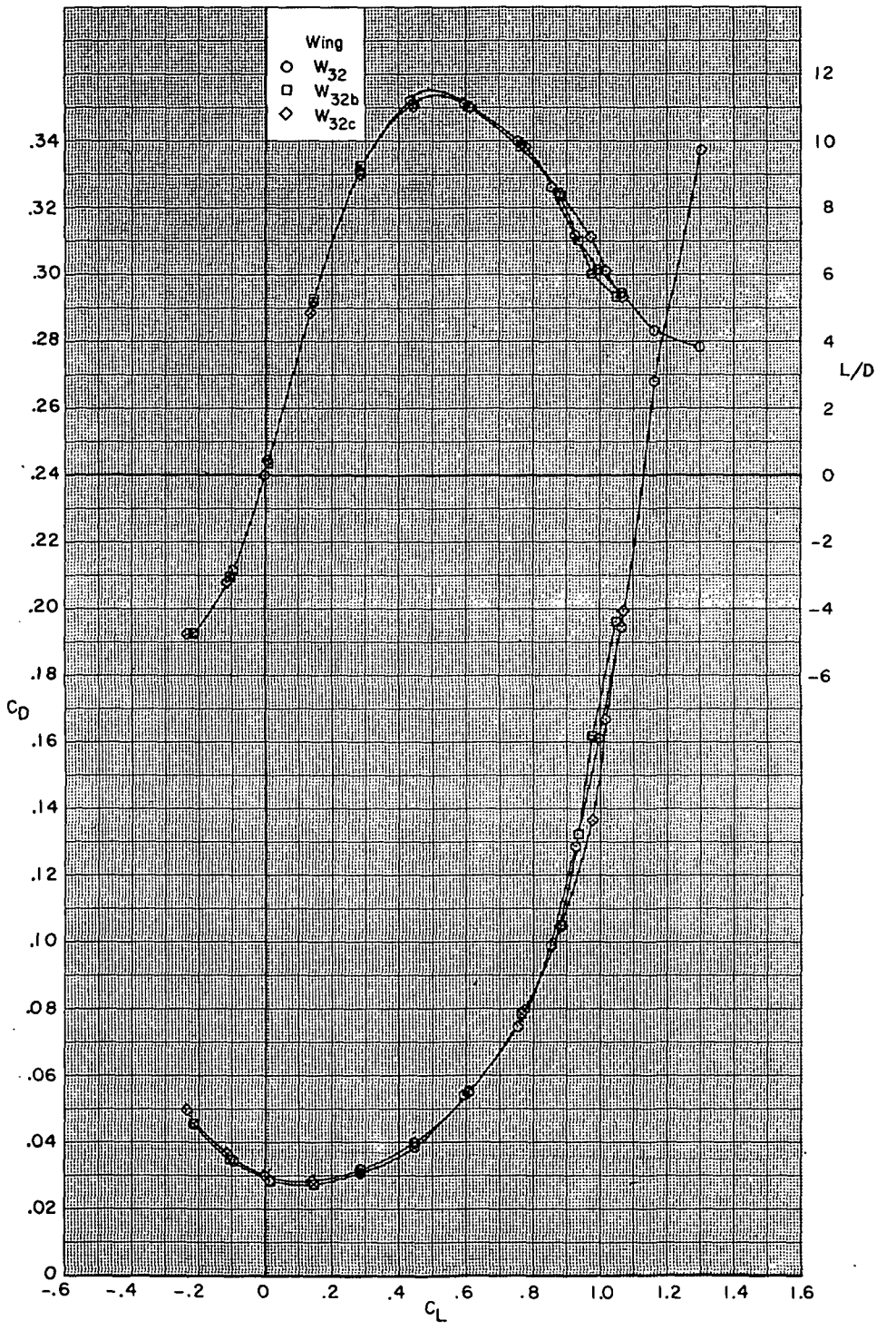

(b) Concluded.

Figure 31.- Continued.

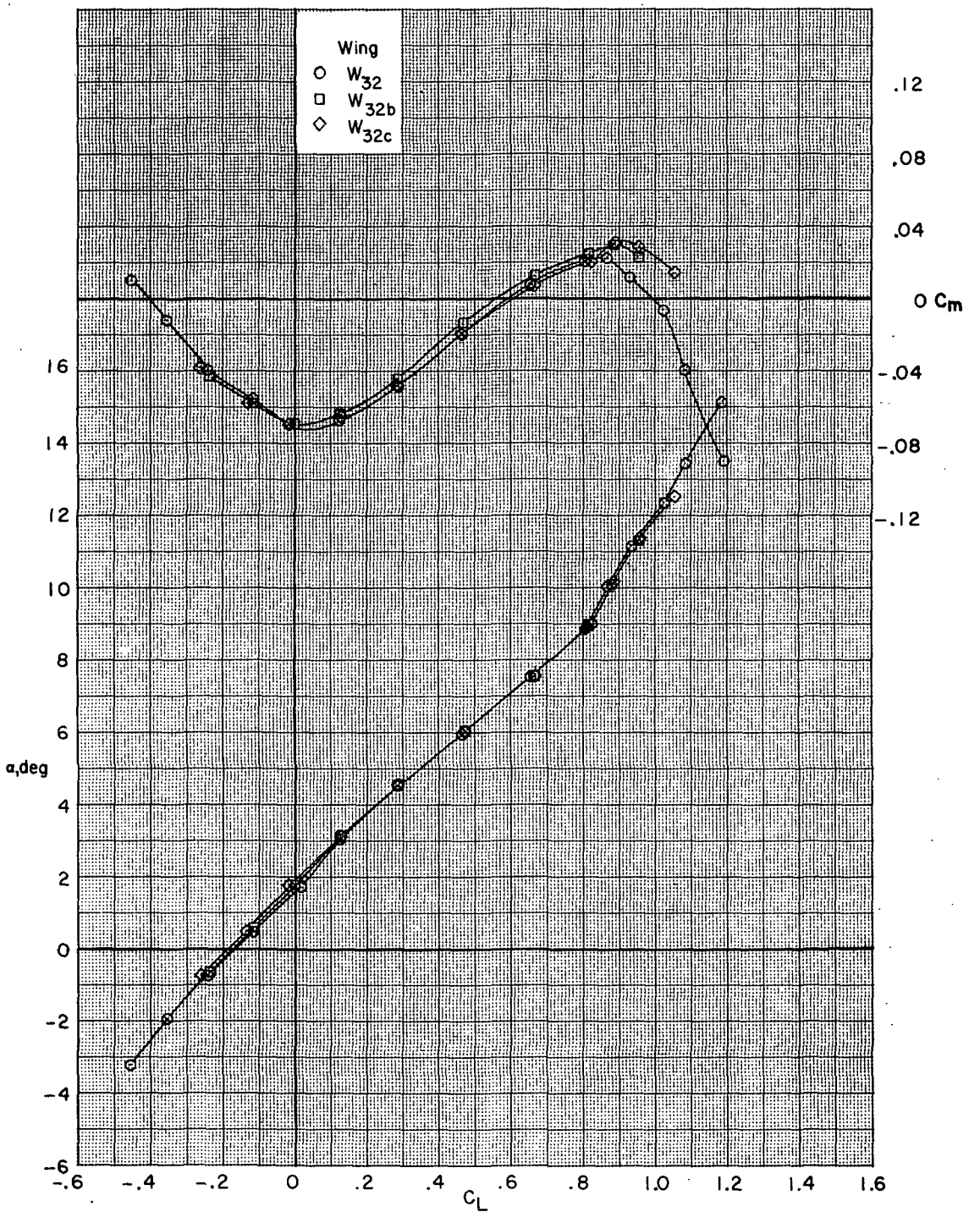

(c) M = 0.85.

Figure 31.- Continued.

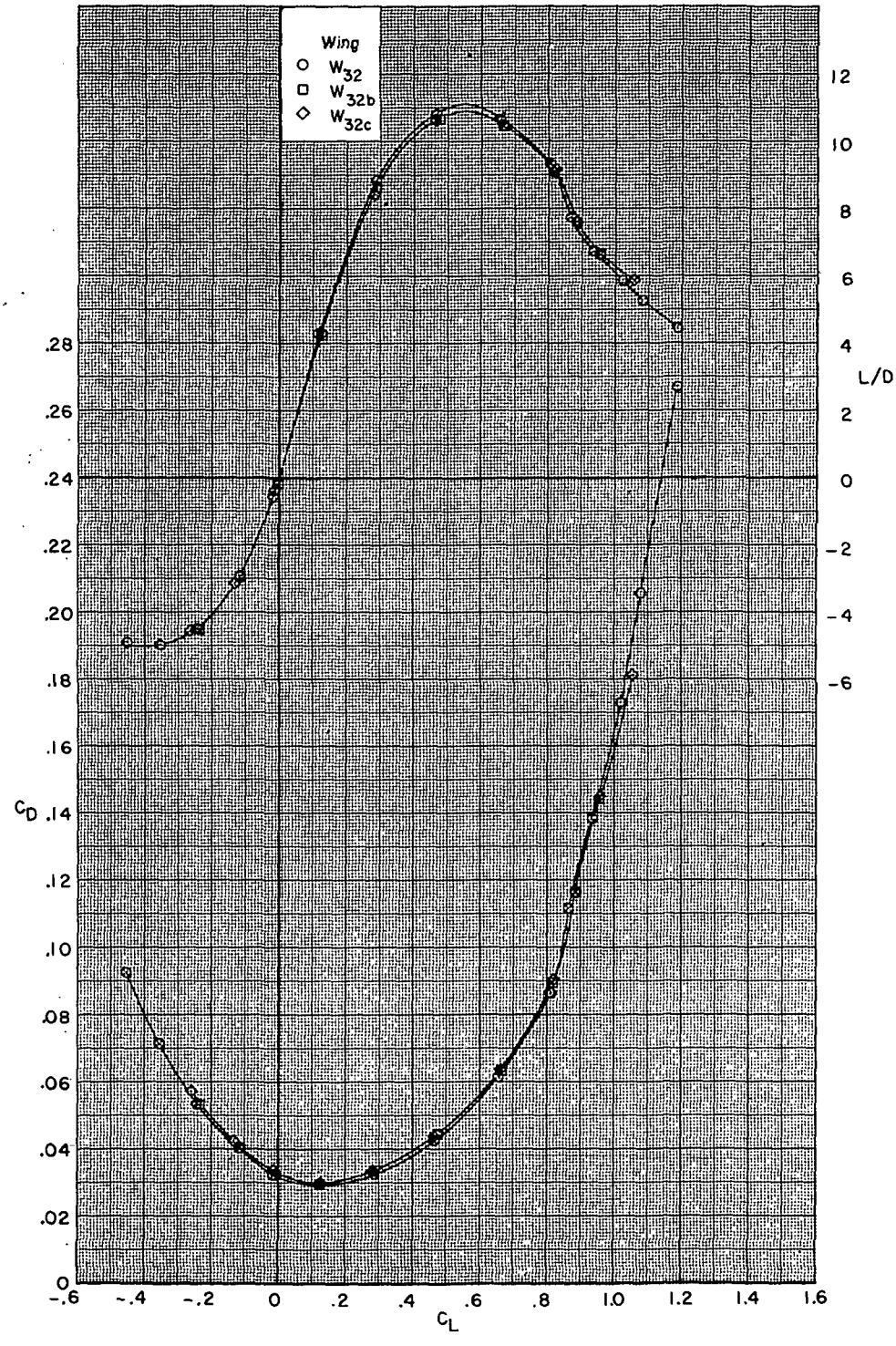

(c) Concluded.

Figure 31.- Continued.

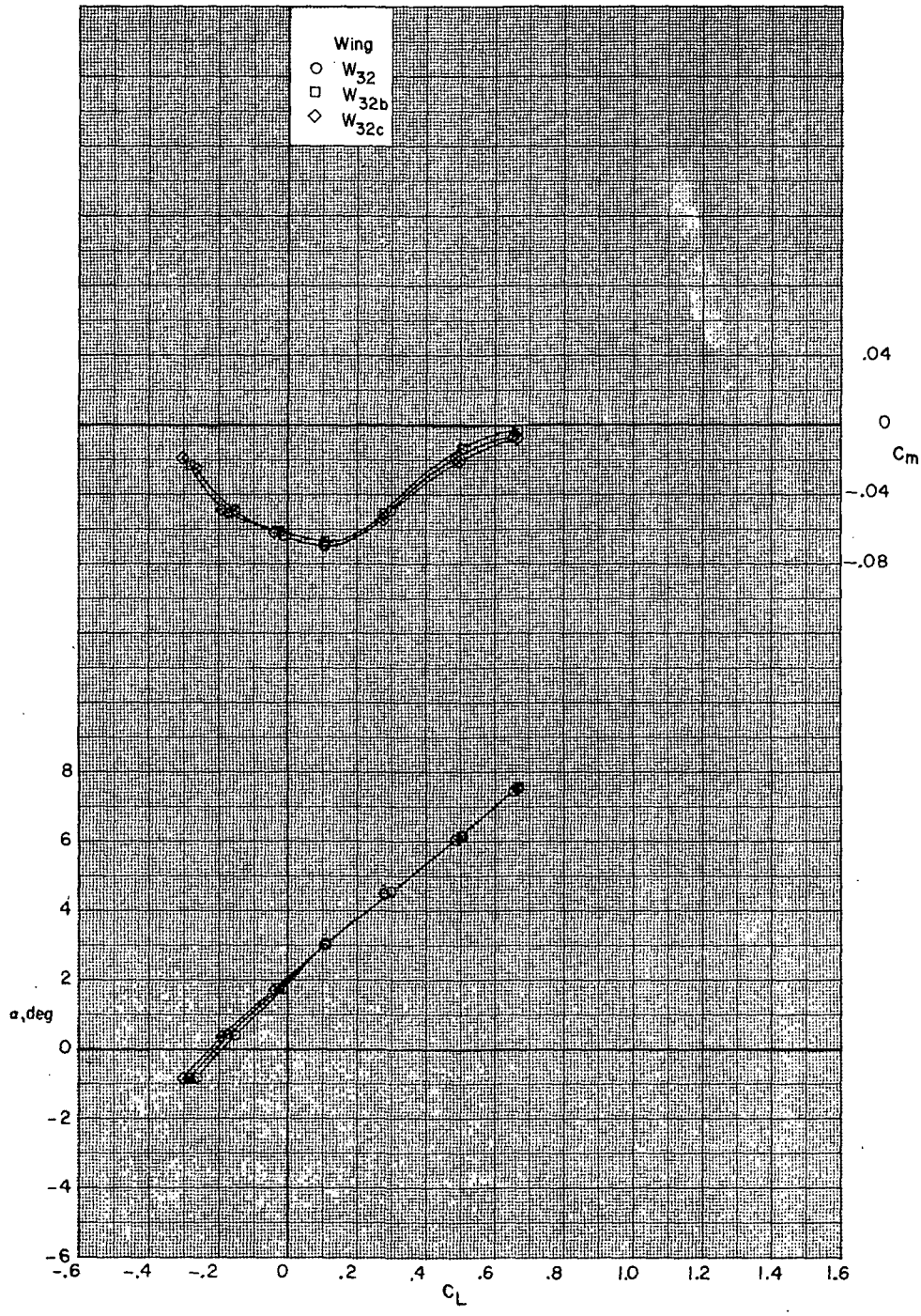

(d) M = 0.875.

Figure 31.- Continued.

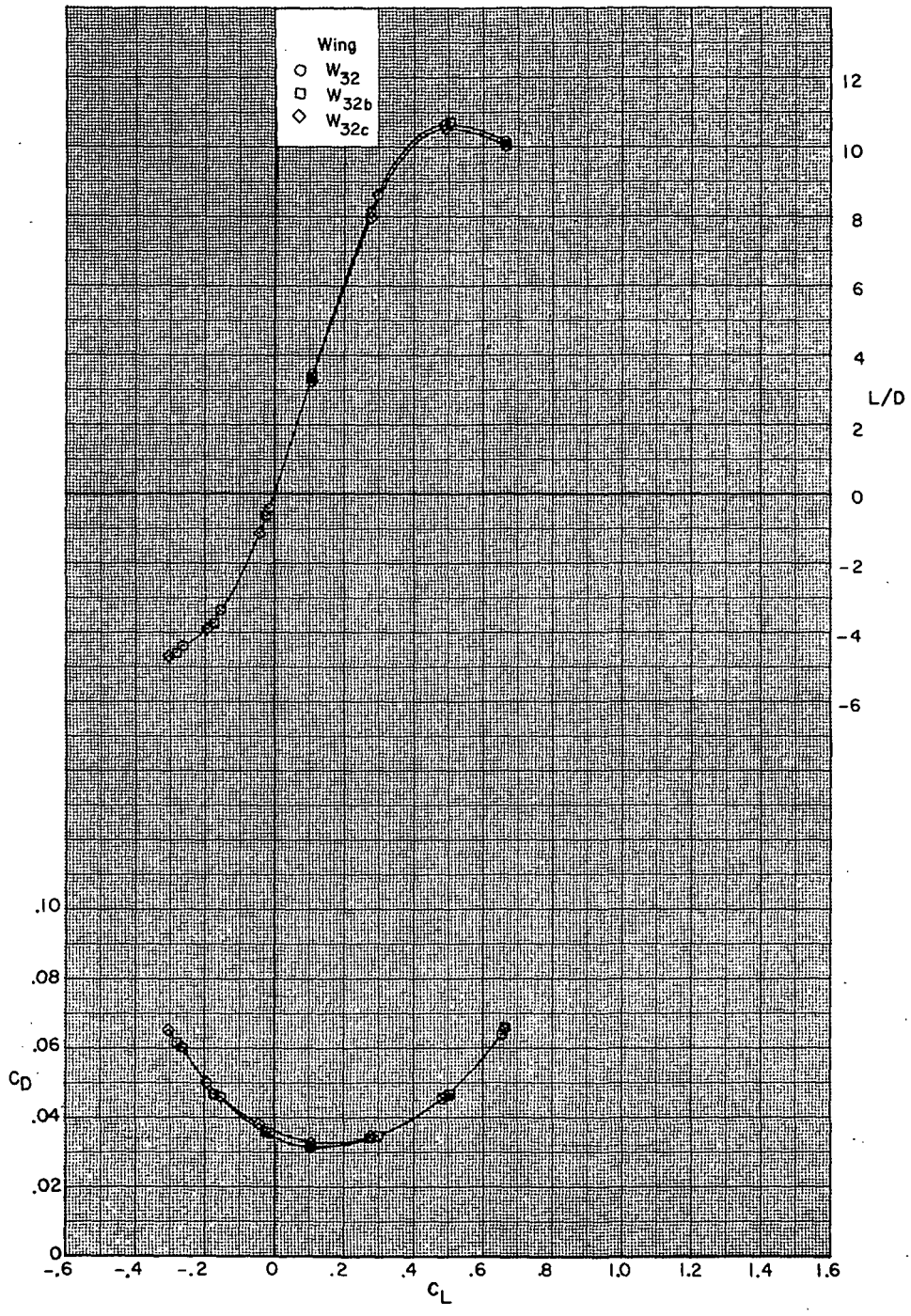

(d) Concluded.

Figure 31.- Continued.

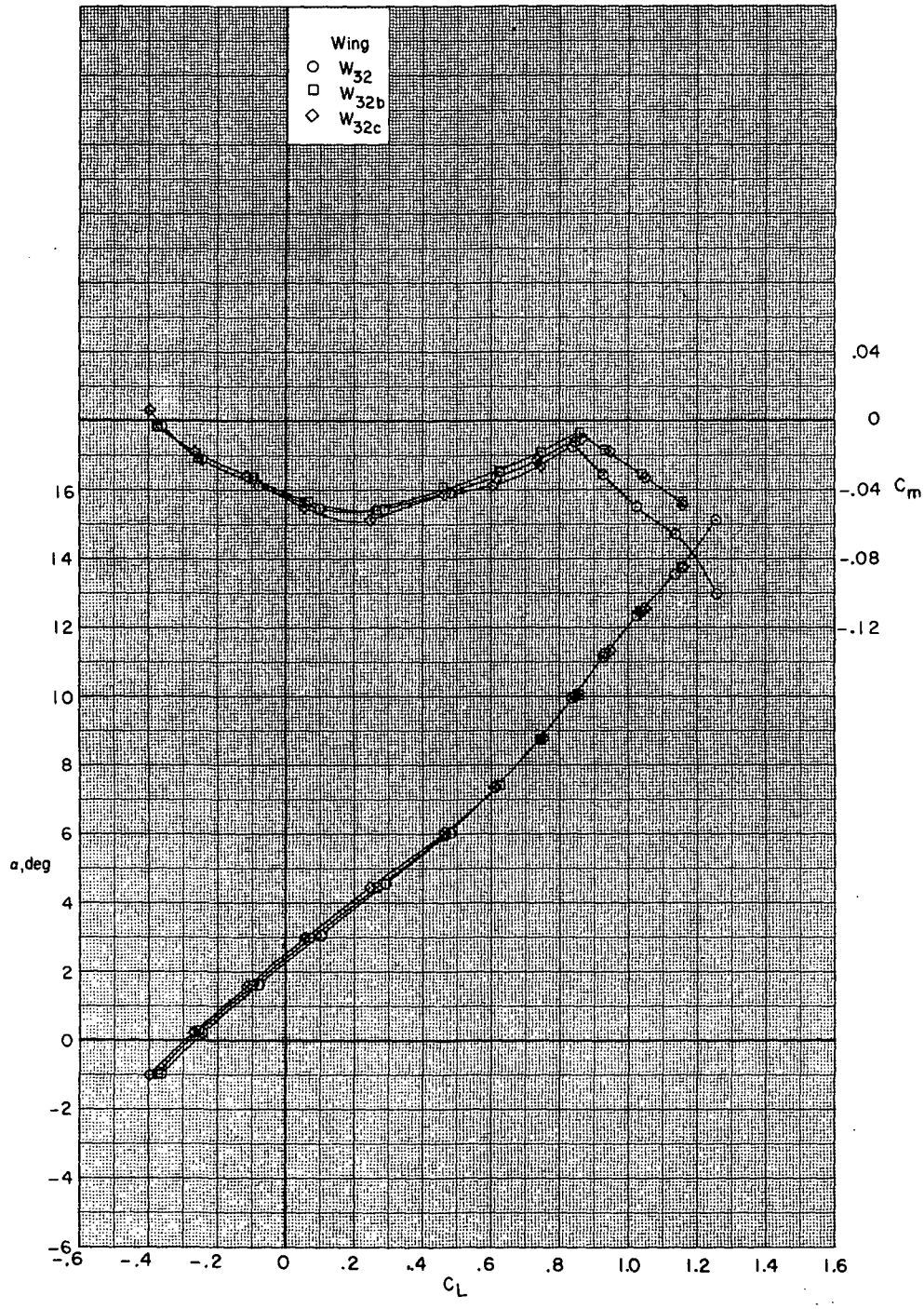

(e) M = 0.90.

Figure 31.- Continued.

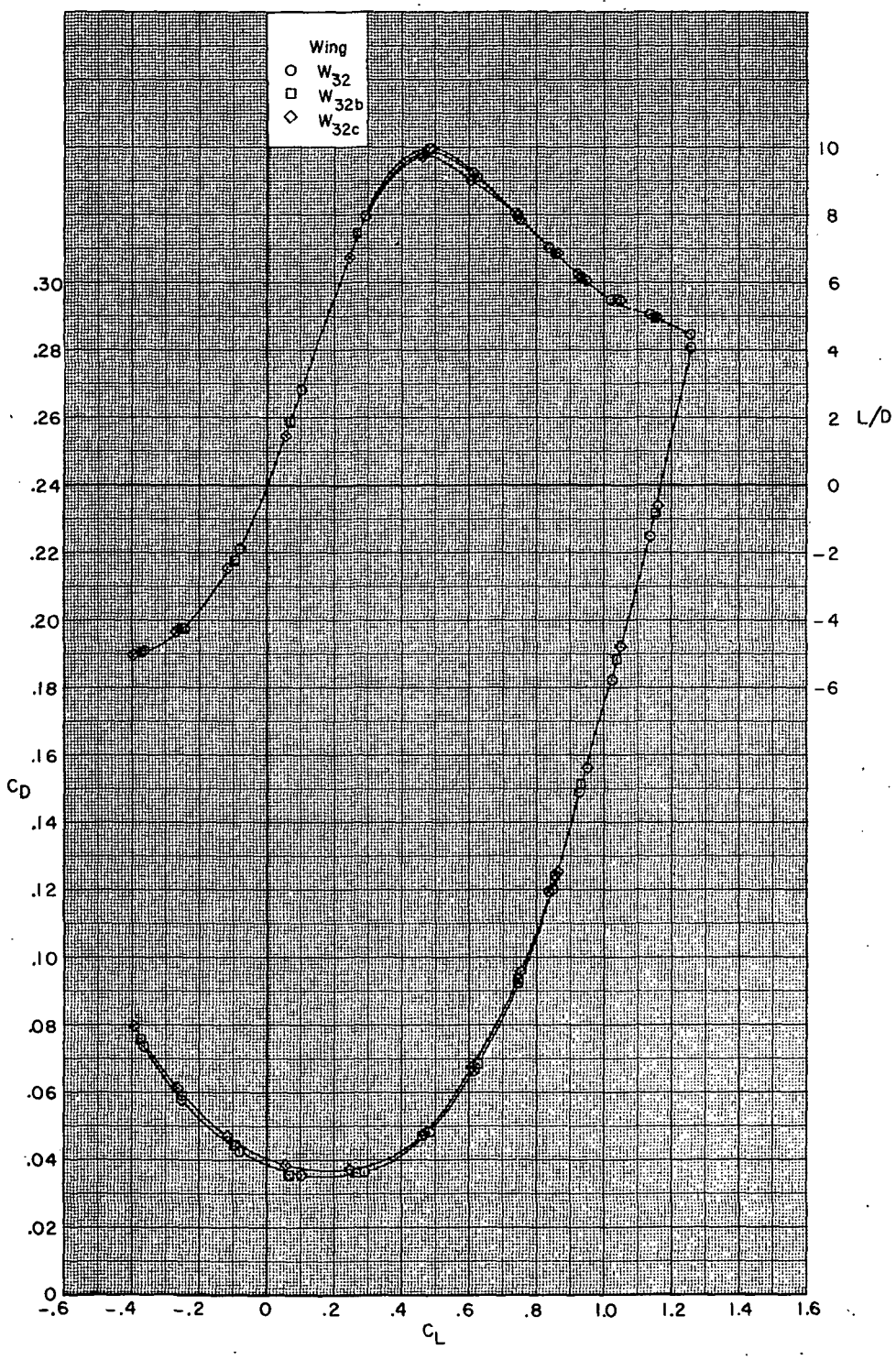

(e) Concluded.

Figure 31.- Concluded.

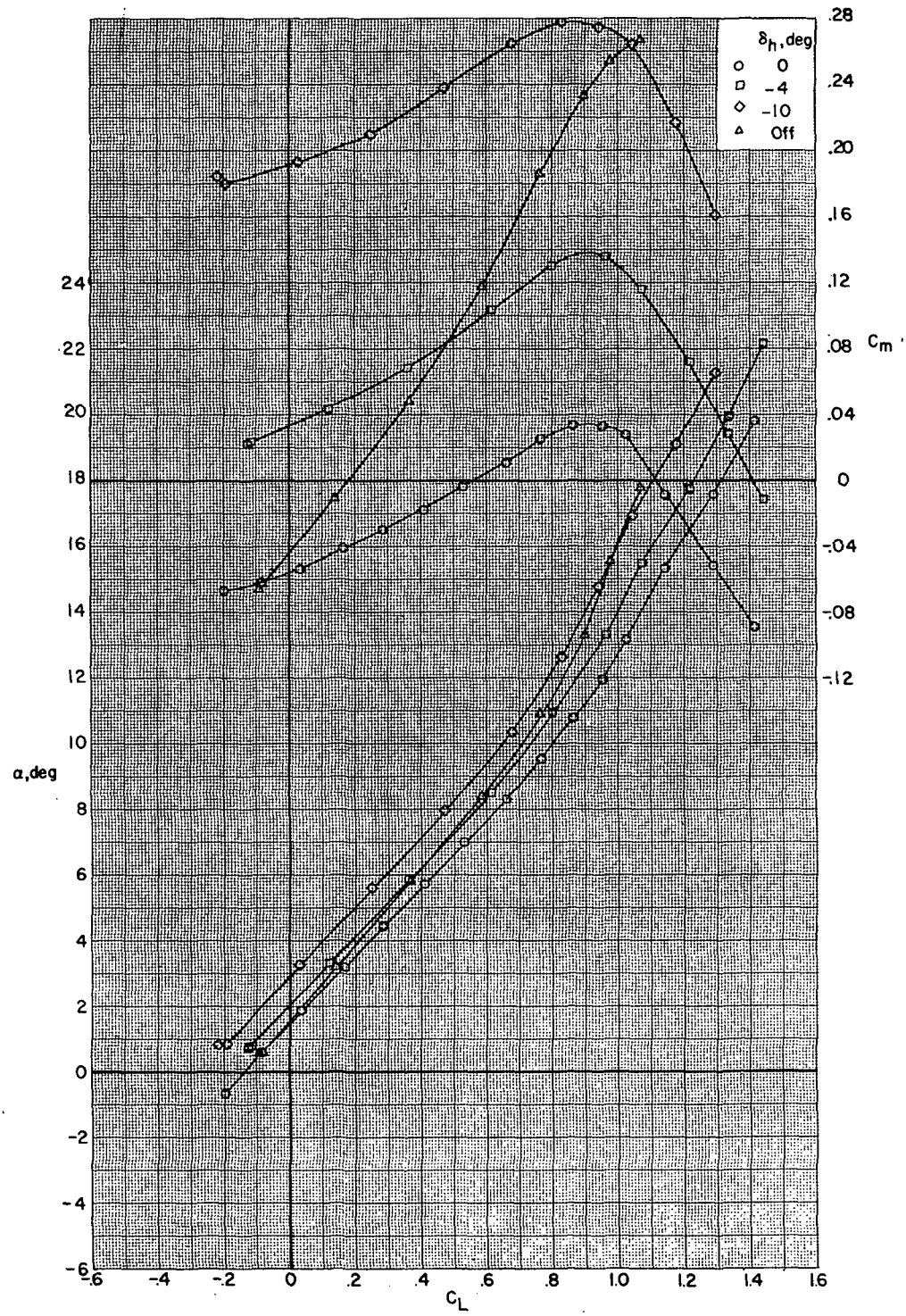

(a) M = 0.70.

Figure 32.- Effect of horizontal tail on aerodynamic characteristics of configuration $B_{80}G_{47}H_{13}I_{71}N^{b}_{32}V_{29}V_{38}W_{32}X_{24}X_{168}$ with wing swept 26.0°.

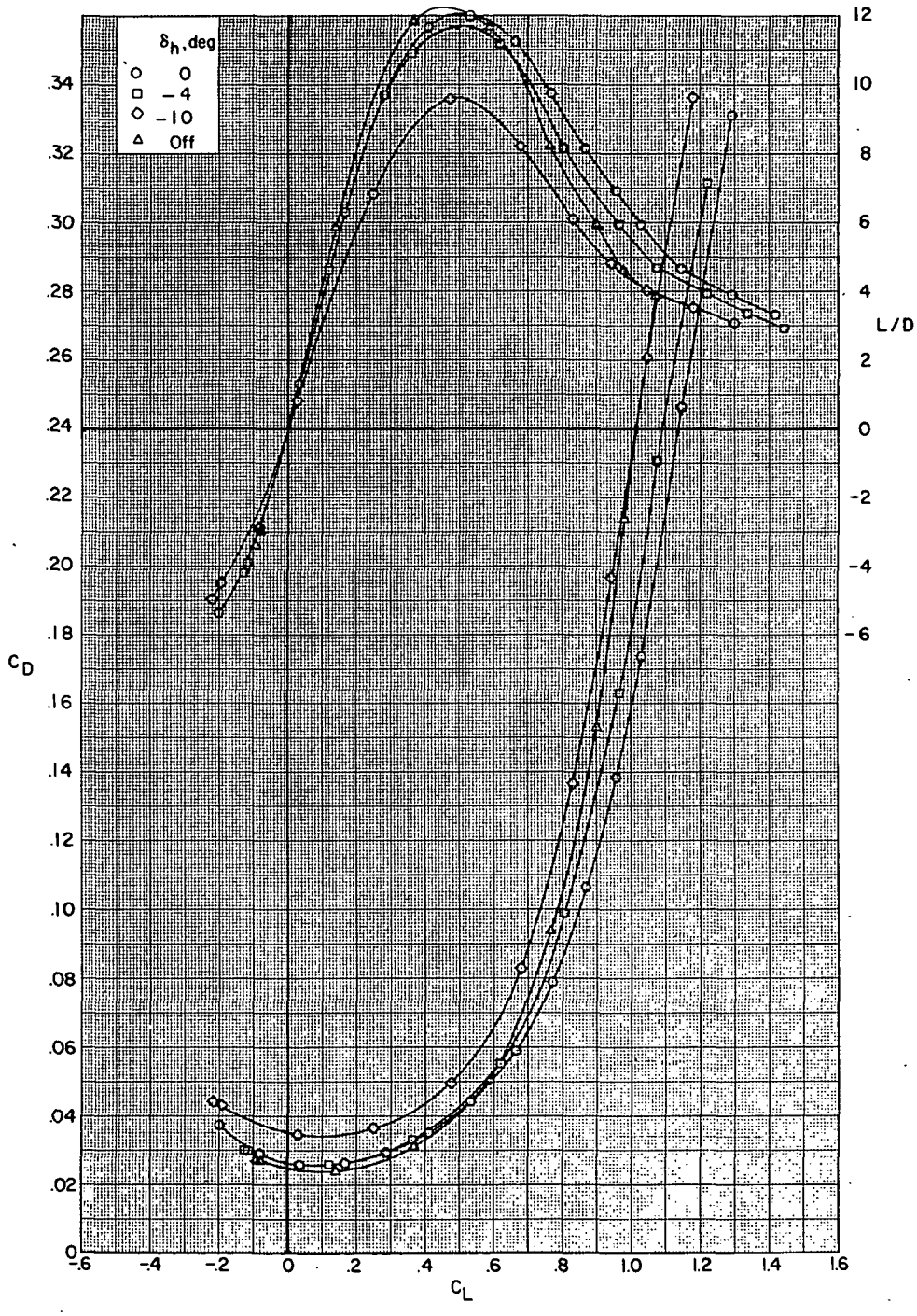

(a) Concluded.

Figure 32.- Continued.

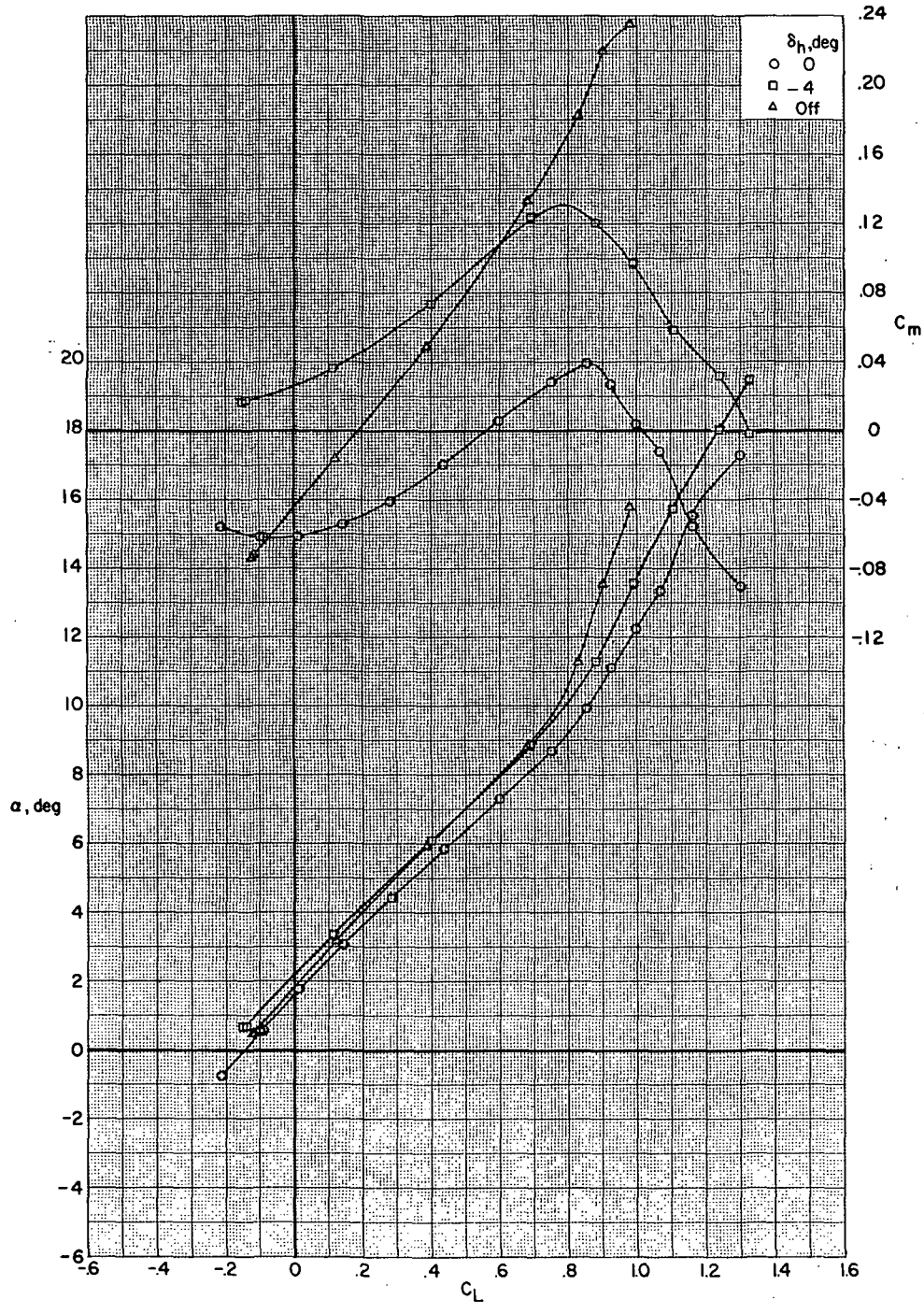

(b) M = 0.80.

Figure 32.- Continued.

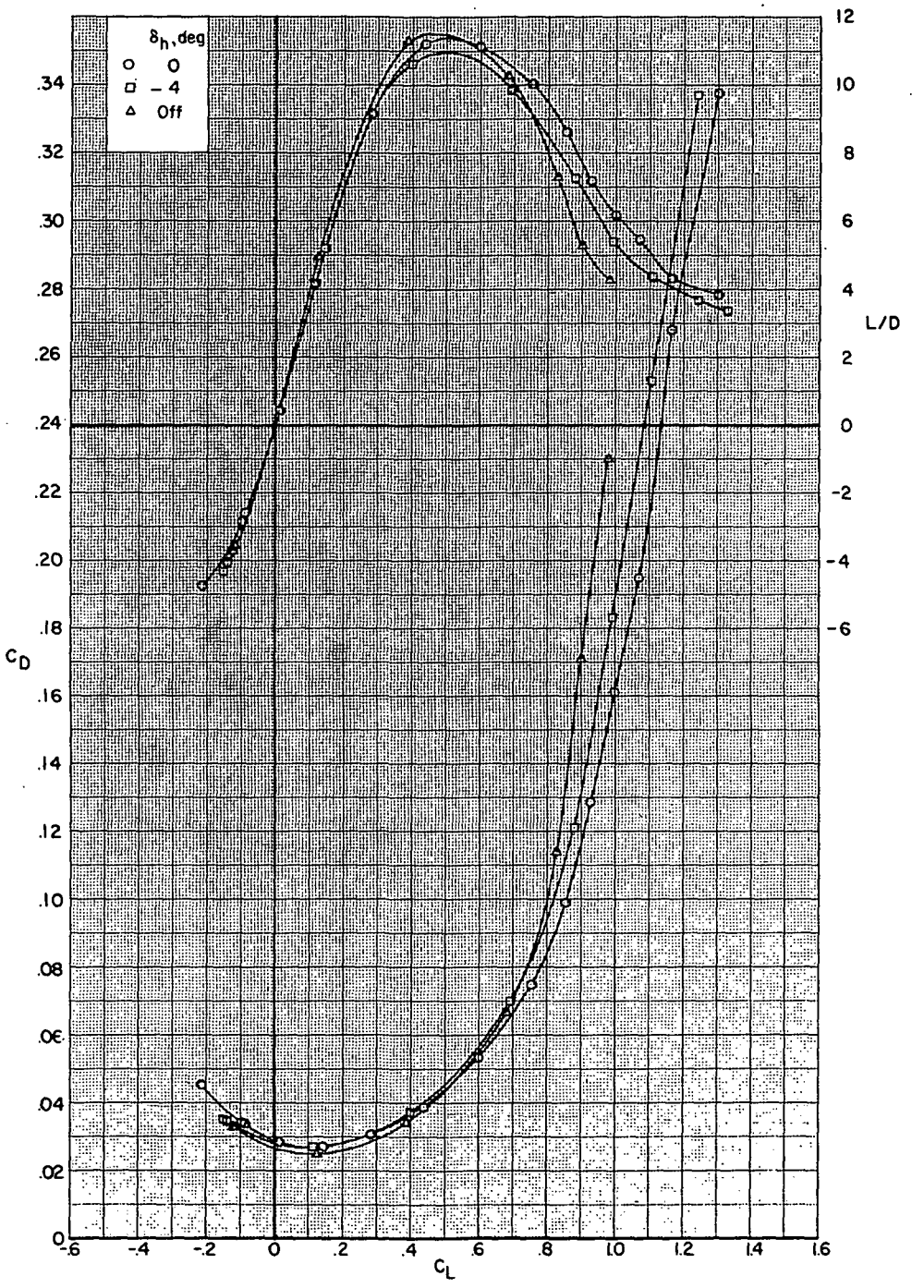

(b) Concluded.

Figure 32.- Continued.

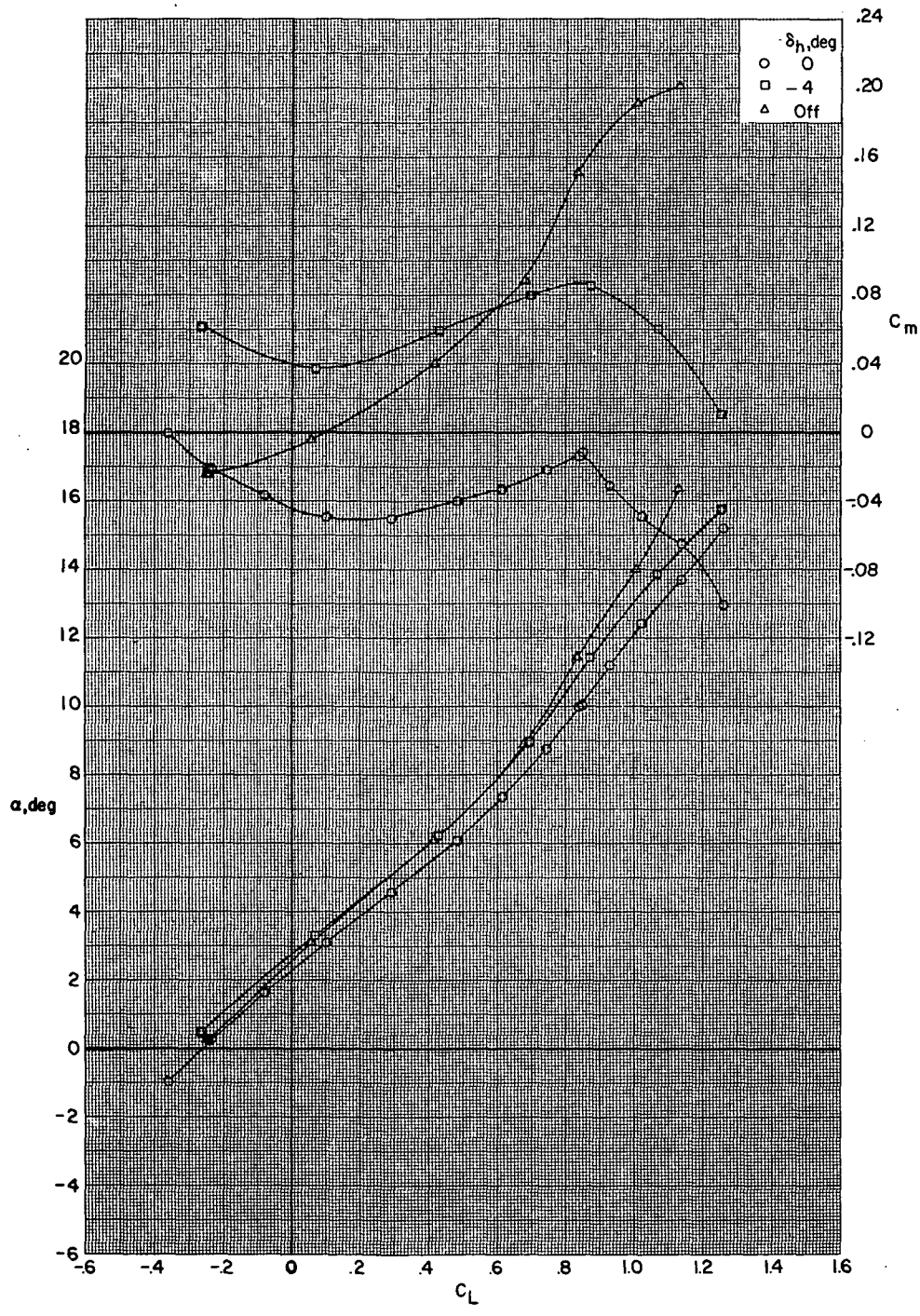

(c) M = 0.90.

Figure 32.- Continued.

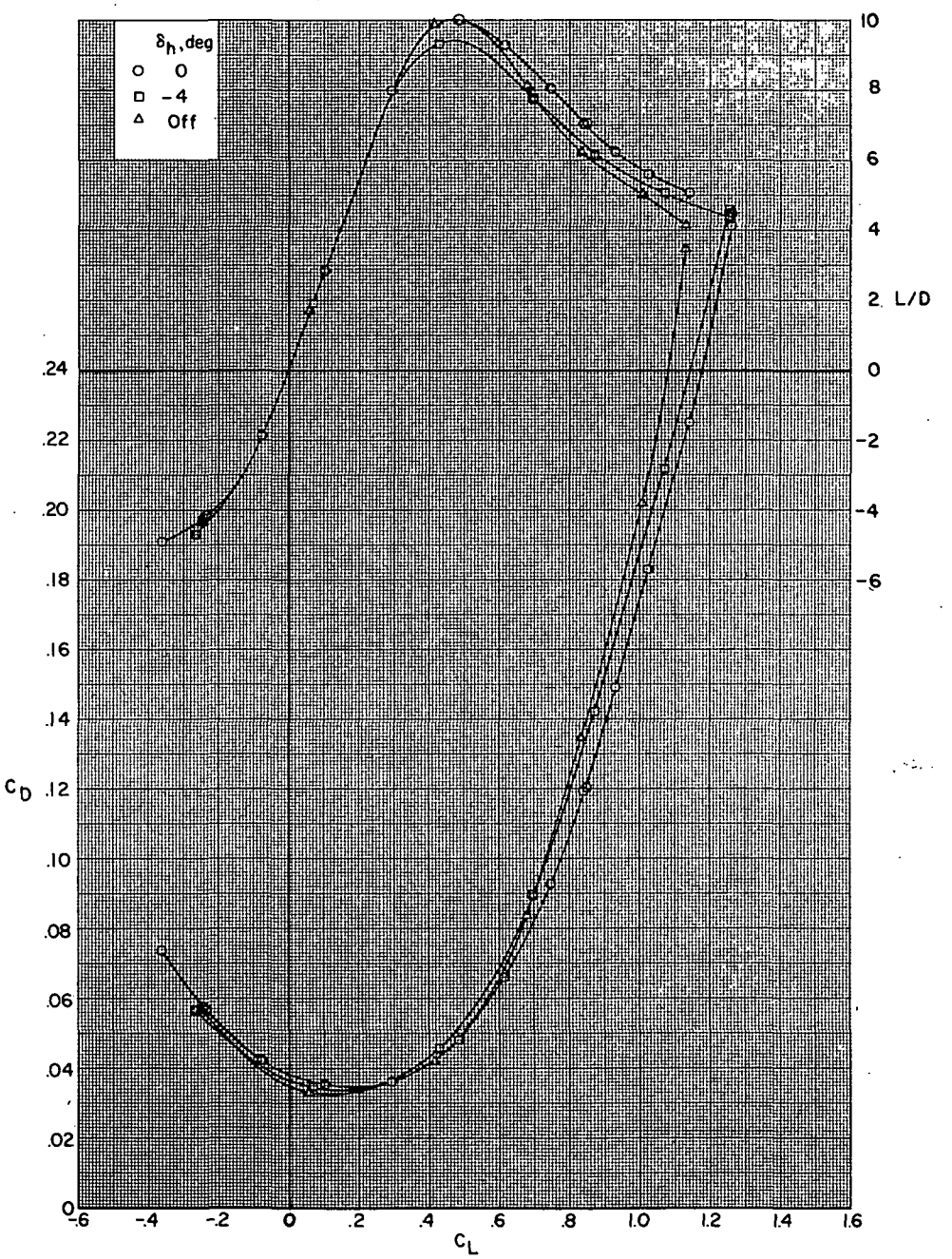

(c) Concluded.

Figure 32.- Concluded.

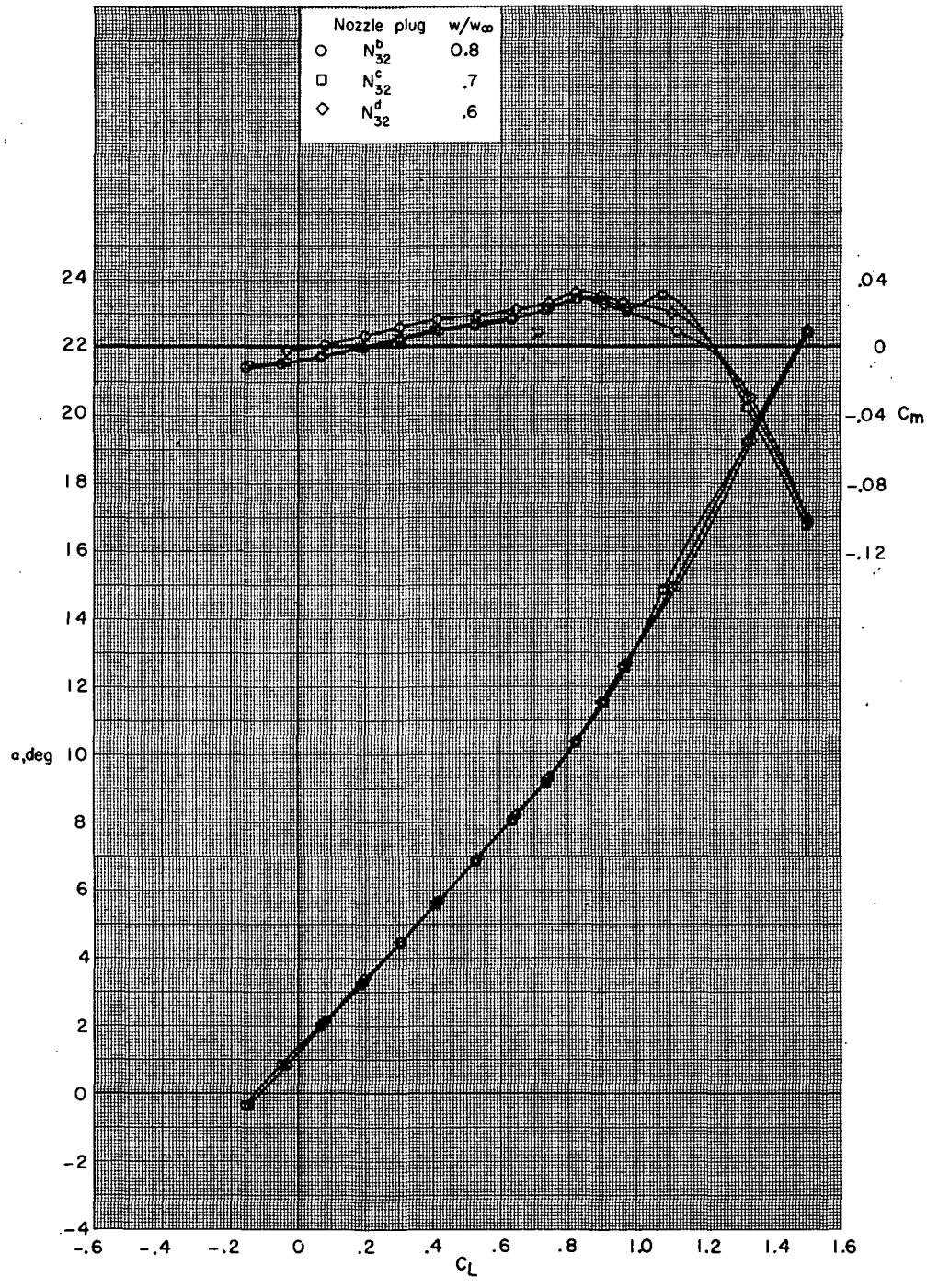

(a) M = 0.60.

Figure 33.- Effect of internal mass-flow ratio on aerodynamic characteristics for configurations $B_{80}G_{49}H_{13}I_{71}N^{X}_{32}V_{29}V_{38}W_{34}X_{24}$ with wing swept 26.0°.

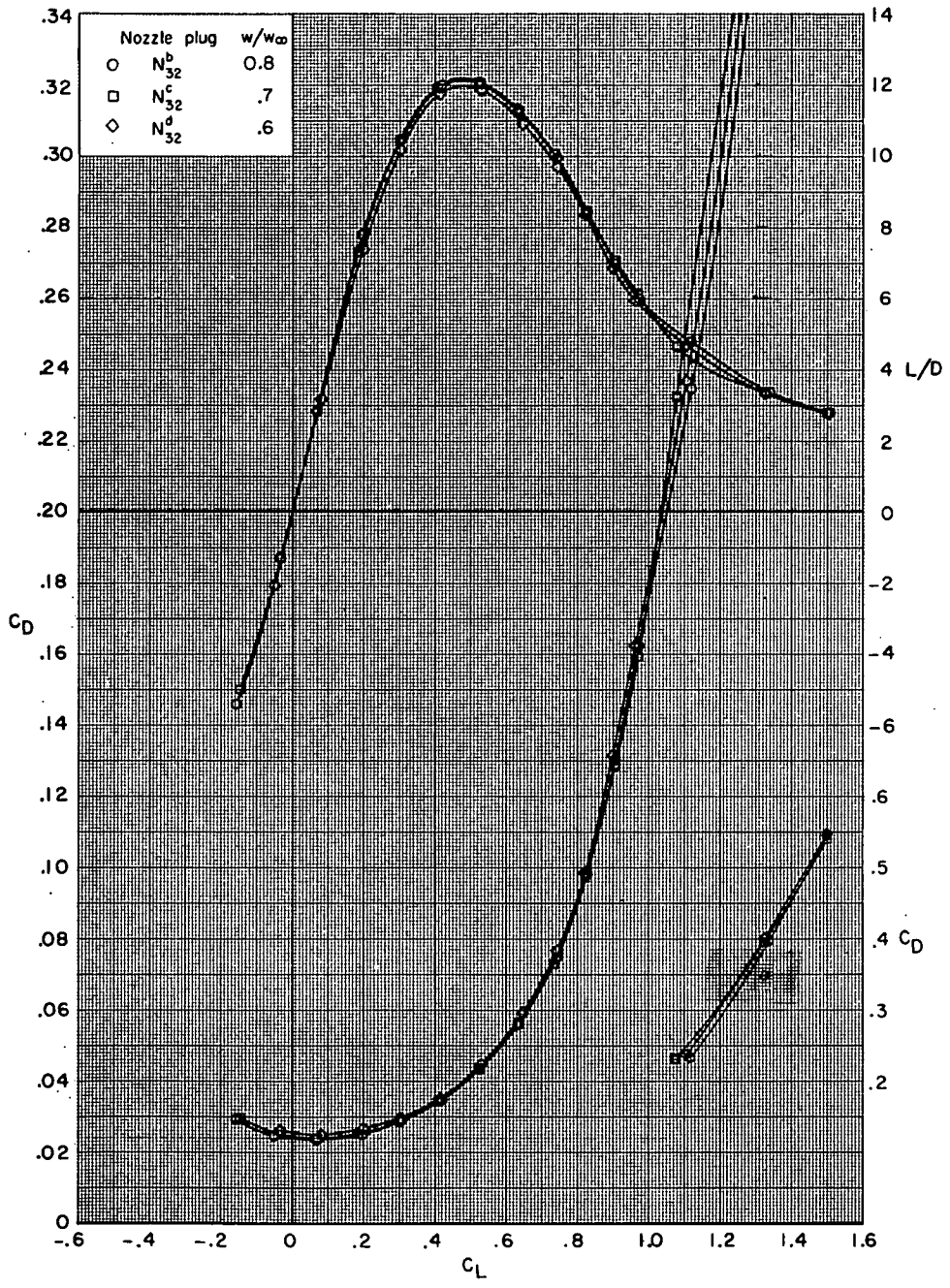

(a) Concluded.

Figure 33.- Continued.

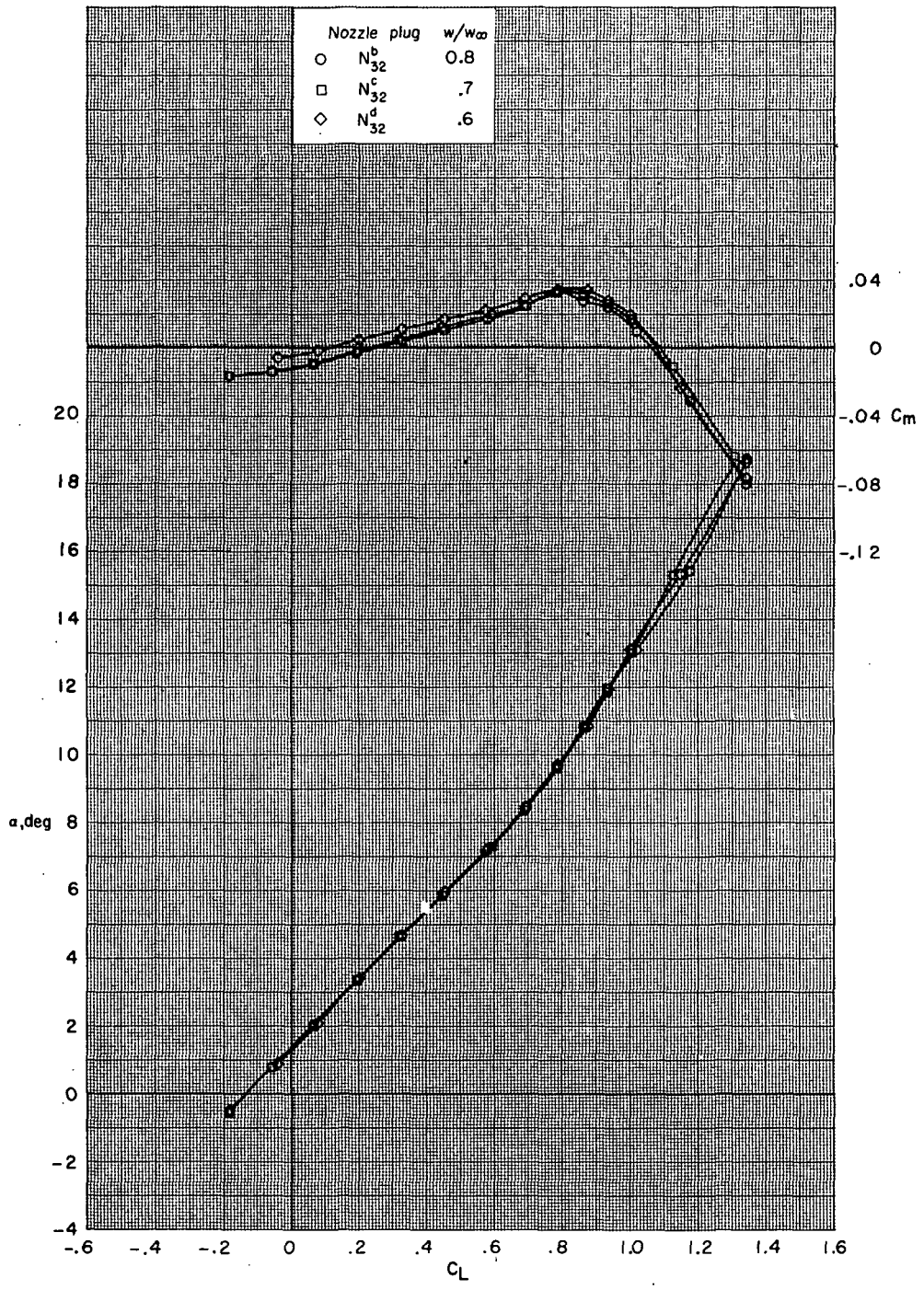

(b) M = 0.70.

Figure 33.- Continued.

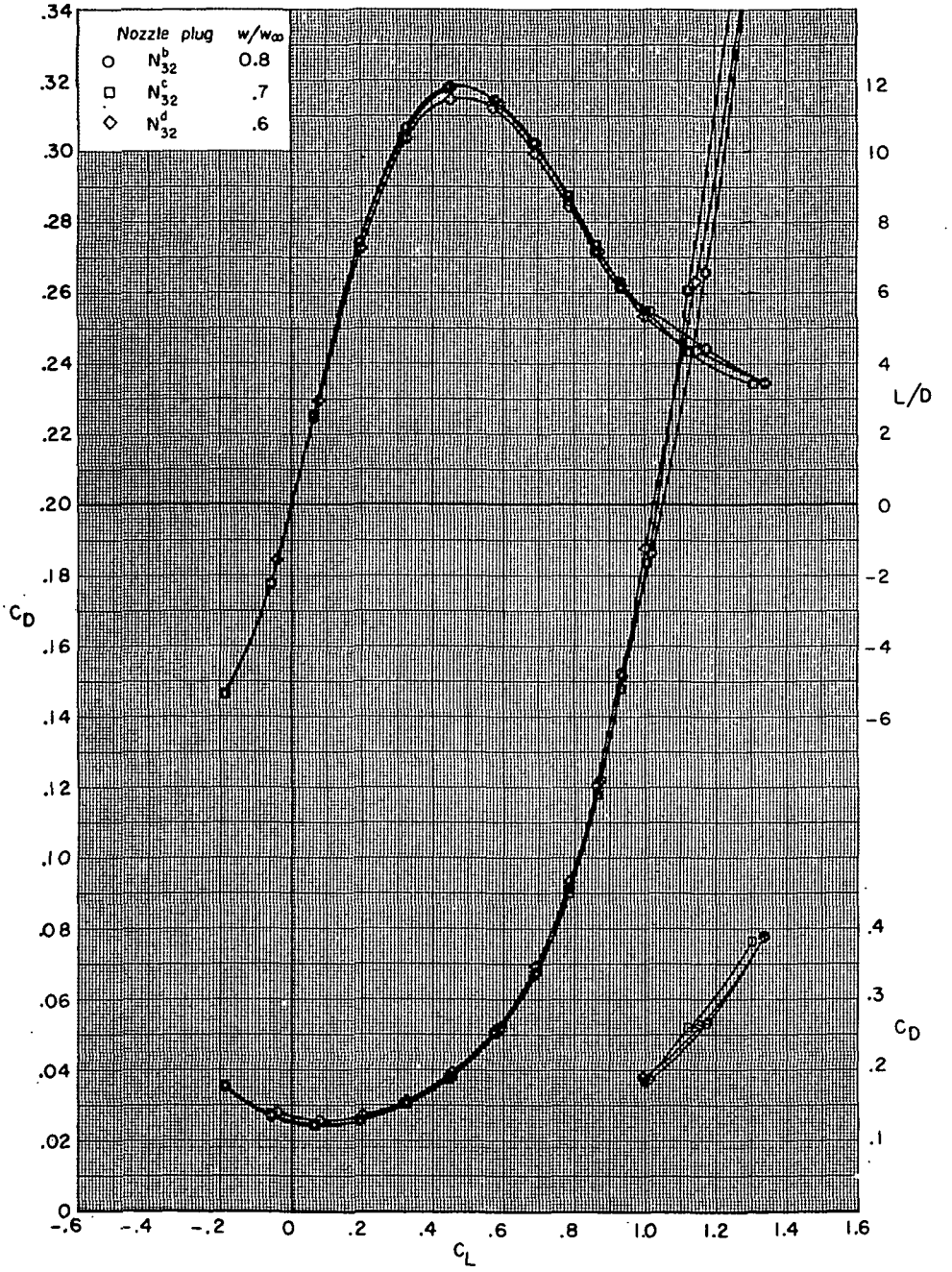

(b) Concluded.

Figure 33.- Continued.

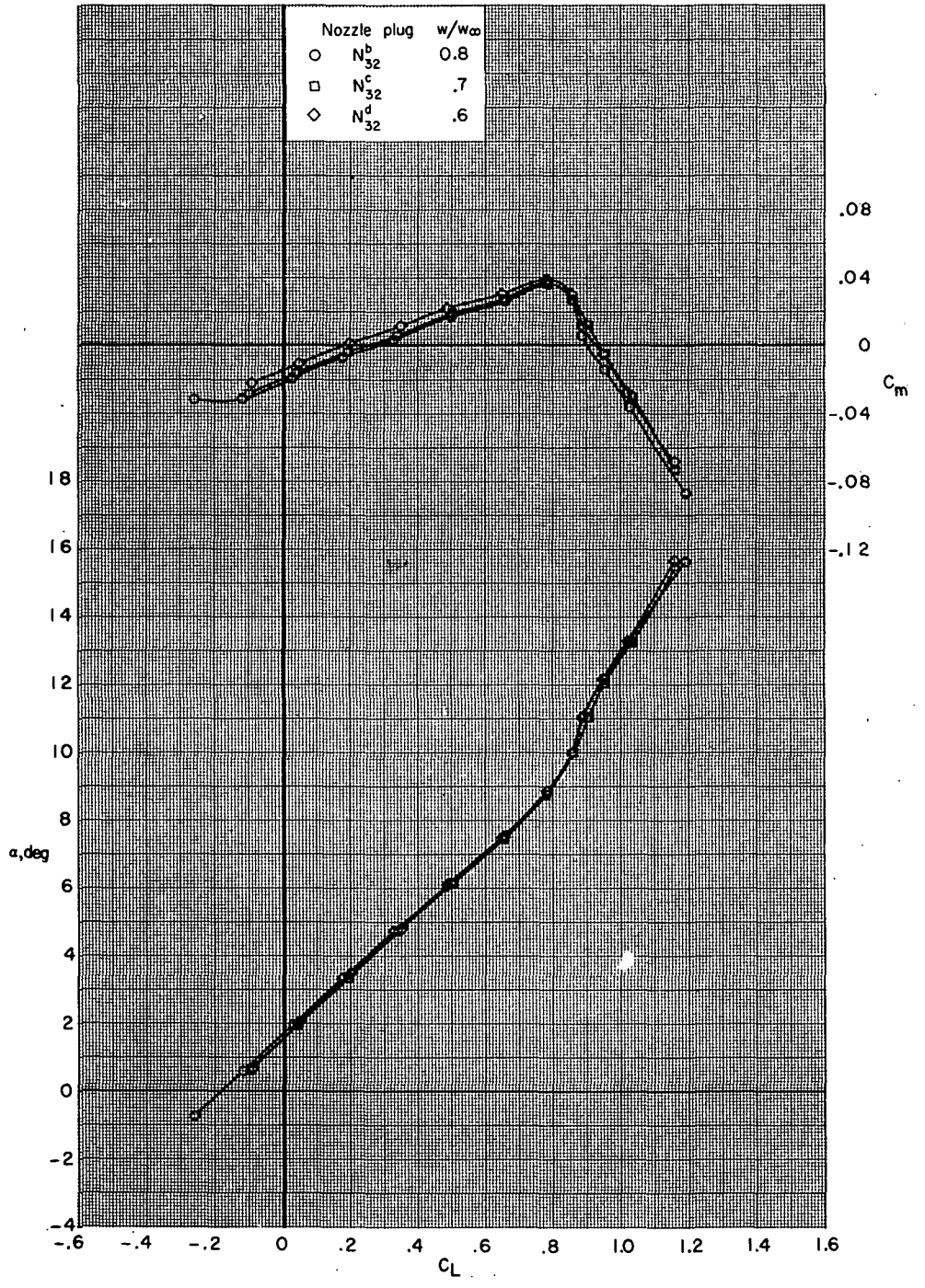

(c) M = 0.80.

Figure 33.- Continued.

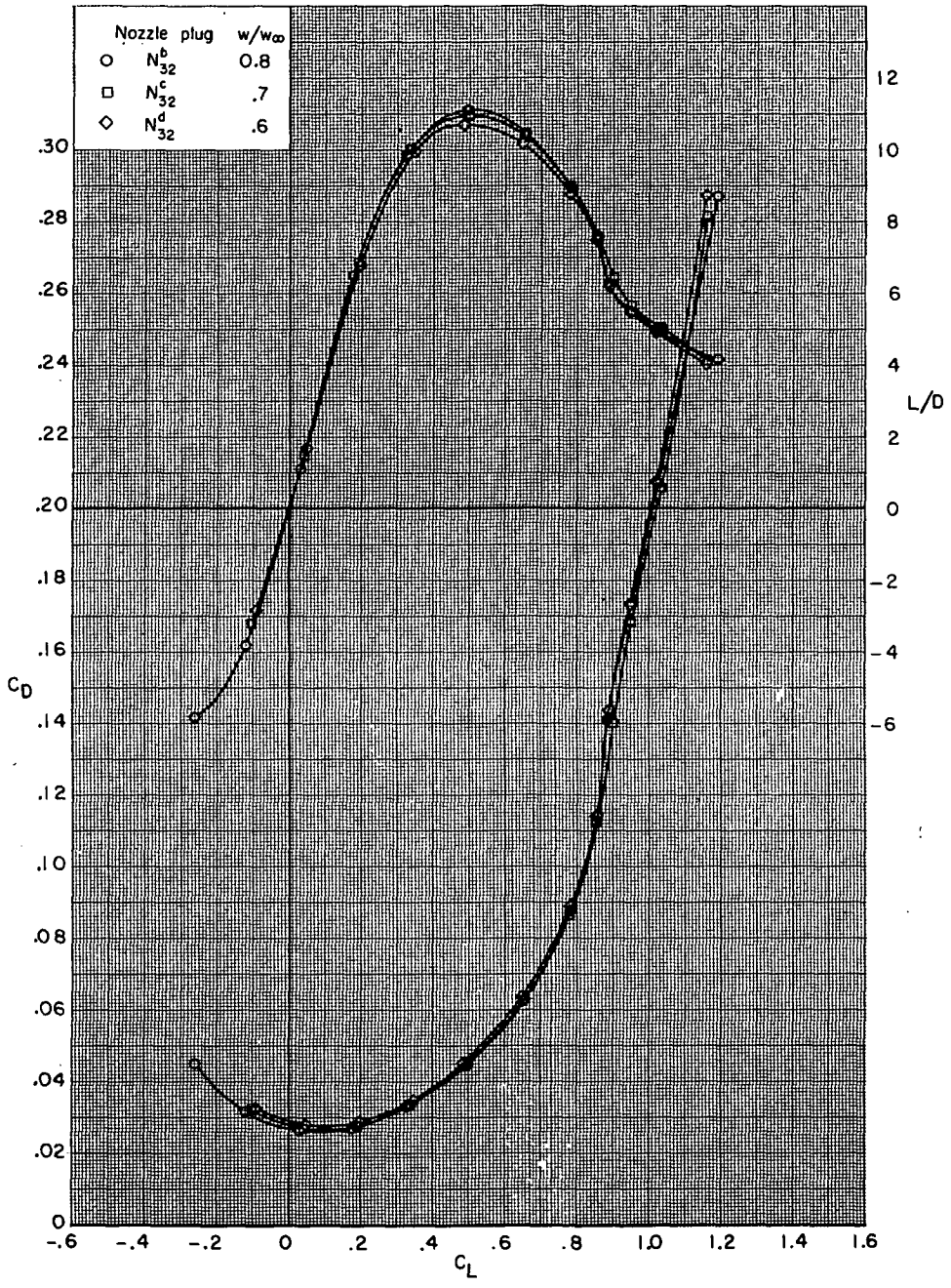

(c) Concluded.

Figure 33.- Continued.

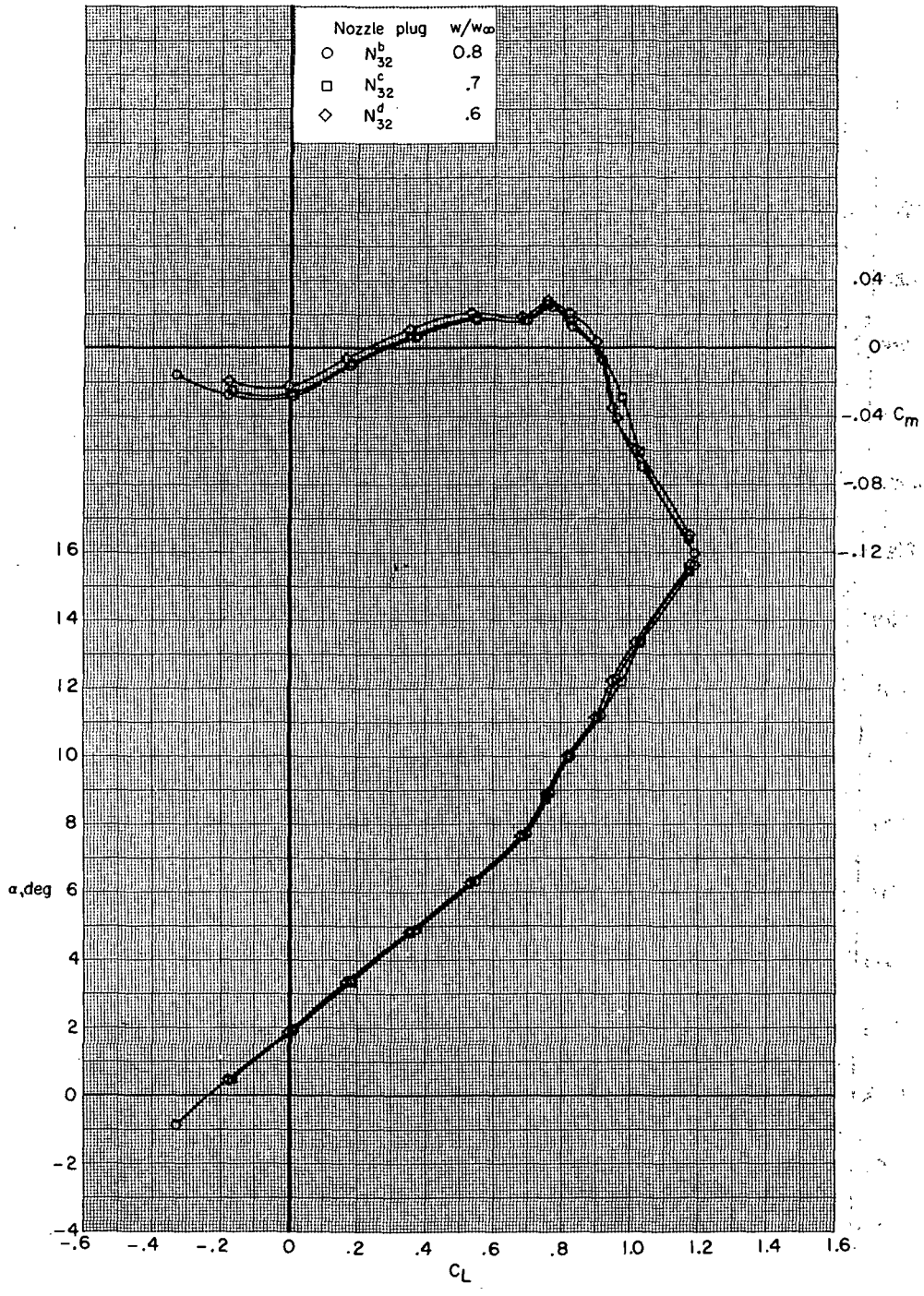

(d) M = 0.85.

Figure 33.- Continued.

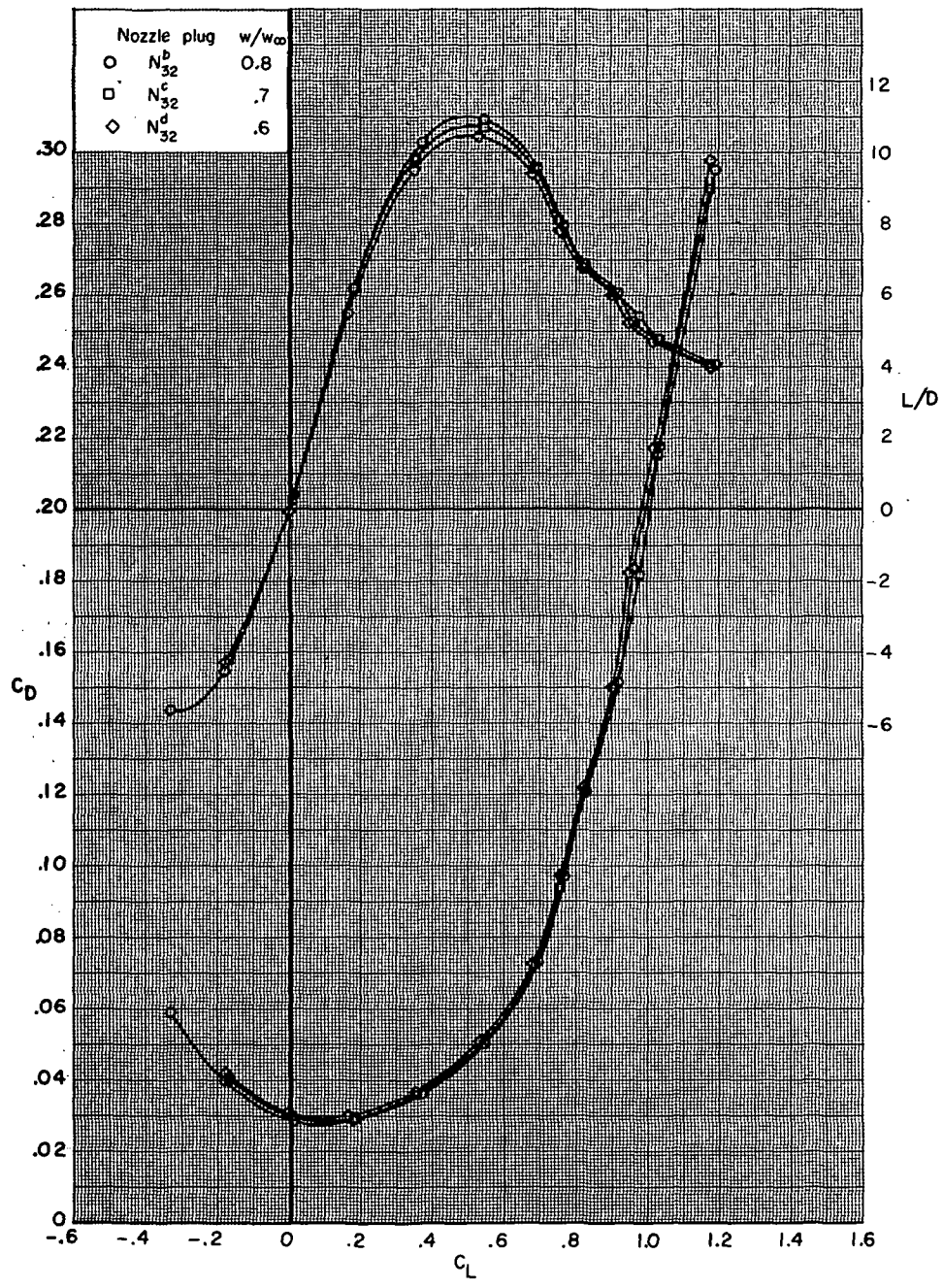

(d) Concluded.

Figure 33.- Continued.

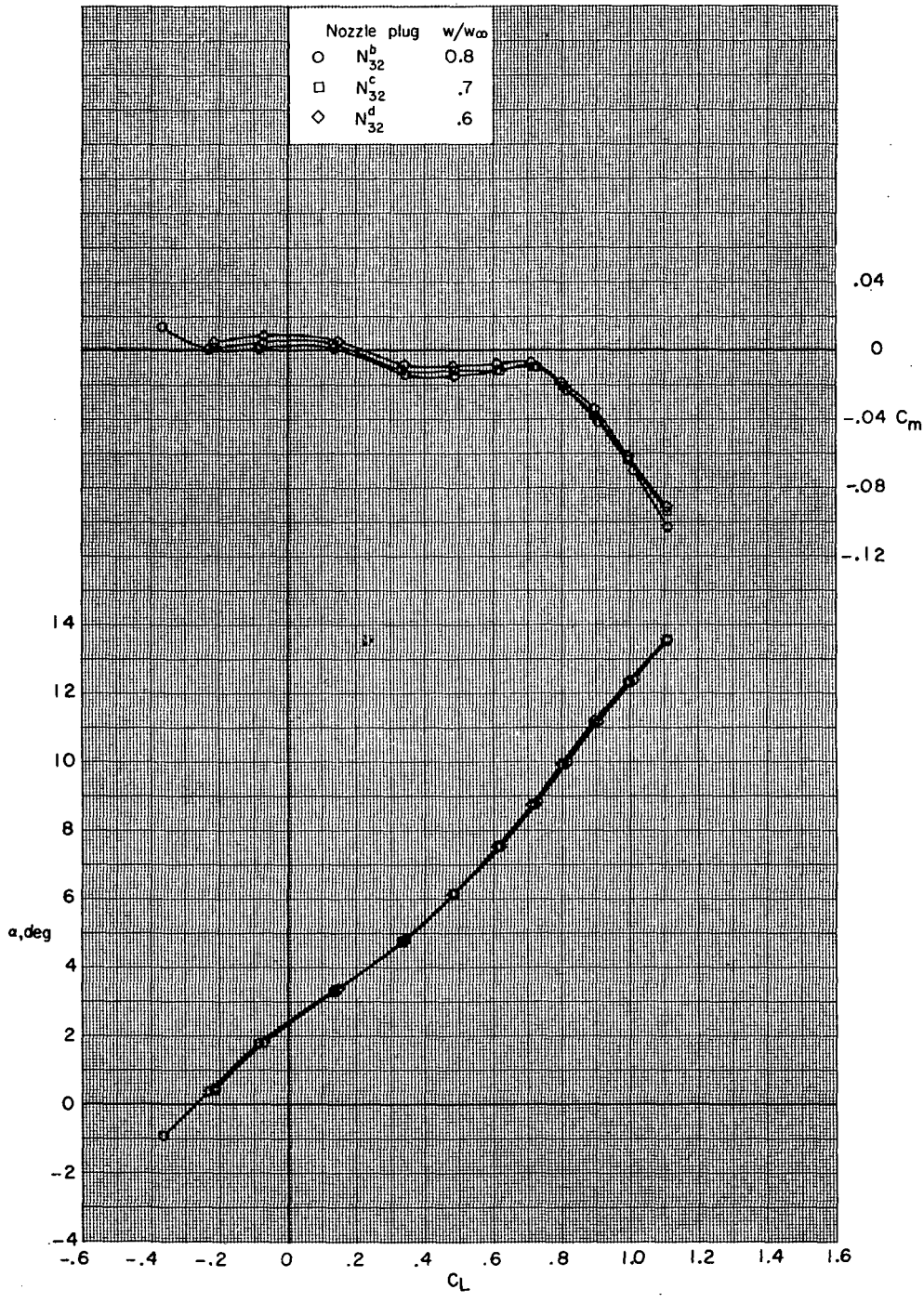

(e) M = 0.90.

Figure 33.- Continued.

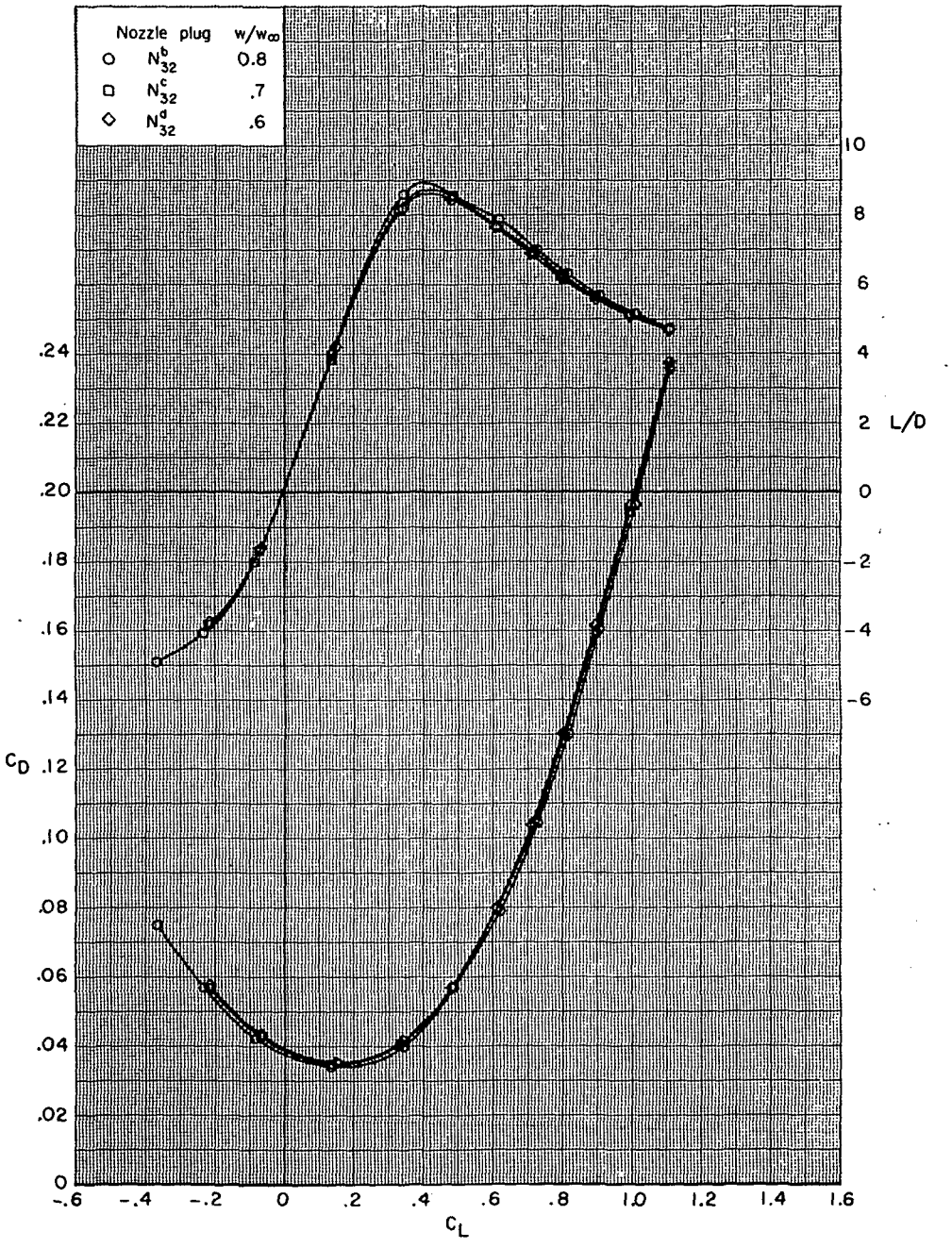

(e) Concluded.

Figure 33.- Concluded.

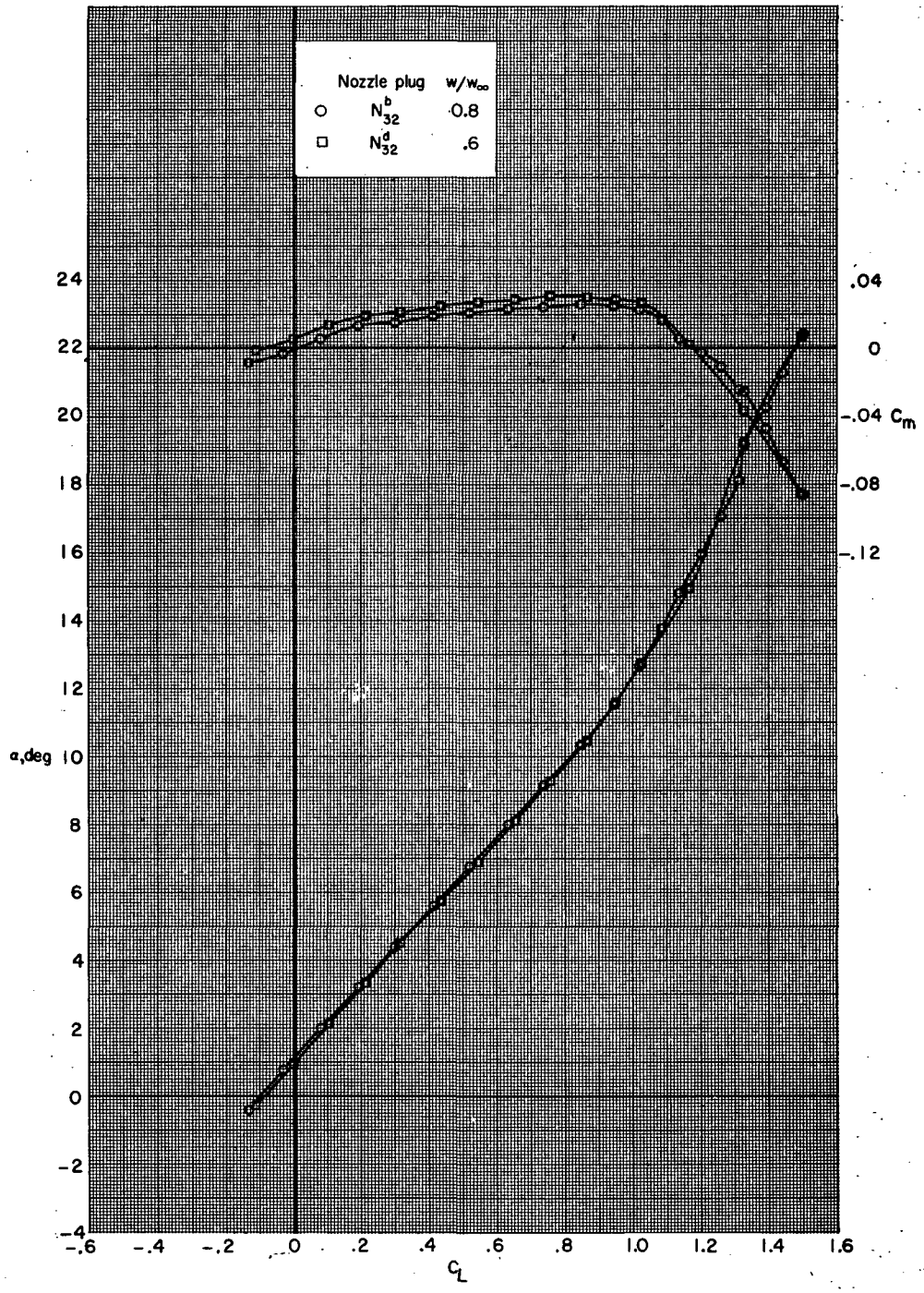

(a) M = 0.60.

Figure 34.- Effect of internal mass-flow ratio on aerodynamic characteristics for configurations $B_{80}G_{50}H_{13}I_{71}N_{32}^{X}V_{29}V_{38}W_{36}X_{24}$ with wing swept 26.0°.

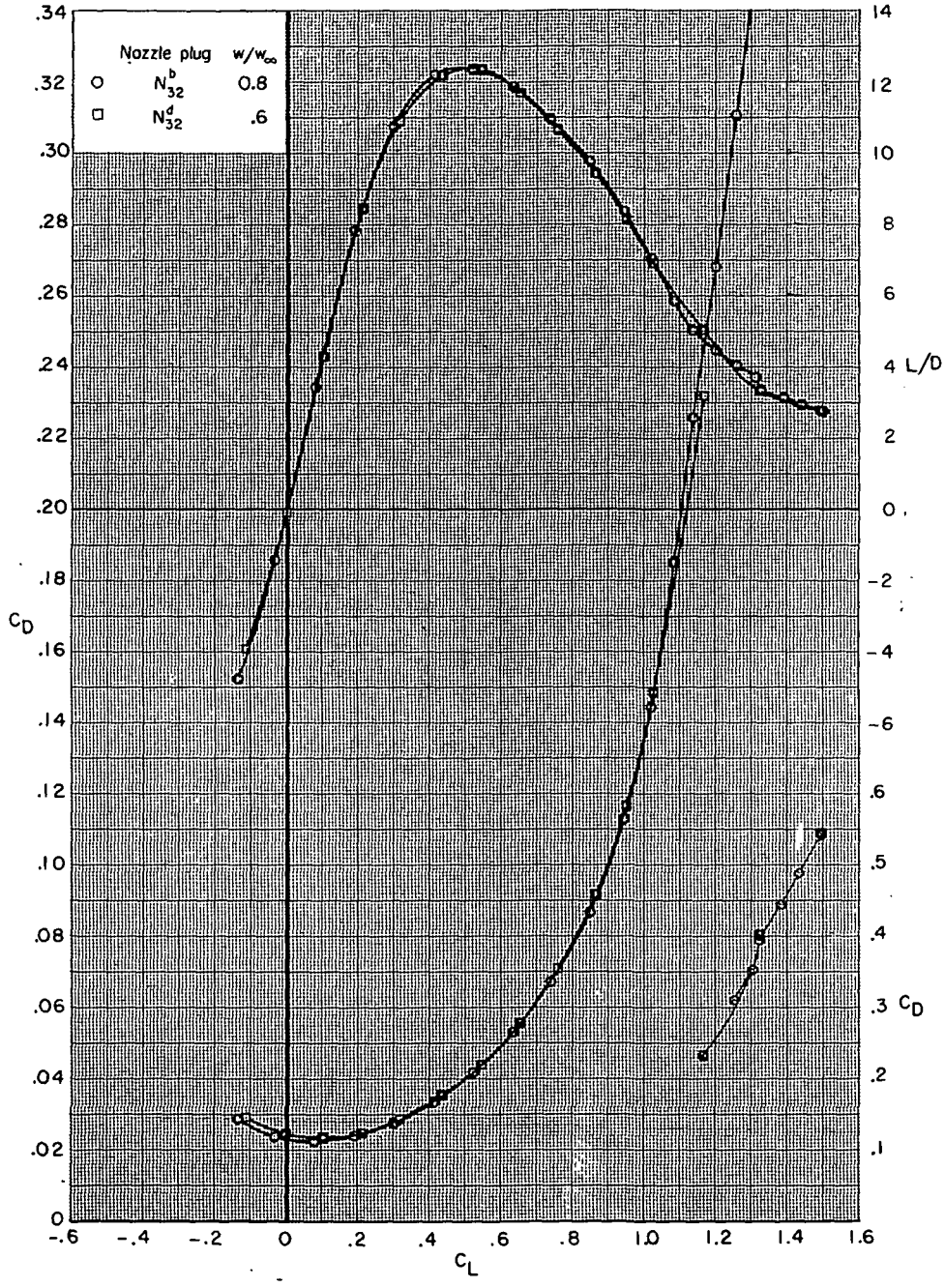

(a) Concluded.

Figure 34.- Continued.

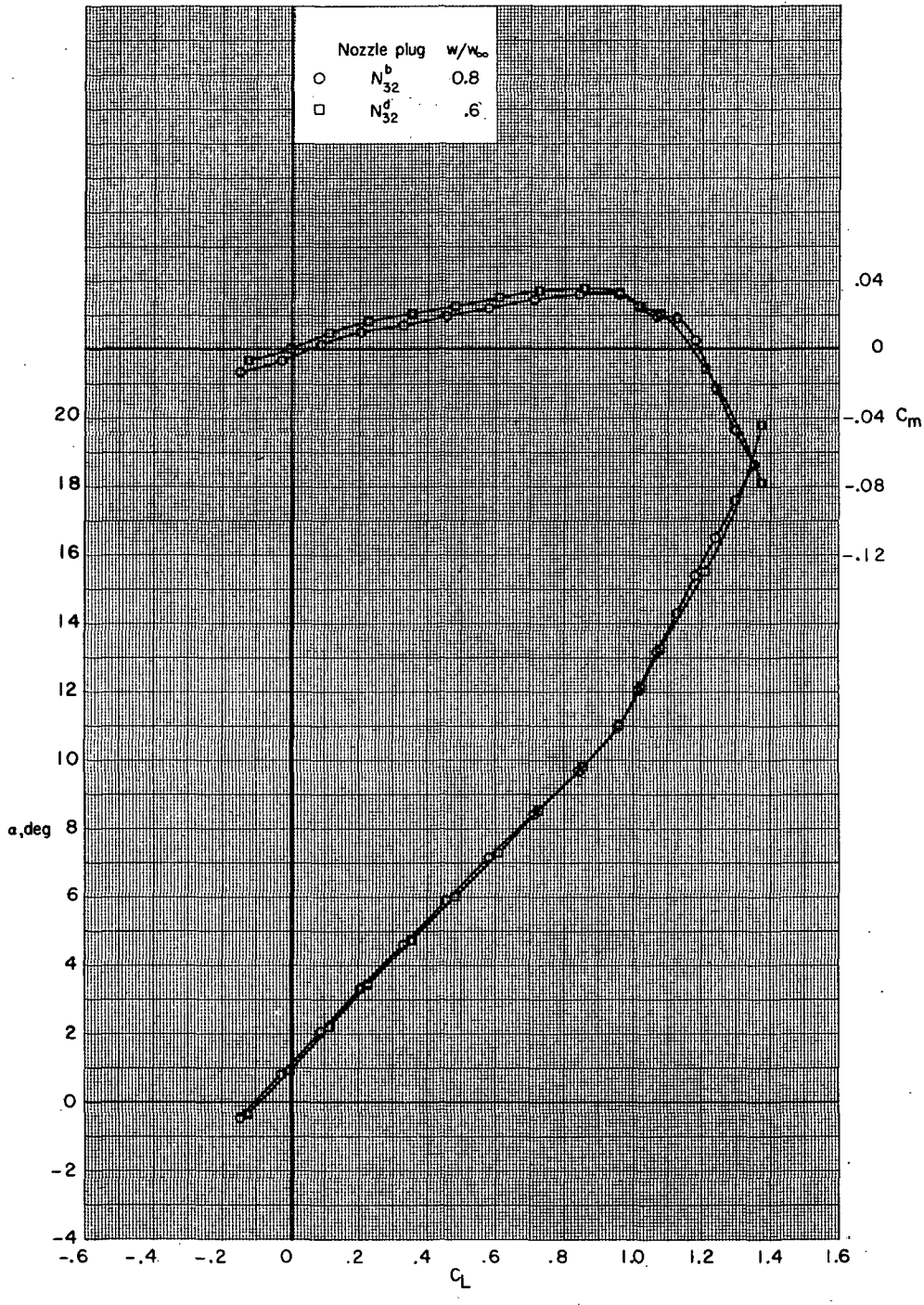

(b) M = 0.70.

Figure 34.- Continued.

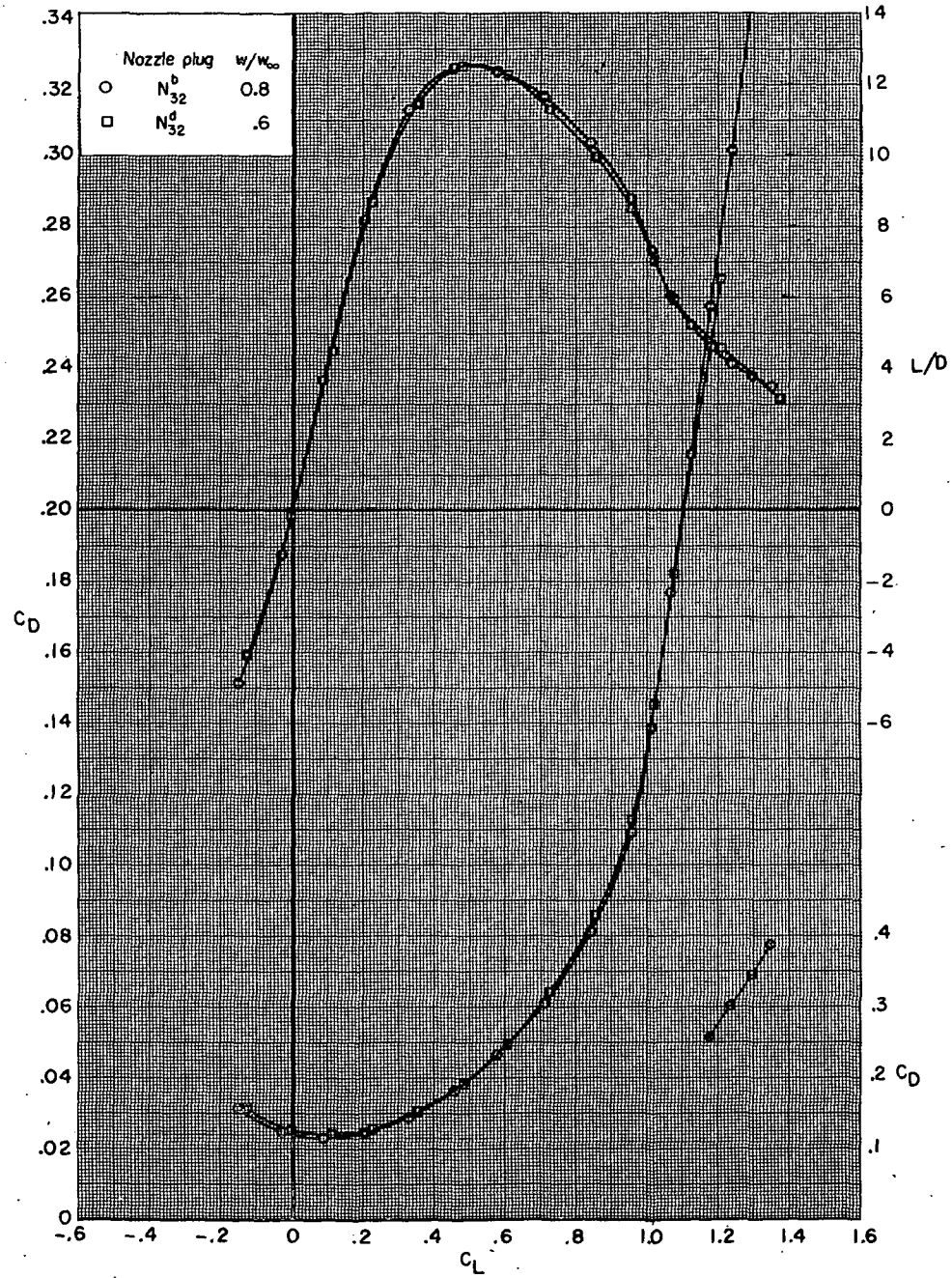

(b) Concluded.

Figure 34.- Continued.

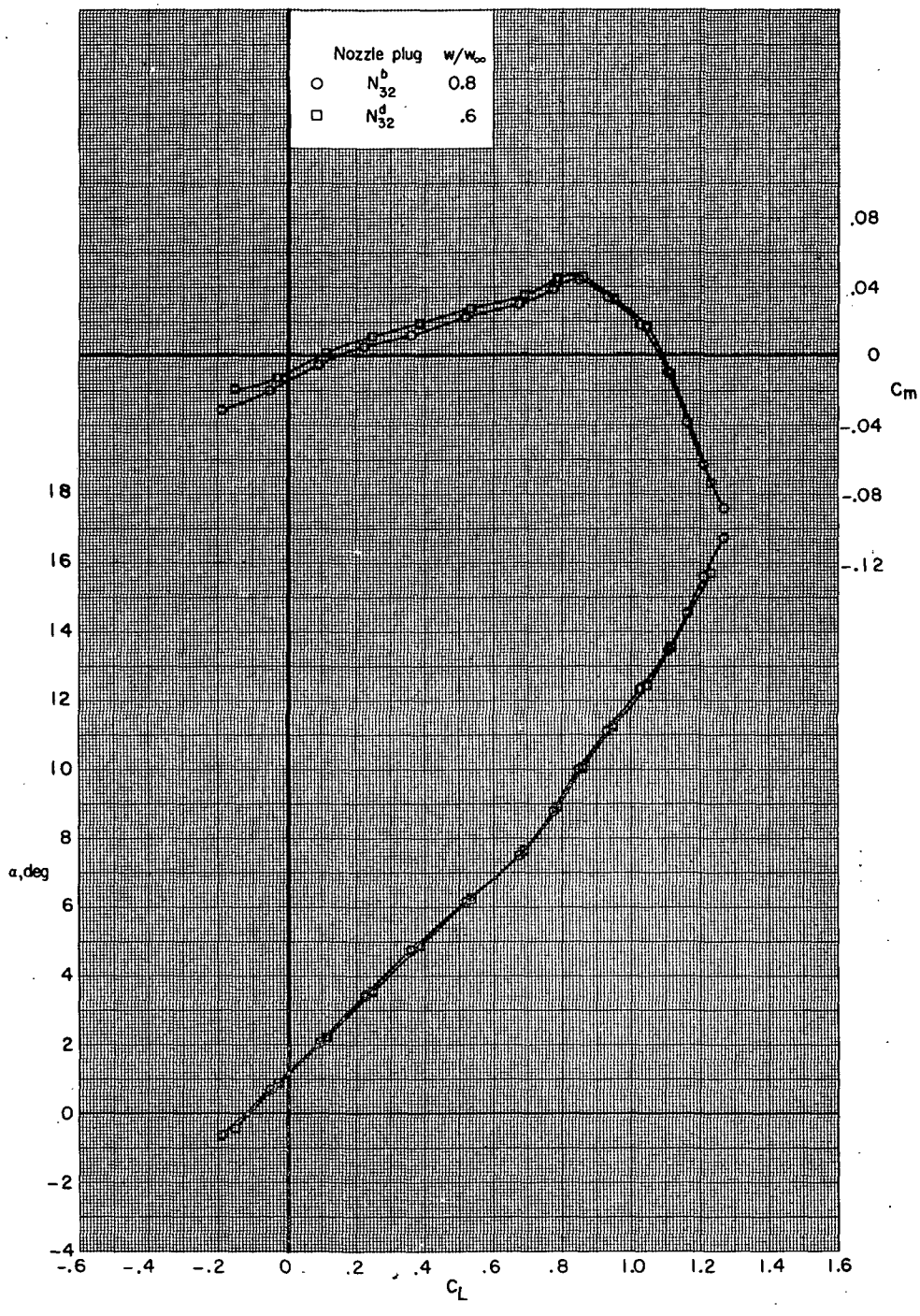

(c) M = 0.80.

Figure 34.- Continued.

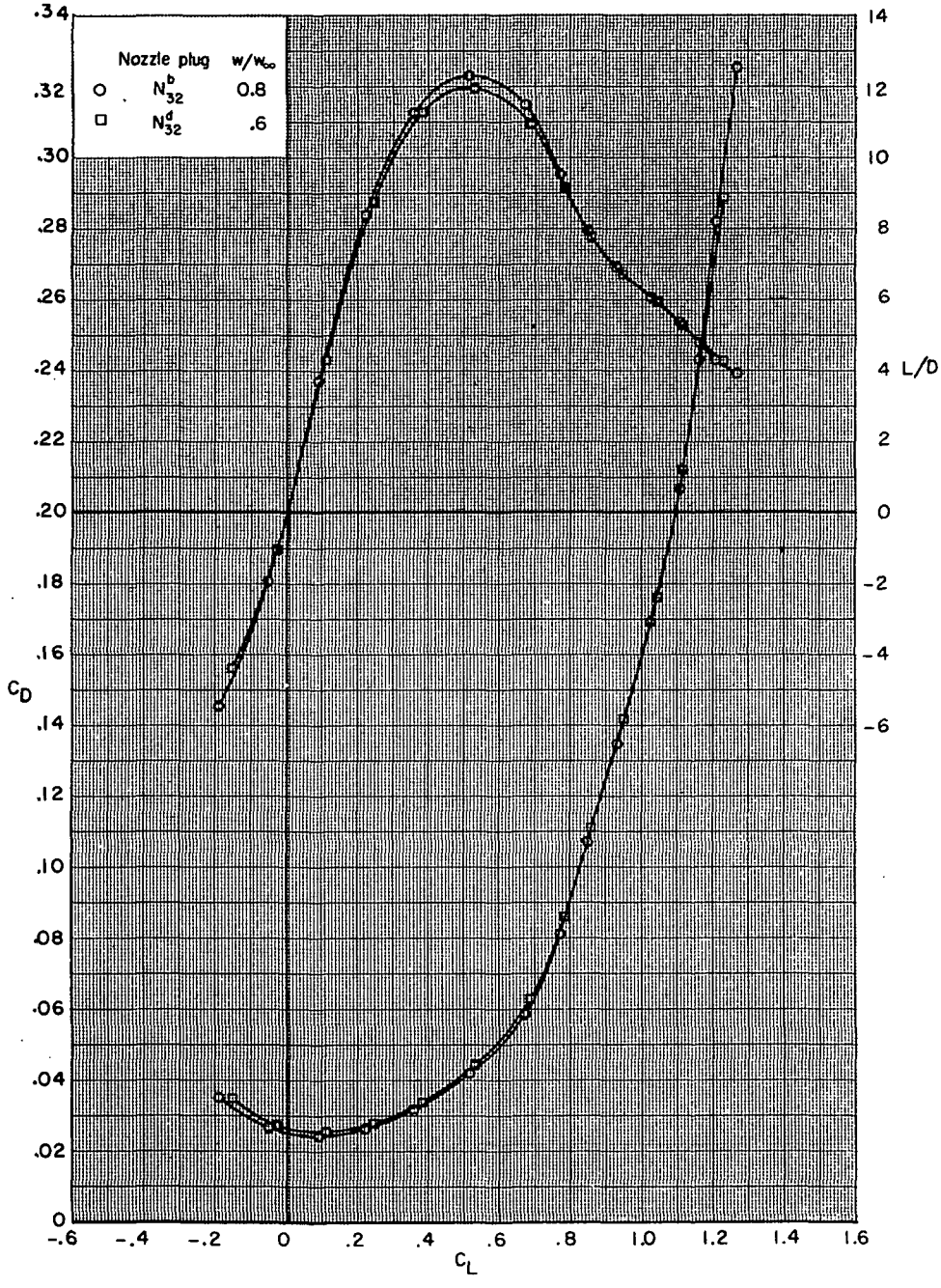

(c) Concluded.

Figure 34.- Continued.

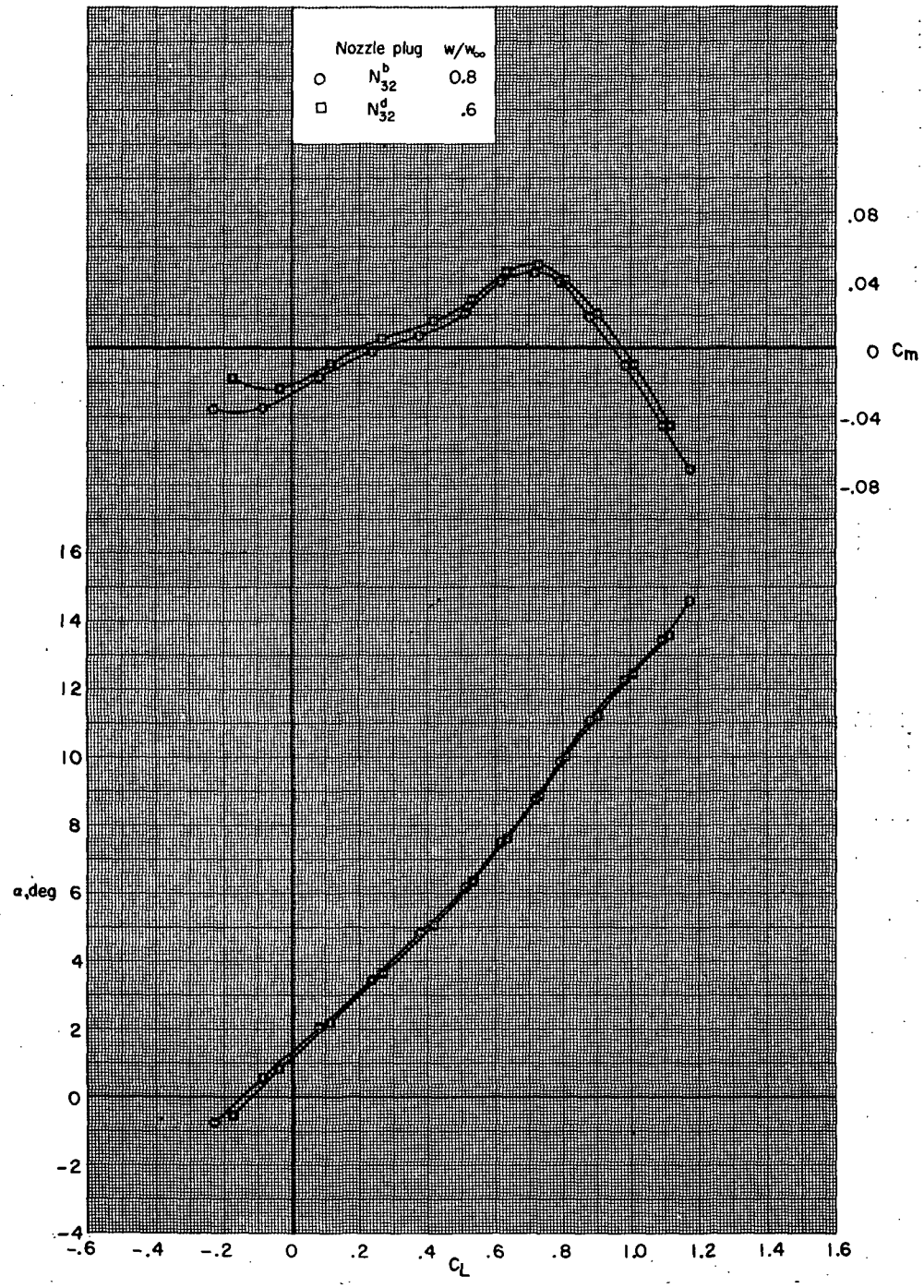

(d) M = 0.85.

Figure 34.- Continued.

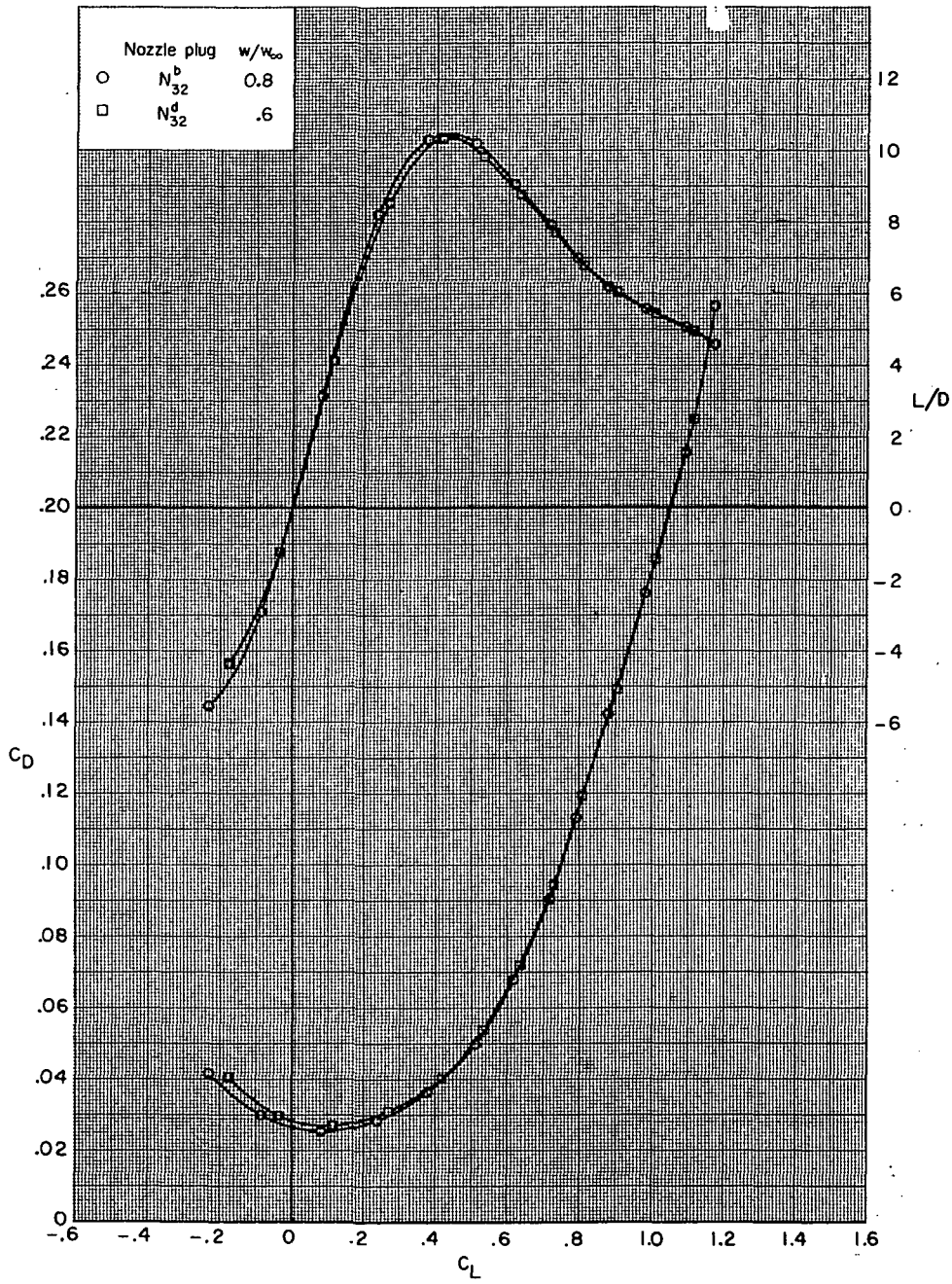

(d) Concluded.

Figure 34.- Continued.

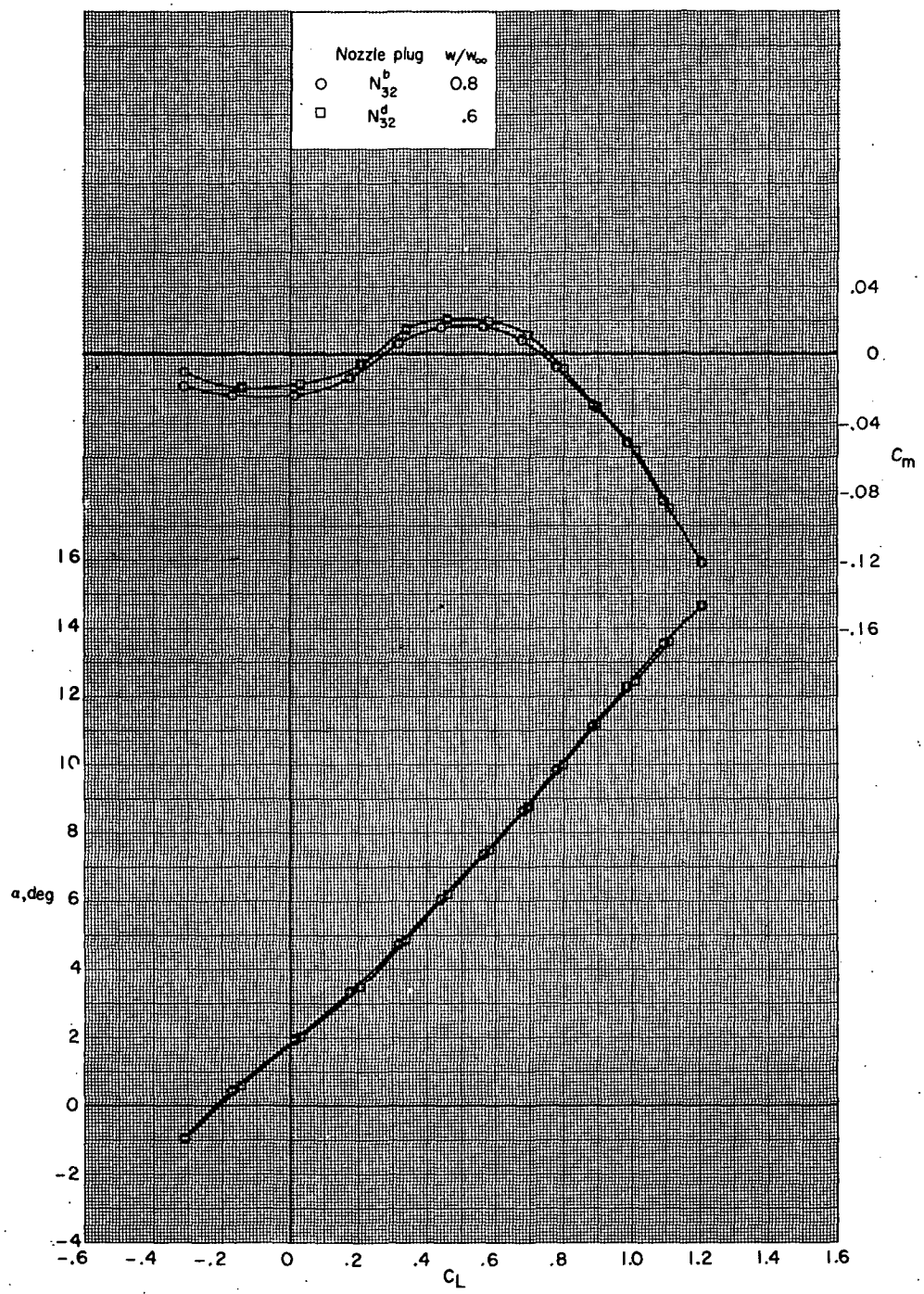

(e) M = 0.90.

Figure 34.- Continued.

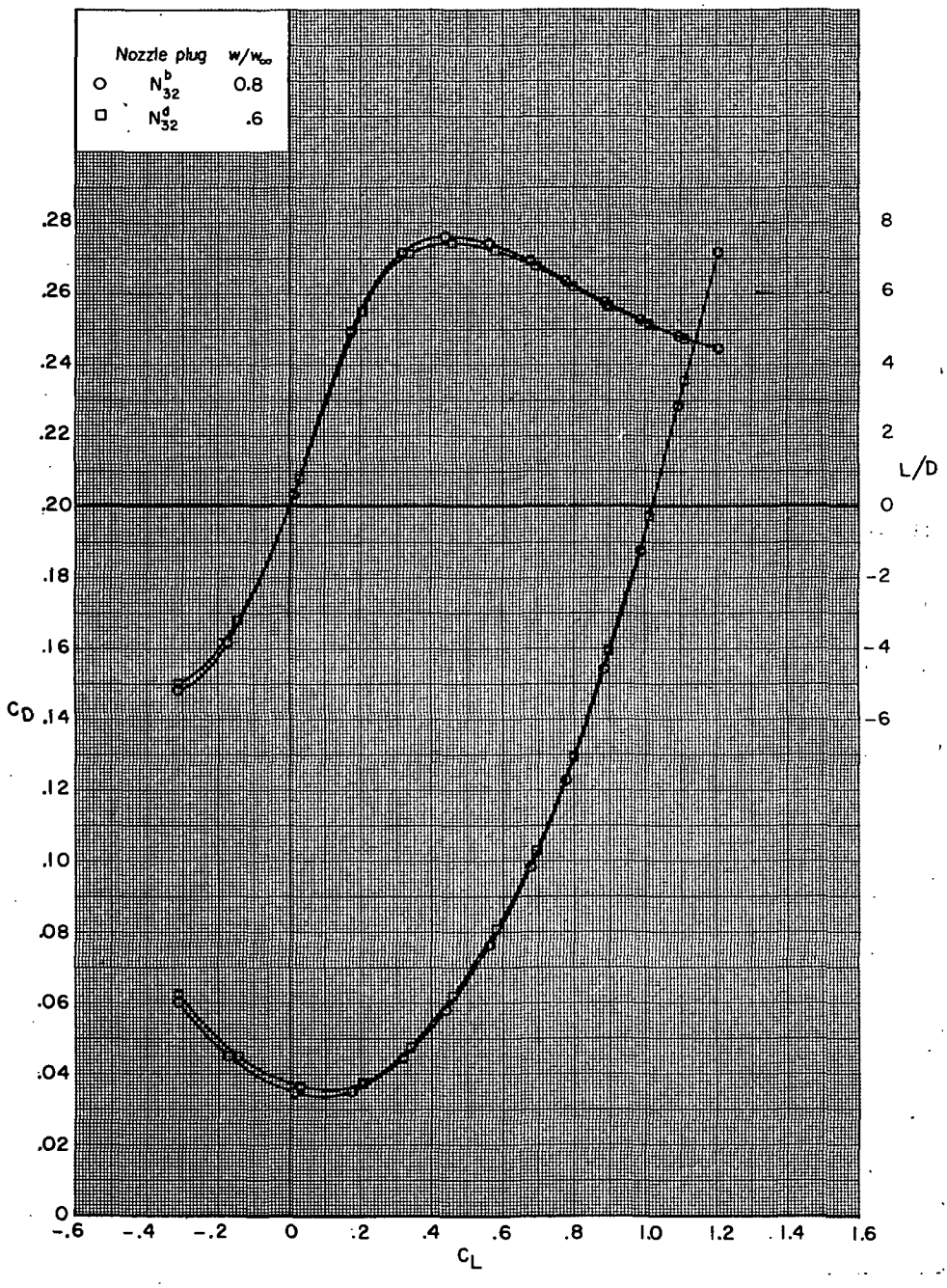

(e) Concluded.

Figure 34.- Concluded.

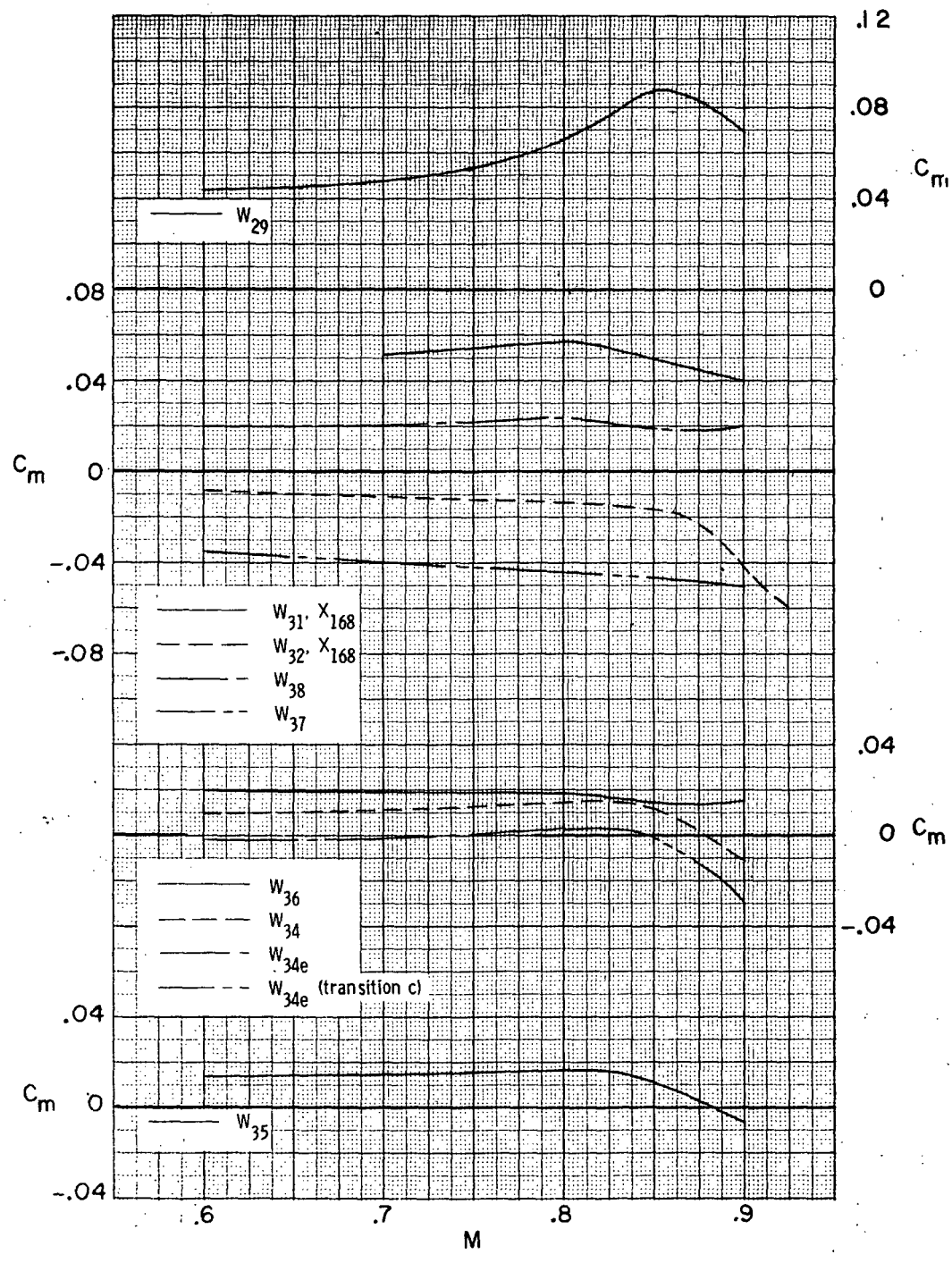

Figure 35.- Variation of pitching-moment coefficient with Mach number. C_L = 0.465; Λ = 26.0°; δ_h = 0°; transition b unless otherwise noted.

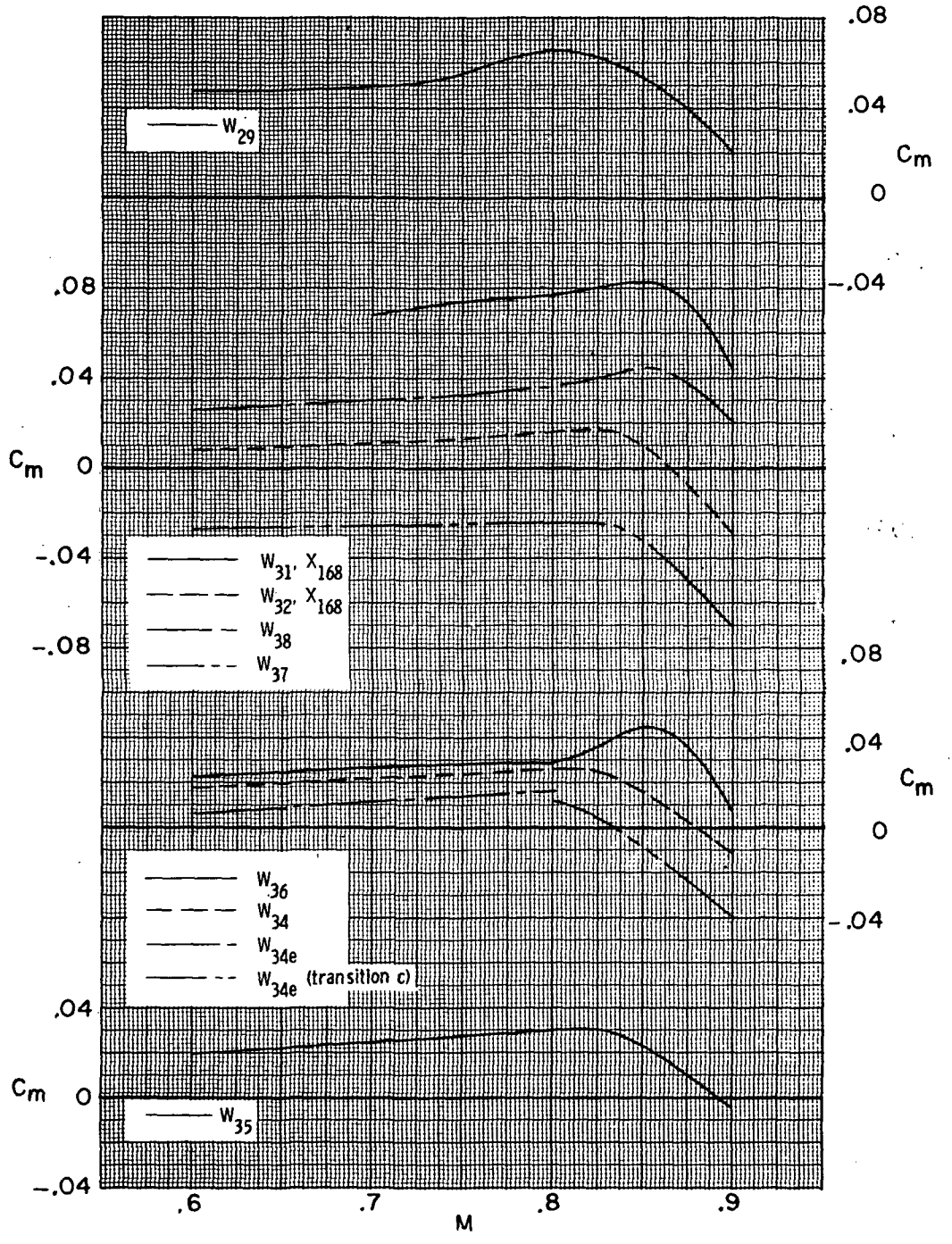

Figure 36.- Variation of pitching-moment coefficient with Mach number. C_L = 0.670; Λ = 26.0°; δ_h = 0°; transition b unless otherwise noted.

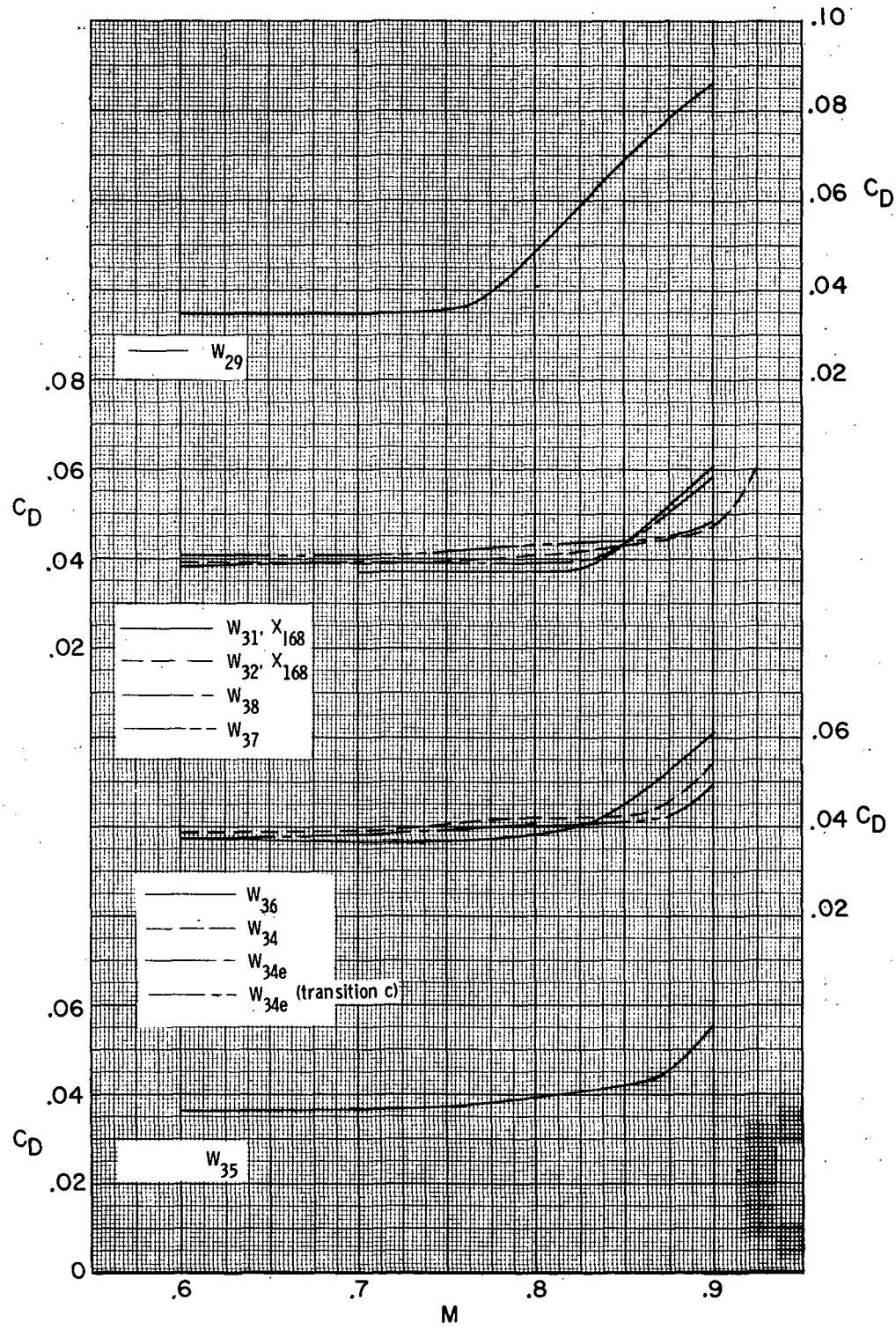

Figure 37.- Variation of cruise drag coefficient with Mach number. $C_L = 0.465$; $\Lambda = 26.0^o$; $\delta_h = 0^o$; transition b unless otherwise noted.

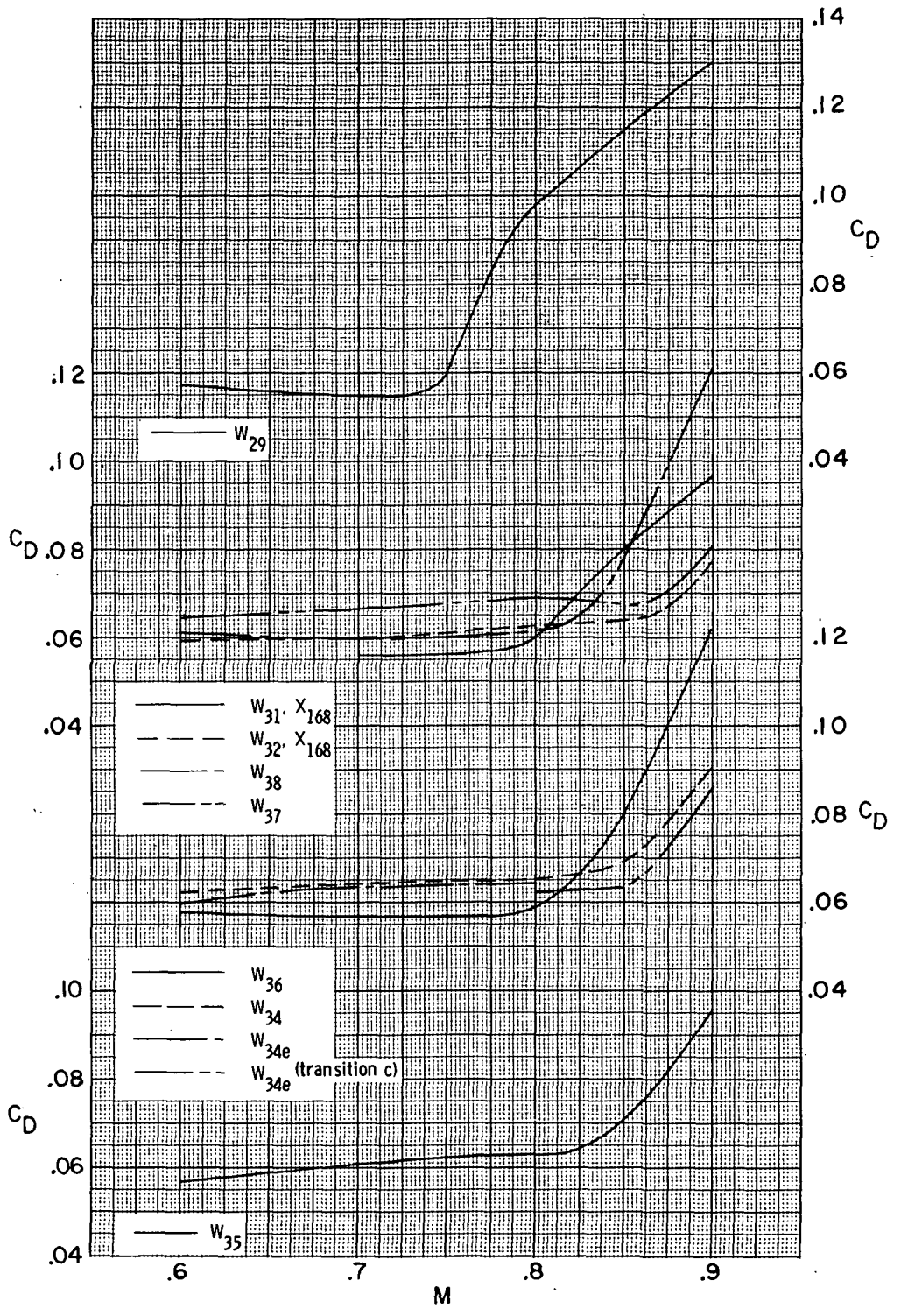

Figure 38.- Variation of maneuver drag coefficient with Mach number. C_L = 0.670; Λ = 26.0°; δ_h = 0°; transition b unless otherwise noted.

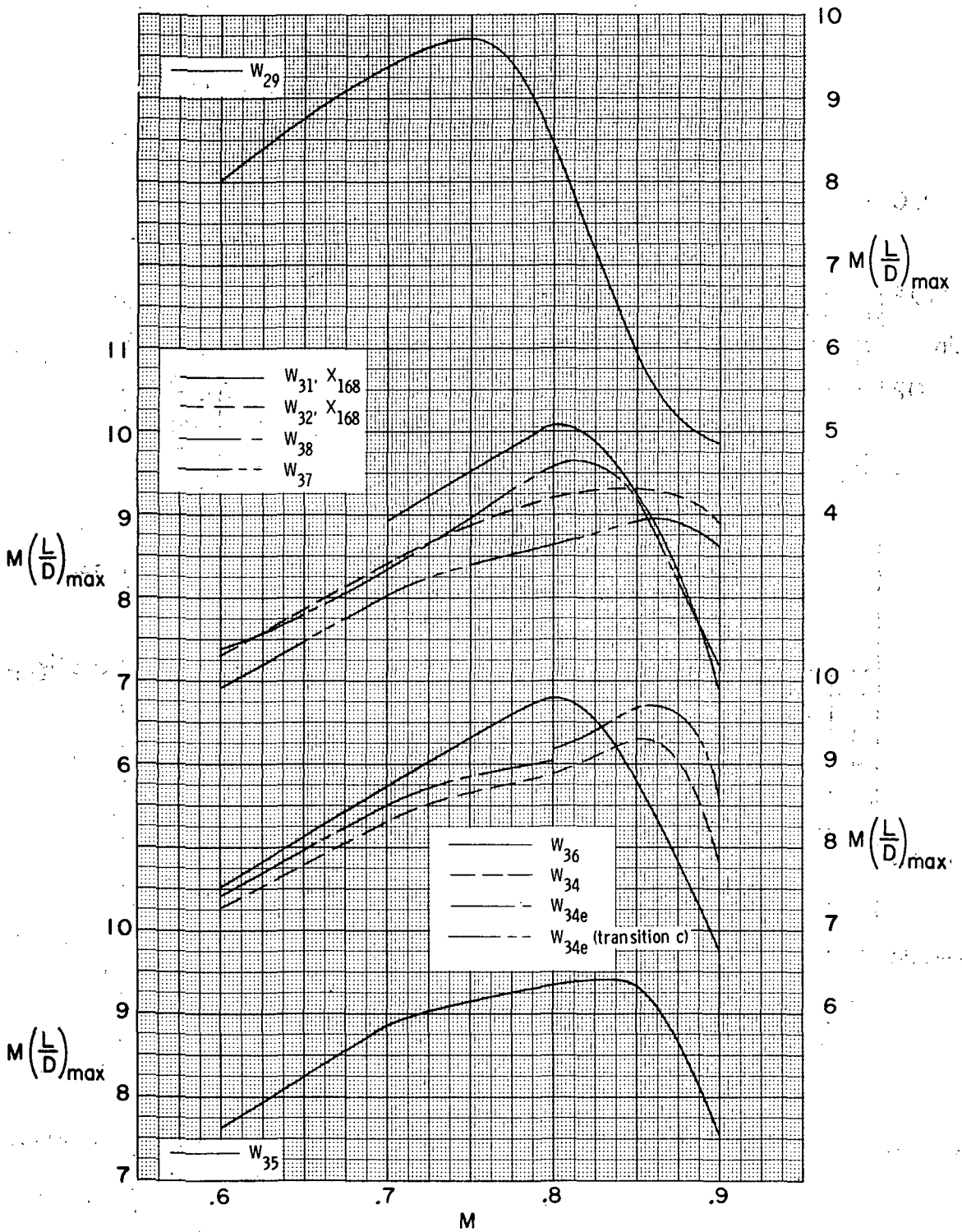

Figure 39.- Variation of aerodynamic range factor with Mach number. Λ = 26.0°; δ_h = 0°; transition b unless otherwise noted.

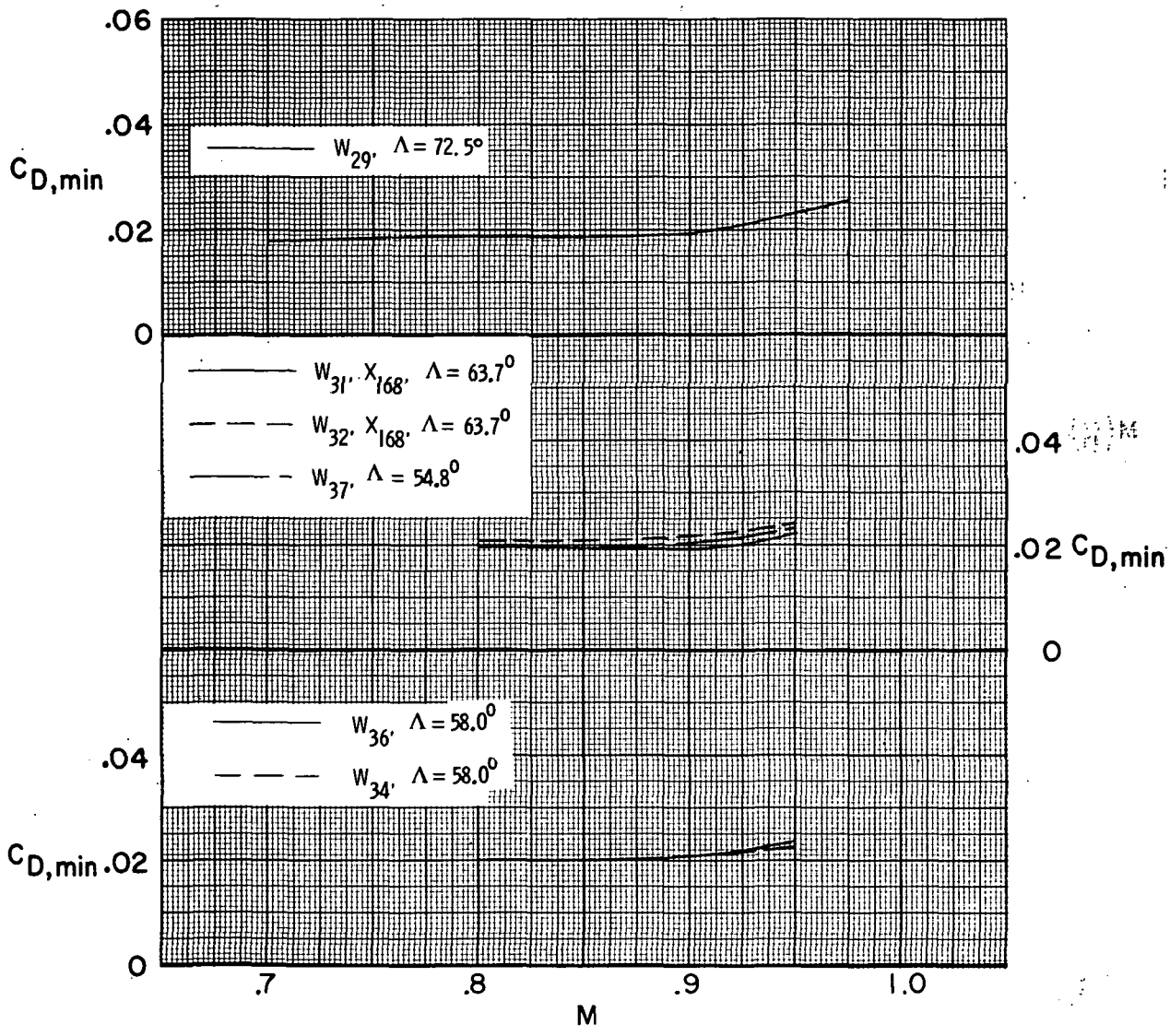

Figure 40.- Variation of minimum drag coefficient with Mach number for maximum wing sweep angle. $\delta_h = 0^o$; transition a.

*U.S. GOVERNMENT PRINTING OFFICE: 1977 - 735-004/20

NATIONAL AERONAUTICS AND SPACE ADMINISTRATION
WASHINGTON, D.C. 20546

OFFICIAL BUSINESS
PENALTY FOR PRIVATE USE $300

SPECIAL FOURTH-CLASS RATE BOOK

POSTAGE AND FEES PAID
NATIONAL AERONAUTICS AND SPACE ADMINISTRATION
451

U.S.MAIL

POSTMASTER: If Undeliverable (Section 158 Postal Manual) Do Not Return

"The aeronautical and space activities of the United States shall be conducted so as to contribute . . . to the expansion of human knowledge of phenomena in the atmosphere and space. The Administration shall provide for the widest practicable and appropriate dissemination of information concerning its activities and the results thereof."

—NATIONAL AERONAUTICS AND SPACE ACT OF 1958

NASA SCIENTIFIC AND TECHNICAL PUBLICATIONS

TECHNICAL REPORTS: Scientific and technical information considered important, complete, and a lasting contribution to existing knowledge.

TECHNICAL NOTES: Information less broad in scope but nevertheless of importance as a contribution to existing knowledge.

TECHNICAL MEMORANDUMS: Information receiving limited distribution because of preliminary data, security classification, or other reasons. Also includes conference proceedings with either limited or unlimited distribution.

CONTRACTOR REPORTS: Scientific and technical information generated under a NASA contract or grant and considered an important contribution to existing knowledge.

TECHNICAL TRANSLATIONS: Information published in a foreign language considered to merit NASA distribution in English.

SPECIAL PUBLICATIONS: Information derived from or of value to NASA activities. Publications include final reports of major projects, monographs, data compilations, handbooks, sourcebooks, and special bibliographies.

TECHNOLOGY UTILIZATION PUBLICATIONS: Information on technology used by NASA that may be of particular interest in commercial and other non-aerospace applications. Publications include Tech Briefs, Technology Utilization Reports and Technology Surveys.

Details on the availability of these publications may be obtained from:

SCIENTIFIC AND TECHNICAL INFORMATION OFFICE

NATIONAL AERONAUTICS AND SPACE ADMINISTRATION

Washington, D.C. 20546